SPACE RESOURCES and SPACE SETTLEMENTS

NASA

NASA SP-428

SPACE RESOURCES and SPACE SETTLEMENTS

Technical papers derived from the 1977 Summer Study at NASA Ames Research Center, Moffett Field, California

Study Director
    Gerard K. O'Neill
    Princeton University, Princeton, New Jersey

Editors
    John Billingham and William Gilbreath
    NASA Ames Research Center, Moffett Field, California
    Brian O'Leary
    Princeton University, Princeton, New Jersey

Manuscript Editor
    Beulah Gossett
    Los Altos, California

NASA

Preface

This publication contains the technical papers from the five task groups that took part in the 1977 Ames Summer Study on Space Settlements and Industrialization Using Nonterrestrial Materials. The study was sponsored by the following NASA Headquarters organizations: Office of Space Science, Office of Aeronautics and Space Technology, and Office of Space Transportation Systems. The NASA Ames Research Center hosted the study and provided administrative support through its Life Sciences Directorate. Expert assistance in the many aspects of the study came from NASA Headquarters, NASA centers, universities, industry, and from individual consultants.

This summer study was the largest and most comprehensive investigation of space manufacturing and habitation to date; forty senior research workers and ten students participated. The six-week study was preceded by several months of planning and preparation, and was followed by extensive work on manuscript checking, review, and assembly. The study topics reflected the research areas requiring the most intensive attention as of mid-1977; they were:

Group I: Regenerative life-support systems and controlled environment agriculture.

Group II: Parametric studies of efficient habitats in space. Time and cost analysis of a space manufacturing program plan.

Group III: Detection and analysis of special classes of asteroids suitable as material resources for space manufacturing; studies of retrieval missions.

Group IV: Electromagnetic mass drivers for use as inter-orbital engines, as devices to launch lunar material into space, and as tugs for the retrieval of asteroidal material.
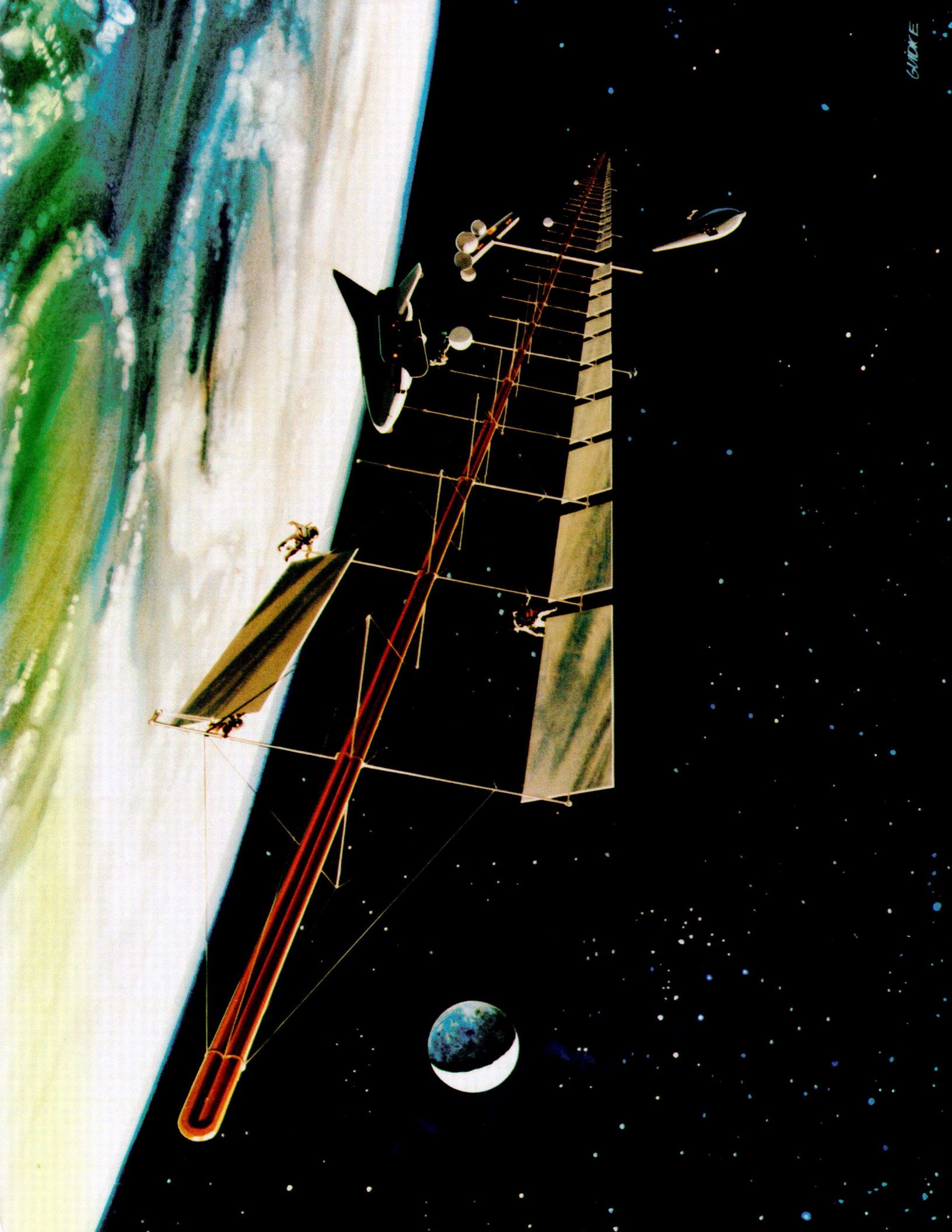
Group V: Chemical processing of nonterrestrial material in space; manufacture of metals and glass fibers, beneficiation, and design of processing plants.

These five task groups each produced two or more technical papers, signed by the contributing members. The papers were subjected to independent peer review by scientists not connected with the study. During the course of the study, frequent formal and informal exchanges of information occurred between task groups, so that the entire effort evolved in a coherent fashion and was directed toward common goals. However, each group remained responsible for the choice of its topics and for its conclusions.

A listing of all the participants is given on pages **vii-x**. It would be inappropriate for me to single out particular people or groups for special mention, since all involved applied their skills with dedication and enthusiasm. Instead, I thank everyone for their contributions to the success of the study, and also for making it a united and warmly cooperative personal experience.

GERARD K. O'NEILL
Study Director

Table of Contents

List of Participants

Director

O'NEILL, GERARD K.
Department of Physics
Princeton University

Special Consultant

CHESTON, STEPHEN
The Graduate School
Georgetown University

Study Coordinator

ZEITMAN, BENJAMIN
Extraterrestrial Biology Division
NASA-Ames Research Center

CLOSED ECOLOGICAL SYSTEMS

Chairman

SPURLOCK, JACK
Engineering Experiments Station
Georgia Institute of Technology

Members

COOPER, WILLIAM
Department of Zoology
Michigan State University

DEAL, PAUL
Extraterrestrial Biology Division
NASA-Ames Research Center

HARLAN, ANNITA
Department of Botany
Pima College (Arizona)

KAREL, MARCUS
Department of Nutrition
Massachusetts Institute of Technology

MODELL, MICHAEL
Department of Chemical Engineering
Massachusetts Institute of Technology

MOE, PAUL W.
Ruminant Nutrition Laboratory
National Agricultural Research Center

PHILLIPS, JOHN
Environmental Research Laboratory
University of Arizona

PUTNAM, DAVID F.
Umpqua Research Co.
Myrtle Creek, Oregon

RAPER, C. DAVID
Department of Soil Science
North Carolina State University

SWAN, ELLIOT G.
Department of Electrical Engineering
Princeton University

TAUB, FRIEDA B.
College of Fisheries WH-I 0
University of Washington

THOMAS, JUDITH
Department of Soil Science
North Carolina State University

ZEITMAN, BENJAMIN
Extraterrestrial Biology Division
NASA-Ames Research Center

Consultants

QUATTRONE, PHILIP
Extraterrestrial Biology Division
NASA-Ames Research Center

WILSON, CHRISTINE
Department of International Health
University of California (Berkeley)

ENVIRONMENTAL PARAMETERS

Chairman

SHETTLER, JOHN
Special Concepts Studio
General Motors Corporation

Members

BILLINGHAM, JOHN
Extraterrestrial Biology Division
NASA-Ames Research Center

BOCK, EDWARD H.
General Dynamics Corporation
San Diego, California

ENGEL, JOSEPH
Department of Systems Engineering
University of Illinois (Chicago)

LAMBROU, FRED
Department of Electrical Engineering
Princeton University

SIMON, MICHAEL
Department of Aeronautics and Astronautics
Stanford University

VAJK, J. PETER
Science Applications Inc.
Pleasanton, California

Consultant

BROOME, TAFT
Department of Civil Engineering
Howard University

MASS DRIVERS

Chairman

O'NEILL, GERARD K.
Department of Physics
Princeton University

Members

ARNOLD, WILLIAM H.
Department of Physics
Hampshire College

BOWEN, STUART
Consultant
Palo Alto, California

COHEN, STEPHEN
Fluid Physics and Chemistry Branch
NASA-Lewis Research Center

FINE, KEVIN
Department of Physics
Massachusetts Institute of Technology

KAPLAN, DAVID
Department of Aerospace Engineering
University of Michigan

KOLM, HENRY
Francis Bitter National Magnet Laboratory
Massachusetts Institute of Technology

KOLM, MARGARET
Department of Mathematics
Haverford College

NEWMAN, JONATHAN
Department of Physics
Amherst College

SNOW, WILLIAM
Department of Physics
Massachusetts Inst. of Technology

ASTEROID RESOURCES

Chairman

O'LEARY, BRIAN
Department of Physics
Princeton University

Members

BENDER, DAVID
Mission Design Section
Jet Propulsion Laboratory

DUNBAR, R. SCOTT
Physics Department
Princeton University

GAFFEY, MICHAEL
Department of Astronomy
University of Hawaii

HELIN, ELEANOR
Division of Geological and Planetary Sciences
California Institute of Technology

ROSS, DAVID L.
Aeronautics and Astronautics Department
Stanford University

SALKELD, ROBERT
Consultant
Malibu, California

Consultants

MASCY, FRED
Planning and Analysis
NASA-Ames Research Center

NIEHOFF, JOHN
Science Applications Inc.
Chicago, Illinois

SKLAREW, RALPH
Science Applications Inc.
San Diego, California

NONTERRESTRIAL EXTRACTION AND CONSTRUCTION

Chairmen

BUNCH, THEODORE
Space Sciences Division
NASA-Ames Research Center

CRISWELL, DAVID
The Lunar Science Institute
Houston, Texas

Members

CHOUDARY, U. V.
Department of Materials
University of Wisconsin (Milwaukee)

ERSTFELD, THOMAS
The Lunar Science Institute
Houston, Texas

GILES, DAVID
Rio Amex Corporation
Denver, Colorado

HO, DARWIN
Department of Aeronautical Engineering
University of Michigan

LEE, STUART
Ford Aerospace and Communications Corp.
Palo Alto, California

McKAY, DAVID
Geology Branch
NASA-Johnson Space Center

RAO, D. B.
Materials and Molecular Research Division
Lawrence Berkeley Laboratory

SOBON, LEON
Shenandoah Winery
Plymouth, California

WILLIAMS, RICHARD
Geochemistry Branch
NASA-Johnson Space Center

Consultants

CHANG, AUSTIN
Department of Materials
University of Wisconsin (Milwaukee)

DEUTSCH, GEORGE
Office of Aeronautics and Space Technology
National Aeronautics and Space Administration

TECHNICAL PLANNING GROUP

Chairman

SADIN, STANLEY
Study & Analysis Office
National Aeronautics and Space Administration

Members

AKIN, DAVID
Department of Aeronautics and Space Technology
Massachusetts Institute of Technology

BURKE, JAMES
Space Program Development
Jet Propulsion Laboratory

CHESTON,STEPHEN
Graduate School
Georgetown University

CULBERTSON, PHILLIP
Office of Space Transportation
National Aeronautics and Space Administration

DEJONG, SUSAN
Hastings College of the Law
San Francisco, California

DRIGGERS, GERALD
Science Applications Inc.
Huntsville, Alabama

FIELDER, DENNIS
Program Planning Office
NASA-Johnson Space Center

GILBREATH, WILLIAM
Materials and Physical Science Branch
NASA-Ames Research Center

HIBBS, ALBERT
Strategic Planning and Studies
Jet Propulsion Laboratory

HOOK, RAY
Systems and Experiments Branch
NASA-Langley Research Center

PELOUCH, JAMES
Propulsion Systems Section
NASA-Lewis Research Center

ROLLINS, ROBERT
Office of Aeronautics and Space Technology
National Aeronautics and Space Administration

STROUD, WILLIAM
Planning Office
NASA-Goddard Space Flight Center

VON PUTTKAMER, JESCO
Advanced Studies
National Aeronautics and Space Administration

VON TIESENHAUSEN, GEORGE
Advanced Systems Office
NASA-Marshall Space Flight Center

Consultants

CONNORS, MARY
SETI Office
NASA-Ames Research Center

GLASER, JACK
Chief Counsel
NASA-Ames Research Center

HORNBY,HAROLD
Planning and Analysis Office
NASA-Ames Research Center

SECRETARIAL STAFF

BUESCHER, VERA
KROHNENGOLD,SHELLY
MICHAUD, KATHY

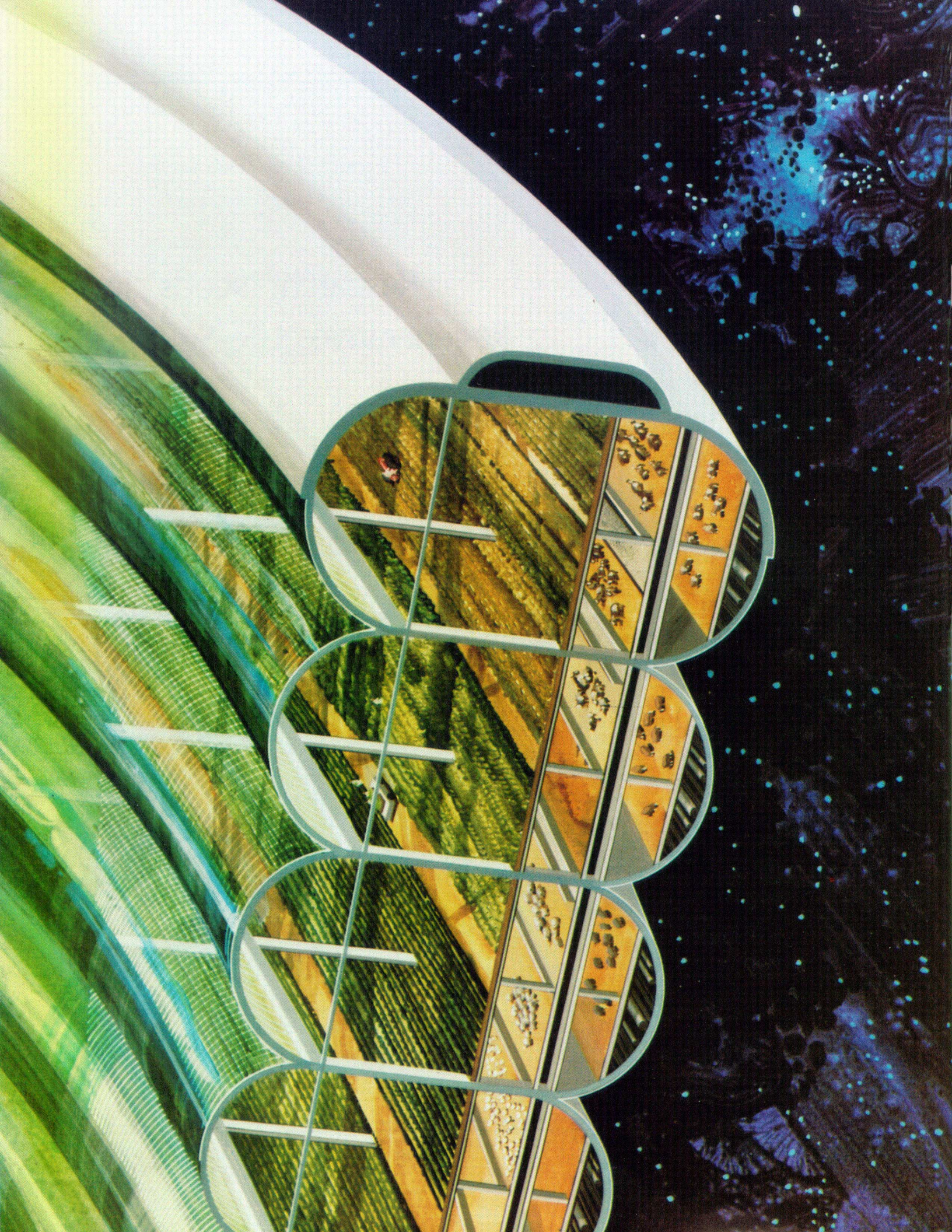## MANUSCRIPT

Graphics

PRZEKOP, MICHAEL

Preparation

OGATA, SARAH

I

Research Needs for Regenerative Life-Support Systems

I-1
Systems Engineering Overview for Regenerative Life-Support Systems Applicable to Space Habitats

JACK SPURLOCK and MICHAEL MODELL

The Life-Support Systems Group of the 1977 NASA Ames Summer Study conducted analyses initially to identify areas where partial or complete closure of the life-support system, for various types of space habitats, should be considered, and to develop a sound methodology for identifying, screening, and evaluating alternative closure schemes. Results of these analyses, including the systems engineering considerations that affect technology-development planning and management for regenerative life-support systems, are discussed. A recommended methodology is also presented as a basis for future technology-development activities in this area.

INTRODUCTION AND OBJECTIVES

The essentials for human survival are commonly referred to as the life-support system (LSS). Requirements for life support on manned space missions include those provisions and accommodations that are necessary to maintain human occupants of the vehicle or space station in a functional state. A functional state is defined as the willingness and physical ability to perform assignments effectively and to accept responsibilities for the duration of the mission. Thus, in general, the necessary provisions and accommodations consist of a primary set (adequate food, potable water, breathable air, and safety from identifiable hazards) and a secondary set (waste disposal, personal hygiene, medical care, and reasonable comfort). It is recognized that these factors affect the psychological, as well as the physiological well-being; however, the focus of this paper is on physiological considerations.

This report was prepared by the Life-Support Systems Group of the 1977 NASA Ames Summer Study on "Space Settlements and Industrialization Using Nonterrestrial Materials." This report summarizes the group's analyses and recommendations concerning several issues that were derived from the objectives of the group's study activity. These objectives included:

- Identification of the areas where partial or complete closure of the life-support system (LSS) loop should be considered
- Development of a sound methodology for identifying, screening, and evaluating candidate biological and physicochemical processing components for regenerative life-support systems applicable to space habitats

The 1977 NASA Ames Summer Study was concerned principally with industrial production in space using nonterrestrial materials, housing, and life support for an industrial work force in space, and space settlements per se. The study planners reasoned that the earliest industrial activities in space probably will depend on "open-loop" life-support provisions, including resupply from Earth for food and perhaps some partial regeneration of atmosphere components and water. However, beyond this early transitional period, it is believed that long-term space settlements for space industrialization will require essentially completely regenerative, or "closed," life-support systems. Therefore, the charter of the Life-Support Systems Group for the 1977 Summer Study was to determine the requirements for achieving this closure, including particularly the research that will be necessary over a period of many years.

The group's findings during the summer study are presented in this paper and its companion, subsequent paper entitled "Research Planning Criteria for Regenerative Life-Support Systems Applicable to Space Habitats." The information presented in these two papers represents interim results on systems analysis, the identification of research options, and the formulation of guidelines for the eventual assignment of research priorities. However, follow-up studies are anticipated and they will be reported later with more detailed assessments of research and development options and recommended priorities for resource allocations.

RATIONALE FOR SPECIFYING THE EXTENT OF CLOSURE

With minor exceptions, life-support functions on manned space missions to date have been accomplished by (1) the on-board storage at launch, of food, water, and atmosphere components; (2) removal (but not conversion) of trace contaminants and excess carbon dioxide; and (3) storage and return to Earth of waste residues. Provisions for personal

hygiene and medical care were very limited until the Skylab missions. These life-support procedures to date have at least been inherently reliable and safe if not a source of comfort, convenience, and pleasure for crew members.

The principal focus of prior NASA-sponsored research and development on life-support systems has centered on partial closure of the mass exchange through the use of physicochemical processes for atmosphere revitalization, wash water regeneration (nonpotable use), and waste conversion to veritable gases, reusable (potable) water, and a storable, compact ash. Food production and regeneration have received very little attention for space-mission applications.

Several trade-off determinations combined to provide the rationale for this orientation of LSS design and technology development until the present. These include the following:

- For short-duration Earth-orbit or lunar missions (which include all manned missions to date), the high costs and long lead times required to develop and flight-qualify reliable regenerative systems could not be justified for any components of the LSS, for these missions.
- For longer duration missions (up to some undefined total duration) which involve more crew members (up to some undefined total number), some regeneration could be justified; particularly atmospheric revitalization, water recycling, and waste conversion to carbon dioxide (then oxygen), usable water, and a compact ash, but all food would still be stored on-board at launch, or resupplied periodically.
- For the latter, partially closed-system applications, physicochemical processes were perceived to be more attractive because of high reliability and energy efficiency; the design difficulties associated with photosynthetic processes (e.g., the need for natural light would require large transparent ports in the vehicle's shell, constant orientation toward the Sun, and provisions for light compensation or complex cycle functions when the vehicle operates in the shadow of the Earth); unknown effects of long-duration and low-gravity or zero-gravity exposure on biological systems, etc.
- Beyond the undefined thresholds for mission duration and crew size (for which some regeneration was considered to be desirable), it was perceived that food regeneration, and therefore essentially complete closure of the LSS, very likely could become necessary, particularly for destinations that are relatively remote from the Earth, and that biological processes might have some potential for this application (possibly performing atmosphere-regeneration and water-reclamation functions as well).

Funding priorities for life-support systems research and development are assigned according to projected time frames of need and readiness for mission applications. Therefore, in view of the limited resources that were available for advanced technology development in these areas, research on completely closed systems and, in particular, biological processing components, received little

or no support, except for minor exploratory efforts that decreased to virtually nothing several years ago.

Current interest in self-sustaining, regenerative life-support systems derives principally from the possibility that habitats will be needed in the coming decades to support missions that could well involve a large number of people working in space for long periods of time and, in some cases, at sites that are quite remote from the Earth.

The inputs required to support a person in space are shown in table 1. Over the course of a year, the average person consumes 3 times his body weight in food, 4 times his weight in oxygen, and 8 times his weight in drinking water. Over the course of a lifetime, these items amount to over a 1000 times an adult's weight.

TABLE 1 — INPUTS REQUIRED TO
SUPPORT A PERSON IN SPACE

Type of input	Amounts, kg per person per:		
	Day	Year	Lifetime
Food (dry)	0.6	219	15,300
Oxygen	0.9	329	23,000
Drinking water	1.8	657	46,000
Sanitary water	2.3	840	58,800
Subtotal	5.6	2,045	143,100
Domestic water	16.8	6,132	429,240
Total	22.4	8,177	572,340

As discussed above, for long-term space missions, it will probably be necessary to replenish or recycle supplies on board. The quantities of supplies required increase with the duration of the flight and the cost of supplies required for the journey is proportional to their weight at launch. At some break-even point it will probably be less costly to send up the equipment to recycle the supplies from wastes than to use up the provisions on a once-through basis.

Consider, for example, wash water which is relatively easy to recycle because the contaminant levels are low (about 350 ppm; ref. 1). A number of processes have been investigated for wash water recycle, including systems based on multifiltration, ultrafiltration, reverse osmosis, and vapor compression distillation (ref. 2). A schematic of a system based on reverse osmosis (RO), with vapor compression distillation to concentrate the rejected wastes, is shown in figure 1. Waste water from a storage tank is passed through progressively finer cartridge filters to remove particulates that can foul the reverse osmosis membranes. The filtered water enters a recirculation loop of RO modules, where the water that permeates the membranes is collected and stored at pasteurization temperature. The concentrated "brine" is sent to a vapor compression distillation unit which reduces the contaminants to a concentrated slurry, either to be stored on-board or processed further.

Even a recycling system such as this requires that replacement filters, membranes, and chemical additives be brought from Earth, with their quantity depending on the length of the flight. Thus the total weight at launch of the system increases with flight duration.
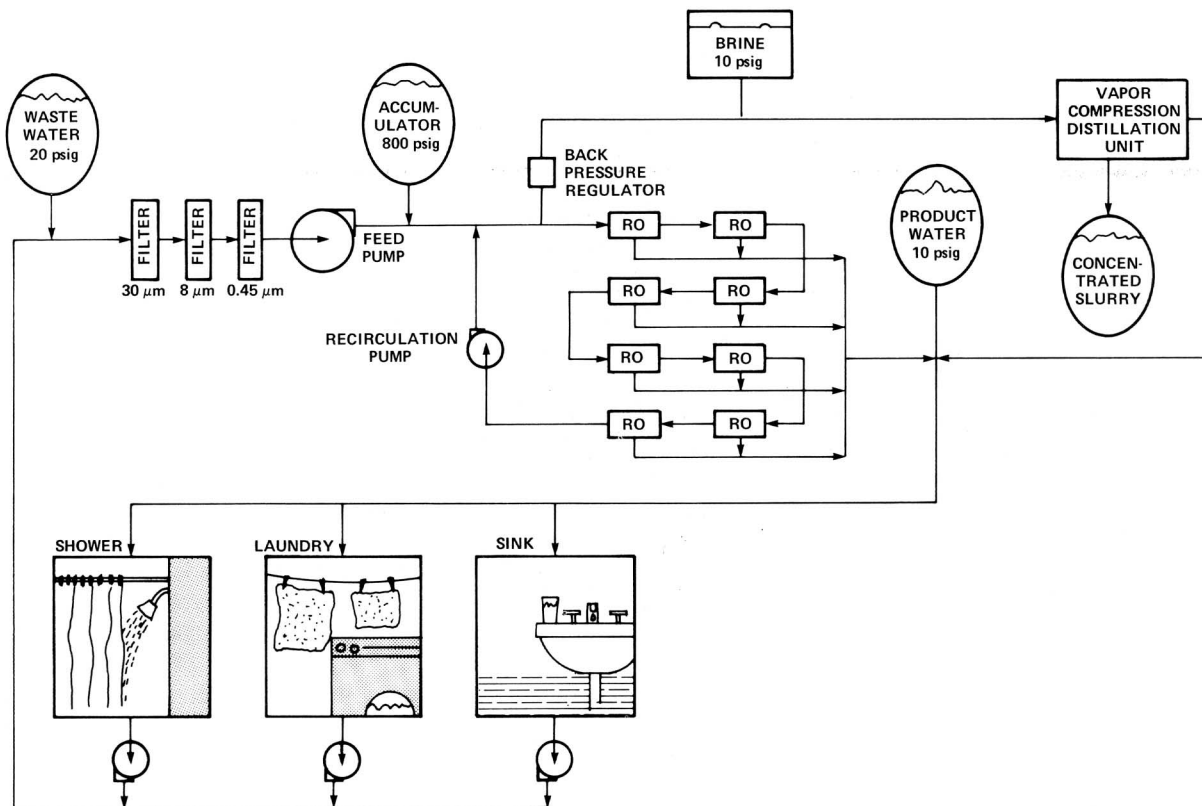
Figure 1 — *Schematic diagram of typical wash-water recycling system (from ref. 3).*

For a six-person crew, launch weight as a function of flight duration is shown in figure 2, for state of the art as well as projected technology. Also shown is the launch weight of an alternative system, multifiltration, based on sequential filtration with cartridge filters, activated carbon, and ion-exchange resins. Based on current knowledge, an RO-type of system for wash water recycle would probably be preferred for a long-duration mission.
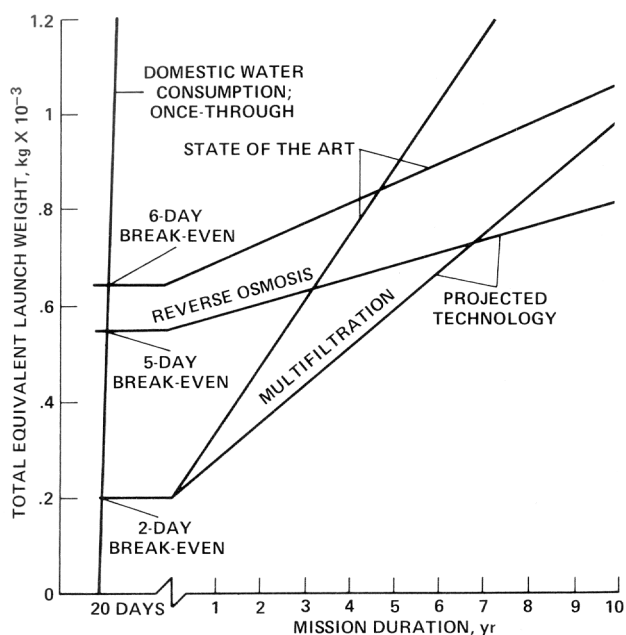
Figure 2 — *Example of attractiveness of wash-water recycling as mission duration lengthens.*

Human wastes and other organic wastes (food wastes and trash) can be turned into carbon dioxide, water, and ash by presently available methods. Wet and dry oxidation systems have been built and tested on a demonstration scale. In wet oxidation, an aqueous slurry is treated at moderate temperatures (150° - 250° C) under high pressures (8.3 X 10^6 to l.5 X 10^7 N/m^2) (ref. 4). In dry oxidation, toilet wastes and aqueous slurries of pulverized trash are first concentrated by evaporation of water, and the concentrate is then incinerated (ref. 5). Water vapor and off-gases from the incinerator are passed through catalytic oxidizer beds to completely convert organic contaminants to CO_2 and H_2O.

A number of physicochemical techniques have been suggested for recycling oxygen from CO_2 (refs. 6, 7). These methods involve separation of CO_2 from air followed by reaction of CO_2 to produce O_2 and carbon by-products (methane in the Sabatier process, or solid carbon in the Bosch process). However, processes of this type are not suitable for a closed life-support system for flights of long duration. Although oxygen is generated for reuse, the carbon present in the food that was consumed is ultimately converted to a solid form and must be stored. To close the system, the carbon must be returned to the food cycle from which it originated.

All of the carbon in human food originates either directly or indirectly (i.e., through animal consumption) from vegetation. Thus, to close the system, all of the carbon in the outputs from living components of the system (e.g., humans, plants, and animals) should be converted back to carbon dioxide so that it can be photosynthesized back into

vegetation. In this manner, it is possible to satisfy simultaneously the recycle requirements for oxygen and hydrogen. For example, if the average carbon, hydrogen, and oxygen composition of vegetation is represented by the formula CH_mO_n, then the stoichiometry of net plant growth (photosynthesis less respiration) is:

$$CO_2 + \frac{m}{2} H_2O = CH_mO_n + 1 + \left(\frac{m}{4} - \frac{n}{2}\right)O_2$$
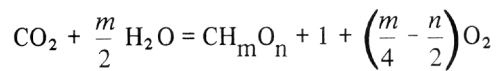
A portion of the edible plant output is oxidized back to CO_2 and H_2O directly by human and animal metabolism. The remainder of the edible portion is partially oxidized to products which appear in urine, feces, perspiration, and exhaled breath. If these partially oxidized products, together with the nonedible portion of the plants, are subsequently oxidized to CO_2 and H_2O, then the net effect of human and animal metabolism plus waste oxidation is the reverse of the net photosynthesis stoichiometry. Thus, incorporation of a process like wet oxidation or incineration for complete conversion of organic wastes to CO_2 and H_2O simultaneously closes the carbon, oxygen, and hydrogen recycle loop.

Figure 3 — *Comparison of transported weight requirements for alternative modes of food supply.*

The logistical basis for the recycling of the wash water, as discussed above and characterized in figure 2, also is applicable to the regeneration of the food supply. Figure 3 illustrates that economic break-even or crossover points occur when comparing the alternatives of ei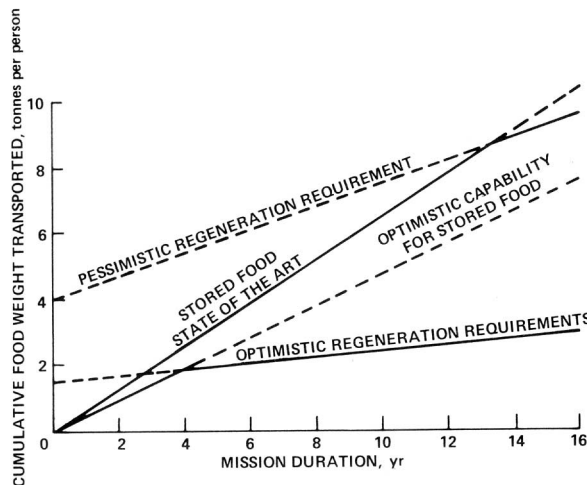ther regenerating food at the space settlement (with some nominal resupply from Earth) or continually resupplying all food from Earth (with no regeneration). The ranges of cumulative food-weight transportation requirements per inhabitant, shown as functions of mission duration (or continuous time in space) in figure 3, are based on best available information. The state of the art for food storage was taken as 650 kg per person per year, which is approximately that for present Space Shuttle food-supply planning. This includes thermo-stabilized and intermediate moisture foods to achieve a level of palatability and general acceptability better than that of the food used on Apollo missions (about 400 kg/person/yr).

TABLE 2 — OPTIMISTIC ESTIMATES FOR STORED WEIGHT OF FOOD IN A REASONABLE DIET FOR SPACE MISSIONS

Food item	Natural	Natural Dry	Natural Freeze-dried and packaged
Cereals	175	154	180
Potatoes	142	114	110
Sugar	75	75	80
Beans and nuts	36	33	38
Vegetables and fruit	608	535	500
Meat	218	88	100
Eggs	76	18	22
Fish	18	6	7
Milk	785	103	110
Fat	55	~55	60
Drinks (dry)	12	12	15
Alcohol	30	30	70
Salts	15	15	16
Total	2,245	1,238	1,308

The optimistic estimate for stored foods is about 475 kg per person per year. This is based on the analysis summarized in table 2, which characterizes a reasonable diet and assumes, optimistically, that technology developments in the future will be able to accommodate the freeze-drying and packaging of these dietary components in an acceptable palatable form within the per-person annual resupply weight value of 475 kg. It should be noted, however, that foods could be chosen differently to minimize the total weight and perhaps reduce this optimistic weight-requirement value by a factor of 2 (i.e., to about 220 kg/person/yr). This weight-conserving food supply does not represent conventional terrestrial diets, however, and its acceptability may be limited. For this reason it was not used in this analysis as the optimistic possibility for food storage.

The optimistic value for food-regeneration requirements shown in figure 3 was taken as 1500 kg/person (total biomass holdup for the self-sustaining, steady-state condition). Therefore, that amount of total food-producing material must be transported from Earth before the food regeneration process can reach this condition. The slope of this line represents an optimistic assumption that only 100 kg/person of resupplied biomass or food must be transported annually from Earth to compensate for supplemental requirements, attrition of material, etc. The initial supply value of 1500 kg/person agrees well with the value presented in the Final Report of the 1975 NASA Ames Summer Study (ref. 8), although this figure was derived independently in a more rigorous manner by members of the Life Support Systems Group of the 1977 NASA Ames Summer Study.

The pessimistic value for food-regeneration biomass requirements was estimated to be 4000 kg/person. This amounts to between 2 and 3 times the optimistic value, and was selected only to obtain some estimate of the sensitivity of the crossover point to the magnitude of the value assigned to food-regeneration biomass requirements. Similarly, the

slope of the pessimistic regeneration line was chosen to be significantly greater than that for the optimistic regeneration line, to portray sensitivity. This slope represents a pessimistic assumption of an annual resupply requirement of 350 kg/person.

Figure 3 illustrates several important points:

1. The point of crossover, on the basis of food weight that would have to be transported, is quite sensitive to the requirement for the biomass supply to sustain food regeneration; nevertheless, a crossover occurs on the state-of-the-art stored-food line for both the optimistic and the pessimistic regeneration lines, with a range of about 3 to about 14 years, and an average of about 8 years.

2. If the optimistic food storage capability can realistically be achieved, food-regeneration technology must be able to provide stable regeneration with a biomass requirement significantly smaller than that represented by the pessimistic line; otherwise, crossover will not occur at a reasonable rnission duration and regeneration of food will not be able to compete with food storage (or resupply).

3. Even if the achievable initial per-person biomass requirement for stable regeneration of food is no better than the pessimistic value, but the annual resupply requirement is at least as low as the optimistic regeneration case (i.e., 100 kg/person), it can be shown that crossovers with the state of the art and the optimistic food-storage lines would occur at about 8 and 12 years, respectively.

At this point it should be emphasized that the food-storage versus food-regeneration comparisons have been based on the required weight to be transported to the space habitat for each case. Assuming transportation cost to be the only significant economic factor, this is a reasonable basis for direct comparisons. However, in reality, the cost of research and development necessary to achieve stable regeneration of food, compared with, for example, the amount of importation of supplies characterized by the optimistic regeneration line in figure 3, might be high enough to greatly change the crossover point to a much longer mission duration in a total-cost comparison of state-of-the-art food storage with resupply. Nevertheless, since the weight (and cost) of subsystems needed to provide atmosphere regeneration and water reclamation are not included for the stored-food cases in figure 3, these comparisons are quite conservative.

Another very significant factor would be the cost of transporting material into space. A greater amount for this cost might significantly offset extensive research and development costs to achieve the optimistic food regeneration capability. Furthermore, consideration must also be given to the extent of transportation cost that might be required to provide equipment for cultivating, harvesting, processing, preparing, and delivering the food in a regenerative system, and for the additional waste processing associated with such a system.

Therefore, the cost-benefit analysis for the comparison of resupply versus regeneration of food is very complex and cannot be accomplished effectively until reliable capability and cost estimates can be made. Even more complex and information-dependent is the selection and design of an integrated regenerative life-support system for a space habitat. Therefore, the information requirements must be fully understood and then satisfied through careful planning.

PHILOSOPHY OF INTEGRATED SYSTEMS DESIGN

Integrated systems design refers to the process of defining the requirements that must be satisfied by a regenerative life-support system, identifying component and subsystem options, screening and selecting among these options for integration into an effective system that satisfies all requirements, and then integrating this life-support system design into the overall habitat design. By far the best approach is to accomplish all of this by way of a total system analysis and design procedure that considers all component and subsystem interactions at the same time. The result has been demonstrated extensively to be superior to the outcome of the alternative procedure of fixing or optimizing one aspect of the design and then trying to retrofit other subsystems into this fixed arrangement such that, typically, the latter subsystems cannot function optimally. The best approach requires careful attention to all identifiable options and the eventual selection of a totally optimum combination of components and subsystems that will meet all performance requirements in a stable, safe, and reliable manner.

This is especially vital for completely regenerative life-support systems which will very likely include biological as well as physicochemical components. The balancing of the input and output streams among the components to maintain stable operation can be expected to be extremely sensitive. This requires detailed consideration of interface constraints inside and outside the system. The task would probably be much easier if only terrestrial conditions needed to be considered. A great deal more is known about the performance of humans, animals, and plants in terrestrial gravity and in an air atmosphere. Almost nothing is known about the effects of long-term zero-gravity or fractional-gravity exposure on plants and animals. In general, this means that enough data will be needed, at a minimum, to support extensive sensitivity analyses for the various systems design scenarios that should be considered. This must include characterization of the effects that choices of external factors (gravity, atmosphere, adjacent activities, etc.) can have on the closed life-support system option, as well as the effects that each life-support system option can have on other elements of the habitat design.

Overall, this requires that mission planners and conceptual designers remain aware of and give adequate consideration to the sensitivity of the regenerative life-support system's selection, design, and performance, and its potential effect on total habitat design. Otherwise, these will be neglected and the life-support system will be developed in a retrofit

mode. This would very likely result in a low probability of optimality in the selection or operation of the life-support system. Furthermore, the consequences could well be disastrous.

As was discussed earlier in this paper, there are various approaches to and degrees of closure. At the present time not enough is known to support the identification of optimum choices. However, a particularly effective procedure for the identification and characterization of options involves the steps shown in figure 4. The procedure begins by selecting a diet scenario which is disaggregated into the types and quantities of food that will be specified to meet the dietary requirements. From this list of required food the resources necessary for producing the vegetables, fruits, and grains on the list are determined. From the agricultural characteristics of these crops the amount of waste that will be generated (i.e., material not consumed by the humans) is estimated. Then the requirements for feed and resources to produce the animal-derived food components of the diet scenario are determined, based on the utilization of the by-products from the crops. The waste generated from the production and processing of the animal-derived food can be estimated at this point.

Next, it is necessary to determine the waste-processing scheme needed to regenerate the required inputs to the plants and animals (i.e., nutrients, water, carbon dioxide, etc.). Processing requirements for food production and preparation can be estimated at this point. These include
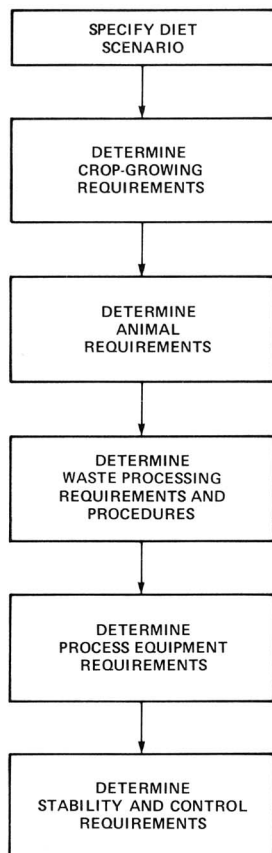
equipment, facilities, and resources (e.g., water and energy) for milking cows, processing the milk and its derivative products, baking bread, processing meat and vegetables, refrigeration, packing, and storing, to name a few. Finally, it is necessary to determine the stability characteristics of the proposed system that has been put together conceptually by this procedure, and identify requirements for monitoring and control.

This latter step provides the basis for the analysis of the system's sensitivity to perturbations at its internal and external interfaces.

The major internal features of the life-support system that can be varied to generate different scenario options are the diet and the method of closure. The method of closure includes both the functions in the system that will be closed and the component biological and physicochemical species that will be employed to accomplish these functions in a closed mode. Although the options that are possible for the variation of these features are many, it would be reasonable to start by selecting a diet that closely represents conventional terrestrial choices of food and then determining the component requirements for full closure of the life-support system. From a baseline case of this type, subsequent analyses can progress to other diet and closure options. For each scenario option, the trade-offs associated with it should be examined carefully in comparison with other proposed options. Analyses of this type are extremely valuable in identifying research required to improve the data base such that the evaluational comparisons will be more reliable.

Several scenarios have been considered and reported to date. The diet associated with the scenarios considered by the 1975 Ames Summer Study team (ref. 8), Henson and Henson (ref. 9), and Soviet researchers (ref. 10) did not closely represent conventional terrestrial choices of food. A scenario based on a more conventional diet is currently being formulated and evaluated by the Bioenvironmental Systems Study Group on NASA Contract No. NASw-2981. The foundation for this diet is presented in the subsequent companion paper prepared by the Life Support Systems Group of the 1977 NASA Ames Summer Study (entitled "Research Planning Criteria for Regenerative Life-Support Systems Applicable to Space Habitats").

It was mentioned earlier in this report that the life-support system also has external "trade-off interfaces." These are defined as environmental or operational conditions that the life-support systems share with other components or systems of the habitat. For example, the gravitational force designed into the habitat is an environmental condition that is shared by all systems; any connections or interlocks between the section of the habitat in which the regenerative life-support system functions and, perhaps, a manufacturing section, would represent shared operational interfaces. Good systems engineering practices require that these interfaces be selected with careful attention to, and adequate knowledge of, the effect of the selected conditions on all systems that share these interfaces. The choice is then optimized with

Figure 4 — *Stepwise procedure for formulation of a candidate regenerative life-support system scenario.*

respect to all these systems through trade-off analyses that are based on a sound rationale.

Typical external interfaces for a regenerative life-support system in a space habitat are discussed below.

Atmosphere Environment

The parameters of atmosphere selection include total pressure, composition, and the individual partial pressures of the principal constituents (oxygen, carbon dioxide, and nitrogen, or other inert diluent). The factors involved in the selection of any atmosphere other than terrestrial air are very complex. Nevertheless, it is very clear that hasty decisions must not be made simply for the convenience of engineering design or other logistical or operational considerations. The health and safety of the habitat's occupants must come first, and this includes the need for a stabilized and optimally performing life-support system. As stated earlier, there is a serious lack of information about the effects of exposure to nonterrestrial atmospheres on humans, plants, and animals. For this reason, pure oxygen or oxygen-rich atmospheres must be avoided until an adequate understanding of the effects of multigeneration exposure of biological species (including microbiological candidates) to such atmospheres has been achieved. Obviously, the length of the time delay and cost incurred in deriving this level of understanding could far outweigh the anticipated benefits from the selection of such an atmosphere, and must be considered in any trade-off analyses. Certainly, from Apollo Project experience, it must be realized that use of such atmospheres involves a significant increase in the risk of fire and imposes severe restrictions on the selection of materials that can be used in the habitat (refs. 11-13).

With respect to the carbon dioxide composition, the current maximum limit for manned spacecraft environments is 7.6 mm of Hg partial pressure with a nominal level of 5 mm of Hg. Research to date by plant researchers in the controlled environments of phytotron chambers indicates that this carbon dioxide level is greater than the maximum level of enrichment of carbon dioxide in terrestrial air for which plant-growth enhancement has been achieved (refs. 14 and 15). Therefore, it does not appear that different atmospheric compositions will be required to satisfy the general needs of humans, plants, and animals. Nevertheless, the optimal level of CO_2 still remains to be determined.

The emphasis expressed above on the advantages of using terrestrial air does not entirely limit considerations to "one standard Earth atmosphere." Stable ecologies exist on Earth at high-altitude locations where the total pressure of the atmosphere is reduced to about 2/3 the standard Earth atmosphere. However, the ratio of oxygen to nitrogen is still about 20/80 (ref. 16), not oxygen enriched. Therefore, these types of atmospheres also qualify for reasonable consideration. The extent of the restrictions, if any, imposed on agriculture (e.g., variety and productivity), on effects on human health and epidemiology, etc., should be investigated thoroughly.

Gravity Environment

The effects of zero-g and low-g exposure on higher plants and food-producing animals are not known. Effects on humans have been documented but not fully explained. This suggests that, at a minimum, the serious consideration of a gravitational environment for the habitat which is other than that on Earth will add significantly to the needed research and development time. Until adequate information can be obtained that ensures the health and safety of the habitat's human occupants in such an environment, and the stability and optimal performance of its life-support system, only terrestrial gravity should be considered for space habitats.

Illumination

The general data base is probably adequate for the specification of illumination requirements for humans, plants, and animals. However, these specifications need to be formulated to provide guidelines for the design of adequate filters or reflectors for the alteration of sunlight, to allow the use of solar illumination in space, or completely artificial illumination using solar energy as a power source. If the habitat must be completely shielded with opaque material to eliminate the cosmic radiation hazard, artificial illumination would be necessary. The results of extensive research show that plants grow very well in artificial illumination (refs. 14, 15). Similar information on illumination requirements (e.g., periodicity, spectral characteristics, and intensity) that are optimum for humans and food-producing animals needs to be compiled.

Special Constraints

These include area, volume and configurational (or shape) limits within which the life-support system must function. Several estimates of area requirements for habitat occupants and their regenerative life-support system have been published (refs. 8, 9), based on different scenarios for regeneration of food. These demonstrate that once the scenario has been quantitatively modeled, various configurations for the arrangement of components of the life-support system can be studied and area and volume requirements for each can be determined. The principal focus of such analyses should be the "packing intensity" potential for various components of each candidate design scenario. In this manner, area, volume, and shape considerations become combined; otherwise the specification of an area requirement alone is quite meaningless since an effective use of an available volume, through higher packing density, can reduce this area requirement. Trade-offs arise, of course, in most layout planning studies. For example, if plants are to be grown with a higher packing density, perhaps involving vertical stacking, provisions for adequate illumination become more complex.

Nevertheless, these problems probably can be resolved from state-of-the-art knowledge and design methodology, and do not require extensive research. Human social and

psychological aspects of spatial planning are another matter, and these must be considered carefully in habitat design. However, for the purposes of this report these factors are not considered to be within the domain of the regenerative life-support system, per se. In a sense, social and psychological factors represent components of a separate system in the habitat which share certain interfaces with the regenerative life-support system.

Radiation Environment

The results of studies on long- and short-term radiation exposure effects show quite conclusively that living systems, particularly humans and animals, must be provided with protection from ionizing radiation that is present in the space environment. Effects of sublethal overexposure include genetic and developmental effects, the production of tumors and leukemia in humans and animals, and generalized life-shortening changes in the vascular and central nervous systems. Therefore, any attempts to reduce the structural weight of a habitat design must not be allowed to compromise the health and safety of human occupants or the stable and optimal operation of the regenerative life-support system by decreasing the radiation shield to even a marginally effective thickness. Further studies will be required to provide the basis for specifying adequate shielding requirements for space habitats. In general, however, life-support systems studies should assume that the radiation environment will not be different from terrestrial conditions.

After several reasonable scenarios for partially or completely regenerative life-support systems have been formulated — based on the selection of internal interfaces, and then analyzed for sensitivity to variations in the external interfaces, perturbations at the internal interfaces (stability characteristics), and the reliability of assumptions — trade-off analyses can be performed to select the most promising options for further consideration. Initially, the trade-off studies can be used to identify auspicious areas of research to improve the data base on performance and stability characteristics. However, as the data base improves as a result of technological developments, the trade-off comparisons should be updated regularly. The results can provide a basis for (1) determining cost effectiveness of the research investment to date; (2) redirecting future efforts; (3) predicting and comparing the time of readiness for use (or "technological maturity") for the various options; and (4) identifying new system-scenario options based on combinations of particularly attractive components or subsystems to form hybrid groupings.

This iterative procedure is strongly recommended as a tool to provide effective management of technologydevelopment programs in the multidisciplinary fields that will contribute to the development of a successful regenerative life-support system for space habitats. Methodology already developed specifically for trade-off analyses for life-support systems components (refs. 17, 18) can readily be adapted for the procedure described above.

SUMMARY AND CONCLUSION

This report has summarized criteria for the closure of the life-support system for space habitats and factors to be considered when assessing the relative benefits and costs of closure in comparison with nonregenerative options. In addition, a methodology was specified for identifying, screening, and evaluating candidate processing components for a regenerative life-support system through an iterative procedure that involves scenario formulation and modeling together with trade-off analyses. The procedure also includes guidelines for effectively managing the associated technology-development program. For all of the above topics of this report, it has been stressed that the limits of the present data base for the relevant areas of technology preclude a priori conclusions, at this time, regarding the ultimate role that regenerative life-support systems will have as a function of time in space habitats or the optimum choices to be made among potential processing components to formulate an "ideal" system scenario. Therefore, the highest priority short-term goal of future studies must be the identification of key data base needs. From there the longer-term research required to satisfy these needs can be specified and prioritized.

REFERENCES

1. Putnam, David F.; and Columbo, Gerald V.: Experimental Study of the Constituents of Space Wash Water. Umpqua Research Co., Myrtle Creek, Oregon, Contract No. NAS2-8239, NASA CR-137735, Sept. 1975.

2. Putnam, D. F.: Development Assessment of Wash Water Reclamation. Umpqua Research Co., Myrtle Creek, Oregon, Contract No. NAS2-8239, NASA CR-137934, Aug. 1976.

3. Modell, M.: Sustaining Life in a Space Colony. Technology Review, vol. 79, July/Aug. 1977, pp. 38-43.

4. Jagow, R. B.: Development of a Spacecraft Wet Oxidation Waste Processing System. ASME Paper 72-ENAv-3, ASME Environmental Control and Life Support Systems Conference, San Francisco, Calif., Aug. 14-16, 1972.

5. Schelkopf, J. D.; Witt, F. J.; and Murray, R. W.: Integrated Waste Management-Water System Using Radioisotopes for Thermal Energy. General Electric Co., Valley Forge, Pennsylvania, Document No. 74 SD 4201 for AEC Contract No. AT(11-1)-3036, May 1974.

6. Reid, Robert C.: University Role in Astronaut Life Support Systems: Atmospheres. Massachusetts Inst. of Technology, NASA CR-1552, May 1970.

7. Quattrone, P. D.: Spacecraft Oxygen Recovery Systems. Astronautica Acta, vol. 18, no. 4, Oct. 1973, pp. 261-271.

8. Johnson, Richard D.; and Holbrow, Charles, eds.: Space Settlements: a Design Study, NASA SP-413, 1977.

9. Henson, H. K.; and Henson, C. M.: Closed Ecosystems of High Agricultural Yield. Princeton Conference on Space Manufacturing, May 1975.

10. Gitelson, I. I.; Kovrov, B. G.; Lisovsky, G. M.; Okladnikov, Y. N.; Rerberg, M. S.; Sidko, F. Y.; and Terskov, I. A.: Problems in Space Biology, vol. 28: Experimental Ecological Systems Including Man, Nauka Press, Moscow, 1975, pp. 1-312; also NASA Technical Translation F-16993.

11. Radnofsky, M. I.: History and Development of Nonflammable Material for Apollo Spacecraft. Aerospace Medicine, vol. 40, Nov. 1969, pp. 1181-1185.

12. Abduragimov, I. M.; and Iantovskii, S. A.: Catastrophe in the Apollo Cabin and Measures for Increasing Prevention of Fires and Explosions During Space Flights. Kosm. Biol. Med., vol. 2, no.6, 1968, pp. 3-9; translated in Space Biol. Med., vol. 2, 1969, pp. 1-8.

13. Huggett, C.: Combustion Processes in the Aerospace Environment. Aerospace Medicine, vol. 40, Nov. 1969, pp. 1176-1180.

14. Downs, Robert J.; and Hellmers, H.: Environment and the Experimental Control of Plant Growth. Academic Press, New York, 1975.

15. Downs, Robert J.: Controlled Environments for Plant Research. Columbia Univ. Press, New York, 1975.

16. von Tiesenhausen, G. F.; Hamaker, J.; and Hilchey, J.: A Review of 'A System Design for a Prototype Space Colony' — M.I.T. Study. Program Development Division, George C. Marshall Space Flight Center, Huntsville, Alabama, June 1977.

17. Spurlock, J. M.; Modell, M.; Putnam, D. F.; Ross, L. W.; and Pecoraro, J. N.: Evaluation and Comparison of Alternative Designs for Water and Solid Waste Processing Systems for Spacecraft. Society of Automotive Engineers, Inc., Warrendale, Penn., Final Report on NASA Contract No. NASw-2439, July 1975.

18. Spurlock, J. M.; Modell, M.; and Putnam, D. F.: Evaluation of Technology for Spacecraft Water Waste Processing Systems. IAF Paper 76-043, 27th Congress of the International Astronautical Federation, Oct. 10-16, 1976, p. 7.

I-2
Research Planning Criteria for Regenerative Life-Support Systems Applicable to Space Habitats

JACK SPURLOCK, WILLIAM COOPER, PAUL DEAL, ANNITA HARLAN, MARCUS KAREL, MICHAEL MODELL, PAUL MOE, JOHN PHILLIPS, DAVID PUTNAM, PHILIP QUATTRONE, C. DAVID RAPER, JR., ELLIOT SWAN, FRIEDA TAUB, JUDITH THOMAS, CHRISTINE WILSON, and BEN ZEITMAN

This paper describes the second phase of analyses that were conducted by the Life Support Systems Group of the 1977 NASA Ames Summer Study. This phase of analyses included a preliminary review of relevant areas of technology that can contribute to the development of closed life-support systems for space habitats, the identification of research options in these areas of technology, and the development of guidelines for an effective research program. The areas of technology that were studied included: (1) nutrition, diet, and food processing; (2) higher plant agriculture; (3) animal agriculture; (4) waste conversion and resource recovery; and (5) system stability and safety. Results of these analyses, including recommended research options and criteria for establishing research priorities among these many options, are discussed in this paper. However, the companion paper that was also prepared by the Life Support Systems Group (entitled "Systems Engineering Overview for Regenerative Life-Support Systems Applicable to Space Habitats," by J. M. Spurlock and M. Modell) should be read first to provide a background on system closure requirements, potential problems associated with the operation of closed systems in the environment of a space habitat, and systems engineering factors that affect technology-development planning and management for closed life-support systems.

INTRODUCTION AND OBJECTIVES

This paper was prepared by the Life-Support Systems Group of the 1977 NASA Ames Summer Study on Space Settlements and Industrialization Using Nonterrestrial Materials. It summarizes the group's analyses and recommendations concerning the following issues:

- A preliminary review of relevant technological efforts to date that provide a promising basis for identifying, evaluating, and developing candidate biological and physicochemical processing components for regenerative life-support systems applicable to space habitats

- Identification of research and development options based on the above components

- Development of guidelines for establishing resource allocation priorities among the options

The 1977 Summer Study was concerned principally with industrial production in space using nonterrestrial materials, with housing and life support for an industrial work force in space, and with space settlements per se. The study planners reasoned that the earliest industrial activities in space probably will depend on "open-loop" life-support provisions, including resupply from Earth for food with perhaps some partial regeneration of atmospheric components and water. However, beyond this early transitional period, it is believed that long-term space settlements will require essentially completely regenerative, or "closed," life-support systems (CLSS). Therefore, the charter of the Life-Support Systems Group (LSSG) was to determine the requirements for achieving this closure, particularly the research that will be necessary over future years.

The efforts of the LSSG were in cooperation with the Bioenvironmental Systems Study Group (BSSG) of the Society of Automotive Engineers, Inc. (The BSSG is sponsored by the Office of Life Sciences, NASA Headquarters, a cosponsor of the 1977 NASA Ames Summer Study.) A major chartered responsibility of the BSSG is to develop recommendations concerning the scope of NASA's future work in regenerative life-support systems for space habitats, including the assignment of research and development priorities to most effectively advance the associated technology. Our joint findings, which must be regarded as interim results, are presented here and in a companion paper, "Systems Engineering Overview for Regenerative Life-Support Systems Applicable to Space Habitats." That paper summarizes criteria for closure of the life-support system for space habitats and factors to consider when assessing the relative benefits and costs of closure in comparison with nonregenerative options. In addition, it specifies a methodology for identifying, screening, and evaluating candidate components through an iterative procedure that involves scenario formulation and modeling, together with trade-off analyses.

As described in the companion report, there are many alternative components from which closed-system scenarios can be postulated. For virtually all of these alternatives, a significant amount of research would be required before any could meet the closure needs of a permanent space habitat. Nevertheless, certain scenarios might show more promise, thereby justifying research emphasis over other options. Presently, the available data base is not adequate to support a priori selections or exclusions from the possible options. In the near future, followup studies will be carried out by the BSSG. Therefore, the review of relevant technology, characterization of research options, and structuring of priorities among these options (as discussed here) are ongoing, iterative processes.

The necessary provisions and accommodations required of life-support systems on manned space missions generally include adequate food, potable water, breathable air, waste disposal, personal hygiene, medical care, safety from identifiable hazards, and reasonable comfort. For this study, the related subtopical areas of regenerative life-support system analysis were designated to be: (1) the dietary basis

for human foodstuffs, (2) how foodstuffs are produced (e.g., grown), (3) how waste products are recycled back into forms that can be used as inputs (i.e., for food production as well as water and oxygen for humans), and (4) how to develop appropriate controls and protective systems to prevent cross-contamination among subsystems and to stabilize the operation of the system. These areas are discussed in detail in subsequent sections.

The LSSG recognizes the fact that the development of a closed regenerative life-support system is an enormously complicated biological problem, particularly with respect to the fundamental ecological issues that must be solved. However, time constraints imposed by the available work period for the 1977 Summer Study required that emphasis be placed on the analysis of problems that would be essentially unique to closed systems, specifically for space habitats. Certainly, the numerous unknowns concerning ecological stability of closed systems in general, which would be common to terrestrial as well as space habitats, must be addressed in significant depth before actual systems designs can be formulated and developed. The reader is cautioned not to conclude from material presented in this paper that such designs are a straightforward undertaking based on present knowledge and data.

BASIS FOR TECHNOLOGY REVIEW

The relevant technology was reviewed so as to delineate the research options. The principal steps in this review procedure were: (1) to identify key technology areas involved in closure of a life-support system for space hatitats; (2) to assess current status of applicable developments for each area; and (3) to identify major technological issues and potential problems that must be addressed in each area.

The basis for identifying key technology areas in closure is illustrated by the qualitative input-output model in figure 1 (ref. 1). Generalized roles for plants and animals in closure
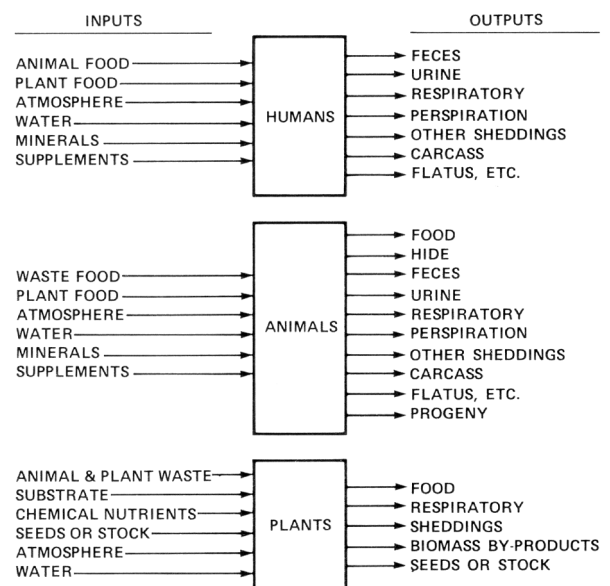
Figure 1 — *Preliminary qualitative input-output model for generalized closed life-support system (ref 1).*
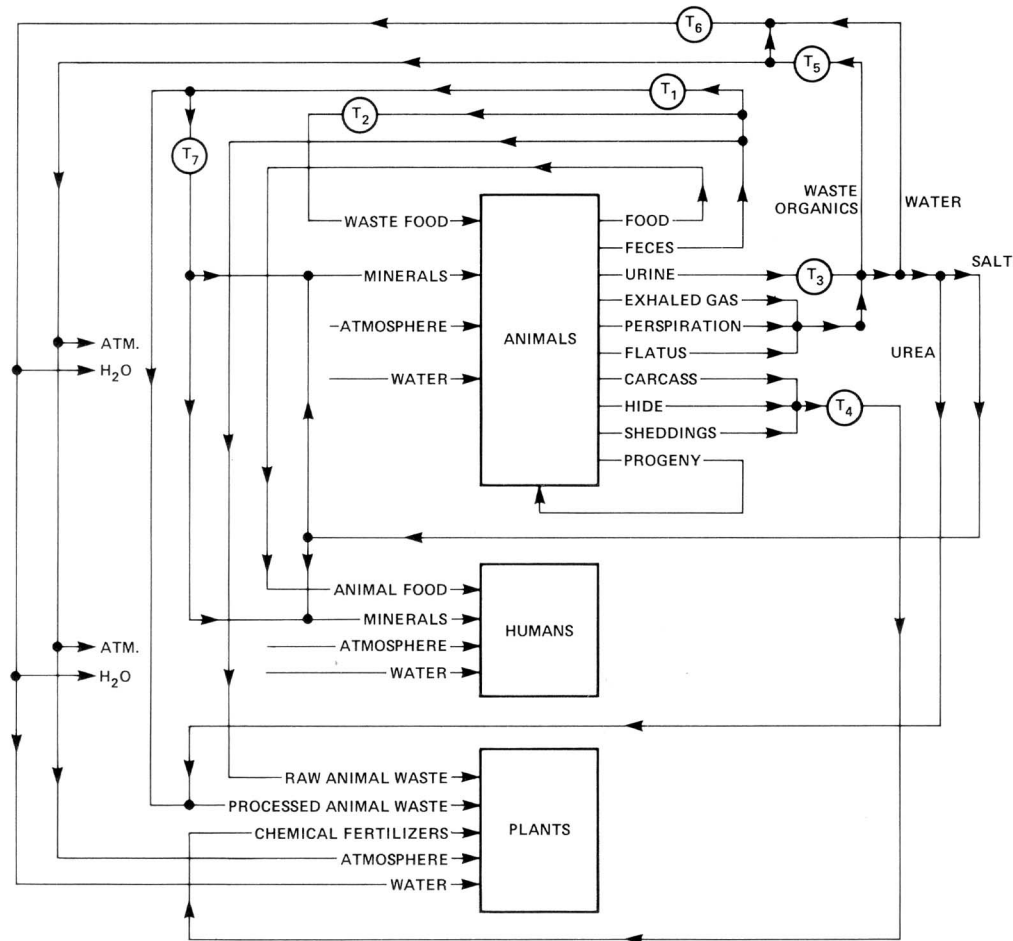
Figure 2 — *Example loop-closing flow sheet for generalized closed life-support system (ref. 1).*

linkages were assumed in the model. Figure 2 illustrates loop-closing possibilities for direct and indirect connections among inputs and outputs for animal outputs and human, plant, and animal inputs. The direct connections between outputs and inputs require little biochemical or physicochemical preprocessing. The preprocesses (or transformations) required for indirect connections are denoted in figure 2 by the encircled symbols T_i. Such flow sheets for connections among all human-plant-animal inputs and outputs (prepared by the BSSG) are useful in visualizing major categories of species subsystems required to accomplish the transformations of indirect connections.

The perceived knowledge and the technological development needs for the major categories of species are discussed in the following sections as the basis for eventual comparison and evaluation of candidate components of a closed system.

NUTRITION, DIET, AND FOOD PROCESSING

Diet Selection

The first criterion for a successful diet is that it provide all nutrients necessary for long-term maintenance of health and work efficiency. Diet determines the agriculture inputs which then flow through the food system, as shown in figure 3. At present, there is no certainty that all necessary components of a human diet have been identified (ref. 2). It

is likely that unrecognized nutrients are contained in the mixed plant and animal diets that have evolved culturally among Earth populations. As engineered foods from a narrow range of plant and animal products are being substituted increasingly into a diet that lacks natural diversity, the danger of missing some trace element or an
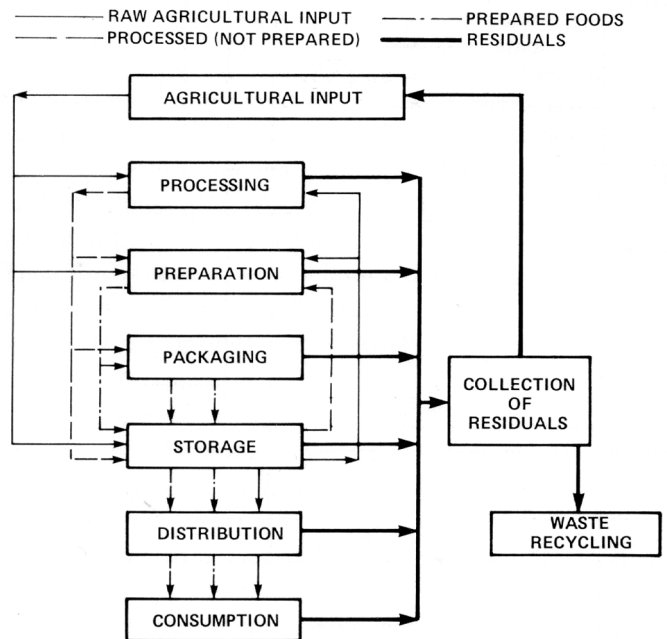
Figure 3 — *Typical food-flow diagram.*

unidentified nutrient also increases. Thus, the development of diet for closed life-support systems must include long-term evaluation of proposed diets that are significantly different from conventional established diet patterns.

Nutritional requirements for CLSS could differ from those of similar terrestrial populations. Construction work might proceed in zero gravity (i.e., extravehicular or extrahabitat activity), and even leisure hours might be spent in only some fraction of full gravity. Therefore, it is of concern that crewmen on long-duration missions such as Skylab showed losses of body mass, water, calcium, and electrolytes, continuing even after months in space (refs. 3, 4). More research under space conditions is necessary to establish whether changes can be normalized by compensatory diet adjustments. Precise information is needed on the individual daily requirements of nutrients for space-habitat personnel before an entirely adequate selection can be made of basic sources of these nutrients. These sources of foodstuffs must be known before the sophisticated existing technology of food processing can be fully utilized to optimize CLSS development.

In anticipating the foods necessary for adequate nutrition, attention must be given to the criteria used to evaluate the complexity of diet that will be acceptable for various periods of time. This is because it can be assumed that the longer the period of habitation in space the more complex will be the dietary requirements. Even in traditional military environments, dietary changes are a major psychological factor. Eating preferences show the need for individual flexibility in diet selection as tastes become jaded and preferences shift (ref. 5).

Food Processing

Diversity in diet requires not only an increase in the number of primary food sources, but also in the forms provided. Processing converts raw materials into a variety of individual ingredients of cuisine, such as the many forms of corn from starch, to meal, to fresh-on-the-cob corn, as in the American diet. Also, processing can produce analogs of traditional ingredients from new materials (e.g., the various "synthetic" products of texturized soy protein). Similarly, nonconventional protein sources such as leaf-protein concentrate, yeast, etc., may be incorporated into the diet through processing into substitutes for traditional food forms (ref. 6). The processes required for such new food sources must be selected and developed, and their complications of acceptance weighed against the problems in expanded agricultural complexity. As new food sources are incorporated into the diet, research is needed to consider the long-term medical and nutritional tolerances.

The conventional technology of food processing has, of course, been developed under terrestrial conditions (ref. 7). Conditions of gravity, atmospheric composition, and Coriolis force can affect the heat- and mass-transfer processes required to process and store food. Research on specific problems is necessary to anticipate and minimize the need for redesign of processing equipment. Furthermore, the existing processing technology must be adapted to the specific space habitat conditions.

Industrial Support for Food-Processing Industry

Even if a minimal food-processing option is selected for space settlements, there will be demands to provide solvents, salts, emulsifiers, bleaching agents, antioxidants (for contingency storage requirements), and other chemicals to process raw agricultural products into usable foods (ref. 8). Without an in situ "chemical industry," many standard food-processing chemicals such as the organic solvents used to extract soybeans will not be available to a CLSS operation. Alternative methods for supplying or eliminating the need for these chemicals must be evaluated. The effects these food-processing alternatives have on the nutritional value of the resulting foods must also be evaluated (ref. 9).

Food Preparation

Terrestrial experience in food service shows that processing, packaging, preparation, and waste disposal streams must all be matched for efficient operation. The extreme efficiency of some types of fast-food service (e.g., "hamburger-fries-shake" meals) suggests possible benefits in CLSS development. Cafeteria vs home cooking vs vending systems should be considered. Equipment inventory and layout, especially if spatial conservation is important, must be tailored to specific scenarios. Diet modifications, methods of processing, and feeding patterns will have important effects on optimal storage, heating, dispensing, and equipment maintenance. A major problem of present-day food service industries is the lack of adequate equipment for intermediate-sized operations, that is, for 1000 to 10,000 people. Hence, methodology that will minimize spatial requirements for feeding a self-contained group of people must be developed (ref. 10).

The size and permanence of the cooking staff are also affected by the food-service component of a given scenario. If it is determined that, for sound psychological reasons, the concept of choice and the principles of variation and change should be built into a system from the beginning, one way to generate these options is to allow individuals to "cook"; that is, to choose from prepared or partially-prepared alternatives.

On Earth, there is renewed interest in water-saving and energy-saving methods of preparation because of various shortages. Research programs in these areas could be doubly rewarding if planning and design are initiated early. It is essential that food-preparation concepts that are deemed potentially appropriate for space use be tested in space environments since those conditions may affect heating, mixing, etc.

Micronutrients and Mineral Toxicity

In closed systems, there exists an added danger regarding control of various elements in metabolism. Since human requirements for trace minerals have not been adequately determined on Earth, and there is often a narrow tolerance

between minimum requirement and toxicity, the artificial levels available in a space habitat might be critically difficult to adjust. A better grasp of requirements and tolerances, and an efficient monitoring system for metals such as copper, chromium, zinc, and cobalt, will be required.

Research and Development Options

Nutritional research and development should follow these steps:

1. Develop diet scenarios of several types and analyze them for nutritional adequacy, suitability to the space environment, and acceptability to the expected inhabitants.
2. Test these diets on animals in multigenerational experiments under conditions closely simulating space environments, and with humans in short-term studies in actual space environments, as well as in longer-term studies on Earth.
3. Reevaluate diets on the basis of data developed in step 2 and retest as necessary, preferably with humans under space-habitat conditions.
4. All of the above studies must be in close interaction with analysis of the processing, storage, and distribution capabilities of the space settlement.
5. It may be necessary to accomplish step 1 and proceed to step 2 in order to develop new information on trace nutrients and trace toxicants (e.g., mineral requirements, tolerable levels of recycled heavy metals, and special requirements of stress conditions).
6. Continue the investigation of various protein resources from nonconventional substrates, with attention to extraction, detoxification, acceptance, and long-term tolerance by humans and/or agricultural animals.
7. In reviewing the various candidate diet scenarios for use in space habitats, consider the complexity and availability of suitable processing technology required to transform raw food-source products into acceptable food for humans.
8. Since schemes used in the United States for large-scale processing will most likely be unsuitable for CLSS, develop processing methods, equipment, and procedures that are adapted specifically for CLSS needs. These schemes should be tested under simulated (or actual) space-environment conditions.
9. Solve specific problems to minimize the need for subsequent redesign; for example, the effect of Coriolis force on heat and mass transfer and on fluid flow in equipment, the best use of the available space vacuum, and the effects of a lowered boiling point (in cases of reduced atmospheric pressure in the habitat).
10. Analyze the storage and distribution requirements of each proposed system scenario and consider needs for preservation, protective packaging, and the special storage environment, including inventory and rotation systems.
11. Adapt preservation methods specifically to CLSS requirements and the types of food to be processed. The same considerations that apply to the development of processing methods will apply to preservation and storage. For example, special problems to consider include different microflora, different entomological hazards, availability of free vacuum for freeze-drying, sunlight, free refrigeration on the dark side, and different heating situations.
12. Analyze the food system, developed and tested above, for its effect on the habitat (e.g., noise, g-location, chemical and odor emanations, ease of distribution, energy and water requirements, and nutrient losses).
13. After this analysis, develop and retest the most promising processing systems.

HIGHER PLANT AGRICULTURE

Plant agriculture is included as an important option in planning CLSS because the photosynthetic process is a conventional means of closing the life-support system. Photosynthesis recycles carbon dioxide, produced by human metabolism, back into organic constituents necessary for human nutrition and into oxygen necessary for respiration. However, in considering plant agriculture as an integral component of a CLSS, it must be recognized that higher plants are a complex and environmentally responsive system. With their thousands of interdependent physiological and morphological processes, they lack the engineered reliability of mechanical and physicochemical systems. Since higher plants are already being grown in controlled environments with both natural and artificial light, although not in a completely closed system, it can be assumed that the minimum technology for intensive plant culture already exists. However, as evidenced by the variability of reported growth and yields (as illustrated in table 1), there is little consistency in productivity. If the demands of a human population can be sustained by higher plant agriculture in a CLSS, then research and development emphasis must center on the technology and tolerable environmental limits for reliable production.

Plant growth occurs as a result of the processes of cell division and cell differentiation in the various meristematic centers and apices of the plant, and the capacity for production and translocation of photosynthetic products to support the expansion of these cells. The morphological and physiological processes are interactively influenced by such environmental parameters as temperature, quality and quantity of light, availability of water and mineral nutrients, atmospheric concentrations of carbon dioxide, oxygen, water vapor, gaseous pollutants, and the presence of certain toxic metal ions in the plant environment (ref. 11). If the technology of crop productivity is to be advanced to the state of reliability required for inclusion of higher plant agriculture in a CLSS, the morphological and physiological responses to all combinations of the environmental parameters must be precisely documented. This is an extensive task when one considers that the magnitude and nature of the responses change with plant age and species.

Simulator Development

The only practical means of approaching this technological competence in assessing and predicting plant responses is to develop comprehensive mathematical models, which would be based on known physiological and morphological principles and would describe environmentally and genetically induced changes in plant growth and development. Modeling would be coordinated with selective experimentation so that the model could be adjusted to simulate the growth of various crop species.

The development of a dynamic crop simulator is recommended for four reasons. First, it establishes a priority for experimental determination of plant responses to environment. The parameters of photosynthetically active radiance (PAR) and temperature form the basis of net carbon fixation; other environmental parameters are then incorporated as regulators of photosynthetic production and partitioning. Second, because predictive ability can be enhanced as the simulator is developed, experimental combinations of environmental variables can be truncated to the few levels necessary to establish and verify a response surface. Similar truncation of environmental combinations are possible for each new growth stage and each species adapted to the dynamic simulator. Third, on a longer-term basis, as the sensitivity of the crop simulator is increased by experimentation, it can become a feed-forward interactive system for controlling the plant environment. Thus, when coupled with the environmental and plant-monitoring system, the crop simulator can project final yield from attained growth and suggest down-the-line environmental alternatives to optimize yield. The fundamental logic for such dynamic plant growth models is already being developed (refs. 12-14), including at least one model capable of multiple crop simulation (ref. 14). Finally, the crop simulator will possess the accuracy needed for final reiterations of whatever input-output model is used for sensitivity studies in developing the ultimate CLSS.

Data-Base Requirements

Crop simulators can only be as precise as the data base underlying their development. Systematic data collection at frequent intervals during plant growth is required to adapt a crop species to the model. These data must include: (1) accurate monitoring of the physical and chemical environment, (2) detailed plant chemical analysis of inorganic nutrients and organic plant constituents of physiological importance, and (3) thorough descriptions of plant morphological development as functions of selected changes in environmental parameters. Such data sets, although being developed for a few crop species (refs. 15, 16), are not available in the literature. However, the controlled-environment research facilities required to generate an adequate data base for the crop simulator are available at the phytotron units of the Southeastern Plant Environment Laboratories at Duke University and North Carolina State University (ref. 17), the Environmental Research Laboratory at the University of Arizona (ref. 18), and the Biotron at the University of Wisconsin. Utilization

of these existing facilities for fundamental research into plant growth dynamics can greatly expedite the development of a prototype crop simulator. They can also be used to develop cultural and nutrient delivery systems (aeroponics, artificial substrates, etc.) for higher plant agriculture in the CLSS.

Development of Completely Closed Facilities

The existing controlled-environment facilities are open systems in which some portion of the conditioned atmosphere is continually replaced from external sources. Hence, they do not have the capacity for research to address three critical questions about the tolerance limits of adapting higher plants to a CLSS for space habitats. The first of these questions concerns the long-term tolerance of higher plants to low gravity. There is no available research on the long-term response of plants to true low-gravity conditions; hence priority must be given to include on the earliest possible long-duration orbiting mission carefully controlled experiments to determine physiological and morphological effects of low gravity. (All effects of low gravity are not necessarily deleterious since a reduced gravitational force on plants may reduce the proportion of nonedible structural biomass.) Meanwhile, attention in terrestrial facilities should be given to the study of proposed hormonal involvement in geotropic responsiveness of plants (ref. 19) to develop chemical or genetical means for counteracting the deleterious effects of low gravity. A second limitation of existing controlled-environment facilities is an inability for long-term regulation of composition of the atmosphere, including toxicants, and changes in atmospheric pressure. Tolerance limits for both environmental parameters must be determined. Special growth rooms must be designed and built for such experimentation. A third concern is the tolerance level of plants to ionizing radiation. Although plants may have a greater tolerance than humans or animals, the long-term effects and resulting requirements for shielding must be determined in experiments in space environments.

Lighting for plants is viewed as a more critical research problem if natural, rather than artificial light is used as the source. Comparisons of growth over extended periods (ref. 20) have shown little difference between natural light, which had a mean daily PAR of 42 Einsteins m^{-2} day^{-1}, and artificial light supplied at fluxes above 17 Einsteins m^{-2} day^{-1}. Furthermore, plants have been grown for several generations with artificial light sources (ref. 21) with no measurable effects on growth. Hence, the use of artificial light for plant growth appears to pose no serious or unknown constraints on crop productivity.

On the other hand, utilization of natural radiation with spectral characteristics unattenuated by the Earth's atmosphere poses questions of possible adverse or mutagenic effects on plants beyond the limits of current predictability. In addition, use of natural light poses problems of photoperiodic control necessary for reproductive development of some plant species (ref. 22). However, problems associated with the use of solar radiation in space may possibly be circumvented by the use of spectral shift and selective transmission of glazings to provide filtered

TABLE 1 — VARIABILITY OF GROWTH AND YIELD DATA

Species	Reference	Edible harvest, g-m^{-2}	Total harvest, g-m^{-2}	Growth period, days	Average growth rate, g-m^{-2} day^{-1}	
					Edible	Total
Cucumbers	23	397	2259	90	4.4	25.1
	18	2850	4350	120	23.8	36.3
CVα		107	45	20	97	26
Soybeans	21	446	1035	120	3.7	8.6
	22	1000	2300	116	8.6	19.8
	22	642	1689	143	4.5	11.8
CV		40	38	12	47	43
Wheat	21	431	1435	100	4.3	14.4
	11	601	2360	63	9.5	37.5
	12	1273	4999	104	12.2	48.1
		58	63	25	46	52
Tomatoes	12	1328	1696	215	6.2	7.9
	18	1034	1320	180	5.7	7.3
		18	18	13	6	6
CV mean		56	41	18	49	32

α Coefficient of variation, in percent.

light that approximates Earth radiation. If glazings are used, control of day length for photo periodically responsive crops can be provided by a system of shutters.

A final question that must be resolved before higher plant agriculture can be included as an integral part of the CLSS is whether the plant agricultural system can maintain a specified level of productivity over long periods of time and several generations of plant culture. An Earth-based model CLSS should be established as a final feasibility study in which all elements of the CLSS are present, and in which reliability of productivity and the interactive crop-environment simulator can be evaluated for several years.

A model evaluation of a CLSS, including linked man and plant systems, was attempted in BIOS-3 by the USSR on a modest scale (ref. 23). They reported deterioration of crop productivity over a 6-month test, but because of their failure to adequately evaluate tolerance limits of plants to changes in the environment, they were unable to diagnose the cause of the partial failure. However, the USSR experience underscores the necessity of a model evaluation of closure in a life-support system.

Novel Concepts

In parallel with a critical evaluation of a CLSS, other research should be undertaken to broaden the options in the ultimate system. This research should include novel concepts such as cultural or biochemical manipulation of plant growth to idealize the plant phenotype of CLSS agriculture. Crop plants possess a certain range of morphological plasticity that potentially can be used to breed plants with a more favorable ratio of edible/total biomass in the stable environments of a CLSS (ref. 21). Similarly, manipulation of environmental factors such as temperature, photoperiod, and partial pressure of oxygen during certain stages of plant development can shift the ratio of total/edible

biomass (ref. 22). The environment not only affects the growth and development of the concurrent generation, but also can affect the viability of the seeds and thus that of several subsequent generations (refs. 24, 25).

Hence, the environmental requirements for plant propagation (e.g., seed production) must be considered separate from the environmental requirements for food-crop production. Since traditional agriculture has been developed within the constraints of a virtually nonmanipulable environment, the flexibilities of the plant system for optimization in controlled-environment agriculture have neither been emphasized nor extensively exploited.

Research and Development Options

Considerable information is being gathered on the effects of environmental systems on higher plant growth and development. However, this research has been conducted within the context of terrestrial agricultural problems. Before the technological base and experimental systems can be applied to developmental problems in adapting higher plant agriculture to CLSS, three specific research requirements must be considered: (1) What are the tolerance limits of higher plants to reduced gravity and can the possible effects be countered by biochemical manipulation? (2) What are the tolerance limits of higher plants to lower atmospheric pressures and gaseous compositions different from those normally encountered in terrestrial systems? (3) What are the tolerance limits of higher plants to ionizing radiation and what amount of shielding is required for growth?

Research and development to resolve these questions are critical to a determination of the feasibility of including higher plant agriculture as an integral part of the CLSS. The design of such experiments should be carefully controlled and coordinated so that they can be integrated into the terrestrial technology base.

Other pertinent options for research and development are:

1. Systematic determination of detailed changes in plant morphology and chemical composition due to variations in individually-controlled environmental variables.
2. Use of these data to develop a dynamic crop simulator model with multiple crop capacity and feed-forward interactive capabilities for optimizing the plant environment.
3. Evaluation of cultural and genetical manipulation to idealize plant phenotypes for CLSS agriculture.
4. Determination of specific environmental requirements for seed production which may be distinct from requirements for edible yield.
5. Development of an Earth-based model CLSS for a final evaluation of the feasibility and reliability of higher plant agriculture in a closed system.

ANIMAL AGRICULTURE

There is some question concerning the need for a livestock component in a CLSS. This fundamental consideration relates to many aspects of CLSS design such as mass, area, and volume requirements, waste and atmospheric recycling, epidemiology, and nutritional adequacy of the diet provided for humans.

The question is difficult to resolve because of the complexity of the trade-offs involved. Several design studies have shown that the inclusion of animals in the food-production subsystem of a CLSS will increase area requirements substantially. Questions have been raised about the additional complexity of the total system, the need to provide additional plant-growing area for feed and forage production and special areas for animal production, as well as the processing and storage requirements for animal products. The use of animals in a CLSS will also place additional burdens on the waste recycling and atmospheric regeneration systems. In particular, grave concern has been expressed concerning the additional risk involved in using animals that may serve as vectors for human pathogenic organisms.

The primary justifications for including animals in a CLSS appear to be their nutritional value, dietary variety for humans, and the possibility that animal components will result in a more balanced, stable ecosystem with enhanced closure characteristics. Animal products do provide high-quality protein in a very acceptable form.

In addition, milk and milk products provide most of the essential minerals, such as calcium, in American diets. Since some animal production is possible by feeding them by-products and plant residues from plants grown for human consumption, limited meat and milk may be made available without additional plant agricultural requirements. The extent to which additional animal products should be included in the diet will be determined by the balance between the esthetic and nutritional value of these products and the cost in terms of plant-growth requirements to produce any additional feed required, spatial and equipment requirements for animal culture, etc.

Ruminants

The primary animal type most suited for converting inedible plant material into animal products will be ruminants; that is, dairy cows for milk production and additional cattle for meat. Swine, chickens, and turkeys can be fed partially from table scraps and noncellulosic plant by-products, but most feed consumed by these animals could also be consumed directly by humans (i.e., competitive consumption).

Cellulosic materials such as plant roots, tops, brans, and hulls, can only be effectively used by ruminants. Microorganisms in the rumen of these animals allow them to digest these fibrous materials and convert them into fatty acids that are absorbed as a primary source of energy for their metabolism. Although the digestion processes are similar for both dairy and beef animals, the overall efficiency of converting feed energy into milk energy is several times greater than feed to beef because of the high rate of daily production possible (ref. 26).

The efficiency of both dairy and beef animals is influenced most by voluntary food intake and by the digestibility of the diet. Because of the intense production rate that would be required by agriculture in a CLSS, these factors will become increasingly important. Increasing from 45 to 75 percent the digestibility of plant residues that are high in lignin and structural carbohydrates can reduce by 40 percent the amount of feed required per unit of milk produced. Of even greater consequence is the concomitant reduction of 73 percent in undigested animal waste voided. Improved digestibility would also permit substantially increased voluntary intake with a resulting gain in gross efficiency (e.g., increasing the intake of a growing steer from 5.0 to 7.2 kg/day would double the rate of edible meat produced).

The removal of constraints on voluntary feed intake and rate and extent of digestion of cellulosic materials has high priority in the development of an animal agriculture compatible with the requirements of the space settlement.

Aquatic animal resources — As suggested, the animal component in space agriculture may perform the functions of a biological recycling agent, converting a portion of useless plant wastes to useful protein and releasing the remaining plant material as egesta. The egesta from the terrestrial animal component of a CLSS must be recycled eventually to plant nutrients and carbon dioxide in order to regenerate the food-production cycle. The same process must be performed for unconsumed plant material and for human wastes. Conventionally, this recycling can be accomplished by the use of some form of physicochemical oxidation process. Another potential option exists, however, to further augment protein production in a CLSS by incorporating an aquatic production process as a supplementary organic recycling system to handle a portion of the wastes generated by humans, animals, and plants.

Aquatic recycling processes have been the subject of considerable research effort in recent years (refs. 27-30). This research has demonstrated that such processes can purify effluents to acceptable standards while producing

valuable, high-protein biomass as a by-product. The possible role of aquatic processes for food production and waste recycling in space applications merits additional investigation.

Small-animal resources — The possible role of small animals for food production in space settlements should be examined. In many ways, they offer substantial production advantages over the large ruminants. Some small animals that should be considered include milk goats, rabbits, ducks, and geese.

Small animals have an advantage in production systems because they reproduce more often and reach maturity more quickly. They have a more efficient overall feed/protein conversion ratio because they are maintained only through the exponential growth phase; therefore less biomass is used in maintenance. For many small animals, feed requirements need only be marginally competitive with the human diet, consisting predominantly of table scraps, vegetable by-products, and small supplements of grain or forage. Lastly, small animal production components may enhance the safety, stability, and reliability by increasing the species diversity of any animal production subsystem.

Epidemiology

Diseases of domestic animals are an important consideration because they may dramatically disrupt the foodproduction process. Also, in some instances, there exists a direct danger to the human population from disease organisms that may infect both human and animal hosts. Terrestrial experience in high-density, confined animal husbandry has documented the need to consider epidemiology and to safeguard animal populations by appropriate sanitation and disease-control measures. At times, the routine administration of antibiotics is recommended. Procedures and facilities should be designed to isolate disease outbreaks. All livestock products must be routinely inspected to ensure their safety for human consumption.

Research and Development Options

The currently recognized limitations to the use of total available plant material by animals must be removed. Voluntary intake of some residues may be limited by use of chemical components that reduce palatability. To remove this limitation:

1. Identify the chemical compounds in specific feed plants, and develop techniques for removing or masking these compounds. Voluntary intake and nutritive value of residue plant materials are limited by structural carbohydrates that decrease the rate and extent of microbial degradation in the digestive tract of ruminant animals.
2. Identify plants according to their readily fermentable residue materials and also develop techniques for the appropriate physicochemical treatment of resistant residue materials (e.g., lignin) that limit the rate of degradation.

3. Examine rumen bacteria for criteria that govern the degradation rate of cellulose and other structural carbohydrates; if applicable, develop methods for providing the rumen bacteria with supplemental minerals and nitrogen sources to achieve maximal fermentation rates.
4. Improve food-production efficiency by reducing the ratio of fat/edible carcass; to accomplish this objective, identify the physiological mechanism that regulates the rate of protein deposition.
5. Examine the management factors and feed additives for their true relationship to the composition and rate gain in the growing animal.
6. Identify the potentially toxic and organoleptically undesirable compounds that exist in residues of some plants grown for human consumption.
7. Undertake a detailed chemical analysis (i.e., nutrient composition) of candidate plants for CLSS growing conditions for both human and animal diets.
8. Explore some unknown aspects of intense animal production in a CLSS.
9. Identify the volatile compounds that will accumulate; examine them for their effect on the humans and animals, and remove them by some appropriately developed method.
10. Develop a minimum-volume system for animal production. To accomplish this task, minimum-volume requirements must be established, including minimum levels of animal exercise required for efficient breeding and milking stock.
11. Develop adequate health management methods to prevent epidemics and catastrophic diseases in CLSS animal agriculture.
12. Collate and compare data from currently available resources to evaluate the potential of animal agriculture in a CLSS.
13. Quantify table wastes and food-processing by-products, which would be quite acceptable as animal feed; delineate fish culture, which is another viable option in a CLSS (ref. 31).
14. Study poultry excreta as a nitrogen source for ruminants before consideration for a CLSS.
15. Analyze more thoroughly the specific nutrient requirements of animals in a CLSS to prevent potential nutritional problems.
16. Describe specific plants to be used as feed sources for animal production on the basis of total digestible mass per unit weight of plant growth resources; consider the processing requirements of these plants for feed, with special reference to CLSS labor and management procedures.
17. Evaluate the advantages of using small animals such as milk goats, rabbits, and poultry; they have possible competitive advantages over cattle for milk and meat production from vegetable wastes and by-products (i.e., noncompetitive with humans).

18. Review current literature and experience with aquatic waste recycling to determine its potential relevance to food production and waste recycling for CLSS; consider aquatic microcosms as a possible research tool for exploring the most promising aquatic recycling/food-production systems.

WASTE CONVERSION AND RESOURCE RECOVERY

The primary objectives of waste processing in a recycling life-support system are to remove waste materials before they build up to toxic levels and to convert them into life-sustaining inputs. In a CLSS, the gaseous, solid, and liquid outputs of food-producing and processing operations must be dealt with in addition to human wastes. Waste can be processed using physicochemical techniques, by bioregeneration, or by some combination of these two approaches.

Current Physicochemical Alternatives

Among waste management concepts, the following are relevant to current research objectives.

Water reclamation technology deals primarily with the processing of lightly contaminated water (humidity or condensate, wash water) or highly contaminated water (urine, fecal water). Ongoing research and development activities are focusing on improved reliability of these processes.

Handling and either storing or treating solid wastes (food waste, wet waste, and fecal matter) probably will require extensive research and development effort. Four processing approaches have been investigated to date for manned spacecraft (ref. 32). One is a dehydration process using space vacuum to achieve a dried, stabilized mass. This method was adapted for use on Skylab and is being developed for the Space Shuttle. The other three approaches involve oxidation. Two of these combine concentrated waste water with solid wastes, the wet oxidation (ref. 33) and the RITE process (ref. 34), respectively. Wet oxidation uses an aqueous slurry contacted with oxygen at elevated temperatures and pressures to produce a stabilized sterile ash and sterile water that requires further treatment. RITE combines solid waste and liquid residues and processes the evaporated water (vapor) by catalytic oxidation. The remaining solid wastes are then pyrolized, incinerated, and their gases removed (for subsequent processing), leaving a sterile solid ash. The other oxidative process involves dry incineration of solid waste which produces a sterile ash after pyrolysis and subsequent oxidation of its vapors (ref. 35).

Any oxidative process offers potentially feasible approaches to solid-waste management. Each has been operated in the batch mode, but the problems of transporting wastes to the processing units for a continuous operation have not been solved. Significant data are lacking on the design and performance of catalytic oxidation units (ref. 32). In addition, applications in CLSS will require specific processes for the selective removal and separation of mineral constituents in the solid-ash residue from the oxidation of the wastes. These minerals are vital nutrient components for humans, plants, and animals, and they must be made available in acceptable form as input constituents.

Biological Alternatives

In addition to the physicochemical methods reviewed previously, there are various bioregenerative systems that use microorganisms, aquatic vascular plants, aquatic animals, and other organisms either singly or in combination (cf. section on Animal Agriculture). This area of technology has received very little research attention for spacecraft applications. Most of the technological developments to date are the products of research and applicational practice relating to municipal waste processing. There is an enormously large body of literature that must be screened eventually to identify any approaches that might offer options feasible for use in CLSS applications.

Research and Development Options

The design of waste processing components for CLSS applications must be integrated with the design of the entire life-support system because it must interface with other components and subsystems to satisfy a complex, interrelated set of input and output requirements (fig. 2). In general, however, the following options now seem to be key data-base expanders that can provide an important basis for the identification, design, and development of appropriate concepts.

1. Characterize the average and range of composition of gaseous, liquid and solid wastes, and their amounts, that are likely to occur in realistic CLSS scenarios, as a basis for specifying the inputs to waste processors.
2. Develop methods for effectively and efficiently converting these wastes into useful inputs for the other CLSS components. Specifically evaluate the relative attractiveness of physicochemical and biological processing techniques, and processes for the selective recovery for reuse of mineral constituents.
3. Give particular attention to the problem of trace elements that may become concentrated to toxic levels because of the waste recycling process; establish levels of tolerability and toxicity for all living components of the CLSS.
4. Develop methods for monitoring and controlling all phases of waste collection and treatment.

SYSTEM STABILITY AND SAFETY

Research options associated with system stability and safety must emphasize those areas of contamination, safety, health, and reliability that are uniquely associated with the design and environmental features of CLSS scenarios; for example, confinement with minimum ecological buffering against hazards. Various possible areas of concern, from which research options might be derived, and a preliminary list of options that should be given further consideration during the early phases of CLSS scenario analysis, are discussed below.

Microbiology

The microbial component of the habitat can reside in several areas: humans, agriculture, water supply, food subsystems, atmosphere, waste processors, and some structural materials of the habitat. The relationships among these are very complex and interdependent. These components form inescapable elements of the ecosystem in the form of pathogens, symbionts, and commensals with humans, plants, and domestic animals.

Compared to terrestrial plant, animal, and soil ecosystems, the habitat will provide a simplified, largely synthetic environment. New biological relationships will undoubtedly form. Also, in new or drastically altered environments, biological change is likely to be abrupt, dramatic, and unpredictable (ref. 36).

Human, animal, and plant pathogens can, in part, be controlled in the habitat by the conventional techniques of quarantine, screening for carriers, and immunization. However, some diseases are so common and the carriers so difficult to identify that exclusion from the habitat may not be possible. Soviet investigators observed major microbial changes in enclosed ecosystems intended to provide human life support (ref. 23). Species composition and population numbers changed throughout the time these simulations were in operation and possibly degraded the performance of some components in the systems. Habitat design may involve problems similar to those encountered in hospital design, but with contamination problems intensified by the impossibility of bringing in "outside" air from a huge external pool and using it as a sink for contaminants. Rigorous microbiological security of the water supply will also be necessary because of the ease with which organisms can reproduce in the aquatic environment and the readiness with which they might be transmitted (refs. 23, 37, 38).

One of the most common methods of microbial control is the use of chemical biocides (e.g., chlorine in water supplies, bacteriocides, fungicides, and algacides in industrial plumbing and tankage, pesticides in agriculture, chemical disinfectants in hospitals and homes, and preservatives in foods). However, the hazards associated with the use of any toxic substance in the space habitat must be thoroughly understood before its application can be rationally contemplated.

Toxic Chemicals

The fragile, synthetic environment of a habitat will probably be highly sensitive to a large array of hazardous organic and inorganic compounds. Since habitats will not have large areas of sediments or volumes of atmosphere to dilute toxic compounds, special measures must be taken to avoid environmental contamination. These measures may include prohibiting the use of many chemicals. Even though prohibited, toxic inorganics could accumulate in the food chain from the processing of nonterrestrial materials that contain trace metals. The severity of this problem increases as the ecological system approaches closure.

The current Environmental Protection Agency (EPA) list of possibly dangerous compounds includes some 30,000 substances. To analyze the effects, transport, and fates of toxic materials in the Earth environment, considerable resources are being committed by EPA, the National Institute of Health, the Food and Drug Administration, the National Cancer Institute, and various industries. A comparable effort is required for the space habitat. Every product, either transported from Earth or synthesized in space, must be evaluated in terms of manufacture, use, and disposal or recycling.

Environmental Monitoring

Biological systems are difficult to monitor. Sensitive detectors for the rapid measurement of pH, temperature, and a variety of compounds such as H_2S, SO_2, and CO_2, and sensors for toxic organic compounds, heavy metals, and microorganisms have been developed for on-line control. However, much labor-intensive analysis is involved using routine microbiological techniques and modern analytical chemistry techniques, such as combined gas chromatography/mass spectrometry, electron microprobe, or atomic absorption spectrometry. Because biological transformations occur very rapidly, computer-compatible monitoring systems must be developed for real-time analysis of trace quantities of organic, inorganic, and biological components. These computer systems should include anticipatory problem-predictive capabilities so that control measures can be implemented while there is still time to avert calamity.

The computerized monitoring systems may be augmented with sensitive biological indicator species; the coal miner's canary is the classical example. It may be possible to develop genetic strains that are sensitive to specific toxic conditions. These biological sensors might provide more efficient early warning against specific or synergistic toxic effects than could either electrical or mechanical monitoring systems.

Considerable interest exists in developing indices of pathologies for ecosystems comparable to those used by physicians. For example, infrared scanners might be used to determine changes in respiration patterns in controlled agricultural systems or shifts in the ratio of chlorophyl/carotenoid pigments could be monitored to indicate changes in algal populations.

Some environmental characteristics might be clustered to the extent that only one component may be measured. The other components may then be predicted with reasonable confidence. By perturbing synthetic ecosystems with known toxins, these diagnostic methods can be evaluated.

Fire Hazard

In a large space habitat with a terrestrial atmosphere, many of the conventional techniques of fire protection can be used. However, a priority must be placed on fire prevention because even a limited fire could have a devastating effect. An uncontrolled or smoldering fire would pose a serious

threat to the structural integrity of the habitat because of the extensive heat and pressures produced. The constraints of habitat design have two important consequences in fire situations: egress will be limited and few items on board will be expendable.

Atmospheric contamination will occur from toxic, corrosive, and flammable residuals of combustion and pyrolysis. Therefore, fire safety will depend on careful material selection. Attention must be given to fire resistance, toxicity, and smoke evolution properties of all proposed materials. Fire detection and rapid automatic control will be the key issues. Combustion products from sustained burning could overwhelm even the most conservatively designed life-support system. This problem normally does not occur on Earth because the atmosphere provides a means of rapid dispersal. In addition, many conventional flame-retardant materials and extinguishing agents are themselves toxic (e.g., halogenated organics) and would pose an added threat to the life-support system.

Radiation Hazard

The wide spectrum of radiation in the space environment will pose a serious health hazard to man and to the biological components of the space ecosystem (as discussed in the companion paper prepared by the LSSB). The shielding requirements for all candidate biological subsystems should be investigated further. Design shortcomings must not compromise the safety and well-being of humans functioning in space.

Noise Hazard

Current EPA noise standards for community and industrial areas are 70 and 90 dB, respectively. In the enclosed structure of a space habitat, the propagation of sound and vibration throughout the hull will pose a unique problem. In addition, the echo effect could be severe. Skylab astronauts experienced both these difficulties and also complained that differential heating of the spacecraft was a major source of noise (ref. 39).

Clearly, a comprehensive design strategy must be developed to limit noise pollution aboard a space habitat. This capability is represented by state-of-the-art submarine technology: the use of acoustic material to combat echos, and specially designed equipment mounts and foundation structures to isolate sources of vibration (refs. 40, 41). Mechanical oscillation can be dissipated as heat if the foundation structure is properly damped and its resonant modes avoided. In a space habitat, an alternative means to combat the problem of noise would be to physically separate industrial and community living areas.

Gravitational and Rotational Problems

The only practical means for providing pseudogravity to a space habitat is to rotate the habitat structure. Greater economy is reached at higher rotation rates (ref. 42); however, it has been shown that living in a rapidly rotating system can cause severe physiological disturbances due to Coriolis force (refs. 43, 44). Upon head rotation, out of the plane of vehicle rotation, semicircular canal fluids will undergo cross-coupled accelerations. This can result in motion sickness and disorientation (ref. 43). Vestibular physiologists have determined that most people can adapt to rotational rates up to 4 rpm (ref. 43). Although adverse symptoms usually disappear after a few days, some individuals are less tolerant. To avoid rotation-rate sensitivity as a constraint in crew selection, a maximum of 1 rpm has been adopted as an engineering guideline for large habitats ($\sim 10^6$ inhabitants) (J. Billingham, NASA Ames Research Center, personal communication, July 1977).

The syndrome of space motion sickness, on exposure to zero gravity, is well known from Apollo and Skylab experience. Susceptible astronauts have required 2 to 5 days to adjust to zero gravity, during which they suffered from effects similar to motion sickness. This illness has been thought to result from conflicts that arise between perceptions of the visual and vestibular systems. It is not yet known what the effect will be of moving between the rotating and zero-gravity habitat regions (ref. 43). Functioning in the two environments will require two modes of vestibular operation. Conceivably, workers involved in extravehicular or zero-gravity activities may have to reside in zero gravity for additional periods to minimize vestibular symptoms.

Research and Development Options

Early emphasis should be placed on the investigations listed below.

1. Develop a data base for those microbiological functions that will produce usable end products or generate residuals in quantities large enough to affect ambient environmental conditions.
2. Develop a predictive model for the rate of genetic change expected in candidate microbial populations, specifically as they relate to space-habitat conditions. Correlate results with experiments in controlled environments, involving single and multispecies microcosms.
3. Review disease control techniques and develop a rationale for their application to the space habitat; develop an interface between disease control specialists and habitat design engineers.
4. Develop a comprehensive data base on Earth-based technology that is applicable to space habitats in the following areas:
   a. Disease control in plants and animals
   b. Aerosol biology and atmospheric contamination control
   c. Aquatic microbiology and water pollution control
   d. Food preservation technology
   e. Microbial toxic by-products and microbial transformations of industrial materials
   f. Quarantine and containment methodology
   g. Sterilization and decontamination technology including both physical and chemical techniques.

5. Develop, with the aid of the EPA, a list of all toxic compounds and products that contain these toxic compounds; design strategies for controlling toxic compounds released from products.

6. Develop an on-line, real-time system to monitor critical inorganic, organic, and biological activities; develop anticipatory problem-predictive computer models that have adequate response times; test a prototype computer control system in environmental chambers; test advanced systems on the Shuttle.

7. For long-term space settlements, investigate the use of specimen banks of key organisms, tissues, and materials so that an adequate environmental baseline "library" can be available to facilitate effective control measures.

8. Develop genetic strains of micro- and macroplant and animal species for use as sensitive environmental indicators; test these indicator species in environmental chambers that simulate proposed habitat conditions.

9. Develop monitors and test procedures for environmental pathologies; test these procedures in synthetic environments that simulate proposed habitat ecosystems.

10. Develop fire-retardant and extinguishing agents to reduce toxicity of combustion and pyrolysis products; determine which toxic combustion residuals are more compatible with candidate life-support systems.

11. Investigate radiation shielding requirements for man, plant, and microbe populations during long-term spaceflight experiments.

12. Investigate human sensitivity to rotating environments, as well as the effects of alternating between rotating and zero-gravity systems.

13. Determine the optimum environmental conditions for plant, animal, microbial, and human components of the habitat; explore the extent to which modularization, for isolation and retreat from catastrophic events (or separate environmental control of sectors), will be more advantageous than an undivided system; perform economic and reliability analyses with respect to advantages of redundancy over maintaining a single integral system.

CRITERIA FOR ESTABLISHING RESEARCH PRIORITIES

A principal conclusion of this study is that it is premature to prescribe priorities for resource allocation among the research options presented here. However, a procedure was developed to assign priorities in a carefully planned manner. The major elements of this recommended procedure are summarized below.

1. Scenarios for closed life-support systems, comprised of various promising combinations of biological and physicochemical species, should be formulated, quantified, evaluated, and compared according to the methodology discussed in the preceding companion paper.

2. The scenarios should consider terrestrial as well as nonterrestrial atmospheric and gravitational conditions, conventional as well as unconventional diet bases, etc. Sensitivity analyses should be performed for each scenario to characterize its stability features, potential problem areas, and performance limitations in optimum as well as nonoptimum modes of operation. The resulting characterizations can then be used to define pacing research needs.

3. Potential research and development costs and time requirements should be estimated for each scenario. Where these estimates are very sensitive to the accuracy of technical estimates that are not reliable at present, research requirements to refine these latter estimates should be indicated.

4. Research priorities should be assigned to studies that show the highest cost-effectiveness potential and the most universally valuable potential results.

5. A national colloquium of experts in all key technology areas related to closed life-support systems should be conducted as soon as possible to refine the list of research options. This will permit planning based on larger representation of relevant expertise than was available during this study.

REFERENCES

1. Spurlock, J. M.: Review of Technology Developments Relevant to Closed Ecological Systems for Manned Space Missions. Final Report, NASA Contract No. NASw-2981, CR-153000, SAE, New York, 1977.

2. Calloway, D. H.: Basic Data for Planning Life Support Systems. Ch. 1 in Foundations of Space Biology and Medicine, vol. III (Joint USA/USSR Publications in three volumes), general editors, Melvin Calvin (USA) and Oleg G. Gazenko (USSR), NASA SP-374, 1975, pp. 3-21.

3. Popov, I. G.: Food and Water Supply. Foundations of Space Biology and Medicine, vol.111, NASA SP-374, 1975, pp. 22-55.

4. Rambaut, Paul C.; Smith, Malcolm C., Jr.; Leach, Carolyn S.; Whedon, G. D.; and Reid, J.: Nutrition and Responses to Zero Gravity. Fed. Proc., vol. 36, no. 5, April 1977, pp. 1678-1682.

5. Peryam, David R.; Polemin, B. W.; Kamen, J. M.; Eindhoven, J.; and Pilgrim, Francis J.: Food Preferences of Men in the U.S. Armed Forces. Quartermaster Res. and Engineering Command, QM Food and Containers Inst., Jan. 1960.

6. Scrimshaw, Nevin S.; Wang, Daniel I. C.; and Milner, Max: Protein Resources and Technology: Status and Research Needs. Prepared for NSF Research Applications Directorate, RANN, Dec. 1975.

7. Karel, M.; Fennema, O.; and Lund, D.: Physical Principles of Food Preservation. Marcel Dekker, New York, 1975.

8. Peterson, M. S.; and Tressler, D. K.: Food Technology the World Over. vols. I and 11, Avi Pub. Co., Inc., Westport, Conn., 1963.

9. Harris, R. S.; and Karmas, E.: Nutritional Evaluation of Food Processing. Avi Pub. Co., Inc., Westport, Conn., 1975.

10. Bustead, R. L.; and Livingston, G. E.: Mass Feeding in Remote Areas. Activities Rept., vol.29, no. 1, Research and Development Associates for Military Food and Packaging Systems, Inc., 1977, pp. 66-69.

11. Downs, R. J.; and Hellmers, H.: Environment and the Experimental Control of Plant Growth. Academic Press, London, 1975.

12. deWitt, C. T.; Brouwer, R.; and deWries, F. W. T. P.: The Simulation of Photosynthetic System. In Prediction and Measurement of Photosynthetic Product, 1970, pp. 47-70.

13. Fick, G. W.; Williams, W. A.; and Loomis, R. S.: Computer Simulation of Dry Matter Distribution During Sugar Beet Growth. Crop Science, vol. 13, no. 4, July/Aug. 1973, pp. 413-417.

14. Wann, M.; Raper, C. D., Jr.; and Lucas, H. L., Jr.: A Dynamic Model for Plant Growth: a Simulation of Dry Matter Accumulation for Tobacco. Photosynthetica, vol. 12, no. 2, 1978, pp. 121-136.

15. Thomas, J. F.; and Raper, C. D., Jr.: Morphological Response of Soybeans as Governed by Photoperiod, Temperature, and Age at Treatment. Botanical Gazette, vol. 138, no. 3, Sept. 1977, pp. 321-328.

16. Raper, C. D., Jr.; Parsons, L. R.; Patterson, D. T.; and Kramer, P. J.: Relationship Between Growth and Nitrogen Accumulation for Vegetative Cotton and Soybean Plants. Botanical Gazette, vol. 138, no. 2, June 1977, pp. 129-137.

17. Downs, R. J.; and Bonaminio, V. P.: Phytotron Procedural Manual for Controlled-Environment Research at the Southeastern Plant Environment Laboratories. North Carolina Agricultural Experiment Station Technical Bulletin 224, Oct. 1976, p. 37.

18. Collins, W. L.: The Day After Tomorrow: The Objectives and Projects of the University of Arizona, Tucson. Environmental Res. Lab. Rept., 1977.

19. Galston, A. W.: Responses to Gravity in Plants: a Summary. Gravity and the Organism, Solon A. Gordon and Melvin J. Cohen, eds., Univ. of Chicago Press, Chicago, Illinois, 1971, pp. 453-467.

20. Flynt, R. W.; Raper, C. D., Jr.; and York, E. K.: Comparative Pre-Floral Growth of the Flue-Cured Tobacco in Field and Controlled Environments. Agronomy Journal, vol. 70, 1978, pp. 555-559.

21. Evans, L. T.: The Physiological Basis of Crop Yield. Crop Physiology, Cambridge Univ. Press, N.Y., 1975, pp. 327-355.

22. Raper, C. D.; and Thomas, J. F.: Photoperiodic Alteration of Dry Matter Partitioning and Seed Yield in Soybeans. Crop Science, vol. 18, no. 3, July/Aug. 1978, pp. 654-656.

23. Gitelson, I. I.; Kovrov, B. G.; Lisovsky, G. M.; Okladnikov, Yu N.; Rerberg, M. S.; Sidko, F. Ya; and Terskov, I. A.: Problems in Space Biology. Vol. 28: Experimental Ecological Systems Including Man. Nauka Press, Moscow, 1975, pp. 1-312; also NASA Technical Translation F-16993.

14. Heydecker, W., ed.: Seed Ecology. The Pennsylvania State Univ. Press, University Park, Pa., 1973.

25. Thomas, Judith F.; and Raper, C. David, Jr.: Seed Germinability as Affected by the Environmental Temperature of the Mother Plant. Tobacco Science Yearbook, vol. 19, 1975, pp. 104-106.

26. Reid, J. P.: Future Role of Ruminants in Animal Production. Physiology of Digestion and Metabolism in Ruminants, A. T. Phillipson, ed., Oriel Press, 1970, pp. 1-22.

27. Oswald, W. J.; and Golueke, G. G.: Harvesting and Processing of Waste-Grown Microalgae. Algae, Man and the Environment, D. F. Jackson, ed., 1968, pp. 371-389.

28. Ryther, J. H.; Dunstan, W. M.; Tenore, K. R.; and Huguenin, J. E.: Controlled Eutrophication — Increasing Food Production From the Sea by Recycling Human Wastes. Bioscience, vol. 22, no. 3, 1972, pp. 144-152.

29. Wolverton, B. D.; and McDonald, R. C.: Water Hyacinths for Upgrading Sewage Lagoons to Meet Advanced Wastewater Treatment Standards. Part 1, NASA TM X-72,729, Oct. 1975.

30. Wolverton, B. C.; Barlow, R. W.; and McDonald, R. C.: Application of Vascular Aquatic Plants for Pollution Removal, Energy and Food Production in a Biological System. NASA TM X-72,726, 1975.

31. McGinnis, J.: Potential of Non-Ruminants. Role of Animals in the World Food Situations. Rockefeller Foundation, 1975, pp. 59—60.

32. Spurlock, J. M.; Modell, M.; Putnam, D. F.; Ross, L. W.; and Pecoraro, J. N.: Evaluation and Comparison of Alternative Designs for Water and Solid Waste Processing Systems for Spacecraft. Society of Automotive Engineers, Inc., Warrendale, Penn., Final Report on NASA Contract No. NASw-2439, Engineering Experiment Station, Georgia Institute of Technology, Atlanta, Georgia, June, 1975.

33. Jagow, R. B.: Design and Development of a Prototype Wet Oxidation System for the Reclamation of Water and the Disposition of Waste Residues Onboard Space Vehicles. NASA CR-112151, Lockheed Missiles and Space Co., Inc., Contract No. NASI-9183, May 1972.

34. Schelkopf, J. D.; Witt, F. J.; and Murray, R. W.: Integrated Waste Management: Water System Using Radioisotopes for Thermal Energy. General Electric Co. Rept. 74SD4201 (U.S. Atomic Energy Commission Contract AT(11-1)-3036), May 1974.

35. Fields, S. F.; Labak, L. J.; and Honegger, R. J.: Development of an Integrated, Zero-g Pneumatic Transporter/Rotating Paddle, Incinerator/Catalytic Afterburner System for Processing Human Wastes Onboard Spacecraft. NASA Contract NAS2-6386, General American Transportation Co., NASA CR-114764, June 1974.

36. Odum, Eugene P.: Fundamentals of Ecology. 3rd ed., W. B. Saunders Co., Philadelphia, Pa., 1971.

37. MacEven, J. C.: Toxicology. Bioastronautics Data Book. 2nd ed., J. F. Parker and V. R. West, eds., 1973; NASA SP-3006, pp. 455-487.

38. Gall, Lorraine S.: Significance of Microbial Interactions in Control of Microbial Ecosystems. Biotechnology and Bioengineering, vol. XII, no. 3, May 1970, pp. 333-340.

39. Cooper, Henry S. F.: A House in Space, Holt, Rinehart & Winston, New York, 1976.

40. Kakaley, Edward: Theoretical and Experimental Studies of Noise Energy Dissipation and Absorption Materials and Techniques — A Survey and Bibliography. Naval Ship Research and Development Center, NSRDC, 2431, June 1967.

41. Thomas, E. V.: Development of Highly Damped Submarine Machinery Foundation. The Shock and Vibration Bulletin, Feb. 1965, pp. 205-209.

42. Johnson, R. D.; and Holbrow, C., eds.: Space Settlements: a Design Study. National Aeronautics and Space Administration, Washington, D.C., NASA SP-413, 1977.

43. Billingham, J.: Physiological Parameters in Space Settlement Design. 3rd Princeton/AIAA Conference on Space Manufacturing Facilities, Princeton, NJ., May 9-12, 1977, AIAA Paper 77-549.

44. O'Neill, Gerald K.; and Driggers, Gerald W.: Observable Effects in and Human Adaptation to Rotating Environments. In Space-Based Manufacturing from Nonterrestrial Materials. Progress in Astronautics and Aeronautics, vol. 57, AIAA, New York, 1977, pp. 173-176; also NASA TM X-73,265, Aug. 1977.

II
Habitat Design

II-1
Effect of Environmental Parameters on Habitat Structural Weight and Cost

EDWARD BOCK, FRED LAMBROU, JR., and MICHAEL SIMON

Space settlement conceptual designs have previously been accomplished using "Earth-normal" physiological conditions. The purpose of this paper is to quantify the habitat weight and cost penalties associated with this conservative design approach. These penalties are identified by comparison of conservative Earth-normal designs with habitats designed to less than Earth-normal conditions. Physiological research areas are also recommended as a necessary prerequisite to realizing these potential weight and cost savings. Major habitat structural elements, that is, pressure shell and radiation shielding, for populations of 10^2, 10^4, and 10^6, are evaluated for effects of atmospheric pressure, pseudogravity level, radiation shielding thickness, and habitat configuration. Results show that broader habitable g-ranges, reduced atmospheric pressure, and detached radiation shielding all have a significant effect in reducing habitat costs. Also, a minimum cost per person is discovered for a habitat with a population of about 10^5, and this cost is independent of habitat configuration.

INTRODUCTION

The design of space habitats is highly dependent on both the physiological conditions needed to support life and the psychological conditions conducive to enjoyable living. The physiological requirements for a breathable atmosphere, cosmic radiation protection, and pseudogravity have a direct effect on the structural weight and cost of the habitat. Psychological conditions also have an important, although less readily assessable, influence on weight and cost through variations in habitat configurations and interior design. This paper addresses only the physiological effects on habitat structural designs. The results obtained, however, should support subsequent livability analyses by supplying sensitivities for evaluating alternative habitat configurations and interior designs.

The minimum environmental requirements for short-duration life support in space are fairly well understood. Less well known are long-term effects under less than Earth-normal conditions. Conceptual space-settlement habitat designs proposed to date have eliminated this concern by use of the conservative design philosophy of Earth-normal conditions. The questions which this paper addresses are (1) How much does this design conservatism cost from a structural standpoint? (2) Which areas of physiological research into less than Earth-normal conditions offer the greatest potential decrease in habitat construction and operating costs? (3) Do the combined results of sensitivity studies performed during this investigation lead to a recommended habitat configuration that offers the best potential for satisfying physiological requirements at minimum cost?

To address these questions, the following approach has been taken: First, the established range of human tolerance limits has been defined for those physiological conditions which directly affect habitat structural design. Second, these entire ranges, or portions thereof, were set as habitat design constraints as a function of habitat population and degree of ecological closure. Third, calculations were performed to determine the structural weight and cost associated with each discrete population size and its selected environmental conditions. These calculations were performed on the basis of habitable volume equivalence for four basic habitat configurations: sphere, cylinder with hemispherical ends, torus, and crystal palace.

Sufficient point designs were analyzed to permit graphical comparison of habitat structural weights and costs due to a broad range of environmental and population conditions. Those environmental parameters that then offered the greatest economic benefits when reduced to less than Earth-normal conditions (but within established human tolerance limits) were readily identified.

It should be emphasized that the work contained in this paper is not an analysis of a total habitat system; rather, it is limited to environmental and configuration sensitivity analyses of the habitat pressure shell and radiation shielding, plus considerations of habitat illumination and atmospheric composition. Except for their gross influence on the basic habitat structural design, such habitat subsystems as the following have not been evaluated or costed as part of this work: internal secondary structures (buildings); furnishings and personal effects; life-support equipment such as air conditioning, water supply, sewage treatment, etc.; photovoltaic power arrays and waste heat radiators; and spin alignment bearings, hub airlock, and docking facilities.

During performance of work at the 1977 Ames Summer Study relating to this paper, two study team leaders made

significant contributions: Dr. Gerard O'Neill suggested the structural analysis approach used for comparing alternative habitat configurations, and provided an example derivation upon which the generation of structural formulas was based. Dr. John Billingham provided guidance on physiological conditions and was an excellent source for reference materials. Both Doctors O'Neill and Billingham contributed to the selection of representative physiological design constraints for the three habitat populations investigated.

PHYSIOLOGICAL CONDITIONS

Human tolerance limits have been defined for physiological conditions that directly influence habitat structural design requirements. Those environmental parameters which directly affect the habitat structure include internal personal space and furnishings, atmospheric pressure, and gravitational acceleration. Other environmental features that can influence structural mass due to implementation options are radiation protection and illumination techniques. Additional features such as noise abatement or vibration control, which do not directly influence structural mass, have not been included in this analysis. (For a more complete general discussion of environmental parameters and habitat sensitivity philosophy, see ref. 1.)

Personal Space and Furnishings

Habitats must be designed to provide comfortable living, service, social, and recreational facilities. These needs can be analyzed in terms of area, volume, and internal mass requirements per person, as a function of population size, duration of stay, habitat remoteness, etc. Three population sizes (10^2, 10^4, and 10^6) were selected for evaluation to encompass a broad range of habitat volumes. These populations span communities ranging from early space construction facilities to large, relatively self-sufficient settlements.

Volume and area requirements for "military-type" spacecraft and submersible vehicles have been established for relatively short durations (less than 12 months) (ref. 2). Use of these data for space settlements would be inappropriate, because these data apply to temporary assignments in which personnel return home when the tour of duty is completed. Although this same reasoning also applies to short-duration civilian habitats, a significant increase in volumetric allocation per person should be allowed. No real data are available for modern, long-duration (>1 year), remote civilian habitats, but information from the 1975 Ames Summer Study on Space Settlements (ref. 3) was used in conjunction with the existing short-duration data to provide the civilian volumetric requirement curves shown in figure 1.

The 10^4 population design point is obtained directly from detailed analyses conducted during the 1975 Ames Summer Study on Space Settlements. The data point for a 10^2 population habitat was derived from the same source; table 1 summarizes the details pertaining to both configurations.

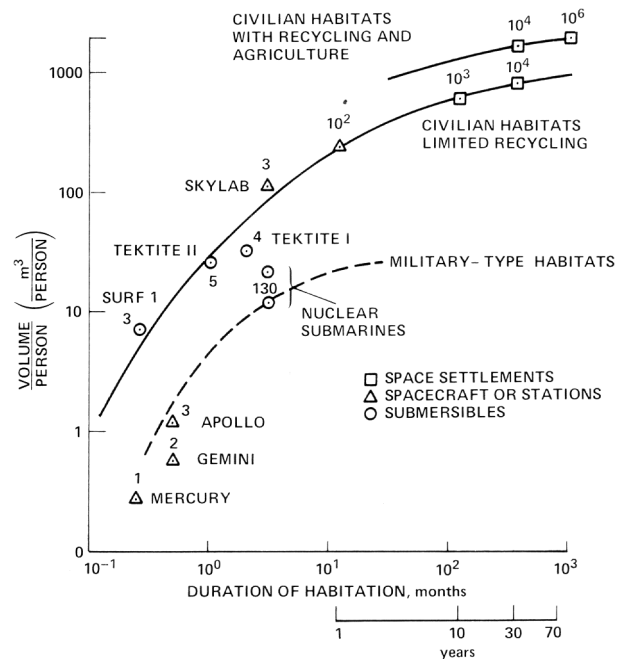The location of these points on the duration abscissa in figure 1 was based on space manufacturing population

Figure 1 — *Habitat volumetric requirements.*

buildup projections (refs. 4, 5). Early habitats with small populations will probably exchange personnel annually or biennially. Larger (10^4) intermediate habitats are expected to receive Earth-trained personnel who will spend their productive years in space, but will return to Earth for retirement. Populations one or two orders of magnitude greater will probably spend their entire lives (vacations excepted) in the habitats. The transition point from an Earth-resupplied habitat to one that is mostly self-sufficient is expected to occur in the 10^4 to 10^5 population range, with substantial on-site food-production experiments performed somewhat earlier. The largest volume/person requirements curve in figure 1 reflects the additional volume needed for food production.

As mentioned previously, both volume and area requirements are important measures of habitat livability. When comparing alternative habitat configurations, however, only one of these measures of personal space can be used as the independent variable. Most previous efforts to define habitat configurations have imposed very strict limits on g-level variations (0.9 to 1.0 g), and have used area as the independent variable. For this comparison, wide g ranges will be studied (including zero g) which makes area a very poor criterion for comparison (essentially meaningless for zero g). All habitat population sizes and geometries have therefore been configured and analyzed on a volume equivalence basis, that is, a fixed volume per person for each habitat population, independent of habitat geometry.

Internal habitat mass per person is a measure of housing and furnishing, and of personal effects allocation. Unfortunately, little appropriate Earth data exist to aid in evaluating this parameter because (1) the cost of Earth-based housing materials, which comprise the largest percentage of personal habitat mass, is generally inversely proportional to their mass, that is, concrete and construction lumber, and (2)

TABLE 1 — COMMUNITY AREA AND VOLUME ALLOCATIONS

Space use	100-person habitat			10,000-person habitat		
	Surface area required, m²/person	Estimated height, m	Volume, m³	Surface area required, m²/person	Estimated height, m	Volume m³
Residential	49	2.5	122.5	49	3	147
Business	2.3	2.5	5.8	3.4	4	13.6
Public space	8.4	6	50.4	14.2	36.5	518.3
Service industry	2.5	2.5	6.3	4	6	24
Storage	5	2.5	12.5	5	3.2	16
Transportation	3.1	2.5	7.7	12	6	72
Mech. subsystem	5.5	4	22	5.0	4	20
Miscellaneous	3.2	4	12.8	3.5	4	14
Subtotals	79.1		240	96.1		824.9
Agriculture						
Plant growing	0		0	44	15	660
Animal area	0		0	5	15	75
Food processing	0		0	4	15	60
Agriculture drying	0		0	8	15	120
Totals	79.1		240	157.1		1739.9

a large percentage of habitat internal mass will be manufactured from "leftover" lunar material, resulting in designs and material uses significantly different from their Earth functional counterparts. The best estimate of habitat internal mass available in current literature is found in the 1975 Ames Summer Study (ref. 3). Since the internal mass requirements should be relatively independent of total population size or volumetric allocation, fixed values for limited recycling (43,000 kg/person) and maximum recycling (53,000 kg/person) habitats were selected.

Pseudogravity and Rotation Rate

The physiological effect of long-term weightlessness is not fully understood. The Skylab 4 astronauts, who were weightless for 84 days, experienced progressive bone decalcification. It is unclear whether these losses stabilize for longer exposures. If they do not, then some level of artificial gravity will be required to prevent severe osteoporosis (ref. 1).

The only way to establish pseudogravity in a space habitat is by rotation. This rotation, however, can cause disorientation and motion sickness due to influence of the Coriolis effect on the vestibular system if the rate of rotation is too high. Because studies in rotating rooms on Earth have shown that most personnel adapt to rotation rates of 3 rpm (ref. 1), this rate will be chosen as the guideline for small, selective, 100-person habitats. For the adaptability and comfort of a general population habitat (10[6]), it is generally accepted that rates above 1 rpm should be avoided. Since the 10[4] habitat will not be as selective as the earlier habitat but more selective than the 10[6] habitat, it is reasonable to consider 2 rpm as its rotation rate.

Radiation and Shielding

Radiation poses a major problem in space-settlement development because of the constant presence of galactic

(cosmic) rays. This type of low-level radiation is isotropic and consists of about 87 percent protons (low Z) and 13 percent heavier nuclei (high Z). "Z" is the charge on the particle, which determines its ionizing power or the quantity of chemical bonds broken by its passage through human tissue. The other source of space radiation, solar flares, is normally at an insignificantly low level, but can occasionally rise to extremely high levels for periods of a few hours or a few days (refs. 6-8).

The best protection against radiation is the use of passive shields. Active "plasma radiation shields" have also been proposed (ref. 3), but are currently speculative and require further substantiation. Figure 2 shows the galactic dose rate as a function of passive shielding thickness. Since nuclear interactions are the primary attenuation mechanism, secondary emission products are a major concern. These secondary products consist of four main types: cascade protons, cascade neutrons, evaporation protons, and evaporation neutrons. Of these four, only the cascade products are significant since the effects of evaporation products are approximately two orders of magnitude smaller than those of the primary protons (ref. 6).

Current U.S. standards for whole-body radiation are 5 rem/yr for radiation workers and 0.5 rem/yr for the general population. Since the inhabitants of the early habitats (100 and 10,000 people) will be selected adult groups with short to intermediate stay times (1 to 30 yr), we can consider them to be radiation workers and design the shielding for 5 rem/yr. To achieve this protection from galactic radiation, 280-g/cm² shielding is required.

The problem of solar flares, however, must still be addressed. Figure 3 shows the total radiation dose as a function of shield thickness for the proton component of an anomalously large flare approximating the intensity of the August 1972 flare. The secondary products are included in this calculation, but the dose from alpha particles is ignored.
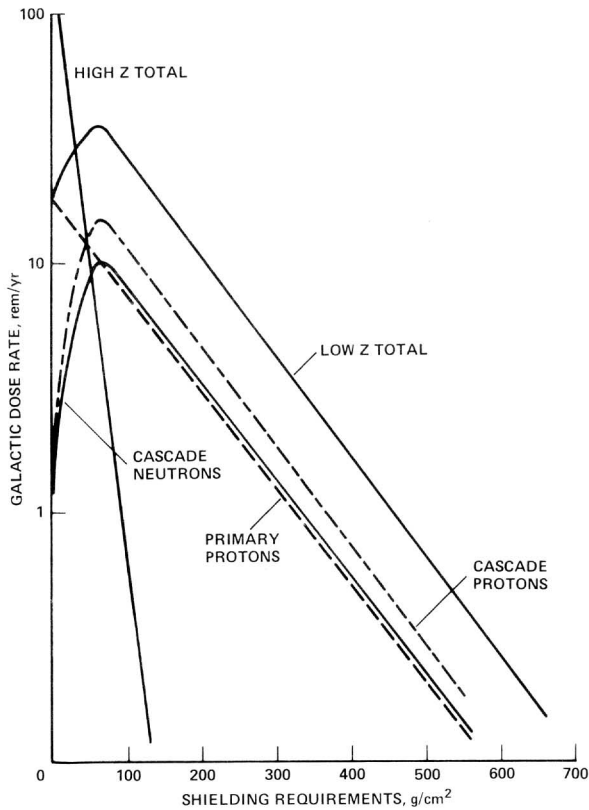
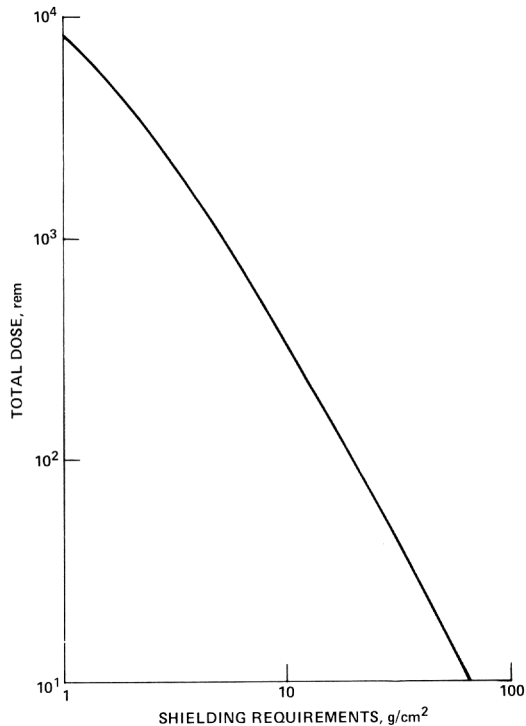Figure 2 — *Galactic dose rates with passive shielding.*

Figure 3 — *Solar flare dose rates with passive shielding.*

The alpha flux, however, is less than 20 percent of the primary rem dose (ref. 9). Thus, 280-g/cm² shielding would attenuate the radiation well below the current U.S. standard for a single emergency exposure of 25 rem. However, on 23 February 1956, the largest flare on record took place. It has been estimated that during this flare people shielded by

approximately 500 g/cm² would have received 25 rem (ref. 10). Fortunately, a flare of this magnitude occurs only once in 20 years. Thus, since people will only live in the 100-person habitat for about 1 year, there would be little need for any additional protection. However, because of the longer duration of the 10,000-person habitat, a flare shelter with an additional 220 g/cm² of shielding will be necessary.

The 10^6-person habitat has an unselected general population. Thus the radiation level must not exceed 0.5 rem/yr. To achieve this, shielding of 550 g/cm² is required. Not only does this protect against galactic

radiation, but it also attenuates the radiation of the largest solar flare to below the maximum permissible for a single emergency exposure. A shelter still might be desirable, however, to protect young children and pregnant women.

Atmosphere

In considering the structural design of a habitat, the total atmospheric pressure is important since it is one of the most significant loads. The lowest pressure will result when the atmosphere contains pure oxygen at a partial pressure similar to that in Earth's atmosphere. Figure 4 shows the pure oxygen atmospheric pressure required for human lungs to physiologically achieve an equivalent Earth altitude. To obtain an Earth sea-level equivalent, 25.3 kPa of pure oxygen is required. This can probably be reduced to 20.0 kPa for the early 100 person habitat since the personnel will be highly selected and could reasonably be expected to function normally in an atmosphere equivalent to 2400 m (8000 ft) above sea level. The inhabitants of the intermediate 10,000-person habitat would also be selected, but to less stringent criteria, so they could operate at an equivalent 1200-m (4000-ft) level or 22.5 kPa pure oxygen.

The desire to operate at such low pressures might be tempered, however, by the fact that sound does not travel well at low pressure (Refs. 11, 12). For instance, the Skylab astronauts, who lived in a total pressure of 34.4 kPa (0.33 atm) said that the limit of a loud speaking voice was about 5 m. This often left them hoarse (ref. 11). Another possible problem with low pressures is diminished effectiveness of the cough mechanism (refs. 12, 13).
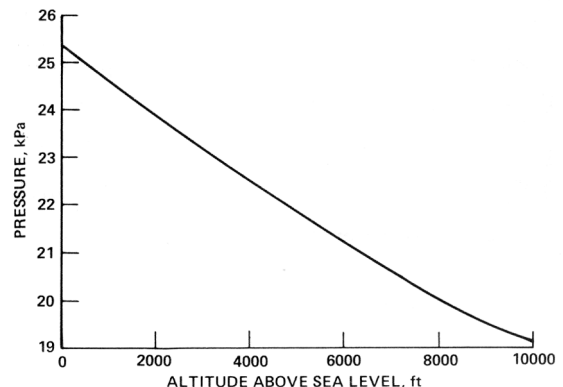

Figure 4 — *Pure oxygen atmospheric pressure at equivalent Earth altitude.*

TABLE 2 — ILLUMINATION REQUIREMENTS FOR 10,000-PERSON HABITAT

Space use	Percentage of time space is used	Required space,[a] m²/person	Lighting required, fc/task	Lighting required, W/m²	Total wattage, W/person maximum	weighted
Residential	50	49	50	11	539	269.5
Business						
Shops	50	2.4	100	22	52.8	26.4
Office	50	1	100	22	22.0	11
Public						
Schools	50	1	100	22	22	11
Hospitals	100	0.3	150	33	10	10
Assembly	50	1.5	40	9	13.5	6.8
Recreation	100	1.4	75	16.5	16.5	16.5
Public open space	100	10	20	4.4	44	44
Service industry	50	4	60	13.2	52.8	26.4
Storage	50	5	40	8.8	44	22.0
Transportation	100	12	15	3.3	39.6	39.6
Mechanical subsystems						
Switching	100	0.3	60	13.2	4.0	4.0
Water treatment	100	4.5	30	6.6	29.7	29.7
Electrical supply	100	0.2	30	6.6	1.3	1.3
Miscellaneous	100	3.5	50	11	38.5	38.5
Subtotals		96.1			929.7	556.7
Agriculture						
Plant growing	50	44	—	250	11,000	5500
Animal	80	5	—	10	50	40
Food processing	80	4	—	10	40	32
Plant drying	100	8	—	15	120	120
Subtotals		61			11,210	5692
Totals		157.1			12,139.7	6248.7

a Data obtained from table 1.

For these reasons, and to reduce fire danger, it is desirable to increase the total pressure by adding a relatively inert gas. Considerable experience has been obtained with nitrogen, Earth's atmosphere diluent, and helium. Although nitrogen is our natural atmospheric diluent, it has one disadvantage: under fast decompression, nitrogen bubbles are released, causing the bends. The best alternative inert gas, helium, reduces man's susceptibility to the bends. Helium also inhibits atelectasis, the tendency for lung collapse, better than nitrogen, but since both helium and nitrogen are superior to pure oxygen, this difference becomes insignificant (refs. 13, 14). Because helium is much less dense than nitrogen its use could lead to significant reductions in transportation cost. Its major disadvantage is severe voice distortion.

The most important function of a diluent gas is to reduce fire danger. Fire hazards in O_2-rich environments have been studied extensively. It has been demonstrated that the burning rate of filter paper in 0.2 atm of pure oxygen is approximately twice that in 1.0 atm of 21 percent O_2 + 79 percent N_2 (ref. 15). Furthermore, many conventional flame-proofed materials burn readily in 30 percent to 40 percent O_2 (ref. 16). Helium diluent is not as effective in reducing the burning rate as is nitrogen (refs. 14, 16). The major factor in overall fire safety, however, is not to control the burning rate but to prevent ignition (ref. 17). As the percentage of O_2 in the atmosphere increases, the minimum pressure required for ignition decreases dramatically.

Figure 5 shows the components of oxygen-nitrogen mixtures that are physiologically equivalent to sea-level air as a function of total pressure. To reduce the total pressure to 0.5 atm, the O_2 partial pressure must be increased to 50 percent. The trade-off between decreased total pressure and increased fire danger must be fully considered before final selection of a space habitat atmosphere is made.
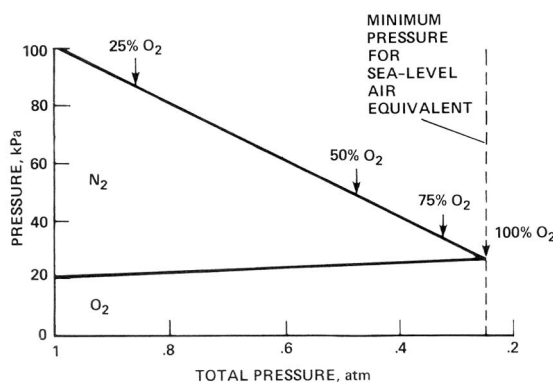

Figure 5 — *Composition of oxygen-nitrogen mixtures equivalent to sea-level atmosphere as a function of total pressure.*

Illumination

The most important component of man's sensory apparatus is his visual system. This makes it particularly important for space-settlement inhabitants to have proper lighting in their work, rest, and living areas. One of the largest habitability problems aboard Skylab was the lack of proper illumination. In fact, the lighting was so poor the astronauts were unable to read a book (ref. 11).

The amount of lighting required depends on the specific task being performed. Table 2 presents illumination requirements for the 10,000-person habitat. As shown, the maximum power required is 929.7 W/person for living and work areas and 11,210 W/person for agricultural areas. These numbers were calculated assuming that the lights are on constantly. A more useful number can be obtained by calculating the percentage of time a particular area will be used, that is, when lights are on. Conservative estimates for these requirements are: 556.7 W/person for living and work areas and 5692 W/person for agricultural areas — a total illumination requirement of 6248 W/person.

These values are conservatively high. The values were converted from lumens to watts by assuming a luminous efficacy of 50 lumen/W. Furthermore, the light reflected from walls, ceilings, and furnishings, which can have a significant effect on illumination intensity, was ignored. These surfaces become secondary sources of illumination, thus lowering the primary light-source intensity requirement (refs. 18, 19).

Studies have shown that the best light for reducing eye fatigue in industrial work is diffused or reflected. Reflected light depends on the properties of the work area surface. Reflection from a matte surface is diffuse while that from a polished surface is specular. Mirrorlike surfaces tend to glare, which greatly increases eye fatigue. Furthermore, the overall color climate of the habitat can have great physiological and psychological effect (ref. 19). Thus, the detailed design of a space habitat must consider these factors.

DESIGN CONSTRAINTS SUMMARY

The tolerable environmental range for satisfying basic human physiological needs has now been established. This range was constrained on the basis of total habitat population. Early construction facilities with small populations will be inhabited by carefully selected crew members and their mission durations limited by reasonable exchange periods. As the population and size of habitats increase, environmental conditions should be changed toward Earth normal, so increased livability and comfort permit extended stay times. This trend is important since personnel selection criteria will be progressively relaxed, and transportation costs for frequent large population exchanges will be excessive.

Table 3 summarizes the physiological design constraints selected for the three habitat populations investigated. These populations represent the full growth range from early

TABLE 3 — PARAMETRIC DESIGN CONDITIONS

Parameters	Stay time, yr		
	1 or 2	30	80
Habitat population	10^2	10^4	10^6
Maximum rotation, rpm	3	2	1
Radiation, rem/yr	5	5	0.6
Atmospheric pressure, kPa			
Maximum	101.3	101.3	101.3
Intermediate	51.7	51.7	51.7
Minimum	20.0	22.5	25.3
Volume/person, m^3			
Limited recycling	240	825	—
Maximum recycling (agriculture)	—	1740	2000
Internal mass/person, kg			
Limited recycling	43,000	43,000	
Maximum recycling		53,000	53,000

construction shacks for space manufacturing to large "ecologically closed" settlements for unselected space immigrants.

Rotation rates for providing pseudogravity decrease from a maximum 3 rpm for a small carefully selected crew to a rotation rate ≤ 1 rpm for a more general population. Similarly, radiation worker dosages of 5 rem/yr are constraints for the 10^2 and 10^4 habitats, while general population dosage limits of 0.5 rem/yr are used for the largest habitat.

A range of three atmospheric pressures has been selected for comparative purposes. Full and approximately half sea-level pressures are the maximum and intermediate selections for all three populations. The minimum pressure is a 100-percent oxygen physiological equivalent to the partial pressure of oxygen at 2400 m (8000 ft), 1200 m (4000 ft), and sea level on Earth for populations of 10^2, 10^4, and 10^6, respectively.

All habitats are limited to a maximum g level of 1.0; minimum g levels ranging from 0 to 0.7 are used as design constraints. These minimum g levels, combined with volumetric requirements, serve to define the habitat geometry for each of the four configurations investigated. The appearance of these volumetrically equivalent geometries varies as a function of how close the spherical configuration approaches the g_{max} limit at the maximum allowable rotation rate, as shown in figure 6. The example on the left depicts a sphere where the radius required to obtain the specified habitable volume is not close to the g_{max} limit. For this case an equivalent cylinder does not exist, the equivalent torus has a circular cross section, and the crystal palace has multiple layers. Habitable volume for the torus and crystal palace configuration is equal to their respective total volumes.

The example on the right in figure 6 shows a sphere for which the radius required to meet volumetric requirements would result in g levels exceeding g_{max} if the sphere were to rotate at the maximum allowable rate. To satisfy all design constraints, the radius is increased and the rotation rate
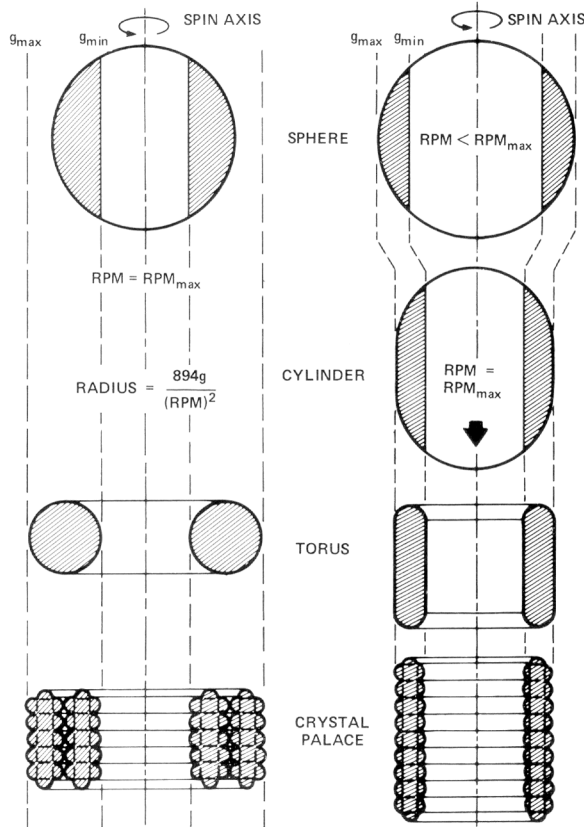
Figure 6 — *Volume equivalence configuration comparison.*

decreased until the habitable volume just fits within the g_{max}/g_{min} limits. For this case, an equivalent cylinder rotating at the maximum rate does exist, as well as a toroidal design with cylindrical walls. The equivalent crystal palace has fewer layers (only one layer is depicted) to remain within the g limits.

The appearance of an "equivalent" torus with cylindrical inner and outer walls imposes one additional design constraint. To prevent the inside cylindrical wall from buckling because of atmospheric-pressure-imposed compressive stresses, the "gravity load" on this surface can be made equal to or greater than the pressure load. This can be accomplished by suspending the entire internal mass from the interior wall and/or adding attached radiation shielding. An alternative approach provides compressive load-carrying capability by structurally stiffening the interior wall.

Radiation shielding is required on all habitats to protect the population from cosmic rays and solar flares. A choice exists, however, as to how this shielding is integrated with the structural shell. Direct attachment is undesirable because centrifugal loading added by the rotating shielding has a major influence on the structural shell thickness (and mass) requirements. The alternative is to mount the shielding outside the structural shell so that it either remains stationary, or counterrotates at a reduced angular velocity to obtain a net zero angular momentum for the entire habitat. This requires that alignment/positioning devices (i.e., mechanical bearings) be used to maintain a positive separation distance between the shell and shielding. To permit structural comparison of these two alternatives, both

attached and detached shielding options were investigated.

SENSITIVITY ANALYSES

Both mass and cost sensitivity analyses were conducted for selected habitat elements. The structural mass sensitivities are presented first, followed by cost sensitivities for structural configurations (pressure shell and radiation shielding), atmospheric composition, and illumination implementation. All cost estimates were based on common ground rules which assumed use of lunar materials, unless the required elements were unavailable in lunar feedstock, in which case these materials were obtained from Earth. Asteroidal resources were not considered. Mass estimates were obtained by performing structural analyses of habitat pressure shell and radiation shielding configurations as a function of population, atmospheric pressure, minimum g level, and shielding integration techniques.

Structural Analyses

As the initial step of the habitat structural design trade, geometries were determined for the sphere, cylinder with hemispherical ends (when applicable), torus, and crystal palace on an equivalent habitable volume basis. The geometric relationships used are summarized in figure 7. Dimensions and important geometric parameters for the 65 shapes included in this analysis are listed in table 4. These characteristics were obtained by applying the design constraints identified in table 3.

Each of these habitat shapes was investigated for structural effects caused by the full range of established design constraints. Membrane stress-analysis techniques were used for the spherical, cylindrical, and toroidal monolithic geometries. For the modular crystal palace, element techniques based on O'Neill's work were used (ref. 20). The membrane analysis was accomplished by resolving all shell loads (atmospheric pressure, skin inertial, internal furnishings inertial, and attached shielding inertial) into combined normal and tangential distributed loads. This enabled the required structural material thickness to be determined by the relationships:

$$\sigma_w = \frac{p_{normal}R}{2t_s} + \frac{q_{tangential}}{t_s} \qquad \text{(sphere)}$$

$$\sigma_w = \frac{p_{normal}R}{t_s} \qquad \text{(cylinder)}$$

$$\sigma_w = \frac{p_{normal}r}{t_s} \frac{2R\text{-}r\sin\theta}{2(R\text{-}r\sin\theta)} + \frac{q_{tangential}}{t_s} \quad \text{(torus)}$$
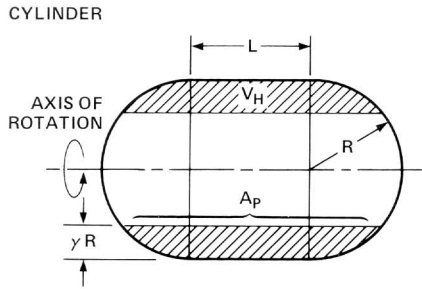
SPHERE
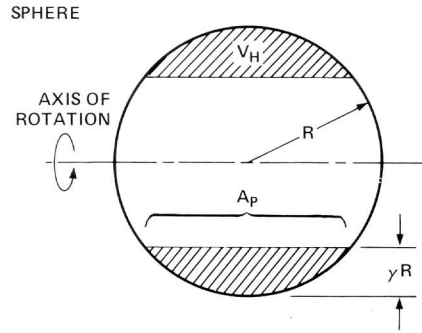
$$V_T = \frac{4}{3}\pi R^3 \qquad\qquad A_S = 4\pi R^2$$

$$V_H = \frac{4}{3}\pi R^3 \left(2\gamma - \gamma^2\right)^{3/2} \qquad \text{WHERE} \quad \gamma = \frac{\Delta g}{g}$$

$$A_P = 4\pi R^2 (1-\gamma)\sqrt{2\gamma - \gamma^2} \qquad \begin{array}{l}\text{FOR} \quad \gamma \geqslant 0.293 \\ A_P = 2\pi R^2 \end{array}$$
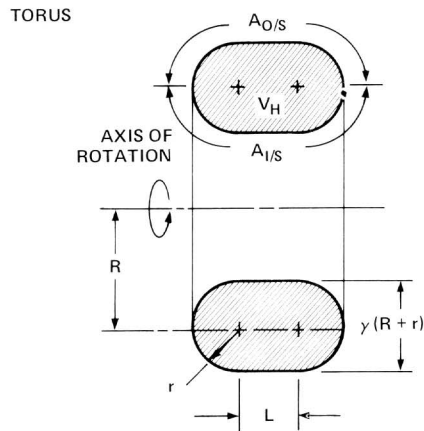
CYLINDER

$$V_T = \pi R^2 L + \frac{4}{3}\pi R^3 \qquad A_S = 2\pi RL + 4\pi R^2$$

$$V_H = \pi R^2 L \left(2\gamma - \gamma^2\right) + \frac{4}{3}\pi R^3 \left(2\gamma - \gamma^2\right)^{3/2}$$

$$A_P = 2\pi R (1-\gamma)\left(L + 2R\sqrt{2\gamma - \gamma^2}\right) \qquad \gamma = \frac{\Delta g}{g}$$

TORUS

$$V_T = 2\pi^2 R r^2 + 4\pi LRr \qquad\qquad V_T = V_H$$

$$A_S = 4\pi^2 Rr + 4\pi LR$$

$$A_{\substack{\text{OUTER}\\ \text{SURFACE}}} = 2\pi^2 Rr + 4\pi r^2 + 2\pi L (R+r)$$

$$A_{\substack{\text{INNER}\\ \text{SURFACE}}} = 2\pi^2 Rr - 4\pi r^2 + 2\pi L (R-r)$$

$$A_P \approx 2\pi R (L + 2r)$$

CRYSTAL PALACE
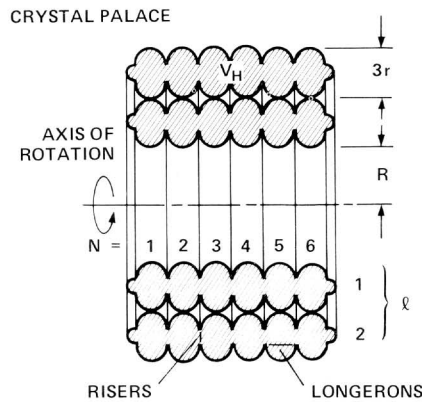
$$V_T = (2\ell R + 3\ell^2 r)\left[Nr^2 (\pi^2 + 2\pi) + \frac{\pi^2 r^2}{4} \right]$$

$$A_{\substack{\text{OUTER}\\ \text{SKINS}}} = 2\pi^2 rN\left[\ell R + \left(\frac{3\ell^2 + \ell}{2}\right)r\right] + 4\pi N\ell r^2$$

$$A_{\substack{\text{INNER}\\ \text{SKINS}}} = 2\pi^2 r N\left[\ell R + \left(\frac{3\ell^2 - \ell}{2}\right)r\right] - 4\pi N\ell r^2$$

$$A_{\text{LONGERONS}} = 4\pi N r (2\ell R + 3\ell^2 r)$$

$$A_{\text{RISERS}} = \pi r (N+1)(2\ell R + 3\ell^2 r)$$

$$A_P \approx 4\pi r N \left(R + \frac{3}{2}r\ell\right)$$

Figure 7 — *Habitat geometric relationships.*

TABLE 4 — DESCRIPTION OF CONFIGURATIONS EVALUATED

10^2 population, V_H = 240 m³/person, 3 rpm (max)

Shape	g_{min}	g_{max}	R	r	L,ℓ	N	A_p/person	V_H/V_T
Sphere	0.70	0.723	71.82	...	...	...	156.5	0.02
	.50	.532	52.82	...	...	...	112.0	.04
	.35	.394	39.12	...	...	...	78.3	.10
	.25	.294	29.22	...	...	...	48.0	.23
	0	0	17.89	...	...	...	20.1	1.0
Cylinder	{.70	...	...	...	...	...	...	...
	.50	...	...	...	...	...	...	...
Torus	.70	.782	73.61	4.064	...	...	37.59	1.0
	.50	.595	54.41	4.727	...	...	32.32	1.0
	.35	.461	40.27	5.495	...	...	27.80	1.0
	.25	.376	31.09	6.253	...	...	24.43	1.0
Crystal palace	.70	.79	69.55	2.952	1	1	27.44	1.0
	.50	.58	49.68	2.540	1	2	34.15	1.0
	.35	.42	34.78	2.474	1	3	35.90	1.0
	.25	.33	24.84	2.500	1	4	35.93	1.0

10^4 population, V_H = 825 m³/person, 2 rpm (max)

Shape	g_{min}	g_{max}	R	r	L,ℓ	N	A_p/person	V_H/V_T
Sphere	0.70	0.90	201.41	...	...	...	24.9	0.24
	.50	.75	168.09	...	...	...	17.8	.41
	.35	.66	147.92	...	...	...	13.7	.61
	.25	.61	137.32	...	...	...	11.8	.76
	0	0	125.35	...	...	...	9.9	1.0
Cylinder	{.70	...	...	...	50.33	...	...	...
	.50	...	...	...	...	...	...	...
Torus	.70	1.00	190.04	33.54	...	...	14.02	1.0
	.50	.95	162.50	50.72	...	...	10.36	1.0
	.35	.85	134.08	55.83	...	...	9.41	1.0
	.25	.79	115.93	60.04	...	...	8.75	1.0
Crystal palace	.70	1.00	156.50	7.452	3	8	14.24	1.0
	.50	.97	111.78	8.694	4	5	8.96	1.0
	.35	.96	78.25	9.151	5	4	6.76	1.0
	.25	.95	55.89	8.731	6	4	5.90	1.0

10^4 population, V_H = 1740 m³/person, 2 rpm (max)

Shape	g_{min}	g_{max}	R	r	L,ℓ	N	A_p/person	V_H/V_T
Sphere	0.70	1.00	225.10	...	...	...	31.8	0.36
	.50	.88	195.77	...	...	...	24.2	.55
	.35	.80	178.65	...	...	...	20.1	.73
	.25	.76	170.40	...	...	...	18.4	.83
	0	0	160.75	...	...	...	16.2	1.0
Cylinder	{.70	1.00	223.57	...	4.40	...	31.8	.37
	.50	...	...	...	...	...	...	...
Torus	.70	1.00	190.04	33.54	164.58	17	27.66	1.0
	.50	1.00	167.67	55.89	59.96	10	18.09	1.0
	.35	1.00	150.91	72.66	12.14	8	14.93	1.0
	.25	.97	136.31	80.42	...	8	13.78	1.0
Crystal palace	.70	1.00	156.50	7.424	3	17	30.12	1.0
	.50	.98	111.78	8.952	4	10	18.62	1.0
	.35	.98	78.25	9.420	5	8	14.10	1.0
	.25	.97	55.89	8.976	6	8	12.33	1.0

10^5 population, V_H = 1900 m³/person, 1.5 rpm (max)

Shape	g_{min}	g_{max}	R	r	L,ℓ	N	A_p/person	V_H/V_T
Sphere	0.70	1.00	499.39	...	...	...	15.67	0.36
	.50	1.00	411.80	...	...	...	10.65	.65
	.35	.99	394.07	...	...	...	9.76	.74
	.25	.94	373.54	...	...	...	8.77	.87
	0	0	356.63	...	...	...	7.99	1.0

10^6 population, V_H = 2000 m³/person, 1 rpm (max)

Shape	g_{min}	g_{max}	R	r	L,ℓ	N	A_p/person	V_H/V_T
Sphere	0.70	1.00	1094.45	...	...	...	7.53	0.36
	.50	1.00	902.51	...	...	...	5.12	.65
	.35	.94	841.37	...	...	...	4.45	.80
	.25	.92	818.92	...	...	...	4.21	.87
	0	0	781.59	...	...	...	3.84	1.0
Cylinder	{.70	1.00	894.26	...	709.42	...	7.84	.42
	.50	1.00	894.26	...	28.83	...	5.14	.65
Torus	.70	1.00	760.12	134.14	1557.8	92	8.72	1.0
	.50	1.00	670.70	223.57	710.24	63	4.88	1.0
	.35	1.00	603.62	290.63	450.69	55	3.91	1.0
	.25	1.00	558.92	335.35	322.37	51	3.49	1.0
Crystal palace	.70	1.00	625.98	9.912	9	92	8.71	1.0
	.50	1.00	447.13	9.880	15	63	5.24	1.0
	.35	1.00	312.99	9.651	20	55	4.02	1.0
	.25	1.00	223.57	9.707	23	51	3.47	1.0

10^7 population, V_H = 2000 m³/person, 1.0 rpm (max)

Shape	g_{min}	g_{max}	R	r	L,ℓ	N	A_p/person	V_H/V_T
Sphere	0.70	1.00	2357.92	...	...	...	3.49	0.36
	.50	1.00	1944.39	...	...	...	2.38	.65
	.35	1.00	1797.59	...	...	...	2.03	.82
	.25	1.00	1739.11	...	...	...	1.90	.91
	0	0	1683.89	...	...	...	1.78	1.0

where

σ_w	allowable working stress for the structural material (218,000 kPa for aluminum)
p_{normal}	combined pressure load normal to shell membrane, kN/m²
t_s	shell thickness, m
R	major radius, m
r	torus minor radius, m
$q_{tangential}$	combined running tangential load, kN/m²

Derivation of these equations is illustrated by the example for the spherical shell skin inertial loading due to centrifugal force depicted in figure 8.

The inertial force of the skin is

$$F_{skin} = V_{skin}\rho_s g = (t_s R^2 \sin\theta \, d\theta \, d\phi)\rho_s(\omega^2 R \sin\theta)$$

$$p_{normal} = \frac{F_{skin}\sin\theta}{A} = t_s\rho_s\omega^2 R \sin^2\theta$$

$$F_{tangential} = F_{skin}\cos\theta$$

accumulated along the $R\sin\theta\,d\phi$ band.

Integrating, the tangential force equals

$$t_s R^3 \rho_s\omega^2 d\phi \int_0^\theta \sin\theta\,\cos\theta\,d\theta = \frac{t_s}{3}R^3\rho_s\omega^2 d\phi \sin^3\phi$$

Therefore,

$$q_{tangential} = \frac{F_{tangential}}{width} = \frac{t_s}{3}R^2\rho_s\omega^2\sin^2\theta$$
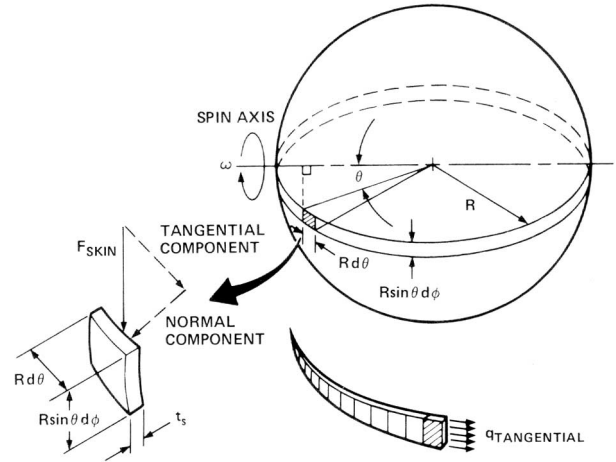
Figure 8 — *Spherical shell analysis.*

where

V volume, m³

ρ_s density of structural material, kg/m³

g pseudogravity level, dimensionless

ω angular velocity, rad/s

Components for internal furnishings inertia and attached radiation shielding inertia are similarly derived. These components are grouped and added together, substituted into the appropriate formula, and the resulting expression extensively manipulated to obtain the final equations listed in figure 9.

SPHERE
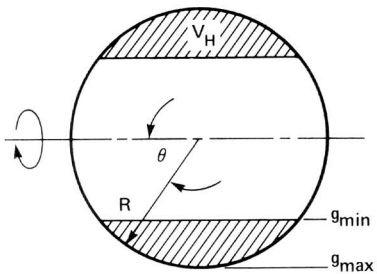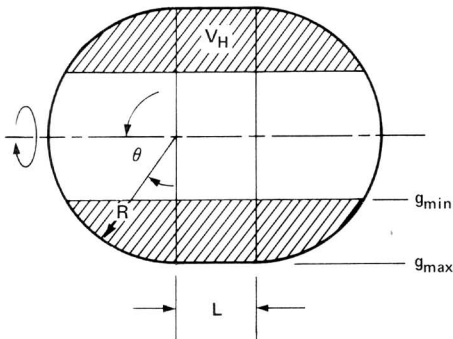
$$t_s = \frac{R}{\sigma_w - \frac{R\rho_s g_{max} k \sin^2\theta}{1200}}\left[\frac{p_A}{2} + \frac{(IM)\,g_{max}\,k\,R}{V_H(1000)}\left\{\frac{7}{20}\sin^4\theta\right.\right.$$

$$\left.- \frac{5}{12}\left(\frac{g_{min}}{g_{max}}\right)^2\sin^2\theta + \frac{1}{15\sin\theta}\left(\frac{g_{min}}{g_{max}}\right)^5\right\}FOR\,\theta > \sin^{-1}\left(\frac{g_{min}}{g_{max}}\right)$$

$$\left.+ \frac{\rho_{rad}\,g_{max}\,k}{1200\,R}\,t_{rad}\left(R + \frac{t_{rad}}{2}\right)\sin^2\theta\right]$$

$$m_s = \rho_s\,VOL = \rho_s\,\Sigma\,4\pi R^2\sin\theta\,\Delta\theta\,t_s$$

CYLINDER

FOR HEMISPHERICAL ENDS USE SPHERE EQUATIONS

$$t_s^{CYL} = \frac{R}{\sigma_w - \frac{R\rho_s g_{max} k}{1000}}\left[p_A + \frac{(IM)\,k\,(g_{max}^2 - g_{min}^2)}{2.2365\,V_H\,(RPM)^2}\right.$$

$$\left.+ \frac{\rho_{rad}\,g_{max}\,k}{1000\,R}\,t_{rad}\left(R + \frac{t_{rad}}{2}\right)\right]$$

$$m_s^{CYL} = \rho_s\,VOL = 2\pi\rho_s\,RL\,t_s$$

WHERE

k 9.80665 m/sec² (ACCELERATION OF EARTH GRAVITY)

Figure 9 — *Habitat structural shell formulas.*

TORUS
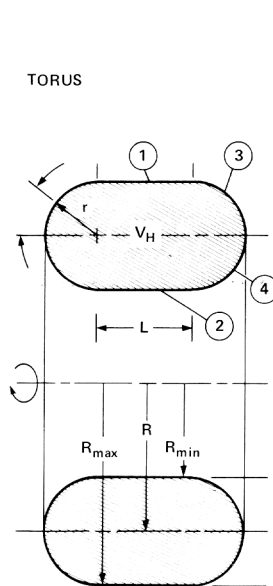
NOTE:
ASSUMES THAT ALL INTERNAL
MASS IS SUSPENDED FROM THE
INSIDE WALLS ② AND ④.

$$\overset{①}{t_s} = \frac{R_{max}}{\sigma_w - \frac{\rho_s \, g_{max} \, k \, R_{max}}{1000}}\left[p_A + \frac{\rho_{rad} \, t_{rad} \, g_{max} \, k \left(R_{max} + \frac{t_{rad}}{2}\right)}{1000 \, R_{max}}\right]$$

$$\overset{①}{m_s} = \rho_s \, A \overset{①}{t_s} = \rho_s \, 2\pi R_{max} \, L \overset{①}{t_s}$$

$$\overset{②}{t_{s\,min}} = \frac{(R_{max}^2 - R_{min}^2)}{\sigma_w \, 2 \, (R_{max} + R_{min})} \, p_A \quad\Big\}\quad \text{WHERE:} \quad p_{rad} + p_{IM} = p_A$$

$$\overset{②}{t_s} = \frac{R_{min}}{\sigma_w + \frac{\rho_s \, g_{min} \, k \, R_{min}}{1000}}\left[\frac{(IM)\,(g_{max} + g_{min})\,k\,r}{1000 \, V_H} + \right.$$

$$\left. \frac{\rho_{rad} \, g_{min} \, k \, t_{rad}}{1000 \, R_{min}}\left(R_{min} - \frac{t_{rad}}{2}\right) - p_A\right] \quad\Big\}\quad \text{WHERE:} \quad p_{rad} + p_{IM} > p_A$$

$$\overset{②}{m_s} = \rho_s \, A \overset{②}{t_s} = \rho_s \, 2\pi R_{min} \, L \overset{②}{t_s} \longleftarrow \text{FOR LARGEST } \overset{②}{t_s}$$

$$\overset{③}{t_s} = \frac{A + (B + CD) \sin\theta + C(E + F) \sin^2\theta + C(G + H) \sin^3\theta}{\sigma_w \, R + (\sigma_w \, r - JD)\sin\theta - JE \sin^2\theta - JG \sin^3\theta}$$

$$\overset{④}{t_s} = \frac{A + (CD - B)\sin\theta - C(E + F)\sin^2\theta + [MN + C(G + H)]\sin^3\theta - MP \sin^4\theta}{\sigma_w \, R - (\sigma_w \, r + JD)\sin\theta + JE \sin^2\theta - JG \sin^3\theta}$$

$$\overset{③}{m_s} = \rho_s \sum \frac{\pi^2 \, \overset{③}{t_s} \, r}{4.5}(R + r\sin\theta) \qquad\qquad \overset{④}{m_s} = \rho_s \sum \frac{\pi^2 \, \overset{④}{t_s} \, r}{4.5}(R - r\sin\theta)$$

WHERE:

$A = r p_A R$		$E = \dfrac{5Rr}{2}$		$J = \dfrac{r\rho_s \, g_{max} \, k}{1000 \, R_{max}}$	
$B = \dfrac{r^2 p_A}{2}$		$F = \dfrac{3R t_{rad}}{4}$		$M = \dfrac{r^2 R(IM) \, g_{max} \, k}{1000 \, V_H \, R_{max}}$	
$C = \dfrac{r t_{rad} \, \rho_{rad} \, g_{max} \, k}{1000 \, R_{max}}$		$G = \dfrac{5r^2}{6}$		$N = \dfrac{8R}{3}$	
$D = 2R^2$		$H = \dfrac{5 r t_{rad}}{12}$		$P = \dfrac{3r}{2}$	

CRYSTAL PALACE
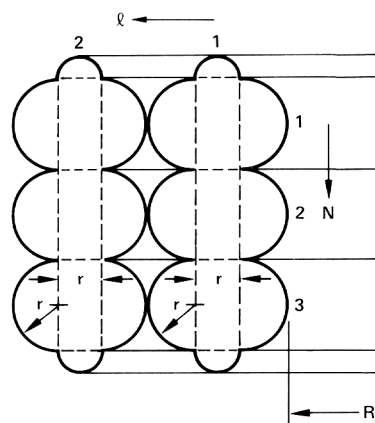
$$t_{LONGERON} = \frac{p_A \, r}{2\sigma_w}$$

$$m_s = \rho_s \, \Sigma At$$

$$t_{OUTER\,SKIN} = \frac{p_A \, r + \dfrac{(IM)\,k\,(RPM)^2}{894,260 \, V_H}\left[R + \dfrac{3r}{2}(\ell+1)\right]^2}{\sigma_w - \dfrac{\rho_s k \,(RPM)^2}{894,260}\left[R + \dfrac{3r}{2}(\ell+1)\right]^2}$$

$$t_{INNER\,SKIN} = \frac{p_A \, r}{\sigma_w + \dfrac{\rho_s k \,(RPM)^2}{894,260}\left[R + \dfrac{3r}{2}(\ell-1)\right]^2}$$

$$t_{RISER} = \frac{p_A \, r + \dfrac{(IM)\,k\,(RPM)^2}{894,260 \, V_H}\left[R + \left(\dfrac{3\ell-1}{2}\right)r\right]^2}{\sigma_w - \dfrac{\rho_s k \,(RPM)^2}{894,260}\left[R + \left(\dfrac{3\ell-1}{2}\right)r\right]}$$

$$m_{CABLES} = \frac{\rho_s m_H k\left[R + \left(\dfrac{3\ell-1}{2}\right)r\right]^2 (RPM)^2}{894,260 \, \sigma_w}$$

WHERE　　$m_{HABITAT} = m_s + (IM)\,(POPULATION)$

Figure 9 — *Concluded.*

The crystal palace equations, also shown in figure 9, were obtained from O'Neill's work (ref. 20) by setting $h = r$ and incorporating the effects of skin inertial loading. Cable mass was calculated by neglecting the additional cable cross section needed to support its own inertia (this assumption results in underestimated cable mass for larger habitats). Attached radiation shielding was not considered for the crystal palace configuration. Employment of these crystal palace formulas presupposes that the minor radius r is much smaller than the major radius R. To remain within this constraint, a maximum minor radius of 10 m was selected. The crystal palace "r" radii shown in table 4 are obtained by selecting suitable integer values for the number of modules (N and ℓ) and solving for the required habitable volume.

Results of these structural shell analyses are presented in figures 10 through 17. Figures 10 through 13 show habitat structural shell mass as a function of minimum g level for fixed populations and atmospheric pressure.
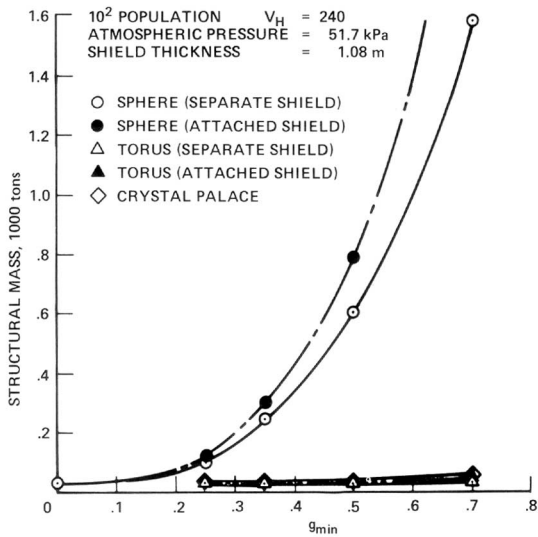
Figure 10 — *Structural mass as a function of* g *level,* 10^2 *population.*

The intermediate 51.7 kPa (half Earth normal) pressure was selected, since representative structural sensitivity to the full pressure range is contained in figures 14 through 17.
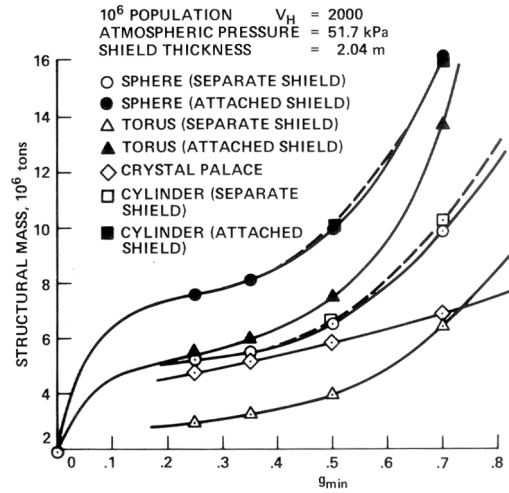
Figure 13 — *Structural mass as a function of* g *level,* 10^6 *population.*
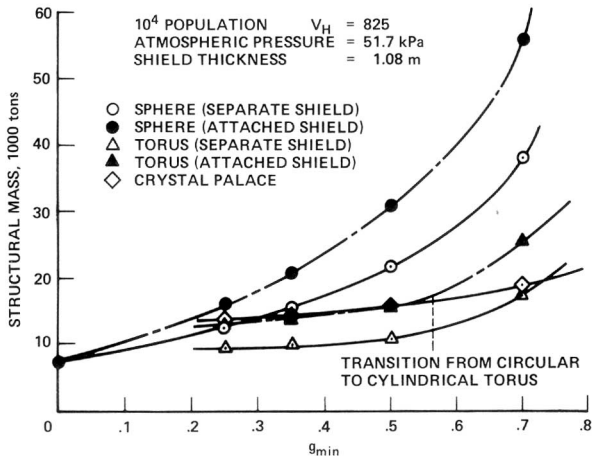
Figure 11 — *Structural mass as a function of* g *level,* 10^4 *population;* $V_H = 825.$
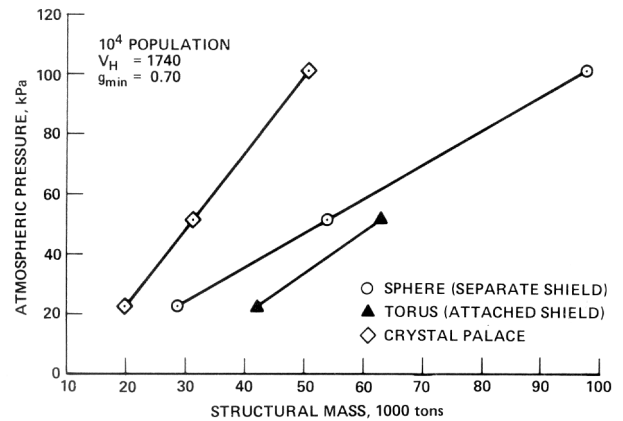
Figure 14 — *Structural mass as a function of pressure,* 10^4 *population;* $g_{min} = 0.70.$
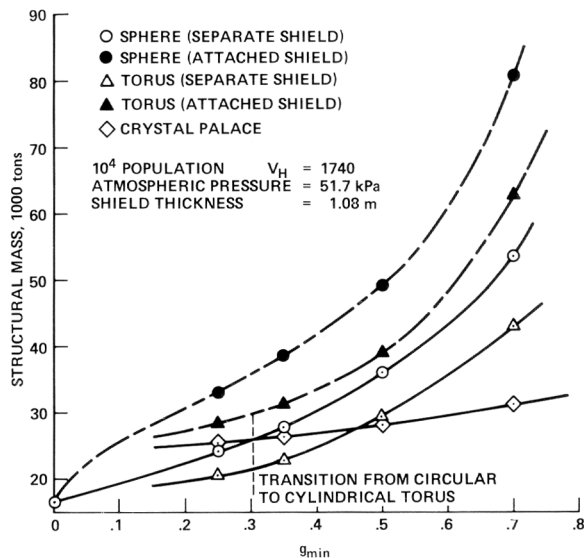
Figure 12 — *Structural mass as a function of* g *level,* 10^4 *population;* $V_H = 1740.$
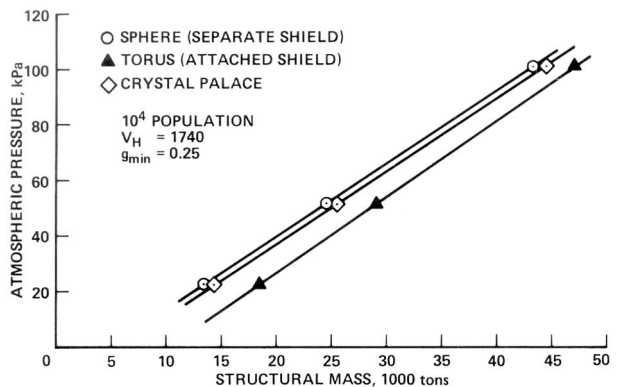
Figure 15 — *Structural mass as a function of pressure,* 10^4 *population;* $g_{min} = 0.25.$
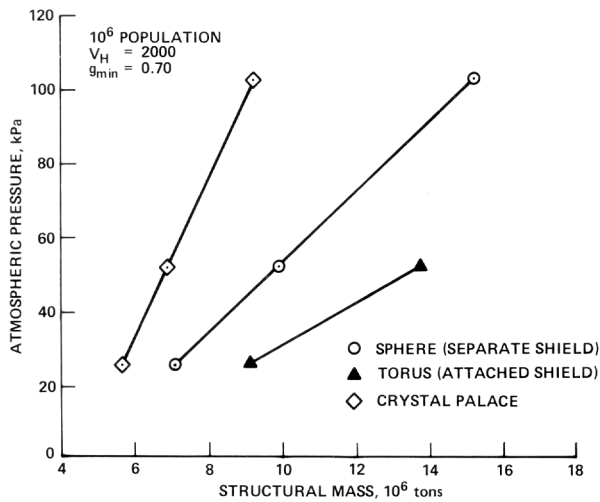
Figure 16 — *Structural mass as a function of pressure, 10^6 population; $g_{min} = 0.70$.*

The following general trends were obtained from data generated:

- At lower populations, the structural mass of spherical habitats is more sensitive to g_{min} than are other configurations (fig. 10).
- Attached shielding results in a substantial structural shell weight penalty.
- The structural penalty per person for attached shielding increases with population (habitat size).
- For larger habitats (figs. 12 and 13), the curves for toroids with attached and unattached radiation shielding bracket the "spherical habitat with unattached shielding" curve. This is important since the "torus with separate shielding" structural mass has been derived by neglecting
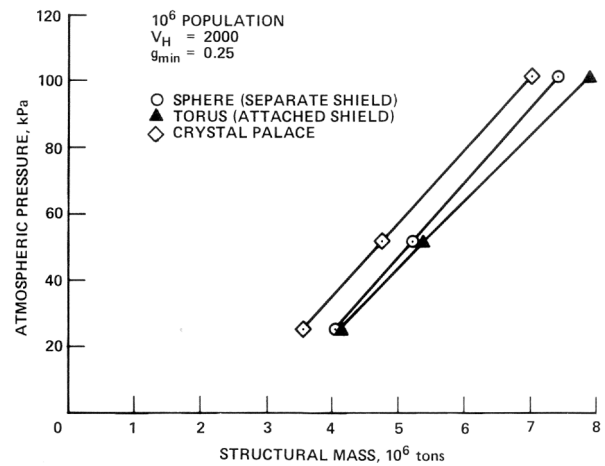
Figure 17 — *Structural mass as a function of pressure, 10^6 population; $g_{min} = 0.25$.*

the compressive loading condition of the inner cylindrical wall. Correction of this condition will shift this curve (increase the mass) closer to the spherical habitat curve.

Referring now to figures 14 through 17:

- Habitat structural mass increases linearly in proportion to internal pressures.
- With a broad habitable g range (0.25 to 1.0), habitat pressure sensitivity is independent of configuration for larger populations.
- For larger habitats with a constrained g range (0.70 to 1.0), pressure sensitivity is configuration-related, with the crystal palace showing the least sensitivity due to "fixed" cable mass.

ATTACHED SHIELDING

$$m_{rad} = \rho_{rad}\, t_{rad} \left[4\pi \left(R + \frac{t_{rad}}{2} \right)^2 + 2\pi \left(R + \frac{t_{rad}}{2} \right) L \right]$$

SEPARATE SHIELDING

$$m_{rad} = \rho_{rad}\, t_{rad} \left[4\pi \left(R + \frac{t_{rad}}{2} + 1.5 \right)^2 + 2\pi \left(R + \frac{t_{rad}}{2} + 1.5 \right) L \right]$$

ATTACHED SHIELDING

$$m_{rad} = \rho_{rad}\, t_{rad} \left[4\pi^2 R \left(r + \frac{t_{rad}}{2} \right) + 4\pi\, RL \right]$$

SEPARATE SHIELDING

$$m_{rad} = \rho_{rad}\, t_{rad} \left[4\pi^2 R \left(r + \frac{t_{rad}}{2} + 1.5 \right) + 4\pi\, RL \right]$$

SEPARATE SHIELDING

$$m_{rad} = 2\pi \rho_{rad}\, t_{rad} \left[(R + 3r\, \ell + 2.25)^2 + (R + 3r\, \ell + 2.25)(2rN + r + 4.5) \right]$$

FOR DEFINITION OF r, ℓ, N SEE FIGURE 9
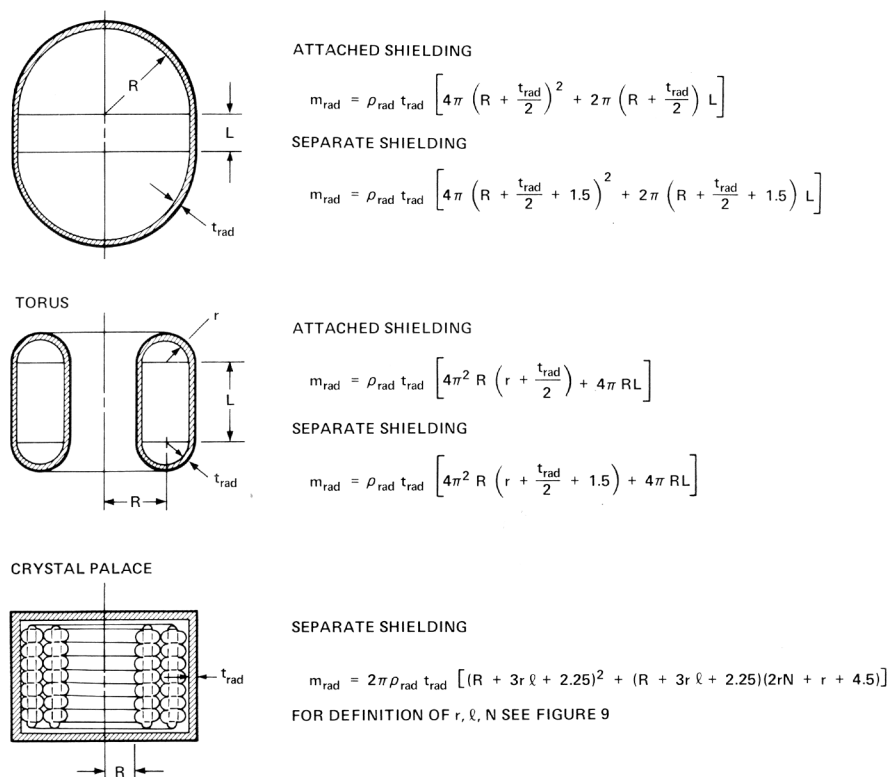
Figure 18 — *Habitat radiation shielding mass equations.*

Shielding masses for each of the habitats were obtained via the equations in figure 18 for the following alternatives:

1. Sphere or cylinder — Shielding can either be attached or detached for all cases, and surrounds the structural shell.
2. Torus — Circular cross-section toroids can have either attached or detached shielding. Torii with cylindrical walls also have an attached/detached option, but must either have sufficient shielding on the inner wall to equalize the internal pressure, or additional shell structure must be incorporated to sustain these compressive loads. All shielding configurations investigated were toroidal and surrounded the structural shell.
3. Crystal palace — Only detached shielding was evaluated for the crystal palace. Since the crystal palace employs cables to react centrifugal loads, cylindrical rather than toroidal shielding was used.

All attached shielding was assumed to be immediately adjacent to the structural shell. Detached shielding was separated by 1.5 m. Owing to the increased area of separated shielding, its mass ranges from about 0.2 to 4 percent more than that for attached shielding. The following general shielding mass trends were obtained from separated shielding data shown in figures 19 through 22.

- Shielding mass sensitivity increases as the habitable g range is constrained ($g_{min} \rightarrow 1$).
- Spheres exhibit greater sensitivity to shielding mass at lower populations than do other configurations.
- The shielding mass is two to three orders of magnitude greater than habitat structural mass for small habitats (10^2 population), but is only one order of magnitude greater for large habitats (10^6 population).

Figure 21 — *Radiation shielding mass as a function of habitat g level, 10^4 population; $V_H =1740$.*

Figure 19 — *Radiation shielding mass as a function of habitat g level, 10^2 population.*
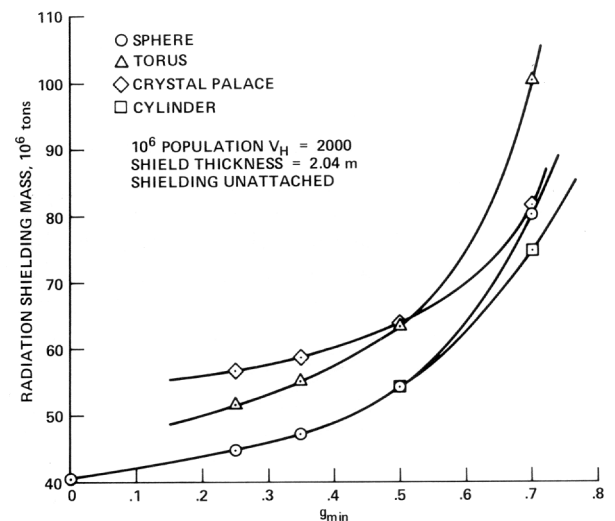
Figure 22 — *Radiation shielding mass as a function of habitat g level, 10^6 population.*

Cost Comparison Ground Rules and Assumptions

The assessment of alternative habitat design concepts can best be accomplished by cost comparison. Our analysis shows considerable cost differences owing to overall habitat material requirements, and between terrestrial supplies and the various products manufactured in space from lunar material. Habitat cost comparison has been conducted by assuming that all habitat atmospheric oxygen, pressure shell structure, and radiation shielding are derived from lunar resources. It was also assumed that other items such as

Figure 20 — *Radiation shielding mass as a function of habitat g level, 10^4 population; $V_H = 825$.*

lighting fixtures are required in sufficient quantity so that they can be economically manufactured from lunar materials. The only materials or products imported from Earth are those which are either unavailable in lunar resources, or which because of complicated manufacturing operations requiring expensive facilities coupled with relatively small quantity requirements can be more economically obtained from Earth. Since the sensitivity studies in this analysis were conducted at a major subsystem rather than a component level, no complicated Earth products of this sort were included. The special ground rules and assumptions used for costing of lunar and Earth habitat construction materials are as follows:

1. Space processing and fabrication costs are obtained from data generated for the 11-year space manufacturing buildup period for the construction of solar power satellites from lunar resources (ref. 5). This information was used in lieu of equilibrium data because it was obtained by more rigorous methods and is better documented. This approach is conservative for comparison with Earth imports because space manufacturing equilibrium costs should be somewhat lower.

2. Space processing and fabrication costs are based on the conversion of 1737 ktons of lunar material into useful products. A total of 5745 man-years and $6.45 billion are expended to perform this conversion, that is, personnel cost (including transportation and all support), equals $1.123 million/man-year.

3. Material processing costs and fabrication costs constitute 25 and 75 percent of this total expenditure, respectively (R. Williams, personal communication, 1977).

4. Costs for each major space-manufactured product obtained from lunar material are shown in table 5. The constituents of lunar material shown reflect some lunar beneficiation prior to delivery to the space manufacturing facility (SMF). The processing and fabrication factors reflect the relative difficulty of manufacturing that particular product (R. Williams, personal communication, 1977).

5. Transportation costs from Earth to the SMF were derived for equilibrium conditions using third-generation launch vehicles. This approach is purposefully optimistic so that cost comparisons with space-manufactured products will be more conservative.

6. A single-stage to orbit vehicle delivers payload in low Earth orbit (LEO) at $47.06/kg, and a heavy massdriver reaction engine provides LEO to SMF transfer at

$10.16/kg, for a total transportation cost of $57.22/kg (J. Engel, Dept. of Systems Engineering, Univ. of Illinois at Chicago, personal communication). For most items, this transportation cost will be an order of magnitude above the Earth purchase price, which has therefore been neglected.

Habitat Structural Cost Comparison

Habitat structural elements included in this comparison are the pressure shell and radiation shielding. Windows for illumination are evaluated later in this paper. Internal furnishings were not included because their allocated mass per person was assumed to be equal for all populations within each of the two habitat classes. The smaller habitat class, 10^2 and 10^4 populations without agriculture, used 43,000 kg/person internal furnishings. The larger class, 10^4 and 10^6 populations with agriculture, all used 53,000 kg/person.

To provide better cost sensitivities for the larger-class habitats, the radiation shielding thickness for the 10^4 population configurations with agriculture was increased from 1.08 to 2.04 m. In addition, spherical habitats with 10^5 and 10^7 populations and shielding 2.04 m thick were also included in an attempt to establish the habitat size for minimum cost per person. A geometric definition of these added habitats is included in table 4.

The cost comparison performed assumes that all materials needed for the structural shell and radiation shield are obtained from processed lunar soil. The shell is assumed to be aluminum with a working stress of 218,000 kPa at a cost of $7.05/kg, and the shielding, molded industrial slag at $0.21/kg from table 5. If a significant percentage of shell alloying elements must be imported from Earth to meet the assumed working stress, then the shell costs must be increased accordingly.

All cost comparisons shown in figures 23 through 28 are for habitats with unattached shielding and an intermediate atmospheric pressure of 51.7 kPa. Unattached shielding and intermediate atmospheric pressure were both previously shown to result in reduced structural shell material requirements. Figure 23 shows the cost per person of the shell and shielding structural components for spherical habitats as a function of habitat size (population) and minimum g level. The shaded bands show the cost range from $g_{min} = 0$ to $g_{min} = 0.7$. It is interesting to note that the shielding cost exceeds shell cost up to a population of about 10^5; for larger populations the reverse is true. Similar results were obtained for toroidal and crystal palace habitats.

TABLE 5 — COST OF SPACE-MANUFACTURED MATERIALS

Product	Glass	Silicon	Oxygen	Shielding	Titanium	Iron	Aluminum
Percent of lunar material	2.25	12.67	19.80	46.63	4.43	5.12	9.10
Processing factor	2	2	0.5	0.1	1	1	1
Processing cost, $/kg	2.95	2.95	0.74	0.15	1.47	1.47	1.47
Fabrication factor	2	2	0.05	0.01	1	1	1
Fabrication cost, $/kg	11.16	11.16	0.28	0.06	5.58	5.58	5.58
Total mfg. cost, $/kg	14.11	14.11	1.02	0.21	7.05	7.05	7.05

Figures 24 through 27 show cost as a function of habitat size (population) for various habitat configurations at fixed minimum g values. The smaller-class habitats (radiation shielding thickness = 1.08 m) are characterized by a very wide configuration cost spread at 10^2 population, narrowing to $20,000/person difference at 10^4 population for all values of g_{min}. For the larger-class habitats (radiation shielding thickness = 2.04 m),

the minimum cost per person always occurs between populations of 10^5 and 10^6 except for the special case of zero-g spheres, where the cost per person continues to decrease as population increases. The data for zero-g spherical habitats can be obtained by summing the left-hand curves of figure 23. For most values of minimum g, toroidal habitats show a significant cost advantage ($10,000 to $20,000/person) over spherical and crystal palace habitats. It must be noted, however, that both toroidal and crystal palace habitat configurations require additional hub structures, which have not been included in this analysis. These hub features include cargo vehicle docking provisions, personnel access structure, and shielding alignment support structure, all of which are inherently provided by a spherical geometry. Also, as noted previously, the geometric constraints employed for this comparison result in toroids with cylindrical sections. With unattached shielding, these inner toroidal habitat cylindrical walls are compressively loaded. The additional structure required to prevent buckling was not included in the "detached shielding" structural weights used.

Large class habitat costs as a function of minimum g level are shown in figure 28. All geometries and populations exhibit lower cost per person for reduced minimum g.
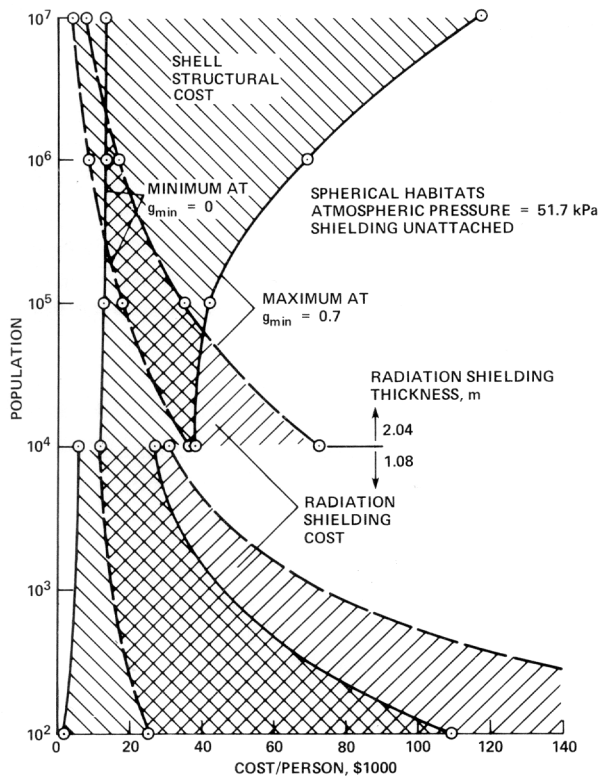
Habitat Atmosphere Cost Comparison

The combination of habitat configuration, atmospheric pressure, and atmospheric composition have a significant effect on the total habitat atmospheric mass and its acquisition cost per person. Toroidal and crystal palace habitats are efficient from an atmospheric volume standpoint, and spherical and cylindrical habitats are inefficient since their total pressurized volumes exceed the habitable volumetric requirements of their populations.

Possible habitat atmospheric compositions of oxygen and diluent were previously established as a function of total pressure and population (see figs. 4 and 5 and table 3). The oxygen for the habitat atmosphere will be recovered during lunar material processing at the space manufacturing facility. Since it is produced in large quantities at the habitat construction site, the cost of oxygen is a reasonable $1.02/kg.

Possible inert atmospheric constituents include nitrogen or helium. During early space-settlement efforts, these diluents will probably be imported from Earth, with a delivery cost of $57.22/kg. Since the cost of atmospheric inerts is 56 times that of an equal quantity of oxygen, their use for large habitats will either be limited or a nonterrestrial source will be developed. Some scientists have suggested that volatiles may exist in frozen form at the lunar poles, but a more probable source is asteroidal material. It has been estimated that up to 0.3 percent of the mass of carbonaceous chondrite asteroids could be nitrogen (ref. 21). If nitrogen can be recovered from a convenient extraterrestrial source, its cost should be approximately equal to that of oxygen.

Figure 23 — *Cost spread of spherical habitat structural components.*
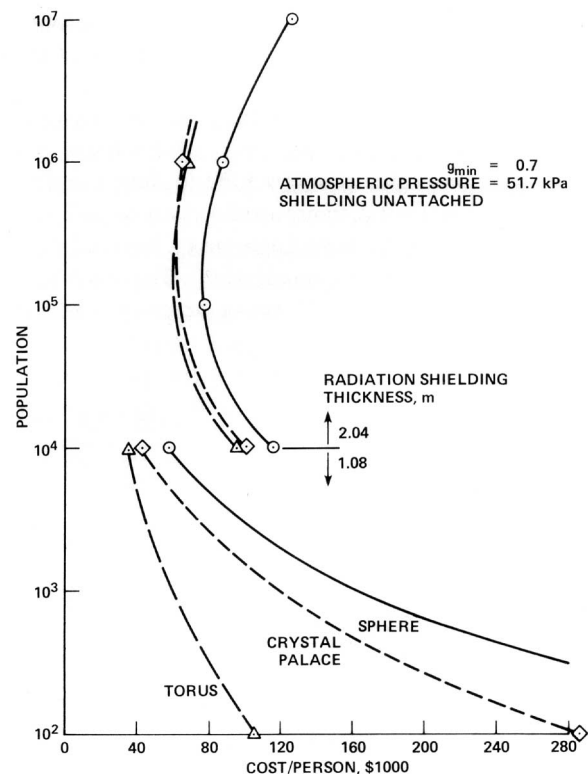
Figure 24 — *Habitat cost comparison for $g_{min} = 0.70$.*
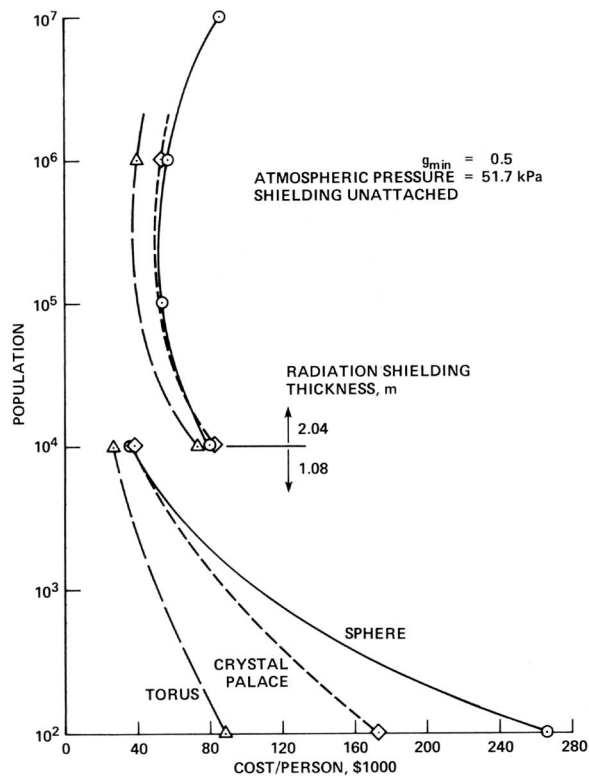
Figure 25 — *Habitat cost comparison for* $g_{min} = 0.50$.
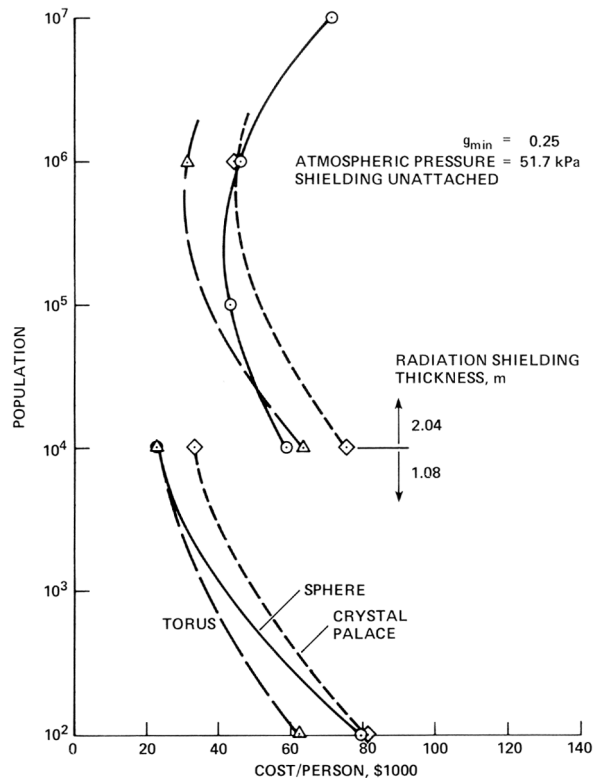
Figure 27 — *Habitat cost comparison for* $g_{min} = 0.25$.
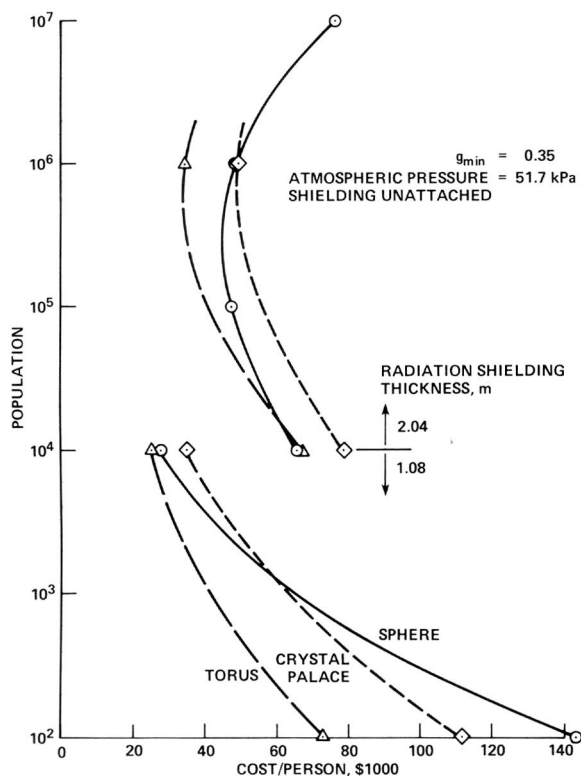
Figure 26 — *Habitat cost comparison for* $g_{min} = 0.35$.
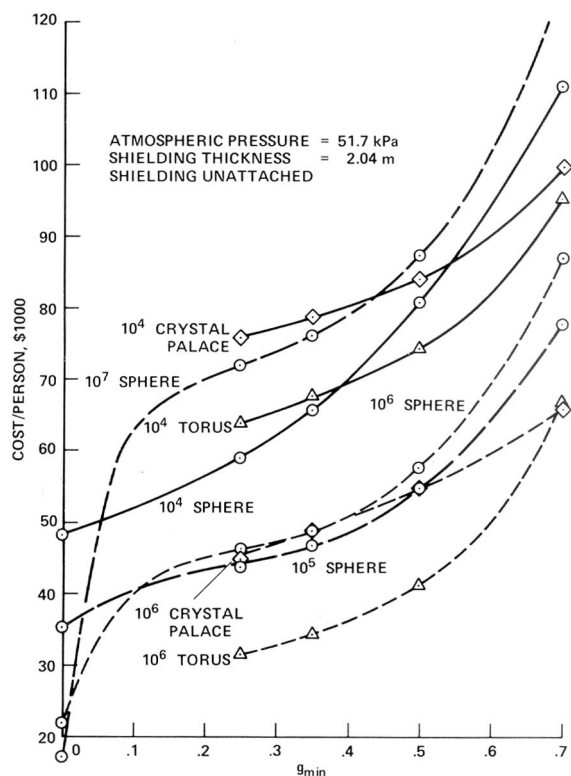
Figure 28 — *Habitat cost comparison as a function of minimum g level.*

Figure 29 shows atmospheric cost sensitivity assuming that either nitrogen (N_2) or helium (He) diluents are imported from Earth. The cost of an O_2/He atmosphere is significantly lower than an equivalent O_2/N_2 atmosphere since, at equal pressure, nitrogen is 7 times more dense, and

is therefore equivalently more expensive to transport. All the curves in figure 29 are for habitats with total volume equal to habitable volume. Spheres and cylinders usually have total volumes greater than the habitable volume as shown in the right-hand column of table 4. For example, a
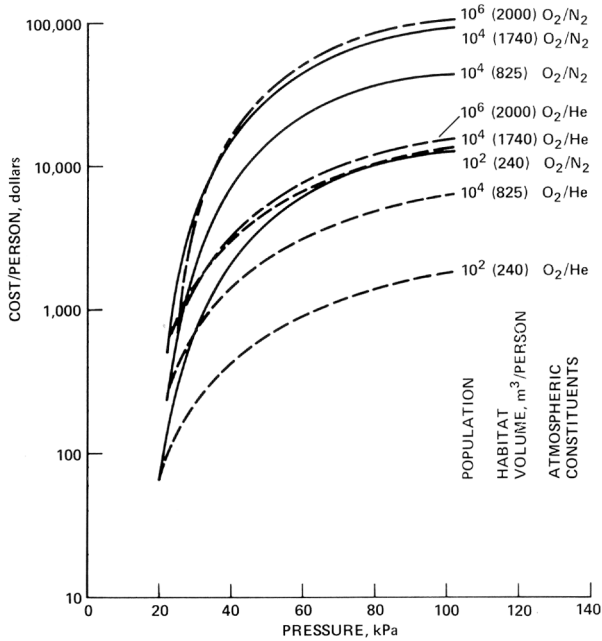
Figure 29 — *Habitat atmosphere cost sensitivity to composition and pressure.*

large spherical habitat (10^6 population), with a 51.7-kPa atmosphere of O_2/N_2 and minimum pseudogravity one-half Earth-normal, will have a volume 1.5 times greater than shown, or a cost revision from \$36,600 (shown in fig.29) to \$56,300/person.

The primary conclusion reached from this cost comparison is that if a significant percentage (>20 percent) of a settlement atmosphere is imported from Earth, then the cost of these diluents may be a major contributor to total habitat cost.

Habitat Illumination Cost Comparison

The interior of a space habitat can be illuminated by either artificial lights powered by photovoltaic cells, or by natural sunlight admitted through windows. This study evaluated the costs of these alternative lighting methods for one representative habitat configuration. Since the natural illumination choice is probably reasonable only for larger habitats, the 10,000-person spherical habitat was selected for this evaluation. This sensitivity analysis was performed only

TABLE 6 — HABITAT ILLUMINATION COMPARISON

System and component data		Area illuminated		
		Living	Agricultural	Total
Artificial light				
Requirement, kW/person		0.56/0.93	5.69/11.21	6.25/12.14
Photo-voltaic array	Area, m²	27,800	284,000	312,400
	Mass, kg	44,900	459,000	503,900
	Cost, \$M	0.41	4.21	4.62
Distri-bution	Mass, kg	281,700	3,397,000	3,678,700
	Cost, \$M	2.58	31.15	33.73
Total cost, \$M		3.0	35.4	38.4
Natural sunlight				
Requirement, kW/person		1.86	5.69	7.55
Glass window	Area, m²	610	1860	2470
	Mass, kg	84,000	257,000	341,000
	Cost, \$M	1.19	3.63	4.82
Mirrors and other equipment	Area, m²	54,200	165,300	219,500
	Mass, kg	10,800	33,100	43,900
	Cost, \$M	0.08	0.23	0.31
Addi-tional shield	Area, m²	610	1860	2470
	Mass, kg	3,220,000	9,850,000	13,070,000
	Cost, \$M	0.68	2.07	2.75
Total cost, \$M		1.95	5.93	7.88

for photovoltaic versus natural illumination, independent of habitat configuration and population variations. Further work should consider possible configuration and population effects.

Artificial lighting — Recent solar photovoltaic array estimates use a specific power generation factor of 138 W/kg (ref. 22). To account for power transmission, conditioning, and control equipment, an efficiency of 90 percent was assumed for an effective array output of 124 W/kg. Photovoltaic array cost was based on space-manufactured components of 30 percent silicon and glass and 70 percent aluminum and other metals. The cost for light bulbs and fixtures was estimated using a specific weight of 0.03 kg/W of rated fixture output. Space-manufactured components were selected over Earth imports owing to the estimated acquisition cost ratio of 1/6. Table 6 displays the weights and costs for the various illumination system components. These calculations were based on the power requirements obtained from table 2. Weighted values were used for array sizing and maximum values for distribution fixtures. The use of maximum power requirements for fixtures reflects the difficulty in moving them as lighting needs vary. As indicated, the cost of illuminating the agricultural area is an order of magnitude higher than that for the living area. Of particular interest is the overwhelming influence of distribution costs, which account for 88 percent of the total artificial lighting cost. If Earth-imported fixtures had been assumed, the distribution cost would have exceeded $200 M, instead of the $33.73 M used.

Natural illumination — The corresponding analysis for determining weight and cost of illuminating with natural sunlight is more difficult because of the many implementation options available. To reduce weight and the possibility of meteorite damage, it is desirable to minimize the window area. This can be done by concentrating the sunlight before it enters the habitat, but the concentration is limited by the 800 K softening temperature of window glass. It was assumed that the maximum window temperature should be less than 600 K (337° C). To maintain this temperature, the absorptivity of the glass must be balanced by its conductivity. The energy admitted to the habitat is also a function of window absorptivity; specifically (refs. 23, 24):

$$HA\alpha = KA (t2 - t1) / d \quad \text{and} \quad Q = HA(1 - a)$$

where

H flux of concentrated sunlight, cal/sec-cm²
A window area, cm²
α absorptivity of glass
K thermal conductivity of glass,
        0.0025 cal-cm⁴/cm-sec-° C
t_2 window temperature, 337° C
t_1 temperature of surrounding structures, 21° C
d window thickness, cm
Q required power in habitat, cal/sec-person
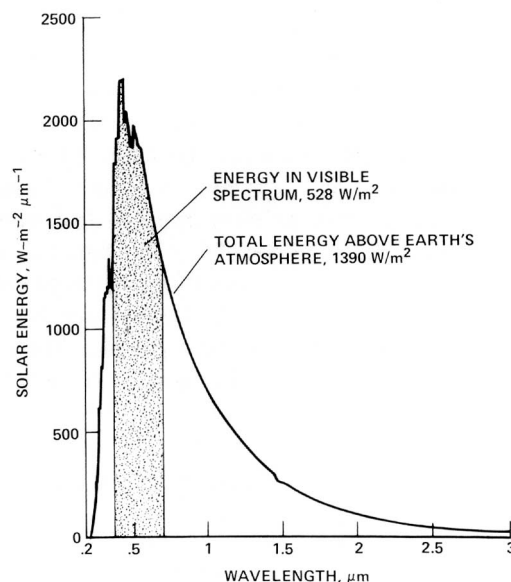
Figure 30 — *Solar energy spectrum.*

Only sunlight in the visible waveband is useful for habitat illumination. This constitutes 38 percent of the total solar radiation (fig. 30). Admitting energy outside this band into the habitat results in many penalties, including the requirement for larger windows and increased internal thermal control capacity. It is therefore desirable to use concentration mirrors that selectively reflect sunlight in the visible spectrum into the habitat for illumination. The degree of allowable concentration is influenced by glass thermal limits and absorptivity, which are functions of glass thickness. The thickness of the window is determined by structural requirements. Based on terrestrial manufacturing experience, the practical window weight limit is about 1 ton. A weight of 0.5 ton per window was selected or volume = Ad = 0.2 m³, where the glass density is 2450 kg/m³. This equation is solved simultaneously with the structural equation for a pressure-loaded square plate with simply supported edges:

$$\sigma_{max} = pA/(3.48d^2)$$

where

σ_{max} working stress (16.5 MPa for tempered window sheet)
p pressure, 51.7 kPa
A window area, cm²
d window thickness, cm

The solution resulted in a window 5.65 cm thick with an area of 3.5 m². The transmissibility of 5.65-cm-thick glass is 0.84 in the visible wavelengths (ref. 25). Since the sum of reflectivity, absorptivity, and transmissibility must equal 1, an absorptivity of 0.16 may be conservatively assumed.

The total energy transmitted through the windows by selective mirrors is therefore 36.5 kW/m². This is equivalent to a solar visible energy concentration factor of 70. Window areas, weights, and costs are delineated in table 6. Illumination requirements were again obtained from table 2 with the following assumptions. Since distribution in living

areas may be cumbersome, twice the maximum energy/person allocation was used. Agricultural areas are relatively open and a simple swiveling mirror can control light, so the weighted power requirement was used.

The mirror estimates shown in table 6 were derived assuming 90 percent efficiency, a total concentration plus distribution factor of 80, and aluminum mirrors and support structure weighing $0.20 \, kg/m^2$.

There are several ways to provide radiation protection for habitat windows: one alternative employs very thick glass windows that supply all the shielding necessary; this is undesirable, however, since the thickness must be 1.02 or 1.92 m to meet the 5.0 or 0.5 rem/yr dose rate requirements, respectively. This increases the total absorptivity, and these windows weigh and cost more than 20 times those that are only 5.65 cm thick. Another approach is to use shielding constructed from lunar slag in a chevron configuration to protect thin windows. Comparable thicknesses are still needed but material costs are 67 times lower and manufacturing requirements are greatly simplified. Chevron construction requires about twice the amount of normal shielding, but as shown in table 6, the cost remains below that for thin-glass windows.

The results of the preceding discussion and a comparison of total costs in table 6 lead to several conclusions:

1. If natural illumination is used, it should be concentrated with selective mirrors before it is transmitted into the habitat.
2. Thick glass windows that supply radiation protection are expensive and impractical.

3. Natural illumination should be used for agricultural areas since its cost is 1/6 that of artificial lighting.
4. Natural illumination should also be considered for living/working areas unless distribution becomes awkward or expensive.

CONCLUSIONS

The introduction to this paper posed three questions to be addressed and, it is hoped, answered by these habitat structural/cost sensitivity analyses. Sufficient habitat options have been evaluated to obtain a quantitative answer to the initial question: How much do "Earth-normal" physiological conditions cost when applied to a space habitat structural design? Obviously, many "less than Earth-normal" design options are possible, but a representative example should be illustrative.

The data in table 7 compare 10^6 population habitats having identical habitable volumes (2000 m^3/person), internal furnishings (53,000 kg/person), and radiation protection (0.5 rem/yr). The variables noted in the table are limited to habitat configuration, atmospheric pressure, atmospheric composition, and the range of pseudogravity in the habitable volume.

The total costs obtained offer some interesting comparisons between conservative and reduced cost designs, as well as for alternative configurations. As shown, when only habitat structure, shielding, and atmosphere are compared, the conservative to reduced cost design ratio is 7.5, 4.8, and 3.5 for spherical, toroidal, and crystal palace habitats, respectively. The answer to the first question is that design

TABLE 7 — EXAMPLE HABITAT COST COMPARISON

Environmental parameter		Earth normal conservative designs			Representative reduced-cost habitat designs		
		Sphere	Torus	Crystal palace	Sphere	Torus	Crystal palace
Atmospheric pressure, kPa		101.3			51.7		
Atmospheric composition		O_2/N_2			O_2/He		
Minimum g level		0.7			0.35		
Habitat structure	Mass, kT	15,300	9,300	9,200	5,500	3,200	5,200
	Cost, $B	107.6	65.3	65.1	38.6	22.7	36.3
Separate radiation shielding	Mass, kT	80,200	100,700	81,600	45,500	55,200	58,700
	Cost, $B	16.8	21.1	17.1	10.0	11.6	12.3
Atmosphere volume ratio		2.78	1.00	1.00	1.25	1.00	1.00
	Cost, $B	293.0	105.5	105.5	7.2	5.8	5.8
Total cost, $B		417.4	191.9	187.7	55.8	40.1	54.4

Notes: 10^6 population; V_H = 2,000 m^3/person; IM = 53,000 kg/person; t_{rad} = 2.04 m (dosage limit of 0.5 rem/yr); atmosphere volume ratio = total volume/habitable volume.

costs associated with Earth-normal conservatism are at least significant and may, in fact, be excessive. Also, table 7 cost data shows that the cost dispersion for conservative designs varies by more than a factor of 2.2 due to configuration differences, but the dispersion for reduced cost designs varies by only 1.4. This reduction in configuration sensitivity demonstrated by the lower cost habitat designs is due primarily to the reduced effect of their atmospheric costs.

The second question asks which "less than Earth-normal" physiological conditions offer the greatest habitat cost savings. Minimum g-level constraints and atmospheric pressure have strongly synergistic effects on structural shell design requirements and costs. The selected habitable g range significantly affects the overall structural shell geometry as demonstrated in table 4, while pressure affects the structural shell thickness. When evaluated independently, these influences are of the same magnitude. The structural mass difference for a 10^6 population spherical habitat is 4.7 X 10^6 tons for a g_{min} range from 0.7 to 0.25. This difference is due to geometry effects; it is not caused by a change in rotation rate, which varies only between 0.9 and 1.0 rpm. Similarly, the mass difference over the 76 kPa atmospheric pressure range is 8.1 X 10^6 tons and 3.7 X 10^6 tons for g_{min} values of 0.7 and 0.25, respectively. Similar results are obtained for toroidal and crystal palace habitat geometries. Shielding mass and its resultant cost at a fixed population and radiation requirement are influenced solely by habitat geometry, which is a function of minimum g-level. The relative importance of structural shell and radiation shielding costs is also a function of habitat population. Below 10^5 inhabitants, shielding costs are higher, but above 10^6 inhabitants, structural shell costs are dominant.

The quantity of atmosphere diluent imported from Earth has the largest potential influence on habitat cost.

The mass which must be imported depends on excess habitat volume, total atmospheric pressure, and the inert gas selected. These factors combined produce a cost factor of 40 for the spherical habitat example given in table 7.

Illumination alternatives also exhibit substantial habitat cost effects. The use of unselected/unconcentrated natural solar lighting results in window plus extra shielding costs similar in magnitude to those for the basic habitat structure. The costs for this technique are two orders of magnitude higher than for a selected/concentrated natural illumination system.

The third question, regarding identification of a recommended habitat configuration, has not been fully resolved by the limited analyses conducted during this investigation. Each habitat shape offers benefits for certain applications, and configuration selection may well depend on design considerations outside the scope of this study. These considerations include implementation of life-support functions, power supply, waste heat dissipation, shielding alignment, docking functions, and illumination for each of the habitat configurations.

Although an overall best habitat configuration has not been recommended, some interesting configuration comparisons can be made:

1. Torus — Offers the lowest habitat basic structural cost (pressure shell and detached radiation shielding) for almost all combinations of population and g_{min}. It is also volumetrically efficient and contains only as much atmosphere as required. Unfortunately, several parts of the torus structure were not included in this analysis: spokes, hub, shielding alignment, and additional stiffening needed in compressively loaded cylindrical sections. Also the distribution of illumination in a torus appears cumbersome. These factors will combine to increase the basic torus structural cost so that its cost per person approaches that for spherical habitats.

2. Crystal Palace — Has attributes and disadvantages similar to the torus. Its basic structural cost always exceeds that for the torus and is less than that for spheres when g_{min} exceeds 0.5. It is atmospherically efficient but has illumination distribution difficulties and requires unestimated spoke and hub structures. The crystal palace cylindrical radiation shielding, which contributes to its high basic structural cost, also offers several potential advantages. Its flat ends provide structure for spin axis alignment, and also radiation protection for the unpressurized volume within the crystal palace's inner structural wall. If additional facilities for space manufacturing were placed within this volume, they would be provided free radiation protection.

3. Sphere — Has a basic structural cost which exceeds that of the torus and crystal palace over most of the population and g_{min} ranges. It also exhibits an inefficient volume ratio, which results in high atmosphere costs. Its advantages include straightforward illumination distribution and no need for separate hub or shielding alignment structure. The sphere's excess pressurized and shielded volume could become advantageous by locating space manufacturing facilities in this region.

One important discovery about habitat configurations was made during this work: based on habitat basic structural cost, the cost per person has a minimum for habitats in the 10^5 to 10^6 population range. Even more interesting is the fact that this minimum is independent of habitat configuration; spheres, toroids, and crystal palaces all had minimum costs in this population range. This minimum is obviously dependent on the ground rules and scope of this investigation, but an equivalent minimum should also exist for revised ground rules and for more extensive habitat subsystem considerations.

RECOMMENDATIONS

Physiological research should be concentrated in those areas where less than Earth-normal conditions offer the greatest savings in habitat cost. Based on the work conducted during these sensitivity analyses, recommended research falls into

two categories: (1) that necessary to validate our assumptions and (2) that highlighted by our results. Our assumptions included allowable habitat rotation rates for pseudogravity, and the use of a broad range of habitable g levels. Since higher angular velocities and broad habitable g ranges result in smaller, less massive, and lower cost habitats, it is very important that we fully understand the long-term physiological effects of these conditions. Specifically, the following research is needed:

- Rotation rates: The angular velocities used for this study were based on work performed in a 1 g (Earth surface) environment. Initial human adaptation, long-duration habitability effects, and transition effects between rotating and nonrotating enclosures must be obtained in a reduced g environment.
- g-level variations: As inhabitants move radially within a settlement with a broad habitable-g band (0.25 - 1 g), they will be subjected to continuous or stepped g-level variations. This effect, with special emphasis on human adaptation and transition, must be investigated.
- Low-g tolerance: More knowledge is required on long-duration physiological effects of low- and zero-g habitation. Experimental data are limited to those obtained during the 84-day Skylab mission.

The results of our sensitivity analyses indicate that the combined influence of atmospheric pressure and composition have potentially the most significant effect on habitat cost. Therefore the following research is recommended:

- Low atmospheric pressure: Perform extended duration and adaptability testing for O_2/N_2 mixtures at less than sea-level pressure. Evaluate speech transmission effects in addition to respiratory effects.
- Low-density diluent: Conduct tests similar to those above for O_2/He atmospheres at less than sea-level pressure.

As repeatedly pointed out in the preceding text, this habitat sensitivity investigation was limited to the basic habitat structure (pressure shell and radiation shielding) plus some considerations of atmospheric composition and habitat illumination. It is recommended that additional habitat sensitivity studies be performed to expand this work. The following sensitivity investigations should be accomplished to gain a better understanding of certain habitat design conditions and subsystem options on overall habitat mass and cost.

- Influence of secondary structures, such as spokes, hub, shielding alignment, and additional stiffening in compressively loaded sections, on overall habitat structural mass and cost comparisons.
- A detailed look at habitat illumination sensitivity for various configurations. Illumination implementation appears to be fairly important and should be treated in much greater depth than was possible in this paper.
- The effect of fixed personnel area requirements on habit structural weight and cost. (The work described in this paper assumed a fixed volumetric requirement.)
- Habitat heat rejection sensitivity as a function of habitat

shape and radiation shielding design.
- Evaluation of life support function integration in various habitat configurations. These functions include air circulation and conditioning, power, water and sewer services.

REFERENCES

1. Billingham, J.: Physiological Parameters in Space Settlement Design. Third Princeton/AIAA Conference on Space Manufacturing Facilities, Princeton, N.J., Paper 77-549, May 9-12, 1977.
2. Marton, T.; Rudek, F. P.; and Miller, R. A.: Handbook of Human Engineering Design Data for Reduced Gravity Conditions. NASA CR-1726, Oct. 1971.
3. Johnson, Richard D.; and Holbrow, Charles, eds.: Space Settlements, a Design Study. NASA SP-413, 1977.
4. O'Neill, G.: The Low (Profile) Road to Space Manufacturing. Astronautics and Aeronautics, AIAA, May 1978, pp. 24-32.
5. Vajk, J. Peter; Engel, Joseph H.; and Shettler, John: Habitat and Logistic Support Requirements for the Initiation of a Space Manufacturing Enterprise. Space Resources and Space Settlements, NASA SP-428, 1979, pp. 57-74.
6. Haffner, James W.: Radiation and Shielding in Space. Academic Press, New York, 1967.
7. Bevan, John S.: Radiation and Radiation Protection. Space Research and Technology, vol. 1: The Space Environment, American Elsevier Publ. Co., Inc., New York, 1969, pp. 94-142.
8. Curtis, S. B.; and Wilkinson, M. C.: Study of Radiation Hazards to Man on Extended Missions. NASA CR-1037, May 1968.
9. Kline, R. L.: Space Station Habitability Issues. AIAA/MSFC Symposium on Space Industrialization, May 1976, pp. 38-53.
10. French, Francis W.: Solar Flare Radiation Protection Requirements for Passive and Active Shields. Journal of Spacecraft and Rockets, vol. 7, no. 7, 1970, pp. 794-800.
11. Cooper, Henry S. F.: A House in Space. Holt, Rinehart, and Winston, New York, 1976.
12. Parker, J. F., Jr.; and West, V. R., eds.: In Bioastronautics Data Book, 2nd ed., NASA SP-3006, 1973.
13. Physiology in the Space Environment, vol. II, Respiration. National Academy of Sciences, National Research Council, Washington, D.C., 1967.
14. Coe, C. S.; Rousseau, J.; and Shaffer, A.: Analytical Methods for Space Vehicle Atmospheric Control Processes. Tech. Rept. ASD-TR-61-162, pt. II, 1962.
15. Woods, F. J.; and Johnson, J. E.: Flammability in Unusual Atmospheres, Part 2 — Selected Materials in Oxygen-Nitrogen and Oxygen-Helium Mixtures at Pressures Up to 315 psia. Naval Research Lab., Washington, D.C., 1967.
16. Galasyn, Valentine D.: A Survey of Fire Prevention Problems in Closed Oxygen-Containing Environments. U.S. Naval Submarine Medical Center Rept.

SMRL-526, May 1968.

17. Parker, John A.; Kourtides, Demetrius A.; Fish, Richard H.; and Gilwee, William J., Jr.: Fire Dynamics of Modern Aircraft from a Materials Point of View. Journal of Fire and Flammability, vol. 6, Oct. 1975, pp. 534-553.

18. IES Lighting Handbook, Illuminating Engineering Soc., New York, 1952. John E. Kaufman, ed., 5th ed., in 1972.

19. Petrov, Yu A.: Habitability of Spacecraft. In Foundations of Space Biology and Medicine, vol. 3, NASA SP-374, 1975, pp. 157-192.

20. O'Neill, G. K.: Maximum-Strength Minimum-Mass Structures, in Space-Based Manufacturing from Nonterrestrial Materials. Progress in Astronautics and Aeronautics, vol. 57, AIAA, New York, 1977, pp. 161-171; also NASA TM X-73,265, Aug. 1977.

21. O'Leary, B.: Mass Driver Retrieval of Earth-Approaching Asteroids. Third Princeton/AIAA Conference on Space Manufacturing Facilities, 1977.

22. Anon.: Final Review of Conceptual Design Study of 200 W/kg Solar Array for Space Applications. General Electric, JPL Contract 954393, Valley Forge, PA, 1977.

23. Miller, Franklin, Jr.: College Physics. 3rd ed. Harcourt, Brace, and Jovanovich, Inc., New York, 1972.

24. Holman, Jack P.: Heat Transfer. McGraw-Hill Book Co., New York, 1963, pp. 174-180.

25. Handbook of Chemistry and Physics, 49th ed. The Chemical Rubber Co., Cleveland, 1968.

II-2
Habitat and Logistic Support Requirements for the Initiation of a Space Manufacturing Enterprise

J. PETER VAJK, JOSEPH H. ENGEL, and JOHN A. SHETTLER

A detailed scenario for the initiation of a space manufacturing enterprise using lunar materials to construct solar power satellites (SPS) has been developed, with particular attention to habitat design and logistic support requirements. If SPS's can be constructed exclusively from lunar materials, the entire enterprise can be initiated in a 7 year period of launch activity (beginning as early as 1985) using the Space Shuttle and a low-cost, Shuttle-derived heavy lift vehicle. If additional chemical feedstocks must be imported from Earth in significant quantities, it may be necessary to bring the next-generation launch vehicle (single-stage-to-orbit) into operation by 1991. The scenario presented features use of the mass-driver reaction engine (MDRE) for orbit-to-orbit transfer of cargos and makes extensive use of the expendable Shuttle external propellant tanks.

INTRODUCTION

During the last 3 years, a number of studies have shown the technical feasibility of manufacturing solar power satellites (SPS) at a space manufacturing facility (SMF) using lunar materials during the next two decades (refs. 1-5). These and related studies have provided conceptual designs and analyses for large-scale habitats in the Earth-Moon system, for chemical and metallurgical extraction and processing from lunar materials, and for a mass driver, an electromagnetic catapult to be installed on the lunar surface to launch raw materials into space at rates up to 600,000 metric tons per year (refs. 6-10). In addition, a bench-top prototype mass driver has been designed, built, tested, and publicly demonstrated (ref. 11).

Here we report on a study of the logistical feasibility of starting such a space manufacturing enterprise within the constraints of the Space Shuttle and of a simple Shuttle-derived heavy lift vehicle (SD/HLV) of higher payload capacity during the period 1985 through 1991. In addition, we have investigated the logistic support required to sustain such an enterprise in a steady state thereafter. This scenario and the dates given above are purely hypothetical, serving principally to indicate that such an enterprise need not be relegated to a distant future and to provide a detailed baseline for trade-off studies.

A key element in the system is the use of a mass-driver reaction engine (MDRE) as an upper stage for the Space Shuttle to carry large payloads from low Earth orbit (LEO) to high Earth orbits or to low lunar orbit (LLO) (ref. 12). Since the MDRE can accept any solid or liquid substance as

a propellant, it can be optimized to use powder fabricated from the expendable external liquid propellant tank of the Space Shuttle. Thus optimized, an MDRE can deliver to lunar orbit the payloads from nearly 30 Shuttle launches in a round trip of 6 months duration. The mature Shuttle system is expected to provide 30 launches every 6 months, beginning about 1985. Each MDRE payload to lunar orbit can thus total 850 metric tons, expending 1050 tons of reaction mass fabricated from 30 external tanks.

The entire space manufacturing system thus consists of (1) a lunar mining and launching base to deliver raw materials into space; (2) a catcher in space to collect the materials launched from the lunar surface; (3) a space manufacturing facility that extracts useful materials from the lunar ores and fabricates solar power satellites and other objects required to support and expand the system; (4) a staging base in LEO that provides an interface between the Earth-launch vehicles and the interorbital vehicles; (5) habitats at each of these locations; and (6) logistic support for the entire operation.

Logistic support includes (1) Earth-launch vehicles (beginning with the Shuttle); (2) a fleet of MDRE's to transfer cargos between various space facilities; (3) chemically propelled orbital transfer vehicles (OTV) to transport people between space facilities; (4) chemically propelled lunar transfer vehicles (LTV) to soft-land cargos on the lunar surface and to transport people between lunar orbit, the lunar surface, and the catcher; and (5) passenger modules to carry large numbers of passengers in the Shuttle and on the OTV. In addition, the enterprise must have a large infrastructure on Earth to provide administration and control, recruitment and training of personnel, coordination of research and development activities, procurement of matériel and services, and marketing of solar power satellites and maintenance services for them.

A fairly detailed step-by-step consideration of how the entire operation can be initiated has been carried out for the first 8 years of launch activities. The result of this effort has been to show the logistical feasibility of initiating a space manufacturing enterprise within the constraints of the Space Shuttle, a Shuttle-derived heavy lift vehicle, and the MDRE during the period 1985 through 1990, with advanced launch vehicles brought into operational use by 1991; to detail personnel and hardware requirements during this initial period; to determine the habitat requirements for each space facility in the system; to highlight certain key problems for intensive research and development which would facilitate or improve the system; and to provide cost estimates for research and development, for matériel and services procurement, for crew selection, training, and employment, for administration and other overhead costs, and for transportation.

We are grateful for the assistance of Edward H. Bock, Fred Lambrou, Jr., and Michael Simon. Joe W. Streetman of General Dynamics/Convair Division provided extensive assistance in the analysis of chemically propelled vehicles and their missions.

SCENARIO DEVELOPMENT

The scenario for the initiation of a space manufacturing enterprise has been developed around three key milestones:

1. Establishment of the lunar base and operation of the lunar mass driver at a launch rate of 30,000 metric tons/yr.
2. Establishment of an initial space manufacturing facility with a processing capacity of 30,000 metric tons/yr.
3. Expansion of the entire system to a capacity of 600,000 metric tons/yr with a work force of 3000 at the SMF producing 2.4 solar power satellites per year, each with a capacity of 10 GW.

To minimize the total time and total costs incurred before investment return, the second milestone is phased to coincide with the first delivery of lunar materials at the SMF. Thereafter, the entire system is bootstrapped to higher levels by diverting some of the lunar materials delivered to the SMF into reaction mass for the MDRE fleet, permitting more rapid expansion of the system than would be possible if the only source of reaction mass were the Shuttle external tanks.

The scenario was developed by working backward from each of the major milestones described above. The total masses required to achieve the first two milestones are sufficiently large to justify establishment of an inhabited station at LEO where MDRE's can be assembled, payloads from Earth-launch vehicles can be reconfigured, and large space structures such as habitats can be built. The establishment of the LEO station is thus a "zeroth" milestone.

The basic working assumptions used to develop the scenario were as follows:

1. The entire enterprise is self-contained, that is, no assumption is made that an essential piece of hardware (such as the LEO station) will already be in place as a result of some other space program. Only the basic Space Shuttle system is given.
2. Once launch operations begin, the entire program is to be carried out as rapidly as possible within the constraints of available transportation systems.
3. Each Shuttle or SD/HLV brings its expendable external tank into orbit. To the maximum extent possible, these tanks are to be utilized for MDRE propellant or for pressure hulls.
4. Initial masses at each facility are to be kept as small as reasonably possible.
5. Research, design, development, and procurement are to be paced by deployment schedules, even if this results in higher technical risk due to high levels of concurrency.

To describe the scenario and its generation, the following sections will describe the initial operations at the Moon, at LEO, and at the SMF.

INITIAL LUNAR OPERATIONS

A site for the initial lunar base must naturally be selected before the first crew arrives at lunar orbit to begin soft-landing equipment and supplies. At the present time, the likely site for the initial base is in the vicinity of the lunar equator and long. 33.1° E. This location permits launch of lunar materials via a family of achromatic trajectories that arrive with minimum dispersion at a moving spot in space in the neighborhood of the second Lagrange libration point L2 some 63,000 km behind the Moon on the Earth-Moon axis (ref. 13). If precise site selection has not been accomplished by prior lunar orbiter missions, the first MDRE payload arriving at lunar orbit (nearly 1 year before arrival of the first lunar crew) can include one or more lunar orbiters totaling several tons. These could provide detailed spectrographic and topographic mapping of candidate sites and high-resolution maps (down to 1 m or less) of the final site.

The initial lunar crew, arriving at lunar orbit aboard a chemical OTV at the same time as the last MDRE payload of initial lunar base supplies and equipment arrives, begins a series of LTV flights down to the main lunar base shortly after sunrise at the main lunar base on 4 March 1987. (Dates for sunrise and sunset at the lunar base (lunar long. 33.1° E, lat. 0°) were computed from ref. 14.) During this period of a few days to a week, the crew continues to live in the OTV passenger module until the lunar base is habitable. The first payload to be landed on the Moon includes the photovoltaic arrays and energy storage systems needed to provide power for the lunar habitats throughout the lunar day and night. The entire energy system must be deployed rapidly to accumulate sufficient energy to support the crew through the first lunar night. At the present time, fused silica flywheels appear to offer the least massive energy

storage system, storing about 0.87 kWhr/kg of flywheel, but trade-off studies against alternatives should be performed. The next task at the main lunar base is to dig trenches for the habitats and to bury them under several meters of lunar soil to provide radiation shielding and thermal insulation. Meanwhile, a smaller contingent of the lunar crew soft-lands equipment and supplies at a second site about 150 km downrange where the velocities of the packages of lunar material launched by the mass driver will be fine-tuned in ballistic flight by electrostatic means (ref. 10). A smaller habitat is established there in the same manner.

During the next two lunar days, the crew surveys both sites, installs the mass driver and the electrostatic trajectory correction equipment, surveys an initial mining site near the mass driver, and tests the mass driver system. The mass driver would be preassembled at LEO into 30- or 40-m-long sections, thereby minimizing installation time. Initial mining activities consist of one small bulldozer and two small trucks working one 8-hr shift every 24 hr during the lunar day, providing 30,000 tons of sieved material per year for launch by the mass driver. The downrange crew returns to the main lunar base for the lunar night, using a fleet (for redundancy) of long-range surface vehicles.

Analogies with terrestrial excavation and construction projects suggest that this work schedule can be accomplished by an initial crew of 24. The mass budget for the habitats, energy systems, consumables (food; gases and water to make up for losses in recycling through leaks and by airlock inefficiencies), lunar surface vehicles, and mass driver system components is summarized in table 1. (Mass estimates for habitats, energy systems, etc., are discussed in a later section.)

Soft-landing this equipment on the lunar surface requires a substantial amount of chemical propellants in lunar orbit. No studies have been made to optimize the capacity of a lunar transfer vehicle (LTV); we have arbitrarily assumed a large cargo and personnel LTV as described in table 2. Eleven round trips are needed for the main base and two round trips for the downrange station; allowing three more trips between LLO and the surface for unforeseen contingencies, 896 tons of prcpellant are needed to start lunar surface operations.

The packages of lunar materials launched by the mass driver must be collected in space with high efficiency. As described earlier, the dispersion of packages arriving at the catcher can be minimized by selecting a suitable launch site and catcher orbit. The catcher orbit thus selected is approximately a circle of radius 10,000 km around L2 in a plane normal to the Earth-Moon axis. To track this orbit while compensating for the momentum imparted to the catcher by arriving packages, a small fraction of the captured lunar materials can be used as reaction mass. Either a mass driver or a rotary pellet launcher could be used for this purpose (see ref. 2, pp. 80, 129-132), but engineering trade-offs remain to be done. The catcher would thus be designed to operate automatically under normal conditions, with remote monitoring and capabilities for remote override and control.

TABLE I — MASS BUDGET FOR INITIAL LUNAR SURFACE OPERATIONS

Component	Mass budget, metric tons
Main lunar base (24 persons)	
Habitat (two LHZ tanks, furnished)	72
Energy system (photovoltaic arrays, flywheels)	128
Surface vehicles and tools	25
Spare parts	2
Consumables (3 kg/day/person)	25
Mass driver and power supply (ref. 12	625
Total	880
Downrange station (12 persons, part-time occupancy)	
Habitat (one LHz tank, furnished)	40
Energy system	45
Surface vehicles and tools	12
Spare parts	2
Consumables (lunar day only)	7
Mass driver trajectory correction system (ref. 12)	50
Total	156
Crew and personal baggage (300 kg/person)	7.2

Nonetheless, maintenance of the catcher and transfer of accumulated lunar materials to a MDRE for transport to the SMF requires human operations on the catcher for a few days at a time. The catcher thus includes a habitat that can accommodate small crews (up to about 12). Crews for this work travel to the catcher from the lunar surface once a lunar day (13 lunar days per year) for routine maintenance when mass-driver operations cease for the lunar night at the main lunar base. A small LTV can be used for this purpose, with characteristics as shown in table 2. The LTV refuels in lunar orbit both on ascent and on descent. Allowing two additional contingency flights per year, the propellants required for this purpose amount to 186 tons/yr, supplied from LEO initially.

One additional system requires chemical propellants in lunar orbit, namely, the OTV for personnel transport between LEO and LLO. Given the advantages of using the MDRE for cargo transportation beyond LEO, the OTV can minimize its propellant requirements by refueling in lunar orbit for the return trip to LEO. One such flight must be provided at the end of a 1-year tour of duty in space for the lunar crew to return to Earth. For emergencies and unforeseen contingencies, we have allowed two additional flights per year. The OTV specifications assumed are given in table 2. For simplicity, we have assumed a single-stage vehicle; no trade-off has been done against a two-stage vehicle with refueling at LEO and at LLO. Total propellants at lunar orbit amount to 165 tons for the first year.

The catcher is delivered to lunar orbit along with equipment and supplies for the lunar surface aboard the MDRE. After delivery of the final payload to lunar orbit, the MDRE carries the catcher out to the vicinity of L2 and waits there with the catcher. Initial launch begins at sunrise of the fourth lunar day (1 June 1987) at a rate of 30,000 tons/yr. At sunset on the eighth lunar day (11 October 1987), the MDRE departs for the SMF site with a cargo of 11,700 tons of lunar materials. The MDRE also carries along one empty propellant storage depot whose contents have been expended in soft-landing the lunar base equipment and supplies. This depot will be refilled at LEO.

Since the chemical propellants must be stored in space for periods of many months, suitable long-term cryogenic depots must be provided. A Shuttle external tank set has a capacity of 703 tons of liquid oxygen and liquid hydrogen propellants. By adding multilayered insulation, reliquefication systems to convert hydrogen and oxygen vapors back into liquid form, and equipment inside the tanks to permit extraction of the propellants from these tanks in zero-gravity conditions, these tank sets can be converted into long-term storage depots. The extra insulation and equipment totals about 4.15 tons for each such depot.

The total mass to be delivered to lunar orbit to initiate lunar operations (as just described) is 2700 tons (table 3). This includes 125 tons of Shuttle external tankage, so that only 2575 tons must be delivered to LEO in the Shuttle cargo bay. Since the MDRE can obtain the reaction mass for the return leg of its last trip from lunar materials at the catcher,

TABLE 2 — SPECIFICATIONS FOR CHEMICALLY PROPELLED SPACE VEHICLES

Large lunar transfer vehicle	
Stage mass	7 tons[a]
Propellant mass (LLO to surface and return)	56 tons
Stage mass fraction	0.89
Payload down to lunar surface	81 tons
Cabin (pressurizable for crew of two)	5 tons
Flight time (LLO to surface or return)	0.93 hr

N.B. In normal operations, the cabin would not be pressurized. All crew members and passengers would wear EVA suits. Passengers in excess of the cabin capability would ride on top of the LTV in lightweight seats enclosed by a lightweight transparent canopy to protect the EVA suits from lunar debris thrown up by the rocket exhaust.

Small lunar transfer vehicle	
Stage mass	2 tons
Propellant mass (LLO to catcher and return)	3.5 tons
Propellant mass (LLO to surface and return)	8.9 tons
Cabin (same as for large LTV)	5 tons
Flight time (LLO to catcher or return)	40.1 hr

N.B. The flight controls of both the large and small LTV should be designed to "feel" the same, permitting concurrent proficiency in both.

Orbital transfer vehicle	
Stage mass	6.5 tons
Propellant mass (LEO to LLO or return)	55 tons
Stage mass fraction	0.89
Propellant mass (LEO to SMF or return)	49 tons
Passenger module (up to 30 passengers for 10 days)	23.4 tons
Flight time (LEO to LLO or return)	122.4 hr
Flight time (LEO to SMF or return)	9.8 hr

N.B. Propellant requirements have been computed on the basis of liquid oxygen and liquid hydrogen at a mixture ratio of 6:1. Specific impulse of 462 sec was assumed for major burns, 400 for midcourse maneuvers, and 220 for attitude control. (These specific impulses are slightly conservative, allowing for some propellant losses by boiloff.). A common engine can be used for all of these vehicles, except that the engine throttling system required for the LTV's is not installed on the OTV engines.

a All in metric tons.

the propellant mass required for this leg can be used on the outbound leg for about 150 tons of additional cargo. The total mass of 2700 tons can thus be accommodated on three MDRE flights with payloads of 850, 850, and 1000 tons, respectively. Once the zeroth milestone has been reached, 88.8 Shuttle payloads of 29 tons each are required to assemble the initial lunar orbit payloads at LEO. The liquid hydrogen tanks from four Shuttle external tank sets are used to build habitats; two complete external tank sets are converted into propellant depots; and 85.7 external tank sets (including unused portions of those tank sets used for habitat construction) are ground up for MDRE reaction mass.

TABLE 3 — MASS BUDGET FOR
INITIAL LUNAR OPERATIONS

Component		Mass budget, metric tons
Mass in lunar orbit		
Main lunar base		880
Downrange station		156
Propellants		1247
Large LTV	896	
Small LTV	186	
OTV	165	
Propellant storage depots (2)		75.2
Shuttle external tank set	33.45	
Conversion materials	4.15	
Catcher ensemble		250
Habitat	45	
Energy system	20	
Consurnables	7	
Catcher	168	
Large lunar transfer vehicles (2)		24
Small lunar transfer vehicles (2)		14
General contingency		63.8
Total payloads for MDRE		2700
Shuttle external tanks		-125
Total payloads for Shuttle		2575
Mass at LEO		
Orbital transfer vehicles (2)		13
Propellants		165
Propellant depot conversion materials		4.15
Total payloads for Shuttle		182

The lunar crew must also be transported to lunar orbit to arrive simultaneously with the third MDRE flight, approximately 5 months after departure of the MDRE from LEO. During the intervening time, a chemical propellant depot must be prepared at LEO, chemical propellants electrolyzed and liquefied from water brought up aboard the Shuttle, and two chemical orbital transfer vehicles brought up from Earth. One OTV is sufficient to deliver the initial lunar crew of 24 from LEO to LLO aboard a passenger module that can fit inside the Shuttle cargo bay, but a second OTV is essential for rescue capability. Propellants required for the first year of OTV operations (matching those provided at lunar orbit) total 165 tons. The total mass required in LEO for crew delivery to the lunar base is also shown in table 3.

INITIAL LEO OPERATIONS

Before launch of supplies and equipment for the initial lunar operations can begin, facilities must be established in LEO to provide a staging base for assembly of lunar orbit payloads. During the year and a half of Shuttle launches required to transport the lunar supplies into orbit, the crew at the LEO station must refurbish four liquid hydrogen fuel tanks into habitats for the lunar surface bases and for the catcher; convert two complete external tank sets into

long-term propellant storage depots; grind 85.7 external tanks into powder for MDRE reaction mass; electrolyze nearly 1250 tons of water; liquefy the resulting hydrogen and oxygen; assemble the lunar mass driver and its enclosing tunnel into sections 30 or 40 m long; assemble the catcher ensemble; and bolt all of these payloads together into predetermined configurations designed for ease of transfer to the LTV, with due consideration for weight and balance limits both of the MDRE and the LTV. Assembly and checkout of the MDRE are also essential tasks for the LEO crew during this period.

Some of this work involves assembly of prefabricated components; most of it requires tending and maintaining automated or semiautomated equipment (such as the electrolysis and cryogenics units that produce chemical propellants). Refurbishing one liquid hydrogen tank for a habitat (as seen below in the discussion of habitat design) is comparable to assembling three prefabricated houses of 1800 ft^2 each, a task of a few weeks for a few skilled workers. Such considerations suggest that a crew of 24 is sufficient during the 18-month period required to assemble the initial lunar orbit payloads, with an average productivity requirement of 460 kg/day/worker.

As shown below, the work force at LEO must be expanded to about 48 sometime after departure of the third MDRE payload for lunar orbit. Four liquid hydrogen tanks can adequately house this size crew; 6 tanks would be ample, leaving room for further expansion to 84. We have adopted a six-tank configuration. Construction of the LEO station begins by refurbishing a single tank, working out of the Shuttle at first. Five workers can ride aboard the Shuttle as passengers on 6- to 8-day flights, with minimal decrease in cargo bay payload capacity. Using the LEO station's own solar panels to supplement the Shuttle power supply, the Shuttle would provide life support initially until habitability is established for at least one liquid hydrogen tank.

Interior fittings such as antislosh baffles must be stripped out of the tank, and air-conditioning ducts, prefabricated floor and wall panels, and other interior fittings must be moved inside. This can be done through a special hatch installed before launch or cut in the tank in LEO for later installation of an airlock. Additional holes must be cut for attachment of the environmental control/life-support system (EC/LSS) pods; these pods and the airlock welded to the hull; photovoltaic arrays and radiators mounted; and the entire hull pressurized. Installation of floors, walls, air-conditioning ducts, plumbing, electrical wiring, elevators, and furnishings can then proceed in a shirtsleeve environment, with structural attachments made to the interior ribs of the tank. Once minimum habitability for 5 has been reached, the 5 workers aboard the current Shuttle flight can remain in orbit, the remainder of the initial LEO crew of 24 joining them during the next four Shuttle flights. The hydrogen tank can then be separated at leisure from the rest of the external tank set which is ground up into MDRE reaction mass.

During the following weeks, refurbishing of the first tank is completed, and work can begin on the other five tanks for the LEO station, beginning, in these cases, by separating the hydrogen tank from the rest of the external tank set. The hydrogen tanks are connecfed by a tunnel, a docking hub, and cables, and rotated to provide 1 g in the hydrogen tanks themselves. Completion of this and subsequent habitats would be facilitated by use of a "space caisson," a collarlike structure that encircles a Shuttle external tank to provide a shirtsleeve environment for work outside the pressurized tank simultaneously with work in progress inside. The caisson has inflatable cuffs to form an airtight seal with the exterior of the tank and contains arc-welding equipment and assorted machines and construction tools for cutting holes through the tank wall to install view ports, air-locks, and other apertures.

Other equipment to be launched to the LEO facility includes the pelletizer for chewing up external tanks into MDRE propellant; the electrolysis and liquefication systems for making liquid oxygen and hydrogen for chemical propellants; consumables for the crew for the first year; and a set of trusses and booms to provide temporary tiedown storage for Shuttle cargo items and external tanks and to serve as a basic construction yoke. In addition, the first MDRE must be brought to LEO before accumulation of lunar cargos can begin in earnest.

Table 4 summarizes the estimated mass budget required in LEO to attain the zeroth milestone. The total mass of 464 tons can be accommodated in 16 full Shuttle payloads. Six liquid hydrogen tanks and one complete external tank set must be reserved for constructing the LEO station. The mass required to complete the interior refurbishing of tanks for expansion to 48 persons is also shown in table 4, requiring 4.8 additional Shuttle payloads, but no additional external tanks.

The schedule to attain the zeroth and first milestones is as follows:

1. First Shuttle launch for this enterprise occurs early in January 1985.
2. Shuttle launch No. 16 completes delivery of equipment and supplies for the LEO station and for the first MDRE late in March 1985.
3. Shuttle launch No. 106 completes delivery to LEO of supplies and equipment to be delivered to lunar orbit, with departure of the third MDRE flight to lunar orbit in October 1986. (One Shuttle flight in January 1986 has been used to resupply consumables for the LEO station.)
4. The third MDRE flight to lunar orbit arrives there early in March 1987, simultaneously with an OTV flight carrying the initial lunar crew.
5. The lunar base begins routine launch of materials into space at the rate of 30,000 metric tons/yr shortly after sunrise at the lunar base on 1 June 1987, completing the first milestone.

TABLE 4 — MASS BUDGET FOR LOW
EARTH ORBIT STATION

Component	Mass budget, metric tons
Initial station (24 persons)	
Habitat refurbishing	142
Energy system	16
Electrolysis and liquefication systems	25
Pelletizer	25
Space caisson	25
Cargo tiedown, construction yoke	10
Spare parts	5
Consumables (one year supply at 3 kg/person/day)	27
General contingency	15
Mass driver reaction engine (ref. 12)	174
Total payload for Shuttle	464
Expansion to 48 persons	
Habitat refurbishing	100
Energy system	11
Consumables (one year supply for 24)	27
Total payload for Shuttle	138

Departure of the third MDRE flight from the LEO station does not, of course, imply shutdown of LEO operations. Accumulation of supplies and equipment for expansion of the lunar base, for assembly of the initial SMF, and for expansion of the MDRE fleet begin in mid-November 1986, after nearly five Shuttle payloads have been used to expand the LEO station.

We suggested above that the MDRE would remain at the catcher for four lunar days after launch of lunar materials begins in June 1987 to permit accumulation of a reasonable cargo of lunar materials for delivery to the SMF. Departure to the SMF would then occur on 11 October 1987, with arrival at the SMF site (discussed below) in February 1988. The waiting period is arbitrary since no optimization studies have been made. A shorter waiting period would permit earlier SMF operation with a smaller supply of raw materials; a longer period would postpone initial SMF operation still further by prolonging the time enroute for the MDRE because of its increased payload. The present choice seems reasonable but nonetheless arbitrary.

If the SMF is to begin operation in February 1988, the last cargo of equipment and supplies for the initial SMF must depart LEO aboard an MDRE in October 1987. Thus everything necessary for the initial SMF must be delivered to LEO and assembled in about 11 months (mid-November 1986 to October 1987), with several Shuttle flights reserved for resupply of consumables for LEO, for delivery of the first lunar crew in an OTV passenger module, and for additional MDRE's. As shown below, some 1980 metric tons of payload must be delivered to LEO for the initial SMF alone, equivalent to more than 14 months of Shuttle launch operations. It is thus appropriate to upgrade the surface-to-LEO transportation system at this stage of operations.

A relatively inexpensive upgrading of the Shuttle system can be achieved with a 5-year development program. Some of the basic characteristics of such a Shuttle-derived heavy lift vehicle (SD/HLV) are shown in table 5, along with similar data for the Shuttle itself and for a more advanced reusable single-stage-to-orbit (SSTO) launch vehicle. Assuming development of the SD/HLV begins between 1980 and 1982 as part of the total R&D effort for the space manufacturing enterprise, it is reasonable to expect that a fleet of four SD/HLV's could be operational beginning in January 1987, with 80 launches/yr in parallel with 60 Shuttle flights per year. With this combination of launch vehicles, the mass delivered annually to LEO would increase from 1,740 to 10,780 tons. This sixfold increase would not, however,

TABLE 5 — EARTH-TO-ORBIT VEHICLES

Space Shuttle
  Configuration: airplanelike Shuttle orbiter contains main engines. Cabin can accommodate flight crew of two plus up to five mission and payload specialists. Cargo bay can accommodate cargos within a cylindrical volume about 5 m in diameter by nearly 20 m in length. Orbiter is launched vertically, attached to side of a large (expendable) external tank carrying liquid oxygen and liquid hydrogen for the Space Shuttle main engines. Two solid-propellant boosters (recoverable) are strapped alongside the external tank.
  Estimated price per launch: $20 million (1975 dollars)
  Payload: 29 metric tons
  Launch price per kilogram: $690

Shuttle-Derived Heavy Lift Vehicle (SD/HLV) (ref. 15)
  Configuration: Shuttle orbiter replaced by cargo enclosed in disposable aerodynamic shroud atop Space Shuttle main engines enclosed in reentry capsule for reuse. Same external liquid propellant tank as used in basic Shuttle. Four solid propellant boosters used instead of two.
  Development time: approximately 5 years, beginning from operational Shuttle.
  Development cost: $1.3 billion (1975 dollars)
  Estimated price per launch: $19.6 million (1975 dollars)
  Payload: 113 metric tons
  Launch price per kilogram: $173

Single-Stage-to-Orbit Vehicle (SSTO) (ref. 16)
  Configuration: delta-winged vehicle with dual-mode engines. Mixed cargo and passenger capability, with vertical launch/horizontal landing. Overall length in launch configuration: 90 m. Anterior payload shroud collapsible for reentry and landing, with overall length in touchdown configuration of 70 m. Completely reusable system.
  Development time: about 10 years, requiring some advanced technologies.
  Development cost: $7 billion (1975 dollars)
  Estimated price per launch: $3.6 million (1975 dollars)
  Payload: 227 metric tons
  Launch price per kilogram: $15.86

require a sixfold expansion of the LEO crew, for two reasons: first, some of the assembly work for the SMF can be postponed until the SMF crew arrives at the SMF site; second, the larger payload capacity of the SD/HLV will reduce the assembly work required per ton of payloads delivered to LEO. Should further study show that a crew of 48 is insufficient, the LEO station we have provided can accommodate a total of 84 workers, with some adjustments required in payload scheduling to bring up more furnishings and more consumables per year.

With this expansion in Earth launch capabilities, the number of expendable Shuttle external tanks also increases from 60 tanks/yr to 140 tanks, providing propellants for delivery of somewhat more than 2.4 times as much mass per year to high orbit for reasons that will emerge below. The MDRE fleet thus must be expanded in parallel with assembly of the initial SMF and with expansion of the lunar base. The first priority, however, is to provide the initial SMF.

DEPLOYMENT OF INITIAL SPACE MANUFACTURING FACILITY

Although the objective of the entire space manufacturing enterprise is to produce solar power satellites from nonterrestrial materials, as yet no one has developed a credible SPS design optimized for nonterrestrial materials. In this sense, the end product of the SMF is poorly defined so that the designs of the chemical processing plant and of the fabrication plant are subject to major uncertainties. As a point of departure for logistical planning purposes, we have adopted a conceptual design for the SMF factory developed during the 1976 NASA Ames/OAST Summer study on space manufacturing (refs. 7, 8).

In that design, it was assumed that the lunar materials arriving at the SMF would be completely unselected (except for choices between mare and highland soils). Present thinking suggests that it would be much more efficient to perform extensive beneficiation operations on the lunar surface before launch by the mass driver (ref. 17). The initial lunar operations would not include beneficiation; equipment for beneficiation would be added during expansion of the lunar base to full capacity (as discussed below).

Raw materials arriving at the SMF would thus consist of separate cargos of (1) unselected (but sieved) lunar materials for radiation shielding or for MDRE refueling, (2) plagioclase concentrates from lunar highland soils, and (3) ilmenite concentrates from mare soils (ref. 17). The chemical processing plant required to extract oxygen, silicon, glass, iron, aluminum, and titanium from these concentrates is far simpler than that described in references 7 and 8; nonetheless, for conservatism, we have used the mass estimates given there. For a processing plant with an annual capacity of 600,000 metric tons, the chemical processing plant totals 2770 tons; the energy system (photovoltaic arrays and radiators), 3852 tons; and the fabrication plant, 5000 to 6800 tons. The entire factory then totals 11,600 to 13,400 tons, exclusive of radiation shielding.

The first lunar materials delivered to the SMF are unselected soil. Approximately 10,000 tons of this material are needed for radiation shielding of the initial habitat, and an additional 4500 tons are required for reaction mass for the MDRE fleet to expand the lunar base and the SMF during the year following initial operation of the SMF. The initial factory includes equipment to extract oxygen from the unselected lunar soil by reduction with hydrogen, with water vapor collected in a cold trap. The hydrogen is recovered by electrolysis, and the oxygen can be used either for life support or liquefied for use in the OTV and the LTV. The factory also includes equipment to sinter the lunar soil into several shapes of large slabs for radiation shielding. Most of the factory mass is taken up by chemical processing equipment and fabrication machinery for the production of structural sheets, plates, and beams and of glass to permit rapid expansion of the SMF factory and habitat as soon as concentrated ores begin to arrive. (This equipment may possibly be used, at much lower efficiencies, to extract metals and glass from the unselected soil provided in the early deliveries.)

To bootstrap the entire enterprise from a minimum initial mass, as much as possible of the final factory and habitat masses should themselves be manufactured at the SMF. Portions of the pressure hulls, photovoltaic arrays, radiators, and massive foundry components could be fabricated readily with the same equipment used to build the SPS's. As a preliminary (and highly uncertain) working estimate, we have assumed that 9 percent of the mass of any finished products manufactured by the SMF must be imported from Earth in the form of complicated components or of raw materials to be used, for example, in alloying structural materials, doping semiconductors, or as special optical coatings (refs. 7, 8 estimate about 9 percent imports for the manufacture of SPS's). Initially, the factory will have only a limited capacity to contribute to its own expansion; as the factory approaches full size over a 3-year period, however, we assume it will approach a 91-percent contribution toward the mass required to complete the SMF factory and habitat. We thus estimate that an additional 4670 tons of factory components must be imported from Earth over the 3-year growth period, with 6900 tons provided by the factory itself from lunar materials. Similar considerations apply to habitat interior furnishings and airlocks. Shuttle external tanks (as shown below) continue to be available for use as pressure hulls until the end of 1990, but detailed trade-offs remain to be made to determine whether the optimum use of these tanks is as reaction mass for the MDRE fleet or as pressure hulls at the SMF.

The estimated masses for the initial SMF and for its expansion over the subsequent 3 years to reach full capacity (600,000 metric tons/hr) are shown in table 6. An initial crew of 150, including administrative, maintenance, galley, and medical personnel, should be sufficient, with productivity of 100-110 kg/hr/person required to process 30,000 tons/yr. A modular habitat design using 14 liquid hydrogen tanks from the Shuttle external tank sets was assumed, with maximum commonality of design with the habitats at LEO and at the catcher. (See the discussion of

TABLE 6 — MASS BUDGET FOR THE SPACE MANUFACTURING FACILITY

Component	Mass budget, metric tons
Initial SMF (30,000 tons/year)	
Habitat (14 LH$_2$ tanks, pressurized and furnished for crew of 150, expandable to 252)	583
Energy system for habitat	40
Structural cable to support radiation shielding	140
Consumables (1 year supply for 150)	165
Propellant depot	38
Propellants	294
Chemical processing plant (60,000 tons/year)	230
Fabrication plant (60,000 tons/year)	250
Energy system for factory	415
Spare parts	20
General contingency	90
Total MDRE payload	2225
Shuttle external tanks	-236.5
Shuttle or SD/HLV payload	1988.5
Expansion to full capacity (600,000 tons/year)	
Interior furnishings for 154 more LH$_2$ tanks (or equivalent)	1650
Environmental control/life support system (EC/LSS) units; airlock pumps and seals	1320
Chemical processing plant equipment	860
Fabrication plant equipment	3000
Miscellaneous components and special materials	810
Shuttle or SD/HLV payload	7640

habitat design below.) Such a configuration readily accommodates 150 persons initially. Completion of interior refurbishing work will allow expansion to 234 to 252 persons, depending on assumptions about the amount of community space required and about sharing of private quarters.

Based on a consideration of the energy and reaction mass needed to transport large masses of lunar soil from the catcher to the SMF and to subsequently transport solar power satellites from the SMF to geosynchronous orbit, a previous study identified the 2:1 resonance orbit as a highly desirable site for the SMF (ref. 13). Additional factors, however, must also be included in optimizing the SMF site, especially in the early stages of a space manufacturing enterprise. Since the MDRE is to be used to deliver cargos from LEO to the initial SMF site, its operating characteristics must be taken into account. A continuous, low-thrust propulsion system (such as the MDRE) is ill-suited for orbital transfers between a circular orbit such as the LEO station and a highly eccentric orbit such as the 2:1 resonance orbit. Both time enroute and total propellant mass for the MDRE will be less for a circular orbit SMF site. Optimization of the SMF site (both in the initial stages of the space manufacturing enterprise and in a late, mature stage) will also depend strongly on the ratio of mass that must be imported from Earth to the mass brought from the Moon to produce SPS's, and of these two masses to the mass of the

SPS which must be moved to geosynchronous orbit. These factors were not considered in the earlier optimization.

Geosynchronous orbit might seem a natural choice for an SMF; unfortunately, the outer portions of the Van Allen radiation belts are sufficiently intense at geosynchronous distance to create serious problems. Without performing the careful trade-off needed to optimize the system, we have somewhat arbitrarily selected a 2-day circular orbit at 10.6 Earth radii (67,500 km) for the initial SMF site. Should the 2:1 resonance orbit or some other highly eccentric orbit prove to be the optimum site for the SMF in a mature system, the entire SMF can be relocated at leisure, using MDRE "tugs," perhaps 5 or 10 years after initial operation of the SMF.

On its way to lunar orbit, the MDRE reaches 2-day circular orbit about 4 months after departure from LEO; on the return voyage, it passes through this orbit about 3 weeks before arrival at LEO. An identical MDRE could thus depart from LEO with increased payload and decreased reaction mass, completing a round trip to the SMF in a travel time about 5 weeks shorter than the 6 months required for the round trip to lunar orbit. The propellant requirements for a round trip to lunar orbit to deliver 850 tons amount to 30 external tanks expended more or less uniformly over the duration of the flight. If the total mass at departure from LEO is the same for both missions, the MDRE flight to the SMF site can deliver 1025 tons while expending less than 25 external tanks as reaction mass. Once the MDRE can refuel at SMF (less than 175 tons of lunar materials will suffice to return the unloaded MDRE to LEO), 1200 tons can be delivered to the SMF using fewer than 20 external tanks in the same round-trip time of slightly less than 5 months.

Refueling at the SMF can also increase the effective capacity of the MDRE in transporting cargos to lunar orbit, requiring fewer than 20 external tanks at LEO and 175 tons of lunar materials at the SMF of the outbound voyage to deliver 1200 tons at the expense of about 1 week more for the outbound flight. Propellants for the return trip from the catcher to the SMF would, again, be provided from the cargo of lunar materials.

For MDRE flights arriving at the SMF site after February 1988, the above improved performance figures were used. In addition, we have estimated that an MDRE can deliver to LEO a cargo of lunar materials for a reaction mass equivalent to about 30 Shuttle external tanks (1050 tons) in 4 months, expending 850 tons enroute. This procedure is a somewhat inefficient way to supplement the supply of external tanks but is occasionally necessary to avoid excessive bottlenecks in orbital transfer. Detailed study is required to evaluate whether it would be more effective to reoptimize the MDRE for the SD/HLV's higher ratio of payload mass to external tank mass.

LUNAR BASE EXPANSION

The initial lunar base installation was limited in its productive capacity to 1/20 the capacity of the mass driver,

both by the limited power available for the mass driver and by the limited mining equipment. Expansion to full capacity (600,000 metric tons launched per year) has been examined in detail by Williams et al. (ref. 17), who estimate that a permanent crew of about 48 will be sufficient to mine, process, and launch lunar materials at full capacity. The initial habitat (two liquid hydrogen tanks from the Shuttle external tank sets) must be replicated. Besides the equipment required for the expanded mining and beneficiation operations, additional photovoltaic arrays must be provided to power the mass driver and the mining and beneficiation equipment. We have added two more items to the list: an oxygen extraction plant to replace oxygen lost from the habitats by leakage, and a small factory to spin fiberglass sacks for the lunar soil to be launched by the mass driver. The total mass requirements are summarized in table 7.

While most of the mining and beneficiation equipment is very specialized and has thus been assumed to be imported from Earth, more than half the total mass is photovoltaic arrays. As the entire space manufacturing enterprise expands, production of photovoltaic cells at the SMF will grow. We have assumed that about 1225 metric tons (of the 1805 tons total required) can be provided by the SMF, reducing the net payload to be transported to LEO by the Shuttle or the SD/HLV. Giving credit for the liquid hydrogen tanks used to construct the additional habitat facilities, we find that the total equipment to be launched to LEO amounts to 2271 tons. Chemical propellants and propellant storage depots were not included in this figure, but appear elsewhere.

We have not analyzed in detail the relative merits of using lunar oxygen in the lunar transfer vehicles (LTV's) versus continuing to provide all propellants for LTV operations at lunar orbit. Tanking up with hydrogen at the lunar orbit propellant depot and tanking up with oxygen at the lunar

TABLE 7 — MASS BUDGET FOR LUNAR BASE EXPANSION

Component	Mass budget, metric tons
Habitat (two LHz tanks, pressurized and furnished for crew of 24)	200
8 mining trucks	154
1 bucket-wheel extractor	460
5 ore beneficiation modules	385
2 conveyor belt systems	96
Maintenance sheds	100
Oxygen extraction plant	125
Fiberglass sack factory	125
General contingency and spare parts	75
Photovoltaic arrays	1805
Total	3525
Photovoltaic arrays manufactured at the SMF	-1225
Two liquid hydrogen tanks	-29
Net Shuttle or SD/HLV payloads	2271

surface would provide a major reduction in the total propellant mass required to be delivered to lunar orbit by the MDRE, with hydrogen coming from Earth and oxygen from the SMF beginning in 1990. On the other hand, the payload deliverable by the LTV in this mode of operation would be reduced, so that more LTV flights would be required. We have conservatively assumed that all propellants continue to be provided in lunar orbit.

For the first year of lunar operations, when a crew of 24 was used to establish the main and downrange stations, a total of 32 tons of consumables was provided (25 at the main base; 7 at the downrange station which would be occupied by no more than 12 during the lunar day only). With expansion of the lunar base to 48 people early in 1988, the consumables are increased to 60 tons/yr until oxygen is supplied at the lunar surface, cutting the consumables budget in half. Similarly, provisions for the catcher habitat initially include 7 tons for the first year of operations. After operations at the catcher have become more routine, 5 tons/yr should suffice, with a further reduction to 3 tons/yr when oxygen becomes available at the SMF.

We have assumed that the lunar crews have a 1-year tour of duty in space (i.e., 1 year from launch to LEO until reentry into the Earth's atmosphere). If the lunar base expansion to a crew of 48 is staggered 6 months from the date of rotation of the first 24, the main lunar base need never be unoccupied. A total of three OTV's (with passenger modules large enough for 24 to 30 persons) is sufficient to provide emergency evacuation capability for the entire lunar crew with one of these OTV's parked in LEO for emergency backup. The OTV fleet used to transport crews to and from the SMF provides additional backup. Thus two OTV round trips must be provided for each year, with contingency propellants at LEO and at lunar orbit for two more flights per year. These propellant requirements, together with the propellants required for soft-landing supplies, equipment, and personnel on the lunar surface and the propellants needed for monthly trips with the small LTV to the catcher, are given in table 8.

For the first chemical propellant storage depots, we minimized the time and labor of converting Shuttle external tanks by keeping the basic external tank structure intact. Once oxygen and hydrogen are supplied from different sources (LEO for hydrogen from Earth, SMF for oxygen

from lunar soil), it is more practical to separate the oxygen and hydrogen tanks and to discard the intertank section, reducing the mass of each complete depot by about 8 tons.

The expansion of the lunar base to full capacity would be completed by mid-1990, with a total of 4530 metric tons of equipment soft-landed at the two surface stations. Continuation of the lunar surface operations at this level requires soft-landing 30 tons of consumables per year, 14.4 tons of crew and baggage, plus an ample allowance of replacement parts and supplies. We have arbitrarily allotted 195.6 metric tons/yr for this purpose (about 4 percent of the total installed mass), so that three trips per year by the large LTV will suffice.

The mass budget we have provided above will provide the lunar base with the capability of launching 600,000 metric tons/yr into space with daytime operations only. Some consideration should be given to ways of extending lunar base operations through the lunar night. The possibility of several large reflector satellites placed in high-inclination orbits around the Moon to provide full daylight illumination for the lunar base should be examined. Such satellites could be manufactured at the SMF and placed in lunar orbit with minimal consumption of propellants, significantly reducing the total mass of the energy systems which must be softlanded on the lunar surface, and nearly doubling the launch capacity of the lunar base (ref. 18).

SMF EXPANSION AND OPERATIONS

The final milestone for the space manufacturing enterprise considered here is to produce 2.4 solar power satellites per year, each with a capacity of 10 GW. Previous studies of Earth-launched solar power satellites estimate that 750 to 800 man-years of assembly work must be done in orbit for each such satellite (H. P. Davis, NASA, Johnson Space Center, Houston, TX, private communication, 1977). In the case of the space manufacturing system considered here, assembly work should be comparable, but additional labor must be provided for chemical processing and for fabricating basic structural components and active elements (such as photovoltaic cells or thermal-cycle radiators). Chemical processing and basic foundry and milling operations are generally much more automated (when measured in tons produced per worker per year) than are assembly operations in terrestrial industries. We have thus assumed that a total

TABLE 8 — PROPELLANT REQUIREMENTS FOR LUNAR OPERATIONS[a]

Year of delivery to LEO	Propellants loaded on OTV at LEO	Propellants loaded on OTV at LLO	Propellants for large LTV	Propellants for small LTV	Total Earth-supplied propellants at LLO	Total SMF supplied propellants at LLO
1986	60.5	165	896	186	1247	—
1987	269.5	220	896	186	1302	—
1988	220	220	952	186	1358	—
1989	220	32	136	27	195	—
1990	32	33	27	92	1170	
1991	32	32	33	27	92	552
1992	32	32	33	27	92	552

    a   In metric tons.

of 1250 man-years will be needed at the SMF to produce each SPS. The target of 2.4 SPS's per year thus requires an SMF crew of 3000.

We have assumed that the SMF crew is initially exchanged after a 1-year tour of duty, as were the LEO station crew and the lunar base crew. Once the total crew at the SMF reaches 1000, however, we have assumed that the tour of duty can be extended to 2 years because of the larger physical size of the SMF and because the larger size of the community affords more opportunity for each person to establish satisfactory social interactions. The schedule of crew buildup and exchange and the numbers of OTV's and the masses of propellants required at LEO and at SMF for personnel transportation between LEO and the SMF, are shown in table 9. A number of contingency flights have also been budgeted, as well as a number of spare vehicles at LEO. As a minimum, we have ensured that sufficient propellants and vehicles are available at the SMF at all times to evacuate to LEO all SMF personnel (up to 252) living in one cluster of 14 converted liquid hydrogen tanks.

LIFE-SUPPORT AND POWER REQUIREMENTS

A space habitat must provide equipment for extracting potable water from human wastes and washing water; for maintaining atmospheric temperature, humidity, and composition within an acceptable range; and for storing or disposing of waste materials. A modular design for an environmental control and life-support system (EC/LSS) was adopted for use in all space habitats in this space manufacturing system. Carbon dioxide is concentrated by a molecular sieve and then reduced to carbon ash and free oxygen by the Sabatier process. Each EC/LSS unit, with a mass of 10.4 metric tons, supports 12 people with 100-percent redundancy, and fits in a cylindrical pod (3 m in diameter, 2.5 m long) large enough to provide interior access for repairs and maintenance (E. H. Bock, General Dynamics, Convair Division, San Diego, CA, private communication regarding a design adapted from ref. 19). With efficient oxygen recovery, a space station using such a system would require about 1.5 kg/person resupply per day (including food as well as water, oxygen, and nitrogen losses through leaks and during EVA). Without oxygen recovery, such a system would require 2.05 kg/person/day. We have assumed 3.0 kg/person/day for consumables imported from Earth until lunar oxygen becomes freely available in 1990, when the consumables resupply is reduced to 1.5 kg/person/day. All waste materials are stockpiled for later use in agriculture.

Radiation protection is an important issue in habitat design. For the LEO station (below the Van Allen belts), we have provided no shielding additional to that afforded by the walls and furnishings of the converted Shuttle tanks. The lunar habitats can be shielded readily by burying them under several meters of lunar soil. The habitat at the catcher can be shielded several years after initial operation against cosmic rays and solar flares, but the expense of providing shielding very early would be difficult to justify because of the very limited times during which it will be occupied by small crews.

For the SMF, on the other hand, cosmic-ray shielding must be provided early. This can be done using the unselected lunar soils provided in the first few deliveries from the catcher during the first 6 months of occupancy. Solar flares, however, pose a serious threat to the SMF crew during this early period. Stowing the consumables for the first year around the walls and between flooring in the galley and mess hall areas of the communal tanks can provide an adequate shelter for solar storms lasting several days, should they occur before the entire habitat is shielded properly.

Estimates of power requirements per person in space stations have been extremely variable. In Skylab, electrical power for life support, environmental control, cooking, refrigeration, and lighting was 2.87 kW/person (average power). Most of the astronauts who flew Skylab complained that lighting was inadequate (ref. 20). Allowing for the limited EVA of the Skylab missions in comparison with the space manufacturing enterprise considered here, we have allowed 9 kW/person (average power) throughout the system, except that the main lunar base provides only 8 kW/person during the lunar night when little EVA is expected, and the downrange station on the lunar surface provides only 3 kW/person during the lunar night for emergencies, since it is expected to be occupied only during the lunar day. Photovoltaic arrays have been sized accordingly, assuming peak power of 200 W/m² under normal incidence of full sunlight and a mass of 1.61 kg/m². Radiator systems to remove heat dissipated by use of electrical power and from human metabolism were assumed to require 170 kg/person with a radiator area of 68 m²/person. Energy storage is provided by flywheels at the lunar surface habitats and at the LEO station, with an energy storage density of 870 W-hr/kg, and a highly conservative 70-percent overall efficiency. Research and development costs for the photovoltaic arrays, radiators, and flywheels can be minimized by modular designs sized for a few persons, just as the EC/LSS pods were sized for 12 persons, providing maximum commonality throughout the system.

HABITAT DESIGN

For the space manufacturing system described here, habitats are required in four different sets of environments and operational conditions:

1. LEO station: permanent occupation, minimal radiation protection needed, prompt return to Earth possible by means of the Shuttle, small crew, frequent visitors
2. SMF: permanent occupation, full radiation shielding required early, rapid return to LEO possible (but expensive) by means of OTV, large crew, no visitors
3. Catcher: infrequently occupied for short periods by very small crews, 40 hr travel time to LLO and lunar surface
4. Lunar surface: permanent occupation at main base, intermittent long occupations of downrange base, small crews, prolonged isolation remote from Earth, 1/6

TABLE 9 — CHEMICAL OTV LOGISTICS FOR SMF PERSONNEL TRANSPORTATION

Date	Crew at SMF	Crew increase	Crew exchange	Total outbound passengers	No. of flights outbound (full)[a]	Earth-supplied propellants loaded at LEO (metric tons)	No. of OTV's in active use	No. of spare OTV's at LEO	Total inbound passengers	No. of flights inbound (full)[a]	No. of flights inbound (empty)[b]	Earth-supplied propellants loaded at SMF (metric tons)	Earth-supplied propellants delivered to LEO for later use at LEO (metric tons)	Earth-supplied propellants delivered to LEO for later use at SMF (metric tons)	SMF-supplied oxygen delivered to LEO for later use at LEO (metric tons)
1987.0	0														
		---	---	---	---	---	---	---	---	---	---	---	319	441	---
1988.0	0														
		300	0	300	10+3	91 H_2 546 O_2	10	3	0	0+13	0	91 H_2 546 O_2	700	852	---
1989.0	300														
		540	300	840	28+5	231 H_2 1386 O_2	20	5	300	10+5	8	142.7 H_2 856.3 O_2	1526	518.2	---
1990.0	840														
		1500	840	2340	78+5	581 H_2	50	5	840	28+5	20	325.2 H_2	495	417.6	4286
1991.0	2340														
		684	1670	2354	79+5	588 H_2	51	5	1670	56+5	22	530.6 H_2	489	459	3528
1991.7	3024														
1992.0	3024														
		0	1512	1512	51+5	392 H_2	51	5	1512	51+5	0	392 H_2	392	392	2352
1993.0	3024														
		0	1512	1512	51+5	392 H_2	51	5	1512	51+5	0	392 H_2	392	392	2352
1994.0	3024														

a Each flight is assumed to carry 30 passengers and consume 49 tons of propellants. Scheduled flights and contingency flights are indicated before and after the plus sign, respectively. Fuel requirements are computed assuming that all contingency flights are actually used. Unused propellants provide additional launch space to LEO in the following year, reducing the numbers shown in the last two columns year by year.

b To the extent that outbound flight requirements exceed inbound flights plus increases in the OTV fleet at LEO, some empty flights must be made from the SMF back to LEO, consuming 33 tons of propellants per flight.

normal gravity, early protection required against radiation and thermal extremes

Because the Shuttle external propellant tank is an existing piece of hardware that can be delivered into orbit at minimal cost and because it was designed to sustain very heavy loads under launch accelerations, we have based all our habitat designs on the use of the liquid hydrogen tank as the basic structural frame and pressure vessel. This approach also permits a high degree of commonality throughout the system and seems to provide a reasonable compromise between the safety features of small modular habitats in the early stages of growth and the economies of scale of large monolithic structures. The extensive structural ribbing along the tank walls provides easy attachment of internal partitions and structures, permitting simple installation of the habitat interiors. (Some years ago, a proposal to use spent fuel tanks from Saturn rockets for space station shells was considered. The cryogenic insulation for those tanks, however, was on the inside of the tanks, and outgassing of hydrogen from the insulation for prolonged periods seemed to be a sufficiently severe problem that the proposal was rejected. For the Shuttle tanks, there is no such problem since the insulation is on the outside.)

The liquid hydrogen tank is 31 m long and 8.5 m in diameter (96 by 27.5 ft). For the orbital habitats, we have adopted a "condominium tower" configuration, dividing each tank into 10 levels of circular floor plan, with 2.6 m (8 ft) ceiling heights, leaving more than 0.5 m of subflooring space for utilities and storage. (Reducing the subfloor storage space to 0.2 m would allow 11 levels per tank with the same ceiling height.) A central shaft (1.8 min diameter) runs the entire length of each tank, containing a dumbwaiter-like continuous belt elevator and ladders for access to all levels.

For the LEO station and the SMF habitat, several residential tanks would be clustered around a communal tank. The lowest level (in the bottom hemispherical dome of the tank) of each tank would be used for storage and for maintenance equipment. In the residential tanks, seven of the levels would be divided into three segments surrounding the elevator shaft to provide three studio apartments per level. Each apartment would have 17.5 m² (188.5 ft²) of floor space, sufficient for one or two persons. One level (in the middle of the tank) would provide toilet, bath, and laundry facilities, while the top level (in the upper hemispherical dome) would be used as a leisure and social area (game room, observation deck).

In the communal tanks, the lowest level would be used for storage and maintenance. The next three levels up would provide recreational facilities (gymnasium, games, library, music room). A pantry and a galley would follow on the next two levels, with the following three levels used for dining rooms. (The dining rooms would double as assembly halls and movie theaters as well.) The topmost level would be used for EVA preparation, providing lockers for storage of EVA suits and facilities for recharging oxygen tanks and repairing EVA suits.

The top level and one lower level of each residential tank would be connected to the corresponding levels of the communal tank and of each adjacent residential tank. When fully occupied, each residential tank (21 persons) requires two EC/LSS pods (12 persons each). These can be nestled between adjacent hydrogen tanks, with short tunnels connecting each pod to both hydrogen tanks to provide access to the EC/LSS equipment for maintenance as well as to provide alternative emergency passageways between tanks. All passageways would be equipped with airtight hatches to permit isolation of any tank.

Two identical clusters of residential tanks and a communal tank can then be assembled with a 140-m-long tunnel between them to form a dumbbell-like configuration. Rotation at 3 rpm then provides Earth-normal gravity at the bottom level of each tank and 0.7 g at the top level. The tunnel is stress-free, the hydrogen tanks being supported from the docking hub at the middle of the connecting tunnel by a set of cables. Each tank has an emergency airlock at the top level, with routine entry into the habitat through two airlocks in the hub. One of the dining room levels (of the six provided in the two communal tanks) would be used instead for a medical clinic/emergency operating room.

The Shuttle tank sets, designed to carry 700 metric tons under launch accelerations exceeding 2 g, are structurally capable of supporting the loads contemplated here with a very large safety factor. The internal loads would be borne by the tank ribbing and by three or more tie bars running the length of the elevator shaft which transmit their load to the cables suspending the entire tank from the hub. With a rotation rate of 3 rpm, crew selection for adaptability to rotation would be essential but would not pose a serious problem for most people (ref. 21).

For the LEO station, two residential tanks and one communal tank would be placed at each end of the dumbbell, providing facilities for as many as 84 persons. For the SMF habitat, each end of the dumbbell would consist of six residential tanks encircling a communal tank. The top level of the communal tank provides access to both the elevator system within that tank and a second elevator system running up to the hub. Because the SMF has a lower ratio of communal space to population than does the LEO station, some reallocation of space different from that described above may be necessary. Several levels among the six residential tanks could be changed from apartment levels into communal facilities. The total occupancy might be reduced from 252 to as low as 234 or the reduction in space could be compensated by some doubling up of crew members. (Alternatively, the 11-level design could be adopted from the start, increasing the total mass somewhat.) Spinning up the SMF habitat dumbbell to 3 rpm requires only 1 metric ton of propellant, a mass sufficiently small to be omitted from the mass budgets shown in the tables. (Figure 1 shows a design for the SMF habitat.)

For the catcher habitat, only one tank need be provided, using a mixture of levels from residential and communal tanks. A crew of 12 would be amply accommodated by four apartment levels; one toilet and laundry level; one

pantry/galley/dining level; one recreation level; one level for workshops used to maintain and repair the catcher; one storage level; and one level for EVA preparation. This single tank does not provide pseudogravity, so no elevator is installed in the central shaft, crew members using ladders instead. The consistent vertical orientation throughout the 10 levels, required for the rotating habitats at LEO and at the SMF, would ease adaptation to the weightlessness of the catcher habitat (ref. 20). The habitat tank would be placed directly behind the catcher itself to protect the habitat from stray projectiles of lunar materials.

Furniture and personal belongings for a small one- or two-person apartment in the United States may total 1000 to 3000 lb (including refrigerator, carpets, and drapes). Instead of attempting to give a detailed breakdown of masses for furniture, toilets, shower stalls, laundry equipment, and galley equipment, we have allowed 1000 kg (2200 lb) of furniture for each of the nine furnished levels of the residential tanks, and 60 percent more for the communal tanks where galley equipment and chairs and tables for dining rooms would require more mass than average. Table 10 summarizes the mass estimates for refurbishing the liquid hydrogen tanks for the orbital habitats at LEO, at SMF, and at the catcher.

For the lunar surface habitats, a different design approach is required because of the necessity of burying the habitats. Instead of a condominium tower configuration, the liquid hydrogen tanks must lie flat on their sides. The interior configuration is then a long two-story bungalow. Setting ceiling heights at 2.6 m (8 ft) leaves ample room for storage, ducting, wiring, and plumbing along the full length of the top and bottom of the tank and between the two levels in the subflooring space. Leaving space for a companionway the full length of each level, with spiral stairways between levels, each level would provide six studio apartments approximately 3.1 m by 4.5 m (10 by 14 ft), with about 11 m of tank length on each level for communal facilities (galley, toilets and baths, laundry, dining room, recreation facilities,

and EVA preparation). Each tank would have two airlocks, and the two tanks at the initial main lunar base would be connected by a tunnel to make a single habitat unit. When the main base is expanded, the third and fourth tanks can be similarly connected to the first two.

Each tank thus provides private space for 12 persons instead of 21. The floor area per person is somewhat smaller, but this is psychologically compensated (in part) by daily work on the surface. With only 1/6 Earthnormal gravity, structural masses for flooring are smaller than would be the case in the orbital habitats. We have thus estimated only 10 metric tons per tank for structure and furnishings; if two airlocks and one EC/LSS pod are added, the total mass per tank is 37.5 tons. The energy system to support 12 persons totals 62.5 tons (4.5 tons for photovoltaic arrays, 2.2 tons for radiators, 55 tons for flywheels, 0.8 ton for motor/generators and for the control system).

VEHICLE REQUIREMENTS

In an earlier section, we discussed the logistics of transporting lunar and SMF crews from LEO by means of a chemically propelled OTV. A passenger module (including EC/LSS hardware and the OTV flight deck) that can fit in the Shuttle cargo bay and that can accommodate 30 passengers enroute to the SMF (a 9.8-hr flight) or 24 passengers enroute to lunar orbit (a 5-day flight) would have a dry weight of about 14.2 metric tons. Allowing 300 kg/passenger (including baggage) leaves room for a 27.5-day supply of consumables for a lunar trip or a 2.2-day supply for the trip to the SMF within the 23.4-metric-ton payload capability of the OTV. Conditions aboard would be distinctly crowded, but such conditions can be tolerated for a voyage of strictly limited duration. One passenger module must be provided for each OTV in the fleet. The passenger modules used for the lunar crews must differ somewhat from those used for SMF crews because of the greater duration of the lunar transfer, with more extensive galley and toilet facilities, consistent with the reduction in the number of
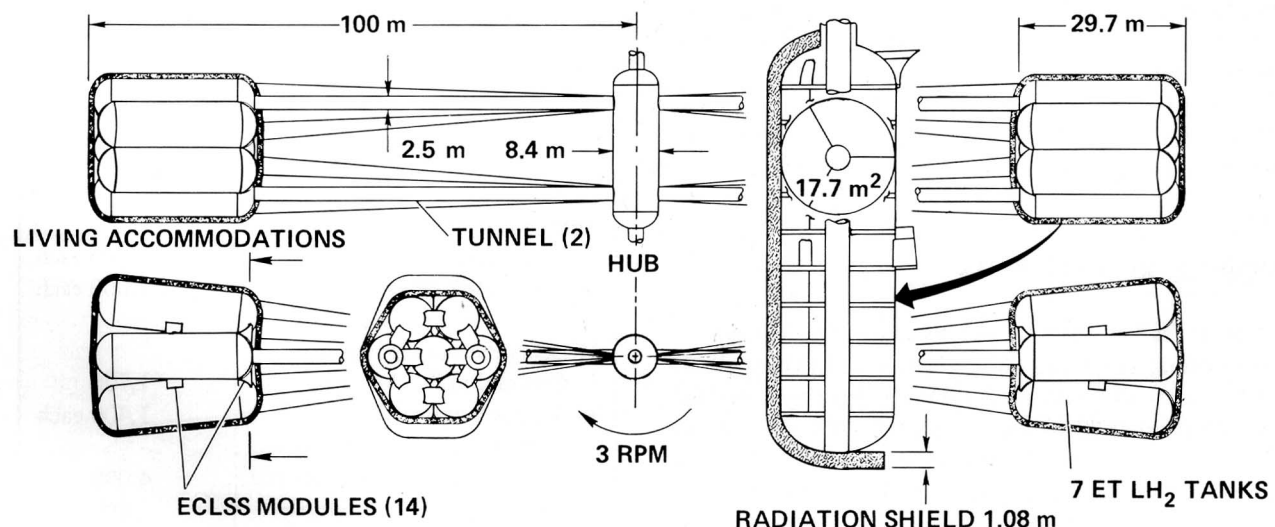

Figure 1 — *Habitat design for the SMF. Two clusters of seven liquid hydrogen tanks from the Shuttle external tank sets provide comfortable living facilities for up to 252 people with pseudogravity ranging from 0.7 to 1.0 gravities provided by rotation at 3 rpm.*

TABLE 10 — MASSES FOR ORBITAL
HABITAT INTERIORS

Component	Mass, kg
Component	Mass, kg
Central shaft for each tank:	
Vertical tie rods (in tension)	440
Continuous belt elevator system	400
Total	840
For each level:	
Structural flooring (12 panels)	800
Outer edging and attachments to tank	45
Inner ring and attachments to tie rods	10
Radial beams (12)	90
Ducting and plumbing	100
Lighting fixtures	100
Partitions and wall finishings	400
Acoustic ceiling	120
Carpeting or tiling	75
Total	1,740
Total internal shell:	
Central shaft	840
9 floors, at 1740 kg	15,660
Total	16,500
Furnishings:	
Communal tanks	14,200 each
Residential tanks	9,000 each
Miscellaneous components:	
Central hub	1,700
Airlock	1,400 each
Tunnels from hub to communal tanks	4,000
Elevator system to hub	800
Cables (per tank)	2,300
EC/LSS pod (completely redundant)	
for 12 persons	10,400 each

passengers. The OTV passenger modules, however, would seldom be used aboard the Shuttle since the Shuttle payload capacity is considerably larger than the total mass of a fully loaded passenger module. Most of these modules would be delivered to LEO aboard the SD/HLV, with the passenger cabin filled with such cargos as consumables for LEO or SMF.

During the first year or two of launch operations before the lunar base begins operation, crews for the LEO station can ride to and from orbit in the Shuttle cabin, 4 or 5 at a time. Later on, when LEO crews and lunar crews are exchanged in lots of 24, and the SMF crews are exchanged in groups of 150 or so, this mode of operation becomes impossible. Two or three Shuttle-bay passenger modules designed for a total flight time of 1.5 to 3 hr would suffice, with double-deck, high-density seating provided for 60 passengers at a time, plus baggage. These Earth-launch modules should be provided in 1987, and could be expected to weigh no more than the OTV modules since the life-support requirements are considerably simpler.

MDRE FLEET EXPANSION

Once the lunar base has been established, the pace of transporting supplies and equipment into orbit is sharply accelerated. A second MDRE is added to the fleet late in 1986, and four more are added in 1987. Because of the higher payload of the SD/HLV, there is a tendency for payloads for high orbit to accumulate faster than the requisite external tanks for MDRE reaction mass. Late in 1987, in anticipation of the arrival of the first cargo of lunar soils at the SMF, the first of eight large MDRE's (LMDRE) is delivered to LEO. Table 11 compares this vehicle with the original MDRE, making some assumptions about economies of scale possible for the larger machine.

The first LMDRE is delivered to the SMF as cargo aboard two MDRE flights shortly after initial operation of the SMF in February 1988. After assembly and checkout are completed, the LMDRE makes a round trip to LEO to deliver 2100 tons of lunar material, enough reaction mass for three MDRE flights to the SMF (fully loaded with 1200 tons of cargo each time). Since the LMDRE is operating far below maximum capacity on this flight, only 2400 tons of reaction mass are required to complete the round trip in about 2 months. The LMDRE is then used to haul larger masses of lunar soil from the catcher to the SMF since the launch rate at the lunar base begins to increase by mid-1988 to rates exceeding the capacity of the MDRE fleet.

During 1988, 2000 metric tons of LMDRE components and subassemblies are delivered to the SMF which contributes 1200 tons of manufactured components (solar cells, cables, structural members) to complete two more LMDRE's. During 1989, assuming that the SMF can now contribute 50 percent of the mass of an LMDRE, 4000 tons of imported components and parts permit expansion of the LMDRE fleet by five more units.

The fleet of eight LMDRE's is required to transport lunar materials from the catcher to the SMF; to transport liquid oxygen for chemical propulsion from the SMF to both LEO and LLO; to transport lunar material to LEO for the MDRE and LMDRE fleets; and to transport (if necessary) chemical

TABLE 11 — MASS DRIVER SPECIFICATIONS

	Metric tons	
MDRE		
Dry weight at LEO	174	tons
Reaction mass consumption rate	175	
tons/month		
Reaction mass required for 4-month trip		
from LEO to SMF with refueling at SMF	700	tons
Payload delivered from LEO to SMF	1,200	tons
LMDRE		
Dry weight at LEO	1,600	tons
Reaction mass consumption rate	1,700	
tons/month		
Reaction mass required for 4-month trip		
from LEO to SMF with refueling at SMF	6,800	tons
Payload delivered from LEO to SMF	12,000	tons

feedstocks for the manufacture of solar power satellites at the SMF. We have arbitrarily assumed that 9000 metric tons of raw materials must be imported from Earth for each SPS totaling 100,000 metric tons when completed. Annual transportation requirements for these chemical feedstocks would then total 21,600 tons, which can be accommodated in two LMDRE flights. More detailed trajectory analyses are required to optimize the MDRE/LMDRE fleet and to confirm some of the mass and flight time estimates used here.

EARTH LAUNCH REQUIREMENTS

Table 12 summarizes the total launch requirements for the scenario described here. The greatest single uncertainty concerns the question of how much mass must be imported from Earth to supplement lunar raw materials in the manufacture of products such as solar power satellites. The lift requirements can be met in many ways; table 13 shows an aggressive launch schedule using the Shuttle, the SD/HLV, and the SSTO to meet the milestones on the schedule described here. After 1987, when a fifth SD/HLV is added, the Shuttle is used only for crew transportation with a passenger module in the cargo bay.

Should it be possible to manufacture SPS's without any imports from Earth, the number of launches by the Shuttle

and the SD/HLV would be considerably reduced. The right half of table 13 shows the launch schedule that results from eliminating the chemical feedstocks column in table 12. Redistribution of the remaining cargos to produce a more even launch schedule has not been attempted, nor have we considered in any detail the changes in MDRE fleet size that would also result. Use of the LMDRE to bring lunar materials to LEO for reaction mass would have to be accelerated because of the reduction in expendable Shuttle tanks.

Table 14 summarizes the allocation of Shuttle tanks over the period 1985 to 1990. Each liquid hydrogen tank weighs 14.5 tons, while a complete tank set weighs 33.45 tons. Thus the tank allocations must be converted to "equivalent tanks" to account for use of the rest of a tank set for reaction mass after the hydrogen tank has been converted into a habitat.

If the reduced launch schedule shown on the right side of table 13 is attainable, deployment of the singlestage-to-orbit vehicle (assumed to operate in a mixed passenger and cargo mode) could be postponed indefinitely, although costs per ton would be higher in that case. After a number of years, the increased costs of using the Shuttle and the SD/HLV would begin to rival the discounted costs for development of the SSTO.

TABLE 12 — SUMMARY OF LIFT REQUIREMENTS TO LEO[a]

Year	Equipment and supplies for:			Vehicles			Chemical propellants	Crew and baggage	Subtotal	Chemical feedstocks	Total
	LEO	SMF	LLO	OTV	MDRE	LMDRE					
1985	290	—	1266	—	174	—	—	9.2	1,739.2	—	1,739.2
1986	169.2	—	66.3	13	174	—	1307.5	9.6	1,739.6	—	1,739.6
1987	70	4173.5	1159.6	43.2	696	1600	2331.5	34.4	10,108.2	621.8	10,730
1988	86.6	3490	1284.6	277.2	—	2000	3130	203	10,471.4	981.6	11,453
1989	70	3540	1318	250.8	—	4000	2459.2	464	12,102	1,838	13,940
1990	43	2980	231.6	627	—	—	1036.6	1189	6,107.2	8,542.8	14,650
1991	43	1600	231.6	20.9	—	—	1072	735	3,702.5	18,797.5	22,500
1992	43	1600	231.6	—	—	—	908	482.4	3,265	21,600	24,865
1993	43	1600	231.6	—	—	—	908	482.4	3,265	21,600	24,865

a   Metric tons.

TABLE 13 — LAUNCH SCHEDULE (EARTH TO LEO)

Year	Total payload[a] (including chemicals), metric tons	Number of flights			Total launch capacity, metric tons	Total payload[b] (excluding chemicals), metric tons	Number of flights			Total launch capacity, metric tons
		Shuttle	SD/HLV	SSTO			Shuttle	SD/HLV	SSTO	
1985	1,739.2	60	—	—	1,740	1,739.2	60	—	—	1,740
1986	1,739.6	60	—	—	1,740	1,739.6	60	—	—	1,740
1987	10,730	60	80	—	10,780	10,108.2	60	75	—	10,215
1988	11,453	7	100	—	11,503	10,471.4	7	91	—	10,486
1989	13,940	16	120	—	14,024	12,102	16	107	—	12,575
1990	14,650	41	120	—	14,749	6,107.2	41	45	—	6,274
1991	22,500	—	—	100	22,700	3,702.5	28	26	—	3,750
1992	24,865	—	—	110	24,970	3,265	—	—	15	3,405
1993	24,865	—	—	110	24,970	3,265	—	—	15	3,405

a   Assuming 9% terrestrial chemical feedstock requirement.
b   Assuming no terrestrial chemical feedstock requirement.

TABLE 14 — ALLOCATION OF SHUTTLE EXTERNAL TANKS

Year	LH$_2$ tanks for habitats at:				Equivalent complete tanks	Chemical propellant storage depots	MDRE reaction mass	Total external tanks available
	LEO	SMF	Lunar base	Catcher				
1985	6	—	2	1	4.4	3	52.6	60
1986	—	28	2	—	13.2	3	43.8	60
1987	—	28	—	—	12.4	3	124.6	140
1988	—	28	—	—	12.4	14	80.6	107
1989	—	42	—	—	18.6	—	117.4	136
1990	—	42	—	—	18.6	—	142.4	161

CONCLUSIONS

We have examined the logistic feasibility of establishing a space manufacturing enterprise for the construction of solar power satellites in high Earth orbit, using lunar materials, operating within the constraints of Space Shuttle and Shuttle-derived launch vehicle technologies. Such a system, it seems, could be deployed in less than 8 years of launch activities maintained at an aggressive pace; the launch activities follow 4 or 5 years of dedicated development and hardware procurement. If the program commences at full speed in 1980 or 1981, the first 10-GW SPS's could be on-line late in 1990; the second, late in 1991; and the third, early in 1992.

Crew selection and training requirements and an economic analysis of the program have also been carried through. These results will be reported elsewhere.

Depending on a variety of assumptions about interest rates, discount rates, costs for competing sources of electrical powerplants, and research and development costs, the total investment for the period 1980 to 1992 (when the third SPS is sold) lies roughly between $50 billion and $100 billion, equivalent (in 1977 dollars) to one or two times the Apollo program.

A key technical problem that must be resolved at an early date is the design of an SPS using only lunar materials. Should it prove impractical to design such an SPS or to design a factory to manufacture such an SPS, the use of asteroidal materials (with a much greater diversity of chemical elements available, especially such volatiles as hydrogen, carbon, and nitrogen) would be favored.

The use of the mass driver as a reaction engine for cargo transportation beyond LEO provides significant advantages over chemical propulsion systems, as can be seen from an examination of the extensive propellant requirements for personnel transportation alone, a small fraction of the total mass required to be transported beyond LEO.

Habitat designs based on use of the Shuttle external tank seem to offer numerous advantages and simplifications in the system considered. The orbital habitats (except for the intermittently occupied habitat at the catcher) all provide near-Earth-normal gravity from the beginning.

The location for the space manufacturing facility must be optimized after the SPS design has been settled. During the early stages of the enterprise, however, a high circular orbit appears to be strongly favored because of logistic considerations.

The detailed scenario presented here is only one of many possible design approaches, but it serves to show that a space manufacturing enterprise is logistically feasible in the Shuttle era, albeit with significant technical risks in such an aggressive program. The feasibility of undertaking such a program in the public sector or along conventionally organized lines in the private sector has not been addressed here.

REFERENCES

1. O'Neill, Gerard K.: Space Colonies and Energy Supply to the Earth. Science, vol. 190, Dec. 5, 1975, pp. 943-947.

2. Johnson, Richard D.; and Holbrow, Charles, eds.: Space Settlements — A Design Study. NASA SP-413, 1977.

3. Grey, Jerry, ed.: Space Manufacturing Facilities: Space Colonies. Proceedings of the Princeton AIAA/NASA Conference, May 7-9, 1975, American Institute of Aeronautics and Astronautics, New York, 1977.

4. O'Neill, Gerard K., ed.: Space-Based Manufacturing from Nonterrestrial Materials. Progress in Aeronautics and Astronautics Series, vol. 57, AIAA, New York, 1977; also NASA TM X-73,265, Aug. 1977.

5. Third Princeton/AIAA Conference on Space Manufacturing Facilities, Princeton, New Jersey, May 9-12, 1977.

6. O'Neill, Gerard K.: Engineering a Space Manufacturing Center. Astronautics and Aeronautics, vol. 14, no. 10, October 1976, pp. 20-28, 36.

7. Phinney, William C.; Criswell, David; Drexler, Eric; and Garmirian, James: Lunar Resources and Their Utilization, in Space-Based Manufacturing from Nonterrestrial Materials. Progress in Aeronautics and Astronautics, vol. 57, AIAA, New York, 1977, pp. 97-123; also NASA TM X-73,265, Aug. 1977.

8. Driggers, Gerald W.; and Newman, Jonathan E.: Establishment of a Space Manufacturing Facility, in Space-Based Manufacturing from Nonterrestrial Materials. Progress in Aeronautics and Astronautics, vol. 57, AIAA, New York, 1977, pp. 135-160; also NASA TM X-73,265, Aug. 1977.

9. Chilton, F.; Hibbs, B.; Kolm, H.; O'Neill, G. K.; and Phillips, J.: Electromagnetic Mass Drivers, in Space-Based Manufacturing from Nonterrestrial Materials. Progress in Aeronautics and Astronautics, vol. 57, AIAA, New York, 1977, pp. 37-61; also NASA TM X-73,265, Aug. 1977.

10. Chilton, F.; Hibbs, B.; Kolm, H.; O'Neill, G. K.; and Phillips, J.: Mass-Driver Applications, in Space-Based Manufacturing from Nonterrestrial Materials. Progress in Aeronautics and Astronautics, vol. 57, AIAA, New York, 1977, pp. 63-94; also NASA TM X-73,265, Aug. 1977.

11. Fine, Kevin: Basic Coaxial Mass Driver Construction and Testing. Third Princeton/AIAA Conference on Space Manufacturing Facilities, May 9-12, 1977, AIAA Paper 77-535, 1977.

12. O'Neill, Gerard K.: The Low (Profile) Road to Space Manufacturing. Astronautics and Aeronautics, vol. 16, no. 3, March 1978, pp. 24-32.

13. O'Leary, Brian; Heppenheimer, T. A.; and Kaplan, David: Trajectory Analyses for Material Transfer from the Moon to a Space Manufacturing Facility, in Space-based Manufacturing from Nonterrestrial Materials. Progress in Aeronautics and Astronautics, vol. 57, AIAA, New York, 1977, pp. 21-36; also NASA TM X-73,265, Aug. 1977.

14. Meeus, Jean: Syzygies Tables. Kesselberg Sterrenwacht (observatory publication). Kessel-Lo, Belgium, 1963.

15. Systems Concepts for STS-Derived Heavy-Lift Launch Vehicles. Final Rept., Boeing Co., NASA study contract NAS9-14170.

16. Henry, B. Z.; and Eldred, C. H.: Advanced Technology and Future Earth-to-Orbit Transportation Systems. Third Princeton/AIAA Conference on Space Manufacturing Facilities, May 9-12, 1977, AIAA Paper 77-530, 1977.

17. Williams, Richard J.; McKay, David S.; Giles, David; and Bunch, Theodore E.: Mining and Beneficiation of Lunar Ores. Space Resources and Space Settlements, NASA SP-428, 1979, pp. 219-229.

18. Criswell, David: The Initial Lunar Supply Base. Space Resources and Space Settlements, NASA SP-428, 1979, pp. 168-181.

19. Nelson, W. G.; and Cody, J.: Life Support System Definition for a Low-Cost Shuttle-Launched Space Station. Paper 72-ENAv-17, presented at the Environmental Control and Life Support Systems Conference, San Francisco, Calif., August 14-16, 1972, American Soc. of Mechanical Engineers.

20. Cooper, Henry S. F., Jr.: A House in Space. Holt, Rinehart & Winston, Inc., New York, 1976.

21. Billingham, John: Physiological Parameters in Space Settlement Design. Third Princeton/AIAA Conference on Space Manufacturing Facilities, May 9-12, 1977, AIAA Paper 77-549, 1977.

III

Dynamics and Design of Electromagnetic Mass Drivers
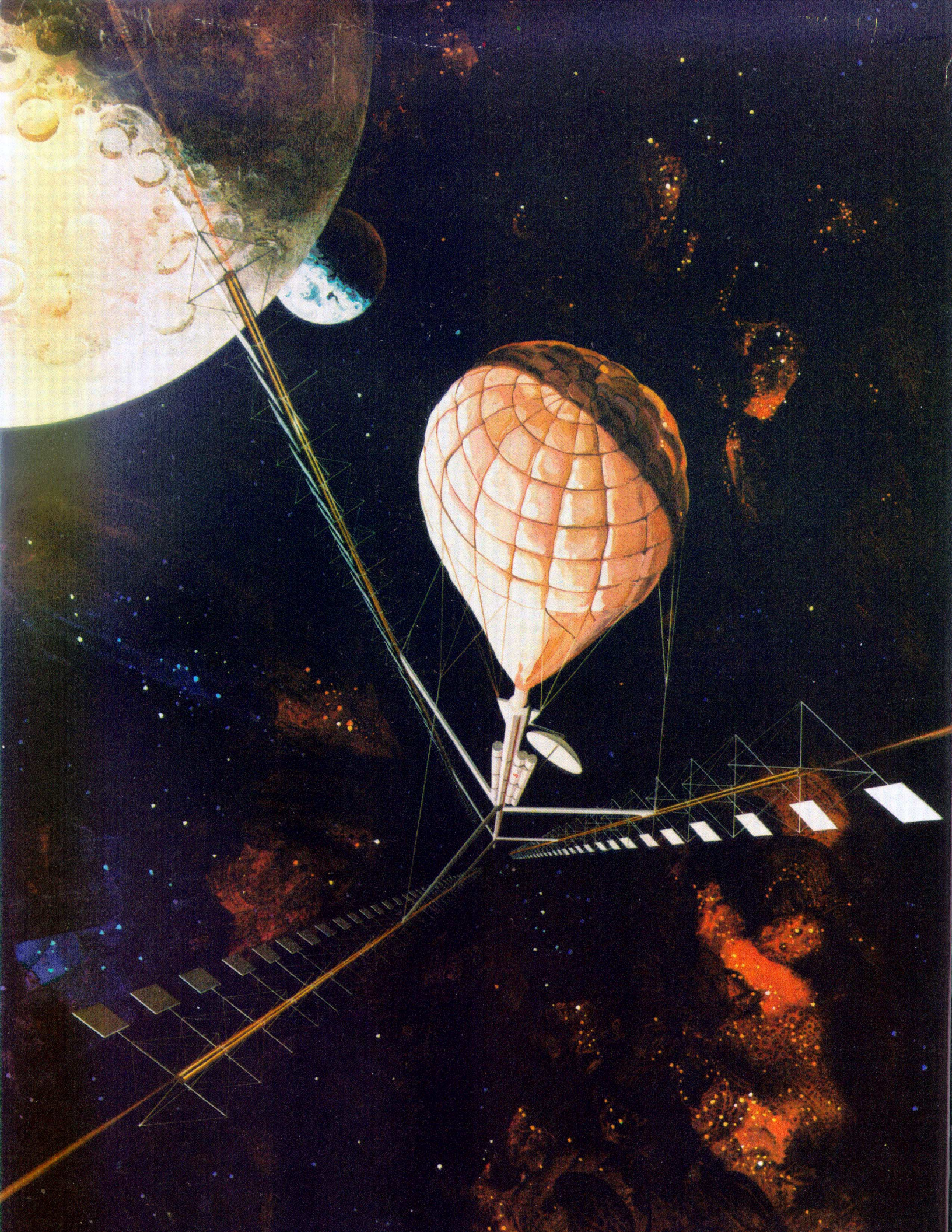
III-1
Mass Drivers I:
Electrical Design

WILLIAM H. ARNOLD, STUART BOWEN, KEVIN FINE, DAVID KAPLAN, MARGARET KOLM, HENRY KOLM, JONATHAN NEWMAN, GERARD K. O'NEILL, and WILLIAM SNOW

A mass driver is an electrical device used to accelerate payloads of any rnaterial to a high velocity. Small vehicles (called "buckets ") containing superconducting coils carry the payloads. These buckets are accelerated by pulsed magnetic fields, timed by information on their position, and are guided by induced magnetic fields set up in a surrounding guideway. Upon reaching the correct velocity, the buckets release their payloads, then they are slowed for recirculation to be reused. A rationale is presented that leads to a relatively simple and near-optimum design, as well as basic programs for calculating acceleration. The transverse oscillation frequencies are found to be invariant to guideway transverse dimensions. A detailed optimization of system mass and a discussion of all structural questions are presented in other papers of this summer study.

INTRODUCTION

The theoretical development of mass-driver designs has intensified since this concept was first published by O'Neill (refs. 1, 2). Much recent work is contained in unpublished notes. The three papers on mass drivers in this Special Publication are therefore written to summarize the present body of knowledge; this introduction contains references to the main sources of relevant information presently known.

After the first publication on mass drivers, the next substantial design effort occurred during the 1976 NASA-Ames Study on Space Manufacturing. In that study, there was active participation by professionals with experience in linear synchronous motors and magnetic flight.

Two mass-driver configurations were considered at the 1976 study: planar and axial. The planar system, a flattened, double-sized version of the M.I.T. magneplane (ref. 3), had served as the basis for the first mass-driver reference design, partly because calculations could be checked against existing computer programs. The axial configuration (fig. l) was eventually recognized as superior, particularly for reaction

engine applications involving maximum exhaust velocity and minimum total system mass. Axial geometry permits tighter inductive coupling between vehicle and drive coils and therefore higher acceleration for the same total system mass. Basic formulas for mass optimization, general enough to apply to a wide variety of mass drivers (both planar and axial designs), are given in references 4 and 5.

The 1976 study served to verify and extend the basic mass-driver concept, to reveal the advantages of axial geometry, to produce the mass-optimization formulas, and to develop a method for payload guidance after release. It yielded the important result that accelerations of the order of 10^4 m/sec^2 are almost certainly realizable in mass drivers of moderate transverse dimensions.

Building on this foundation, substantial advances were made during the 1976-77 academic year. In a series of four seminars,[1] the basic design for a mass driver of high performance (6,000 to 10,000 m/sec) and low system mass (100-200 tons) was developed for application to reaction engines in space. In the seminar series, the transverse oscillation scaling laws were derived, a simple program for calculating acceleration was written, and improvements were made in obtaining maximum drive for minimum power loss in the drive windings. These results were summarized concisely, without derivations, at the 1977 Princeton/AIAA Conference on Space Manufacturing (ref. 6). In that paper, the concept was applied to an engine used to move large amounts of equipment from low Earth orbit (LEO) to lunar orbit.

During the same period, the first mass-driver model was designed and built at M.I.T.: construction was directed by
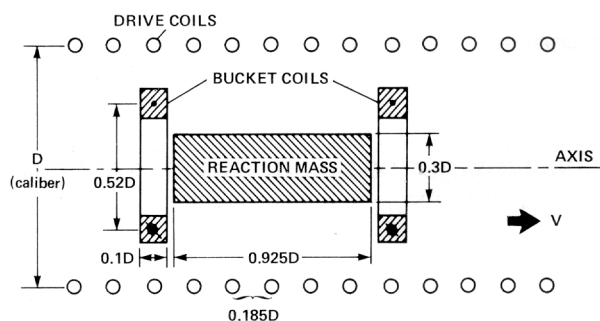

Figure 1 — *Axial configuration for mass driver. Two coils are used in the bucket; drive coils energized separately to maximize acceleration and efficiency.*

1   O'Neill, G. K.: Space Flight via Maxwell's Equations. Special Seminar Series, Department of Aeronautics and Astronautics, M.I.T., 1977 (unpublished work).

Henry Kolm and a number of the authors of this paper took part in the assembly and testing. The model, 2 m long with simplified circuits, demonstrated acceleration only; no attempt was made to combine a test of magnetic flight. It operated successfully in the acceleration range of tens of gravities and was widely demonstrated. Its design is covered in reference 7 and its construction, in reference 8.

The state of the art of the theoretical design of mass drivers as of September 1977 was summarized at the International Astronautical Federation Conference of that year (ref. 9).

EARLIER WORK ON AXIAL SUPERCONDUCTING ACCELERATORS

It has come to our attention that, in addition to the extensive bibliography listed in reference 5, a "traveling-wave accelerator" for superconducting solenoids was proposed and studied earlier by F. Winterberg and co-workers at the Desert Research Institute, University of Nevada, Reno (refs. 10, 11).

In discussing the differences between the mass-driver concept and the Winterberg traveling-wave accelerator, we should note the several key elements of the mass-driver system: a linear *synchronous* motor for acceleration, guidance by magnetic flight, and recirculation of the accelerated vehicle, with *only* the payload leaving the system. Winterberg's system differed from the mass driver in that he made no provision to maintain synchronization by silicon-controlled rectifier (SCR) switching on the basis of position sensing. Instead, the coils and capacitors were selected to form a lumped parameter transmission line having a local phase velocity that provides uniform acceleration of the traveling wave. This was accomplished by making $1/[(LC)^{-2}]$ (where L and C are inductance and capacitance per unit length) equal to the correct local velocity. Winterberg showed by approximate analysis that phase stability should be achieved. He also found that resonance (in phase) should be confined to a very small region at the beginning of the track, and that angular instability should be controllable by the relative position of the center of thrust and the center of mass of the accelerated solenoid.

He concluded, however, that there will be inherently unstable transverse translational motion because, in his system, the vehicle always rode the front crest of the traveling step function. In the axial mass driver, the bucket is first attracted and then repelled by each drive coil. Attraction has a centering effect, while repulsion has a destabilizing effect. The net stability is therefore neutral under completely symmetric timing conditions. If, however, the wave form is made asymmetric so that the attractive pulse is of larger amplitude than the repulsive pulse, then the net effect will be stabilization of lateral motion. In the latest mass-driver circuit design, it is easy to achieve stabilizing asymmetry by making the dc feeder voltages (capacitor charge) unequal to the extent required.

DESIGN RATIONALE

There are many possible choices in the design of mass drivers, and optimizations will change both as the result of further refinements in design and of improvements in materials (especially superconductors) and components (capacitors and SCRs in particular). We do not wish to halt that process of continual refinement, but we feel that the present state of knowledge is sufficient to justify setting out a "nominal" family of designs, for which the potential user can calculate performance, system mass, and sensitivities to changes in materials, components, and the main variables of payload size, repetition frequency, maximum velocity, and acceleration. Here we consider the electrical design of a particular family of mass drivers (axial geometry, with a specified value for the ratio of bucket to drive coil radii) in the approximation that accelerations are calculated for currents taken to be thin filaments. In reference 12, we consider large-scale structural questions; in reference 13, we present optimization formulas and programs.

Table 1 presents the nomenclature used in all three papers. Where the notation had already been chosen in earlier publications, we adopted the same notation. For easy reference, table 1 also contains the specific design choices corresponding to our family of designs (discussed below). With our design choices, all main dimensions of the bucket and all transverse dimensions of the drive system are fixed when the drive coil diameter D is chosen (where D is referred to as the "caliber," but it is not equal to the clear diameter through which the bucket passes; that clear diameter is smaller than D because of the finite cross section of the drive coil, necessary insulators or supports, and finite thickness of the guideway).

In table 1, several approximations are implicit. The minimum velocity is approximately zero in calculating t_a, S_a, S_d, and S_{tot}. Drift space and bucket deflection space (peel-off length) required to separate the bucket from the payload after release are neglected in calculating S_{tot}. As defined, S_{tot} is the correct parameter to use in mass-optimization formulas, but it is smaller than the physical length of the complete mass-driver system. The term L_w is based on a simple calculation of self-inductance and mutual inductance, and does not take full account of the detailed changes in currents in the drive coils adjacent to the coil whose inductance is calculated.

TRANSVERSE SCALING

For our family of designs, we have chosen to leave $\alpha = r/R$ fixed at 0.52. This choice is arbitrary; a reasoned choice would require knowledge we do not yet have, as we now show.

The magnetic-flight guidance forces are restoring for the two orthogonal position oscillations in the transverse direction and the two orthogonal angular oscillations. To first order, longitudinal motion depends only on the drive currents, and there is no restoring force for the roll mode. A practical

mass driver might be wound with bucket and drive coils slightly noncircular to provide a restoring torque for roll.

We chose, in our family of designs, to scale all linear dimensions of the bucket with caliber D, and now calculate the approximate transverse oscillation frequency for $D = 5.0$ cm. We consider the guideway to be composed of eight strips of equal width and approximate the bucket coil as octagonal (see fig. 2). Assume that a particular current element of the bucket of length y is influenced only by the parallel guideway strip nearest to it. Thus, for each of the eight bucket coil sides, only a single image current is needed to describe the force F felt by that side. When the bucket is centered,

$$F = (\mu_o i_B^2 y) / (2\pi)$$

where $y = 2\alpha D$ (tan $45°/2$) and μ_0 is the permeability constant. To sum the forces on all sides of the bucket when the bucket is displaced a distance x from the centerline position, the restoring force that acts to return the bucket to the centered position is

$$F = (4\mu_o i_B^2 xy) / (2\pi s^2)$$

Here half of the contribution to the restoring force comes from sides 1 and 5, while half comes from side 4, 6, and 8. The corresponding spring constant 2000 N/m. For $s = 0.3$ $D/2$, leaving a distance 0.18 $D/2$) for the finite half-thickness of the drive coils, for insulation, and for the finite thickness of the guide strips, the restoring force for larger displacements is given figure 3. For bucket mass given by our nominal design, the corresponding oscillation frequency is 37.3 Hz. The notation in this derivation, as in table 1, is that of reference 4.

Consider next the effect on bucket transverse motion caused by scaling mass-driver linear dimensions proportional to D. The dimensions R, r, s, and y all scale linearly with D. The cross-sectional area of the bucket coil is D^2. If it is assumed that the current density in the superconducting bucket coil remains constant, the current flow i_B will also scale as D^2. By substituting these scaling factors, the restoring force on the bucket scales as D^4.

The spring constant K will vary as D^3 since it is the restoring force F divided by the linearly scaling distance s. The bucket mass will also increase as D^3. Consequently, the frequency of bucket oscillation, equal to $(K/m_B)^{-2}$, will be invariant to the caliber D, and so the maximum tolerable angle of bucket motion relative to the axis will also scale as D.

In the absence of active feedback from steering coils placed at intervals along the guideway, the bucket oscillation amplitude would slowly build up as a result of misalignments along the accelerator. There is an extensive literature treating such oscillations, as a result of the 30 years of previous development of particle accelerator theory and practice. At a more sophisticated level of design knowledge on mass drivers, it will be necessary to investigate how the misalignments that drive oscillation buildup scale with D. At our present level, we must close the argument at this point with the comments that we lack sufficient knowledge
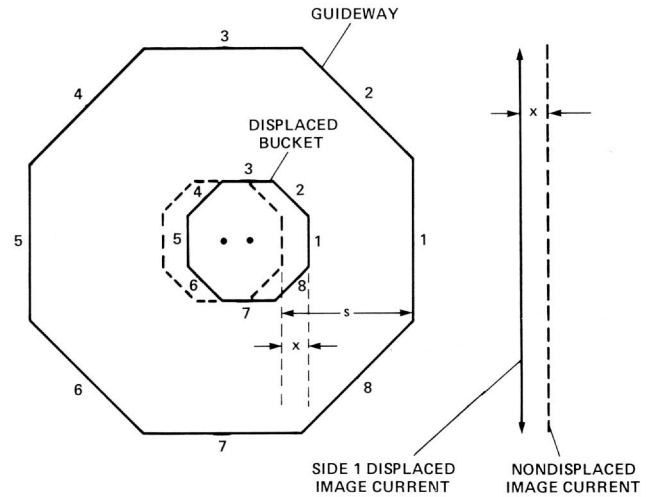

Figure 2 — *Geometric approximation used in calculating to first order the guidance forces in magnetic flight of bucket through guideway.*
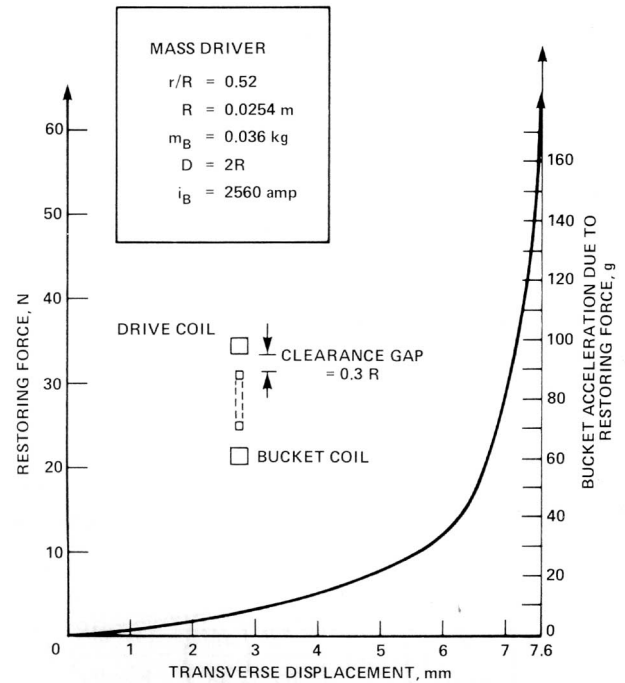

Figure 3 — *Restoring force profile as calculated in approximation represented by figure 2.*

to proceed further, and that active feedback should be much easier in our case than for particle accelerators: we are dealing with a macroscopic bucket, of fixed shape, whose position can be measured to very high precision by optical scanning. The bucket moves very slowly compared to the velocity of light, so there is ample time to measure, calculate, and feed back correction currents to steering coils located at intervals along the guideway. In reference 13, we show that the mass of a total optimized accelerator changes only slowly as a function of D so long as the mass flow dm_1/dt and v_{max} are held constant. Therefore, the choice of D does not appear to be critical and can be deferred until a more thorough understanding of misalignments is reached.

TABLE 1 — NOTATION AND DESIGN PARAMETERS FOR MASS DRIVER

Symbol		Design choice
Bucket		
i_B	current in each coil, A	$2.5 \times 10^6 D^2$
m_B	mass of empty bucket, kg	$296D^3 = 2.263m_1$
m_{BL}	mass of loaded bucket, kg	$3.263m_1$
m_{BC}	mass of each coil, kg	$74D^3$
m_1*	mass of expelled segments, kg	m_1
n_C	number of bucket coils	2
r	radius of bucket coil from axis, m	$0.26D$
V_{BC}	volume of each coil, m^3	$1.634 \times 10^{-2} D^3$
W_B	width of square bucket coil, m	$0.1D$
Drive system		
A_{DO}	cross-sectional area of drive winding, m^2	To be optimized
A_{fo}	cross-sectional area of feeder lines, m^2	To be optimized
a	acceleration delivered to m_{BL}, m/s^2	a
D	mean diameter of drive coil $\equiv$ caliber, m	$0.197m_1^{1/3}$
f_m	microduty cycle, s^{-1}	1
f_R*	repetition (launch) rate, sec^{-1}	f_R
i	feeder current, A	i_D/n_2
i_D	ampere turns peak, each drive winding, ampere-turns	$0.435m_1a/D^2$
L_w	single-turn inductance of drive winding including mutual, henries	$2.004 \times 10^{-6} D$
ℓ_m	inductance length = drive coil spacing, m	$0.185D$
ℓ_P	phase length or wavelength $\equiv 4\ell_m$, m	$0.74D$
ℓ_s	sector length, m	To be optimized
ℓ_w	length of drive winding (circumference), m	πD
N_w	total number of drive windings per phase	$1.351 V_{max}^2/aD$
n_w	number of simultaneously excited drive windings per sector capacitor with bridging	2
n_2	number of turns each drive winding	
R	mean radius of drive coil from axis, m	$D/2$
S_a	acceleration length, m	$V_{max}^2/2a$
S_d	deceleration length, m	$m_B/m_{BL}S_a = 0.694S_a$
S_{tot}	total length of driver, m	$1.694S_a$
t_a	acceleration time, sec	V_{max}/a
V	local velocity of bucket, m/sec	V
V_{max}*	launch or exhaust velocity, m/sec	V_{max}
α	ratio of radii of bucket and drive coils	$r/R = 0.52$
ϕ	number of phases	2
ω_{LC}	ringing frequency (= $2\pi V/\ell_p$), sec^{-1}	$1/\sqrt{2L_wC}$
ω_{max}	maximum ringing frequency, sec^{-1}	$8.489 V_{max}/D$

* Denotes fundamental mass-driver mission variable.

Radius Ratio

Tighter coupling would be obtained with a higher value of the radius ratio r/R. However, this would reduce the clearance gap between bucket and guideway. For $\alpha = 0.52$ (from ref. 4) and for bucket and drive coil widths of $0.1D$, the total allowance for insulation, guide strips, clearance, and thermal insulation surrounding the superconducting coil is $0.14D$, or 0.7 cm for $D = 5$ cm. It does not seem realistic to reduce clearance by using a much higher value of α; the dependence of the peak gradient of mutual inductance on r/R is shown in figure 4, along with the peak mutual inductance with respect to r/R, which also does not justify a tighter coupling.
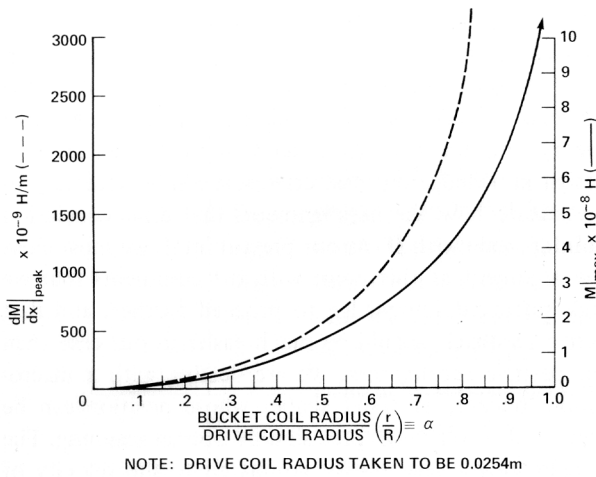
Figure 4 — *Variation of peak value of dm/dx, mutual inductance axial gradient, with* r/R *of bucket/drive coil radii.*

Bucket Coil Cross Section

We chose square coils of width $0.1D$. If the coils were much thicker, the drive current pulse could not be timed to optimize the drive simultaneously on all parts of the drive coil, and therefore the efficiency would be lost. Our choice could probably be altered by ± 25 percent.

Superconducting Cable Density and Current

We chose 25,000 A/cm² at an average density of 4.53×10^3 kg/m³, the same values discussed in reference 5. The choice rests on practical operating experience with the M.I.T. magneplane model.

Drive Frequency, Coil Spacing, and Energy Transfer

The instantaneous force on one bucket coil due to one drive coil is $i_B(dM/dx)i_D(t)$, where $i_D(t)$ is the value of the ampere-turns in the drive coil at time t (ref. 4). In reference 6, it was found convenient to integrate the drive force over the x region of drive coil excitation, to obtain the total energy change imparted to each bucket coil in traversing each drive coil. During the same interval, the energy loss in the drive coil is proportional to $\int i_D^2(t)\,dt$. We therefore obtain maximum energy transfer to the bucket, at minimum power loss in the drive coil, by maximizing $[\int i_B(dM/dx)i_D(t)\,dx]/\int i_D^2(t)\,dt$. The problem is slightly complicated by the fact that the induced EMF caused by the moving bucket coil in the drive coil affects di_D/dt; the current cycle in the drive winding is therefore not exactly sinusoidal when a charged capacitor is connected to the winding.

Although our actual basic drive circuit consists of two drive coils, separated by the spacing of the bucket coils and operated in series from a capacitor, that circuit is equivalent to the simpler one shown in figure 5; that is, a single drive coil with its self-inductance, mutual inductance, and internal resistance, across a capacitor, with an additional generator corresponding to the induced EMF due to bucket motion. The differential equations that describe the current variation in that circuit are
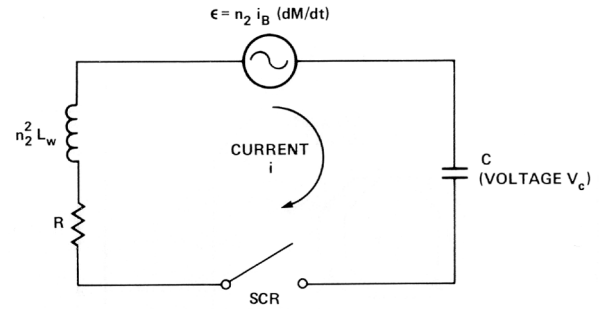

Figure 5 — *Equivalent circuit for electrical drive; single coil shown represents two adjacent drive coils of one phase, connected through a neutral bus.*

$$V_c - n_2{}^2 L_w\left(\frac{di}{dt}\right) - n_2 i_B\left(\frac{dM}{dt}\right) - iR = 0$$

$$v = \frac{dx}{dt}$$

$$i = C\left(\frac{dV_c}{dt}\right)$$

where t is time, dM/dt is the time rate of change of the mutual inductance between the total current of one bucket coil and one turn of the drive coil, and R is the resistance of a drive winding having n_2 turns. By the chain rule,

$$n_2 i_B\left(\frac{dM}{dt}\right) = n_2 i_B\left(\frac{dM}{dx}\right) v$$

For numerical computation, we put these formulas into difference-equation form with V_c and i as functions of x rather than of t and solve for Δi and ΔV_c:
for stepwise integration with a step interval Δx. The velocity

$$\Delta i = \left(\frac{\Delta x}{vL_w n_2{}^2}\right) V_c - \frac{(\Delta x)i_B}{L_w n_2}\left(\frac{dM}{dx}\right) - \frac{(\Delta x)R}{vL_w n_2{}^2}\, i$$

$$\Delta V_c = -\frac{(\Delta x)}{vC}\, i$$

v is considered to be constant over the short interval in x over which one drive coil acts — an excellent approximation for all but the first few drive coils of the accelerator. Cast in this form, dM/dx is an explicit function of x, independent of n_2 but dependent on the caliber D. For purposes of calculation, the four constants appearing in the difference equations are called successively a_1, a_0, a_3, and a_4.

The calculation can be carried out with high accuracy by use of a program for dM/dx (see appendix A), combined with a difference-equation routine. Alternatively, a good approximation is obtained much more compactly by a simpler program (see footnote 1) (appendix B). This program carries out the stepwise integration of the difference equations for V_c and i, and yields the total energy transfer to the bucket coil; the program occupies less than 50 program steps and so can be run on even a small programmable calculator.
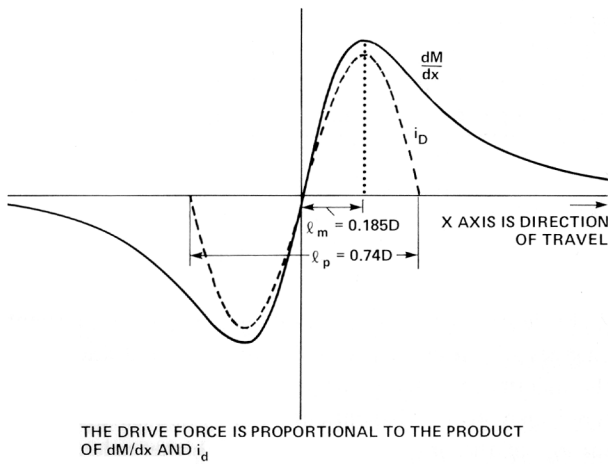
dM/dx CURVE AND DRIVE CURRENT WAVEFORM

$\frac{dM}{dx}$

i_D

$\ell_m = 0.185D$

$\ell_p = 0.74D$

X AXIS IS DIRECTION OF TRAVEL

THE DRIVE FORCE IS PROPORTIONAL TO THE PRODUCT OF dM/dx AND i_d

Figure 6 — *Matching of the drive current wave form to shape of* dM/dx *curve, for approximate maximization of drive efficiency.*

By use of this simple program, it was found in the paper in footnote 1 and noted in reference 6 that a very good, although not necessarily an ideally optimized, solution is obtained by matching the peak in the $i(x)$ curve to the peak in the curve of dM/dx (fig. 6). If that is done, the sine wave of the drive current is turned on when the bucket coil is a distance $0.37D$ before the drive coil. We call the distance $0.185D$, the "inductance length," ℓ_m.

We obtain a particularly simple geometry and drive circuit by choosing a spacing between drive coils equal to the inductance length. In that case, successive coils carry currents 90° apart in phase. Only two independent circuits are needed to feed all coils in a given region of the accelerator, one circuit for even-numbered coils, another circuit to feed odd-numbered coils.

Number of Bucket Coils

With progressive refinement of our understanding, we have adopted a drive system in which each coil is separately excited (ref. 5) through its own switches (SCR's). For historical reasons, the number of bucket coils previously chosen was four, in the case of axial symmetry. However, with each drive coil separately excited, we consider anew the question of the optimum number of bucket coils.

For stability against pitch and yaw, the minimum number of bucket coils is two. A possibility (not considered further here) is that one of these two coils might carry most of the total current, the other having low mass and current and intended only to provide stability. Consider two alternative bucket designs, of the same total superconductor mass, divided in one case into four coils and, in the other, into only two coils, To provide equal total energy transfer to the moving bucket, the drive currents required are the same in both cases because that energy transfer is proportional to the product of peak drive current, current per bucket coil, and number of bucket coils. However, for two coils, each drive winding need only be excited for two complete sine waves, while for four coils, four cycles of excitation are needed.

Therefore, the power loss is reduced one-half with two coils, for equal drive-winding mass. Our choice is thus $n_c = 2$.

Feeder losses are also reduced in the two-coil case. For full drive in these drive windings, current must precede and follow each bucket coil. In the notation in reference 5, the number n_w of windings simultaneously excited is reduced from six for four coils to four in the case of two coils. In the section on drive circuit, we reduce n_w to two. Figure 7 traces the winding currents as the bucket moves.

Bucket Length

The spacing between the two bucket coils could be any multiple of the spacing between drive coils. We adopt a specific value, with the note that changing to a longer bucket to accommodate a low-density payload would have little effect on bucket mass and no effect on accelerator mass. Given sufficient built-in flexibility in the coil triggering system, it may be possible to accommodate different bucket lengths even in a single accelerator.

Limits on Drive-Coil Spacing

We have chosen for simplicity a two-phase drive system, with the spacing between coils equal to ℓ_m. All coils are connected in the same sense, and the bipolar feeder always sends current to two adjacent coils of one phase, which are connected by a common neutral (fig. 8). From the viewpoint of placing the drive currents in the best possible geometric location, drive windings should probably be distributed uniformly, in a thin layer forming a continuous solenoidal coil. That alternative will be studied in the future. We consider here the practical limits on coil spacing set by the simplicity of the circuit we have adopted, but allowing for the possibility of a multiphase drive (more than two phases).

FIRST SNAPSHOT

PUSH
PULL

PHASE

PHASE 1
PHASE 2

BUCKET COIL   VELOCITY

SECOND SNAPSHOT, 45° LATER
IN PHASE: CURRENTS 0.707 OF PEAK.

PHASE 1   PHASE 2

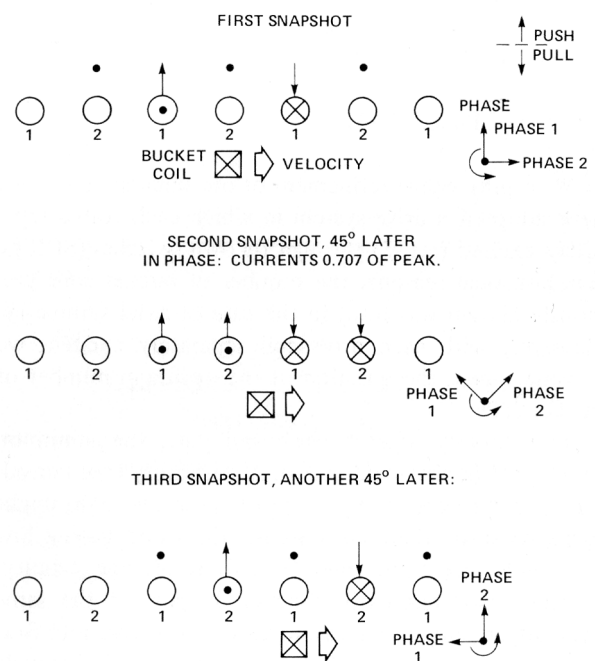THIRD SNAPSHOT, ANOTHER 45° LATER:

PHASE 2

PHASE 1

Figure 7 — *Phase and amplitude of drive currents as bucket moves through drive coils.*
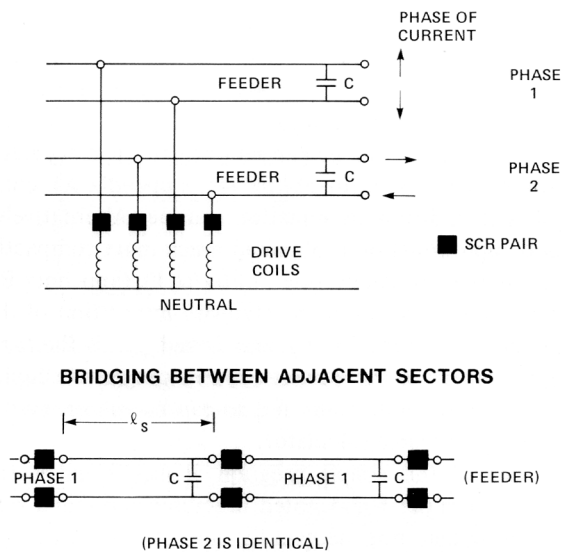
Figure 8 — *Electrical circuit for bipolar two-phase system, with bridging switches between sectors to reduce the optimized mass of capacitors and feeders.*

In the mass optimization for the entire mass driver, feeder and capacitor mass can be saved by operating with each drive winding subdivided into n_2 turns, with n_2 as large as possible. For typical mass-driver parameters, the most serious limit on n_2 is set by the mutual inductance M_D between drive windings. For drive ampere-turns i_D, the induced voltage from this source is $(n_2 M_D))\omega_{LC} iD$. This effect increases the SCR standoff voltage by a certain fraction, independent of acceleration.

The fractional induced voltage is approximately inversely proportional to spacing. For an actual multiphase system, it is necessary to sum the effects of all coils appropriately phased, as summarized below for $n_2 = 1$.

Drive coil spacing, cm	Total induced voltage as fraction of applied voltage
1.0	0.28
.6	.72
.2	2.24
.1	4.4

Evidently, the induced voltage caused by current changes in adjacent drive coils limits n_2 and also limits the minimum spacing between drive coils. Our choice (equivalent to the 1.0-cm entry) allows moderate values for n_2, of the order of 2 or 4. Much higher values of n_2 would result in a much-increased standoff requirement for the SCR's.

Payload Dimensions

The bucket length ℓ_B is chosen as six drive coil spacings ($6\ell_m = \ell_B = 1.11D$). The length of the payload is chosen to be $5/6$ of this or $0.925D$. To provide a reasonable clearance gap between the payload and bucket coils (to accommodate magnetic shielding, insulation, payload holder, etc.), the radius of the cylindrical payload is chosen as $r_p = 0.3R$. Thus the clearance gap between the outer surface of the payload and the bucket coils is $0.12R = 0.06D$. The ratio of

bucket length/diameter is thus 1.95 (taking into account the finite thickness of the bucket coils) and the ratio of payload length to diameter is 3.08.

For a payload of density ρ_p, the caliber D is then

$$D = 3 \sqrt{m_1 (6.54 \times 10^{-2}) \rho_p}$$

We assume a nominal $\rho_p = 2 \times 10^3$ kg/m³.

Drive Circuit

There are two bipolar feeder lines (two split phases) plus one neutral line, and the two feeders are in quadrature, that is, their currents differ in phase angle by 90°. Drive coils are all identical and are connected to the neutral line on one side, their other side being connected to the four feeders of alternating side and alternating phase (fig. 8). The resulting phasor diagrams are also shown in figure 8. Note that there are only four simultaneously excited coils during the passage of one bucket coil, and that there are always two coils connected *in series* across one bipolar feeder pair, although the coil connections progress in a leapfrog fashion along the feeder pair. Each coil is fired independently by its own bipolar SCR, which conducts during one entire 360° cycle, whose period is matched approximately to the local velocity by the choice of local LC product.

Bridging SCR's connect adjacent feeder pairs so long as a bucket occupies one of them. This arrangement eliminates the need to double the capacitor energy of individual sector capacitors to allow for the fact that two bucket coils will occupy each sector most of the time. Bridging SCR's allow each bucket to derive energy from two adjacent feeder sectors, and the average conduction distance remains unchanged. Feeder power loss is unaffected, and the number of windings simultaneously driven by one sector capacitor n_w is reduced to two.

The ringing frequency of the drive circuit (ω_{LC} in previous terminology) is chosen to make the coil spacing or inductance length equal to one-quarter wavelength:

$$f = \frac{\omega_{LC}}{2\pi} = \frac{v}{4\ell_m} = \frac{v}{\ell_p}$$

The "microduty cycle" defined in reference 6 is now unity. The feeders carry continuous current.

SUMMARY

In this discussion of mass-driver electrical design, several small improvements have been made relative to our previous studies. The bucket design is simplified by reducing the number of coils to two. That change reduces winding losses by $1/2$ and feeder losses to $2/3$ the previous value. Feeders are reduced from three phases to two. Bridging SCR's offer savings by a factor of 2 in the total capacitor energy storage required. Our application of these changes to the reoptimization of total system mass is treated in reference 13. At a later time, it would be worthwhile to consider a wider class of designs than those we treat here. Although it

seems unlikely that large improvements are yet to be made, it may well be that our design is as much as 20% away from an optimum system mass.

APPENDIX A

MUTUAL INDUCTANCE OF TWO COAXIAL COILS

This program computes the mutual inductance of a pair of coaxial circular coils as a function of the two radii and their axial separation (see tables 2-4). All units are MKS. The geometry of the coils is shown in sketch to the right.
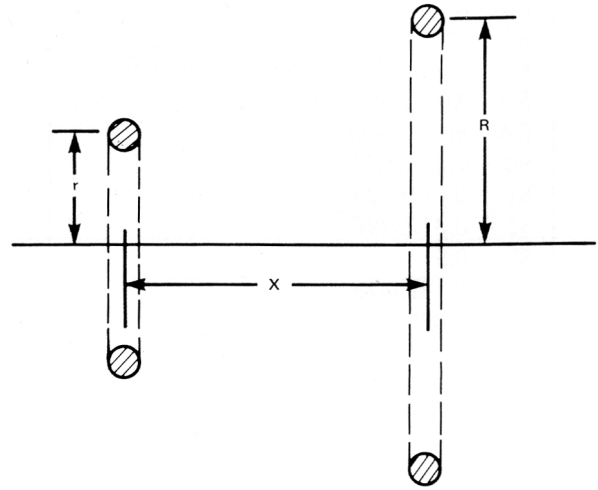
TABLE 2 — INSTRUCTIONS FOR USE

Step	Instructions	Input data/units	Keys	Output data/units
Step	Instructions	Input data/units	Keys	Output data/units
1	Load sides 1 and 2.			
2	Load data card containing constants into secondary for evaluation of elliptic integrals (all dimensions in m).			
3	Enter first coil radius	r	ENT	
4	Enter second coil radius	R	ENT	
5	Input coil spacing	x	A	M
	After coil radii have been input once, the variation of M with x can be found as follows:			
6	Enter coil spacing	x	D	M

TABLE 3 — REGISTERS USED IN MUTUAL INDUCTANCE PROGRAM

R0	First coil radius
R1	Second coil radius
R2	Coil spacing
R3	Ratio of coil radii
R6	k
R7	$m = k^2$
R8	$E(m)$, elliptic integral of first kind
R9	$K(m)$, elliptic integral of second kind
RA	$m_1 = 1 - m$
S0	1.3862944
S1	0.1119723
S2	0.0725296
S3	0.5
S4	0.1213478
SS	0.0288729
S6	0.4630151
S7	0.1077812
S8	0.2452727
S9	0.0412496

M= mutual inductance of coil pair (henries)

$$= \frac{8\pi \times 10^{-7}\sqrt{rR}}{k}\left[\left(1 - \frac{k^2}{2}\right)K - E\right]$$

where

$$k^2 = m = \frac{4rR}{[(R + r)^2 + x^2]}$$

Complete elliptic integrals of the first and second kind are

$$E(m) = \int_O^{\pi/2} \sqrt{1 - m \sin^2\theta}\ d\theta$$

$$K(m) = \int_O^{\pi/2} d\theta/\sqrt{1 - m \sin^2\theta}$$

The test case is: $r = 0.2$, $R = 0.25$, and $x = 0.1$, which should be inserted as follows: 0.2 [ENT↑] 0.25 [ENT↑] 0.1 [A] → 2.4877 X 10^{-7} at $x = 0.2$ m, 0.2 [D] → 1.23945 X 10^{-7}. Rational approximations to $K(m)$ and $E(m)$ are from reference 14.

APPENDIX B

CALCULATION OF REQUIRED DRIVE CURRENT i_D

In the text, a difference equation is obtained from which the energy transfer from the drive to the bucket coil can be found as a function of i_D, with the circuit constants n_2, L_w, and C, and velocity v as parameters. The program in this appendix solves the difference equations, with the help of an approximation for dM/dx. The entire program is designed to run on an HP-25 pocket calculator with 49 program steps. Given a larger calculator or computer, one could generalize the program by using a more exact expression for dM/dx or (more usefully) by including the finite cross sections of the drive and bucket coils.

TABLE 4 — CALCULATOR PROGRAM FOR MUTUAL INDUCTANCE OF TWO COAXIAL COILS

Step	Key entry	Comments	Step	Key entry	Comments	Step	Key entry	Comments
001	*LBL A		040	RCL 1		080	RCL A	
	STO 2	x		x			1/x	
	R↓			√			LN	
	STO 1	R		x			x	
	R↓			8			+	
	STO 0	r		x			P⇌S	
	*LBL a			π			STO 9	$K(m)$
	RCL 0			x			P⇌S	
	RCL 1			RCL 6			RCL 7	
010	÷			÷			RCL A	
	STO 3	$\alpha = r/R$	050	EEX		090	x	
	RCL 0			CHS			RCL 6	
	RCL 1			7			+	
	+			x			RCL A	
	x^2			RTN			x	
	RCL 2			*LBL E			1	
	x^2			RCL 7			+	
	+			1			RCL 9	
	1/x			–			RCL A	
020	4			CHS			x^2	
	x		060	STO A		100	x	
	RCL 0			P⇌S			RCL 8	
	x			RCL 2			RCL A	
	RCL 1			RCL A			x	
	x			x			+	
	STO 7	$k^2 = m$		RCL 1			RCL A	
	√			+			1/x	
	STO 6	k		RCL A			LN	
	GSB E			x			x	
030	1			RCL 0			+	
	RCL 7		070	+		110	P⇌S	
	2			RCL 5			STO 8	$E(m)$
	÷			RCL A			RTN	
	–			x			*LBL D	
	RCL 9			RCL 4			STO 2	
	x			+			RCL 0	
	RCL 8			RCL A			GTO a	
	–			x		117	RTN	
	RCL 0			RCL 3				
				+				

The simple program consists of four subroutines:

- Update x
- Calculate dM/dx
- Solve difference equation
- Test for zero current

In normal use, registers R5 and R7 (summation of $i(dM/dx)$ and i) are initialized to zero. Register 6 (V_C) is set to the initial voltage on the capacitor. The calculator is started, and the program then traces the half-cycle of oscillation from the starting value of x (normally a negative number stored in R1) until current i goes negative. The summation is then recalled from R5, and the calculation is repeated with different values of V_C until the correct value of the sum, corresponding to the desired energy transfer to the bucket, is found. The peak drive current i_D is then obtained from

$$CV_C{}^2 = L_w i_D{}^2$$

For still higher accuracy, the curve of i_D is traced point-by-point by slightly modifying the program: step 47: pause, step 48: pause.

In this program, one or two minor tricks are used to save register space: the constant a_1, which equals a_3/R, is stored as a sequence of four key strokes in steps 31-34. Register 2 contains a constant whose integer and fractional parts are both used in the dM/dx subroutine. The step interval Δx appears as a sequence of four key strokes in steps 01-04. (All

TABLE 5 — REGISTERS USED IN ENERGY TRANSFER PROGRAM

R0	$a_0 = (\Delta x) i_B / L_w n_2$
R1	Initial value of position x (in m) at which drive coil switch is closed. Zero is allowed, but constant should be chosen so that x update subroutine never finishes with zero. R1 stores updated x.
R2	a_2 = const used in dM/dx subroutine. For $D = 5.0$ cm, a_2 = -184.000138 (i.e., INT = -184, FRAC = -0.000138). For other calibers D, INT and FRAC are proportional to D.
R3	$a_3 = (\Delta x) R / v L_w n_2{}^2$. Drive winding resistance R appears only in this constant.
R4	$a_4 = (\Delta x)/vC$. Resonant capacity C appears only in this constant and is equal to the sum of capacities on two adjacent sectors of the actual mass driver.
R5	Initialize to zero; stores updated $\Sigma i (dM/dx)$.
R6	Peak voltage to which capacitor is charged before drive circuit switches on; R6 stores updated capacitor voltage V_c.
R7	Initialize to zero; stores updated current i.

constants are in MKS units.) In detail, the registers store information as shown in table 5.

As normally used, the program calculates the energy transfer for a half-cycle of oscillation. The total energy transfer for a two-coil bucket, corresponding to the passage of both bucket coils through one drive coil, is then $(\Delta x)(4n_2 i_B)$ (summation of $i_D M/dx$ in register 5).

Typically, a step interval Δx of 1 mm is used, 0.001 in program steps 01-04. Each step interval requires 3.75 sec on an HP-25, and about twice that time on an HP-67, so a half-cycle of oscillation with $D = 5.0$ cm requires a little over 1 min (see table 6).

REFERENCES

1. O'Neill, Gerard K.: The Colonization of Space. Physics Today, vol. 27, no. 9, Sept. 1974, pp. 32-40.
2. O'Neill, Gerard K.: Summarization of Conference: The Colonization of Space, in Space Manufacturing Facilities (Space Colonies). 1975 Princeton/AIAA/NASA Conference (including May 1974 Princeton Conference on Space Colonization), Jerry Grey, ed., March 1, 1977, AIAA, pp. A-61-69.
3. Kolm, H. H.; Thornton, R. D.; Iwasa, Y.; and Brown, W. S.: The Magneplane System. Cryogenics, vol. 15, no. 7, July 1975, pp. 377-384.
4. Clulton, F.; Hibbs, B.; Kolm, H.: O'Neill, G. K.; and Phillips, J.: Electromagnetic Mass Drivers, in Space-Based Manufacturing from Nonterrestrial Materials. Progress in Astronautics and Aeronautics, vol. 57, AIAA, New York, 1977, pp. 37-61; also NASA TM X-73,265, Aug. 1977.
5. Chilton, F.; Hibbs, B.; Kolm, H.; O'Neill, G. K.; and Phillips, J.: Mass-Driver Applications, in Space Based Manufacturing from Nonterrestrial Materials, Progress

TABLE 6 — CALCULATOR PROGRAM FOR ENERGY TRANSFER TO MOVING BUCKET

01	}	ΔX stored in four keystrokes
02		
03		
04		
05	STO + 1	(updates X)
06	RCL 1	(X + ΔX)
07	RCL 2	Start
08	FRAC	
09	X	
10	RCL 1	dM/dx subroutine. Starts with X in $\underline{X}$ and in register 1. X = 0 illegal
11	ABS	
12	1	
13	.	
14	1	
15	7	
16	y^X	
17	RCL 2	
18	INT	
19	X	
20	e^X	
21	X $-(dM/dx)$	END
22	↑	START
23	↑	
24	RCL 7	$\underline{X} = i$ y - $\underline{z}$ = t
25	X	$= -dM/dx$
26	ST – 5	Update + $\Sigma i (dM/dx)$
27	↑↓	
28	RCL 0	
29	X	
30	RCL 6	
31	}	a_1 Stored in four keystrokes
32		
33		
34		
35	X	Difference equation subroutine
36	+	
37	RCL 3	
38	RCL 7	
39	X	
40	–	Δi
41	ST + 7	update i
42	RCL 7	
43	RCL 4	
44	X	ΔV_c
45	ST – 6	update V_c END
46	RCL 7	
47	X < 0	Test for zero crossing
48	STOP	
49	GTO 01	

in Astronautics and Aeronautics, vol. 57, AIAA, New York, 1977, pp. 63-94; also as NASA TM X-73,265, Aug. 1977.
6. O'Neill, G. K.: Mass-Driver Reaction Engine as Shuttle Upper-Stage, AIAA Paper 77-536, 1977.
7. Kolm, H.: Basic Coaxial Mass Driver Reference Design, AIAA Paper 77-534, 1977.
8. Fine, K.: Basic Coaxial Mass Driver Construction and Testing, AIAA Paper 77-535, 1977.

9. Kolm, H.; and O'Neill, G. K.: Mass Driver for Lunar Transport and as a Reaction Engine. International Astronautical Federation Paper 77-74, XXVIIIth Congress, Prague, Sept. 1977.

10. Winterberg, F.: Magnetic Acceleration of a Superconducting Solenoid to Hypervelocities. Plasma Physics, Part C, vol. 8, 1966, pp. 541-553.

11. Anderson, D.; Claflin, S.; and Winterberg, F.: On the Acceleration of a Superconducting Macroparticle in a Magnetic Travelling Wave Accelerator Z. Naturforschung, vol. 26A, issue 9, 1971, pp. 1415-1424.

12. Arnold, W.; Bowen, S.; Fine, K.; Kaplan, D.; Kohn, H.; Kolm, M.; Newman, J.; O'Neill, G. K.; and Snow, W.: Mass Drivers II: Structural Dynamics. Space Resources and Space Settlements. NASA SP-428, 1979, pp. 86-100.

13. Arnold, W.; Bowen, S.; Cohen, S.; Fine, K.; Kaplan, D.; Kolm, H.; Kolm, M.; Newman, J.; O'Neill, G. K.; and Snow, W.: Mass Drivers III: Engineering. Space Resources and Space Settlements. NASA SP-428, 1979, pp. 100-130.

14. Abramovitch, Milton; and Stegun, Irene A.: Handbook of Mathematical Functions with Formulas, Graphs, and Mathematical Tables. Dover Publ., New York, 1965.

III-2
Mass Drivers II:
Structural Dynamics

WILLIAM H. ARNOLD, STUART BOWEN, KEVIN FINE, DAVID KAPLAN, MARGARET KOLM, HENRY KOLM, JONATHAN NEWMAN, GERARD K. O'NEILL, and WILLIAM R. SNOW

Various structural and dynamical problems related to both small-scale forces between the drive coils and within the bucket structure as well as the overall combined large-scale dynamical interaction of the bucket stream and MDRE structure are examined. The large-scale dynamics appear weakly stable. Finally, MDRE operation in an inverse-square law gravitational field is discussed and the required curved shape of the guideway is computed.

INTRODUCTION

In the following sections we discuss various structural and dynamical problems associated with operation of mass drivers. First, because of the very large accelerations ($\sim 10^3$ - 10^4 m/s^2) we are concerned with the various forces and stresses between the drive coils and within the bucket; in particular, the stresses on the super-conducting coils. We then compute the "tear-off point," that point along the MDRE at which the feeder structure alone can no longer support the imposed axial stress, and supplemental strengthening must be incorporated, probably in the form of steel cables.

We next examine the large-scale dynamical interaction of the bucket stream with the primary load bearing MDRE electrical structure. The bucket stream is modeled as a fluid stream whose acceleration along the limp MDRE structure provides the tension force in both the acceleration and deceleration section. The transverse oscillations of this structure are computed. Finally some consideration is given to the problems of steering a MDRE and the requirements for operation in an inverse-square gravitational field. In particular the necessary changes to the nominal straight form of the MDRE in free space are computed for operation in a gravitational field.

SMALL-SCALE FORCES AND STRESSES

Mass Driver Structure

Viewed in the macroscopic scale, the mass-driver (MD) structure experiences an overall tension which is due to the gross acceleration of buckets down the length of the track. Under closer examination, however, the forces that act on the support structure between individual drive coils are seen to behave in a manner such that both local compression and local tension are experienced. To determine the stresses to which the support structure between drive coils will be subjected, and hence must be designed to withstand, it is necessary to first determine a time-dependent description of the small scale forces acting on any individual drive coil. With this in hand, it will then be possible to come to some conclusion concerning the forces exerted on the structure between two adjacent drive coils.

Due to the triggering mechanism in the electric circuit, current is permitted to flow in a drive coil only when a bucket coil is within a distance of $2\ell_m$ from that drive coil. During the period in which it is on, the drive coil will experience inductive forces not only with the bucket coil, but also with other neighboring drive coils which themselves have current flow. Calculations reveal that the reaction force on the drive coil due to the bucket coil is actually an

order of magnitude smaller than the reaction forces due to the other neighboring drive coils.

The force interaction between the bucket coil and the drive coil is described by the equation (ref. 1):

$$F = i_B i_D \, dM/dx \quad (1)$$

where i_B is the constant current in the bucket; i_D is the time-varying current in the drive coil; and dM/dx is the gradient of the mutual inductance between drive and bucket coils and is a function of distance separating the coils. Figure 1 plots the reaction force felt by a drive coil due to the passage of a bucket coil. While the force calculations presented are made for the specific case of a mass driver reaction engine of caliber 0.0508 m (ref. 2), they are nonetheless typical of all mass drivers in terms of general behavior (though not necessarily in terms of magnitude). Because of the antisymmetry of both the i_D and dM/dx curves, the bucket coil receives twin impulses from the drive coil — first it is pulled toward the drive coil as it approaches, and next it is shoved away from the drive coil as it departs downstream.

The second source of forces acting on the drive coil results from inductive interactions with other active neighboring drive coils. These forces are described equally well by equation (1) if the neighboring drive coil current is substituted for the bucket current and a different dM/dx curve, one applicable to equal radii coils, is used.

Over a short distance (typically several centimeters), it is reasonable to assume that bucket velocity V is constant. With a fixed drive coil spacing (ℓ_m), then, the time the bucket coil takes to travel from one drive coil to the next, t, is also constant and equal to ℓ_m/V. The current flow in each drive coil is sinusoidal, and designed to have a period of $4t$. Consequently, any two adjacent drive coils, if active, will be 90° out-of-phase with each other, and at any particular moment, current will be simultaneously flowing in four contiguous drive coils. Figure 2 indicates which drive coils will be active during each of four quarter-wave phases of a reference drive coil. The appendix documents the specific
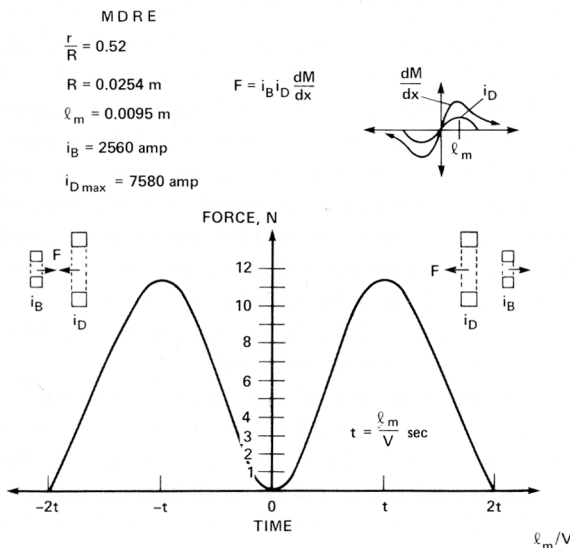
force equations and presents a calculator program to solve those equations. The results from the appendix are plotted in figure 3.

Through the superposition of the force exerted on a drive coil due to passage of a bucket coil and the force exerted on that drive coil due to its neighboring drive coils, a complete description of the total force exerted on the drive coil may be ascertained. A plot of this is shown in figure 4, from which it may be seen that the coil experiences forces in both the positive and negative directions.

With a knowledge of the behavior of the force on the individual drive coil, attention may now be focused on the stresses applied to the structure between any two adjacent drive coils. Consider a section of the mass driver track in which the bucket velocity is substantially less than the speed of sound for the support structure material (for aluminum, approximately 5000 m/sec). If the velocity of the bucket is assumed to be constant, then each drive coil will propagate identical stress waveforms with identical periods, and the net force felt by a structural member joining two adjacent drive coils will be the difference in the instantaneous force exerted on each coil individually. Figure 5 graphically displays this difference in force (assuming constant bucket velocity) for the example mass-driver reaction engine. From this figure, it may be observed that the tension to be sustained in the material is roughly twice as great as the compression and is of a magnitude approximately double that of the maximum force acting on an individual drive coil.

If the bucket velocity is equal to or in excess of the speed of sound for the structural material, then the stress wave caused by the passage of a bucket coil will never reach the following sequential drive coil before the time that that coil starts to propagate its own stress wave. Considering the bucket
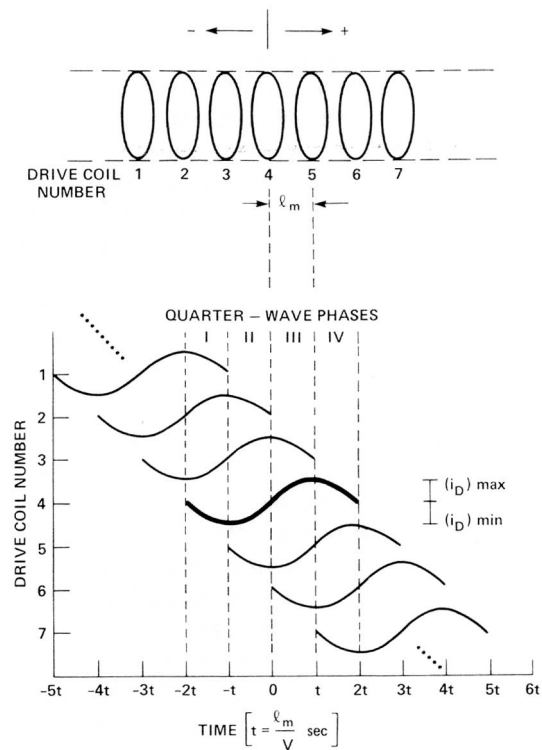

Figure 1 — *Force on drive coil due to bucket coil.*

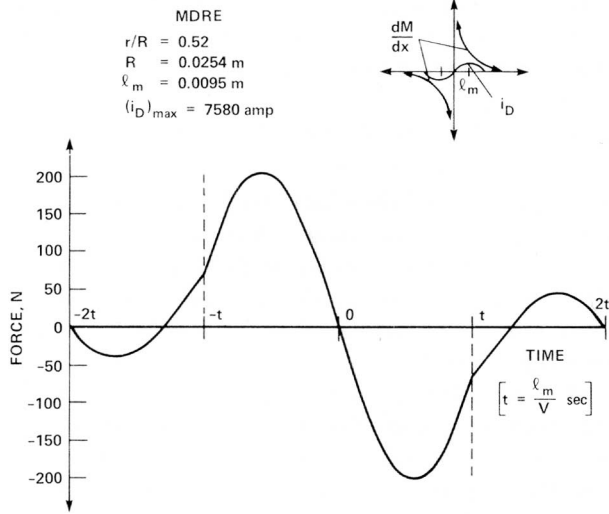Figure 2 — *Drive coil current flow.*

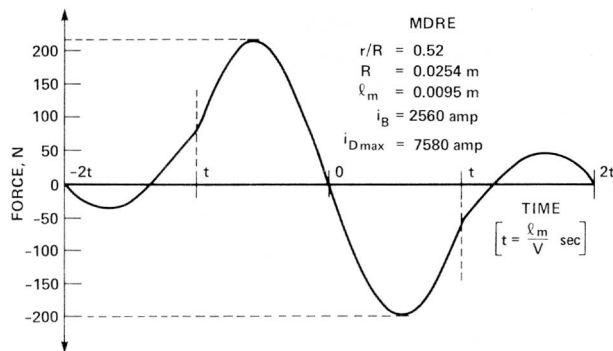Figure 3 — *Force on a drive coil due to neighboring drive coils.*

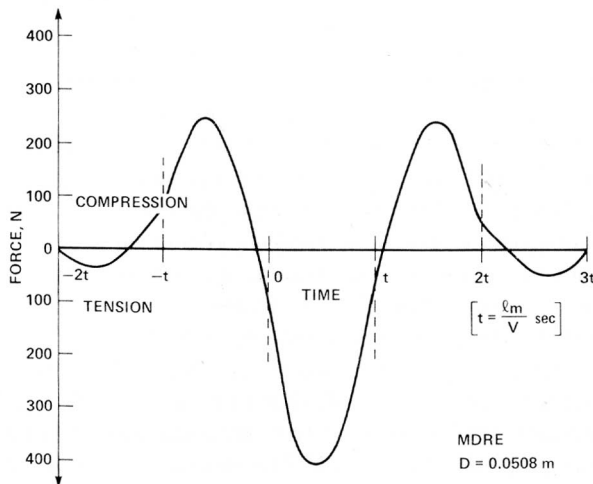Figure 4 — *Total force on a drive coil.*

Figure 5 — *Relative force between drive coils.*

velocity to be constant, all drive coils will experience the same forces within the same length of time. Hence, all coils will propagate the same tension waves in one direction and the corresponding compression waves in the other.

Since these waves all propagate at the same velocity, no wave will "catch up" to the one in front of it. However, tension stress waves traveling in one direction will pass through compression stress waves moving in the other direction. The additive behavior of these complementary waveforms will give the maximum stress in the local

structure. This behavior is well understood and maximum stresses are easily predicted.

Unfortunately, the assumption of constant bucket velocity over significant portions of the mass-driver track is not reasonable (indeed, it is contrary to the concept of a linear accelerator). The velocity increases, and the time during which the forces act on the drive coil decreases. Consequently, the stress waves propagated by contiguous drive coils will have increasingly shorter periods. An analytical or numerical analysis of the constructive or destructive interference of these stress waves is beyond the scope of this study and considerations of how their effects behave along the length of the track must be left for future study.

In summary, calculation of the forces exerted on any drive coil lead to the conclusion that the structural members joining two drive coils will be subjected to both local tensions and local compressions. Over small lengths of the track, bucket velocity may be taken as constant and hence the stress waves propagated by drive coils will be identical. Over these short regions, forces acting on the structural members joining adjacent drive coils can be determined. However, a complete analysis of the structural load forces between drive coils must include changing bucket velocity and the consequent interference patterns caused by nonidentical stress waves. It must be noted that only the first few coil sections will be subjected to a net compression since as one progresses along the MD the intercoil forces shown here are superimposed on the increasing tension, $T(x) = m_{BL}f_R\sqrt{2ax}$

Bucket Structure

The mass-driver bucket is subjected to various forces which must be evaluated in designing the bucket. Considered here are the forces on the bucket coils: the "hoop stress" which keeps the coil in tension, the forces between the two coils, and the stress associated with connecting the payload to the superconducting coil.

Hoop stress — A radial force in the outward direction is experienced by any current-carrying loop. This force is equal in magnitude to $d$energy$/dR = (1/2)I(2L/R)$ where I = current, R = radius, and L = self-inductance of the loop. The force per unit length is then $I^2L/4\pi R^2$ which results in a tension on the wire of $I^2L/4\pi R$.

For a bucket coil with thickness 0.1 D and radius 0.26 D, L = $(6128.46 \times 10^{-9})D$ (henries). Current is 2.5×10^8 A/m$^2 \times$ $(0.1\ D)^2$ and R is 0.26 D, yielding tension as a function of caliber:

$$T = 11723.33\ D^4\ (\text{newtons})$$

The stress on the loop material is:

$$\sigma = T/(0.1\ D)^2 = 1.172 \times 10^6\ D^2\ \text{Pa}$$

Even for a large 0.5-m caliber mass driver, the hoop stress is 2.931×10^5 Pa.

Force between coils — An attractive force will exist between two coaxial coils carrying current in the same direction. The magnitude of the force is $I_1 I_2 (dM/dx)$ where I is current and M is mutual inductance. For the specified bucket geometry, in which both bucket coils are of equal radii and the ratio of radius to distance between them is always 0.26 $D/1.11D$, dM/dx is a constant 1.3903 X 10^{-8}. $I = 2.5$ X 10^8 A/m² X $(0.1D)^2$, so the force between bucket coils is:

$$F = (2.5 \text{ X } 10^6)2(1.3903 \text{ X } 10^{-8})D^4$$

For a 0.0508-m caliber model, this force is 0.58 N. For a 0.5-m caliber machine (larger than any currently being considered) the force would be 5430 N, less than one-third the force of the accelerated payload mass on the bottom of the bucket; this force is not a limiting factor in bucket design.

Load attachment forces — In order to minimize heat loss from the superconducting coil, the bucket coils will have to be attached to the payload at the minimum possible number of points with the smallest possible connection. The penalty, of course, is in stress on the coils at the attachment points.

The sections of the coil between attachment points are comparable to curved, double-cantilevered beams which are being loaded with a uniform force normal to the plane of curvature. Calculations for such beams have been done and enable us to deduce that, for a coil attached at eight evenly spaced points, the transverse shear force at the attachment points will be wR (0.3927), where w is the loading in force/unit circumferential length of winding, and R is coil radius. For a coil attached in only four places, the force is wR (0.7854).

Supposing that one coil had to accelerate the total combined mass of payload and bucket at an acceleration a, then $F = (M_1 + M_B)a = W(2\pi R)$; $m_1 = (D/0.197)^3$ and $m_B = 2.263(D/0.197)^3$, so $wR = (1/2\pi)xax$ 3.263$(D/0.197)^3$. The force on the attachment points is then proportional to D^3 and to a.

$$F = 53.35 \text{ X } D^3 \text{ X } a \qquad \text{for four attachment points}$$

$$F = 26.67 \text{ X } D^3 \text{ X } a \qquad \text{for eight attachment}$$

points

This force will act upon connections which will probably be kept quite cold, and hence brittle, by their proximity to the superconducting coil. Attachment that will distribute the transverse force so as to keep stress within acceptable limits while minimizing mass and heat loss is one of the engineering problems of actual bucket design. These considerations affect mass driver design insofar as that the stress placed on the coils increases proportionally to D. Once the stress limits of the material have been reached, either the proportion of load attachment area must be increased with D for large-scale mass drivers or acceleration must be decreased (held constant with respect to $1/D$).

A sample calculation: for a 0.4-m caliber mass driver, accelerated at 1000 g's by one coil, with four attachment points which distribute the load equally over four sections of the coil, each spinning a 10° arc, the stress on the coil tubing is about 2.31 X 10^7 Pa.

Tear Off Point

We compute the "tear-off" point, that is the position along the MDRE where the stress placed on the feeders alone requires additional strengthening to sustain the axial tension.

The tension is

$$T(x) = m_{BL} f_R \sqrt{2ax}$$

and the feeder area is

$$A(x) = A_{fo}\sqrt{L/x}$$

where m_{BL} = payload + bucket mass, and L = acceleration length.

The stress is

$$\sigma(x) = \frac{T(x)}{A(x)} = \frac{m_{BL} f_R}{A_{fo}} \sqrt{\frac{2a}{L}} \, x$$

If $\sigma = \sigma_{ult}$ at the tear-off point, then we can write the above as

$$\frac{x}{L} = \frac{\sigma_{ult} A_{fo}}{m_{BL} f_R V_e}$$

where $V_e = \sqrt{2aL}$. Since $m_{BL} = m_1 [1 + (m_B/m_1)]$, $\dot{m} = m_1 f_R$, and $T = \dot{m} V_e$ = thrust force

$$\frac{x}{L} = \frac{\sigma_{ult} A_{fo}}{\left(1 + \dfrac{m_B}{m_1}\right) T}$$

If $x/L > 1$, tear-off is beyond the attachment point; if $x/L < 1$, tear-off occurs prior to attachment point and additional strengthening must be provided.

For $A1$ 2024 $T4$:

$$\sigma_{ult} = 4.27 \text{ X } 10^8 \text{ N/m}^2$$

Steel:

$$\sigma_{ult} = 1 \text{ X } 10^9 \text{ N/m}^2$$

For OPT-4:

$$1 + m_B/m_1 = 3.263$$

In figures 6 and 7, x/L is shown as a function of the exhaust velocity V_e for various propellant accelerations as computed from the OPT-4 formulas. The tension at the attachment point = 3.263 T where T is the MDRE thrust.
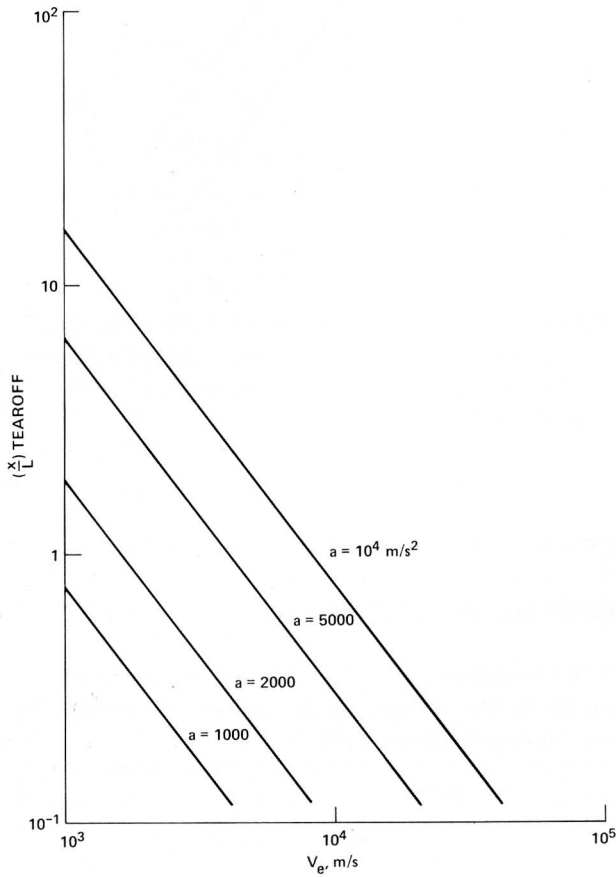
Figure 6 — *Tear-off point based on feeder area OPT-4, as a function of exhaust velocity and bucket acceleration; propellant lump mass = 3.8 kg, $\sigma_{ult} = 4.27 \times 10^8$ N/m².*
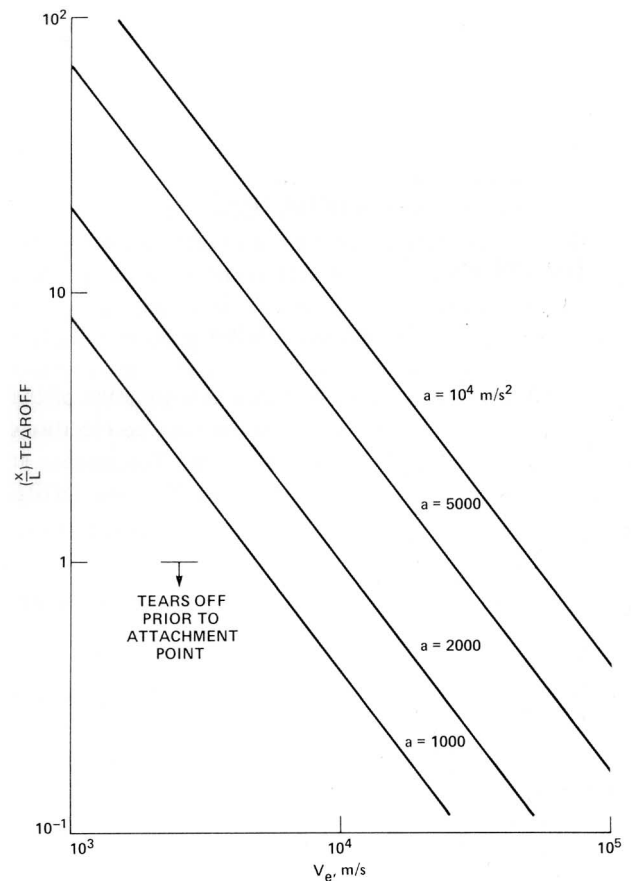

Figure 7 — *Tear-off point based on feeder area OPT-4, as a function of exhaust velocity and bucket acceleration; propellant lump mass = 0.016 kg, $\sigma_{ult} = 4.27 \times 10^8$ N/m².*

LARGE-SCALE DYNAMICS AND STABILITY

Bucket Stream in a Curved Tube

To understand the combined effects of the bucket stream on the stability of the mass driver we consider the following sample problem.

We imagine a curved section of tube containing two frictionless ball streams moving in opposite directions within the tube and which elastically rebound from the end walls of the tube. The momentum change of the ball streams at each end provides a tension force T which will tend to straighten the curved tube.
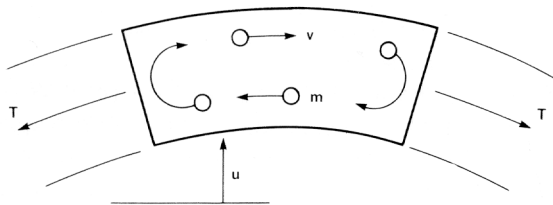
The mass flow of each ball stream is $\dot{m} = \mu_B V$ where $\mu_B =$ mass of balls per unit length and $V =$ velocity of each ball. The momentum per ball is $p = mV$ where $m =$ ball mass. The momentum change per ball due to the elastic rebound at the end is $\Delta p = 2mV$ so that the momentum change per second $\Delta \dot{p} = 2\dot{m}V = 2\mu V^2$ which must equal the tension force T. If the curvature of the section is u'', where u is the

displacement of the tube, the net downward straightening force on the section is:

$$Tu'' = 2\mu_B V^2 u''$$

Opposing this straightening force are the centrifugal forces of the two ball streams which tend to increase the curvature of the tube. If $R = 1/u''$ is the radius of curvature then the upward centrifugal force due to the curvature of the two ball streams is:

$$2\mu_B V^2/R = 2\mu_B V^2 u''$$

which exactly balances the straightening forces. Therefore, the curved tube-ball stream structure is dynamically neutral, neither straightening itself nor curving itself more strongly.

Additionally, one can easily show that the total downward force on the section given on $2/Tu'$ is exactly balanced by the total upward force exerted by the ball streams on the tube $4\mu V_B^2 u'$ where u' is the slope of the curved tube at the ends. Hence, bending the tube does not give a net upward or downward force, which we also know from Newton's Third Law.
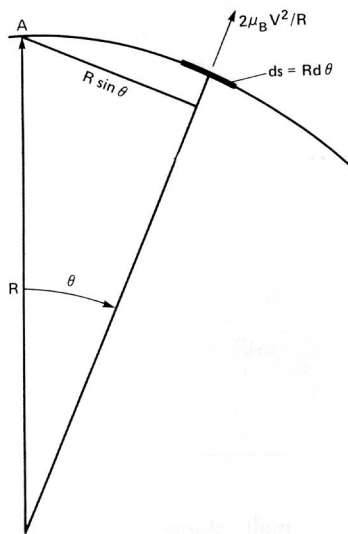
Another way to arrive at the neutral curvature stability is to consider the moment of the tension and centrifugal forces taken about the center of the curved tube at A.
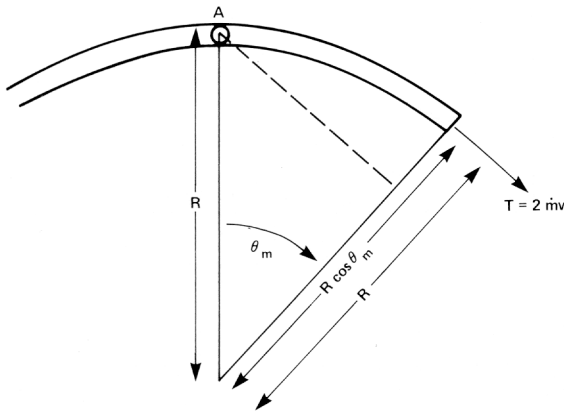
The clockwise moment of the tension force about the point A is:

$$M_{ccw} = T(R - R\cos\theta_m) = 2mVR(1 - \cos\theta_m)$$

The counterclockwise moment of the centrifugal force due to an element of tube $ds = Rd\theta$ about point A.

due to the two ball streams is

$$dM_{cw} = R\sin\theta\mu_B (V^2/R)\, ds$$

So

$$M_{cw} = 2\dot{m}VR \int_O^{\theta m} \sin\theta\, d\theta$$

$$= 2\dot{m}VR(1 - \cos\theta_m)$$

Since these are the same there is no net moment tending to bend or straighten the tube-ball stream structure.

Large-Scale Dynamical Stability

Mass-driver reaction engine structure — The MDRE structure is typically a very long (3-10 km) and at least for the electrical components, quite thin (≤1 m) structure operating in tension. Transverse oscillations will travel very slowly along the structure at velocities of ~10-50 m/sec. Typical payload launch rates are 10 Hz and are considered

high frequencies. We therefore consider the following as a useful limiting model to describe the combined mass-driver bucket stream interaction for large-scale, low-frequency dynamical motions.

1. The mass-driver electrical structure (stringers, feeders, drive coils, capacitors, etc.) is averaged over and replaced by a continuously variable mass per unit length.
2. Because of the extreme length-to-diameter ratios, and because we are interested in the basic stability of the primary load-bearing electrical structure-bucket interaction, we ignore any beam bending moments tending to straighten the overall structure. Thus the MDRE is a variable density "rope," unable to sustain any buckling or compressive forces and must remain in tension to be stable. For small-scale, high-frequency phenomena such as the transverse impulses imparted to separate the payloads and buckets in the peel section, beam bending moments must be included.
3. The tension forces applied to the "rope" are supplied by the reaction forces of the drive coils accelerating the buckets and payloads. Since the number of buckets between the zero velocity point and any point depends on the position along the MDRE, the tension forces are variable depending on position.
4. The tension forces appearing in the MDRE accelerate the bucket stream. Since the launch rate is large compared to the natural frequencies of interest for the large-scale dynamical motion, we replace the discrete buckets with a continuum bucket stream variable having a position-dependent velocity and mass per unit length.

Thus the problem to be solved in this approximation is that of a variable-tension, variable-mass-per-unit-length rope, which is tensioned by accelerating a variable mass per unit length of a varying-velocity fluid "bucket" stream attached to the rope.

Continuum treatment of bucket flow — If $\dot{m}$ = the mass flow of buckets and payloads considered as a fluid, $\dot{m} = \rho AV$, V = bucket velocity, then $\mu_B = A\rho$ = bucket and payload density per unit length.

For uniformity accelerated motion

$$V(x) = \sqrt{2ax}$$

Using f_R = bucket repetition rate, Hz, $\dot{m} = m_{BL}f_R$, m_{BL} = bucket and payload mass, $\dot{m} = \mu_B V$, and $\dot{m} = \mu_B\sqrt{2ax}$. Hence

$$\mu_B = \frac{M_{BL}f_R}{\sqrt{2ax}} = \frac{\dot{m}}{\sqrt{2ax}}$$

If $n(x)$ = number of buckets between 0 and x, the mass of buckets between 0 and x is:

$$\int_O^x \mu_B(x)dx = m_{BL}f_R\sqrt{\frac{2x}{a}}$$

and hence

$$n(x) = \frac{\int_O^x \mu_B(x)dx}{m_{BL}} = \frac{\text{mass of buckets between } o \text{ and } x}{\text{mass per bucket}}$$

$$= f_R \sqrt{\frac{2x}{a}}$$

The tension at x is $T(x) = m_{BL}an(x) = m_{BL}f_R\sqrt{2ax} = m_{BL}f_RV(x)$, and $T(x) = \dot{m}V(x)$.

Mass-driver transverse motion — In the sketch below, let $u(x,t)$ = transverse displacement of the rope, x = distance from free end, t = time, $T(x)$ = tension in the rope, $\mu(x)$ = mass per unit length of the rope, $\mu_B(x)$ = mass per length of the bucket stream, and $V(x)$ = velocity of the bucket stream along the rope relative to the rope.
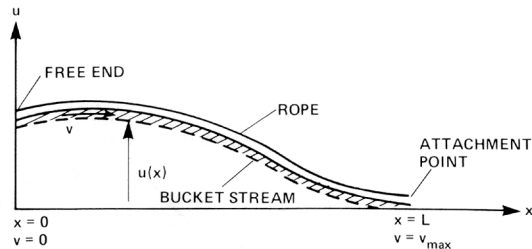

We will ignore longitudinal motion of the rope in the x direction and assume the bucket stream coincides with the rope.

The transverse equation of motion governing the transverse displacement $u(x,t)$ of the rope is derived using the momentum theorem applied to an incremental control volume of length dx enclosing both the rope and the bucket stream.

The momentum theorem can be written as:

$$\frac{\partial}{\partial t} \iiint_V \rho\bar{v}\, dV = -\iint_S \rho\bar{v}\bar{v} \cdot d\bar{A} + \bar{F}$$

| rate of increase of momentum in side volume V | rate of momentum gain by convection of momentum inward across the surface S enclosing volume V | external forces acting on volume V |

where ρ is the volume density of the material having velocity v.
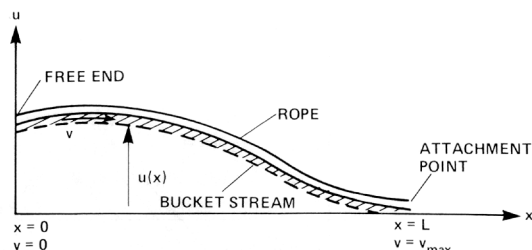
We assume small slopes and curvatures so that $\sin u' \sim u'$ where $u' = \partial u/\partial x$ and $\cos u' \cong 1$.

In the above sketch, ① and ② refer to the surfaces at x and $x + dx$, respectively, across which buckets are flowing.

For the rope

$$\bar{v} = O \cdot \hat{i} + \dot{u}\hat{j} \qquad (2)$$

where $\dot{u} = \partial u/\partial t$ and $\hat{i}$ and $\hat{j}$ are unit vectors in the x and y directions.

For the bucket stream

$$\bar{v} = V\hat{i} + (Vu' + \dot{u})\hat{j} \qquad (3)$$

$\dot{u}$ is the transverse rope velocity and vu' is the transverse bucket velocity relative to the rope.

The continuity equation for the control volume is

$$\frac{\partial}{\partial t} \iiint_V \rho\, dV = - \iint_S \rho\bar{v} \cdot d\bar{A} \qquad (4)$$

The total mass inside the control volume is

$$\iiint \rho\, dV = \mu_B\, dx + \mu\, dx$$

and is independent of time. Hence the left-hand side of equation (4) is zero and

$$\iint_① \rho\bar{v} \cdot d\bar{A} + \iint_② \rho\bar{v} \cdot d\bar{A} = 0$$

Now

$$\iint_① \rho\bar{v} \cdot d\bar{A} = -\mu_B V$$

is the mass flow of the bucket stream across the surface 1 at x. The minus sign occurs since v and dA are in opposite directions.
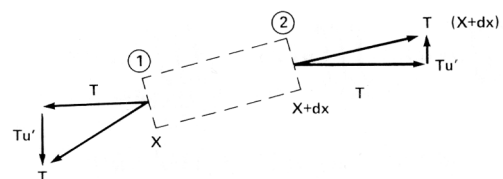
Similarly

$$\iint_② \rho\bar{v} \cdot d\bar{A} = \mu_B V$$

It is convenient to write the mass flow of buckets along the rope

$$\dot{m} = \mu_B V = \text{constant}$$

External forces

These are due only to tension and if we are in free space

$$\vec{F} = \hat{i}\,[T(x + dx) - T(x)] + \hat{j}\,[(Tu')_{x+dx} - (Tu')_x]$$

Since

$$T_{x+dx} = T(x) + \frac{\partial T}{\partial x}\,dx$$

$$(Tu')_{x+dx} = (Tu')_x + \frac{\partial(Tu')}{\partial x}\,dx$$

$$\vec{F} = \hat{i}T'\,dx + \hat{j}\,\frac{\partial}{\partial x}\,(Tu')dx \qquad (5)$$

Momentum flow: Now

$$\iint \rho\vec{v}\vec{v}\cdot d\vec{A} = \iint \vec{v}\,d\dot{m}$$

On surface ① in the preceding sketch, $\dot{m} = -\mu_B V$ so

$$\iint_① \rho\vec{v}\vec{v}\cdot d\vec{A} = -[V\hat{i} + (Vu' + \dot{u})\hat{j}]\mu_B V'$$

while on surface ② $\dot{m} = \mu_B V$ so

$$\iint_② \rho\vec{v}\vec{v}\cdot d\vec{A} = \left\{\left(V + \frac{\partial V}{\partial x}\,dx\right)\hat{i}\right.$$

$$\left. + \hat{j}\left[Vu' + \dot{u} + \frac{\partial}{\partial x}(Vu' + \dot{u})dx\right]\right\}\mu_B V$$

The total momentum flow is thus

$$\iint_S \rho\vec{v}\vec{v}\cdot d\vec{A} = \mu_B V\left[\hat{i}\,\frac{\partial V}{\partial x} + \hat{j}\,\frac{\partial(Vu' + \dot{u})}{\partial x}\,dx\right] \qquad (6)$$

Momentum inside control volume

$$\vec{M} = \iiint \rho\vec{v}\,dV = \underbrace{\iiint \rho\vec{v}\,dV}_{\text{rope}} + \underbrace{\iiint \rho\vec{v}\,dV}_{\text{buckets}}$$

$$= \mu\,dx(0\hat{i} + \dot{u}\hat{j}) + \mu_B\,dx\,[V\hat{i} + \hat{j}(Vu' + \dot{u})]$$

$$= \hat{i}(\mu_B V\,dx) + \hat{j}\,[u\mu + \mu_B(Vu' + \dot{u})]\,dx$$

$$= M_x\hat{i} + M_y\hat{j} \qquad (7)$$

In the transverse direction we have:

$$\frac{\partial M_y}{\partial t} = -\mu_B V\,\frac{\partial}{\partial x}\,(vu' + \dot{u})dx + \frac{\partial}{\partial x}\,(Tu')dx$$

Subtracting for M_y, canceling the common dx, noting $\mu_B V = \dot{m}$ is a constant independent of x or t, and that v, μ, and μ_B are functions of x but not of t, we finally have

$$(\mu + \mu_B)\,\frac{\partial^2 u}{\partial t^2} = -2\dot{m}\,\frac{\partial^2 u}{\partial x\partial t} - \mu_B V^2\,\frac{\partial^2 u}{\partial x^2}$$

$$- \mu_B V\,\frac{\partial V}{\partial x}\,\frac{\partial u}{\partial x} + T\,\frac{\partial^2 u}{\partial x^2} + \frac{\partial T}{\partial x}\,\frac{\partial u}{\partial x} \qquad (8)$$

It is interesting to note several limits to equation (8).

1. In the limit of a very light bucket stream $\mu_B = 0$

$$\mu\,\frac{\partial^2 u}{\partial t^2} = \frac{\partial}{\partial x}\,(Tu')$$

which is the wave equation for a variable tension, variable density rope.

2. If we have zero speed buckets $V = 0$ with μ_B remaining finite

$$(\mu_B + \mu)\,\frac{\partial^2 u}{\partial t^2} = \frac{\partial}{\partial x}\,(Tu')$$

which again is the wave equation on a rope having an increased mass per unit length.

Form of various terms: the rope tension due to the bucket stream can be written as

$$T(x) = \dot{m}V(x) = \mu_B V\,V$$

$$= \mu_B V^2$$

Hence the terms in equation (8) involving u' cancel. Also since

$$T' = \mu_B V\,V'$$

$$T'u' = \mu_B V\,V'u'$$

the terms involving $u'v'$ also cancel in equation (8) leaving

$$(\mu + \mu_B)\,\frac{\partial^2 u}{\partial t^2} = -2\dot{m}\,\frac{\partial^2 u}{\partial x\,\partial t} \qquad (9)$$

Since $v = \sqrt{2ax}$ = bucket velocity

$$\mu_B = \frac{\dot{m}}{\sqrt{2ax}} \qquad (10)$$

For reasons of constant power dissipation per unit length, the rope density μ is also proportioinal to $1/\sqrt{x}$. Thus we let

$$\mu + \mu_B = \mu_T\sqrt{L/x} \qquad (11)$$

where μ_T = mass per unit length of buckets and rope at the attachment point $x = L$. If we assume harmonic motion

$$\mu(x,t) = W(x)\,e^{i\omega t}$$

then equation (9) becomes

$$\frac{dW}{dx} + i \frac{C}{\sqrt{x}} W = 0 \qquad (12)$$

which has the solution

$$W(x) = D\, e^{i2c\sqrt{x}}$$

$$= D[\cos(2c\sqrt{x}) - i\sin(2c\sqrt{x})] \qquad (13)$$

where

$$c = \frac{\mu_T \omega \sqrt{L}}{2m} \qquad (14)$$

The eigenfrequencies are obtained by applying the boundary condition that

$$u(t,L) = 0$$

$$\therefore W(L) = 0$$

Hence

$$\cos(2c\sqrt{L}) = 0$$

$$\omega_n = \frac{\dot{m}(n + 1/2)\pi}{L\mu_T} \qquad (15)$$

the complete solution is

$$u(x,t) = \sum_n D_n \cos\left[W_n t - \left(n + \frac{1}{2}\right)\pi \sqrt{\frac{x}{L}}\right] \qquad (16)$$

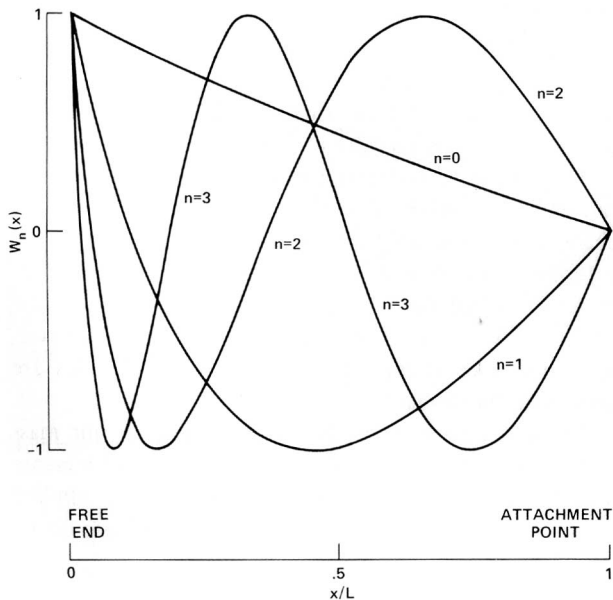A plot of the fundamental $n = 0$ and the first three harmonics is shown in figure 8.

Figure 8 — *Fundamental and first three harmonics of MDRE.*

The total mass of the acceleration or deceleration section is:

$$M = \int_o^L [\mu_B(x) + \mu(x)]\, dx$$

$$= \frac{1}{2} \mu_T L$$

so that the period of the nth harmonic can be written as

$$\tau_n = \frac{2\pi}{\omega_n} = \frac{M}{\dot{m}(n + 1/2)}$$

that is, proportional to the mass-driver mass divided by the mass flow through the mass driver.

Comments Regarding MDRE Solution, Equation (16)

1. The eigenfrequencies of the MDRE structure are very small. For an asteroid class MDRE of acceleration length 10.6 km, $m = 10 \times 3.8 = 38$ kg/sec; $\mu = 150$ kg/m, $\mu_B = 2.76 \times 10^{-2}$ kg/m at attachment point, $V_e = 5000$ m/sec, the first few eigenfrequencies are (OPT-4)

n	ω_n, rad/sec	period, hr
0	1.36×10^{-4}	12.83
1	4.09×10^{-4}	4.27
2	6.81×10^{-4}	2.56
3	9.54×10^{-4}	1.83

2. Because of these long periods it is clear that a beam term

$$-\frac{\partial^2}{\partial x^2}\left(EI \frac{\partial^2 u}{\partial x^2}\right)$$

will need to be included in the right-hand side of equation (9). The inclusion of the fourth-order term will allow satisfaction of the following boundary conditions:

$$u(L,t) = 0$$
$$u'(L,t) = 0$$
$$u''(0,t) = 0$$
$$u'''(o,t) = 0$$

Values appropriate to EI for external stress structures must be obtained to proceed further. The effective transverse moment $I \sim$ (transverse dimension)^4 while Young's modulus can be changed using active tensioners. Adding springs through an external structure will give a tension in addition to the tension due to accelerated bucket stream. This will leave a u" term in equation (16), as will an initial tension T_0 at $x = 0$ due to the bucket turn around at finite speed either for insertion into the acceleration section or removal from the deceleration leg of the mass driver.

3. The eigenfrequencies of the acceleration and deceleration sections can be made the same. Since the force exerted on the buckets is the same, in each section, the acceleration ratio is

$$\frac{\ddot{x}_{accel}}{\ddot{x}_{decel}} = \frac{L_{decel}}{L_{accel}} = \frac{m_b}{m_B + m_1} \qquad (17)$$

The requirement for ω_n to be the same in the two sections is

$$\omega_n = \frac{m_{accel}(n + 1/2)\pi}{L_{accel}\,\mu_{T,accel}} = \frac{\dot{m}_{decel}(n + 1/2)\pi}{L_{decel}\,\mu_{T,decel}}$$

Using

$$\dot{m}_{accel} = f_R(m_B + m_1)$$

$$\dot{m}_{decel} = f_R m_B$$

then

$$\frac{L_{decel}}{L_{accel}} = \frac{\mu_{T,accel}}{\mu_{T,decel}} \frac{m_B}{m_B + m_1} \qquad (18)$$

which is the same as equation (17) provided $\mu_{T,decel} = \mu_{T,accel}$, generally, $\mu \gg \mu_B$.

4. The solutions $W_n(x)$ form an orthogonal set on x using a new variable $z = x^{-2}$ Thus, given an initial $u(x,0)$ and/or $u(x,0)$ the constants in equation (16) can be determined using the Fourier sieve. Since the higher harmonics are not integral multiples of the fundamental, the overall shape of the MDRE composed of a summation of the initial eigensolutions will not repeat itself. Each normal node has one more node than the preceding one and the nodes crowd together toward the free end where the tension is small. The slope at the attachment point is finite.

5. Since the variable x occurs as x^{-2} in the sine or cosine, transverse waves are dispersive, the wave speed depending on frequency. For moderate period waves (~1-0.1 Hz) the local wave speed can be written as

$$V_{wave} \simeq \sqrt{\frac{T}{\mu}} = \sqrt{\frac{mV_e}{\mu_T L}}\ \sqrt{x}$$

$$= 0.346\ \sqrt{x}$$

for the asteroid MD discussed in reference 5. The wave speed varies from 10.9 m/sec for $x = 1$ km up to 34.6 m/sec at $x = 10$ km.

6. We conclude from the weakly oscillatory nature of the solutions to the free space MDRE electrical structure-bucket interaction that the MDRE is stable. The driving term on the right-hand side of equation (9) is proportional to the bucket mass flow and hence the external truss structure will need to be sized in some manner related to the mass flow.

7. The most important parameter of the external structure is its mass. From a viewpoint of overall efficiency, the external structure should be as light as possible. When this factor is entered into the overall optimizations, it

will undoubtedly tend to shorten mass driver length to decrease overall mass. This has not been done at the present time because of ignorance of appropriate structural mass values.

Even if we do not have figures on structural mass, we can still determine how these masses will scale with changes in total length. Assume that our mass driver external structure is made from a long chain of identical sections, so that the value of EI does not change over the length. If we change the total length of the mass driver, how must we change EI so that the deflections are geometrically similar?

We will assume that the forces acting on our mass driver are gravitational tidal forces, which will increase linearly with the length. This means that the applied forces will also be geometrically similar. The basic differential equation describing the deflection is

$$EI\ \frac{\partial^2 u}{\partial x^2} = \text{applied moment}$$

If we change the length by a factor ℓ_2 the applied force at a point increases as ℓ_2, and the applied moment increases as ℓ_2^2. Defining

$$x_0 = x/\ell_L$$

$$u_0 = u/\ell_2$$

$$\mu_0 = \mu/\ell_L^2$$

then the deflection is described by the nondimensional equation

$$\frac{\partial^2 u_0}{\partial x_0^2} = \frac{\mu_0\,\ell_L^3}{EI}$$

For a similar deflection, $\partial^2 u_0/\partial x_0^2$ must be the same, which implies that the factor ℓ_L^3/EI must be constant. But EI increases as r (transverse size of external structure) to the fourth power. Thus for similar deflection

$$r\ X\ \ell_L^{3/4}$$

But mass and length of the track increase as r^2. This implies that mass and length of the structure will increase as $\ell_L^{9/16}$ and total mass as $\ell_L^{25/16}$. So total mass increases with increased length not only because a longer structure is needed, but also because this structure must be more solidly built.

This model assumes that the major loads applied to the MDRE are gravitational. It may be that they will in fact be due to internal mechanic motions (mating of pellets, etc.). As long as it is known how these forces scale with total length, this kind of analysis can be applied. If applied moments are constant with length, for example, then mass increases as $\ell_L^{17/16}$; very nearly a power of one.

Steering the MDRE

A requirement exists for changing the thrust vector orientation during both orbital and free space operations. One method for accomplishing this steering is to utilize the torque produced when the thrust vector does not pass through the center of mass of the entire system. It must be recognized that the application of the torque so produced to the very long, basically flexible MDRE to produce the desired overall angular acceleration without undue bending, constitutes a major yet unsolved structural problem, probably requiring active structural control. Clearly there will be upper limits of the overall angular acceleration and bending that will still allow passage of the buckets through the guideway without their scraping the guideway edges.

We dynamically represent the MDRE by a long uniform rigid rod with the propellant and payload masses arranged as shown:
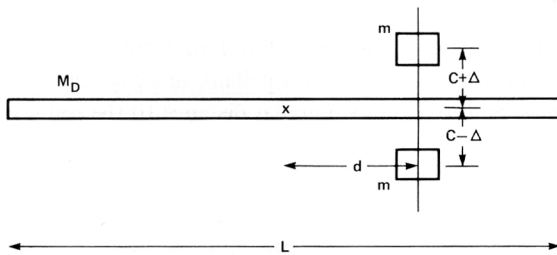
We let

m_D electrical and external structural mass of MDRE "uniform rod"

$2m$ total propellant and payload mass

L total length, acceleration and deceleration of MDRE "rod"

$2c$ distance between the two separated payload and propellant masses, perpendicular to the rod

d axial separation between the payload and propellant masses at the attachment point and the center of the MDRE

Δ offset distance, the perpendicular distance between the thrust vector and the center of mass of the propellant and payload mass

The moment of inertia of the combined system about the center of the rod is

$$I_{zo} = \frac{1}{12} m_D L^2 + m[d^2 + (c + \Delta)^2 + (c - \Delta)^2]$$

$$= m_D \left[\frac{L^2}{12} + \frac{1 - \nu}{\nu} (d^2 + c^2 + \Delta^2) \right]$$

where

$$\nu = m_D/(m_D + 2m)$$
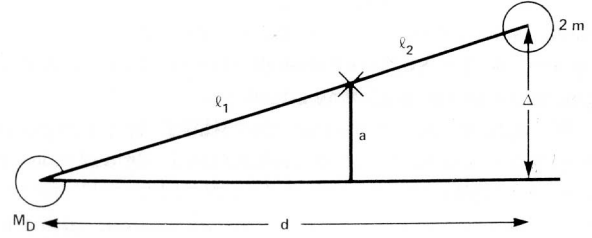
The position of the overall system center of mass lies a distance ℓ_1 toward the propellant and payload center of mass and has a perpendicular distance to the rod given by a.

Now

$$\ell_1 + \ell_2 = \sqrt{d^2 + \Delta^2}$$

$$\frac{\ell_2}{\ell_1} = \frac{\nu}{1 - \nu}$$

$$\frac{\Delta}{a} = 1 + \frac{\ell_2}{\ell_1}$$

Hence, the moment arm between the overall system center of mass and the thrust vector which is assumed coincident with the MDRE axis is

$$a = (1 - \nu)\Delta$$

Using the Lagrangian transfer theorem to find the system moment of inertia about the displaced center of mass and noting

$$\ell_1 = (1 - \nu)\sqrt{d^2 + \Delta^2}$$

we find

$$I_z = I_{zo} - (m_D + 2m)\ell_1{}^2$$

$$= m_D \frac{L^2}{12} + \frac{1 - \nu}{\nu} (d^2 + c^2 + \Delta^2) - \frac{(1 - \nu)^2}{\nu} (d^2 + \Delta^2)$$

The angular acceleration is then

$$\dot{\omega} = \frac{T(1 - \nu)\Delta}{I_z}$$

when T = thrust of MDRE. The required offset is

$$\Delta = \frac{\dot{\omega} I_z}{T(1 - \nu)}$$

Note that $\Delta^2 \ll d^2$ so Δ^2 can usually be neglected in the expression for I_z.

The required angular acceleration for tangential thrusting in a nearly circular orbit is computed in the following section.

As an example consider a MDRE in a circular orbit at an altitude of 200 km requiring $\dot{\omega} = 1.22 \times 10^{-10}$ rad/sec^2. If $T = 560$ N, $m_D = 200 \times 10^3$ kg, $2m = 1900 \times 10^3$ kg, $L = 10.3$ km, $d = 3.537$ km, $c = 10$ m then $\nu = 0.0952$, $I_z = 4.023 \times 10^{12}$ kg/m^2 and the required offset $\Delta = 0.97$ m.

Rather than using the entire propellant and payload mass for the active control mass, a smaller mass could be moved through a greater distance to provide the required torque.

As a second example we compute the offset needed for an asteroid retrieval mission utilizing the moon with perilune 87 km above the surface and $V_\infty = 0.84$ km/sec for which we have computed $\dot\omega = 7.62 \times 10^{-7}$ rad/sec^2.

For a typical Opt 4.0 asteroid retrieval $T = 1.5 \times 10^4$ N, $m_D = 3.512 \times 10^5$, $d = 345$ m, $c = 50$ m, $2m = 1.832 \times 10^8 + 1.500 \times 10^8 = 3.332 \times 10^8$ kg, we find $I_z = 1.300 \times 10^{12}$ kg/m^2 so the offset $\Delta = 66$ m, which is larger than the separation c. Hence, either one needs a larger separation or a larger perilune and/or smaller V_∞ which will give a smaller $\dot\omega$.

MDRE OPERATION IN A GRAVITATIONAL FIELD

Angular Acceleration

We compute the angular acceleration required for operation in the inverse-square gravitational field around a central body.

The angular rate of revolution in a circular orbit at radius r around a central body is

$$\omega = \sqrt{\frac{K}{r^3}} \qquad (19)$$

where K is the gravitational parameter. For a low-thrust orbit in which the velocity is essentially the local circular value at all times, this is also the required pitching rate for the MDRE to remain tangent to the orbit path. The radial velocity for a low-thrust spiral is (ref. 5, eqn. 3):

$$\dot r = \frac{2ar^{3/2}}{\sqrt{K}} \qquad (20)$$

where a = tangential acceleration = thrust/mass.

To find the angular acceleration, that is, the rate of change of the pitching rate, we differentiate equation (19), with respect to time and substitute equation (20) to find

$$\dot\omega = -\frac{3a}{r} \qquad (21)$$

Since $a = a_0/(1 - a_0 t/V_e)$ where V_e is the exhaust velocity, a_0 is the initial acceleration = T/m_0, m_0 is the initial mass, we can integrate equation (21) by separating variables to find

$$\sqrt{\frac{K}{r_0}} - \sqrt{\frac{K}{r}} = -V_e \ln\left(1 - \frac{a_0 t}{V_e}\right)$$

and

$$a = a_0 \exp\left[\frac{1}{V_e}\left(\sqrt{\frac{K}{r}} - \sqrt{\frac{K}{r_0}}\right)\right]$$

or

$$\dot\omega = -\frac{3a_0}{r_0}\exp\left[\frac{1}{V_e}\left(\sqrt{\frac{K}{r}} - \sqrt{\frac{K}{r_0}}\right)\right]$$

Another case of interest in asteroid retrieval missions is the angular accelerations required during a hyperbolic encounter with the Moon or a planet. We characterize the hyperbolic orbit by the nondimensional velocity at infinity $V_\infty = V_\infty/V_0$ and the nondimensional periapsis distance $r_p = r_p/r_0$ where V_0 is the circular velocity about the primary at radius r_0. The unit of time $t_0 = r_0/V_0$. The nondimensional angular momentum is given by

$$\hat h = \hat r_p \hat V_p = \hat r^2 \theta'$$

and the total velocity is

$$\hat V^2 = \hat r^2 + (r\theta')^2$$

$$= \hat r^2 + \left(\frac{\hat h}{\hat r}\right)^2$$

where $(\ )' = d(\ )/dt_0$, and θ = true anomaly. For constant angular momentum

$$2\hat r\hat r'\theta' + \hat r^2\theta'' = 0$$

so that the nondimensional angular acceleration of the true anomaly is

$$\theta'' = -\frac{2\hat r'}{\hat r}\theta'$$

$$= \frac{2\hat h}{\hat r^3}\sqrt{\hat V^2 - \left(\frac{\hat h}{\hat r}\right)^2}$$

Using the vis-viva relation

$$\hat V^2 = \frac{2}{\hat r} + \hat V_\infty{}^2$$

$$\theta'' = \frac{2}{\hat r^3}\left\{[2\hat r_p + (\hat V_\infty\hat r_p)^2]\left[\hat V_\infty{}^2 + \frac{2}{\hat r_p} - \frac{2\hat r_p + (\hat V_\infty\hat r_p)^2}{\hat r^2}\right]\right\}^{1/2}$$

$$= \frac{2}{\hat r^3}\left\{[(2\hat r_p + (\hat V_\infty\hat r_p)^2]\left[\hat V_\infty{}^2 + \frac{2}{\hat r_p} - \frac{2\hat r_p + (\hat V_\infty\hat r_p)^2}{\hat r^2}\right]\right\}^{1/2}$$

During hyperbolic encounter one may simply orient the MDRE along the radius vector so the angular acceleration required is given by the above. Using the Moon ($r_0 = 1738$ km, $V_0 = 1.679$ km/sec) with $r = 1.05$, that is, 87 km altitude perilune, $V_\infty = 0.50$ so $V_\infty = 0.8395$ km/sec, the peak $\theta'' = 0.9217$ at $r = 1.2$ and hence:

$$\dot\omega = \frac{\theta''}{t_0{}^2} = \frac{0.9127}{1035^2}$$

$$= 8.52 \times 10^{-7} \text{ rad/sec}^2$$

For a MDRE in circular orbit at an altitude of 200 km above the Earth with $T = 560$ N, $V_e = 8000$ m/sec and $m_0 = 2.1$ X 10^6 kg,

$$a_0 = 2.67 \text{ X } 10^{-4}$$

and

$$r = r_0 = 6578 \text{ km}$$

so

$$\dot{\omega} = 1.22 \text{ X } 10^{-10} \text{ rad/sec}^2$$

with

$$\omega = 1.18 \text{ X } 10^{-3} \text{ rad/sec}$$

Mass-Driver Shape in Orbit

The nominal shape of the mass driver reaction engine in free space will be a straight line. However, when the MDRE is operating in orbit about the Earth or Moon the nominal shape will deviate from a straight line. This arises from the fact that the bucket is moving at a different orbital velocity from that of the main structure of the MDRE. If left to itself the MDRE would tend to deflect downward (in a rotating coordinate frame) when V_e is such as to give retrograde elliptical orbits for the released pellets. Thus, the thrust would not be tangential for a straight MDRE and additional forces on the guideway would result in the bucket scraping the walls. Therefore, the nominal shape of the MDRE must coincide with the trajectory of the accelerating bucket with the additional constraint that at release the pellet velocity is tangential to the orbit.

The reference frame used moves in a circular orbit of radius r as shown below.
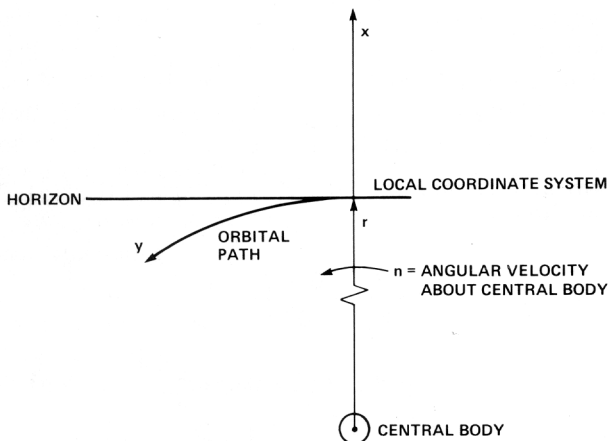
Hill's equations for the motion relative to a coordinate system in uniform circular motion with the x direction along the radial direction are (ref. 3)

$$\ddot{x} = a_x + 2n\dot{y} + 3n^2x$$

$$\ddot{y} = a_y - 2n\dot{x}$$

where a_x, a_y are the applied accelerations. The constraint that the acceleration is tangential to the local shape of the MDRE requires

$$a_x/a_y = \dot{x}/\dot{y}$$

Since

$$a^2 = a_x^2 + a_y^2$$

$$a^2 = a_y^2\left(\frac{\dot{x}}{\dot{y}}\right)^2 + a_y^2$$

Then

$$a_y = a\left[\left(\frac{\dot{x}}{\dot{y}}\right)^2 + 1\right]^{-1/2}$$

Now Hill's equations become

$$\ddot{x} = a\left(\frac{\dot{x}}{\dot{y}}\right)\left[\left(\frac{\dot{x}}{\dot{y}}\right)^2 + 1\right]^{-1/2} + 2n\dot{y} + 3n^2x$$

$$\ddot{y} = a\left[\left(\frac{\dot{x}}{\dot{y}}\right)^2 + 1\right]^{-1/2} - 2n\dot{x}$$

with

$$n = \sqrt{\frac{K}{r^3}}$$

where

$$K = GM = \text{gravity parameter of the central body}$$

To obtain the shape of the MDRE as given in figure 9 these two equations must be numerically integrated to obtain x and y. To accomplish this and to meet the constraint that at the V_e point the velocity vector be tangent to the orbit, these equations are integrated backward in the acceleration section with the final launch conditions becoming the initial conditions.

We compute the shape of a MDRE in a 200-km altitude spiral orbit about the Earth with the following performance.

$$V_e = 8000 \text{ m/sec}$$

accel. $a = 5000$ m/sec^2 ; $L = 6400$ m
decel. $a = 8205.1$ m/sec^2 ; $L = 3900$ m

The deceleration section shape was found by integrating forward with initial conditions being the final conditions from the accelerator section. A second-order Runge-Kutta
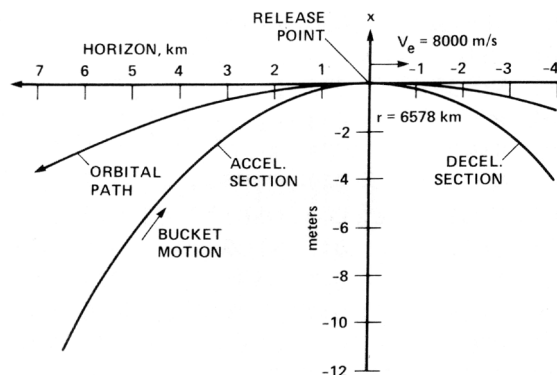

Figure 9 — *MDRE shape in a 200-km orbit (departing) about Earth.*

program was used to integrate these with a step size of 0.05 sec for a duration of 1.6 sec for the acceleration section and a step size of 0.025 sec for a duration of 0.975 sec for the deceleration section.

APPENDIX A

FORCE EXERTED ON A DRIVE COIL DUE TO NEIGHBORING DRIVE COILS

During the passage of a bucket coil, a sinusoidal current flow described by the equation

$$i_D = (i_D)_{max} \sin(\omega t + \phi)$$

will appear in each drive coil. The angular frequency, ω of the flow will be 2π/period, where the period equals $4\ell_m/V$ with ℓ_m being the spacing between drive coils and V being the bucket velocity. At any moment, there will be four contiguous drive coils having a current flow within them. Every current will be 30° out of phase with that in each of the adjacent drive coils. Figure 2 illustrates the current flows in neighboring coils during the activation of a particular reference drive coil (coil no. 4). The equations describing the current flows with respect to that reference drive coil current are as follows:

Coil no. 1 $\qquad i_D = (i_D)_{max} \sin\left(\omega t + \dfrac{3\pi}{2}\right)$

Coil no. 2 $\qquad i_D = (i_D)_{max} \sin(\omega t + \pi)$

Coil no. 3 $\qquad i_D = (i_D)_{max} \sin\left(\omega t + \dfrac{\pi}{2}\right)$

Coil no. 4 $\qquad i_D = (i_D)_{max} \sin(\omega t), \quad -\pi \leqslant \omega t \leqslant \pi$

Coil no. 5 $\qquad i_D = (i_D)_{max} \sin\left(\omega t - \dfrac{\mu}{2}\right)$

Coil no. 6 $\qquad i_D = (i_D)_{max} \sin(\omega t - \pi)$

Coil no. 7 $\qquad i_D = (i_D)_{max} \sin\left(\omega t - \dfrac{3\pi}{2}\right)$

The force experienced by any two active coils will be given by the product of the instantaneous current in each coil multiplied by the gradient of their mutual inductance (dM/dx) at the distance of their separation:

$$F_{ab} = i_a i_b \, dM/dx$$

This force will be attractive between coils with currents of the same sign, and repulsive between coil currents of opposite sign.

Refer again to figure 1 and consider the forces acting on the reference coil no. 4. During its first quarter-cycle ($-\pi \leqslant \omega t \leqslant -\pi/2$), coil no. 4 will interact repulsively with coil no. 1, repulsively with coil no. 2, and attractively with coil no. 3.

At exactly $\omega t = \pi/2$, a weakly felt coil no. 1 (a distance $3\ell_m$ away) will turn off and a much closer coil (coil no. 5 only a distance ℓ_m away) will be activated. Because the force on coil no. 4 due to coil no. 5 is stronger than was the force from coil no. 1, a discontinuity in the gradient of the force acting on coil no. 4 will exist. During the second quarter-cycle ($-\pi/2 \leqslant \omega t \leqslant 0$), coil no. 4 will feel a repulsion from both coils nos. 2 and 3, and an attraction to coil no. 5. Through considerations of symmetry, the forces exerted on coil no. 4 in the third quarter-cycle are the negative of those exerted during the second quarter-cycle. Similarly, forces felt during the fourth quarter-cycle are the negatives of those experienced during the first quarter-cycle. Over the complete cycle, then, a drive coil receives no net force from its neighboring drive coils.

The program listed below is designed to calculate the reaction force on a drive coil due to all other active drive coils in its neighborhood as a function of the time from which that coil was turned on. It is written to be run on a Hewlett-Packard HP-67/HP-97 calculator.

It is assumed that bucket velocity may be taken as constant during the passage of the bucket through any four successive drive coils (a distance of only a few centimeters). Hence, the angular frequency ω will be constant.

The program is initialized by the input of three pieces of information: key in the dM/dx between drive coils separated by a distance ℓ_m; ENTER; key in dM/dx at a distance of $2\ell_m$; ENTER; key in dM/dx for a distance of $3\ell_m$ (ref. 4). Initiate the program by pressing the button labeled [A]. Program execution will begin. Very quickly, the program will pause for a second and the display will show "1.0." During this pause, key in the maximum drive coil current. (This value will default to 1.0 if no entry is made; in this case, all final answers will actually be $F/i_a i_b$.)

The program will then loop, displaying a zero for a second and then blurring for a second. At any instant when the machine has paused with a zero showing, key in a value of ωt and the reaction force of the drive coil at that instant will be calculated. The program accepts values of ωt expressed in degrees rather than radians. The range of valid values are $-180° \leqslant \omega t \leqslant 180°$.

Once a force has been calculated, the answer (in Newtons) is displayed for 10 sec. The program then branches to the zero/blur input mode, ready to have the next value of ωt keyed in.

001	*LBLA	012	PSE	023	*LBL2
002	DEG	013	F3?	024	X<0?
003	STO3	014	X²	025	SF2
004	R↓	015	STO4	026	ABS
005	STO2	016	CF3	027	STO5
006	R↓	017	*LBL1	028	1
007	STO1	018	CLX	029	8
008	CF3	019	PSE	030	0
009	1	020	F3?	031	-
010	STO4	021	GTO2	032	X>0?
011	PSE	022	GTO1	033	GTOe

034	RCL5	057	F2?	080	RCL4
035	9	058	CHS	081	x
036	0	059	PRTX	082	ABS
037	-	060	PRTX	083	RTN
038	X<0?	061	GTO1	084	*LBLc
039	GTOB	062	*LBLa	085	RCL5
040	GSBc	063	RCL5	086	SIN
041	STO0	064	SIN	087	RCL5
042	GSBb	065	RCL5	088	COS
043	ST-0	066	COS	089	x
044	GSBa	067	x	090	RCL1
045	ST-0	068	RCL3	091	x
046	GTO3	069	x	092	RC L4
047	*LBLB	070	RCL4	093	x
048	GSBc	071	x	094	ABS
049	ENT↑	072	ABS	095	RTN
050	+	073	RTN	096	*LBLe
051	CHS	074	*LBLb	097	CLX
052	STO0	075	RCL5	098	1/X
053	GSBb	076	SIN	099	RTN
054	ST-0	077	X²	100	R/S
055	*LBL3	078	RCL2		
056	RC L0	079	x		

REFERENCES

1. Kolm, H.: Basic Coaxial Mass Driver Reference Design. Space Manufacturing Facilities II, Proceedings of 1977 Princeton /NASA/ERDA/GE Conference on Space Manufacturing, AIAA, New York, 1977.
2. O'Neill, G. K.: Mass Driver Reaction Engine as a Shuttle Upper-Stage. Space Manufacturing Facilities II, Proceedings of 1977 Princeton/NASA/ERDA/GE Conference on Space Manufacturing, AIAA, New York, 1977.
3. Kaplan, Marshall H.: Modern Spacecraft Dynamics and Control. John Wiley & Sons, New York, 1976, p. 111.
4. Arnold, W.; Bowen, S.; Fine, K.; Kaplan, D.; Kolm, H.; Kolm, M.; Newman, J.; O'Neill, G. K.; and Snow, W.: Mass Drivers I: Electrical Design. Space Resources and Space Settlements, NASA SP-428, appendix A, 1979, p. 83.
5. Arnold, W.; Bowen, S.; Kaplan, D.; Fine, K.; Cohen, S.; Kolm, H.; Kolm, M.; Newman, J.; O'Neill, G. K.; and Snow, W.: Mass Drivers III: Engineering. Space Resources and Space Settlements. NASA SP-428, 1979, pp. 100-130.

III-3
Mass Drivers III: Engineering

WILLIAM H. ARNOLD, STUART BOWEN, STEVE COHEN, DAVID KAPLAN, KEVIN FINE, MARGARET KOLM, HENRY KOLM, JONATHAN NEWMAN, GERARD K. O'NEILL, and WILLIAM R. SNOW

This paper is the last of a series of three by the Mass-Driver Group of the 1977 Ames Summer Study. It develops the engineering principles required to implement the basic mass-driver design defined in paper I and as presented previously in the literature. Optimum component mass trade-offs are derived from a set of four input parameters, and the program used to design a lunar launcher. The mass optimization procedure is then incorporated into a more comprehensive mission optimization program called OPT-4, which evaluates an optimized mass-driver reaction engine and its performance in a range of specified missions. Finally, this paper discusses, to the extent that time permitted, certain peripheral problems: heating effects in buckets due to magnetic field ripple; an approximate derivation of guide force profiles; the mechanics of inserting and releasing payloads; the reaction mass orbits; and a proposed research and development plan for implementing mass drivers. This paper also considers further optimization that depends on advances in component technology beyond the present state. It is concluded that significant advantage can be gained in the case of small reaction engines with high emission velocity by developing lightweight packaging technology for silicon-controlled rectifiers (SCR's).

INTRODUCTION

The fundamental physics of electromagnetic mass drivers and the rationale for the basic design that has evolved are described by Arnold et al. (ref. 1, and prior literature referred to there). This paper deals primarily with the engineering principles involved in implementing the basic design, and the application of those principles to both mass-driver lunar launchers (MDLL) and mass-driver reaction engines (MDRE).

This embryonic engineering text represents, of course, a first approach, subject to perhaps as much subsequent refinement as was the engineering work of the Wright brothers or of Professor Goddard. It is rather remarkable that precise engineering principles can be formulated at all at such an early stage, considering for comparison the amount of work that had to be done in thermodynamics, fluid dynamics,

applied metallurgy, etc., before the first text on aircraft turbines could be written. Mass drivers are unique in that they derive very directly from the straightforward and well-understood principles of electromagnetic theory.

This paper first develops the formalism for deriving the optimum trade-off among design decisions for a given set of four input parameters; then certain peripheral problems that appear to be important are considered. Bucket-heating effects, which result from magnetic field ripple, turn out to be entirely manageable, and guide force profiles turn out to rise steeply enough to provide reasonable assurance against physical contact. Payload insertion and release do not appear to present serious problems, even at the significantly higher launch repetition rates utilized in the present designs. The conditions for safe (i.e., short-lived) reaction mass orbits seem clearly definable.

Capacitor mass must be higher than previously assumed to permit the high repetition rates imposed by optimization conditions, that is, maximum use rate conditions. The higher capacitor masses do not appear to affect total system mass very significantly.

SCR mass, on the other hand, represents a crucial problem that requires further research. Presently available SCRs involve package masses from 50 to more than 1000 times heavier than the silicon wafer masses. This circumstance does not reflect a physical necessity, but only the fact that little attention has so far been paid to this problem. From the viewpoint of mass-driver design, the high mass of SCR's is unimportant for lunar launchers and for the large, low-mission-velocity reaction engines intended for use in asteroid retrieval. On the other hand, for high-velocity reaction engines, SCR mass has overwhelming effect. It should be possible to take advantage of the extremely short pulse duration and the relatively low pulse repetition rate involved in order to develop SCR's approaching the actual mass of the active silicon wafers.

Another important consideration involving SCR's, about which very little data are available, is the effect of ambient operating temperature on their short pulse rating. It turns out that the total mass of power supply and radiators could be reduced by 32 percent if the overall system temperature were permitted to run at 400 K rather than 300 K. Unfortunately, this optimum system temperature is so close to the present operating limit of SCR's that their pulse rating would be seriously reduced. Thus, there are two substantial incentives for devoting some research to the packaging and rating of SCRs for space applications. It is quite likely that much could be gained by the development of a heat pipe cooling system for SCRs, for space applications other than mass drivers.

The design procedures, optimization programs, and example design results presented here are conservatively based on existing component technology. They are intended to supply a reliable data base for evaluating mass-driver performance and usefulness in relation to the entire range of possible missions now envisaged.

Our conclusions justify a serious development effort aimed toward the implementation of mass drivers. If such a program is started immediately, following the suggested baseline scenario, an operational mass-driver reaction engine could be launched in 1985.

MASS-DRIVER DESIGN PRINCIPLES

Input Parameters

The basic electrical and mechanical design of a mass driver is governed by the choice of three mission-related variables and one internal design variable.

Choice 1 — Mass m (kg) and density ρ_p (kg/m³) of the cylindrical propellant lump or payload carried in the bucket. Because the volume of the payload has been set, m_l varies only with the density of the material used. For all calculations shown here, we have arbitrarily chosen $\rho_p = 2 \times 10^3$ kg/m³, which is somewhat less than the density of ordinary rock (about 2.5×10^3 kg/m³).

Choice 2 — Repetition or launching rate of payload masses f_R (sec⁻¹ or Hz). The product of f_R and m_l is equal to the mass throughput $dm/dt = \boldsymbol{m}$ of the mass driver; f_R is known once $\boldsymbol{m}$ and m_1 are chosen. Mass throughput $\boldsymbol{m}$ is the relevant parameter for determining mission performance, but must be separated into f_R and m_l for purposes of design optimization.

Choice 3 — Exhaust or emission or launch velocity v_e (m/sec) ($v_e = V_{max}$), that is, the velocity with which the payload masses leave the mass driver. The product $\boldsymbol{m}v_e = f_R m_1 v_e$ is equal to the thrust of the mass driver when it is considered as a reaction engine.

Choice 4 — Acceleration a (m/sec²) imparted to the loaded bucket by the magnetic drive force. Once the configuration has been selected, as was done in reference 1, acceleration is simply proportional to the product of bucket and drive coil currents. The bucket current is limited by the critical current density of the superconducting material at the magnetic field and temperature conditions prevailing, while the drive coil current represents a trade-off, subject to optimization, between component mass (powerplant and radiators, capacitors, and SCR's). Assuming equal accelerating and decelerating forces, the total length of the mass driver (accelerating and decelerating sections) is given by the simple relation $[1 + (m_B/m_{BL})]$ $(v_e^2/2a)$, where m_B is the mass of the unloaded bucket and $m_{BL} = m_B + m_1$ is the mass of the loaded bucket. This relation expresses the very reasonable result that, for fixed v_e, the greater the acceleration, the shorter the driver.

Design Rationale

The mass-driver design flow chart given in figure 1 traces the logic that leads the designer from his initial choices of m_l, f_R, v_e, and a to the optimized mass-driver system mass and efficiency. In this section, we discuss in detail the logic tree presented in figure 1.
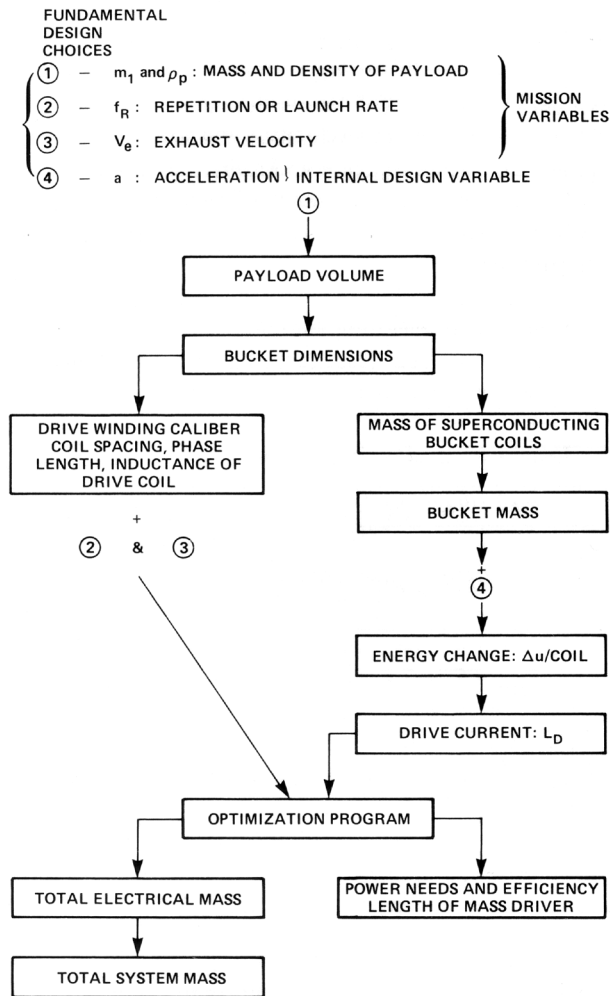
Figure 1 — *Mass-driver design logic.*

From choice 1: Once the mass and density of the individual payloads m_l and ρ_p are specified, the dimensions of the bucket drive coils and coil spacing can be determined as explained in the payload dimensions section of reference 1. The length of the payload is $0.925D$ (where D, the mean diameter of the drive coils, is the "caliber"), while its diameter is $0.3D$. Hence the volume of the payload is (in MKS units)

$$V_p = \pi r_p^2 \ell_{pay} = 6.538 \times 10^{-2} D^3$$

Since $m_l = v_p \rho_p$, the caliber D can be determined; assuming $\rho_p = 2 \times 10^3 \ kg/m^3$,

$$D = \left(\frac{m_1}{6.538 \times 10^{-2} \rho_p} \right)^{1/3} = 0.197 \ m_1^{1/3}$$

Once the caliber is known, the following design parameters with dimensions of length can be determined from the design decisions defined in reference 1:

Bucket coil width = build:
$$W_B = 0.1D = 0.0197 \ m_1^{1/3}$$

Effective radius of bucket coil:
$$r = 0.26D = 5.122 \times 10^{-2} \ m_1^{1/3}$$

Length of single-turn drive winding:
$$\ell_W = \pi D = 0.619 \ m_1^{1/3}$$

Inductance length = drive coil spacing:
$$\ell_m = 0.185D = 3.645 \times 10^{-2} \ m_1^{1/3}$$

Phase length or wavelength of drive current oscillation:
$$\ell_p = 4\ell_m = 0.146 \ m_1^{1/3}$$

Volume of individual bucket coils:

$$V_{BC} = \pi W_B \left[\left(r + \frac{W_B}{2} \right)^2 - \left(r - \frac{W_B}{2} \right)^2 \right]$$

$$= 1.634 \times 10^{-2} \ D^3 = 1.249 \times 10^{-4} \ m_1$$

Mass of a single bucket coil:

$m_{BC} = V_{BC}\rho_s = 0.566 \ m_l$ since the density of the niobium-tin superconductor is $4.53 \times 10^3 \ kg/m^3$

From these results and design choices mentioned earlier, we obtain:

Total coil mass per bucket:
$$m_{super} = 2m_{BC} = 1.132 \ m_l$$

Empty bucket mass:
$$m_B = 2m_{super} = 2.263 \ m_l$$

Loaded bucket mass:
$$m_{BL} = m_B + m_1 = 3.263 \ m_1$$

Ratio of unloaded to loaded bucket mass:
$$m_B/m_{BL} = 0.694$$

Current in each bucket coil:
$i_B = 2.5 \times 10^6 \ D^2 = 9.702 \times 10^4 \ m_1^{2/3} \ A$ based on a current density of $2.5 \times 10^8 \ A \ m^{-2}$, achieved in the M.I.T. magneplane model

Single-turn self-inductance of a drive coil:
$$L_S = 2.004 \times 10^{-6} \ D, \ H$$
$$= 3.948 \times 10^{-7} \ m_1^{1/3}, \ H$$

Note that the above inductance value was computed using reference 2 (p. 95), assuming the drive coil cross section to have a width and build each equal to $0.05D$. If we assume instead a value of $0.1D$, then we obtain: $L_S = 1.572 \times 10^{-6} \ D = 3.097 \times 10^{-7} \ m_1^{1/3}$ H, equivalent to multiplying by a factor of 0.78. This alternative will be referred to later.

From reference 1, the equivalent circuit for the electrical drive is a series LRC combination in addition to a voltage generator for the back emf due to bucket passage. The actual drive circuit consists of eight drive coils, four per phase, the two phases being in quadrature. It is beyond the scope of this article to analyze this circuit completely; the interactions between sine-wave currents switched on for single cycles and of differing phases in nearby drive coils require a more detailed analysis. For the circuit given in reference 1 the inductance L_W, consists of the self-inductance of a drive coil and the effect of all relevant mutual inductances. In the simplified case of only one phase

operating, $L_W = L_S - M_2$, where M_2 = mutual inductance between drive coils with a spacing of $2\ell_m$.

From choices 2 and 3: Together with the choice of m_l and ρ_p, the exhaust velocity v_e and the repetition rate f_R determine the following additional mission parameters:

Mass throughput:
$$dm/dt = \dot{m} = f_R m_1$$

Thrust:
$$\dot{m} v_e = f_R m_1 v_e$$

Kinetic energy of payload:
$$(1/2) m_1 v_e^2$$

Jet power or kinetic power:
$$(1/2)\dot{m} v_e^2 = (1/2) m_1 f_R v_e^2$$

The ringing frequency of the drive circuit, ω_{LC}, is related to the velocity of the bucket and the phase length by

$$\omega_{LC} = 2\pi v/l_p$$

At the maximum velocity end of the driver, $\omega_{LC} = \omega_{max}$ and $\omega_{max} = 43.1 v_e m_1^{-1/3}$.

From choice 4: The choice of acceleration together with the choice of m_1, f_R, and v_e determine the remaining parameters:

Length of accelerating section:
$S_a = v_e^2/2a$ (assuming equal accelerating and decelerating forces)

Length of decelerating section:
$$S_d = (m_B/m_{BL})(v_e^2/2a) = 0.347(v_e^2/a)$$

Total length of mass driver:
$$S_{tot} = S_a + S_d = [1 - (m_B/m_{BL})]\,(v_e^2/2a) = 0.847\,v_e^2/a$$

Total number of drive windings per phase:
$$N_W = S_{tot}/\phi\ell_p = 11.62 v_e^2 a^{-1} m_1^{-1/3}$$

Finally, the drive current i_D (in ampere-turns, $i_D = n_2 i$) must be calculated. As described in reference 1, the required drive current is obtained from the energy change Δu which each drive coil must impart to a bucket. However, an approximate method was used in this article (not in ref. 1) to determine i_D. Given that $\Delta u = \int i_B (dM/dx) i_D(x)\, dx$, the expressions for dM/dx and $i_D(x)$ were approximated by: $dM/dx = dM/dx(\max)\,\sin[(\pi v/2\ell_m)x]$ and $i_D = i_D(\max)\sin[(\pi v/2\ell_m)x]$. In this approximation, the integral for Δu can be solved in closed form in terms of caliber D. Typically this gives an error of less than 10 percent from the correct value determined by the method described in reference 1.

Once all the design parameters are computed, the masses of the various electrical components, total system mass, power requirements, and system efficiency can be determined. The formulas that give the minimized electrical component masses and total system mass were derived in the 1976 Ames Study report (ref. 3). These formulas have been modified in certain details because of the change from a three-phase to a split two-phase system and the elimination of the "local duty cycle" (now unity). Consult references 3 and 4 for a derivation of these formulas; we discuss here only modifications to these formulas.

Dependent Parameters

1. Total SCR mass, M_S:

$$M_S = (4/3)\,N_W(VA)_{max}m_s$$

where

$(VA)_{max} = i_D \omega_{max} L_w$
ms = specific SCR mass
$= 5 \times 10^{-9}\ kg/VA_{peak}$

This formula is a factor of 2/3 less than that derived in references 3 and 4, the result of reducing the number of phases in the mass driver from 3 to 2. When M_S is computed in terms of the relevant design parameters,

$$M_S = 1.656 \times 10^{-10} v_e^3 a m_1^{1/3}$$

This relation assumes a certain drive coil cross section (as discussed in the previous section) and is also based on SCR technology (see section on SCR technology).

2. Total winding mass, M_W and M_{PRW}:

$$M_W = 4N_W \ell_W A_{DO}\rho kG$$

where

$$A_{DO} = \left[\frac{n_C \ell_P f_R i_D^2 \rho_R (m_P + m_R)}{4\rho_{kG}v_e} \right]^{1/2}$$

where ρR and ρ_{kG} are the electrical resistivity and mass density of aluminum, respectively; A_{DO} is the minimized drive winding cross section; n_C is the number of coils per bucket; m_R is the specific powerplant mass; and m_R is the specific radiator mass. The formula for M_W is reduced by a factor of 2/3 because of the reduction from three phases to two. The expression for A_{DO} omits the term $(f_m)^{-2}$ because f_m, the so-called micro-duty cycle, becomes unity in the two-phase system. When M_W is computed explicitly in terms of parameter values,

$$M_W = 0.122 v_e^{3/2} m_1^{1/2} f_R^{1/2}\ \text{for mass-driver reaction}$$
engines (MDRE)
$$= 0.142 v_e^{3/2} m_1^{1/2} f_R^{1/2}\ \text{for mass-driver lunar}$$
launchers (MDLL)

In the optimized case (refs. 3, 4), the mass of the powerplant and waste heat radiators associated with the drive windings M_{PRW} is equal to M_W, the winding mass.

3. Total feeder mass, MF, and MC and MpRF:

$$M_F = 8Af_0 S_{tot}\rho_{kG}$$

where

$$A_{f0} = \frac{1}{8}\left[\frac{n_w{}^3 L_w i_D{}^4 m_c \rho_R f_R (m_P + m_R)}{2 n_2{}^2 \rho_{KG}{}^2 v_e}\right]^{1/3}$$

where n_w is the number of windings simultaneously excited per phase associated with one bucket coil, A_{f0} is the minimized feeder cross section, and m_c is the specific capacitor mass. The formula for M_F is reduced by a factor of 2/3 because of the reduction from three phases to two. The expression for A_{f0} is less by a factor of $n_w{}^{2/3} f_m{}^{1/3}$ because the number of bucket coils was reduced from four to two and $f_m = 1$ was chosen. When M_F is computed explicitly in terms of the parameter values,

$$M_F = 7.196 \times 10^{-4} v_e{}^{5/3} a^{1/3} m_1{}^{5/9} f_R{}^{1/3}$$
$$\text{(for reaction engines)}$$
$$= 7.97\,3 \times 10^{-4} v_e{}^{5/3} a^{1/3} m_1{}^{5/9} f_R{}^{1/3}$$
$$\text{(for lunar launchers)}$$

These figures again assume $L_W = 3.948 \times 10^{-7} m_1{}^{1/3}$ (see note in previous section concerning inductance). For the larger coil cross section, $L_W = 3.097 \times 10^{-7} m_1{}^{1/3}$, and M_F must be multiplied by a factor of 0.92; in this case, the factors in the above relation become 6.637×10^{-4} for MDRE and 7.353×10^{-4} for MDLL. In the optimum case, the mass of the capacitors connected across the feeders, m_c, and the mass of the powerplant and waste heat radiators associated with the feeders, M_{PRF}, are both equal to M_F (see refs. 3, 4).

4. Kinetic power mass, M_{kin}:

$$M_{kin} = 0.5(dm/dt) m_p v_e{}^2 = 0.5 f_R m_1 m_p v_e{}^2$$

There is no change in this expression for M_{kin}. In terms of the parameter values, we obtain:

$$M_{kin} = 0.0025 f_R m_1 v_e{}^2$$
$$\text{for reaction engines (mp = 0.005 kg/W)}$$
$$= 0.007 f_R m_1 v_e{}^2$$
$$\text{for lunar launchers (mp = 0.014 kg/W)}$$

5. Total electrical mass, M_{el}:

$$M_{el} = M_S + M_W + M_{PRW} + M_F + M_C + M_{PRF} + M_{kin}$$
$$= M_S + 2M_W + 3M_F + M_{kin}$$

This expression remains unchanged.

6. Total structural mass, M_{st}:

$$M_{st} = 0.5 M_{el}$$

This value represents a first estimate subject to further refinement. It includes the total mass of all buckets, mass of the electrical components in the return track, mass of all sensing and control devices used in the driver, and mass of all structural members.

7. Total mass of mass-driver system, M_{tot}:

$$M_{tot} = M_{el} + M_{st}$$

8. Mass-driver power requirements, P_{tot}: The total power required to operate a mass driver is the sum of the kinetic power ($P_{kin} = (1/2)\boldsymbol{m} v_e{}^2$, electric power required to accelerate the payload to the exhaust velocity) and the power required to supply $i^2 R$ losses in the feeders and drive windings. The term P_{tot} is given by

$$[(M_{kin})\,(1/m_p) + (M_W + M_F)(1/(m_p + m_R))]$$

which, in terms of the parameter values, is

$$P_{tot} = (0.5)(f_R m_1 v_e{}^2) + 40[(0.122 v_e{}^{3/2} m_1{}^{1/2} f_R{}^{1/2})$$
$$+ (7.196 \times 10^{-4} v_e{}^{5/3} a^{1/3} m_1{}^{1/2} f_R{}^{1/2})]\ \text{(MDRE)}$$

$$P_{tot} = 0.5(f_R m_1 v_e{}^2) + 29.41[(0.142 v_e{}^{3/2} m_1{}^{1/2} f_R{}^{1/2})$$
$$+ (7.973 \times 10^{-4} v_e{}^{5/3} a^{1/3} m_1{}^{5/9} f_R{}^{1/3})]\ \text{(MDLL)}$$

(again, refer to the note concerning inductance in the preceding section).

9. Waste power, PW (power lost in feeders and windings):

$$P_W = (M_W + M_F) + 1/(m_p + m_R)$$

with the explicit values given on the right-hand side of the above expressions.

10. Mass-driver efficiency, η:

$$\eta = (P_{tot} - P_W / P_{tot} = 1 - (P_W / P_{tot})$$

Example Design: Lunar Launcher

The design principles developed previously and in reference 1 have been translated into an HP 67/97 program, readily adaptable to any other computer (described in detail in appendix A). The program derives optimized component masses, total mass, overall length, power requirements, and waste power, and efficiency on the basis of the four input parameters that have been defined. One essential parameter does not appear explicitly in this program — the caliber. It depends directly on payload mass m_l and, as explained in reference 1, is

$$D = 0.197 m_1{}^{1/3}$$

where m_1 is the payload (in kilograms) and D is the caliber (in meters). This relationship is based on our assumed payload density of 2×10^3 kg/m³.

The program was used to compute an optimized lunar launcher. Requirements were specified as an annual throughput of 650,000 metric tons, assuming 49 percent operating time — which allows for total shutdown during the lunar night and 1-percent downtime for emergency repairs. This requires a 42-kg/sec throughput. At a given throughput, the total system mass is found to be quite insensitive to variations in launch frequency and payload mass, within practical limits. We have therefore arbitrarily chosen payload mass and launch frequency as 10.5 kg and 4 Hz, respectively. The launch velocity is 2,400 m/sec, the lunar escape velocity. Acceleration is chosen as 1000 Earth gravities or 10,000 m/sec². The following optimized parameters are obtained:

SCR mass	5.03×10^4 kg
Winding mass	1.08×10^5 kg
Feeder mass	4.33×10^4 kg
Kinetic power mass	1.69×10^6 kg
Total electric mass	2.09×10^6 kg
Total mass	3.13×10^6 kg
Total length	4.88×10^2 m
Waste power	4.46×10^6 W
Total power	1.25×10^8 W
Efficiency	96.4 percent

Note that if the acceleration is decreased by a factor of 10 to 100 gravities or 1000 m/sec², there will be a 4-percent savings in total mass, the efficiency will rise slightly to 97 percent, but the total length of the launcher increases by a factor of 10 to nearly 5 km. The caliber of the assumed launcher is $D = 0.197 m_1^{1/3} = 0.431$ m (17 in.).

The program can also be used to optimize the mass of mass drivers used as reaction engines, subject to the slight change in assumed boundary conditions as indicated in the program description (appendix A). However, mass-driver reaction engines must be optimized in terms of overall mission requirements and, therefore, the input parameters that form the basis for the present optimization no longer represent the independent variables. A more fundamental mission optimization program will therefore be developed in the following section.

MISSION OPTIMIZATION

In the preceding section, we solved the problem of designing an optimized mass driver, that is, one of minimum total mass, on the basis of four input parameters: payload mass and density, launch repetition rate (which together determine mass throughput and required size), exhaust velocity, and acceleration. This optimization program is adequate for the design of lunar launchers, but a more comprehensive optimization process is required to design the optimized mass-driver reaction engine for a given mission in space. We have developed such a comprehensive mission optimization program, called OPT-4. The rationale of this procedure is described here and a number of selected mission performance curves are presented. An HP 67/97 version of the OPT-4 program is described in appendix B.

Equivalent Free-Space Velocity Increment

A space mission is characterized predominantly by its velocity increment, which is defined as

$$\Delta V = \int_O^{t_B} a(t) dt \qquad (1)$$

where $a(t)$ is acceleration as a function of time and t_B is the total thrusting time. This parameter can be defined for motion in an inverse-square gravitational field in the limit of low-thrust spiral orbits typical of mass-driver performance as follows.

We assume the velocity to be equal to the local circular velocity at all times. The total energy per unit mass, kinetic

plus gravitational, is

$$E = (V^2/2) - (K/r) \qquad (2)$$

where $K = GM_{primary}$ and r is the orbit radius.

The local circular velocity in an orbit is $v_c^2 = K/r$ (orbit condition) and, since $v = v_c$, $E = -K/2r$. The rate of change of energy per unit mass, that is, the power per unit mass, is

$$dE/dt = (K/2r^2) \, dr/dt$$

If $a =$ force per unit mass $=$ acceleration, then the power supplied per unit mass is $a \cdot v = dE/dt$. Assuming v parallel to a (tangential thrust) and $v^2 = K/r$, we find:

$$dE/dr = 2ar^{3/2}/K^{1/2} \qquad (3)$$

as the radial velocity due to the tangential acceleration.

Separating variables, we obtain:

$$\int_O^t a \, dt = \sqrt{\frac{K}{2}} \int_{r_O}^r \frac{dr}{r^{3/2}}$$

and

$$\Delta V = \sqrt{K/r_O} - \sqrt{K/r} = v_{c,O} - v_{c,f} \qquad (4)$$

Thus, the equivalent free-space ΔV for low thrust spiraling in an inverse-square-law field is the difference in circular velocities for the initial and final orbits. This analysis does not apply for plane-changing or highly elliptical orbits.

Another quantity of interest is the relation between ΔV, the initial acceleration a_0, and the exhaust velocity v_e. Let $M(t)$ be the overall mass of the vehicle and T be the thrust force, then $a(t) = T/M(t)$, where $M(t) = M_0 - \dot{m}t$ and M_0 is the initial mass. Since $T = \dot{m}v_e = M_0 a_0$, we find

$$a(t) = a_0/[1-(a_0/v_e)t]$$

and hence

$$\Delta V = \int_O^{t_B} a(t)dt = -v_e \ln(1 - a_0 t_B/v_e)$$

or

$$\frac{a_0 t_B}{v_e} = 1 - e^{-\Delta V/v_e}$$

where t_B is the thrusting time.

From low Earth orbit (LEO), at an altitude of 200 km, to geosynchronous orbit at radius = 42,243 km, $\Delta V = 7.785 \times 10^3 - 3.072 \times 10^3 = 4.713 \times 10^3$ m/sec.

Externally Powered Rocket Equations

Electromagnetic mass drivers differ from other propulsion systems in that the propellant mass flow is decoupled from the energy per unit mass of propellant flow, since propellant represents only reaction mass, power being supplied from a separate source, the Sun. Optimization will therefore be governed by the relative value of time and reaction mass, energy consumption entering only in the sense that it

determines the mass of power supply and heat radiators.

Let

M_{pay} payload mass
M_{pow} powerplant and associated structure mass
M_{prop} propellant mass
M_{tot} total mass-driver mass

The initial mass is

$$M_0 = M_{pow} + M_{pay} + M_{prop} \tag{5}$$

the final burnout mass is

$$M_B = M_0 - M_{prop} \tag{6}$$

Let P = powerplant power and α = overall powerplant specific mass of the mass-driver reaction engine (in kg/W). The power that appears as kinetic energy in the jet is

$$P_K = \dot{m}(v_e^2/2) \tag{7}$$

where v_e is exhaust velocity and $\dot{m}$ is the propellant mass-flow rate. We define an efficiency of conversion η as the fraction of the electrical power P that appears as exhaust kinetic energy:

$$\eta = P_K/P \tag{8}$$

The thrust force is

$$T = \dot{m}v_e \tag{9}$$

where

$$\dot{m} = M_{prop}/t_B = m_1 f_R$$

is the propellant mass-flow rate and t_B is the mission thrusting time. The jet power can also be written as

$$P_K = \eta P = T v_e/2 \tag{10}$$

The free-space velocity increment is, from the rocket

$$\Delta V = v_e \ell n(M_0/M_B) \tag{11}$$

In the following, we assume $\dot{m}$ and v_e are constant throughout the mission. From the definition of specific power $M_{pow} + P\alpha$, we find:

$$\frac{M_B}{M_O} = \frac{M_{pow}}{M_O} + \frac{M_{pay}}{M_O} = \frac{\alpha P}{M_O} + \frac{M_{pay}}{M_O}$$

$$= \frac{mv_e^2}{2\eta M_O} + \frac{M_{pay}}{M_O} = \frac{\alpha v_e^2}{2\eta t_B}\left(1 - \frac{M_B}{M_O}\right) + \frac{M_{pay}}{M_O} \tag{12}$$

or

$$\frac{M_{pay}}{M_O} = \exp\left(\frac{-\Delta V^*}{v_e^*}\right) - v_e^*\left[1 - \exp\left(\frac{-\Delta V^*}{v_e^*}\right)\right] \tag{13}$$

where

$$\Delta V^* = \Delta V/v_c \tag{14}$$

$$v_e^* = v_e/v_c \tag{15}$$

and

$$v_c = \text{mission characteristic velocity} = \sqrt{2\eta t_B/\alpha} \tag{16}$$

Equation (13) gives the payload fraction delivered at the end of the mission. The propellant fraction is

$$\frac{M_{prop}}{M_O} = 1 - \exp\left(\frac{-\Delta V^*}{v_e^*}\right) \tag{17}$$

while the powerplant fraction is

$$\frac{M_{pow}}{M_O} = v_e^{*2}\left[1 - \exp\left(\frac{-\Delta V^*}{v_e^*}\right)\right] \tag{18}$$

Thus, if we compute α and η from the input parameters by the program developed in the preceding section and specify a particular mission characterized by the free-space velocity increment ΔV and mission time t_B, we can compute not only the mass-driver component masses, but also the payload mass returned and other mission performance parameters. These quantities can be crossplotted as required. Since the overall vehicle initial acceleration is

$$a_O = \frac{v_e}{t_B}\left[1 - \exp\left(\frac{-\Delta V^*}{v_e^*}\right)\right] = \frac{T}{M_O} \tag{19}$$

where $T = mv_e$, the initial mass M_0 is given by

$$M_0 = T/a_0$$

and the payload delivered then follows from equation (13), the propellant used from equation (17).

Reaction Engine Component Masses, System Mass, and Efficiency

Using the OPT-4 program, we determined and plotted the efficiency, overall system mass, specific system mass, and separate component masses as a function of mission velocity, v_e, and acceleration a for two typical mass-driver reaction engines:

1. A small-caliber, high exhaust speed engine to be used for LEO-GEO tug; $m_1 = 0.016$ kg, $D = 0.05$ m
2. A large-caliber, moderate exhaust speed engine to be used for asteroid retrieval; $m_1 = 3.8$ kg, $D = 0.307$ m

The launch frequency f_R was 10 Hz for both engines.

The bare power plant specific mass was set at 0.005 kg/W, and the specific radiator mass, at 0.020 kg/W. The payload/bucket-mass ratio was 2.263 (see figs. 2-5).

Mission Performance Curves for Selected Input Parameters

We now present curves showing the dependence of mission performance parameters for various missions characterized by ΔV, as a function of exhaust velocity for various values of propellant acceleration a. The following parameters are plotted (see figs. 6-13):

a	acceleration
M_0	initial mass
M_{pay}	payload mass (final mass at destination)
M_{prop}	propellant mass
m_l	pellet mass
t_B	mission duration
v_e	exhaust velocity

(a) 3.8-kg load pellets.

(b) 0.016-kg load pellets.
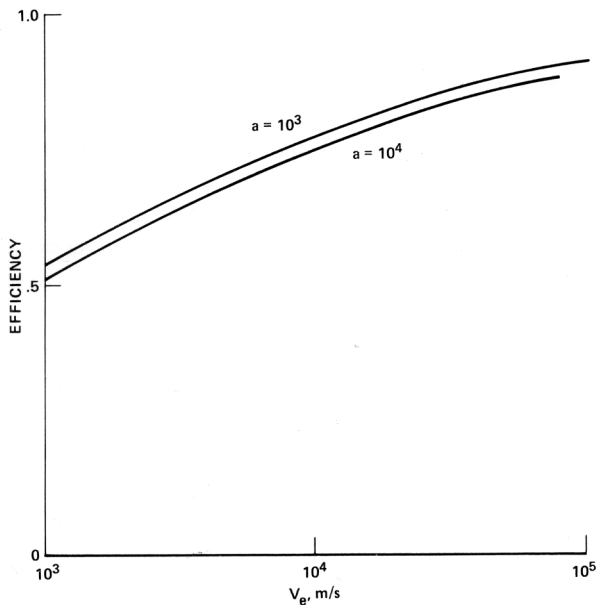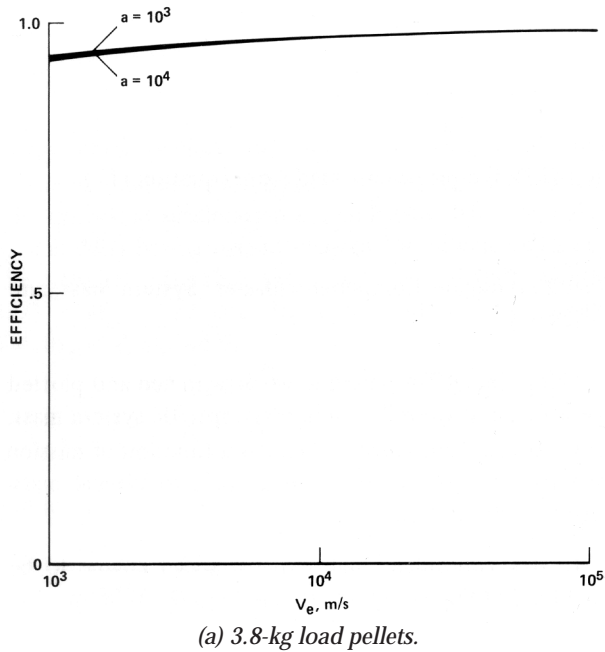
Figure 2 — *Efficiency vs exhaust velocity.*

(a) 0.016-kg pellets.
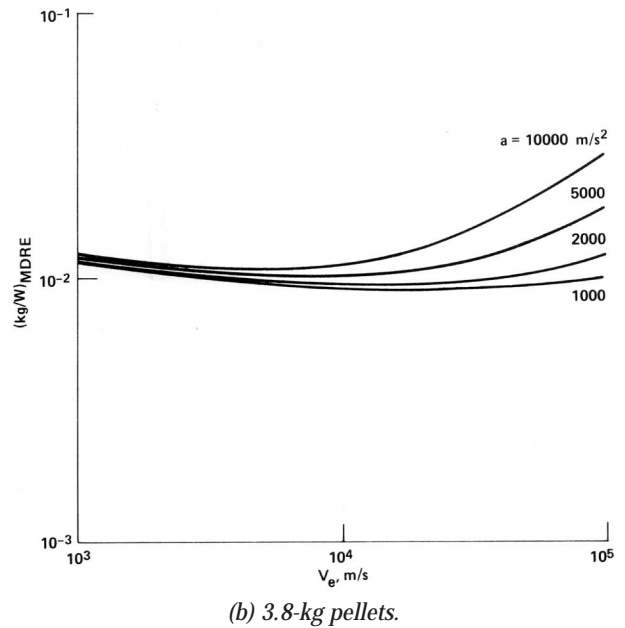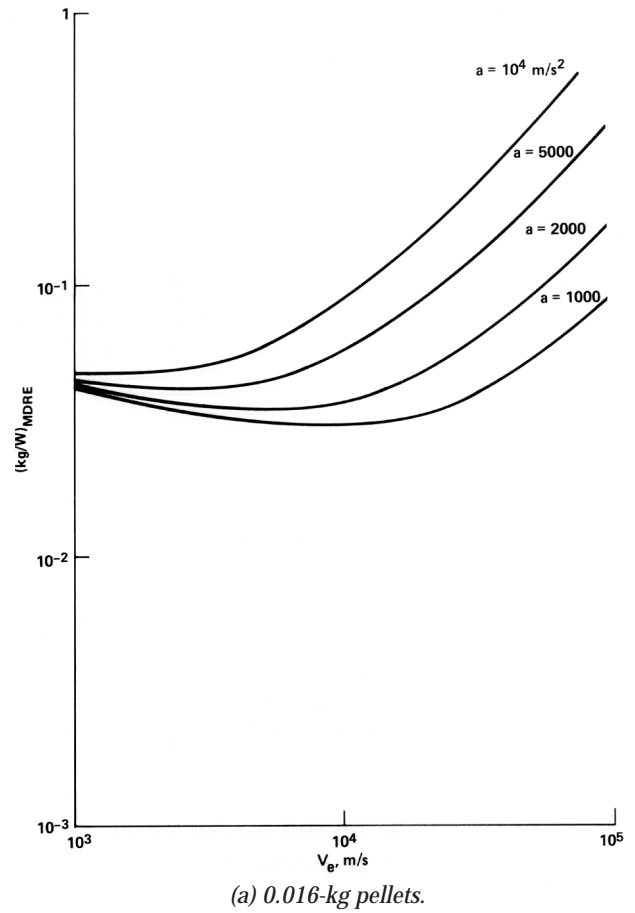
(b) 3.8-kg pellets.

Figure 3 — *Specific MDRE mass (kg/W) vs exhaust velocity;* a = 1, 2, 5, and 10 X 10^3 m/sec².
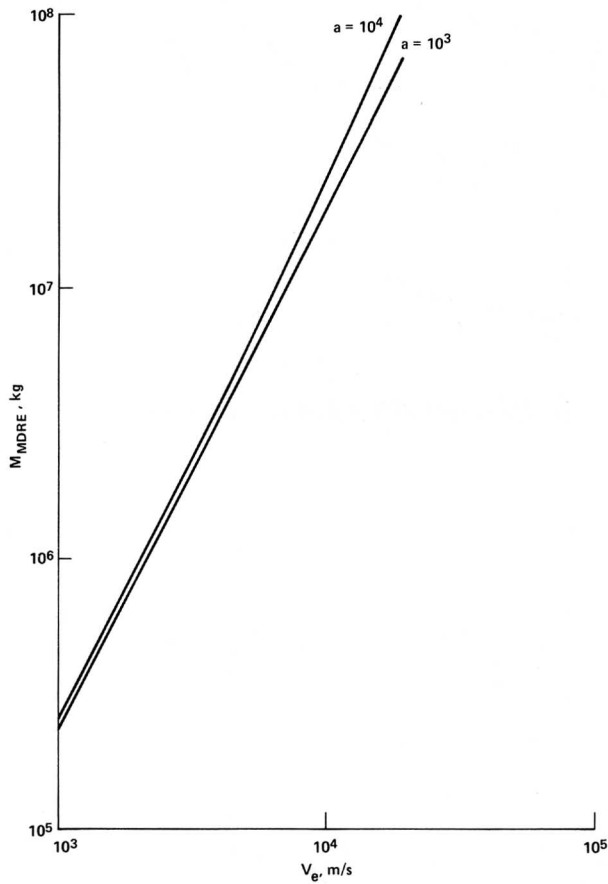
(a) 3.8-kg pellets, a= 1,000 and 10,000 m/sec².
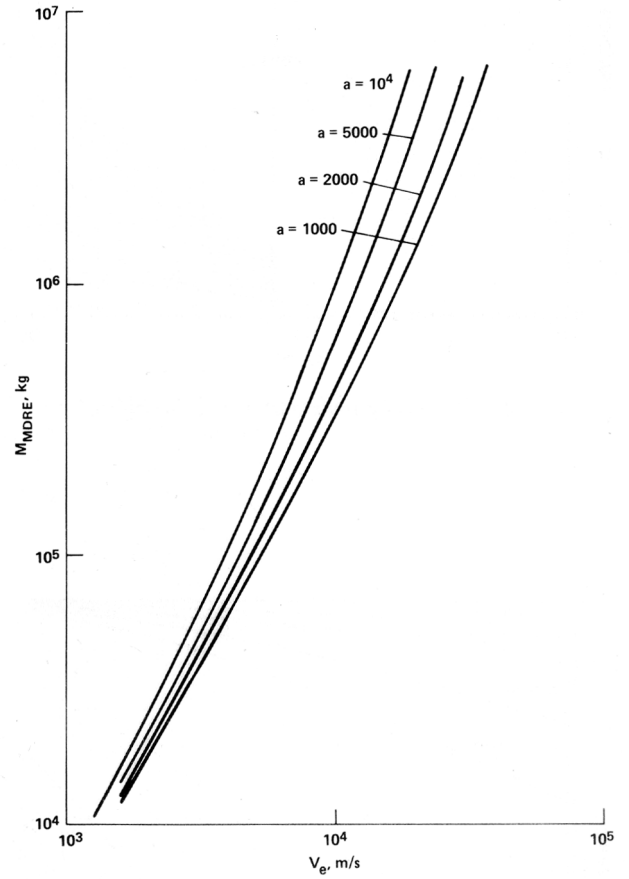
(b) 0.016-kg pellets, a= 1, 2, 5, and 10 X 10³ m/sec².
Figure 4 — *MDRE mass (kg) vs exhaust velocity.*
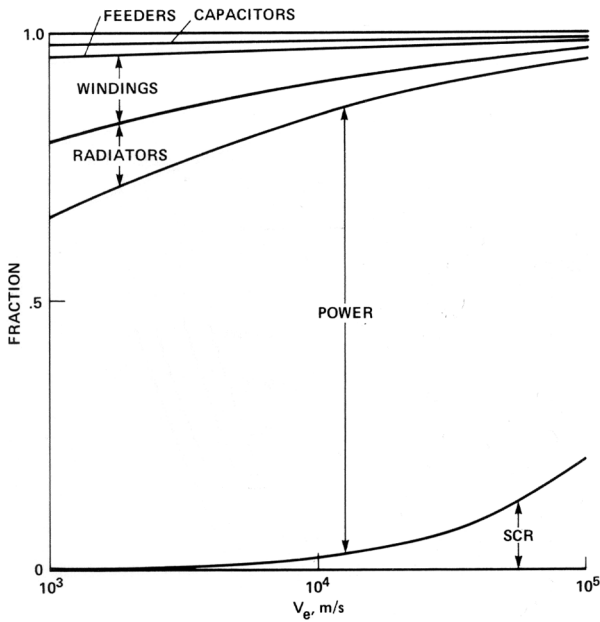
(a) Ejecting 3.8-kg pellets at a = 1,000 m/sec².
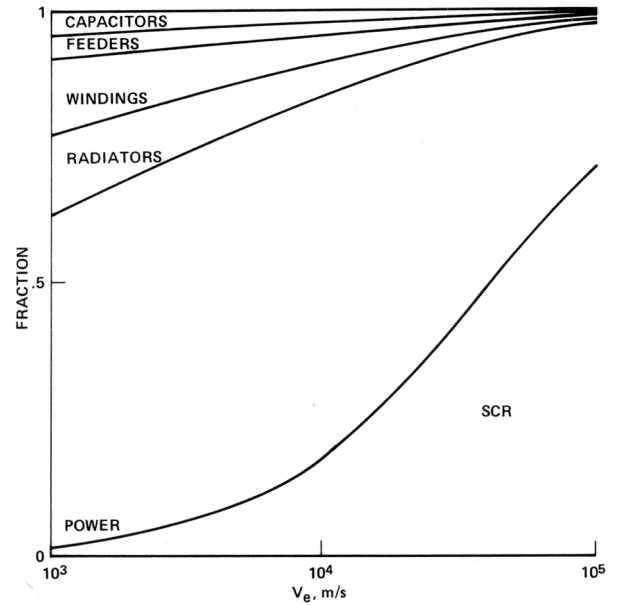
(b) Ejecting 3.8-kg pellets at a = 10,000 m/sec².
Figure 5 — *Component masses (SCR, power, radiators, windings, feeders, and capacitors) vs exhaust velocity for MDRE.*
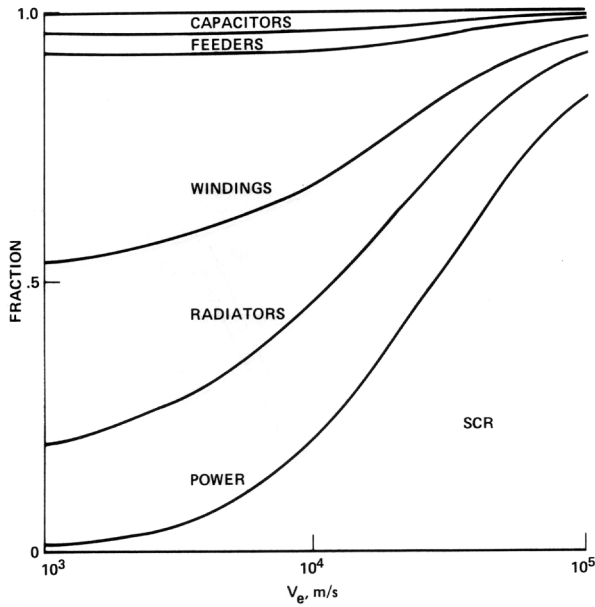
(c) Ejecting 0.016-kg pellets at a = 1,000 m/sec².
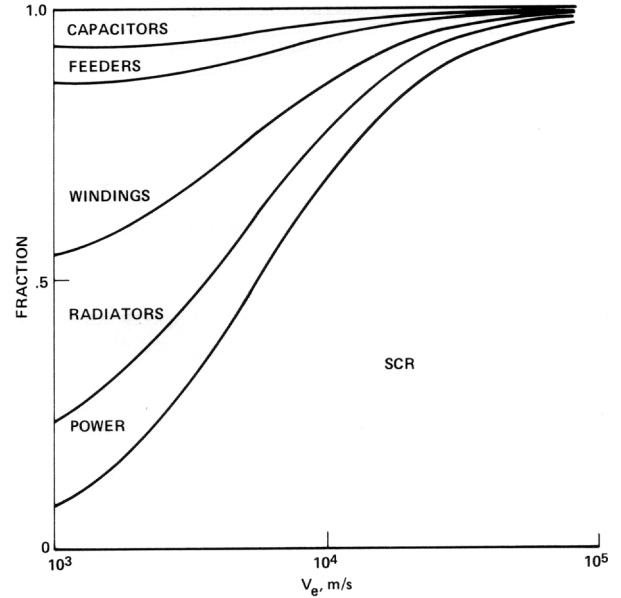
(d) Ejecting 0.016-kg pellets at a = 10,000 m/sec².

Figure 5 — *Component masses (SCR, power, radiators, windings, feeders, and capacitors) vs exhaust velocity for MDRE.*
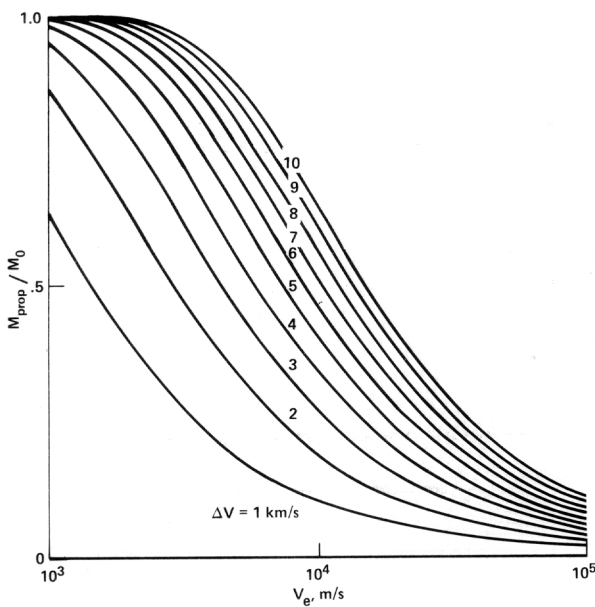
Figure 6 — *Propellant/initial mass ratio vs exhaust velocity for MDRE ejecting 3.8-kg pellets at a = 10,000 m/sec², assuming a 365-day mission at ΔV = 1, 2, 3, 4, 5, 6, 7, 8, 9, and 10 km/sec.*
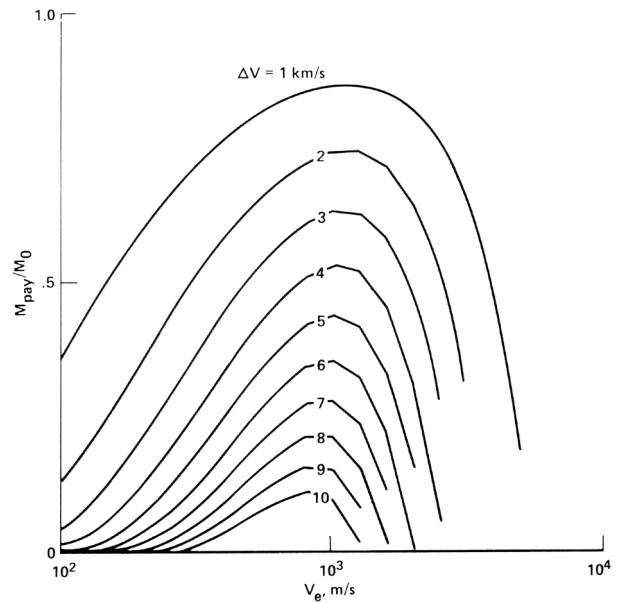
(a) a = 10,000 m/sec², assuming a 150-day mission at ΔV = 1, 2, 3, 4, 5, 6, 7, 8, 9, and 10 km/sec.

Figure 7 — *Payload/initial mass ratio vs exhaust velocity for MDRE ejecting 0.016-kg pellets.*
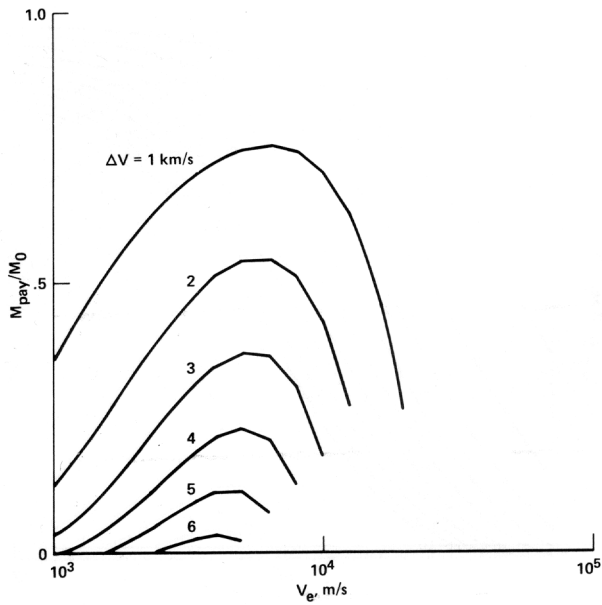
(b) a = *10,000 m/sec², assuming a 30-day mission at* ΔV = *1, 2, 3, 4, 5, and 6 km/sec.*
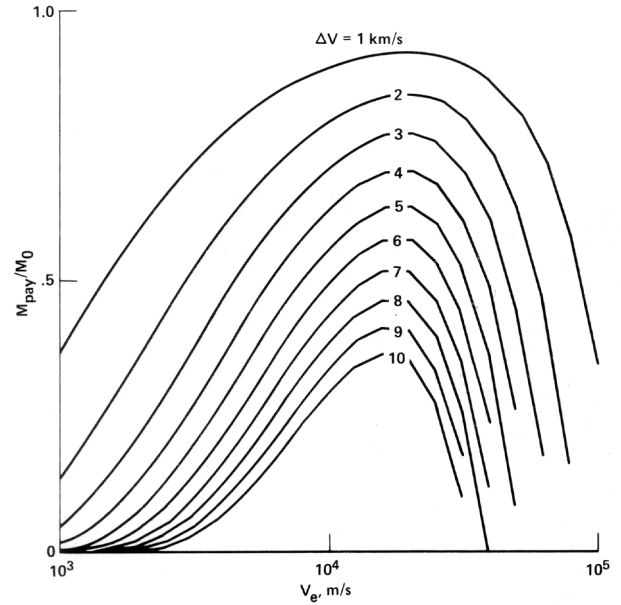
(c) a = *5,000 m/sec², assuming a 365-day mission at* ΔV = *I , 2, 3, 4, 5, 6, 7, 8, 9, and 10 km/sec.*
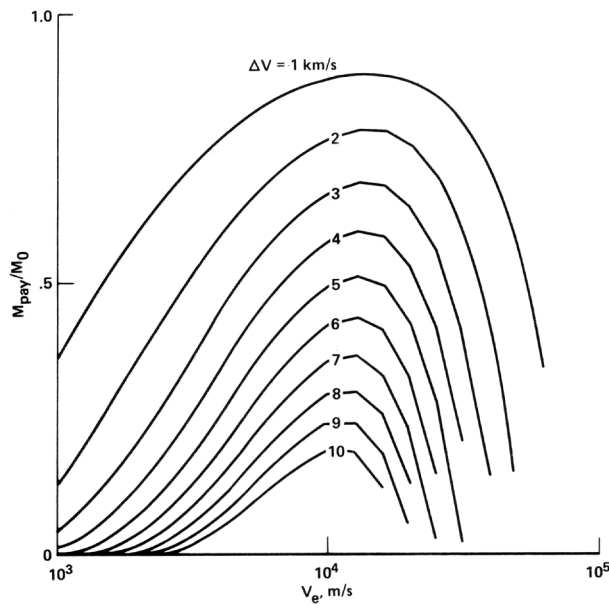
(d) a = *5,000 m/sec², assuming a I50-day mission at* ΔV = *1, 2, 3, 4, 5, 6, 7, 8, 9, and 10 km/sec.*

Figure 7 — *Payload/initial mass ratio vs exhaust velocity for MDRE ejecting 0.016-kg pellets.*
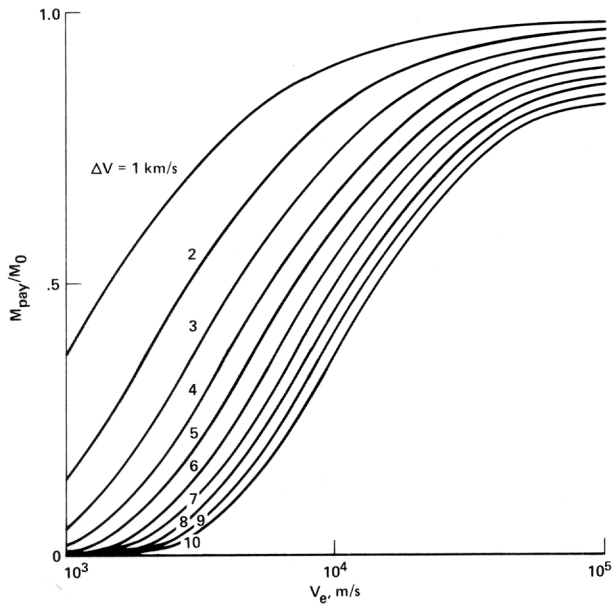
(a) Ejected at a= 1,000 m/sec², assuming a 730-day mission at ΔV = 1 to 10 km/sec.

(b) Ejected at a = 1,000 m/sec², assuming a 365-day mission at ΔV = 1 to 10 km/sec.

(c) Ejected at a = 5,000 m/sec², assuming a 365-day mission at ΔV = 1 to 10 km/sec.

(d) Ejected at a = 10,000 rn/sec², assurnlng a 7.3U-clay mission at ΔV = 1 to 10 km/sec.

Figure 8 — Payload/initial mass ratio vs exhaust velocity for MDRE ejecting 3.8-kg pellets.

(e) Ejected at a = 10,000 m/sec², assuming a 365-day mission at
ΔV = 1 to 10 km/sec.

Figure 8 — *Payload/initial mass ratio vs exhaust velocity for*
MDRE ejecting 3.8-kg pellets.

Figure 9 — *Payload mass vs exhaust velocity delivered by MDRE*
ejecting 3.8-kg pellets at a *= 10,000 m/sec², assuming a 730-day*
mission at ΔV = 1 to 10 km/sec.

Figure 10 — *Payload mass vs exhaust velocity delivered by a*
MDRE ejecting 0.016-kg pellets at a *= 10,000 m/sec² for a 150-day*
mission at ΔV = 1 to 10 km/sec.

(a) 3.8-kg pellets, assuming a 730-day mission.　　　　*(b) 0.016-kg pellets, assuming a 150-day mission.*
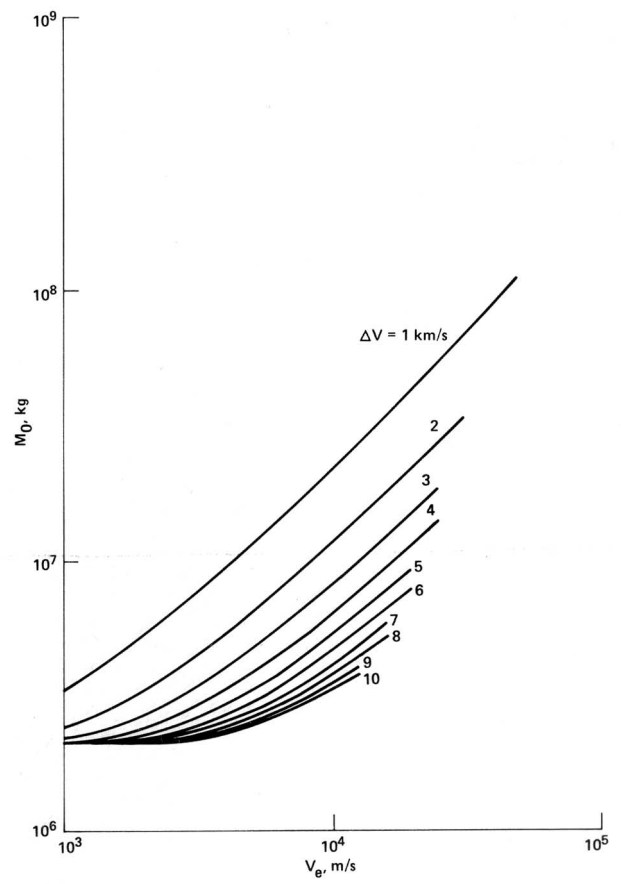
Figure 11 — *At* a *= 10, 000 m/sec² and* ΔV *= 1 to 10 km/sec, initial mass vs exhaust velocity for MDRE ejecting pellets of various masses.*
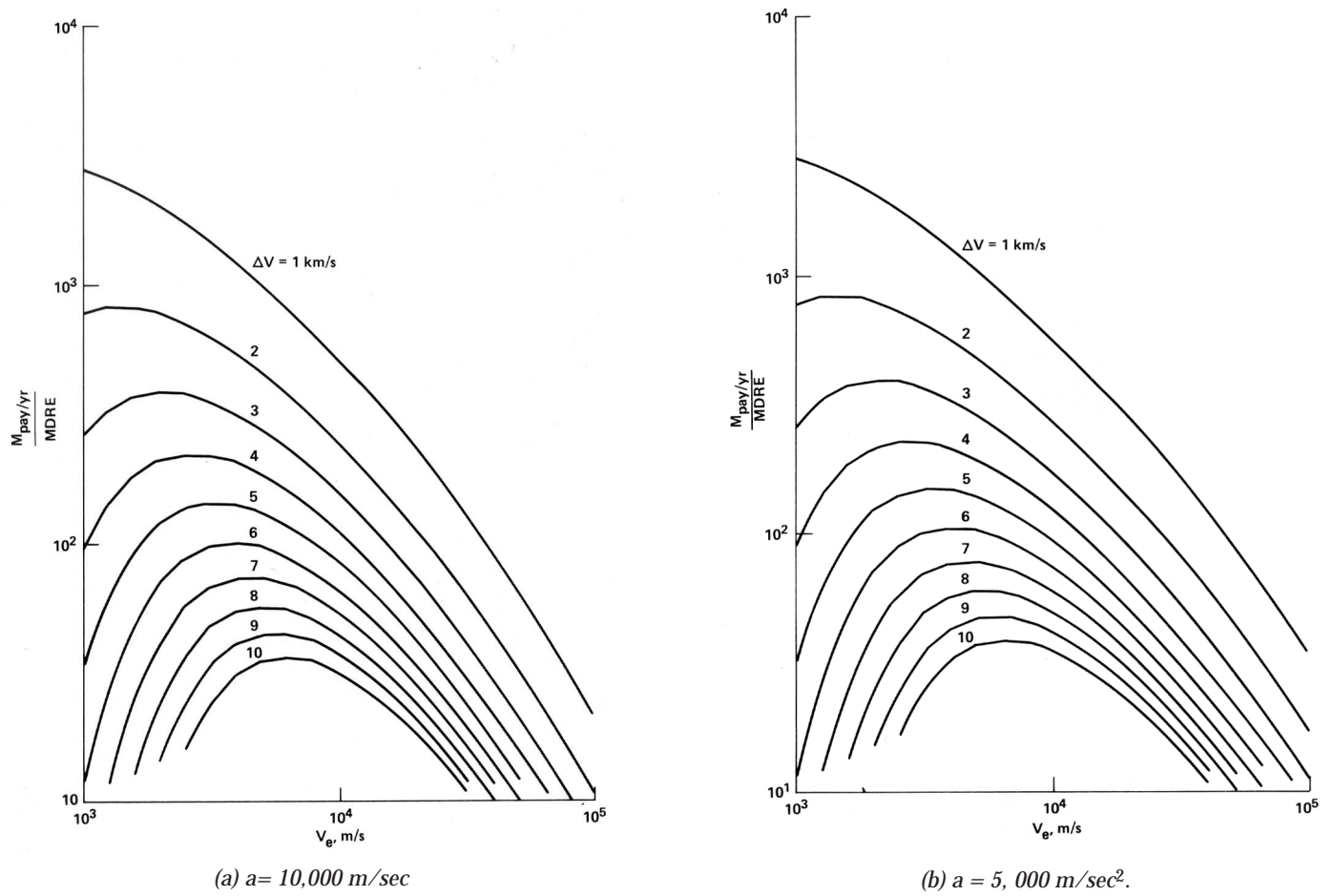
(a) a= 10,000 m/sec

(b) a = 5, 000 m/sec².

Figure 12 — *Payload fraction per year vs exhaust velocity delivered by MDRE ejecting 3.8-kg pellets for a 730-day mission at $\Delta V = 1$ to 10 km/sec.*
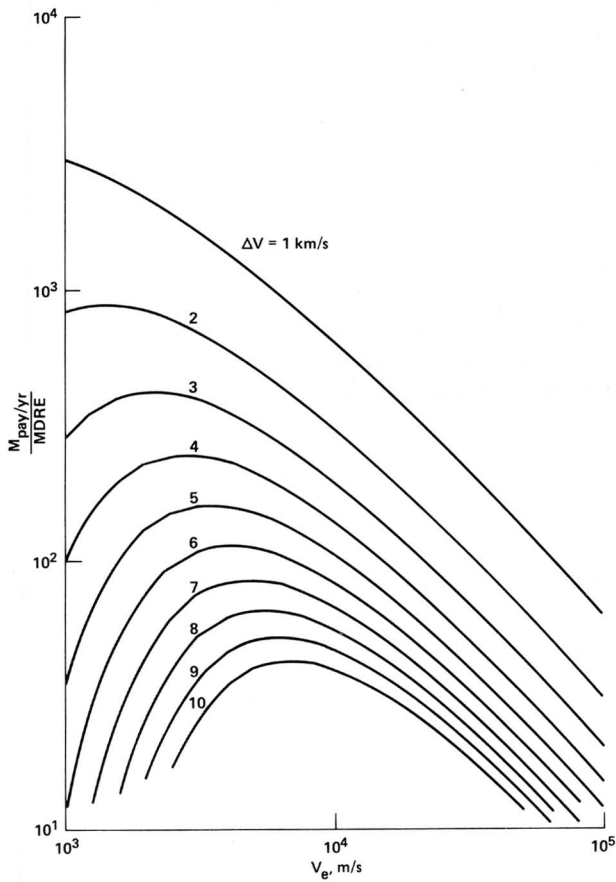
(c) a= 1,000 m/sec².

Figure 12 — *Payload fraction per year vs exhaust velocity delivered by MDRE ejecting 3.8-kg pellets for a 730-day mission at ΔV = 1 to 10 km/sec.*
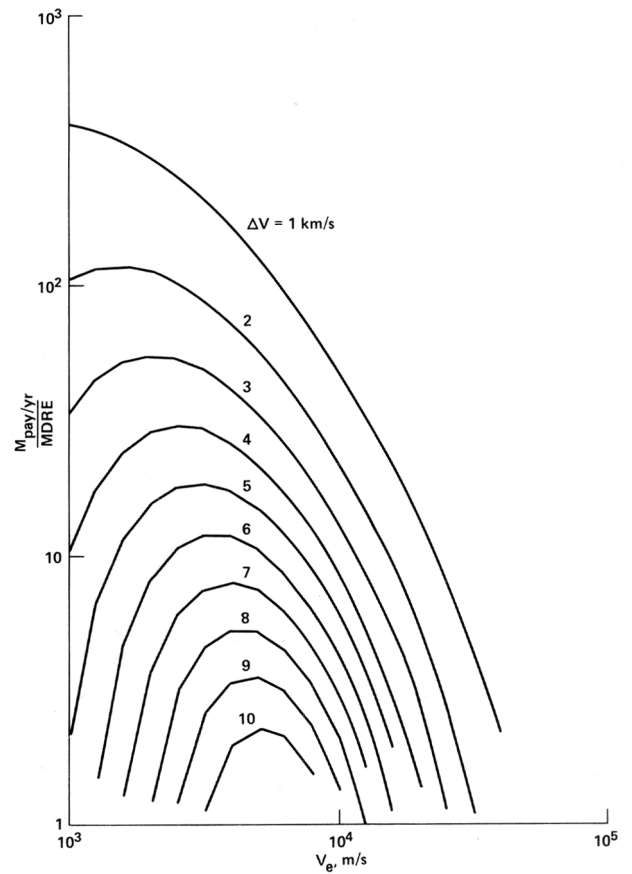
(a) a = 10,000 m/sec².

Figure 13 — *Payload fraction per year vs exhaust velocity delivered by MDRE ejecting 0.016-kg pellets for a 150-day mission at ΔV = 1 to 10 km/sec.*

(b) a = 5,000 m/sec².

Figure 13 — *Payload fraction per year vs exhaust velocity delivered by MDRE ejecting 0.016-kg pellets for a 150-day mission at* ΔV = *1 to 10 km/sec.*

HEATING EFFECTS IN BUCKET

Losses due to the drag component of the magnetic-flight guidance forces occur in the guideway conductors rather than in the moving bucket, and so are not considered in this section. As the bucket accelerates, however, it is acted on by fields that vary with time, as seen in the coordinate system of the bucket. These time-varying fields cause induced currents within the bucket and corresponding losses. We now compute those losses to determine whether they will cause an unacceptable heat input.

There is a question, not investigated here, whether the superconducting windings must be protected from time-varying fields. The fields of the drive coils are not very strong, typically about 500 G (0.05 T), and the time variation in the bucket frame is only a small fraction of the amplitude. Although no protection is likely to be required, we take the precaution of providing an eddy current shield around the superconductor. We consider the specific case of a mass-driver reaction engine used as the Shuttle upper stage. The drive windings have a mean diameter (caliber) of 5 cm, with a nominal peak drive current of 15,000 A-turns, corresponding to an acceleration of 1000 gravities. For single-turn drive and bucket windings, the mutual inductance is 0.015-μH peak and the bucket coil inductance is 0.03 μH.

An upper limit to bucket heating is the case of the bucket coil anchored in position in the plane of the drive coil, which corresponds to the "locked rotor" case of an electric motor. At the v_e end of the mass driver, the drive frequency is 2.5 X 10^5 Hz, for $v_e = 10^4$ m/sec and a wavelength of 4 cm (two-phase bipolar drive with a 1-cm spacing between drive coils). We assume that each bucket coil is surrounded by thermal radiation shields and an outermost unbroken aluminum jacket serving as eddy current shield. To satisfy electromagnetic principles, the current flowing in the current shield must cancel any flux change induced by the drive coils. The corresponding condition is

$$M(di_D/dt) + L(di_B/dt) = 0$$

where i_D is the drive coil current, i_B is the bucket coil current, and t is time. The corresponding current in the current shield would be 7200 A, which is intolerably high, as might be expected in the locked rotor case.

The realistic situation is a bucket moving along the accelerator, triggering the drive coils at the correct times as it advances. If the drive coils were distributed uniformly, corresponding to an infinite number of phases, the bucket coil would ride a moving wave of nonvarying magnetic field in the manner of a surfboard and would experience no change in flux linkage. In the real case, there is some variation due to the ripple in the drive system. We recall that, for 60 Hz, the ripple frequency is 120 Hz for single phase or 360 Hz for three phase. Correspondingly, the ripple frequency is four times the drive frequency in the two-phase case. It suffices to calculate the current over 180° of phase at this ripple frequency, half the distance between drive coils. We verify that statement by noting that all drive coils act identically, and that their action is symmetrical forward and backward, so that the longest unrepeating distance along the machine must be half the distance between coils.

We have used the curve for dM/dx to calculate the energy change imparted to each bucket coil by passage through each drive coil. To calculate the ripple, we need the curve for M itself (fig. 14) to obtain the change in flux linkage in the absence of current in the current shield.
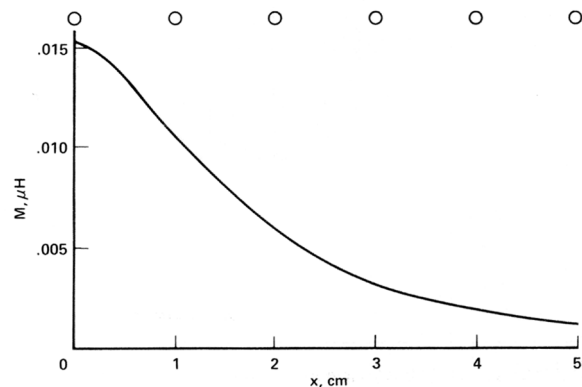
Figure 14 — *Mutual inductance between drive and bucket coils vs bucket position for 5-cm caliber MDRE, for calculation of field ripple in bucket frame of reference.*
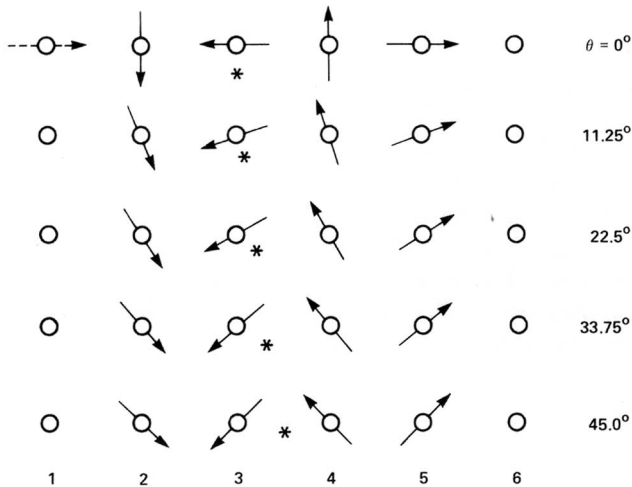
Figure 15 — *Vector representation of drive current in six drive coils at different values of the phase angle.*

We carry out the bookkeeping of drive currents by use of figure 15, where the current in each drive coil is represented by the projection onto the y axis of a vector of length i_d rotating at the drive frequency. The vector switches on when $\theta = 0°$ (positive horizontal axis), when the bucket coil is two coil spacings (half a wavelength) from the drive coil. The vector goes through a complete 360° change of direction in the mathematically positive sense (counterclockwise) and switches off after that one rotation when the bucket coil is a half wavelength on the opposite side of the drive coil. The flux ϕ linking the driven coil (in the absence of shielding currents) is then obtained from

$$\phi = i_D \sum_n M_n \sin \theta_n$$

over all coils whose currents are nonzero. Table 1 summarizes the calculation. As expected, the ripple frequency corresponds to a wavelength equal to the drive coil spacing. The peak current is l/58 of the drive current and must be carried by the shield in order that the superconducting coil experience no flux linkage.

The skin depth δ in the shield is $\delta = (2\rho/\omega\mu)^{-2}$, where ω is the ripple frequency (for 10^6 Hz) and ρ, the resistivity. For aluminum, $\delta = 8.5 \times 10^{-5}$ m. The resistance of a solid shield would be excessive, so the shield must be in Litz wire form. In that case, if we devote 1 g of aluminum to each of the two current shields in the bucket, the average power in each shield during acceleration will be 18 W for a shield major diameter of 2.6 cm. For a track 10 km long, the acceleration time is 2 sec, and the heat rise is 40° C, which is quite tolerable. During the long, slow return, the shield will have time to cool back to room temperature if it is left free to radiate to the cold of space.

We conclude therefore that no serious heating effects will occur in the bucket as a result of induced currents or fields during acceleration so long as accelerations are of the order of 1000 gravities. At higher accelerations, in the range of several thousand gravities, such effects might become more serious and might require the use of a larger number of phases, that is, more closely spaced drive coils.

GUIDE FORCE PROFILES

In reference 1, the guidance or restoring force on the bucket was calculated for small displacement from the equilibrium trajectory to determine the resonant frequency of transverse oscillations and its scaling with caliber.

TABLE 1 — RIPPLE FLUX LINKAGE CALCULATIONS

n	θ, deg	$|x_n|$, cm	M_n, μH	$\sin \theta_n$	$\sum_n M_n \sin \theta_n$
2	11.25	1.125	0.0100	−0.981	
3	11.25	.125	.0152	−.195	−0.00036
4	11.25	.875	.0114	.981	
5	11.25	1.875	.0063	.195	
2	22.5	1.250	.0094	−.924	
3	22.5	.250	.0148	−.383	
4	22.5	.750	.0122	.924	−0.00055
5	22.5	1.750	.0066	.383	
2	33.75	1.375	.0086	−.831	
3	33.75	.375	.0142	−.556	
4	33.75	.625	.0128	.831	−0.00029
5	33.75	1.625	.0074	.556	

An equally important consideration is whether the restoring force profile for large displacement from equilibrium rises steeply enough to prevent physical contact between the bucket and the guideway surface. The repulsion force becomes infinite, of course, in the mathematical limit when the current filament representing the bucket coil contacts the surface. Because of the physical size of the superconducting coil and the surrounding thermal radiation shield and eddy current shield, contact occurs before the current filament reaches the guideway. The strength of the repulsion force at contact, or the shape of the restoring force profile, represents the ultimate lower limit on the caliber of mass drivers. Ultimately, it will have to be computed exactly or determined by inductance simulation methods. At present, however, we shall calculate the restoring force profile from the octagonal approximation and examine its implication for the two design examples presented earlier: the optimized lunar launcher and the 5-cm caliber reaction engine.

The octagonal approximation is defined in figure 16. The approach is a fair approximation of reality because the guideway will consist of several narrow aluminum strips, possibly eight, located inside the drive coils. These strips might occupy 1/4 to 1/2 the circumference. The restoring force profile must then be scaled accordingly from our calculation, which assumes complete envelopment. (Complete envelopment is impossible because the bucket coils would be shielded from the drive coils; the guideway must consist of relatively narrow strips.)

The force on each of the eight elements of the bucket coil is assumed to be caused only by its mirror image in the nearest guideway surface. The magnetic field at each element due to its image, which is at a distance $2s$ (s being the distance to the reflecting surface) is given by the Biot-Savart law (valid at distances small relative to the conductor length):

$$B = \mu_0 I/(2\pi(2s)) \text{ tesla}; \quad \mu_0 = 4\pi \times 10^{-7} \text{ (rat. MKS)}$$

where I is the current (in amperes) and s is the distance between the bucket coil element and the guideway surface. The Lorentz force per unit length on the current element due to its parallel image current is therefore

$$F = IB = \frac{\mu_0 I^2}{4\pi s} \left(\frac{N}{m} \right) = I^2 \, 8.975 \times 10^{-8} \, \frac{1}{s} \, \ell (N)$$

The length of each current element (each octagonal side, fig. 16) in terms of r, the mean bucket coil radius, is $\ell = 2(2^{-1/2} - 1)r$. We now displace the bucket coil octagon a distance x to the left (dashed line), which causes its image to assume the position shown (dashed line), and express the mirror distances for the four sides labeled ℓ_1, ℓ_5, ℓ_2, and ℓ_4 in terms of the normalized, dimensionless displacement $x/(R - r)$; we also eliminate r in favor of R by using $r/R = 0.52$, as adopted in our design family:

$$s_1 = (R - r) - x = (R - r)\left(1 - \frac{x}{R - r} \right) = 0.48R \left(1 - \frac{x}{R - r} \right)$$

$$s_5 = (R - r) + x = (R - r)\left(1 - \frac{x}{R - r} \right) = 0.48R \left(1 + \frac{x}{R - r} \right)$$

$$s_2 = (R - r) - \left(\frac{x}{\sqrt{2}} \right) = (R - r)\left[1 - \frac{x}{\sqrt{2}(R - r)} \right]$$

$$= 0.48R \left[1 + \frac{1}{\sqrt{2}} \frac{x}{(R - r)} \right]$$

$$s_4 = (R - r) + \left(\frac{x}{\sqrt{2}} \right) = (R - r)\left[1 + \frac{x}{\sqrt{2}(R - r)} \right]$$

$$= 0.48R \left[1 + \frac{1}{\sqrt{2}} \frac{x}{(R - r)} \right]$$
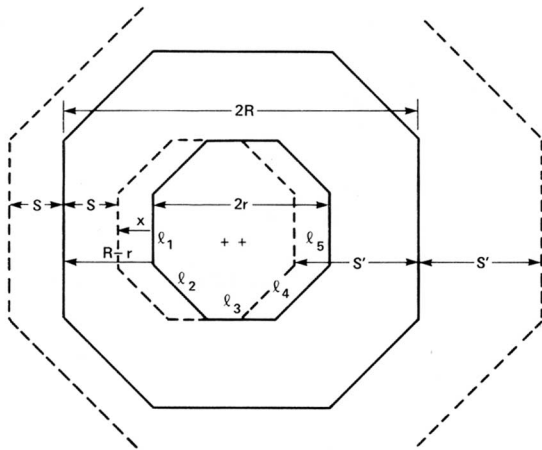
Figure 16 — *Octagonal approximation of bucket coil current and its image current reflected in the guideway surface, when the bucket is displaced a distance* x *toward the left (dashed lines); this model is used to calculate restoring force profiles.*

The total restoring force can be expressed in four terms by substituting these s values into the above expression:

$$\Sigma F = F_1 - F_5 + 2F_2 - 2F_4$$

In figure 17, the restoring force is plotted as a function of the normalized displacement $x/(R - r)$, that is, the displacement expressed as a fraction of the nominal gap. As stated above, this force assumes total envelopment by the guideway and must be scaled to the fraction of the circumference actually occupied by the guideway.
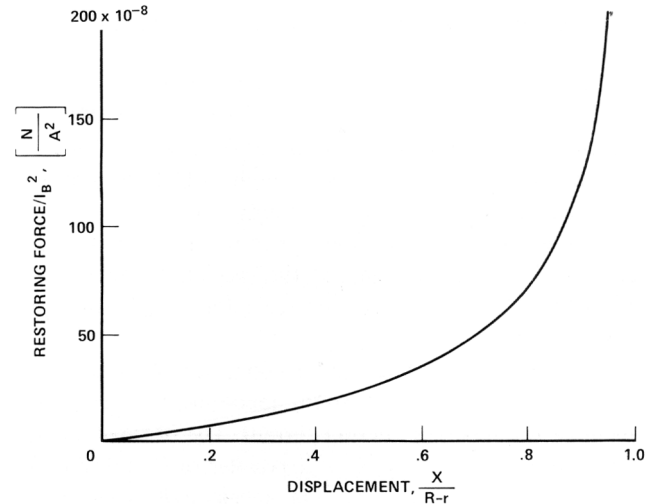
Figure 17 — *Specific restoring force profile (N/A2 vs relative displacement expressed as fraction of clearance gap between theoretical current filaments), as calculated from the octagonal approximation shown in figure 16.*

We now calculate the restoring force at contact for our two example designs, assuming a totally enveloping guideway:

> *Lunar launcher*:
> $D = 0.431$ m; $m_1 = 10.5$ kg; $R = 0.216$ m; $r = 0.112$ m
>
>   Bucket coil width = build = 0.043 m; mass = 5.94 kg
>
>   For bare coil, repulsion at contact = 1.5×10^5 N
>   = 2550 gravities
>
>   With 1-cm shield envelope: 1.1×10^5 N
>   = 1820 gravities
>
> *Reaction engine*:
> $D = 0.05$ m; $m_1 = 0.0164$ kg; $R = 0.025$ m;
> $r = 0.013$m; $R - R = 0.012$m
>
>   Bucket coil width = build = 0.005 m; mass = 0.093 kg
>
>   For bare coil, repulsion at contact = 27.34 N
>   = 170 gravities
>   With 0.5-cm shield envelope: 5.86 N = 36 gravities

The lateral acceleration at contact limits the permissible guideway curvature or kink radius. The limitation might be quite stringent in the 5-cm caliber case, but will depend on the dynamics of the interaction since the guideway is far from rigid.

PAYLOAD MANIPULATION

The manipulation of buckets and payloads has been studied only to the extent necessary to ascertain that no fundamental problems arise, and that the repetition rate of 10 launches/sec is a conservative choice.

Loading and Feeding

For the optimized lunar launcher, buckets that are 0.478 m long will enter the mass driver at the rate of 10/sec. This represents a bumper-to-bumper procession moving at 4.78 m/sec or 10.7 mph, which is bicycle speed, or the speed of many assembly lines.

For the reference reaction engine design, buckets that are 0.056 m long, launched at the rate of 10/sec, would enter the mass driver at 0.56 m/sec, which is 1.24 mph, a leisurely walk.

Individual buckets would be taken out of circulation at intervals of perhaps 1 hr for recooling and readjustment of the superconducting current. The payload could be introduced in the form of a powder or liquid (liquid oxygen) while the buckets are accelerated to feeding speed, and in this case no special containers would be required. Alternatively, the payload might be compacted into a cylindrical pouch having adequate tensile strength, or held in a surrounding structure capable of withstanding the hydrodynamic bursting force under acceleration.

Loading and feeding do not appear to involve any fundamental problems.

Release and Deflection

As the stream of buckets enters the launcher, their separation increases continuously until the launch point is reached. We must ascertain that the empty bucket can be deflected with sufficient lateral acceleration by the available guidance forces to ensure that it will not be struck by the next payload to be launched.

Assuming that the empty bucket is deflected with a radius of curvature R, then the distance of travel required to reach a deflection d is given approximately by

$$d = z^2/2R$$

We assume that the deflection required to clear the next payload is about equal to the caliber D. The centrifugal force F is related to the radius of curvature R by

$$F = mv^2/R \qquad \text{or} \qquad R = mv^2/F$$

the empty bucket mass $m_B = 2.263\ m_1$, the payload mass. Therefore, the travel distance required to achieve a deflection D is given by

$$z = (2RD)^{-2} = v(4.5mD/F)^{-2}$$

The maximum available deflection force F was calculated in the preceding section.

For the lunar launcher,

$m_1 = 10.5$ kg
$D\ = 0.431$ m
$v\ \ = 2.4$ km/sec
$F\ \ = 0.5 \times 10^5$ N

The deflection path is found to be $z = 4.86$ m, compared to the headway distance from the following payload of 240 m — clearly a safe separation.

For the reaction engine,

$m_1 = 0.0164$ kg
$D\ = 0.05$ m
$v\ \ = 10$ km/sec
$F\ \ = 2.9$ N

The separation path is found to be 358 m, compared to a headway of 1000 m, still as safe a separation as prevails on most freeways. In both cases, the available lateral force is based on the assumption of a half-enclosing guideway structure.

It is clear that, with reaction engines, deflecting the empty bucket at high speed will apply a lateral force to the launch end of the mass driver which may produce unacceptable effects. To avoid this situation, it would be simple to split the payload longitudinally and separate the two halves laterally by means of a relatively gentle spring pressure, while the empty bucket is decelerated drastically before being deflected for the slow return travel. It thus appears that no serious problem is involved in the launching operation.

REACTION MASS ORBITS

The reaction mass ejected by a mass-driver reaction engine (MDRE) may be rendered harmless if it consists of liquid oxygen or a loose aggregate of fine powder. If it is a solid pellet, however, it poses a hazard to other spacecraft as well as to itself. We shall therefore examine the conditions that must be satisfied to ensure that the orbit of the ejected reaction mass is short-lived. The mass-driver reaction engine considered here is thrusting tangentially to the orbit as it spirals inward or outward from the central body. The nominal trajectory of the MDRE at an instant is a circular orbit.

When departing from low orbit about the central body, the exhaust velocity is opposite that of the circular orbit velocity. This allows for retrograde orbits with respect to the orbiting MDRE when $v_e > v_c$, where v_e is the exhaust velocity and v_c is the circular orbit velocity. When $v_e < v_c$, the orbits are posigrade.

For the pellets to go into a retrograde parabolic escape trajectory,

$$v_e = \sqrt{K/r}\,(\sqrt{2} + 1)$$

where $K = GM$ =gravity constant of the central body and r is the orbit radius. When $v_e > (K/r)^{-2}(2^{-2} + 1)$, the pellets will travel hyperbolic escape trajectories.

The cases where the periapsis is equal to the radius of the central body and the orbit radius is equal to the apoapsis radius constitute the boundaries for central body intersecting trajectories:

$$\text{Retrograde limit:} \quad v_e = \sqrt{K/r}\,[1 + \sqrt{2R/(R+r)}]$$

$$\text{Posigrade limit:} \quad v_e = \sqrt{K/r}\,[1 - \sqrt{2R/(R+r)}]$$

where R is the radius of the central body. When

$$v_e < \sqrt{K/r}\,[1 - \sqrt{2R/(R+r)}]$$

the pellets will go into elliptical orbits that will not decay for periods ranging from days to many years. This is a forbidden region of operation.

When

$$\sqrt{K/r}\,[1 + \sqrt{2R/(R+r)}] < v_e < \sqrt{K/r}\,(\sqrt{2} + 1)$$

the pellets are in retrograde elliptical orbits also, with decay times ranging from days to many years, also a forbidden region of operation. When

$$\sqrt{K/r}\,[1 - \sqrt{2R/(R+r)}] < v_e < \sqrt{K/r}\,[1 + \sqrt{2R/(R+r)}]$$

the orbits are either posigrade or retrograde, but they all intersect the central body during the first orbit. This is an acceptable region of MDRE operation, with the obvious precautions to be taken.

In figures 18 to 21, the following values are used:

Earth:
$\quad K \quad = 3.986 \times 10^5 \text{ km}^3/\text{sec}^2$
$\quad R \quad = 6378 \text{ km}$
$\quad \text{LEO} = 200 \text{ km altitude}$

Moon:
$\quad K \quad = 4.9 \times 10^3 \text{ km}^3/\text{sec}^2$
$\quad R \quad = 1738 \text{ km}$
$\quad \text{LLO} = 100 \text{ km altitude}$

The two figures for arrival trajectories for the MDRE show the limit for parabolic escape only since v_e is in the same direction as v_c:

$$v_e = \sqrt{K/r}\,(\sqrt{2} - 1)$$

$$v_e = \sqrt{K/r}\,(\sqrt{2} - 1)$$
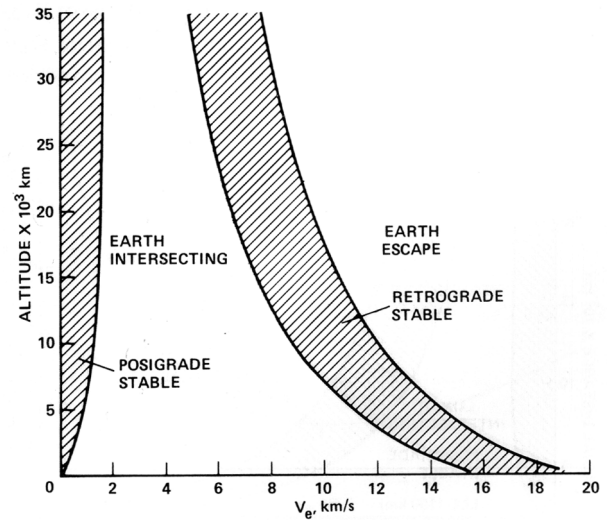
(a) From 0 to 35,000 km altitude.
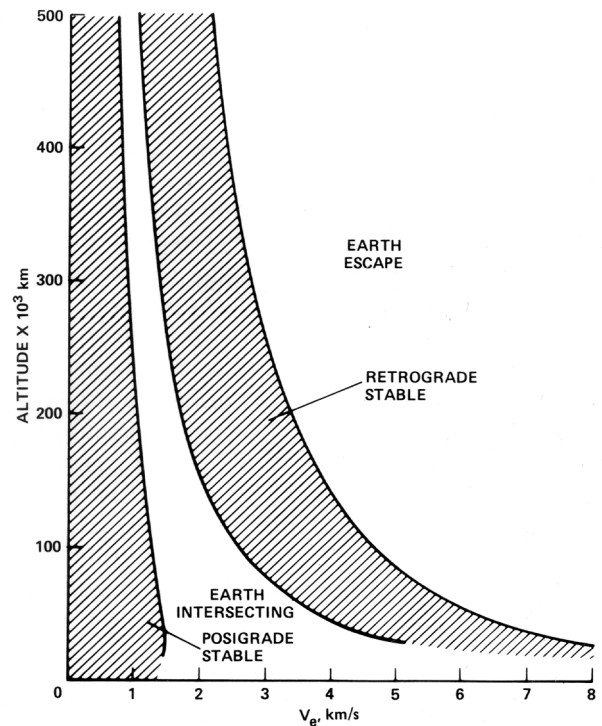
(b) To 500,000 km altitude.

Figure 18 — *MDRE departure velocity zones from LEO with tangential thrusting.*
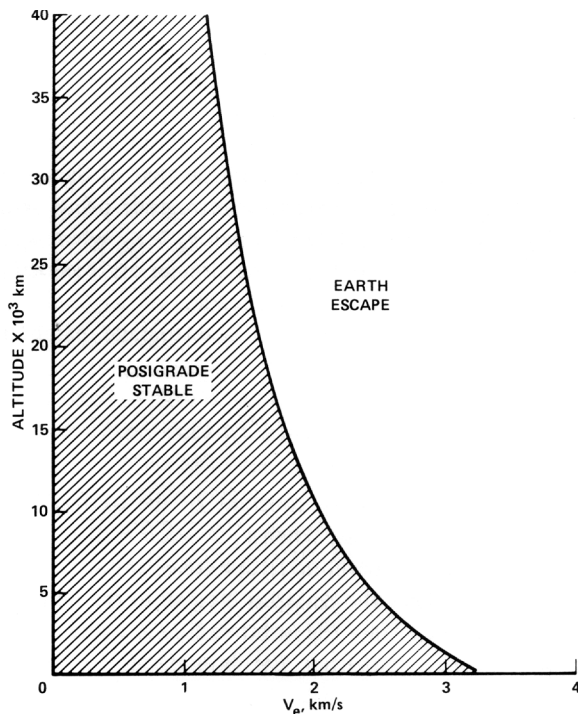
Figure 19 — *MDRE arrival velocity zones to LEO with tangential thrusting.*
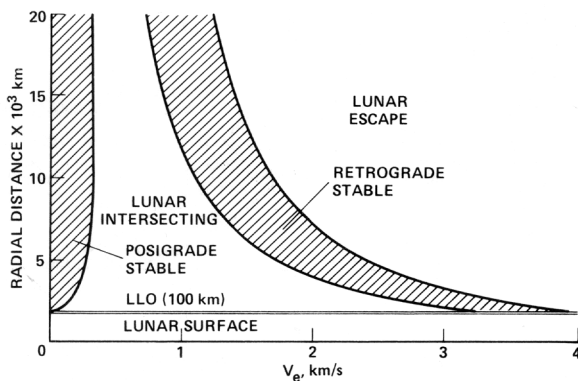
Figure 20 — *MDRE departure velocity zones from LLO with tangential thrusting.*
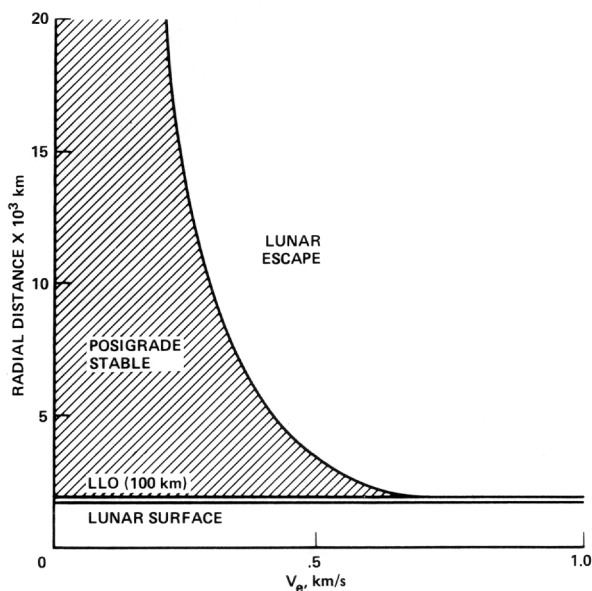
Figure 21 — *MDRE arrival velocity zones to LLO with tangential thrusting.*

FURTHER OPTIMIZATION OF COMPONENT TECHNOLOGY

Radiators

Waste heat produced by the mass driver will be dissipated through radiator panels that can be positioned behind the solar cells and will thus be radiating into the 3 K of deep space. The solar panels and the struts that support the mass-driver structure itself can be used as the framework for the radiators. These radiators will be very similar to the outside radiators developed and used in the Apollo program, so these can be used as models in arriving at mass estimates for mass-driver radiators.

The heat lost from a given radiator is proportional to $(1/T_R^4)$ - $(1/T_s^4)$, where T_R is the radiator temperature and T_s is the temperature of the heat sink into which it radiates. Approximating the temperature of space shaded from the Sun as 0° and using the fact that the Apollo radiators, which operated at 300 K, weighed 0.02 kg/W, the mass of the radiators is found to be

$$m_R = 0.02 \, (300)^4 \, (1/T)^4 \, (kg/W)$$

It is possible that slightly lighter radiators might be designed for the mass driver since these will not have to function at the low temperature which forced the Apollo designers to use special materials with unusual thermal properties; however, the above figure is the one used in all calculations.

Optimized System Temperature

The operating temperature of the mass driver has been arbitrarily assumed in all previous calculations to be about room temperature, that is, 300 K. Since radiator mass varies significantly with temperature and represents a considerable fraction of the total mass, it must be considered whether a significant reduction in optimized total system mass might be attained by allowing the operating temperature of the radiators to rise. This could be accomplished either by running the entire circuit at a higher temperature or by using heat pumps to maintain a higher radiator temperature while operating the electrical circuitry at a lower temperature.

To do this, one must examine the dependence of mass on temperature. Both powerplant and radiator mass vary with temperature, powerplant mass being directly proportional to the power dissipated in the circuit (I^2R, where I is current and R is resistance). Radiator mass, from basic thermodynamics, is inversely proportional to the fourth power of temperature. The overall expression for powerplant and radiator mass is:

$$M \, \alpha \, (I^2R)(m_p + m_R)$$

where

m_p specific powerplant mass; 0.005 kg/W for MDRE's and 0.014 kg/W for MDLL's

m_R radiator mass; $0.02(300/T)^4$ (kg/W)

R resistance, proportional to resistivity,
   $\rho = 2.81 \times 10^{-8}(1.0041)^{T-300}$ (for aluminum)
I current

and R and m_R are functions of T. Then,

   $$M \propto [(2.81 \times 10^{-8})(1.0041)^{T-300}] \, [0.005 + 0.02(300/T)^4]$$

which yields the curve shown in figure 22. The mass savings with increasing temperature are at first substantial, but taper off, with overall mass beginning to level off at about 400 K and reaching an optimum at about 440 K.

Limitations are imposed on the system by the SCR's, which at the present level of technology cannot be operated above 400 K. Were the radiators to be operated above this temperature, therefore, heat pumps would have to be used between radiators and SCR's. Since the mass savings on radiators and power plant become minimal above 400 K (only 3 percent of combined radiator and power-plant mass is saved by running from 400 K up to 440 K), it is apparently not profitable to install the extra hardware necessary to operate radiators a few degrees higher than 400 K.

However, the mass savings resulting from allowing the entire system to function at the upper limit of SCR operating range are considerable; power plant and radiator mass are reduced by 31.8 percent by raising system temperature from 300 to 400 K. Mass-driver design in the future should be based on the assumption that the system will be run at the highest temperature possible for the circuit components. At present, this appears to be about 400 K.

However, the surge rating of SCR's decreases with rising temperature and becomes very low at the operating limit of 400 K; no performance data are available in this region. There is clearly a need for research in the adaptation of SCR technology to space requirements (see SCR section).

Capacitor Technology

Specific capacitor mass has been assumed to be 8×10^{-3} kg/J (or 56.7 J/lb in customary trade units). This is a conservative rating for energy storage capacitors of the "high energy density" class.
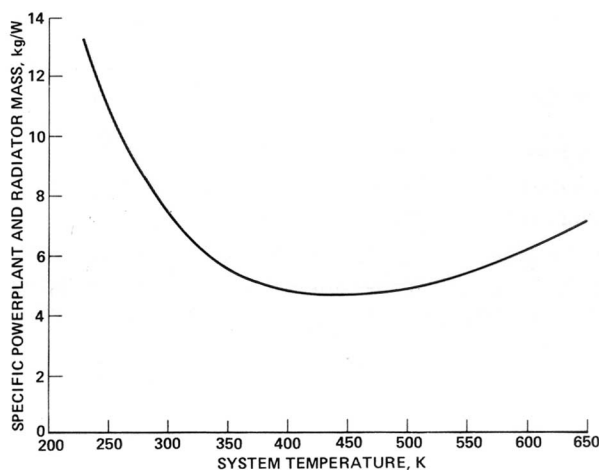
Figure 22 — *Specific powerplant and radiator mass vs system temperature (without heat pumping).*

We have never examined, however, whether such capacitors will withstand the actual operating conditions resulting from optimized sector length, and achieve the required service life of about 10^{10} discharge cycles. It appears that they will not, and that two alternative solutions to the capacitor problem must be compared:

1. Use of capacitors designed for continuous ac duty (powerline capacitors) at the discharge rate and average power flow resulting from optimized sector length, that is, optimized capacitor utilization.
2. Use of high energy density energy storage capacitors, but limiting the sector length to remain below the maximum discharge rate permissible under the particular operating conditions.

The previous optimizations lead to the following conditions: in a 5-cm caliber orbital transfer driver operating at $a = 5000$ m/sec^2 , $v_e = 8000$ m/sec, launch rate = 5 Hz:

Capacitor mass = feeder mass = associated power and radiator mass = 4 percent of total driver mass, or 12 percent altogether

Sector length = 1.25 m, with 40 coils on each capacitor, discharge rate = 800/sec, ringing frequency = 1.95×10^5, duty cycle = 4.1×10^{-3}

In a 17-cm caliber asteroid retriever operating at $a = 1000$ m/sec^2, $v_e = 2400$ m/sec, launch rate = 14 Hz:

Capacitor mass = feeder mass = associated power and radiator mass = 10 percent of total driver mass, or 30 percent altogether

Sector length = 1.4 m, with 15 coils on each capacitor, discharge rate = 412/sec, ringing frequency = 2.6×10^3 , duty cycle = 0.156

An increase in specific capacitor mass would increase the optimum sector length, resulting in even more coils connected to each feeder capacitor, with a corresponding increase in discharge rate. It therefore becomes important to consider in some detail the performance capability of energy storage capacitors.

The Air Force Propulsion Laboratory, Wright-Patterson Air Force Base, Ohio, has already sponsored a serious investigation of high-density energy storage capacitors by two leading manufacturers (refs. 5, 6). A third source of information is Tobe Deutschman Laboratories, Inc. (Canton, Mass.), a small but very innovative manufacturer, and the first to have developed energy storage capacitors for high-voltage, high-rate service (T. Deutschman, Jr., personal communication, 1977; he considers the Maxwell report to be solidly based on experiment, but the TRW report to contain somewhat excessive extrapolations beyond actual testing).

The tests in question were made using 0.00017-in.-thick aluminum foil, separated by four types of dielectric:

Polyester film (Mylar, Scotchpar)
Polypropylene film
Polyvinylidine fluoride (KF polymer)
Kraft paper with castor oil

and immersed in four types of oil:

    Polychlorinated polyphenyls
    Aromatic hydrocarbons
    Ester
    Silicon oils

Repetition rates up to 250/sec were tried where possible, but in most cases burst rates had to be severely limited to prevent excessive temperature rise. The maximum hot-spot temperature permitted was 65° C. Test voltages to 12 kV were used. Duty cycles ranged from 0.1 to 0.004. Reversal voltages of 0 to 31 percent were used. Test units were individual pads, 1 in. in diameter and 6 in. long, and completely packaged 500-J units. Life expectancy was only 10^5 discharge cycles, which satisfied Air Force requirements.

Results indicate that the dominant failure mode was dielectric puncture at foil edge, and that voltage reversal has dramatic effect on life, which varies about with the power of -1.83 of the fractional voltage reversal. A curve taken from reference 6 summarizes life as a function of specific mass (fig. 23).
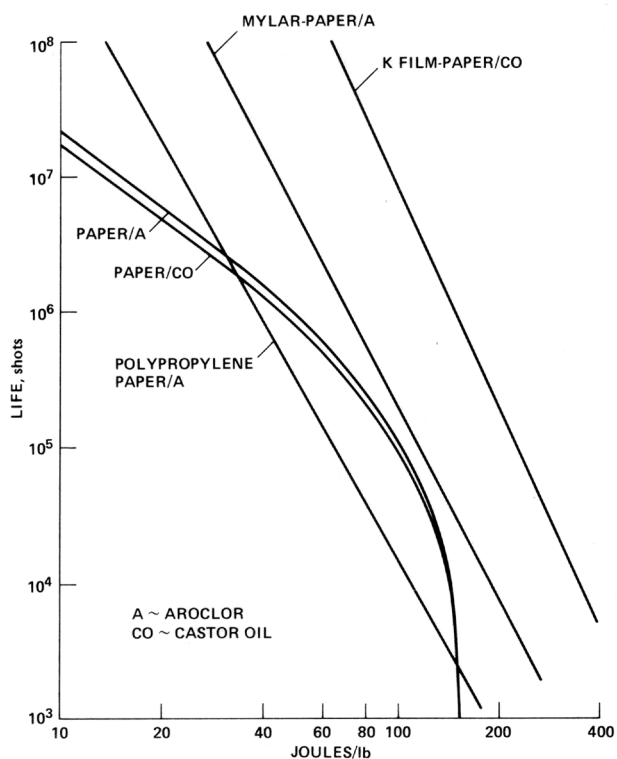
Figure 23 — *Pad life vs energy density for commercial energy storage capacitors (from ref. 3).*

Maxwell Laboratories (W. White, personal communication, 1977) is now undertaking a new investigation for Wright-Patterson AFB to cover high discharge rates (to 500 pps) and longer lifetimes (to 10^9 cycles). They also report having built (for Avco-Everett Laboratory) one unit that approaches our requirements and that also provides a tested value of specific mass: a laser optical pumping unit for laser propulsion studies. The specifications are:

    50-Hz discharge rate, continuous
    25-kV operating voltage, 50-J unit

    10^9 pulse life expectancy
    Specific mass: 5 J/lb

This represents 10 times the specific mass assumed previously (57 J/lb).

Note that this specific mass approaches that value typical of commercial power factor correction capacitors, rated for continuous duty at 60 Hz, with 100-percent voltage reversal. A currently available Westinghouse unit has a specific mass of 2 J/lb. Maxwell Laboratories estimate that 400-Hz line frequency units might have a mass of about 1 J/lb, which is 50 times the assumed specific mass.

Note, as indicated in reference 6, that no capacitor manufactured to date has come close to performing to the limits of the material used. Failure is always associated with manufacturing defects.

Finally, we should consider the use of vacuum capacitors. For mass-driver service, they have the advantage of very long life expectancy and frequency tolerance, and they would have a specific mass no greater than that of powerline capacitors if one assumes that 0.001-in.-thick aluminum foil can be made to support itself. The bulk of such capacitors has always precluded their use on Earth, but they should be investigated in connection with space requirements in general.

It might also be expedient at some point to consider the possibility of using the back surface of solar panels as capacitor area.

SCR Technology

Mass-driver optimizations to date have been based on a "nonrepetitive peak pulse rating" leading to a typical specific mass of 5×10^{-9} kg/VA peak. They represent about 1/3 the total mass of the 5-cm caliber interorbital reaction engine (operating at an acceleration of 5000 m/sec², a launch velocity of 8000 m/sec, a payload of 0.014 kg, and a launch rate of 5 Hz). SCR mass represents a smaller fraction of the 18-cm caliber asteroid-retrieval engine operating at a launch rate of 14 Hz. However, since individual SCR's now fire at a rate of 28 pulses/sec (two bucket coils), their duty cycle begins to approach powerline service conditions and continuous duty ratings must be considered. This suggests a thorough examination of the state of power semiconductor technology.

The functional element of power rectifiers, transistors, and thyristors is a silicon pellet or wafer about 0.008 to 0.020 in. thick, ranging in size from 1.7 in. (44 mm) to 2.8 in. (70 mm) in diameter, with 3-in. (76-mm) and 4-in. (102-mm) pellets, presently under development (D. L. Schaefer, unpublished General Electric report, 1977). The packaging of these elements represents General Electric's primary research priority at the present since it has never received sophisticated attention. Not only does the package mass completely overshadow the functional element mass, but it also increases disproportionately with increasing size. For example, a 33-mm-diameter pellet has a mass of 0.75 g and a package of 200 g (factor 267); a 102-mm pellet has a mass of

2.3 g and a package of 3.1 kg (factor 1348). The only incentive for making larger devices is to eliminate the difficulty of connecting many small ones in series or parallel.

Figure 24 summarizes the specific mass of presently available "Press Pak" or "Hockey-Puck" devices, intended to be clamped between heat sinks at bolting forces ranging from several hundred to several thousand pounds (bolts not included in package weight). Note that these ratings are based on 1000-V standoff, but that 10,000-V ratings would not increase the mass substantially; specific mass values can therefore safely be divided by a factor of 10.
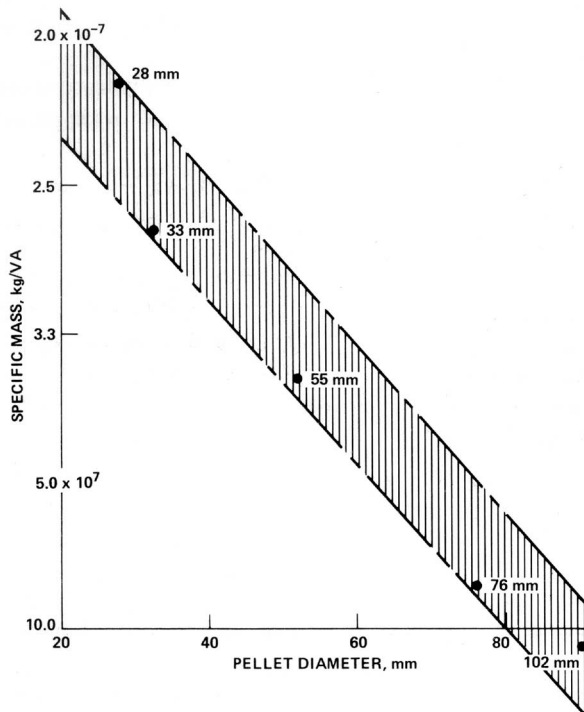
Figure 24 — *Specific mass of packaged, commercial SCR's vs pellet diameter, for 1000-V rating and average power shown in VA (information supplied by General Electric — see text).*

The maximum safe operating temperature of the silicon pellets is 125° to 150° C (398 to 423 K). As mentioned in the section on optimized system temperature, this limits the temperature of the feeder lines to which the SCR's must be connected.

The inordinate packaging mass of power semiconductors represents a crude solution to two basic problems: (1) making good electrical and thermal contact with the pellet surface despite a difference in thermal expansion coefficient by a factor of 7 to 10 (silicon to copper or aluminum) and (2) preventing voltage breakdown or leakage currents at the edge of the very thin pellets.

The contact problem is solved by diffusion bonding the silicon wafer to a massive tungsten or molybdenum pad of low thermal expansion (within a factor of 2 relative to silicon), typically 10 times thicker than the wafer, and then clamping this bonded sandwich between copper electrodes with maximum possible pressure. The dry contact thus achieved is still poor, both electrically and thermally. It is likely that a considerable fraction of the heat to be removed

is generated not in the water body, but ironically at the contact surface.

The voltage problem is solved by coating the lateral wafer surfaces with silicone compounds and encapsulating the wafer hermetically. In certain exceptional applications (high-energy physics) involving high standoff voltages, the wafers have been immersed in Dow-Corning silicone transformer oil No. 704, one of the few liquids found to be compatible with silicon on the long run.

It is clear that a significant mass savings can be realized by finding a more elegant solution to both problems. The subject deserves serious attention, considering the increasing need for power semiconductor devices in space, as well as in airborne terrestrial applications.

For mass drivers, it seems logical to consider the possibility of designing the entire feeder structure as a heat pipe, using the aluminum litz wire filaments as a possible wick material. The silicon wafers could then be immersed directly in the heat pipe fluid. Instead of dry contact, it seems logical to use a graded bond involving several metals of progressively increasing expansion coefficient in order to distribute the inevitable strain over several bonded interfaces with provisions for direct heat removal by immersed fins.

It seems reasonable, for the present purposes, to use a specific SCR mass of 10^{-7} kg/VA average duty; this represents 1/10 of the worst case (largest) 1000-V device included in figure 24.

RESEARCH AND DEVELOPMENT PLAN

Baseline Scenario

No engineering study is complete without some assessment of the cost and time required for implementation. We have attempted to make such an assessment on a conservative basis. We define a "baseline scenario" as an all-out effort based on a national commitment. If this effort is started immediately, using the body of knowledge and expertise developed to date, a lunar mass driver could begin operating in 1985. The proposed baseline schedule is shown in figure 25.
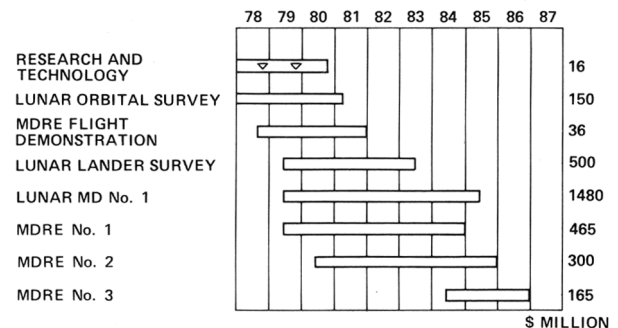
Figure 25 — *Mass-driver development schedule according to baseline scenario.*

The program begins with a series of technology studies to define critical development areas and select certain parameters and techniques for the initial design. These studies include the design and demonstration of two

working models of a mass driver, indicated by triangles. The first of these, a 500-g linear superconducting system that is 10 m long, is to be constructed by Princeton and M.I.T. in 1978-79. The second model would be a prototype interorbital transfer reaction engine of 5-cm caliber operating in a vacuum tunnel. The related research program is outlined in the following section.

Concurrently, potential installation sites would be surveyed from lunar orbit and eventually explored by a manned or unmanned lander. An excellent review of this subject, as well as the mass catching problem, was published recently by Heppenheimer (ref. 7).

The first flight demonstration of a MDRE in LEO might occur in late 1981. Development would continue, culminating in the first operational reaction engine in mid-1985. This reaction engine might serve to transport the first parts of the lunar launcher, which would be ready to begin installation at about that time. Second and third reaction engines would become operational in 1986 and 1987.

Research and Technology Studies

The research and technology studies necessary for the development of operational mass-driver systems have been broken down rather arbitrarily into six broad categories:

Basic research and technology $10 million
1. Mechanical analysis and design $7 million
 Payload loading on LL
 Payload release from LL
 Payload attachment to MDRE
 Reaction mass handling on MDRE
 Reaction mass sanitization
 Bucket recirculation
 Lunar installation design
 Assembly techniques in space
2. Structural analysis and dynamics $1 million
 Structural model
 Bucket-structure interactions
 Thrust vectoring
 Bucket steering
 LL downrange guidance
3. Electrical analysis and design $1 million
 Electrical configurations
 Inductive force modeling
 Higher harmonics
 Oscillation-induced radiation loss
 Effects of Van Allen belts
 Induced voltages on SCR's
 Position sensing of buckets
 Capacitor recharging and
   regenerative braking
4. Miscellaneous considerations $0.5 million
 Systems study and optimization
 Startup and shutdown
 Reaction mass as a heat sink

5. Ground test models $0.5 million
 10-m Princeton -M.I.T. model
 100-m MDRE prototype
6. Component improvements $6 million
 Power supplies
 Capacitors: dielectric, vacuum
 SCR's: alternative packaging
   and cooling
 Superconductors: mechanical
   and electrical containment
 Radiators and heat pipes
 Actuators
Total research and technology $26 million

The first (and costliest) of these categories involves several detailed design problems that are self-explanatory as presented here.

Structural analysis and dynamics is the first research area to be addressed. A structural model is required to explore the limits of static and dynamic stability over the entire range of possible operating parameters. Topics requiring attention include interaction of the structure with the stream of accelerating buckets, thrust vectoring, bucket steering, stabilization of oscillations and perturbations, and downrange guidance for the lunar launcher.

Electrical analysis and design includes the important task of optimizing electrical configurations for both lunar launchers and reaction engines. Other tasks include inductance modeling to determine restoring force profiles, an evaluation of the effects of harmonics in the drive current wave form, oscillation-induced radiation losses, and effects of induced voltages on the SCR's. Studies must be made to determine optimum techniques for recharging the capacitors, returning regenerated brake energy to the system, and sensing the position of buckets. Finally, it must be determined what effects passing through the Van Allen belts will have on the system.

The category of miscellaneous considerations includes first a detailed systems study, such as the study represented by the very crude first approach of the OPT-4 program presented here. The startup and shutdown of reaction engines and lunar launchers have not been considered thus far, but may have a significant effect on the overall system design. One final item in the miscellaneous category which merits early attention is the possibility of using the reaction mass or payload as a heat sink. Considering the very large fraction of total system mass devoted to waste heat radiators, this technique could result in substantial mass reduction, even if it should require the use of a heat pump.

A basic mass-driver model, built at M.I.T. by some of the present authors, was demonstrated at Princeton in May 1977. Its accelerating section is 2 m long and accelerates a 0.5-kg bucket at 33 g to 36 m/sec. This is a single-shot (push only) system using aluminum rather than a superconductor, with an ultimate capability of 100 g.

The next model to be built, the Princeton-M.I.T. model will be 10 m long and will have an acceleration of several hundred g's. It will have a caliber of 13.1 cm, with an

evacuated glass tube located between the drive coils and the bucket. The bucket will have two superconducting coils.

The third model will be 100 m long and reach 960 m/sec at 1000 g. It should represent the first prototype for an orbital transfer reaction engine, including bucket return loop. If operated in an evacuated tunnel, it could serve as a test bed for structural as well as electrical design considerations.

All areas mentioned previously involve the development of mass drivers. It appears that no advances in the technology involved are required to achieve a practical mass driver. There are, however, a number of areas in which significant advances could dramatically improve the performance of mass drivers (as well as other space hardware). For this reason, a modest development effort is proposed for component improvement. Components that appear to offer potential for improvement are:

> Power supplies: photovoltaic, nuclear
> Capacitors: dielectric, vacuum
> SCR's: alternatives in packaging and heat removal
> Superconductors and associated cryogenic structure
> Radiators and heat pipes
> Mechanical actuators

In relation to the proposed flight tests, note that these will be simpler in some respects than terrestrial tests. There is no need for vacuum insulation, and prototype systems will have been reduced to a number of identical modules sized for shuttle transportation (20 m long).

Funding Requirements

The funding requirements are estimated below, based on the optimized system masses derived earlier.

MASS-DRIVER R&D FUNDING REQUIREMENTS (millions of dollars)

Research and technology	
Basic design and technology	$ 10
Component improvements	6
Flight demonstration	36
Site selection for lunar launcher	
Lunar orbital survey	150
Lunar lander survey	500
Ground test facility	25
MDRE no. 1	465
MDRE no. 2	300
MDRE no. 3	165
Lunar launcher	1480
Total	$ 3137

We assume development costs and learning curves typical of other space projects. Our baseline scenario represents an all-out effort and is recognized to be extremely ambitious in terms of both costs and schedule. However, it does seem to be a realistic objective if a national commitment is made and given the required priority. In many respects, the project seems more realistic than did the Apollo program at the time it was embarked upon just 10 years ago.

A very important aspect of the proposed program is the fact that it would provide a badly needed long-term goal. We have not had such a goal for several years. The stimulation provided by a long-term goal very often transcends the ultimate value of the goal itself. Pyramids, cathedrals, and manned spaceflight all serve to confirm this assertion.

REFERENCES

1. Arnold, W.; Bowen, S.; Fine, K.; Kaplan, D.; Kolm, H.; Kolm, M.; Newman, J.; O'Neill, G. K.; and Snow, W.: Mass Drivers I: Electrical Design. Space Resources and Space Settlements. NASA SP-428, 1979, pp. 76-86.
2. Grover, Frederick W.: Inductance Calculations, Working Formulas and Tables. Van Nostrand, New York, 1947.
3. Chilton, F.; Hibbs, B.; Kolm, H.; O'Neill, G. K.; and Phillips, J.: Electromagnetic Mass Drivers, in Space-Based Manufacturing from Nonterrestrial Materials. Progress in Astronautics and Aeronautics, vol. 57, AIAA, New York, 1977, pp. 37-61; also NASA TM-73,265, Aug. 1977.
4. Chilton, F.; Hibbs, B.; Kolm, H.; O'Neill, G. K.; and Phillips, J: Mass-Driver Applications, in Space-Based Manufacturing from Nonterrestrial Materials. Progress in Astronautics and Aeronautics, vol. 57, AIAA, New York, 1977, pp. 63-94; also NASA TM-73,265, Aug. 1977.
5. Hoffman, Paul S.: Capacitors for Aircraft High Power. Report AFAPL-TR-75-19, Maxwell Laboratories, Inc., Final Report, March 1, 1973-Jan. 15, 1975.
6. Dailey, C. L.; and White, C. W.: Capacitors for Aircraft High Power, Report AFAPL-TR-74-79, TRW Systems Inc., July 1974.
7. Heppenheimer, T. A.: The Lunar Mass Transport Problem in Space Colonization, Paper presented at the AAS/AIAA Astrodynamics Specialist Conference, Jackson Hole, Wyoming, Sept. 7-9, 1977.

APPENDIX A

MASS OPTIMIZATION FOR MDRE AND MDLL, DEVELOPED IN SECTION 2

(HEWLETT-PACKARD 67/97 PROGRAM)

Step	Instructions	Input	Key	Output	Units
1	Load sides 1 and 2				
2	Input coefficients	1.66×10^{-10}	STO 0		
	for MDRE	0.122	STO 1		
	for MDLL	0.142			
	for MDRE	7.19×10^{-4}	STO 2		
	for MDLL	7.97×10^{-4}			
	for MDRE	0.0025	STO 3		
	for MDLL	0.007			
3	Rotate registers		P⇔S		
4	Input data	a	ENT↑		m/sec²
		v_e	ENT↑		m/sec
		m_l	ENT↑		kg
		f_R			Hz
5	Start		A		
6	HP97 will print input			a, v_e, m_1, f_R	
	HP67 will store				
				SPACE	
			(for HP67)		
			RCL 1	M_S	kg
			RCL 2	M_W	kg
			RCL 3	M_F	kg
			RCL 4	M_{kin}	kg
			RCL 5	M_{elec}	kg
				SPACE	
			RCL 6	M_{tot}	kg
			RCL 7	S_{tot}	m
			RCL 8	P_W	W
			RCL 9	P_{tot}	W
			RCL 0	Eff	

PROGRAM DESCRIPTION

R1   SCR mass $M_S = 1.66 \; 10^{-10} \; v_e^3 a m_1^{1/3}$

R2   winding mass $M_w = 0.122 \; v_e^{3/2} m_1^{1/2} f_R^{1/2}$ for MDRE

$\qquad\qquad\qquad\quad = 0.142 \; v_e^{3/2} m_1^{1/2} f_R^{1/2}$ for MDLL

    equal to associated power and radiator mass

R3   feeder mass $M_F = 7.19 \; 10^{-4} v_e^{5/3} a^{1/3} m_1^{5/9} f_R^{1/3}$ for MDRE

$\qquad\qquad\qquad\quad = 7.97 \; 10^{-4} v_e^{5/3} a^{1/3} m_1^{5/9} f_R^{1/3}$ for MDLL

    equal to associated power, radiator and capacitor mass

R4   kinetic power mass $M_{kin} = 0.0025 f_R m_1 v_e^2$ for MDRE

$\qquad\qquad\qquad\qquad = 0.007 f_R m_1 v_e^2$ for MDLL

R5   total electric mass $M_{elec} = M_s + 2M_w + 3M_F + M_{kin}$

R6   total mass $M_{tot} = 1.5 \; M_{elec}$

R7   total length $S_{tot} = 0.847 v_e^2 / a$

R8   waste power $P_w = [R2 + R3] \; 1/0.025$ for MDRE;

$\qquad P_w = [R2 + R3] \; 1/0.034$ for MDLL

R9   total power $P_{tot} = [R8] + [R4] \; 1/0.005$ for MDRE;

$\qquad P_{tot} = [R8] + [R4] \; 1/0.014$ for MDLL

R0   efficiency $Eff = [R9 - R8] \; / \; [R9]$

PROGRAM LISTING

001 *LBLA	037 x	073 x	109 RCLA
002 SCI	038 RCLD	074 STO3	110 ÷
003 STOD	039 x^{-2}	075 PRTX	111 .
004 PRTX	040 x	076 RCLD	112 8
005 R↓	041 P⇔S	077 RCLC	113 4
006 STOC	042 RCL1	078 x	114 7
007 PRTX	043 P⇔S	079 RCLB	115 x
008 R↓	044 x	080 x^2	116 STO7
009 STOB	045 STO2	081 x	117 PRTX
010 PRTX	046 PRTX	082 P⇔S	118 RCL2
011 R↓	047 RCLB	083 RCL3	119 RCL3
012 STOA	048 5	084 P⇔S	120 +
013 PRTX	049 ENT↑	085 x	121 4 (2 for LL)
014 SPC	050 3	086 STO4	122 0 (9 for LL)
015 RCLC	051 ÷	087 PRTX	123 .
016 3	052 y^x	088 RCL3	124 0 (4 for LL)
017 1/X	053 RCLA	089 3	125 x
018 y^x	054 3	090 x	126 STO8
019 x	055 1/x	091 +	127 PRTX
020 RCLB	056 y^x	092 RCL2	128 RCL4
021 3	057 x	093 2	129 2 (7 for LL)
022 y^x	058 RCLC	094 x	130 0 (1 for LL)
023 x	059 5	095 +	131 0 (. for LL)
024 P⇔S	060 ENT↑	096 RCL1	132 . (4 for LL)
025 RCL0	061 9	097 +	133 x
026 P⇔S	062 ÷	098 STO5	134 RCL8
027 x	063 y^x	099 PRTX	135 +
028 STO1	064 x	100 SPC	136 STO9
029 PRTX	065 RCLD	101 1	137 PRTX
030 RCLB	066 3	102 .	138 RCL8
031 1	067 1/x	103 5	139 -
032 .	068 y^x	104 x	140 RCL9
033 5	069 x	105 STO6	141 ÷
034 y^x	070 P⇔S	106 PRTX	142 STO0
035 RCLC	071 RCL2	107 RCLB	143 PRTX
036 x^{-2}	072 P⇔S	108 x^2	144 RTN

APPENDIX B

MISSION OPTIMIZATION PROGRAM — OPT-4: MDRE COMPONENTS, FREE-SPACE ΔV MISSION PERFORMANCE

Step	Instructions	Input data/units	Keys
1	load sides 1 and 2		
2	store constants into secondary registers		
	store:	1.656×10^{-10}	STO0
	store one of the following set of constants:		
	MDRE MDLL		
	0.122 0.142		STO1
	7.194×10^{-4} 7.973×10^{-4}		STO2
	0.005 0.014		STO3
3	rotate storage		P⇔S
4	set format SCI 3		
5	store MD values and mission parameters all units MKS		
	propellant acceleration a, m/sec²	a	STOA
	propellant launch rate f_R, Hz	f_R	STOB

	exhaust velocity v_e, m/sec	v_e	STOC
	propellant lump (payload) mass, kg	m_l	STOD
	mission Δv, m/sec	Δv	STOE
	mission thrust time, t_B, sec	t_B	STOI
6	start program. Output data printed as follows:		[A]
	caliber D, m		
	SCR mass, kg		
	winding mass, kg		
	feeder = capacitor mass, kg		
	MDRE total mass, kg		
	total power, W		
	efficiency, fraction		
	total radiator mass, kg		
	overall MD specific powerplant mass, kg/w		
	powerplant, total mass, kg		
	MDRE mass/overall initial mass, fraction		
	payload mass/overall initial mass, fraction		
	initial mass M_0, kg		
	payload mass delivered at destination, M_{pay}, kg		
	propellant mass used, M_{pro}, kg		
note:	last five items apply only to MDRE calculations		
7	for length, m		[B]
8	for thrust, N		[C]

OPT-4 PROGRAM LISTING

001	*LBLA	033	.	065	÷	097	RCL6
002	.	034	5	066	y^x	098	RCL2
003	1	035	y^x	067	x	099	2
004	9	036	x	068	STO3	100	x
005	7	037	RCLD	069	PRTX	101	+
006	RCLD	038	RCLB	070	RCLB	102	RCL3
007	3	039	x	071	RCLD	103	3
008	1/X	040	x^{-2}	072	x	104	x
009	y^x	041	x	073	RCLC	105	+
010	x	042	STO2	074	x^2	106	RCL1
011	PRTX	043	PRTX	075	x	107	+
012	P⇔S	044	P⇔S	076	2	108	1
013	RCL0	045	RCL2	077	÷	109	.
014	P⇔S	046	P⇔S	078	STO8	110	5
015	RCLC	047	RCLC	079	P⇔S	111	x
016	3	048	5	080	RCL3	112	STO5
017	y^x	049	ENT↑	081	P⇔S	113	PRTX
018	x	050	3	082	x	1!4	1
019	RCLA	051	÷	083	STO6	115	RCL9
020	x	052	y^x	084	RCL2	116	RCL8
021	RCLD	053	x	085	RCL3	117	PRTX
022	3	054	RCLA	086	+	118	÷
023	1/x	055	RCLB	087	.	119	-
024	y^x	056	x	088	0	120	STO0
025	x	057	3	089	2	121	PRTX
026	STO1	058	1/X	090	P⇔S	122	RCL9
027	PRTX	059	y^x	091	RCL3	123	5
028	P⇔S	060	x	092	P⇔S	124	0
029	RCL1	061	RCLD	093	+	125	÷
030	P⇔S	062	5	094	÷	126	STO4
031	RCLC	063	ENT↑	095	STO9	127	PRTX
032	1	064	9	096	ST+8	128	RCL5

129	RCL8	152	x^2	175	x	198	RTN
130	÷	153	RCLE	176	RCL1	199	*LBLB
131	STO6	154	RCLC	177	÷	200	RCLC
132	PRTX	155	÷	178	STO8	201	X^2
133	RCL8	156	CHS	179	1/X	202	RCLA
134	P⇔S	157	e^x	180	RCLD	203	÷
135	RCL3	158	P⇔S	181	x	204	.
136	P⇔S	159	STO5	182	RCLB	205	8
137	x	160	CHS	183	x	206	4
138	PRTX	161	1	184	RCLC	207	7
139	SPC	162	+	185	x	208	x
140	RCL0	163	x	186	STO9	209	PRTX
141	2	164	STO4	187	PRTX	210	RTN
142	x	165	PRTX	188	RCL6	211	*LBLC
143	RCL1	166	CHS	189	x	212	RCLB
144	x	167	RCL5	190	PRTX	213	RCLD
145	RCL6	168	+	191	1	214	x
146	÷	169	STO6	192	RCL5	215	RC LC
147	x^{-2}	170	PRTX	193	-	216	x
148	STO7	171	1	194	RCL9	217	PRTX
149	RCLC	172	RCL5	195	x	218	RTN
150	X⇔Y	173	-	196	PRTX	219	R/S
151	÷	174	RCLC	197	P⇔S		END OF PROGRAM

OPT-4 PROGRAM DESCRIPTION (EQUATIONS, VARIABLES)

MDRE constants are used and identified by ( )

caliber (mean diameter of drive coils) = $0.197\ m_1^{1/3}$; m_1 = payload (pellet) mass

SCR mass = $1.656 \times 10^{-10} v_e^3 a\, m_1^{1/3}$

winding mass = $(0.122)\ v_e^{3/2}(m_l f_R)^{-2}$

feeder = capacitor mass = $(7.196 \times 10^{-4}) v_e^{5/3}[a f_R]^{1/3} m_1^{5/9}$

kinetic power = $0.5 m_l f_R v_e^2 = P_{kin}$

kinetic power mass = $(0.005) *$ kinetic power = $M_{kinetic}$

waste power = $[M_{wind} + M_{feed}] / [(0.005) + 0.02] = P_{waste}$

total MDRE mass = $1.5 * [M_{scr} + 2M_{wind} + 3M_{feed} + M_{kin}] - M_{tot}$
        which is also = $1.5 * [M_{scr} + M_{wind} + M_{feed} + M_{cap} + M_{rad} + M_{pow}]$

$P_{tot} = P_{kin} + P_{waste}$

power plant mass = $(0.005) * P_{tot}$

radiator mass = $M_{rad} = 0.02 * P_{waste}$

efficiency $\eta = 1 - P_{waste}/P_{tot}$

overall MD specific powerplant mass $\alpha = M_{tot}/P_{tot}$

characteristic velocity $v_c = (2\eta t_B/\alpha)^{-2}$, $v_e^* = v_e/v_c$

$M_{pay}/M_0 = e^{-\Delta v/ve} - v_e^{*2}(1 - e^{-\Delta v/ve})$

initial acceleration = $a_0 = [v_e/t_B] [1 - e^{-\Delta v/ve}]$

initial mass = $M_0 = m_1 f_R c/a_0$

mission payload mass $M_{pay} = M_0 * M_{pay}/M_0$;

propellant mass $M_{prop} = M_0 [1 - e^{-\Delta v/ve}]$

$m_{bucket}/m_l = 2.263$

overall MDRE length $S_{tot} = 1.694\ v_e^2/2a$

thrust = $f_R m_l v_e$

IV

Asteroids as Resources for Space Manufacturing

IV-1
Round-Trip Missions to Low-Delta-V Asteroids and Implications for Material Retrieval

DAVID F. BENDER, R. SCOTT DUNBAR, and DAVID J. ROSS

Low-delta-V asteroids are to be found among those which have perihelia near 1 AU. From the 50 known asteroids with perihelia less than 1.5 AU, 10 candidates for asteroid retrieval missions were selected on the basis of low eccentricity and inclination. To estimate the ranges of orbital elements for which capture in Earth orbit may be feasible, a survey was made of 180° transfers from a set of orbits having elements near those of the Earth to the Earth. For 2 of the 10 low-delta-V asteroids and for an additional one with elements more Earth-like than any yet known, direct ballistic round trips in the 1980's were computed. A stay time of several months at the asteroid was used. The results show that the total delta V, including that for rendezvous with Earth upon return, for the known asteroids is above 14 km/sec. But if asteroids are found similar to the strawman considered, the total delta V could be as low as 10 km/sec.

To obtain trajectories with lower delta V than the direct ballistic cases, three modifications to the trajectories that use gravity-assisted flybys are considered: a lunar gravity assist at both departure and arrival at Earth, Earth-Venus-Earth flights which can greatly increase or decrease heliocentric energy, and low-thrust Earth-to-Earth transfers to increase or decrease the V_∞ at Earth.

Ballistic studies using Earth-Venus-Earth return trajectories were made for 3 of the 10 low-delta-V asteroids. These studies can form the basis for low-thrust return trajectories, but only one low-thrust case was investigated. Low-thrust mission results are shown for a direct retrieval of the "Earth-like" asteroid and a gravity-assisted retrieval of 1977 HB. Although they have the disadvantage of longer mission times, the gravity-assisted trajectories make available for possible return a much wider range of targets, as opposed to the severely restricted class of orbital elements required for direct missions; for example, the 1977 HB return requires a delta V of only 3.04 km/sec using low thrust and gravity assists.

The final phase of the return of an asteroid is capture by the Earth-Moon system, which is accomplished by a lunar gravity assist even though V_∞ at Earth arrival is as high as 1.5 km/sec. A sample trajectory showing capture into an orbit near the 2:1 Earth-Moon resonance is presented.

With the discovery of new Earth-approaching asteroids for direct missions and more detailed and exhaustive trajectory studies for gravity-assisted missions, it is felt that asteroid round trips with delta-V values as low as 6 km/sec can be found. This work serves only to demonstrate the feasibility of asteroid return missions and to indicate possible directions for future studies.

INTRODUCTION

Many types of asteroid missions, including flybys (refs. 1, 2), rendezvous (ref. 3), and sample return missions (ref. 4) have been discussed previously. Recently, the idea of retrieving all or part of an Earth-approaching asteroid as raw material for space manufacturing has heen proposed. This paper addresses the problems of trajectory dynamics crucial to this scheme and proposes several techniques for conducting such a mission.

Clearly, only those asteroids accessible with the lowest possible delta V to rendezvous will be of interest, at least for the time being. Such low-delta-V asteroids will be those crossing or inside the orbit of Mars, with small eccentricity, low inclination, and a sernimajor axis near 1 AU.

In addition to trajectories that travel directly from Earth to an asteroid and return, the greatest possible use will be made of gravity assists. Earth escape and capture will be facilitated by lunar-gravity assists. In the solar system, flybys of Earth and Venus will be used to shape the trajectory, with a consequent reduction in total delta V. Finally, the possibility of low-thrust trajectories between gravitational encounters will be considered briefly. (However, it was not possible to explore this concept in depth here.)

TABLE 1 — ORBITAL ELEMENTS OF NEAR-EARTH OBJECTS[a]

Asteroid

Number	Name	A	Ecc	Incl	Q1	Q2
1566	Icarus	1.08	0.827	23.0	0.19	1.97
	1974MA (L)	1.76	.760	37.7	.42	3.09
	1936CA Adonis	1.87	.764	1.4	.44	3.30
	1976UA	.84	.451	5.9	.46	1.22
1864	Daedalus	1.46	.615	22.1	.56	2.36
1865	Cerberus	1.08	.467	16.1	.58	1.58
	1937UB Hermes (L)	1.64	.624	6.2	.62	2.66
1981	1973EA	1.78	.650	39.8	.62	2.93
1862	Apollo	1.47	.560	6.4	.65	2.29
	1977HB	1.08	.346	9.4	.70	1.45
1685	Toro	1.37	.436	9.4	.77	1.96
	1976AA	.97	.182	18.9	.79	1.14
	1977HA	1.58	.498	22.8	.80	2.37
	6743P-L (L)	1.62	.493	7.3	.82	2.42
1620	Geographos	1.24	.335	13.3	.83	1.66
	1976WA	2.41	.656	24.3	.83	3.99
	1947XC (L)	2.25	.630	1.0	.83	3.67
	1959LM (L)	1.34	.379	3.3	.83	1.85
	1950DA (L)	1.68	.502	12.1	.84	2.53
1866	Sisyphus	1.89	.540	41.1	.87	2.92
	1973NA (L)	2.39	.633	67.9	.88	3.91
1863	Antinous	2.26	.606	18.4	.89	3.63
	1975YA	1.29	.298	64.0	.91	1.67
	6344P-L (L)	2.58	.635	4.6	.94	4.21
	196DUA	2.26	.537	3.7	1.05	3.48
1915	Quetzalcoatl	2.52	.583	20.5	1.05	3.99
1917	Cuyo	2.15	.505	24.0	1.06	3.23
1943	1973EC	1.43	.256	8.7	1.06	1.80
1980	1950LA	1.71	.365	26.8	1.08	2.33
1221	Amor	1.92	.436	11.9	1.08	2.76

Number	Name	A	Ecc	Incl	Q1	Q2
1580	1972RB	2.17	.492	5.2	1.10	3.23
1627	Betulia	2.20	.490	52.0	1.12	3.27
	Ivar	1.86	.397	8.4	1.12	2.60
	1972RA	2.36	.523	9.0	1.13	3.60
433	Eros	1.46	.223	10.8	1.13	1.78
887	Alinda	2.52	.544	9.1	1.15	3.88
	4788P-L (L)	2.55	.545	10.8	1.16	3.93
719	Albert (L)	2.58	.540	10.8	1.19	3.98
1036	Ganymed	2.66	.542	26.3	1.22	4.10
	1963UA	2.65	.530	11.1	1.24	4.05
1916	1953RA	2.27	.450	12.8	1.25	3.30
1951	Lick	1.39	.062	39.1	1.30	1.48
	1971SC (L)	2.21	.390	12.0	1.34	3.07
	1974UB	2.12	.359	36.3	1.36	2.89
1474	Beira	2.73	.490	26.8	1.39	4.07
	2108P-L (L)	2.32	.385	2.6	1.43	3.21
1134	Kepler	2.68	.467	15.0	1.43	3.93
	4548P-L (L)	2.17	.340	7.5	1.43	2.91
1009	Sirene	2.63	.454	15.8	1.44	3.82
1139	Atami	1.95	.255	13.1	1.45	2.44
	1963RH (L)	2.38	.379	21.1	1.48	3.28
	1975AD	2.37	.375	20.1	1.48	3.26
1198	Atlantis (L)	2.25	.335	2.7	1.49	3.00

Meteoroid

Number	Name	A	Ecc	Incl	Q1	Q2
	40503	2.02	0.642	12.6	0.72	3.31
	Harvard 19816	2.24	.662	12.6	.76	3.72
	Pribram	2.42	.674	10.4	.79	4.05
	Iron Meteor	1.05	.117	13.3	.93	1.17
	Harvard 7946	2.49	.621	18.1	.94	4.04
	Lost City	1.66	.417	12.0	.97	2.35
	40617	2.02	.516	3.3	.98	3.06

a Data supplied by James G. Williams of the Jet Propulsion Laboratory.

LOW-DELTA-V ASTEROIDS

A low-delta-V asteroid is one for which the total impulse to rendezvous, including Earth launch delta V, is among the lowest known. In this study, the return of a significant part of the asteroid is considered and thus the total impulse to return to Earth, including that for rendezvous with Earth, must also be as low as possible. Generally, the outbound and return thrust requirements should be essentially the same, but to return an asteroid, contrary to expectation, the outbound delta V must be nunimized at the expense of the inbound delta V (ref. 5).

The low-delta-V asteroids will be found among those which come near the Earth; such a list is obtained by arranging all the asteroids by perihelion distance (Q1). Orbital elements of the 53 asteroids with perihelion under 1.5 AU are given in table 1. The designation (L) after the name indicates that the asteroid is lost. The elements listed are semimajor axis (A), eccentricity (ECC), inclination to the ecliptic (INCL) and aphelion distance (Q2). Two of the 53 asteroids — 1977 HA and 1977 HB — were discovered in April 1977. In addition, orbital elements for seven large fireballs (meteoroids) are added to indicate a range of orbital elements for large objects that have intersected the Earth's orbit.

In selecting the low-delta-V asteroids from this list, note that a delta V of 6 km/sec for Earth escape to asteroid rendezvous or for return would allow the spacecraft to reach to $\cong 1.8$ AU for $e = 0.45$ and $i = 0$, or to $i = 12°$ for $a = 1$ AU and $e = 0$. These values, namely $a \leq 1.8$ AU, $e \leq 0.45$, and $i \leq 12°$, are used as limits in selecting asteroids although by doing so regions are included for which the ΔV would exceed 6 km/sec. Six asteroids are thus selected from table 1: 1976 UA, 1977 HB, Toro, 1959 LM, 1973 EC, and Eros. Another seven lie near but outside this boundary: Adonis, Hermes, Apollo, 6743 PL, Geographos, Amor, and Ivar. If the three lost asteroids are excluded from this set of 13, 10 may be considered as low-delta-V asteroids (see table 2).

BALLISTIC TRAJECTORIES

To estimate in a general way the delta-V values for return of material from asteroid orbits, we first examined the ballistic equivalent trajectories for a general class of objects with orbital parameters near those of Earth. The range of semimajor axes was from 0.8 to 1.2; of eccentricities, from 0 to 0.4; and of inclination, from 0° to 10°. These limits approximate those developed above by setting a bound on the delta V at Earth of 6 km/sec to produce an elliptical orbit or an inclined orbit. This value is higher than can reasonably be provided by available thrust systems operating on an asteroidal mass, but these limits encompass the ranges of orbital elements that will be of interest.

The delta-V values are computed for 180° ballistic transfer from the asteroid orbit to Earth. For no inclination of the asteroid orbit, the total delta V is known to be optimal. Figure 1 shows delta V at the asteroid as a function of eccentricity and semimajor axis of the asteroid orbit. The contours of constant delta V are marked with the delta V (in kilometers per second) and a symbol to indicate whether the departure is from the aphelion of the asteroid orbit (number within triangle) or from the perihelion (encircled numbers). The delta V at Earth to yield rendezvous is indicated only for 1.5 km/sec, which is taken to be the upper limit of the approach velocity for "free" capture with a lunar gravity assist (dashed lines).

For transfers from inclined orbits to Earth, the first impulse is applied at a node and is assumed to establish a transfer orbit that is coplanar with and tangent to the Earth's orbit 180° from the node. For simplicity, only orbits with the nodes at perihelion and aphelion are considered. By departing from these nodes (which can be characterized as from perihelion or from aphelion), the same kind of curves can be presented for orbits of any single inclination as in figure 1 for coplanar orbits. Figures 2 and 3 show delta V at the asteroid as a function of a and e for inclinations of 2° and 5°, respectively. The dashed lines in figure 1, showing the free capture region, transfer identically to figures 2 and 3 since the transfer orbits are the same for each figure.

For any given semimajor axis and eccentricity, one of the two transfers in figures 2 and 3 will have less total delta V than the other. It can be shown that for various locations of the periapse around the orbit the optimum transfer will lie between these two values.

Of the 10 low-delta-V asteroids from table 2, only 1976 UA lies near the regions plotted in figures 1-3. Its position is indicated in figure 3, but, because it has an inclination of 5.9°, the delta-V values from the graph are too small. In an effort to present an example of a moderate delta-V requirement, a fictitious asteroid, Ames SSS 77, is hypothesized with the following elements: semimajor axis, 1.08 AU; eccentricity, 0.18; inclination, 5°; longitude of ascending node, 0°; argument of perihelion, 45°; and mean anomaly, 0°, on 14 November 1979.

The position of this asteroid is also marked in figure 3, which indicates that the delta-V value to depart from the asteroid to Earth can be as low as 2.3 to 3.4 km/sec (if the relative positions of Earth and the asteroid are those required for the transfer). The capture by Earth should ideally require only a small delta V to reduce the approach speed to the 1.5 km/sec assumed as satisfactory for lunar-assisted capture.

TABLE 2 — ORBITAL ELEMENTS OF THE TEN KNOWN LOW-AV ASTEROIDS

Asteroid	A	Ecc	Incl	Q1	Q2
1976 UA	0.84	0.451	5.9	0.46	1.22
1977 HB	1.08	.346	9.4	.70	1.45
Toro	1.37	.436	9.4	.77	1.96
1973 EC	1.43	.256	8.7	1.06	1.80
Eros	1.46	.223	10.8	1.13	1.78
Adonis	1.87	.764	1.4	.44	3.30
Apollo	1.47	.560	6.4	.65	2.29
Geographos	1.24	.335	13.3	.83	1.66
Amor	1.92	.436	11.9	1.08	2.76
Ivar	1.86	.397	8.4	1.12	2.60

Figure 1 — *Delta V at asteroid for transfer orbit tangent to Earth orbit (inclination = 0°). Note: Arrows indicate boundary above which either asteroid departure ΔV is >3 km/sec or Earth-approach ΔV is >1.5 km/sec.*

Figure 3 — *Delta V at asteroid for transfer orbit tangent to and coplanar with Earth orbit (inclination = 5°). Note: Arrows indicate boundary above which either asteroid departure ΔV is >3 km/sec or Earth-approach ΔV to >1.5 km/sec.*

Figure 2 — *Delta V at asteroid for transfer orbit tangent to and coplanar with Earth orbit (inclination = 2°). Note: Arrows indicate boundary above which either asteroid departure ΔV is >3 km/sec or Earth-approach ΔV is >1.5 km/sec.*

POSSIBILITIES FOR GRAVITY-ASSISTED ASTEROID MISSIONS

Consider a spacecraft moving in the gravitational field of a central body and assume that a moderately massive secondary body is also moving in the field. The spacecraft can be directed to approach the secondary body closely, causing the spacecraft to change its direction and magnitude of velocity in the field of the central body. It is assumed to occur essentially instantaneously at the position of the secondary body. A gravity-assisted flyby uses this change in spacecraft velocity to enhance the mission under consideration.

For asteroid sample return missions, and particularly for asteroid retrieval, a gravity assist by the Moon in the Earth's gravity field would lower the delta-V requirement significantly. It has been shown that capture by the Earth-Moon system can occur for a hyperbolic approach velocity to the Earth as high as 1.85 km/sec (ref. 6). Similarly, an escape velocity of 1.85 km/sec can be achieved on a parabolic trajectory in the Earth's field by a lunar flyby on the outbound leg. These cases require a grazing flyby of the Moon. To provide a safe margin for guidance, V = 1.5 km/sec is used at Earth approach or departure. Multiple flybys of the Earth-Moon system with a lunar gravity assist at each could be used to capture at a higher velocity (ref. 6), but such trajectories considerably lengthen total mission time (1 yr per pass). For two flybys, the upper limit is 2.58 km/sec. An example of a single encounter capture is examined in a section (Lunar Gravity-Assisted Capture).

Multiple flybys of a single secondary body cannot be used to change the magnitude of the hyperbolic approach speed to that body (if its orbit is circular), assuming that no delta V is

Suppose that delta V at the asteroid is limited to 3 km/sec and the Earth approach speed is limited to the "free" capture speed of 1.5 km/sec. Then, from figure 1, a zigzag line across the figure as shown by the arrows shows which regions of *a* and *e* are accessible. In figure 2, the corresponding line is slightly modified from that in figure 1, but for 5° inclination (fig. 3), the available ranges for *a* and *e* are reduced significantly.

applied along the trajectory between encounters. But if the trajectory is modified by a gravity assist at a different body or by impulsive or low-thrust delta V between encounters, dramatic changes can be made. Bender and Friedlander (ref. 2) have shown that, by means of a Venus-Earth gravity-assisted trajectory, almost any asteroid in the main belt can be approached on a ballistic trajectory with lower than direct ballistic energy expenditure. In that study, launch velocities of 3 to 5 km/sec from Earth were considered. The Venus flyby modifies the orbit so that the subsequent Earth flyby is at a higher relative speed. The Earth return speeds used to reach the asteroid belt and beyond were in the range of 8 to 14 km/sec. Moreover, trajectories were found for dates of the Earth return flyby over a large fraction of any synodic period of Earth and Venus.

Presumably, if any asteroid can be reached by an Earth-Venus-Earth trajectory, return trips are also possible with arrival conditions at Earth similar to the low-energy launches considered by Bender and Friedlander (ref. 2). Additionally, for an asteroid to be retrievable by means of Earth and Venus gravity assists, the asteroid must approach Earth or Venus so closely that only a small delta V is required for the first encounter.

A technique little studied to date is to shape a trajectory by low thrust between gravitational maneuvers. This concept is applied here to reduce an Earth flyby speed from 3-5 km/sec at return from Venus to 1.5 km/sec as needed for the final capture. Table 3 shows some test results obtained when the flyby speed was reduced by low-thrust propulsion between two Earth encounters. Equivalent delta V is the total d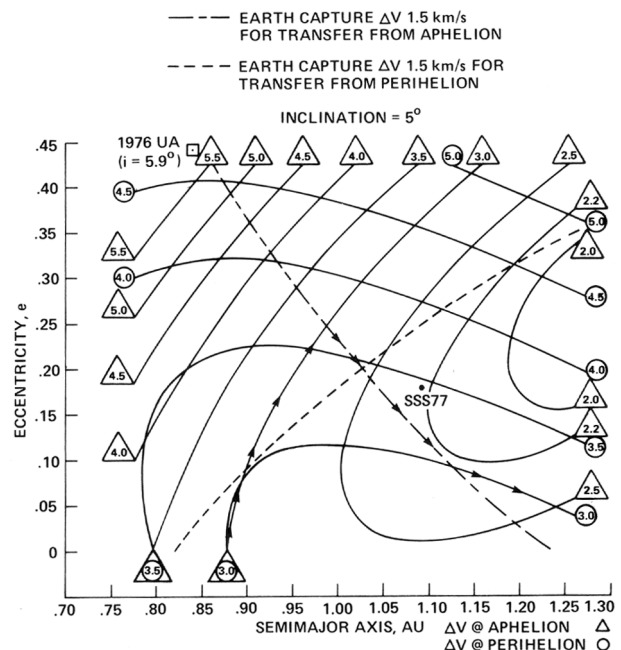elta V supplied by the low-thrust system. Low-thrust propulsion effectively reduces the relative speed at Earth arrival. Capture by the Earth-Moon system can be managed in 410 days or less at approach speeds from 3 to 5 km/sec with a low-thrust delta V that provides from 1 to 2.7 km/sec.

TABLE 3 — EARTH-TO-EARTH FOR LOWERING
V_∞; FINAL V_∞ = 1.5 km/sec

Initial V_∞	2	3	4	5
Equivalent ΔV, km/sec	0.46	0.96	2.13	2.69
Time, days	370	390	390	410

If this capture process is combined with Venus-Earth gravity assists, a great range of asteroid orbits is opened for asteroid retrieval. The low-thrust system is required mainly to provide for the first Earth or Venus encounter and the capture phase. The only requirement is that the total velocity change required to produce a flyby of Earth (or Venus) be small. The known candidates are listed in table 2. A Venus encounter requires that the perihelion distance be less than 0.72 AU; a crossing of the Venus orbit plane at Venus's distance from the Sun is unlikely. An Earth encounter similarly requires that the perihelion distance be less than 1.0 AU. But crossing the Earth orbit plane near 1 AU is very likely since this is essentially the condition required for discovering it. Results of testing a few asteroids from table 1 indicate that a delta V of about 500 m/sec represents the lower range of values for achieving the first

Earth encounter. The total delta V for the return phase of an asteroid retrieval will be from 2-4 km/sec, possibly sometimes as low as 1.5 km/sec.

If the smaller fraction of the total delta V is needed at the start of the retrieval process, it and the navigational delta-V values required to control the flybys might be supplied by a relatively modest mass driver. The final larger delta V, upon Earth return from Venus, could be supplied by a larger mass driver sent to rendezvous with the asteroid in its nearly final and much lower delta-V orbit, provided sufficient time remains to accumulate the required delta V.

BALLISTIC RESULTS

Direct Retrievals

Ballistic mission studies for asteroid sample return were performed for several asteroids, including some of interest for possible asteroid retrievals. Although there is little possibility of ballistic asteroid retrieval, ballistic studies do show the relative costs of reaching and bringing back various asteroids. The delta-V values found will not differ greatly from the low-thrust delta-V values.

Actual ballistic round trips to two asteroids 1977 HB and 1974 EC are shown in table 4. Additional data are shown for the hypothetical asteroid Ames SSS 77 (table 5) in a later opportunity, which is representative of those that might be discovered. The fact that the real departures and arrivals with a considerable stay time at the asteroid have been required means that delta V will be considerably larger than for the ideal two impulse transfer between the orbits. Table 4 is divided into three parts: dates and time intervals, impulses needed, and orbit elements. The impulse to remove V_∞ at Earth is included in the total delta V because the asteroid must be captured. All legs were optimized on total delta V for rendezvous. Ecliptic plane projections of the orbits of SSS 77 and 1977 HB are illustrated in figures 4 and 5 drawn to the same scale so that differences are easily observed. Ames SSS 77 is significantly more accessible than 1977 HB. Note that in table 4 the use of lunar gravity assist on Earth departure and arrival is not included. If this "free" delta V were 1.5 km/sec, the total delta V would be reduced by 3 km/sec. Note also that the total impulse required on the retrieval phase for Ames SSS 77 is 3.76 + 1.68 - 1.5 or 3.94 km/sec, which lies between 3 to 4 km/sec, postulated previously for the minimum total delta V to retrieve an asteroid by direct flight to Earth.

Earth-Venus-Earth Gravity-Assisted (EVEGA) Retrievals

As mentioned in the preceding section, one method for reducing overall delta V during retrieval is to use gravity assists by Earth and Venus. In this technique, the orbital inclination and the high excess hyperbolic velocity at the first Earth encounter can be decreased to values that are amenable to a relatively easy capture maneuver into high Earth orbit. The cost is the flight time to Venus and back to Earth in one to three revolutions. A basic technique of searching for mission opportunities of this kind has been

TABLE 4 — BALLISTIC ROUND TRIPS

Dates and times	1977 HB	1943-1973 EC	Ames SSS 77
Launch	Oct. 18, 1985	May 26, 1992	March 13, 1982
TF, days	242	453	221
Arrival	June 17, 1986	Aug. 20, 1993	Oct. 20, 1983
Stay time, days	202	151	394
Depart	Jan. 5, 1987	Jan. 19, 1994	Nov. 18, 1983
TF,days	192	465	238
Return	July 16, 1987	Apr. 21, 1995	July 12, 1984
Total time, days	626	1069	853
Impulses needed			
Launch ΔV, km/sec	7.89	5.87	3.01
Rendezvous ΔV, km/sec	1.57	.98	1.62
Depart ΔV, km/sec	6.78	2.57	3.76
Earth ΔV (=V_∞ appr.) km/sec	2.83	4.62	1.68
Total ΔV, km/sec	19.07	13.95	10.07
Launch DLA, deg	24.8	41.8	-27.2
Orbit elements			
Semimajor axis, AU	1.08	1.43	1.08
Eccentricity	.44	.26	.18
Inclination, deg	9.4	8.7	5
Longitude of node, deg	32.8	346.0	0
ARG of perihelion, deg	54.9	11.0	45

TABLE 5 — RETRIEVAL OF AMES SSS 77

	Equiv. ΔV, km/sec	Mass fraction delivered
	Equiv. ΔV, km/sec	Mass fraction delivered
Launch Feb. 21, 1987 (V_{AL} = 1.5 km/sec)		
340 days		
Arrival Jan. 27, 1988	4.72	0.389
Stay time in asteroid orbit: 246 days		
Departure Oct. 1, 1988		
900 days		
Earth arrival Mar. 19, 1991 (V_∞ = 1.5 km/sec)	3.61	.406

established but, as expected, a high velocity at the first Earth approach cannot be reduced to low values in two or three revolutions for every date. In the data below, no more than three revolutions were considered.

The scheme of using an EVEGA trajectory to retrieve an asteroid is as follows: (1) the asteroid is driven from its orbit by some sort of propulsion system (high or low thrust) so as to intercept the Earth, (2) the encounter is controlled so that the spacecraft flies on to Venus (ideally, with no intermediate thrusting during the flyby), and (3) it then makes a gravity-assisted flyby of Venus, sending it back to Earth for rendezvous. In searching for mission opportunities of this type, each separate leg was analyzed ballistically in hopes of finding a suitable set of launch/arrival dates so that the hyperbolic excess velocities, $V_{\infty in}$ and $V_{\infty out}$ at each boundary point would be matched as closely as possible and the velocity at the second Earth approach would be minimized (i.e., from 3-5 km/sec). Given the rough boundary dates derived from this survey, the entire case

could be run at once and optimized on total delta V from asteroid to Earth to Venus to Earth. The results of four such cases are given in table 6.

These results indicate that the Earth-Venus-Earth gravity-assist technique will contribute significantly to the retrieval of asteroid material. The flyby velocity at the first Earth encounter on the return trip is sometimes too fast and sometimes too slow to match the "best" value for the gravity-assist geometry that occurs. It is therefore conceivable that, when more asteroids are found, it will be possible to obtain cases for which there is a closer match of $V_{\infty in}$ and $V_{\infty out}$ at Earth. The earth return velocities are sometimes too high, but it is believed that, if only cases for which this velocity is under 5 km/sec are considered, there will still be many opportunities. These are ballistic results and the addition of low-thrust techniques to those of gravity assist will result in successful asteroid retrieval trajectories in almost every case. One such case developed from the 1977 HB results is presented in table 7.
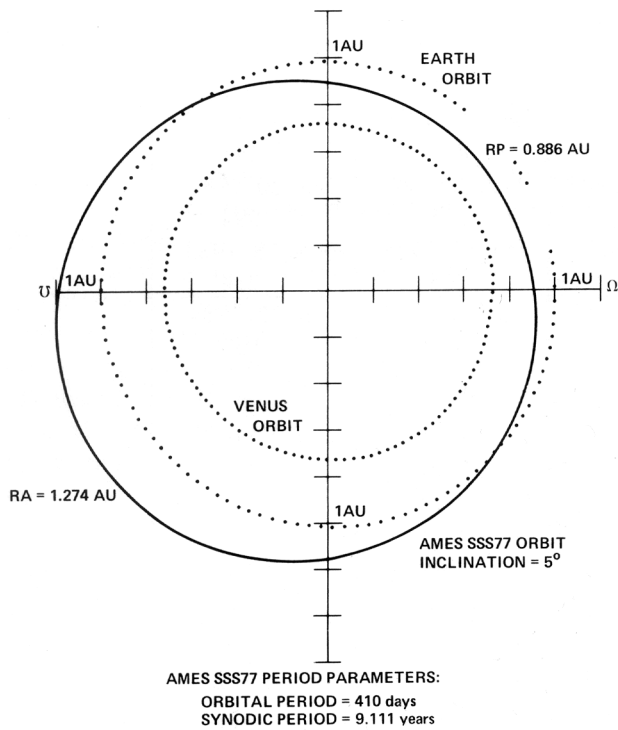
Figure 4 — *Ecliptic plane projection of the orbit of the hypothetical asteroid Ames SSS77.*
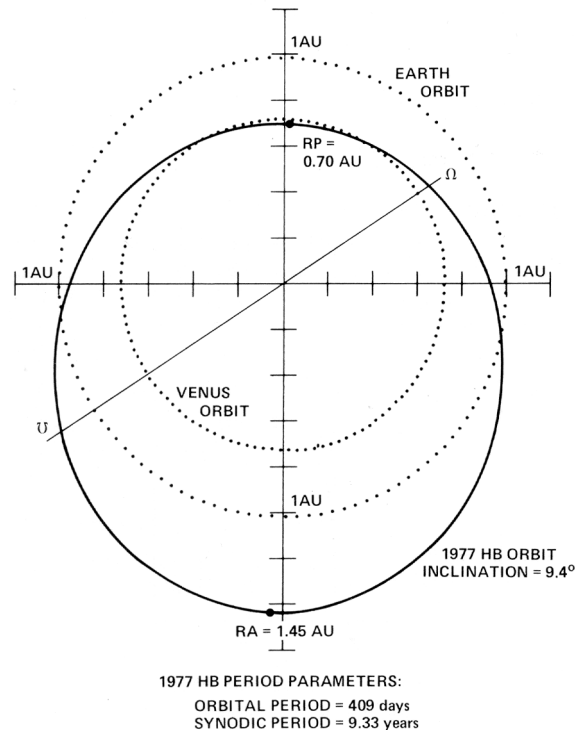
Figure 5 — *Ecliptic plane projection of the orbit of 1977 HB.*

TABLE 6 — ILLUSTRATIVE EXAMPLES OF EVEGA RETRIEVAL TRAJECTORIES

Asteroid	1977 HB	1976 UA	1976 UA	1973 EC
Departure date at asteroid	Oct. 1, 1986	Mar. 19, 1983	Feb. 8, 1990	Feb. 14, 1994
ΔV at asteroid	1.06 km/sec	0.61 km/sec	1.18 km/sec	1.43 km/sec
Earth flyby	Apr. 15, 1987	Oct. 18, 1983	Oct. 17, 1990	May 24, 1995
$V_{\infty in}$	12.29 km/sec	12.62 km/sec	11.90 km/sec	7.01
$V_{\infty out}$	9.24 km/sec	11.46 km/sec	8.36 km/sec	8.95
Rad	3.14 ER	1.66 ER	3.10 ER	1.54
Venus flyby	Mar. 10, 1988	Oct. 6, 1984	July 28, 1991	Mar. 17, 1996
$V_{\infty in}$	5.47 km/sec	7.43 km/sec	5.00	5.38
$V_{\infty out}$	5.47 km/sec	7.43 km/sec	5.00	5.38
Rad	1.61 VR	2.92 VR	6.35	3.06
Earth arrival	Aug. 29, 1988	Mar. 27, 1986	Feb. 9, 1992	Aug. 31, 1996
V_{∞}	3.04 km/sec	6.72 km/sec	5.24 km/sec	3.36 km/sec
Ballistic total ΔV^a to rendezvous	6.721 km/sec	8.276 km/sec	9.411 km/sec	7.432 km/sec
Total time	698 days	1104 days	731 days	929 days

a ΔV at Earth used at periapse, and is less than $|V_{\infty in} - V_{\infty out}|$.

LOW-THRUST RESULTS

It has been shown that the total delta V for retrieving an asteroid is likely to range from 2 to 4 km/sec. To estimate the capability of a mass driver in supplying such a delta V, suppose that delta V is supplied at the rate of 1 km/sec/yr to a 200-m-diameter asteroid with a mass of 10^{10} kg (density = 2.39 g/cm^3). The acceleration is 31.7 X 10^{-6} m/sec^2 and, if the mass is expelled at 5000 m/sec, the power required is 792 MW and the mass flow rate is 63.4 kg/sec. These are strong requirements on the mass-driver system and it may not be possible to meet them. If not, the size of the asteroid would have to be reduced or the flight time increased so that the total delta V would be supplied at a slower initial rate.

Low-thrust techniques can be used to improve the ballistic retrieval trajectories in table 6. A low-thrust trajectory can be used from the asteroid to first Earth encounter in such a way as to supply the proper magnitude of V_{∞} at Earth. For 1977 HB, this technique was combined with an additional revolution about the Sun, that is, by starting one revolution earlier from the asteroid orbit. The Earth flyby encounter and velocity were obtained at a total delta V of 2.04 km/sec supplied in 653 days. This slightly exceeds the acceleration value of 1 km/sec/yr adopted as a nominal upper limit. With a low-thrust Earth-to-Earth trajectory at a delta V of 1.00 km/sec to reduce V_{∞} at capture from 3.04 to 1.5 km/sec (as in table 3), the return of 1977 HB is possible with a total

delta V of 3.04 km/sec. As shown in table 7, the return begins from the asteroid orbit on 1 July 1985, with a 653-day low-thrust transfer to Earth; "free" flybys of Earth, Venus, and Earth in succession; and, finally, a 390-day low-thrust trajectory before final Earth encounter on 23 September 1989.

TABLE 7 — RETRIEVAL OF 1977 HB

Earth launch	Apr. 28, 1984	(6.32 km/sec)
	214 days	
1977 HB (arr)	Nov. 28, 1984	Imp 2.53 km/sec
	216 days	
1977 HB (dep)	July 1, 1985	LT 2.04 km/sec
	653 days	
Earth (F.B.)	Apr. 15, 1987	(9.24 km/sec, 2.78 ER)
	330 days	
Venus (F.B.)	Mar. 10, 1988	(5.47 km/sec, 1.61 VR)
Earth (F.B.)	Aug. 29, 1988	(3.09 km/sec, 3.09 ER)
	390 days	LT 1.00 km/sec
Earth (ret)	Sept. 23, 1989	(1.5 km/sec for capture)
Total time	1,974 days	ΔVout 7.41 km/sec
	5.41 years	ΔVret 3.04 km/sec

Only navigational delta-V values are needed during flyby. However, the low thrust could possibly be applied during the Earth-Venus-Earth portion to further reduce the total delta-V requirement for capture. (No analysis of this variation in the technique was attempted here.)

Finally, searches were made for suitable gravity-assisted opportunities for an outbound trajectory to 1977 HB. Unfortunately, no satisfactory gravity-assisted trajectories could be found using less than three revolutions about the Sun with significantly less delta V than that of the optimum direct impulsive case. Consequently, the retrieval scenario in table 7 for 1977 HB contains the impulsive data for the Earth-to-asteroid portion. The total delta V given in table 7 reflects the assumption that $V_\infty = 1.5$ km/sec represents the launch or capture assistance provided by a lunar gravity assist.

It is realized that the total outbound delta V to asteroid rendezvous is more important than the return delta V in terms of providing the maximum return per unit cost (ref. 5). Unfortunately, the 1977 HB case was developed naively on the basis of minimizing the return delta V. The present outbound results remove it from serious consideration. None of the other cases in table 6 were investigated, but the outbound results for 1977 HB were instructive and indicate that satisfactory cases should be found — especially when more Earth-approaching asteroids are known.

LUNAR-GRAVITY-ASSISTED CAPTURE

As mentioned previously, it is reasonably safe to use a lunar-gravity-assisted maneuver to capture an Earthapproaching body with a V_∞ relative to the Earth of less than about 1.5 km/sec. At 1.85 km/sec, the capture orbit is almost parabolic and there is no freedom in choosing the radius of perigee. In considering the capture problem

ballistically, it is desirable that the radius of perigee of the capture orbit equal the radius of perigee of the final desired orbit so that injection into the desired orbit can be accomplished in one maneuver. Because of its stability and favorable gravitational characteristics, the orbit in 2:1 resonance with the Moon, described by Heppenheimer (ref. 7), was chosen for this example (fig. 6). For a sufficient margin of safety and one that ensures capture of the approaching body into Earth orbit, a $V_\infty = 2^{-2}$ X lunar orbital velocity (= 1.447 km/sec) is considered. The body passes 184 km above the lunar surface, which is considered an adequate margin of safety, and has its orbit relative to the Moon bent 89.5° and its Earth-relative velocity reduced from 2.046 to 1.316 km/sec. It is injected into an orbit having a radius of perigee of 0.3952 X lunar distance.

After the lunar-gravity-assisted flyby, an impulsive velocity change of 292.3 m/sec at the perigee is sufficient for injection into the 2:1 orbit. In practice, since the stability of the 2:1 orbit depends on the avoidance of close lunar approaches by having the body at apogee when the Moon is 90° away, injection into the 2:1 orbit would be a two-stage process. First, a near 2:1 orbit would be achieved and allowed to coast until a suitable relationship with the Moon had been established and a second velocity change performed to lock the orbit into resonance. For a low-thrust mission, the capture orbit would be gradually changed over several periods to accomplish the same thing with a considerably higher equivalent delta V.

This simple scenario ignores two interesting possibilities. The first is the use of continuous thrust after lunar encounter to further retard the body. A body with incoming $V_\infty = 2.25$ km/sec injected into a hyperbola with perigee at 6 Earth radii may be captured with a continuous thrust under 5 microgee (5×10^{-5} m/sec^2) applied during the time the body is within the lunar orbit. Thus bodies with approach velocities considerably higher than the nominal 1.5 km/sec could be captured with minimal effort.

The second interesting consideration ignored by this analysis concerns multiple lunar encounters with a lowthrust interplanetary trajectory between the Earth approaches.
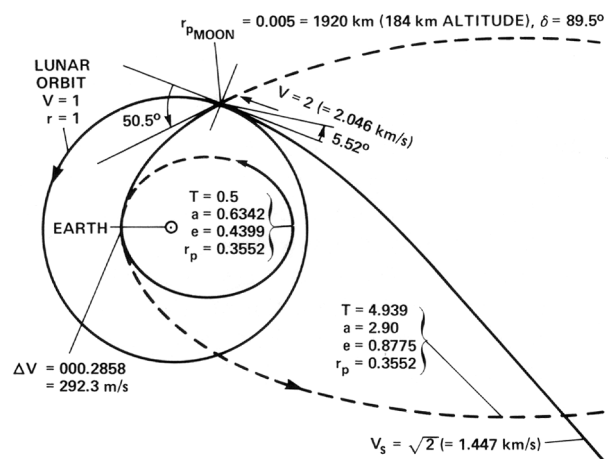
Figure 6 — *Trajectory geometry for lunar-assisted capture into Earth orbit.*

Preliminary investigation indicates this may be very promising, but more thorough analysis is not possible at this time.

CONCLUSIONS

It has been shown that direct round-trip trajectories for asteroid retrieval missions may be possible with a total delta V of the order of 7 km/sec, assuming that lunar-gravity-assisted flybys are used both inbound and outbound. This would require a significant increase in the number of known Earth-approaching asteroids such that several with more favorable orbital elements for this type of mission are found. The total delta V for the real asteroid 1943 is about 11 km/sec.

On the other hand, gravity-assisted trajectories to rendezvous with an asteroid and to return it to Earth may have total delta-V values as low as 6 km/sec. This requires fortuitous timing and geometry so that good Earth-Venus-Earth trajectories are available for both outbound and inbound flights. However, they do not require as limited a class of orbital elements for suitable targets as are needed for direct retrieval. In fact, several candidates are known, and every asteroid discovered by virtue of a close approach to Earth becomes yet another candidate. A return trajectory using low thrust for the asteroid 1977 HB was found with a delta-V requirement of only 3.04 km/sec. Although no satisfactory outbound flight arriving at this asteroid less than 1 year before the return flight was found, it is confidently expected that, as asteroids are studied and more are discovered, cases will be found that do indeed provide retrieval for a total (round-trip) delta V of 5 km/sec.

Another technique involves the use of Earth-to-Earth low-thrust trajectories. These are used to increase the V_∞ of a spacecraft at launch from 1.5 km/sec to 3-5 km/sec (or to decrease V_∞ for Earth approach from 3-5 km/sec to 1.5 km/sec).

Finally, the problem of capture into long-term stable orbits about the Earth was examined. A satisfactory procedure for entering resonant orbits was developed and data presented for entering the 2:1 resonant orbits for $V_\infty = 1.5$ km/sec at Earth approach.

It appears from these studies that a significant amount of asteroidal material can be retrieved by techniques well within the grasp of present technology. More work is needed on the discovery of asteroids, the search for good mission opportunities, and possibly the development of other useful techniques to return an asteroid which will be technically and economically feasible. In addition, precursor missions to establish asteroid composition and structure are essential.

REFERENCES

1. Brooks, David R.; and Hampshire, William F. II: Multiple-Asteroid Flyby Missions. Physical Studies of the Minor Planets. NASA SP-267, 1971, pp. 527-537.
2. Bender, D. F.; and Friedlander, A. L.: Multi-Asteroid Flyby Trajectories Using Venus-Earth Gravity Assists. AAS/AIAA Astrodynamics Specialists Conference, Nassau, Bahamas, July 28-30, 1975.
3. Bender, D. F.; and Bourke, R. D.: Asteroid Rendezvous Missions. Physical Studies of the Minor Planets. NASA SP-267, 1971, pp. 503-511.
4. Mascy, Alfred C.; and Niehoff, John: Sample Return Missions to the Asteroid Eros. Physical Studies of the Minor Planets. NASA SP-267, 1971, pp. 513-526.
5. O'Leary, Brian; Gaffey, Michael J.; Ross, David J.; and Salkeld, Robert: Retrieval of Asteroidal Materials. Space Resources and Space Settlements. NASA SP-428,1979, pp. 142-155.
6. Bschorr, O.; and Leibold, A.: Das Einfaung-und-Katapulvermogen von Planet/Mond-Systemen. Deutsche Luft-Und Raumfahrt, Rept.68-81, NASA TT F-12,330, July 1969.
7. Heppenheimer, Thomas A.: The Lunar Mass Transport Problem in Space Colonization. AAS/AIAA Astrodynamics Specialist Conference, Jackson Hole, Wyo., Sept. 7-9, 1977.

IV-2
Retrieval of Asteroidal Materials

BRIAN O'LEARY, MICHAEL J. GAFFEY, DAVID J. ROSS, and ROBERT SALKELD

Earlier scenarios for mass-driver retrieval of asteroidal materials have been tested and refined after new data were considered on mass-driver performance, favorable delta-V opportunities to Earth-approaching asteroids with gravity assists, designs for mining equipment, opportunities for processing volatiles and free metals at the asteroid, mission scenarios, and parametric studies of the most significant variables. We conclude that the asteroid-retrieval option is competitive with the retrieval of lunar materials for space manufacturing, while a carbonaceous object would provide a distinctive advantage over the Earth as a source of consumables and raw materials for biomass in space settlements during the 1990's. We recommend immediate studies on asteroid-retrieval mission opportunities, an increased search and followup program, precursor missions, trade-offs with the Moon and Earth as sources of materials, and supporting technology.

INTRODUCTION

O'Neill proposed that lunar and asteroidal materials may be economically mined and processed in space for the construction of high orbital habitats (ref. 1) and satellite solar power stations (ref. 2). The 1976 NASA-Ames Summer Study on Space Settlements (ref. 3) corroborated early estimates that these concepts could be carried out on a large scale in the 1990's with an initial investment comparable to that of the Apollo program using present technologies. In the scenario considered, an electromagnetic mass driver on the Moon would propel lunar material into free space for subsequent transfer to a space manufacturing facility (SMF) for chemical processing and fabrication into large structures. The mass driver would also serve as an orbital transfer vehicle, possibly reducing the cost of transport from low Earth orbit, where the external tanks for the Space Shuttle would be pelletized into reaction mass (ref. 4).

O'Leary (ref. 5) explored the possibility of using mass-driver tugs to move Earth-approaching asteroids at opportunities of low-velocity increment to the vicinity of the Earth. Carbon, hydrogen, nitrogen, and free metals, apparently scarce on the Moon, may be abundant on some asteroids; possibly, the retrieval of asteroidal materials may be cost-competitive with that of lunar materials in an early program of space manufacturing. A scenario was developed (ref. 6) where a 100-MW mass driver, assembled in space with about 50 Space Shuttle flights, would retrieve about 22 percent of a 200-m-diameter (1 X 10^7-metric ton) asteroid through a velocity increment ΔV of 3 km/sec in 5 years. Many such objects are believed to be within reach of Earth-based telescopes in ongoing search programs.

The current study tests the assumptions made in earlier work and refines the existing scenario. Two companion papers describe, in detail, (1) delta-V requirements for favorable round-trip missions to currently known candidates and probable future ones (ref. 7) and (2) asteroidal resources and recommendations for expanding the search program,

followup for orbital determination and chemical classification, and identification of precursor missions (ref. 8).

This paper describes scenarios for asteroid retrieval (1) for a real object (asteroid 1977 HB with gravity assists from Earth, Venus, and the Moon) and (2) for a likely hypothetical case, given an increase in the asteroid discovery rate and improved mission-analysis techniques. Several topics are discussed: values for delta V, energy requirements, role of man, design of outbound mass-driver system, assembly and attachment to asteroid, mining operations, timing and logistics of the retrieval operation, the selection of volatiles and free metals, and options for using hydrogen and oxygen processed at the asteroid for fuel. The second section places this scenario in a parametric context, which will identify the most significant variables in comparing the economics of transport, into a stable high orbit, of asteroidal, lunar, and terrestrial materials. This paper concludes with recommendations for a research and development program designed to provide technology readiness for asteroid retrieval by the mid-1980's. An appendix, by Robert Salkeld, presents a cost comparison of asteroidal vs lunar derived materials.

GROUND RULES AND ASSUMPTIONS

First, we assume that it is desirable to minimize the mass of the equipment required to retrieve the asteroid: rendezvous engine and propellants, mining apparatus, equipment for preparing reaction mass at the asteroid and for successfully returning the asteroid (or portions thereof). The mass of the retriever must be kept low because of the large Earth-to-orbit launch costs (at about $700/kg and $240/kg for an upgraded

Space Shuttle) and equipment costs (assumed to be $400/kg or three times that of modern aircraft).

The selection of an optimal exhaust velocity V_e for the asteroid-retriever mass driver depends on various parameters, which were recently revised by the Mass-Driver Study Group of this summer study. The earlier asteroid-retrieval study (ref. 6) considered $V_e \sim 2$ km/sec, which was optimized for maximum returned mass per unit power imparted to the reaction mass through a total one-way delta V of 3 km/sec, a value that appears reasonable for the most favorable known cases (ref. 7). This value suggested commonality in design with the lunar mass driver and mass drivers designed for orbital transfer between high orbits (e.g., long-term SMF orbits, lunar orbit) and geosynchronous orbit. A higher-thrust mass driver would act as a booster to spiral the asteroid retriever from low-Earth orbit to high-Earth orbit, as in the lunar scenario (ref. 4).

However, further consideration of the relationship between exhaust velocity and mass-driver mass for constant thrust and an analysis of the requirements for the outbound leg of the retrieval mission led us to conclude that a single-stage, high-thrust mass driver alone may perform the retrieval. For a nominal delta V from Earth escape of 3 km/sec, in addition to the 6.4 km/sec required to achieve escape from low-Earth orbit by low thrust, $V_e \sim 8$ km/sec appears to be a reasonable value for the mass-driver retriever. Commonality in design is again possible when the former booster becomes the retriever itself.

The use of the same mass-driver design for diverse tasks suggests minimal development costs which would be uniquely attributable to the asteroid retriever. We have assumed that a mass driver would be used for the first asteroid retrieval because of the common design property and because the mass driver has some attractive features not offered by most alternative propulsion systems: high throughput-to-mass ratio, relative ease of preparation and use of asteroidal material as reaction mass (the fuel is "free" at the asteroid), high efficiency of operations, and near-term technology required for timely development.

We have further assumed that the size of the asteroid fragment to be retrieved is about 100 m in diameter (1×10^6 metric tons). Such a fragment is at the lower end of the size range of objects accessible to telescopic search programs. It would provide about 0.5×10^6 metric tons of material in high-Earth orbit, which is comparable to a few years throughput of lunar material in the lunar resource retrieval scenario (ref. 3). This size would be appropriate for first mission(s) where "one-time" development costs would be in reasonable proportion to total mission costs while their sum would be within the scope of current NASA planning and would require moderate, temporary use of an upgraded (class II) Space Shuttle. A more quantitative investigation of this assumption is presented later. If the best initial candidate is more massive than 10^6 metric tons, it would be necessary to break off a piece for the first recovery.

We assume that the first asteroid retrieval mission will be manned. In our opinion, the assembly and mining operations are sufficiently complex, with real-time decisions governing equipment several light-minutes from Earth, that an automated mission would be a formidable task. It follows that the total mission time should be kept as low as realistically possible, with crew changes only about once a year. Such crew changes could be conveniently carried out at times of Earth gravity assist (described later). A minimum round-trip time for an asteroid mission would be about 1 year, corresponding to a one-way Hohmann transfer time of about 6 months from Earth to the asteroid on an Earth-like orbit. But most optimal transfer times are considerably longer, particularly when gravity assists are used (ref. 7). For the optimal retrieval of a 10^6-metric-ton asteroid, a throughput of about 4 kg/sec of reaction mass would be required for a 3-year return time.

VOLATILE AND FREE METAL RETRIEVAL FROM ASTEROIDS

Most ordinary and low-grade carbonaceous chondrite meteorites — and, by inference, asteroids — contain ≥ 10-percent free metals, water, and carbon. Water and carbon dominate this phase in carbonaceous objects of types I and II; metals dominate in ordinary chondrites. One class of carbonaceous objects has appreciable percentages of all three, comprising about 20 percent of the body by weight. At a modest additional cost in the mining operations of the asteroid, the free metals can be sifted out and magnetically separated and H_2O, and CO_2 can be extracted by heating the asteroidal fragments in a solar furnace to about 600° C. After the H_2O and CO_2 are extracted, the remaining material would serve as reaction mass. This operation would be continuous at the asteroid, corresponding to the nominal throughput of 4 kg/sec for a 3-year mission to return about 0.5×10^6 tons of material.

The SMF site would receive about 100,000 metric tons of free metals (mostly Fe/Ni), 50,000 metric tons of water, 20,000 metric tons of carbon compounds with the remainder for reaction mass, shielding, and processing into oxygen, ceramics, glasses, and metals.

The 1977 Summer Study projected that 3100 persons could be in high orbit by 1991 to process, in space, nonterrestrial materials into satellite power stations. If it is assumed that 3 kg/person/day is required for consumables (half of which is water in "wet" food with some additional nitrogen and oxygen to replace airlock leakage) and about 0.5 ton/person of carbon, hydrogen, and oxygen imported for biomass to establish farming operations in space, it follows that about 30,000 tons of water, carbon compounds, and nitrogen will be required for the first decade of large-scale production of satellite power stations from nonterrestrial materials. Unless trapped volatiles are found in permanently shadowed areas on the Moon, these materials must come from Earth or asteroids. Processing a 10^6-ton carbonaceous asteroid for volatiles will provide more than enough material for consumables and for establishing space farms.

A plant will be required to process the appropriate alloys and to fabricate them into useful structures, but the power requirements for this are more than an order of magnitude less than those for extracting aluminum from lunar soil.

The relative energy requirements to produce structural elements from lunar ore (aluminum oxide) and from asteroidal ores (iron-nickel metal grains) can be estimated from basic chemical data. The energy necessary to reduce iron oxide to metallic iron in a blast furnace is about 17×10^6 J/kg (metal) and the theoretical lower limit (heat of formation) is about 7.5×10^6 J/kg (metal). The energy needed to melt metallic iron (heat of fusion, about 10 cal/g; heat capacity, about 0.15 cal/g, 300-1600 K) is about 9×10^5 J/kg (metal). The ratio between the energy required to reduce an oxide and to melt the metal per unit of metal is about 8 (independent of efficiency). The heat of formation ratios to produce metal from an oxide for aluminum versus iron is between 2 (Fe_2O_3) and 3 (FeO). Thus the energy required to produce metallic aluminum from lunar oxide ore is 15 to 25 times higher than that needed to melt a metallic asteroidal ore per unit mass of metal.

The actual relative energy requirements will depend on system designs (e.g., melting by means of solar furnace vs electrolysis and associated electricity-producing efficiency), the number of melt-freeze episodes necessary to refine the iron-nickel to construction grade alloy, and the ratio of metal mass necessary to provide the same structural strength (about 2 to 3 times more favorable for aluminum). The economics should also consider trace element recovery from NiFe (Ni, Co, Ge, Pt, etc.) during the refinement process of iron.

If the asteroidal NiFe metal is used, the mass and complexity of the SMF chemical processing plant may be reduced considerably, reducing the cost of an early program of nonterrestrial material processing. It also appears that virtually all the materials required for SMF operations — consumables, plastics, graphite for radiators, solar reflectors, and possibly germanium for solar cells — would be available. If a lunar program is more feasible at first, the economics of volatile and metal extraction from asteroids may be immediately competitive. If serious problems were to develop with the structural dynamics of mass drivers, water could possibly be used at the asteroid as fuel (liquid oxygen and hydrogen produced from electrolysis) or as a working fluid to return appreciable quantities of asteroidal materials. Details of these concepts are explored later.

SCENARIO FOR ASTEROID RETRIEVAL

A representative scenario was developed for capturing a 10^6-ton asteroid (see fig. 1). A single mass driver is

used to accelerate the crew and the equipment for mining and retrieval to rendezvous with the asteroid. That mass driver is then used to return a large fragment of the asteroid to Earth orbit. The scenario chosen uses a low-thrust delta V of 6.4 km/sec to achieve Earth-escape speed, a lunar gravity assist maneuver, and a further delta V of 3 km/sec to
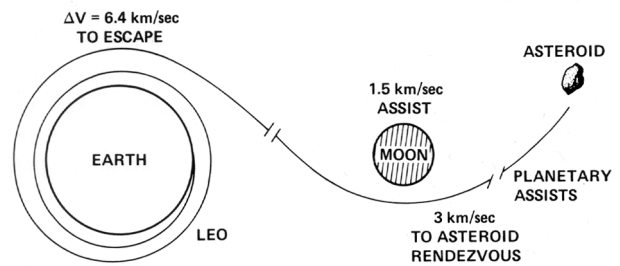
Figure 1 — *Outbound journey.*
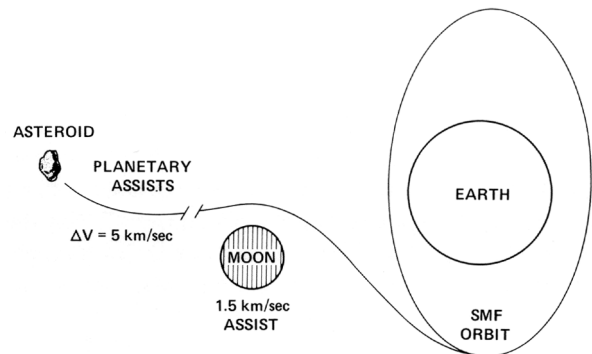
Figure 2 — *Inbound journey.*

intersect and rendezvous with the asteroid. Also, in the outbound trip, one or more gravity-assisted maneuvers are used with Earth and perhaps Venus (ref. 7).

Return delta V is taken to be 5 km/sec, including insertion into a 2:1 resonant SMF orbit (ref. 7) (see fig. 2). A mission to capture a portion of the asteroid 1977 HB was used as a basic mission (ref. 2). The results of this investigation are shown in table 1. In this case, which was not optimized but was arrived at by trial and error, the outbound delta V was intolerably large, even with gravity assist. But the return delta V was between 2 and 3 km/sec (the lower value obtainable with an extra Earth gravity assist). We concluded that, upon further analysis, opportunities will be found for missions to currently known asteroids in which either the inbound or outbound delta V is on the order of 3 km/sec, with the other leg larger. The strategy will be to find opportunities where some combination of both delta V values is minimized. The 5-km/sec return delta V was chosen because lowering the delta V of the initial leg will most likely increase the final-leg velocities. As shown in a later section (Parametric Consideration of Asteroid Capture), these values are not critical to mission economics. Since the primary effort of the mission is to expend moving mass out of the Earth's gravity well, the cost per kilogram of returned asteroidal material will increase only slightly if the delta V values are increased by 2 or 3 km/sec. Nevertheless, the best opportunities should be identified.

Two considerations strengthen the belief that considerably better missions than that shown in table 1 are possible. Missions are found by trial and error and, therefore, finding a good mission depends directly on how many cases are considered. Time severely limited the number of cases we analyzed; with more time, the study of known objects can be extended considerably. An increased discovery rate for this type of object would increase the number of good cases and should therefore be pursued.

TABLE 1 — RETRIEVAL MISSION TO 1977 HB (TOTAL MISSION TIME, 1974 DAYS)

Location	Operation	Date	Delta V required, km/s
Earth	Depart high orbit	April 28, 1984	6.32
1977 HB	Arrive	Nov. 28, 1984	2.53
1977 HB	Depart	July 1, 1985	2.04
Earth	Flyby	April 15, 1987	
Venus	Flyby	March 10, 1988	
Earth	Flyby	Aug. 29, 1988	1.04
Earth	High orbit arrival	Sept. 23, 1989	1.5 (lunar gravity assist)

Given these caveats and uncertainties, we now describe the scenario. The retrieval of asteroidal material includes the following steps: achieve a low-Earth orbit, transfer to high-Earth orbit, lunar gravity assist and departure, intermediate gravity-assisted maneuvers, rendezvous operations, including despinning, mining, and processing operations; and mass-driver coupling and deployment; and return. (Each step is described in detail in the following sections.)

Low-Earth Orbit (LEO)

Components of the asteroid-retriever mass driver, fuel for the outbound leg, and mining and processing equipment would be Shuttle-launched from Earth and the component systems should be assembled and tested in low-Earth orbit. If it is assumed that Shuttle payloads are arranged to be mass-limited rather than volumelimited, and if the Shuttle hydrogen tanks (30 metric tons) are used as mass-driver reaction mass, about 55 metric tons may be lifted to 250-km-altitude orbit per launch. When the assembly and testing phases are completed, the crew is Shuttle-lifted to the waiting vehicle. This 21-man team would live in one or more Shuttle hydrogen tanks similar in design to that envisioned for an early space habitat. Escape from near Earth space is achieved in two stages: first, with a delta V of about 6.4 km/sec, the asteroid-retrieval package is raised to high-Earth orbit by a slow spiral orbit. This stage requires 2 weeks to complete, using a mass driver (or its equivalent) with an exhaust velocity of 8 km/sec. The mass driver is optimized to place the asteroid retrieval package in suitable orbit for the minimum number of Shuttle flights, and ideally would be identical to that designed for low-to-high Earth orbit transport (ref. 4). Recent data provided by the Mass-Driver Group of this study, from conservative assumptions made about the component masses and length, indicate a total mass of 2500 tons at an acceleration of 800 gravities. The propellant throughput is 4 kg/sec. The crew and their life-support system have a mass of 291 tons; the mining facility has a mass of 560 tons. A total outbound delta V of 9.4 km/sec requires the launch of 10,000 tons to low-Earth orbit. With an assumed return delta V of 5 km/sec and an asteroid fragment of 10^6-ton mass, this enables 532,000 tons to be brought to Earth orbit. The second departure phase involves a lunar gravity assist which gives a 1.5-km/sec escape velocity.

Gravity-Assisted Maneuvers

Besides the lunar-gravity-assisted maneuver, other possible maneuvers permit a considerable saving in delta-V requirements and hence in mass lifted to low-Earth orbit. These are described in reference 7 and are summarized as follows. Of the planets, only Earth and Venus are suitable for missions to Earth-approaching asteroids because the other planets are either too small or too far away. The low-thrust EGA technique uses the Earth alone and is therefore always available. After launch from Earth, the mass driver imparts a small delta V to the system and causes it to reintersect the Earth with a higher relative velocity than that with which it departed. These times of close encounter with the Earth offer excellent opportunities for crew rotation, about every 400 days, except during the trips to and from the asteroid. This relative velocity is changed in direction by the close Earth encounter, and the final Sun-centered velocity may be altered greatly.

The second type of gravity-assisted maneuver, called VEGA, uses both Earth and Venus. The mission leaves Earth to intercept Venus. A close Venus encounter rotates the relative velocity vector and directs the retrieval package back to Earth. A second flyby of the Earth bends the relative velocity vector and the final Sun-centered velocity may be greatly increased. The mass driver may improve conditions further by thrusting during the Earth-Venus or the Venus-Earth passage. In all these ways, a considerable saving in delta V and thus in launch mass may accrue. The mission leg from the last planetary encounter will probably require additional thrust to intercept Earth and will certainly require thrust to match orbital velocities. The return trip may use similar gravity-assisted maneuvers to further reduce thrust requirements.

Asteroid Rendezvous Operation

Rendezvous with the asteroid includes the following events (fig. 3): orbital matchings, fragmenting, despinning and bagging the asteroid, establishing the mining and processing operation, and packaging material for reaction mass and for return. Orbital matching is achieved in about 1 day, with a total velocity change of about 1 to 2 km/sec.

After rendezvous, a small jeep will land on the pole and its crew will find a suitable fragment of the asteroid for return to Earth. This fragment, which will have a mass of approximately 10^6 metric tons, will be near the equator and
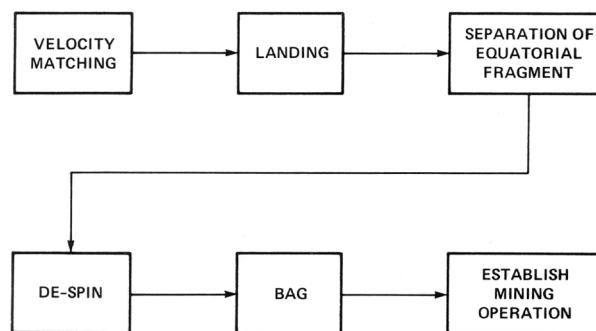
Figure 3 — *Rendezvous operations at the asteroid.*
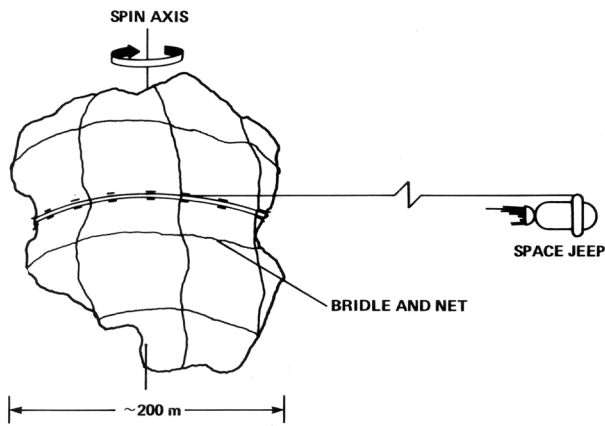
Figure 4 — *De-spinning an asteroid.*

will be separated from the asteroid by a small chemical explosion. The jeep will then land on the detached mass and proceed to despin it. Asteroids rotate at different rates, but 4 revolutions/day may be considered representative of asteroids in the 100-m-diameter size range. A jeep will land at the pole of the fragment and establish a line of small Y-shaped pylons around its equator (fig. 4). These pylons will be either driven into the asteroid (if it is firm enough) or held in place by some kind of anchor. The jeep crew will then wind the asteroid in the direction of its rotation with 5 km of very lightweight cable, using the pilons to hold the cable. One end of this cable will be firmly anchored to the asteroid and the other end to the tug. Launching the jeep with a very minimal velocity to just escape the weak field of the asteroid would result in the cable being unwound as the asteroid rotates. A very tiny thrust from the jeep would be required to keep a light tension on the cable (a few Newtons), which would have a minimal effect on the despin operation. After 2 days, the cable will be unwound and will start to rewind in the other direction. The jeep will thrust against this with 34 N for 4 days (fig. 4). For an exhaust velocity of 4 km/sec, 29 tons of propellant will be used to despin the asteroid completely. Cable and pilons will be stored for return.

After despinning, the asteroid fragment will be bagged along with the entire processing plant. The bag is a slightly pressurized covering constructed of 1-mm composite material resembling fiberglas plastic-coated to make it gas-tight. This bag, with a volume of 10^6 m^3, contains debris and gas produced by mining and processing operations and keeps the surrounding region clean. The asteroid fragment itself is surrounded by a net of 1 km^2 area composed of 0.5-cm aluminum cable spaced 1 m apart. This net will be preassembled and can be rolled out quickly by the crew. The net distributes the thrust loads over the asteroid surface and must be able to withstand the 32 tons of thrust developed by the mass driver. The total mass of the bag and net is 160 tons. The mass driver is now brought alongside the asteroid and coupled to the net. Considerable adjusting will be required to ensure that the mass driver thrusts through the center of mass of the system. Care must be taken in processing the asteroid during return so as not to misalign the thrust by shifting the center of mass.

Mining and Processing Operations

After the asteroid has been cradled, tied down, and bagged, the mining and processing operations must be established (fig. 5). The design requirements for the mining and processing equipment will depend on the character of the asteroidal material being used (ref. 8). Three possible types of material containing abundant volatile and/or free metal phases are listed in table 2.
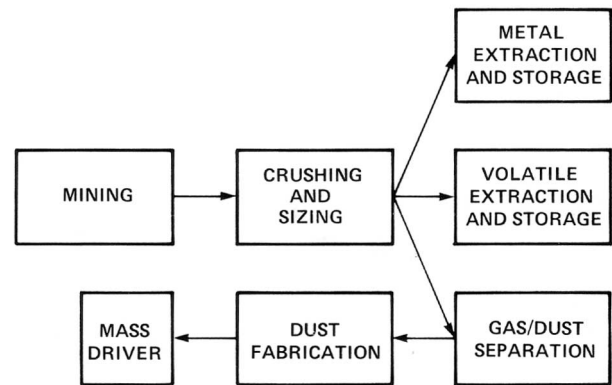
Figure 5 — *Mining operations.*

TABLE 2 — MINERALOGICAL, CHEMICAL AND PHYSICAL PROPERTIES OF THREE POSSIBLE ASTEROIDAL MATERIALS

Type	Metal-rich carbonaceous (~C2)[a]	Matrix-rich carbonaceous (~C1-C2)[b]	Type 3-4, L-H chondrite
Fe^c (metal)	10.7	~0.1	6-19
Ni (metal)	1.4	—	1-2
Co (metal)	.11	—	~0.1
C	1.4	1.9-3.0	~.3
H_2O	5.7	~12	~.15
S	1.3	~2	~1.5
FeO	15.4	22	~10
SiO_2	33.8	28	38
MgO	23.8	20	24
Al_2O_3	2.4	2.1	2.1
Na_2O	.55	~.3	.9
K_2O	.04	.04	.1
P_2O_5	.28	.23	.28
Minerals	Clay mineral matrix Mg Olivine with FeO inclusions	Clay mineral matrix Olivine	Olivene Pyroxene Metal
$\rho(g/cm^3)$ Metal grain size Strength	3.3 ~.2 mm Moderately friable	2.0-2.8 — Weak-moderately friable	3.5-3.8 ~.2 mm Moderately friable

a   Data from metal-rich C2 meteorite Renazzo.
b   Data from C2 meteorite Murchison and average Cl-C2 types.
c   Chemical analysis in weight percent.
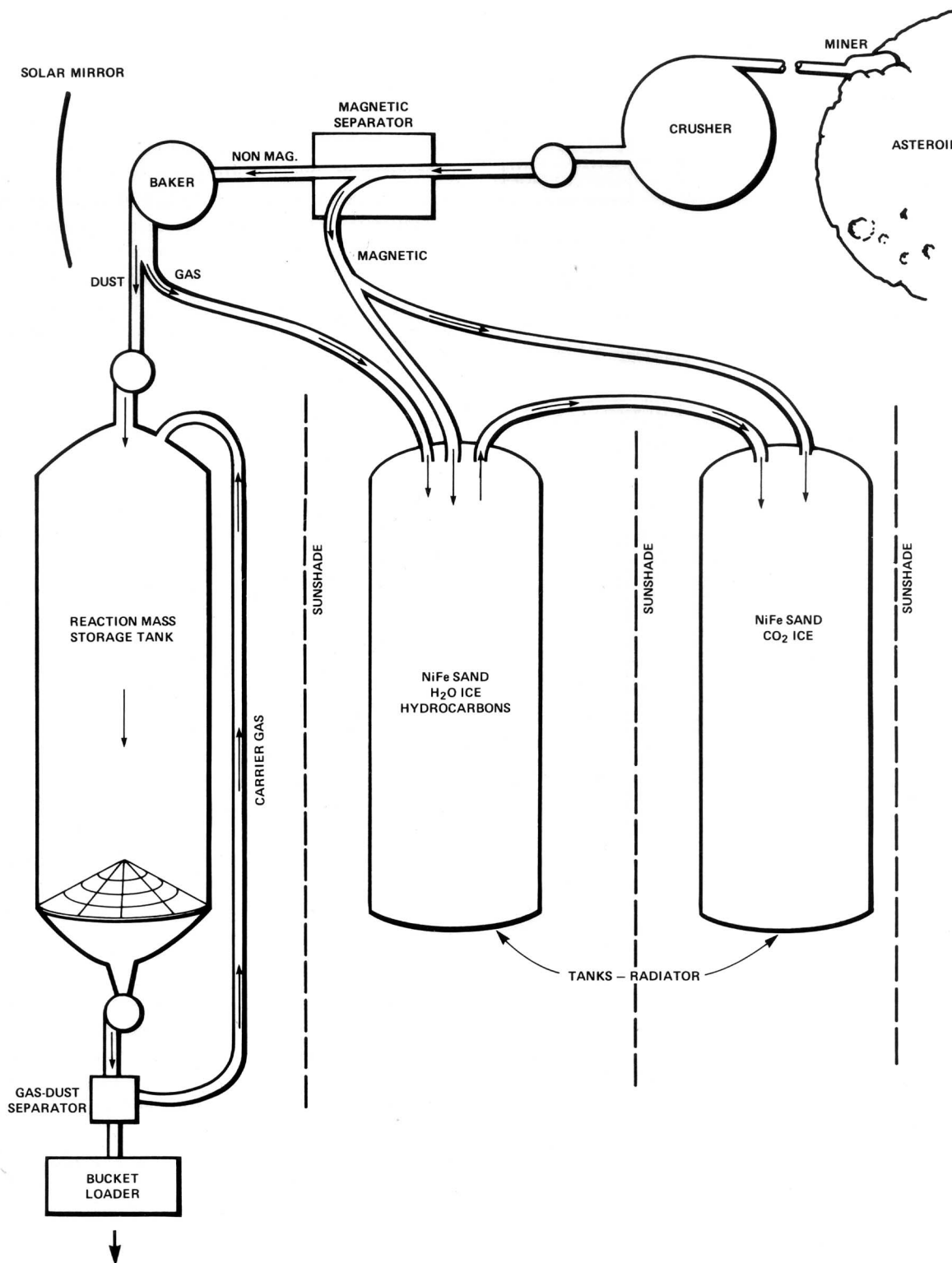
Figure 6 — *Schematic diagram of asteroid processor.*

In this scenario, a metal-rich carbonaceous material is considered to be the most desirable material to recover. We also assume that the metals (NiFe) and volatiles are sufficiently valuable to justify the extra steps necessary to extract or concentrate these materials. There are six major processing steps to follow between the raw asteroidal material and its use as reaction mass in a mass driver: mining, crushing, and sizing; metal extraction and storage; volatile extraction and storage; gas-dust separation; and dust

fabrication for mass-driver use. Figure 6 is a schematic diagram of the asteroid processor.

The physical situation at the asteroid requires special types of processing and handling. For an object in the mass range of interest, the surface gravity is about a few microgravities, which corresponds to a surface acceleration of some thousandths of a centimeter per second per second or a few tens of micrometers per second per second. Initial acceleration proposed for the mass-driver system is about 50

$\mu m/sec^2$ and increases as the body mass decreases. A body of this size in the solar system is almost certainly a collisional fragment (or a portion of one) and will be strength-limited by internal fractures. A relatively simple netting arrangement should suffice to hold it together against the relatively small accelerations contemplated. (This netting was described previously.)

Mining — The major problem in any mining scenario is to hold the cutting equipment against a surface with sufficient force to cut into the fragment. In tunneling operations, pressure can be exerted on the walls to provide stabilization, but for fractured, realtively low-strength rock, tunnels must be spaced to provide relatively thick walls (e.g., about 1 tunnel diameter), which limits the usefulness of this technique, particularly if much of the material is to be used for reaction mass.

An alternate surface technique involves a covered flail excavator that cuts a 5-m-wide, 1-m-deep trench. This excavator is held against the surface by anchor rods driven into the ground around it; the excavator pulls itself forward with these anchors. The forward progress needed to supply 4 kg/sec is about 0.03 cm/sec or about 1.3 m/hr. This device delivers appropriately sized fragments (e.g., ≤20 cm) through a pipe or conveyor system to the main processing facility.

Crushing and sizing — Because the materials being considered are relatively soft, crushing them should be fairly easy. The crushing device used has a rocking jaw arrangement for coarse crushing (≤1 cm) and a series of rollers for fine crushing (fig. 7). The crushing elements are arranged radially in a rotating cylindrical housing to provide a radial acceleration from the hub (input) to the final powder (~0.1 g at 10 rpm of a 3-m-radius device). Mean particle sizes of about 0.2 mm or slightly less are desirable for metal extraction.

Metal extraction and storage — After crushing, it is probably desirable to use gasdynamic transport to move the materials. Gas pressure can be quite low (~1 millibar) and still be effective for transport in this low-gravity environment. A low gas pressure simplifies system construction since leak rates and material strength requirements are minimized.
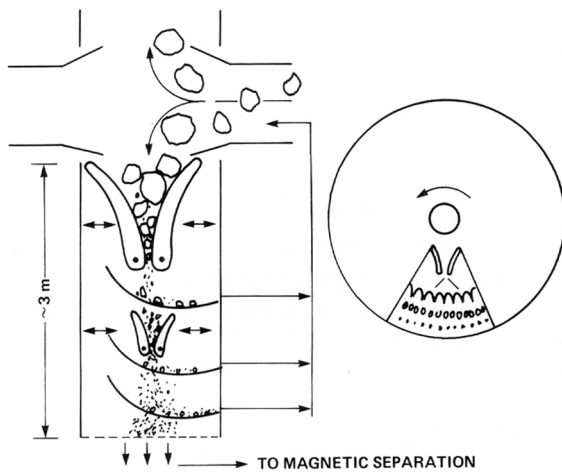
The carrier gas could be either CO_2 or H_2O, both of which are available. Leakage into a moderately contained environment (e.g., the surrounding processing facility) can be minimized by cold-trap pumping in a passive mode.
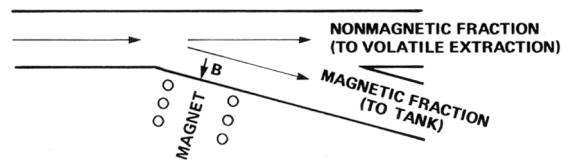
Figure 8 — *Magnetic separation.*

To extract most of the metallic phase, the gas stream and its entrained dust are passed through a magnetic field (fig. 8). An enriched fraction ≥80 percent NiFe) will contain most of the coarse-grained metal particles (~70 percent by weight). This enriched fraction (metal sand) will be diverted to a storage facility (large, relatively weak tank or bag). It is doubtful that any subsequent processing of this metal-rich phase would be economically feasible enroute.

Volatile extraction and storage — To recover the volatile phases (H_2O, CO_2, hydrocarbons), the material must be heated (fig. 9). The temperatures required depend on the desired recovery rate. Water chemically bound into the clay minerals of C1-C2 matrix material begins to come off near 100° C and continues to come off until about 400° C. Carbon dioxide is produced by the disassociation of hydrocarbon compounds and by reaction of elemental carbon with oxide phases (e.g., $C + 2Fe_2O_3 \rightarrow CO_2 + 4FeO$). Hydrocarbons volatilize or break down in the range 100° - 700° C, releasing a variety of compounds, including methane and petroleumlike vapors.

70 m   7 m

DUST

GAS (TO TANKS)

T ~ 700° C
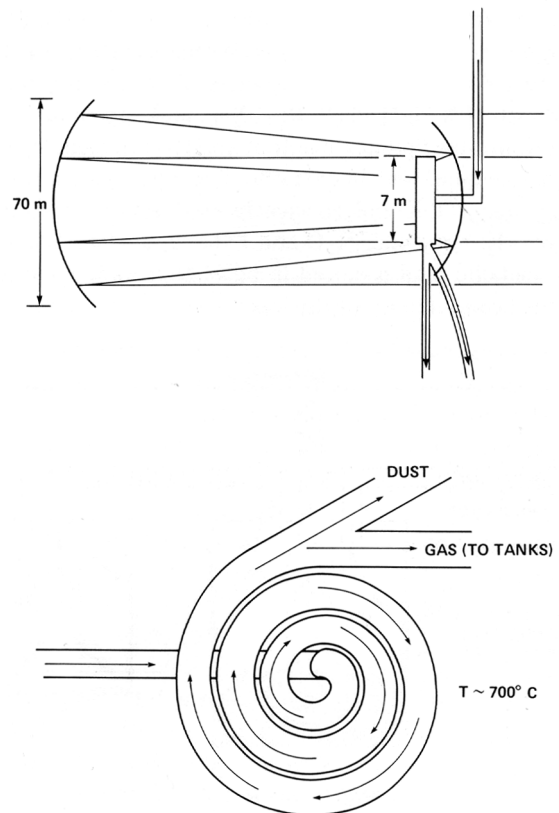
Figure 9 — *High temperature volatile extraction.*

TO MAGNETIC SEPARATION

~3 m

Figure 7 — *Crusher.*

The energy requirements depend on the recovery rate, which is dominated by the heat of vaporization of water. Considering the various heat capacities of the phases, about 200 cal/g are required to raise raw C_2 carbonaceous matrix material to about 700° C and to vaporize the volatile components. A 4-kg/sec throughput would require a solar collector about 60 m on a side focused on a collector area about 6 m across. Dust entrained in a carrier gas ($\sim$2-10 kg/m^3) is introduced into a heat-exchange system at the mirror focus for a period of 30-60 sec. The dust is separated from the gas by a cyclonic separation (dust settles rapidly to the outer wall of a curved conduit). Counterflow of gas and dust is used to heat incoming stream and cool outgoing stream. The gas stream is directed to a shaded heat exchanger and into a storage tank that also serves as a heat exchanger. To condense all products to $\sim$200 K, a radiator area must be about 100 m on a side. The heat released by condensing water may limit the total volatile recovery program. A double condenser system may solve some of this difficulty; the first tank operates near 250 K and precipitates much of the H_2O (depending on vapor pressure) and hydrocarbons. A second tank operating near 150 K and at slightly elevated pressure condenses the remaining H_2O and CO_2 vapors (see fig. 10). The metallic sand is stored in both tanks to increase the thermal conductivity of the ices.
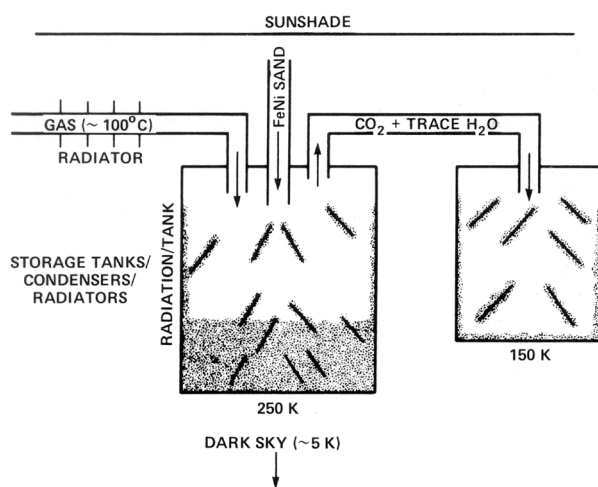
Figure 10 — *Radiatively cooled volatile storage tanks.*

The recovery of volatiles is likely to be limited by the ability to radiate away the heat of condensation of the volatile phases for reasonable tank/radiator mass. In the shade, radiating to a dark sky, an optimum value can be evaluated.

Dust fabrication for the mass driver — The dust fraction of the cooled product is delivered to a storage tank, then to either the mass-driver loading point or to a central fabricating facility. The dust is separated from the entraining gas and is stamped or poured into appropriate molds. The character of these mold requirements is presently unspecified. However, laboratory experience has shown that relatively low pressures are required to form a reasonably solid pellet.

Mass Requirements for Mining, Processing, and Storage

The cost of feasibility of mining and processing an asteroid for reaction mass, volatiles, and metals will depend greatly on the mass and associated costs of transporting equipment to the asteroid to accomplish these tasks. The necessary equipment includes that for mining and processing (crushers, metal and volatile extractors), storage containers, radiators, and support equipment (piping, blowers, "nets," and "bags"). An initial estimate of the mass of the necessary equipment can be made by fixing a preliminary design for each component and by then making a reasonable estimate as to the mass of that component. Certain elements of the proposed system are sized to a particular mass-flow rate. Each component is discussed briefly below and its associated mass is estimated.

Reaction-mass storage and "pumping" facilities include the system needed to store and feed reaction mass for the outbound leg (analogous to a fuel tank). For a throughput of 4 kg/sec, this tank must have a storage capacity of about 20,000 m^3 and is envisioned as a gas-tight ($\sim$1 mbar pressure) bag, 20 m in diameter and 65 m long, opening slightly "downward" with a gas-agitated grating at the bottom. The bag material is assumed to be a composite (canvas and plastic or appropriate substitute of mass 3.75 kg/m^2, e.g., 5-mm-thick composite or 2.5-mm-thick aluminum) with a mass of 25 tons. Gasdynamic transport using blowers (five blowers at 2 tons each with motor), composite pipes (about 1 km, 7 kg/m^2, and with a 2-m diameter weighing about 22 tons), and a gas-dust separator and bucket loader (about 4 tons and 10 tons, respectively). Such a structure would have a mass of about 71 tons, and if we apply a safety factor, the estimate is 120 tons.

"Big bag" is a slightly pressured gas-tight covering for an entire work area (1 mm of composite), which encloses a volume of 10^6 m^3 and has a mass of about 60 tons. The asteroid is enclosed and suspended in a net (1 km^2 of 0.5-cm aluminum cable at 1-m spacing weighing about 100 tons).

The mass of the processing equipment corresponds with the throughput of material. The 50-kg/sec mass flow, considered the maximum case, is discussed here. (For other mass-flow rates, estimates are provided below.) The equipment includes: miners (three at 50 tons), crushers (two at 75 tons), a magnetic separator (10 tons), blowers (five at 2 ions), volatile extraction baker and mirror (200 tons), and volatile storage and radiators (two at 350 tons). The total mass requirements depend on throughput as given below: 0 kg/sec, 300 tons; 4 kg/sec, 560 tons; 10 kg/sec, 650 tons; and 50 kg/sec, 1500 tons.

Alternatives to the Mass Driver

Of any presently known system, the mass-driver concept allows an asteroid mission to return to Earth orbit with the largest amount of material. But other devices are available that could also return large quantities of material. For any asteroid recovery mission, it may be preferable to process the material where it is obtained and to bring only the most

valuable portion back to Earth. The disadvantage of a longer waiting time at the asteroid may be more than compensated for if processing the asteroid in situ allows either a faster manned return or the use of a propulsion system that can be fully automated. We have indicated that establishing machinery to process volatiles and free metals at the asteroid does not impose severe economic penalties.

Two schemes suggest themselves for the return flight: a rocket that uses either water or volatized rock as a working fluid and the solar sail. Solar power could convert water from a carbonaceous asteroid into liquid hydrogen and liquid oxygen by electrolysis. LH_2 and LOX would then be used as fuel and oxidizer in a low-thrust rocket engine that has an extended operating time. Although this is a roundabout way to extract propulsion energy from sunlight, the very high efficiency of the electrolysis makes it feasible. The conversion process would be continuous throughout the return flight, a factor that might enable the return mission to be entirely automated. To avoid the use of large cryogenic storage tanks, the rocket motor would, ideally, also operate continuously on the return flight. This introduces the complication of a long-thrusting rocket motor that uses LH_2 and LOX, but the mass of the rocket motor is negligible compared to either conversion system or payload so that several could be used sequentially.

An in-house General Dynamics study (E. Bock, Convair Division, personal communication, 1977) provided the basic figures for the electrolysis and refrigeration plant. It was assumed that, excluding this plant, the mass of the supporting structures and the rocket motor and its subsidiary systems would not together exceed 300 tons. This latter figure appears reasonable since, if the payload is stored in the shadow of the solar collector, it will be solid condensate and should not require an elaborate bracing system to transfer the modest thrust to it. The exhaust velocity, taking into account various losses, is assumed to be 4400 m/sec and all missions have a 1-year return time. The exhaust velocity is compatible with low delta-V mission requirements. This type of rocket is well configured for a water-retrieval mission. Changing the mission time directly alters the thrust and collector area requirements, but has only a secondary effect on the mass of the system itself. Processing rates are assumed constant for both outbound and return legs and therefore the thrust, but the rocket operates only during a portion of the outbound leg. Since a conventional rocket may be started or stopped easily, this requirement for noncontinuous thrust on the outbound leg presents no serious complication.

Collector area is based on an assumed 10-percent solar collector efficiency and a 95-percent electrolysis efficiency. Both are reasonable, and the possibility of using germanium solar cells with a sunlight concentrator instead of silicon may make the first figure conservative. Collector areas and power requirements are moderate and thrust requirements may be fulfilled with very small engines. For equivalent delta-V values up to 8 km/sec, the mission returns more mass from the asteroid than it used to reach the asteroid. This is necessary if the returned material is primarily water

but is desirable in any case. All scenarios assume a return payload of 10^4 tons of water. For low equivalent delta V values, the mass of water in high Earth orbit may be multiplied many times by this device. The same scenario as presented alone is used here — an outbound delta V of 3 km/sec from high-Earth orbit and a return delta V of 5 km/sec from the asteroid. Power supply and electrolysis plant scales inversely with mission return time. For a 2-year return flight, the solar rocket fully fueled in high-Earth orbit has a mass of 2084 tons. The rocket has a mass of 1054 tons, 463 tons of which are the power supply and electrolysis plant and 291 tons are the crew and their life-support system. The remaining mass is a processing plant for extracting water and other derived mass from the asteroid. For continuous operation, the power requirement is a modest 19 MW. For the return trip in this nonmass-driver scenario, an initial mass of 33,000 tons results in 10,000 tons brought to high Earth orbit, a tenfold increase in the mass of fuel used for the outbound journey.

A second alternative to the mass driver, one that further reduces the mass brought to Earth by a factor of 10 but which could more easily be automated, is the solar sail. This device consists of a very large mirror of thin metal foil or a microlayer of metal or plastic; it relies on solar radiation pressure — caused by momentum transfer at reflection — for propulsion. Although the maximum force available at Earth orbit is only 9.3 N/km², the need for propellant has been eliminated.

The recent development of new sail material with lightness ratios (ratio of solar radiation pressure to solar gravitational force) of 5 or more has returned the solar sail to consideration for low to moderate delta-V lowthrust missions. The lightness ratio is constant regardless of distance from the Sun.

It is assumed that the structural mass excluding the sail is 10 percent of the returned payload. If a 1000-metric-ton (10^6 kg) payload must be returned and if it is assumed that 38 percent of perpendicular thrust can be used, lightness ratios of 5 and 1 both yield satisfactory results. For most missions, the sail area depends very little on sail lightness ratio and therefore the sail area can be varied inversely with mission time.

For the specific scenario used previously, a 2-year return time requires a 22.7-km² sail area and a sail mass of 7.2 tons for a sail lightness ratio of 5, and a 23.4-km² sail area and a sail mass of 37 tons for a sail lightness ratio of 1. In both cases, 1000 tons of material may be brought to Earth orbit. If these devices are automated, a fleet of these may be launched from a suitable asteroid and later retrieved near Earth. While the mass driver promises to be very useful in returning large quantities of asteroid material to Earth orbit, it is not crucial to such a mission. Either alternative presented here appears feasible and there are surely other possibilities. The solar rocket hybrid is within reach of current technology, while the solar sail is not far beyond it.
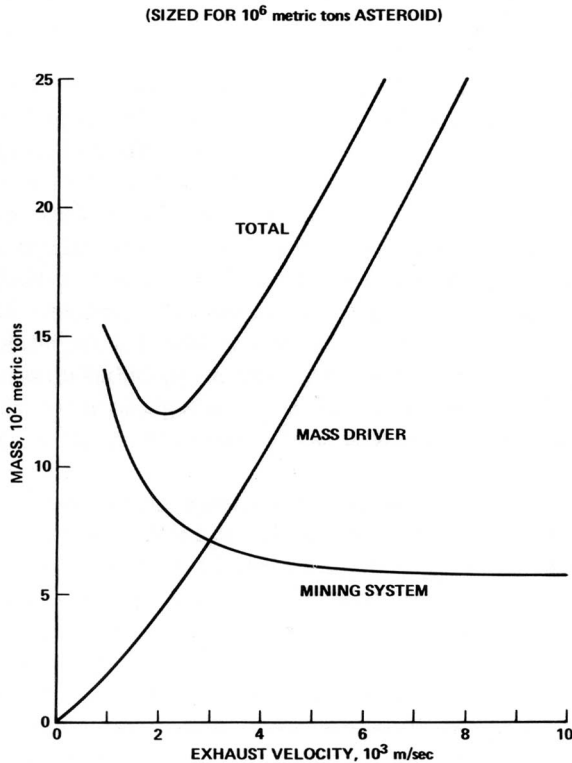
Figure 11 — *Effects of exhaust velocity on asteroid mining vehicle mass.*
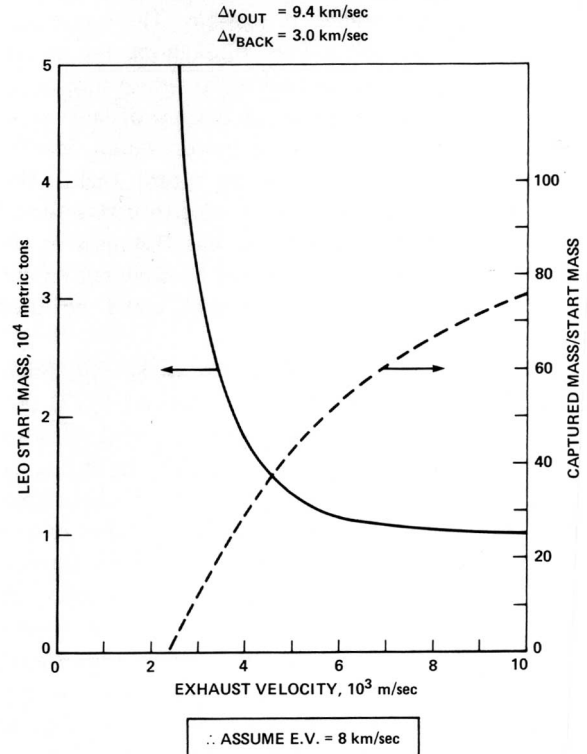
Figure 12 — *Effects of exhaust velocity on start and capture mass.*

PARAMETRIC CONSIDERATIONS OF ASTEROID CAPTURE

The estimated masses of an asteroid mining vehicle sized to capture a 10^6-ton asteroid are shown in figure 11 as a function of mass-driver exhaust velocity. As exhaust velocity increases, the mass-driver mass increases sharply because of increasing power requirements, while the mass of the mining system including personnel accommodations decreases more slowly because the reaction mass throughput decreases.

It is postulated that the asteroid can be captured by a single-stage mining vehicle starting from LEO, which attaches to the asteroid and returns with it to far Earth orbit. The required start mass in LEO is shown in figure 12 as a function of exhaust velocity for a typical mission requiring ideal velocity gain on the outbound trip of 9.4 km/sec (6.4 km/sec for escape and 3.0 km/sec for transit and rendezvous maneuvers) and 3.0 km/sec on the return trip. Since, in the range of feasible exhaust velocities, LEO start mass always decreases with increasing exhaust velocity, a value of 8.0 km/sec was selected and is used henceforth. For this value, the captured mass is 0.535×10^6 tons.

The sensitivity of LEO start mass and capture — the start mass ratio — to variations in outbound and return velocity requirements is shown in figure 13. Note that the post-escape outbound velocity requirement doubles, but there is no more than about a 45-percent increase in LEO start mass and a corresponding decrease in capture mass. Also, a 67-percent increase in return velocity requirement produces only a 21-percent reduction of capture to start mass ratio. Therefore, it can be concluded that a comfortable
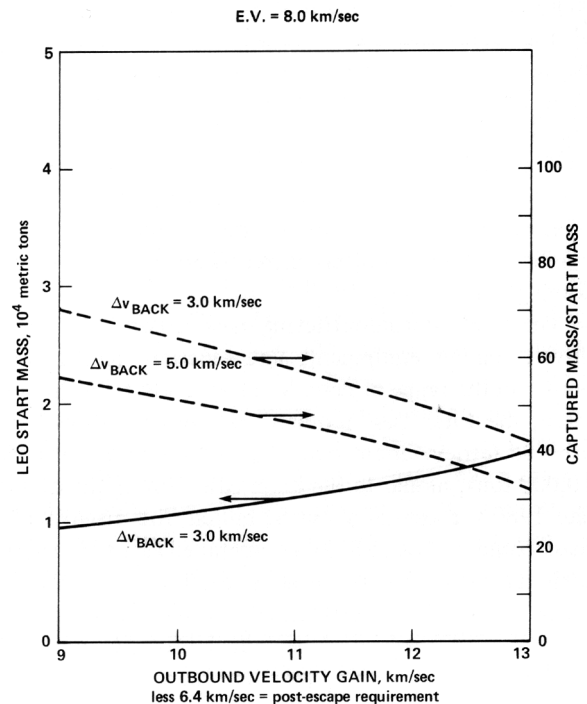
Figure 13 — *Effects of mission velocity on start and capture mass.*

range of potential asteroid orbits can be accommodated without severe losses.

Figure 14(a) is a schematic of the asteroid capture mission; it also includes a parametric cost equation expressing total program costs per kilogram of asteroid captured. Also shown for comparison is a similar expression for the corresponding costs of terrestrial material. In the terrestrial case, it is postulated that the material is procured on Earth, transported to LEO, and then carried to geosynchronous

$$\text{MASS LIFTED TO LEO} = \frac{\text{HARDWARE}}{m_M + m_D} + \frac{\text{REACTION MASS}}{(m_M + m_D)(r_I - 1)}$$

$$\text{PROGRAM COST/kg CAPTURED} = \left[\frac{\text{MINING SYSTEM}}{m_M (Cd_M + Cp_M + C_t)} + \frac{\text{MASS DRIVER}}{m_D (Cd_D + Cp_D + C_T)} \right.$$

$$\left. + \frac{\text{REACTION MASS}}{(m_M + m_D)(r_I - 1) \, Crm} \right] \frac{r_{II}}{mA}$$

TERRESTRIAL MAT'L (REF.)

$$\text{PROGRAM COST/kg CAPTURED} = \left[\frac{\text{MASS DRIVER}}{m_D (Cd_D + Cp_D + C_t)} + \frac{\text{REACTION MASS}}{\frac{m_A}{r_{II}} (r_{GSO} - 1) \, Crm} \right.$$

$$\left. + \frac{\text{TERR. MAT'L.}}{\frac{m_A}{r_{II}} Cp_E} \right] \frac{r_{II}}{m_A}$$
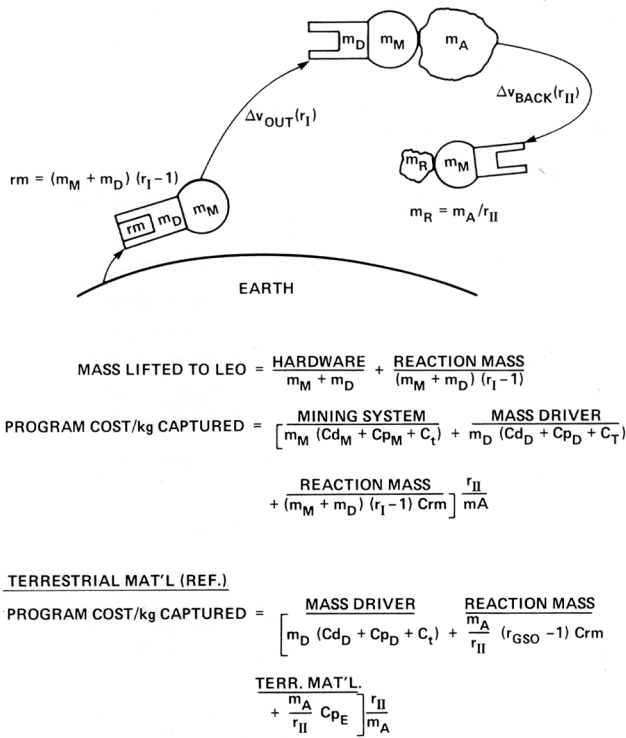
PARAMETERS

NOMENCLATURE		ASTEROID	TERRESTRIAL
Cd_D	RDT&E COST/kg (DRIVER)	2×10^3	2×10^3
Cd_M	RDT&E COST/kg (MINER)	10^4	–
Cp_E	PROCUREMENT COST/kg (TERR. MAT'L.)	–	1
Cp_D	PROCUREMENT COST/kg (DRIVER)	4×10^2	4×10^2
Cp_M	PROCUREMENT COST/kg (MINER)	6×10^2	–
C_{rm}	REACTION MASS COST/kg	(PARAMETRIC)	
C_t	EARTH → LEO TRANSP. COST/kg	(PARAMETRIC)	
m_A	MASS (ASTEROID)	10^9	–
m_D	MASS (DRIVER)	2.5×10^6	2.5×10^6
m_M	MASS (MINER)	5.8×10^5	–
Δv_{OUT}	VELOCITY (LEO → ASTEROID)	(PARAMETRIC)	–
Δv_{BACK}	VELOCITY (ASTEROID → GSO)	(PARAMETRIC)	–
Δv_{GSO}	VELOCITY (GSO − r/t)	–	4.93 (X2)

NOTE: COSTS IN $; MASSES IN kg; VELOCITIES IN km/sec

Figure 14 — *Asteroid retrieval: (a) Parametric schematic, (b) Parameter notation.*

orbit by the same mass driver as used in the asteroid case, which subsequently returns itself to LEO to pick up another cargo. In the terrestrial case, costs are amortized over a cumulative delivered mass equal to the asteroid capture mass, processed to the same degree. (Notation for the equations in fig. 14(a) and numerical values assumed are summarized in fig. 14(b).)

The cost expressions in figure 14(a) are plotted in figure 15 using the values assumed in figure 14(b). Several observations were made:

1. For capture of a 10^6-ton asteroid, estimated total program costs are from $12-14 billion or about $24/kg of captured mass. If RDT&E are excluded, the captured mass cost reduces to about $4/kg. These values assume up-rated Shuttle as the Earth-to-LEO transporter, with transportation costs of $240/kg.

2. These results are only moderately sensitive to Earth-to-LEO transportation cost and reaction mass cost because of the relatively high RDT&E and hardware procurement costs.

3. Delivery to geosynchronous orbit (GSO) of a total mass of terrestrial materials equal to the asteroid capture mass would involve, on the same basis of comparison, a total program cost of about $663 billion and a delivered cost/kilogram of about $355/kg, including RDT&E costs ($343/kg, excluding RDT&E costs).

4. If the asteroid mass were increased, RDT&E and procurement costs would increase somewhat, but capture mass would increase proportionately with asteroid mass, resulting in significant reductions in cost/kg captured. Thus for a 10^6-ton asteroid, cost/kg captured might be reduced to about 50¢/kg.

5. While support operations costs are not considered here, it seems likely that their magnitudes relative to the costs considered would be similar for both cases, and not dominant.

6. This preliminary parametric assessment confirms suggestions that asteroids may be promising sources of materials for support of space activities on a growing scale in the future, and that this possibility should receive increased attention.
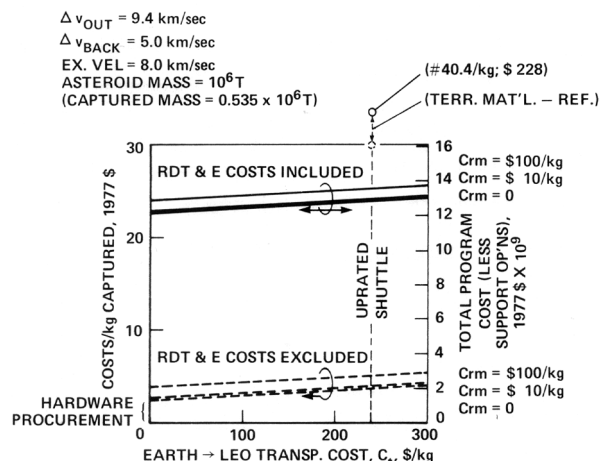
Figure 15 — *Cost of captured asteroid mass.*

CONCLUSIONS AND RECOMMENDATIONS

The present study has determined that, through the techniques of multiple gravity assists by the Earth, Moon, and Venus, the total one-way delta V from Earth escape (or capture) to rendezvous (depart from) existing asteroids, in favorable cases, is from 2 to 4 km/sec. The mission analysis described here indicates that a singlestage, low-Earth orbit to asteroid mass driver with an exhaust velocity of about 8 km/sec may be the most cost-effective alternative. Minimizing delta V in the outbound leg of the mission was found to be more important than minimizing inbound delta V, in terms of the amount of Earth-launched mass required to perform the retrieval mission. A large delta V for the inbound leg (e.g., 5-8 km/sec) increases the mass of the mining operation to prepare reaction mass, thereby reducing the amount of asteroidal material retrievable, but has no significant bearing on the total mass required to start the mission in low-Earth orbit, which appears to be the major cost driver. But a modest increase in the delta V of the outbound leg to values up to 6 km/sec from escape would not impose severe penalties. Therefore, there are mission opportunities to existing targets that can be immediately investigated. Further refinements of mission-analysis techniques for known objects will permit a more precise determination of known opportunities. In addition, opportunities will arise as the number of known objects increases appreciably over the coming years.

The total asteroid-retrieving mass consists of the mass driver, mining equipment, and reaction mass for the boost. In the range of delta V values likely to be encountered, the total mass required for launch to low-Earth orbit to retrieve about half of a 10^6-ton asteroid is near 10,000 tons, similar to the lunar case. During the mid-tolate 1980's, a cost of about $2 billion, this magnitude of mass could be launched by an upgraded (class II) Shuttle with the external tanks used as reaction mass. Development costs (about $10 billion) would dominate and would be absorbed in subsequent, larger-scale asteroidal retrievals. Alternatively, reaction mass could become available in low-Earth orbit in the form of lunar materials obtained in an early, modest program of lunar mining (ref. 4).

Perhaps the most unique aspect of retrieving asteroidal materials is the availability of large quantities of volatiles (water and carbon compounds) and free metals. These materials may not be available in large quantities on the Moon. Since about 30,000 tons of consumables are required for space settlements that support the construction of satellite power stations, most of these consumables preferably could come from the asteroids rather than from Earth. Moreover, free metals separated at the asteroid and alloyed at the space-manufacturing facility (SMF) into useful structures may eliminate many of the complex chemical processing steps required in the lunar case.

Much of the 500,000 tons of asteroidal material that would arrive at the SMF could be water and carbon if a type I or II carbonaceous object at a low to moderate delta V could be discovered. It is possible that the Earthapproaching asteroid Betulia is carbonaceous, and statistical considerations suggest that such a discovery, in an expanded search and followup program, is probable at some time over the next few years (ref. 8). Such an object would obviously be a prime target for a precursor mission.

The retrieval of asteroidal materials for space manufacturing appears to be cost-competitive and contemporary with the retrieval of lunar materials, and considerably less expensive than transporting consumables from the Earth if a type I or II carbonaceous object with reasonably favorable delta-V characteristics could be found. Therefore, the asteroid option for space manufacturing should be kept open. We recommend that the following studies and programs be carried out immediately to better assess the details of this option:

1. Continued studies of retrieval mission opportunities: Late in this study, we recognized that gravity assists in a low-thrust mission significantly reduce the mass requirements and that the delta V in the outbound leg should be minimized; also the economics of asteroid retrieval are not severely affected for moderate delta V values (one way, about 6 km/sec). From an analysis of the asteroid 1977 HB, the inbound delta V was found in one case to be from 2-3 km/sec. Many more cases — and a scheme for selecting the best ones — must be studied. Several known candidate asteroids can be studied over the next few years, and new ones as they are discovered.

2. Increased asteroid search and followup program: The current inventory of 39 Earth-approaching asteroids whose orbits are known can be increased appreciably with a modest investment in dedicated Earth-based telescopes and perhaps orbital telescopes. The followup work of orbital determination and chemical analysis is also important. Such an inventory would identify carbonaceous objects with low-to-moderate delta-V opportunities.

3. Precursor missions: Because of the potential importance of obtaining volatiles — and possibly free metals — from asteroids, clearly, a precursor mission to the prime carbonaceous candidate(s) is paramount. Such a mission is also important to assess mineralogical structure for designing the mining and processing apparatus. We recommend a new start in the NASA budget aimed toward single- or multiple-asteroid rendezvous and landing missions that would answer these questions for one or more objects between 1982 and 1985.

4. Continuing studies of the potentials of asteroidal retrieval: These studies would continue to assess the trade-offs between the retrieval of asteroidal, lunar, and Earth materials for space manufacturing in the light of new information as it comes in.

5. Technology support: Design concepts of asteroid-retriever mass drivers and mining and processing equipment must be further developed; technology development milestones must be established in parallel with the lunar option.

APPENDIX

PRELIMINARY COMPARISON OF ESTIMATED COSTS FOR ASTEROIDAL AND LUNAR MATERIALS

Robert Salkeld

To estimate a common-based comparison of asteroidal and lunar materials costs, both are here placed on the same program basis as assumed for the lunar case (ref. 9). That is, Earth launches are assumed to begin in 1985 using the first generation space shuttle (capacity — 60 flights/yr), phasing in 1987 to a shuttle-derivative heavy-lift vehicle (SD/HLV) for unmanned cargo (capacity — 80 flights/yr), and finally phasing in 1991 to a second generation passenger-cargo single-stage-to-orbit (SSTO) shuttle. Program duration is 10 years (1985-1994), during which about 1 million tons of asteroid material (from the capture of two 1-million-ton asteroids) are returned to the space manufacturing facility (SMF), compared with about 2.4 million tons of lunar materials.

Capture of two asteroids in this time period is based on the estimate of a 5-year out-and-back mission time, and is consistent with the maximum-paced program assumed for the lunar case. Thus, the first generation shuttle launches the asteroid miner and mass driver in sections during 1985-86, contributing in the process all of its external tanks for mass-driver reaction mass. The SD/HVL then phases in to launch a second miner and mass driver, and all the remaining reaction mass for two asteroid expeditions as well as chemical orbital transfer vehicles (OTV) and their propellants for establishing the SMF, during 1987-89. The first expedition leaves lowEarth orbit (LEO) early in 1987 and returns in 1992. When it has successfully reached its target and is homeward bound 1989, the second leaves to

return in 1994. The SD/HVL, SSTO and OTV establish the SMF in 1989-92 so that it is ready to process the first returning asteroid. The chemical OTV is used for SMF rather than a smaller mass driver, to avoid a second mass driver development program, and because the OTV is required in any case for SMF personnel transfer. Use of a mass driver for deploying SMF would reduce total program cost only slightly.

The results of preliminary costing of the asteroid and lunar programs are summarized in table 3. A possible requirement for an LEO station has been included as one consideration, to maintain as comparable basis as possible with the lunar case. Several observations may be made:

1. Costs of asteroidal materials are higher in table 3 than in figure 15 because of inclusion of the SMF and higher cost launch vehicles in the program, to be more comparable with the lunar case.

2. Costs of asteroidal materials are not sensitive to the requirement for an LEO station, since its development, deployment and resupply costs are small in the total picture.

3. The total program cost for the asteroid option is only about half that of the lunar case including nonrecurring research, development, test and engineering (RDT&E) costs; it is only about one-third that of the lunar case if RDT&E costs are excluded.

4. Cost per delivered kg of material is 10-20 percent higher for asteroid materials if RDT&E are included, but 25-30 percent lower than lunar materials on a recurring cost basis. Reasons for this are the relatively high RDT&E costs, but the lower amount of mass-driver throughput for the same delivered mass, for the asteroid than the

TABLE 3 — SUMMARY OF ASTEROIDAL AND LUNAR MATERIALS COSTS (10-YEAR PROGRAM-1985-1994)

Costs 1975 $	LEO station req'd?	Asteroidal, 1.1×10^6 tons delivered to SMF		Lunar, 2.4×10^6 tons to SMF
		No	Yes	Yes
Total program, $ billions	RDT & E included	27.7	31.2	57.0
	RDT & E excluded	11.9	12.6	37.0
Per kg delivered, $/kg	RDT & E included	25.2	28.4	23.8
	RDT & E excluded	10.8	11.5	15.4

lunar case. In addition, the asteroid operation is not burdened with the establishment and operation of anything akin to the mass-catcher or lunar orbit facilities and logistics.

5. These results suggest that for comparable or better economics in terms of cost per kilogram delivered, the asteroid option is significantly more attractive than the lunar option in terms of front-end "price of admission." The relative attractiveness of the asteroid option would of course be further strengthened if asteroidal material compositions are found more favorable than those of lunar materials.

REFERENCES

1. O'Neill, Gerard K.: The Colonization of Space. Physics Today, vol. 27, no. 9, Sept. 1974, pp. 32-40.
2. O'Neill, Gerard K.: Space Colonies and Energy Supply to the Earth. Science, vol. 190, no. 4218, Dec. 5, 1975, pp. 943-947.
3. O'Neill, G. K.: Engineering a Space Manufacturing Facility. Astronautics and Aeronautics, Oct. 1976, pp. 20-28, 36 (Summary); Space-Based Manufacturing from Nonterrestrial Materials, vol. 57, Progress in Astronautics and Aeronautics, AIAA, New York, 1977.
4. O'Neill, Gerard K.: The Low (Profile) Road to Space Manufacturing. Astronautics and Aeronautics, 1977, vol. 16, no. 3, March 1978, pp. 24-32.
5. O'Leary, B.: Mining the Apollo and Amor Asteroids. Science, vol. 197, no. 4301, July 22, 1977, pp. 363-366.
6. O'Leary, B.: Mass Driver Retrievals of Earth-Approaching Asteroids. AIAA Paper 77-528, 1977.
7. Bender, David F.; Dunbar, R. Scott; and Ross, David J.: Round-Trip Missions to Low-Delta-V Asteroids and Implications for Material Retrieval. Space Resources and Space Settlements, NASA SP-428, 1979, pp. 133-141.
8. Gaffey, Michael J.; Helin, Eleanor F.; and O'Leary, Brian: An Assessment of Near-Earth Asteroid Resources. Space Resources and Space Settlements, NASA SP-428, 1979, pp. 155-166.
9. Vayk, J. P.; Engel, J. H.; and Shettler, J. A.: Habitat and Logistic Support Requirements for the Initiation of a Space Manufacturing Enterprise. Space Resources and Space Settlements, NASA SP-428, 1979, pp. 57-74.

IV-3
An Assessment of Near-Earth Asteroid Resources

MICHAEL J. GAFFEY, ELEANOR F. HELIN, and BRIAN O'LEARY

The very large number of small asteroids in near-Earth space provide many opportunities to transfer material to the Earth-Moon system at low cost. On the basis of remote-sensing evidence and meteorite studies, a substantial fraction of these objects should contain abundant volatile (water, carbon, carbon compounds) and/or free metal (nickel-iron) materials. Although there are only about 40 known Earth-approaching asteroids, this number could be increased by at least an order of magnitude in a few years by a dedicated search program with a large telescope (48-in. Schmidt). A discovery rate of 20 objects/yr could be expected from a facility costing about $3 million to establish.

The material these objects contain should be determined, if possible, during the discovery opposition, because of their long synodic periods. Relatively high-resolution, broad-wavelength coverage (0.3-2.0 μm) reflectance spectra could be made for many of these objects with a large ($\sim$ 100 in.) telescope and instruments under development. Such spectra are necessary for detailed mineralogic, characterizations of these asteroids. Low-resolution survey spectra with similar wavelength coverage (UBVRIJHK filters) would provide useful characterizations of fainter objects.

A spacecraft mission should be planned to one or more of these asteroids. Support for programs to locate and characterize the near-Earth asteroids is essential to any program of large-scale space operations since asteroidal bodies appear to be the least expensive source of certain needed raw materials.

INTRODUCTION

In addition to the four terrestrial planets and the Moon, a very large number of minor objects, ranging in size from single dust motes to bodies more than 10 km in diameter, are present in the inner solar system. A small fraction of these asteroids follow orbits that intersect the Earth's orbit, and when collisions occur, meteors, meteorites, and impact craters result (depending on the size of the object).

These asteroids may offer the nearest (in terms of energy) source of raw materials, certainly the nearest beyond the Moon, for any large-scale space activities. The suitability of these asteroids as a resource base will depend on (1) what types of needed materials are available, (2) how the material can be transferred in a useful form to the required area, and (3) how many of these objects have orbits favorable for efficient transfer.

This paper evaluates the potential resources available among the Apollo-Amor objects (those asteroids that cross or approach the Earth's orbit). The orbital distribution of the known Apollo-Amor objects (about 40) and of the expected population (about 200,000 with diameters greater than 100 m) are discussed from both empirical (i.e., observation) and theoretical perspectives. Several programs aimed at locating these bodies are outlined, and their relative cost and discovery rate discussed.

The chemical and physical nature of these bodies can be deduced from an analysis of remote-sensing data, from analysis of meteorites, and from a study of their source regions. A program of telescopic and spacecraft observations to determine the chemical composition and physical characteristics of these objects is outlined. The transfer (delta V) requirements for several members of the Apollo-Amor population were investigated in a separate paper (ref. l). A scenario for moving a 10^6-10^7-metric-ton portion of such an object into Earth-Moon space and the requirements for such a transfer were investigated in a second companion paper (ref. 2).

APOLLO ASTEROID ORBITS AND POPULATIONS

Introduction

The distribution of asteroids in general and of the Apollo-Amor group in particular can be determined from either observational or theoretical considerations. The distribution of known asteroids as a function of distance from the Sun (semimajor axis a) is shown in figure 1. Between 1.8 and 3.5 AU (asteroid belt), this distribution is probably a reasonable representation of the actual distribution, subject to corrections for observational bias against the more distant and lower albedo (fainter) objects in the outer asteroid belt (ref. 3).

The population of known objects with a semimajor axis <1.6 AU (mostly Apollo-Amor objects) is probably not representative of the population as a whole because of the small number of known objects (about 40) and because of observational selection effects that have favored the discovery of certain types of objects. Increasing the number of known Apollo objects to several hundred in a systematic search program will provide a secure basis for evaluating population patterns and for identifying the most suitable bodies for material return.

Based on the discovery rate of Apollo objects in three systematic search programs, it is estimated that the number of bodies larger than 1 km should be 800 ± 400 (ref. 4). This number is comparable to that estimated from rediscovery statistics (refs. 5, 6), impact statistics for large craters on the Earth and Moon (refs. 6, 7), and from the mass yield of meteorites from Apollo objects (refs. 6, 8). Based on the observed scaling law for asteroidal objects and collisional fragments (ref. 9), the number of objects larger than 100 m should exceed 100,000 ($2.0 ± 1.0 \times 10^5$). These objects are unstable against perturbations by, close approaches to, and collisions with the inner planets on a time scale of 10^7 years and must be replenished from an external reservoir.
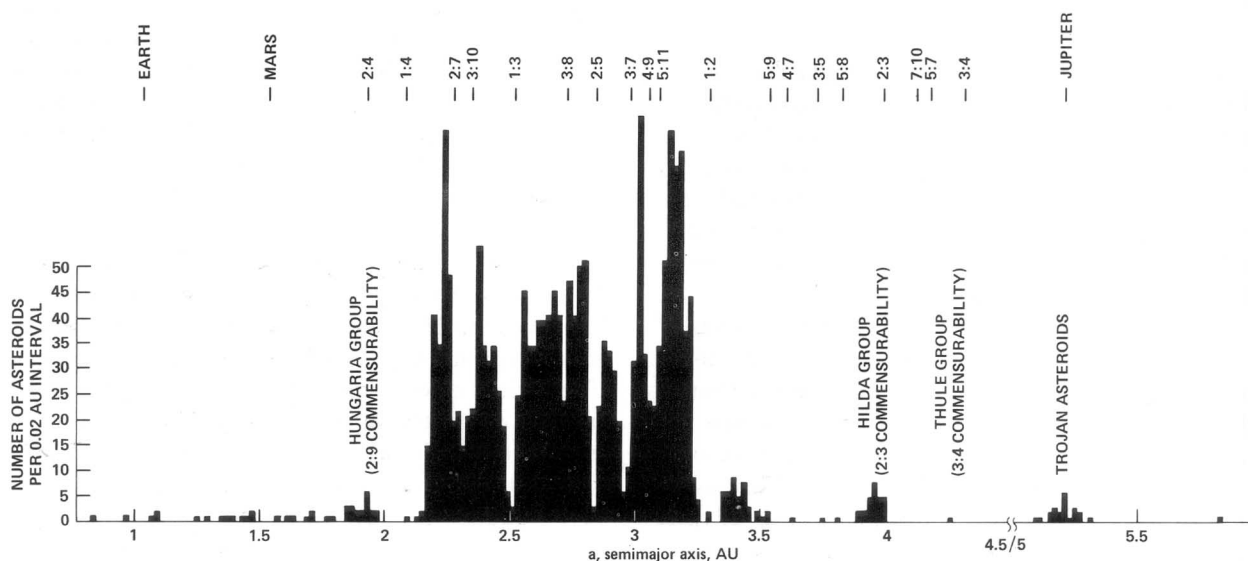
Figure 1 — *Frequency distribution of known asteroids with respect to semimajor axis. Elements of the current Apollo Amor group were provided by Williams (personal communication, 1977).*

History and Discovery Circumstances of Apollo Asteroids

Max Wolf, who had actively pursued a photographic search of asteroids at Heidelberg during the first three decades of the twentieth century, was succeeded by Karl Reinmuth. In 1932, Reinmuth found, on a 2.5-hr exposure plate, a long trail of a close, fast-moving asteroid. The new asteroid was named "Apollo" and became the prototype of a new class of asteroids characterized by a perihelion distance of 1 AU. After the discovery of Apollo, the next 5 years witnessed the discovery of two additional members, Adonis and Hermes.

The next decade was a quiet time in the realm of Apollo discoveries. However, in the late 1940s, two systematic programs were started: one at Mt. Palomar, the National Geographic Sky Survey (1949-1965), and the other, the Lick Observatory Proper Motion Survey. As by-products of these two surveys, several more Apollo asteroids were discovered. It should be understood that any asteroid trails found on these plates were considered undesirable, flawing the otherwise acceptable photographic plate. It was primarily the diligence of certain individuals, who were sufficiently intrigued by the long trails, that led to recovery and followup of the new objects.

After these two surveys were completed, there was another lull in discovery activity. From the early 1950s through the early 1970s, four other Apollo objects were found incidentally in other observational programs. The first systematic search for Earth-crossing asteroids was initiated in 1973 using the 46-cm (18-in.) Schmidt at Mt. Palomar. The results of this ongoing study have been the discovery of four Apollos, five Mars crossers, and another dozen asteroids from inner regions of the main belt. Figure 2 shows the discovery plate for one of the Apollo objects (1976 AA).

This dedicated program has had an influence on other observers in the astronomical community. By acquainting other observers (particularly the regular observers using the 122 cm (48-in.) Schmidt) with the nature and rationale of the search program and its significance, another four Apollos have been discovered. It should be pointed out that, before the 46-cm Schmidt planet-crossing asteroid search, these asteroid trails were ignored. These observers, with a better understanding of the importance of reporting these trailed objects, have been responsible for doubling the total number of Apollo asteroids discovered in the last 4 years.

ASTEROIDAL MATERIALS

Introduction

While a good case can be made that any mass in space is useful (e.g., reaction mass, radiation shielding, etc.), certain raw materials will probably be more in demand than others (e.g., metals, volatiles, carbon, etc.) (ref. 2). It is therefore appropriate to consider the availability of such materials in objects of the near-Earth population. Several perspectives can be used to characterize the material resources on these bodies. The meteorites represent direct samples of extraterrestrial materials that can be studied in the
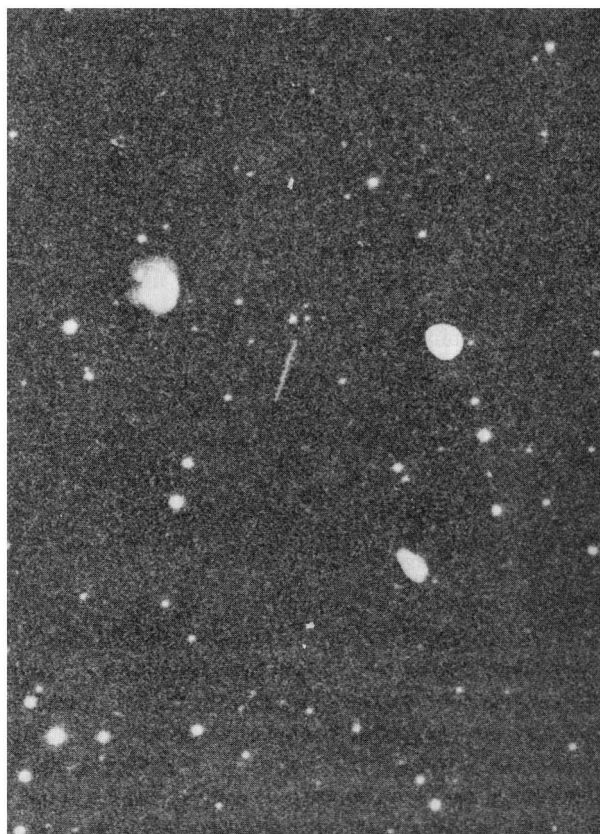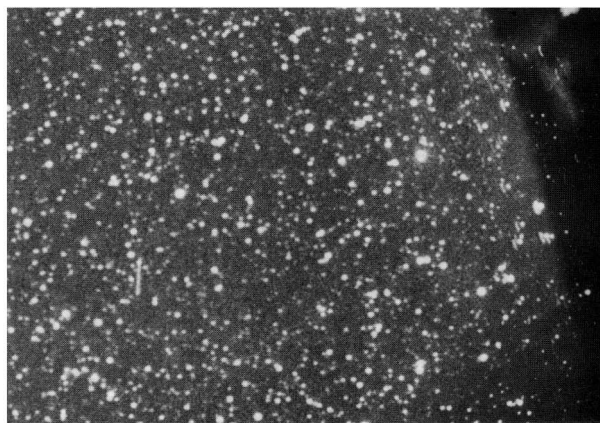
Figure 2 — *Discovery plates (X15) for two recent Apollo objects. (a) 1976 AA, January 7, 1976; (b) 1976 UA, October 25, 1976 (Hale Observatory photographs).*

laboratory. Orbital data from atmospheric meteor paths provide clues concerning the membership of materials in a near-Earth population. Studies of meteor trails provide chemical and physical data for materials that do not survive atmospheric entry. Collections of meteoric dust from high altitudes provide similar information.

Interpretation of reflectance spectra (fraction of sunlight reflected as a function of wavelength) can provide mineralogical characterizations of the surface materials of objects large enough to be measured through a ground-based telescope (refs. 10, 11). This information is available for several of the brighter Apollo-Amor asteroids (refs. 12-14) and indicates the distribution of material types in the Earth-approaching population.

Since the lifetime of an object in the near-Earth population is short (about 10^7 years), these bodies must be continuously replenished from some external reservoir of material (e.g., main-belt asteroids, comets, etc.) (refs. 6, 15). Studies of the nature of these reservoirs and the source mechanisms provide clues to the general nature of the material types present in the near-Earth population.

Availability of Raw Material

Supplies of certain specific raw materials will be required to build or maintain an inventory for processing purposes. The replenishment requirements for basic raw materials consumed (e.g., incorporated in long-lived products, expended, or lost) in large quantities will determine which types of asteroidal material are most useful. The minerals of major significance found in meteorites (refs. 16, 17) and which should be present on Apollo asteroids include: olivine (iron-magnesium silicate), pyroxene (iron-magnesium-calcium silicate; low calcium pyroxenes are termed "orthopyroxenes" because of their crystal structure), feldspar (calciumsodium-potassium alumino-silicate), clay minerals (hydrated iron-magnesium silicate), and metals (nickel-iron alloys). The various meteorite types contain different abundances and compositions of these minerals in a range of structural types which reflects their mode of formation. Four general classes of meteorites are recognized: chondrites, achondrites, stony-irons, and irons.

Chondrites were named for the presence of small spherical inclusions (chondrules). These meteorites contain approximately solar abundance of the nonvolatile elements (e.g., iron, magnesium, silicon, etc.) and apparently represent (essentially) unaltered material formed during the accretion of the solar system. The ordinary chondrites are composed of olivine, pyroxene, and feldspar with varying amounts of NiFe metal (about 15-19 percent H (high iron)-type; about 4-9 percent L (low iron)-type; about 0.3-3 percent LL (low iron, low metal)-type). The carbonaceous chondrites (c. chondrites), despite their name, are not necessarily characterized by abundant carbon. Type C1-C2 (CI-CM or type I-11) meteorites do contain relatively abundant carbon (about 1-5 percent) as graphite and tarlike organic compounds. The bulk of the C1 meteorites consists of a complex clay mineral assemblage and the C2 meteorites contain 15-70 percent olivine as inclusions in a clay mineral matrix. These clay minerals contain about 20 percent water in their structure. Type C3 meteorites consist mostly of olivine and contain only traces of water and carbon (<l percent). The C4 meteorites consist mainly of olivine and magnetite and are essentially devoid of either carbon or water.

The achondrites are silicate-rich meteorites apparently formed by igneous activity in their parent bodies. These consist of various mixtures of olivine, pyroxene, and feldspar and include eucrites and howardites or basaltic achondrites (pyroxene, feldspar) diogenites (pyroxene), nakhlites (olivine, calcic pyroxene), chassignites (olivine) and ureilites (olivine, carbon).

The stony-irons consist of mixtures of nickel-iron metal (30-70 percent) with various silicates: pallasites (olivine), mesosiderites (pyroxene, feldspar), and several other mixtures.

The iron meteorites consist of alloys of nickel and iron ranging from 5 percent to 50 percent nickel with an average near 10 percent Ni. Cobalt (about 0.5 percent) and other siderophile elements (Ga, Ge, etc.) are enriched in many of these meteorites. The irons often contain several percent silicate inclusions. Mason (ref. 16) provides a good introduction to the meteorites. Wasson (ref. 17) has reviewed and summarized recent work.

Two lines of direct evidence define the range of materials available in near-Earth space. First, the meteorites provide direct samples of such material. Wetherill (ref. 6) argues persuasively that most of the meteorite specimens recovered at the Earth's surface must derive from Apollo-Amor group asteroids. Certain select mainbelt asteroids may also be supplying a component of the meteorite flux (refs. 18-20). The pre-encounter orbits of at least three recovered meteorites (Pribram and Lost City, refs. 21-23 and Innisfree, 1977) are consistent with the orbits of members of the Apollo population.

A second line of direct evidence involves mineralogical characterizations of Apollo-Amor group asteroids from remotely obtained spectral evidence. Many important minerals exhibit characteristic features in their reflectance spectra which can be used to identify their presence, composition, and abundance from telescopic spectra (refs. 11, 14, and 24-26). Observational data of varying mineralogical significance are available for 12 Earth-approaching or Mars-approaching asteroids. These bodies and the types of materials associated with each are listed in table 1. With one exception, these are consistent with mafic-silicate (olivine, pyroxene) or mafic-silicate-metal assemblages. The available spectral and meteorite evidence indicates that the near-Earth population is dominated by ordinary chondritic-type materials.

However, in the observational case, one is dealing with the statistics of small numbers where a selection effect of unknown magnitude is operating (i.e., one tends to preferentially discover and observe brighter objects such as those with the highest albedo in any given size range). Anders (ref. 27) noted that it is possible to supply the ordinary chondrites from a very small number of favorably situated parent bodies. There is an additional bias introduced by atmospheric entry which operates against weak structures, such as would be expected for Cl chondrites or cometary debris (ref. 23). Therefore, while it is evident that ordinary chondritic assemblages are present in the near-Earth population, their relative abundance and the character and abundance of other types of meteoritic materials cannot be ascertained on the basis of available data.

TABLE 1 — CHARACTERIZATIONS OF APOLLO-AMOR OBJECTS

Number	Name	Note a, AU	q,a AU	Surface type[b]	Albedo[c]	Diameter,[c] km
Number	Name	Note a, AU	q,a AU	Surface type[b]	Albedo[c]	Diameter,[c] km
433	Eros	1.458	1.13	Olivine, pyroxene, metal (~H Chon) (ref. 13)	0.17	23
887	Alinda	2.516	1.15	Olivine, carbon (~C3)(ref. 26)	.17	4
1011	Laodamia	2.394	1.56	"S"-probably silicate or metal-rich assemblage	.16	7
1036	Ganymede	2.666	1.22	"S"-probably silicate or metal-rich assemblage	—	(~35)
1566	Icarus	1.078	.19	Pyroxene (olivine, metal ?)(ref, 26)	.17	1
1580	Betulia	2.196	1.12	"C"-opaque-rich assemblage, possibly carbonaceous		6
1620	Geographos	1.244	.83	"S"-probably silicate or metal-rich assemblage	.18	3
1627	Ivar	1.864	1.12	"S̲"-probably silicate or metal-rich assemblage	—	(~7)
1685	Toro	1.368	.77	Pyroxene, olivine (ref. 12)	.12	3
1864	Daedalus	1.461	.56	"O̲"-probably silicate or metal-rich assemblage	—	(~2)
1960 UA		2.26	1.05	"U̲" ?	—	—
2062	Aten	.97	.79	"S̲"-probably silicate or metal-rich assemblage	.17	1

a Perihelion distance for each object. By definition, Apollo objects have $q < 1.0$ and Amor objects, $1.00 < q < 1.38$. 1011 Laodamia is included even though it only approaches the orbit of Mars.

b Where adequate spectral data are available, mineralogical characterizations and meteorite equivalents are given. Bracketed numbers indicate the appropriate reference. Where only UBV colors are available, the Chapman-Morrison-Zellner classification of the object as summarized by Zellner and Bowell is given. Underlined classification symbols indicate those based on a single classification criterion. Probable mineral assemblages are indicated.

c Albedos and diameters as summarized by Morrison (ref. 36). The diameters in parentheses were derived assuming an average albedo for the "C-S" class of the object and should be considered as indicative only.

It is clear, however, that the material-population pattern of the main asteroid belt is not applicable to the Apollo population. Chapman et al. (ref. 28) evolved an asteroid classification scheme that utilizes observational properties (UBV colors, polarization, albedo) which, in modified form, has been used to define general population patterns in the asteroid belt (ref. 3). The types described in this system (C = carbonaceous, S = silicaceous or stony-iron, M = metal-rich, etc.) should not be taken as compositional descriptions. Most main-belt C-type asteroids turn out to be similar in spectral signature to carbonaceous type I and II meteoritic materials, but a significant minority of these C-type asteroids are a quite different assemblage (opaque-rich mafic silicate assemblages) (ref. 26).

However, as a classification scheme of limited compositional significance, the C-S system provides some important information concerning asteroid distributions. The relative abundance of S objects increases to nearly 50 percent at the inner edge of the belt, while the C objects constitute about 76 percent of all main-belt asteroids (ref. 3). Of the 12 objects thus far observed that either cross or approach the Earth-Mars orbits, only one (1580 Betulia) has the low albedo and neutral colors of the C group. It is possible, but by no means certain, that this asteroid is made up of material similar to C1 or C2 meteorites. Higher-resolution, broader-wavelength spectral data are needed before the composition of this object can be established.

Source Regions and Mechanisms for Near-Earth Asteroids

The two major candidates for source regions for near-Earth asteroids are the main-belt asteroids and the comets. The major difficulty for an asteroidal source for meteorites (and Apollo asteroids) is to modify the orbit from that of a main-belt object to an Earth-approaching object in as short a time as indicated by the cosmic-ray exposure age of the meteorites, or at a rate sufficient to maintain the Apollo population. The problem is less severe for small (~1 m) bodies than for larger bodies. Collisional injection of material from a body adjacent to a Kirkwood Gap into the gap (ref. 19) or into a secular resonance with Jupiter (ref. 18) provides a way to transfer this material into Earth-crossing orbits. Momentum transfer from sunlight by an absorption-reradiation mechanism (Yarkovsky effect) may transfer small objects (~1 m) into Earth-crossing orbits in relatively short time intervals (~10^7 yr) and might move larger objects into a resonance with Jupiter where relatively rapid orbital evolution can occur (ref. 29).

Asteroids that approach the orbit of Mars can be subjected to small cumulative perturbations and converted into Earth-crossing objects on a time scale of ~1×10^9 to 2×10^9 yr (refs. 30, 31). This rate is apparently too low to replenish the Apollo-Amor group from the available number of Mars-approaching or Mars-crossing bodies (ref. 6). Thus, while material equivalent to most meteorite types (except ordinary chondrites) is present in the asteroid belt and mechanisms for modifying these orbits exist, questions can be raised as to the relative importance of this source.

The capture of comets into the inner solar system by Jupiter is a well-known phenomenon. Wetherill (ref. 6, 20) concludes that, on the basis of dynamical considerations (refs. 15, 32), most (>90 percent) of the Apollo-Amor objects are of cometary origin. In this model, to account for the type of assemblages inferred to be present on the Apollos, it is plausible to assume that some portion of the material in cometary orbits represents the return of inner-solar-system material that was expelled by Jupiter during the early post-accretionary period of the solar system. This cometary hypothesis is not unanimously accepted (ref. 33).

If we assume that these two hypotheses are both correct and that only the relative rates of each are in doubt, then we can define a reasonable qualitative model of the near-Earth population. The asteroid belt should provide material from objects adjacent to resonance surfaces which include achondrite, stony-iron, and C1-C2 and C3 type assemblages. The Mars-approaching asteroids may provide ordinary chondritic or stony-iron assemblages based on the relative increase of S-type objects toward smaller semimajor axes. The cometary source could provide ordinary chondritic, achondritic, and stony-iron materials (ejected inner-solar-system material) and C1 material (devolatilized cometary nuclei). A degassed cometary nucleus should retain a significant amount of trapped volatiles in its deep interior (water, carbon dioxide, methane, and ammonia ices) (ref. 34). The relative abundance of these types cannot be established until a significant number of Apollo-Amor objects have been discovered and observed with sufficient spectral resolution and wavelength coverage to make mineralogical characterizations.

Physical Characteristics and Mechanical Properties

The mechanical properties of an Apollo-Amor object are determined by its composition and previous history. Most of the meteorite types exhibit a degree of coherency, that is, they tend to have reasonable physical strength and are hard to crush. The irons and stony-irons have the greatest strength. Ordinary chondrites tend to become stronger with increasing metamorphic grade. The C1 chondrites are quite friable (weak or easily disaggregated), the C2 reasonably coherent, and the C3 reasonably hard.

How the characteristics of a small specimen scale up to an object 100 m or larger is somewhat difficult to evaluate. Generally, any large fragment resulting from an impact event is likely to be extensively fractured and weak on a large scale. This is supported by meteorite fall evidence which indicates that most large (e.g., 2 m) bodies break up into many smaller ones (~20 cm) very soon after initial atmospheric contact. Typically, a large fall will consist of hundreds of individual objects, each with its own fusion crust, indicating breakup early in reentry. On a larger scale, doublet impact craters on Mars and Earth are more common than impact statistics would suggest, and this could be attributed to preatmospheric breakup under differential gravitational stress near the planet. It seems reasonable to assume that an object 100 m or larger will not withstand significant differential forces or high accelerations.

Devolatilized cometary nuclei are likely to be very porous "fairy-castle" materials with relatively little physical strength. The low density and low physical strength of fireball meteors, generally associated with extinct comets, are evidence of these properties (ref. 23). While there may be relatively dense regions in the interior as a result of weak compressional loading, these objects can generally be considered fragile.

RECOMMENDATIONS FOR GROUND-BASED TELESCOPE SEARCH FOR ASTEROIDS

Introduction

Statistically, it is estimated that there are about 1000 Earth-crossing asteroids larger than 1.0 km, many of which would be of interest for either missions or as the sources of raw material. Yet, as of July 1977, only 24 Apollo-type asteroids (Earth crossers) with well-defined orbits are known. Included in this small number, asteroids 1976 AA, 1976 UA, and 1977 HB are potentially attractive mission objectives. Asteroids 1976 AA and 1976 UA, actually the first of a new orbital class, were discovered in the past year. Besides orbit and delta-V considerations, the physical properties of a particular asteroid (e.g., abundance of volatiles and metals) will play a role in the selection process. Therefore, we need to know about the physical and chemical properties of the Apollo group.

A planned search program, using a 46-cm (18-in.) Schmidt telescope, and the subsequent increased interest generated in the astronomical community has doubled in 4 years the number of known Apollo asteroids. It took 40 years to discover the first 12 members. Since it has been estimated that at least 10 times as many Apollo asteroids should be observed to enable a judicious mission/resource selection, then one would estimate that, at the current rate of discovery, approximately 50 years of diligent effort would be required. This problem can be overcome by employing larger telescopes with more observing time. This approach is addressed here.

A goal of an order-of-magnitude increase in known objects in 5 to 10 years — a reasonable period for planning optimum use of present Space Shuttle capabilities — can be achieved by use of a 122-cm (48-in.) Schmidt telescope 10 days/month with appropriate support at other facilities.

Asteroid Detection Probabilities

The probability of detecting an asteroid in a search program depends on the apparent magnitude or brightness of the object, on the limiting magnitude of the search telescope, and on the amount of time committed to search. Figure 3 shows the surface corresponding to an 18th-magnitude detection limit as a function of opposition angle and object size for two reasonable albedos (0.15 and 0.04) and corresponding phase functions (0.025 and 0.038 magnitude/deg). Figure 4 shows the detection distances for a 1-km object with an albedo of 0.15 and a phase function of 0.023 magnitude/deg. The advantage of searching at or
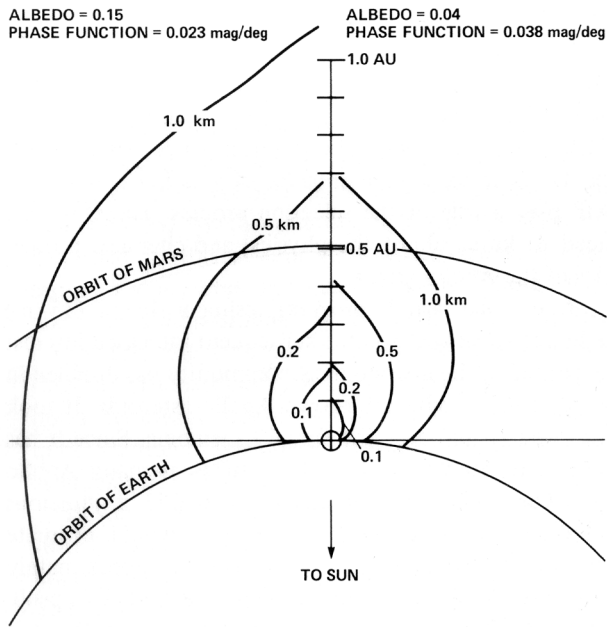
ALBEDO = 0.15
PHASE FUNCTION = 0.023 mag/deg

ALBEDO = 0.04
PHASE FUNCTION = 0.038 mag/deg

Figure 3 — *Detection distances for high- and low-albedo objects as a function of object diameter and opposition angle (Sun-Earth-object angle). An 18th-magnitude detection limit is assumed.*
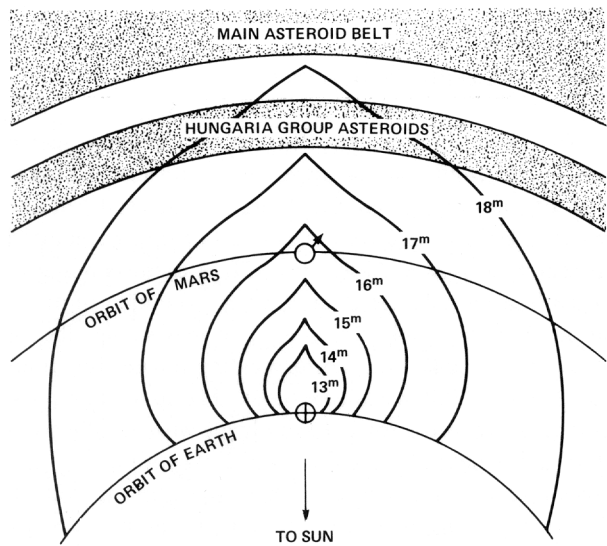
Figure 4 — *Detection distances for a high-albedo asteroid (0.15, 0.023 magnitude/deg), 1 km in diameter as a function of magnitude detection limit,* m, *and opposition angle.*

near opposition is evident. The disadvantage of a search at a high opposition angle (Sun-object-Earth angle β) is that the volume searched per square degree of plate area decreases substantially with increasing opposition angle. For example, at a limiting 17th magnitude for ($\beta = 0°$ - 5.6×10^{-5} (AU^3/deg^2), $\beta = 10°$ - 3.8×10^{-5}, $\beta = 50°$ - 2.1×10^{-5}, $\beta = 70°$ - 1.6×10^{-5}, and $\beta = 90°$ - 1.2×10^{-5}.

The probable discovery rate of Apollo asteroids as a function of telescope size and the characteristics and distribution of appropriate telescopes are given in table 2. Projected discovery rates increase dramatically with increasing telescope size and limiting magnitude. The 46-cm (18-in.) Palomar Schmidt is a telescope currently committed to a search for planet-crossing asteroids. The search program has

led to the discovery of four Apollo asteroids over a 4-year period. Other Apollo asteroid discoveries have been made with large-aperture Schmidt telescopes (100-cm (40-in.) and 122-cm (48-in.)) plates taken for other purposes. Observations with the 100-cm (40-in.) ESO Schmidt have concentrated on the Fast-Blue Survey (FBS) of southern skies, extending the Palomar National Geographic Sky Survey to declinations below -23°. The 122-cm (48-in.) Palomar Schmidt is used for many purposes, but the ongoing monthly program plates that have recorded the Apollo asteroids are the Supernovae Program and the Solar-System Search. Four Apollo asteroids have been incidentally discovered on 122-cm (48-in.) Palomar Schmidt plates. The ESO Schmidt (operated by R. M. West and H. E. Schuster on the FBS) has found one Apollo, but only after several had been lost because the plates were not examined soon enough for followup observations. Too much time had elapsed since the plates were taken, and the fleet object was lost.

If one or two moderate-sized Schmidts (apertures 24, 32, and 36 in.) were dedicated to search systematically during a 7-10-day period each dark of the Moon or if sufficient time were allocated on existing Schmidt telescopes (24- to 48-in. aperture), the current yearly discovery rate could be increased 5 to 10 times (in the last 2 years, three or four Apollo asteroids have been discovered each year). Only four of these asteroids were discovered in a search program designed specifically for their detection. The other discoveries were made on plates taken for other purposes. Hence, if one or two telescopes devoted to serious search were available, one could very conservatively estimate an order-of-magnitude increase in discovered objects. If one uses the present known number of Apollo asteroids (24), it is reasonable to estimate that the number could be doubled in a year of concentrated effort. B. G. Marsden (Smithsonian Astrophysical Observatory, Harvard University, personal communication, 1975) pointed out that there should be two Apollo asteroids discovered each month with the 122-cm (48-in.) Palomar Schmidt telescope during dark runs. With this increase in known objects, it is reasonable (based on the discovery of (1943), 1976 AA, 1976 UA, 1977 HB, and somewhat less suitable, 1975 YA) that 5 to 10 percent of the new discoveries would prove to have orbital characteristics that would qualify them as favorable mission candidates (ref. 35).

Asteroid Search Recommendations — Observation

The search efforts must be accelerated to ensure a dramatic increase in the discovery rate of planet-crossing asteroids. The commitment of any instrument for a dedicated asteroid search should include the detection of all classes of asteroids up to the magnitude limit of the search instrument. To optimize such a search, a strong recommendation would be to secure the use of or financial support for the construction of a large Schmidt telescope (122-cm (48-in.)). The objective of this search, however, would be to detect objects of moderate to fast motion (1/3° per day, upward) and therefore generally close to the Earth. Using the 46-cm

(18-in.) Schmidt telescope, in which 1/3° per day motion was used as a lower limit of motion for followup work, has produced 20 discoveries: 4 Apollos, 5 Mars crossers, 3 asteroids in the Phocaea regions, 2 asteroids in the Hungaria region, and 7 others from the edge of the main-belt region. The limiting factor for increasing the discovery numbers is the detection limit of a given telescope. The limiting magnitude of the 18-in. Schmidt is about magnitude 15 for a moving object.

Based on current numbers, one might expect that about 5 to 10 percent of the new objects would be of interest for rendezvous or sample return missions. This is a conservative estimate, based on only the 24 known Apollos. By committing a large-aperture Schmidt for a 10-day/month search, one could optimally expect to discover about 250 Earth crossers in 10 years or about 500 Earth crossers in 20 years.

Proposed System of Search

A search plan should consist of photographing a series of standard fields distributed along the ecliptic and extending to moderate latitudes north of the ecliptic. A 122-cm (48-in.) Schmidt camera plate is 35.5 X 35.5 cm (14 X 14 in.) and is 6.6 degrees in effective diameter. Monthly (each dark run), a series of fields should be photographed clustered around opposition. Two exposures should be made of each standard field, one of 12-min duration and one of 6 min. Typical planet-crossing objects can be recognized on the 12-min exposures by the amount of elongation or trailing of their images. The 6-min exposures would be used to confirm the detected objects and to determine their direction of motion. Under good seeing conditions, stars to 21^m are recorded in 6-7 min exposures with a variety of plate emulsions (e.g., 103 a-o, a-e). The magnitude limit for detecting moving objects is lower; however, fast-moving planet-crossing asteroids fainter than apparent magnitude 17 to 17.5 would only be marginally discernible.

Exposed plates should be developed immediately and scanned within 24 hr by microscopic examination. Generally, three observer teams would work shifts through an observing run; this intensive effort requires participation by several persons and, if continued through a 10-14-day dark run, would require two or three team shift rotations. Fast-moving objects must be detected promptly and followed for several days or they will be lost. Followup observations should also be obtained at least through the following lunation, if possible, so that the orbits can be computed with sufficient accuracy to recover these objects on their second apparition.

With the immediate goal of an expanded search program to accumulate sufficient observations to derive reliable orbits, the discovery telescope must continue to follow the new discovery. But it is critical that other observatories better located for followup observation be willing to collaborate on securing needed observations.

Asteroid Search Recommendations — Telescopic and Manpower Support

With a large Schmidt telescope and with adequate support, data necessary for the mission/natural resource program can be obtained within an acceptable time. Table 2 shows the presently available telescopes and projected rate of discovery when applied 10 nights/month to this program. To produce the data within a feasible period of time (5 to 10 years), time on a 122-cm Schmidt telescope is required. Table 3 shows a cost breakdown for constructing and supporting such a facility.

Once a principal telescope is available, there is a related significant problem, that is, backup and followup by other astronomical facilities. This support is necessary to secure orbits, particularly when weather or other difficulties render the discovery telescope inoperable on subsequent nights or when the motion of the object carries it beyond the observational range of the discovery instrument (e.g., to high

TABLE 2 — DISCOVERY RATE OF APOLLO ASTEROIDS VERSUS TELESCOPE

Telescope aperture size, cm (in.)	Discovery rate (current)	Potential discovery rate by increasing to 10 nights/ dark run	Threshold magnitude/size for moving objects	Tele-scopes in U.S.	Tele-scopes out-side	Availability of equipment, nights/yr	Cost of new instru-ments, $ millions
46 (18)	1 per year; 48 nights/year	>2	$15^m = 0.5$ km[a]	2		50-60	0.25
50 (20)		>2	15^m5		1		.3
61 (24)		2-3	15^m5		2		.4
81 (32)		3-4	16^m5		1	10-15 nights/year but not now in operation	.9
100 (40)	1-2 per year (incidental)	>4	$16\text{-}17^m > 0.3$ km		1	ESO Southern Sky Survey - by-product	2.25
105 (42)		5-6			1	—	2.75
122 (48)	1 per year (incidental)	>8	$17\text{-}17^m > 0.2$ km	1	2	Standard program by-product	3

a Size estimate corresponds to detection limit of discovery telescope.

negative declinations). With the discovery of relatively large numbers of objects, this could require a significant effort rather than the present somewhat informal effort, often the result of personal contact.

An observational clearinghouse should be established to collect monthly telescope logs from observatories with suitable telescopes. This could be handled simply — the monthly plates of each telescope could be reproduced, punched on cards, and collated on printouts and distributed to interested observers. From this information on known existing plates and their positions, it is possible to check for additional observations of a new discovery either before or after discovery. Locating plates that contain needed positions from a review of Palomar logbooks has revealed additional positions of new objects, extending the arc from a few days to a few months. A substantial increase in secure orbits could be obtained at relatively low cost by the coordinated use of such a clearinghouse for long-exposure, wide-angle plates.

To determine surface compositions, it would be most desirable to discover these bodies before opposition and, ideally, with several weeks or months of lead time so that observation time could be requested on large telescopes. To do this, it would be necessary to search a region near the ecliptic about 90° from the opposition point (forward for objects beyond 1 AU, backward from objects inside 1 AU). This requirement would decrease somewhat the efficiency of a search program. From the point of view of obtaining compositional characterizations of these objects (spectrophotometric or radiometric observations), it would seem worthwhile to partition a portion of any general search effort into a survey of the $\beta = 0$ to $\beta = \pm 90°$ directions. The value of early detection and discovery-opposition spectral work is high for interesting objects whose synodic periods are long (>5 years). Failure to achieve a compositional characterization during the discovery opposition means a wait equal to the synodic period before such a study can be made.

ASTEROID MATERIAL CHARACTER-IZATIONS — RECOMMENDATIONS

Any reasonable scenario for asteroidal resource utilization will require a spacecraft survey mission to a likely candidate body selected on the basis of a preliminary material characterization from Earth-based studies. Even if nonspecific mass is desired, a characterization will be necessary to define the most appropriate recovery program (e.g., type of processing and mining equipment, type and amount of expendables for system operations, etc.). The available techniques for studying these objects can be divided into ground-based (or near-Earth) and spacecraft.

Earth-based characterizations must depend on information contained in reflected sunlight (reflectance spectroscopy) or reflected man-made radiation (radar) or in emitted thermal radiation (thermal infrared, thermal microwaves). Reflectance spectroscopy is most sensitive to surface mineralogy, but a certain minimum spectral resolution and

TABLE 3 — COST ESTIMATES FOR DEDICATION OF A 122-cm (48-in.) SCHMIDT AND ASSOCIATED EQUIPMENT

	Estimated cost, $ millions
Setup cost:	
122-cm (48-in.) facility	3.0
Measuring machine	.04
(14- X 14-in. plate, custom-made size)	
Automatic blink machine	.6
(14- X 14-in. plate size)	
Computer (or buy time)	.12
Establish international clearinghouse to record all astronomical observations and distributing costs	.1
Subtotal	3.86
One-year operation cost:	
Photographic plates (14- X 14 in.) plus chemicals (1-year supply)	0.02
Guest observing charges and reimbursement to other observing facilities	.01
Communication (telex, telegram, telephone, etc.)	.005
Travel (U. S. and foreign) for 3-4 people	.03
Personnel support:	
2-3 full-time astronomical observers	.06
3-4 support technical assistants	.05
Subtotal	0.175
(plus overhead)	
Total	4.035

wavelength coverage is necessary to obtain such characterizations. A spectrum with 1-percent resolution over the interval 0.3-5 μm could provide detailed information (mineral chemistry, abundance, and distribution) on surface materials. In practice, one almost certainly would not be able to obtain such spectral data for the asteroids in near-Earth space. The photon flux from the observed object (magnitude, telescope size, detector sensitivity, the flux onto detector and atmospheric transmission) are the main factors that control the resolution and coverage of spectral data. Low-resolution data (e.g., broad bandpass UBV filters) can be obtained for very faint objects (i.e., 18 magnitude), but are not particularly sensitive to surface composition. High-resolution spectra cannot be made for very faint objects unless longer integration times or lower spectral precision is accepted. Simultaneous detection over a broad spectral region (e.g., dispersion of the spectrum across an array of detector elements — vidicon or CCD spectrometer or interferometer) can alleviate this discrepancy somewhat. Wavelength coverage depends on the additional factors of spectral flux and atmospheric transmission. The spectral flux of almost any object reflecting sunlight peaks in the mid-visible and decreases rapidly toward the UV and IR (e.g., at 1.0-μm flux, it is down to a third of the peak flux and at 2.0 μm, down to 5 percent) following a blackbody curve for ~6000 K object (Sun). This flux loss must be compensated for by increasing integration times or decreasing resolution. Atmospheric absorptions in the near IR (e.g., H_2O vapor at 1.4 and 1.9 μm) effectively block these spectral regions for faint objects.

We recommend a multiple approach to ground-based studies of the near-Earth population of asteroids:

1. A low-resolution, wide-coverage spectral program (UBVRIJHK). These data can provide some indicative compositional information on very faint objects (~17-19 magnitude on large (~100-in. or 2.5 m) telescopes) in an observing period of several days. The IR filters (RIJHK) are essential since they can provide criteria for discriminating metal-rich assemblages from silicate-rich assemblages and may provide a preliminary subdivision of the opaque-rich assemblages.

2. A moderately high-resolution (~3 percent), wide-coverage (0.3-2.0 μm) spectral program. This program can provide detailed mineralogical characterizations for reasonably faint asteroids (~15-16 magnitude) observed with a large telescope (~100 in. or 2.5 m). The instrumentation to make these measurements (vidicon or CCD arrays) are being developed as astronomical instruments.

3. Measurements of the thermal IR can be used to determine the diameter and albedo of faint asteroids (~16-17 magnitude) on the large telescopes. The albedo provides an additional compositional discriminant.

4. Radar reflectances of these asteroids can be obtained only when the object is near Earth and when it is in a portion of the sky accessible to the large radio telescopes, such as Arecibo.

5. Photo polarimetry measurements can be made of reasonably bright objects (~14 magnitude). Measurements near opposition which can determine the shape and depth of the negative branch of the phase-polarization curve can provide clues on the structure and optical density of the surface material.

6. High-resolution spectroscopy (~3 percent) of the thermal infrared should provide indications of silicate chemistry, but previous attempts to apply this to telescopically observed objects have not been successful. Limiting magnitude (~12 magnitude) is probably not faint enough to be of general interest to this program.

7. The compositional significance of thermal microwaves and the limiting magnitude is unclear.

A program of low- and high-resolution, wide-coverage reflectance spectroscopy coupled with broadband thermal IR radiometry should provide a basis for a reasonably precise characterization of asteroid materials. The high-resolution, wide-coverage reflectance spectroscopy is the essential component of such a characterization.

The design of a spacecraft system to characterize an asteroid or several asteroids depends rather critically on the mission profile. Mission options include single- or multiple-asteroid flybys or rendezvous with either ballistic or low-thrust spacecraft. The asteroid studies that can be done with available spacecraft instrumentation and general mission profiles are discussed separately. Experience derived from the design of a state-of-the-art mission for studying the Moon (LPO) is helpful in a discussion of possible asteroid missions.

Experiments that characterize the "chemical" properties of a planetary surface remotely include reflectance, x-ray, gamma-ray, and alpha-particle spectrometers. A spacecraft reflectance spectrometer can provide detailed mineralogical characterizations of each spatial resolution element on the surface of the asteroid. An x-ray spectrometer detects the x-ray emission lines of lighter elements ($Z \leqslant 16$ and, under favorable conditions, $Z \leqslant 30$) that have been excited by solar x-rays to obtain elemental ratios such as Mg/Si. A gamma-ray spectrometer detects gamma-ray emission from (1) the decay of natural radioactive elements, (2) the decay of radioisotopes induced by galactic cosmic-ray bombardment, and (3) decay of excited nuclei in atoms subjected to galactic cosmic-ray bombardment. A gamma-ray instrument will obtain elemental ratios for the naturally occurring radioisotopes (U, Th, K^{40}) and the abundant elements (e.g., Fe, Mg, Si, O, etc.) in the surface material. A gamma-ray spectrometer can also measure the content of water (H) in the surface material of an asteroid. An alpha-particle spectrometer measures the energy of alpha particles emitted by the decay of daughter products of the U-Th series.

Other experiments that remotely characterize surface properties include thermal infrared and microwave radiometers and radar sounders and altimeters. An infrared radiometer measures the temperature distribution across the asteroid surface, which provides an indication of surface (~1-10 cm) conductivity (thermal inertia, texture), while a microwave radiometer can characterize the temperature distribution with depth for the top meter or so of the surface material. A radar sounder/altimeter can measure the texture (particle size) and conductivity of the top meter or several meters (depending on wavelength) of the surface material and can measure the shape of the asteroid with precision.

An imaging system is essential both for terminal guidance during approach to the asteroid and in obtaining high-resolution (~1-10 m) photographs of the body. Photographs are important for locating the ground tracks of high-resolution instruments (e.g., reflectance spectrometer, thermal infrared, and radar) to relate their results to surface features. Photographs also provide size and shape information which can be combined with mass determination to obtain bulk density.

Spacecraft tracking during a flyby can provide a mass determination and, during the orbit about an asteroid, can provide a very precise mass determination, moment of inertia, and density distribution measurements that provide information on the internal structure of the asteroid.

In situ measurements can be made by experiments delivered to the surface either by a soft lander or a penetrator. Chemical (alpha-particle backscattering, neutron activation analysis, x-ray fluorescence) and mineralogical analysis (reflectance spectrometer, x-ray diffraction) can be carried out on the surface. Monitoring the deceleration of the

penetrator on impact provides a measure of physical strength of materials. A soft lander would be needed to acquire a sample for any sample return mission.

The scientific payload on any asteroid mission will depend on the propulsion systems available and the survey goals. For a ballistic trajectory and given propulsion system (e.g., Shuttle plus interim upper stage (IUS)), the total spacecraft mass launched to an asteroid (spacecraft bus, additional propulsion requirements, scientific payload) will depend on the orbit of the target asteroid. A low-thrust propulsion system (after trajectory insertion) can increase payload capacity or enable multiple asteroid rendezvous missions. An ideal mission (neglecting sample return) would probably involve insertion of the spacecraft into an orbit (or station-keeping location) near the asteroid for an extended survey mission (months). With a low-thrust propulsion system, the spacecraft can be inserted into a new trajectory to a second or third asteroid.

We recommend planning studies to optimize a series of spacecraft missions based on the propulsion systems available in the near term (1978-1985) and far term (post-1985) for various asteroid targets.

REFERENCES

1. Bender, David F.; Dunbar, R. Scott; and Ross, David J.: Round-Trip Missions to Low Delta-V Asteroids and Implications for Retrieval. Space Resources and Space Settlements, NASA SP-428, 1979, pp. 133-141.

2. O'Leary, Brian; Gaffey, Michael J.; Ross, David J.; and Salkeld, Robert: Retrieval of Asteroidal Materials. Space Resources and Space Settlements, NASA SP-428, 1979, pp. 142-155.

3. Zellner, B.; and Bowell, E.: Asteroid Compositional Types and Their Distributions. The Interrelated Origin of Comets, Asteroids, and Meteorites. A. H. Delsemme, ed., University of Toledo Publ., 1977, pp.185-197.

4. Shoemaker, E. M.; and Helin, E. F.: Populations of Planet-Crossing Asteroids and the Relation of Apollo Objects to Main-Belt Asteroids and Comets. The Interrelated Origin of Comets, Asteroids, and Meteorites. A. H. Delsemme, ed., University of Toledo Publ., 1977, pp. 297-300.

5. Whipple, Fred L.: Note on the Number of Origin of Apollo Asteroids. The Moon, vol. 8, 1973, pp. 340-345.

6. Wetherill, G. W.: Where Do the Meteorites Come From? A Re-evaluation of the Earth-Crossing Apollo Objects as Sources of Chondritic Meteorites. Geoclumica Cosmochimica Acta, vol. 40 no. 11, 1976, pp. 1297-1317.

7. Shoemaker, E. M.; Helin, E. F.; and Gillett, S. L.: Populations of the Planet-Crossing Asteroids. Geologica Romana, vol. XV, 1976, pp. 487-489.

8. Wetherill, G. W.; and Williams, J. G.: Evaluation of the Apollo Asteroids as Sources of Stone Meteorites. Journal of Geophyscial Research, vol. 73, no. 2, 1968, pp. 635-648.

9. Dohnanyi, J. S.: Collisional Model of Asteroids and Their Debris. Journal of Geophysical Research, vol. 74, no. 10, 1969, pp. 2531-2554.

10. McCord, T. B.; and Adams, J. B.: The Use of Ground-Based Telescopes in Determining the Composition of the Surface of Solar System Objects. Proceedings of Soviet-American Conference on Cosmochemistry of the Moon and Planets, Moscow, USSR, June 4-8, 1974. (Also NASA SP-370, pp. 893-922.

11. Adams, John B.: Visible and Near-Infrared Diffuse Reflectance Spectra of Pyroxenes as Applied to Remote Sensing of Solid Objects in the Solar System. Journal of Geophysical Research, vol. 79, 1974, pp. 4829-4836.

12. Chapman, Clark R.; McCord, Thomas B.; and Pieters, Carle: Minor Planets and Related Objects. X. Spectrophotometric Study of the Composition of (1685) Toro. Astronomical Journal, vol. 78, no. 6, 1973, pp. 502-505.

13. Pieters, Carle; Gaffey, Michael J.; Chapman, Clark R.; and McCord, Thomas B.: Spectrophotometry (0.33 to 1.07 μm) of 433 Eros and Compositional Implications. Icarus, vol. 28, no. 1, 1976, pp. 105-115.

14. Gaffey, M. J.; and McCord, T. B.: Asteroid Surface Materials: Mineralogical Characterizations and Cosmological Implications. Proceedings of the 8th Lunar Science Conference, vol. 1, 1977, pp. 113-143.

15. Opik, Ernest J.: The Stray Bodies in the Solar System. Part I. Survival of Cometary Nuclei and the Asteroids. Advances in Astronomy and Astrophysics, vol. 2, 1963, pp. 219-262.

16. Mason, Brian: Meteorites. John Wiley & Sons, New York, 1962.

17. Wasson, John T.: Meteorites; Classification and Properties. Springer-Verlag, New York, 1974.

18. Williams, J. G.: Meteorites from the Asteroid Belt? (Abstract). EOS Trans. American Geophysical Union, vol. 54, 1973, p. 233.

19. Zimmerman, Peter D.; and Wetherill, G. W.: Asteroidal Source of Meteorites. Science, vol. 182, no. 4107, 1973, pp. 51-53.

20. Wetherill, George W.: Solar System Sources of Meteorites and Large Meteoroids. Annual Review of Earth and Planetary Sciences, Fred A. Donath, ed., vol. 2, 1974, pp. 303-331.

21. Ceplecha, Z.: Multiple Falls of the Pribram Meteorites Photographed. Bulletin of the Astronomical Institute of Czechoslovakia, vol. 12, 1961, pp. 21-47.

22. Clarke, R. S.; Jarosewich, E.; and Nelson, J.: Lost City, Oklahoma, Meteorite: An Introduction to Its Laboratory Investigation and a Comparison with Pribram and Ucera. Journal Geophysical Research, vol. 76, no. 17, 1971, pp. 4135-4143.

23. McCrosky, R. E.; Posen, A.; Schwartz, G.; and Shao, C. Y.: Lost City Meteorite — Its Recovery and a Comparison with Other Fireballs. Journal of Geophysical Research, vol. 76, no. 17, 1971, pp. 4090-4108.

24. Adams, J. B.: Interpretation of Visible and Near-Infrared Diffuse Reflectance Spectra of Pyroxenes and Other Rock-Forming Minerals. Infrared and Raman Spectroscopy of Lunar and Terrestrial Minerals, Clarence Karr, ed., Academic Press, New York, 1975, pp. 91-116.

15. McCord, Thomas B.; and Gaffey, Michael J.: Asteroids: Surface Composition from Reflection Spectroscopy. Science, vol. 186, no. 4161, 1974, pp. 352-355.

26. Gaffey, M. J.; and McCord, T. B.: Asteroid Surface Materials: Mineralogical Characterizations from Reflectance Spectra. Space Science Review, vol. 21, no. 5, 1978, pp. 555-628.

27. Anders, Edward: Interrelations of Meteorites, Asteroids and Comets. Physical Studies of Minor Planets, T. Gehrels, ed., NASA SP-267, 1971, pp. 429-446.

28. Chapman, Clark R.; Morrison, David; and Zellner, Ben: Surface Properties of Asteroids: A Synthesis of Polarimetry, Radiometry and Spectrophotometry. Icarus, vol. 25, no. 1, 1975, pp. 104-130.

29. Peterson, Charles: A Source Mechanism for Meteorites Controlled by the Yarkovsky Effect. Icarus, vol. 29, no. 1, 1976, pp. 91-111.

30. Arnold, James R.: The Origin of Meteorites as Small Bodies. Isotopic and Cosmic Chemistry, North Holland, 1964, pp. 347-220.

31. Arnold, James R.: The Origin of Meteorites as Small Bodies. III. General Considerations. Astrophysical Journal, vol. 141, no. 4, 1965, pp. 1548-1556.

32. Opik, Ernst J.: The Stray Bodies in the Solar System, Part II. The Cometary Origin of Meteorites. Advances in Astron. Astrophys., vol. 4, 1966, pp. 301-336.

33. Anders, Edward: Do Stony Meteorites Come From Comets? Icarus, vol. 24, no. 3, 1975, pp. 363-371.

34. Marsden, B. G.: Evolution of Comets into Asteroids? Physical Studies of Minor Planets, T. Gehrels, ed., NASA SP-267, 1971, pp. 413-421.

35. Helm, Eleanor F.; and Shoemaker, Eugene M.: Discovery of Asteroid 1976 AA. Icarus, vol. 31, no. 4, 1977, pp. 415-419.

36. Morrison, David: Asteroid Sizes and Albedos. Icarus, vol. 31, no. 2, 1977, pp. 185-220.

V

Processing of Nonterrestrial Materials
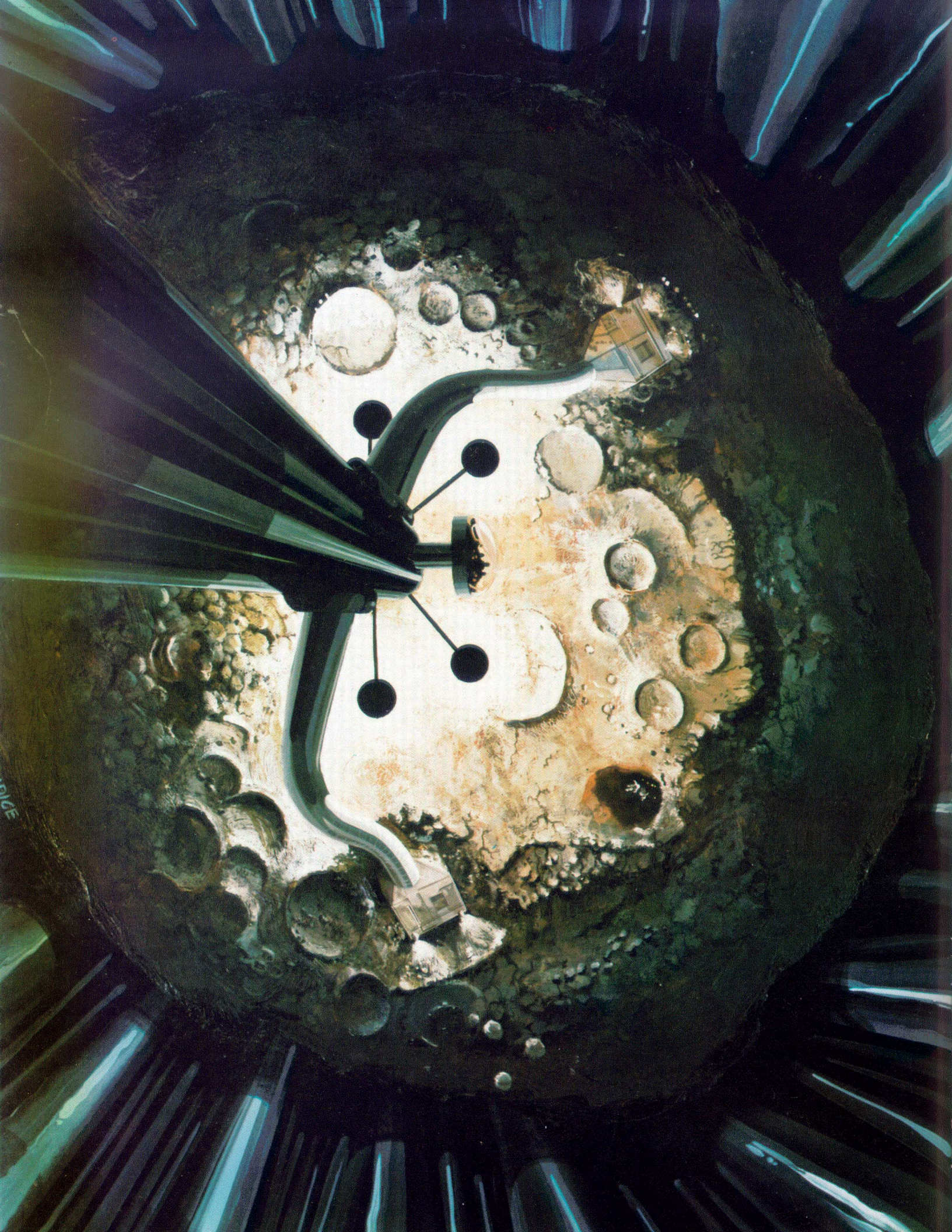
V-1
The Initial Lunar Supply Base

DAVID R. CRISWELL

The initial lunar supply base should have a mass less than 1000 tons, be deployed by 25 persons in 4 months, and be maintained by 10 persons. Output could be expanded 20 times in 5 years to 600,000 tons/yr by a factor of 10 expansion of the area of the solar array on the lunar surface, using low power soil beneficiation, increasing the fleet of mining vehicles, and illuminating the base continuously at night with lunar orbiting mirrors. The space manufacturing facility (SMF) will supply most of the mass (solar cells and orbiting mirrors) necessary for expansion. Several devices and procedures are suggested for development which could further reduce the total mass necessary to transport to the Moon and establish the initial lunar supply base.

INTRODUCTION

The ultimate objective of space industrialization is to create a growing economy in space which can eventually become self-sufficient. Space industry is presently supported by sales of goods with extremely high intrinsic values, such as satellites for communications, research, navigation and reconnaissance. Low-volume production of exotic goods in the zero-gravity and weightless conditions afforded in near-Earth space may broaden the market for space produced goods. However, in all these cases the cost of transporting the goods or raw materials into low-Earth orbit will add $200-$700/kg to the product price for a period of 15 years and thus place a sharp limit on the ultimate terrestrial market (ref. 1). There appears to be a way of circumventing the present high cost of launching materials from the Earth into space. This can be done by acquiring bulk raw materials from the Moon or asteroids and processing them in space into economically valuable products. Initial bulk material costs could be of the order of $25/kg in high-Earth orbit (Salkeld, Part IV-2, Appendix) and the cost would drop with experience. There would be two effects of lower material costs. First, the space economy could begin approaching the richness and cost structures of our present terrestrial economy. Secondly, the range of space products that could be sold for terrestrially-related use either in space or on Earth would be greatly expanded.

The Moon can supply most of the mass needed for large-scale industry in space. There are two ways to approach the proof of this statement. The first is to look in detail at the materials needed to construct specific products in space. At this point in time the production of space solar power stations is an attractive candidate because of the high value per unit mass of such objects and because of the large number of stations which could be required (>200 in next 30 years). Analyses even of designs not optimized for lunar elements reveal that at least 60 percent of the required silicon, aluminum and oxygen could be obtained from the Moon and the total mass lifted from Earth could be reduced about 80 percent by utilizing lunar materials (refs. 2, 3).

Alternatively, one can compare the nonfuel distribution of nonrecoverable elements (weight fraction) utilized in the industrial economy of the United States with elements present in the lunar soil as is shown in table 1 (ref. 4). The fraction of these elements which can be extracted with reasonable and presently available chemical processing techniques from beneficiated lunar ores is the subject of two companion papers by Williams et al. and Rao et al. (Parts V-6 and V-5, respectively) discuss extraction of Si, O, Fe, Al, Ti, and H_2O. Using these and other proposed extraction procedures most of the components of the synthetic molecule of "Demandite" (defined in table 1), which constitute most of the nonfuel material inputs to American industry, could be provided in deep space at less cost per unit mass than the launch cost of the complete suite of the constituent elements directly from Earth in large tonnages until the mid-1990's (ref. 4).

Notice in column 4 of table 1 that the major demandite components (Si, O, Fe, Al, Mg, X, Ca, Na, K, P, and S) are present either in adequate concentrations or in enrichments that are 10 times the specific fractions of the soil. Beneficiation of soil components to enhance and possibly simplify known chemical extraction processes should be achievable using electrostatic, magnetic, dielectric and mechanical techniques and careful site selection. Elements such as Cu, Zn, Pb, H, Cl, N, C, and other trace elements comprise 8.4 percent of the demandite molecule. These elements would be shipped from Earth, eventually located from other sources, such as non-Apollo sites, or other materials substituted for them. In any event, it is clear that of order of 90 percent of the present day inventory of industrial elements can be provided from known lunar soils. Lunar soil processed to provide 90 percent of the demandite complement at $20/kg (i.e., Si, Al, Fe, Mg, Ca, and O) and the remainder supplied from Earth at $300/kg would provide the in-space demandite molecule at a cost of about $50/kg or 17 percent of the direct supply cost (ref. 4).

It is very clear, however, that substitution of materials, which is being required in the terrestrial economy even now,

TABLE 1 — NONFUEL DEMANDITE (U.S., 1958) COMPARED TO ELEMENTARY DISTRIBUTIONS
OF SOIL AT THE APOLLO-15 LANDING SITE (WEIGHT FRACTIONS)

	Nonfuel demandite[a]	Apollo 15 mare-low Ti	Enhancement required	Bulk soil (1 unit)[b]	
				Excess	Deficiency
Si	0.2444	0.2158	1.13	—	0.0286
O	.4547	.4130	1.10	—	.0417
Fe	.0479	.1535	.31	0.1056	—
Al	.0023	.0681	.04	.0523	—
Mg	.0017	.0681	.025	.0664	—
(Cu,Zn,Pb)	.0020	2.2(-5)[c]	90	—	.0020
X[d]	.0030 Σ -.0569	0.0189 Σ-.2951	.15	.0159	—
Ca[e]	.1417	.0696	2.0	—	.0721
Na	.0095	.0023	4.1	—	.0072
S	.0058	.0006	9.7	—	.0052
K[e]	.0021	.0008	2.6	—	.0013
P[e]	.0019	.0005	3.8	—	.0014
Cl	.0147	7.6 (-6)	1934	—	.0147
N[e]	.0083	8 (-5)	103	—	.0083
C[e,f]	.0574	9.5 (-5)	604	—	.0573
H[f]	.0025	6.4 (-5)	350	—	.0025
Other[g]	.0001	.0023	.03	.0022	—
	1.0000	1.0000		(+) 0.2424	(-) 0.2423

a Demandite data supplied in reference 4.
b Formula = (Wt. fraction lunar element) — (Wt. fraction demandite).
c $(N) \equiv 10^N$.
d x ~ Mn, Ti, Cr, Ba, F, Ni, Ar, Sn, Br, Zr.
e Important agriculturally.
f Concentrated in the smaller grains ($<50\mu$).
g Virtually the complete suite of elements is present in these areas, but their contributions (on the ppm and ppb levels) are lost in the errors of the sum over the listed elements. Trace element concentrations may vary greatly from one site to another.

will permit much greater use of lunar materials both in general and for specific products (ref. 5). Thus, the cost of space "demandite" should approach the cost of the lunar processed materials.

The economic value to Earth of the Moon or the asteroids as a source of raw materials is strongly dependent on the total retrieval and elemental separation costs of the raw materials. Figure 1 is a qualitative description of the costs of goods or end-use-material on a dollar per kilogram basis (horizontal axis) versus the differential output of the total value of goods in the U.S. economy in billions of dollars per dollar per kilogram or ($\Delta 10^9$ \$/(\$/kg)) for a total GNP of 10^{12} (ref. 1).

Most goods now sell for less than \$10/kg with most between \$0.1/kg and \$2/kg. Transport into low-Earth orbit (LEO) from the Earth presently adds more than \$500/kg and thus confines goods produced in space to a tiny fraction of the potential terrestrial market (right of arrow 1 in fig. 1). Solar power stations are estimated to be economically feasible at \$140/kg (refs. 3, 6). Supplying the bulk of the required construction material from the Moon at \$20/kg (arrow 2) would clearly improve the economics and decrease the cost of the power supplied to Earth. If sources of industrial

feedstock can be developed in deep space with costs of less than \$0.5/kg (arrow 3) then many of the Earth-produced goods can be considered for potential space manufacture
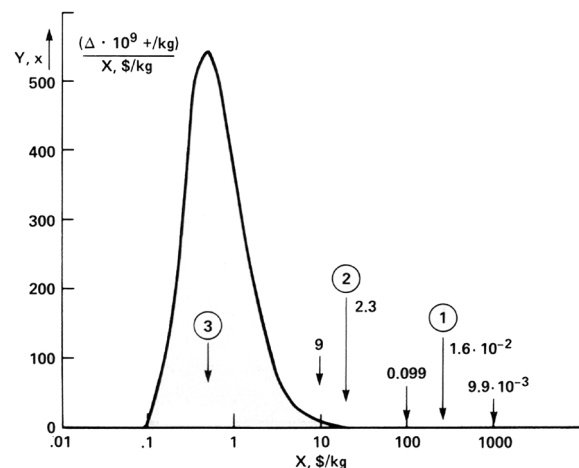
Figure 1 — Differential value of all goods produced in the U.S. (vertical axis) versus the intrinsic unit value (\$/kg) of the goods (horizontal axis). Integral value in \$B of goods with intrinsic values greater than 10, 20, 100, 250, and \$1000/kg are shown at arrows.

(ref. 1). It is conceivable that industrial material can be supplied at such low costs from the Moon or asteroids assuming normal industrial "learning curve" experience occurs.

Previous scientific exploration of the Moon and the vigorous ongoing program of lunar sample research and theoretical analyses allows us to study and plan in detail for obtaining lunar materials and chemically processing them. However, additional research is necessary and should be an ongoing component of the lunar base siting and operation. A general survey of the Moon is necessary — including the polar regions. There should be a close tie-in of the lunar sample and planetary sciences communities, with the engineering communities responsible for research and development of lunar bases and refining schemes. Above all, design of the lunar supply base should be approached so as to minimize total cost and maximize output to provide useful components of the lunar soil at points in deep space at the lowest possible cost per unit mass.

The following sections describe one approach toward a lunar base of minimal size which could be expanded in launch capacity from 30,000 tons/yr (bulk soil) to 600,000 tons/yr (beneficiated soil components) over a 5-year period making maximum use of lunar materials to minimize shipping from the Earth.

LUNAR BASE TOUR

Conceptions of mankind's first permanent installation on the Moon have tended to evoke paintings of either immense facilities containing hundreds of persons and enormous rocket traffic between the Earth and the Moon (ref. 7) or, on the other hand, simple and isolated extensions of the Apollo lunar module with little space, with limited capability and operated by only three or four persons. Concepts evolved during this study project a different style — one dominated for at least the first 5 years by the severe demands of utility and cost effectiveness. The principal function of the base is providing a supply of minimally-processed lunar materials to a collection point in deep space at the lowest possible initial cost, greatest reliability (attainable principally through simplicity of design) and with a straightforward plan for expansion of base output capacity by a factor of 20 over 5 years.
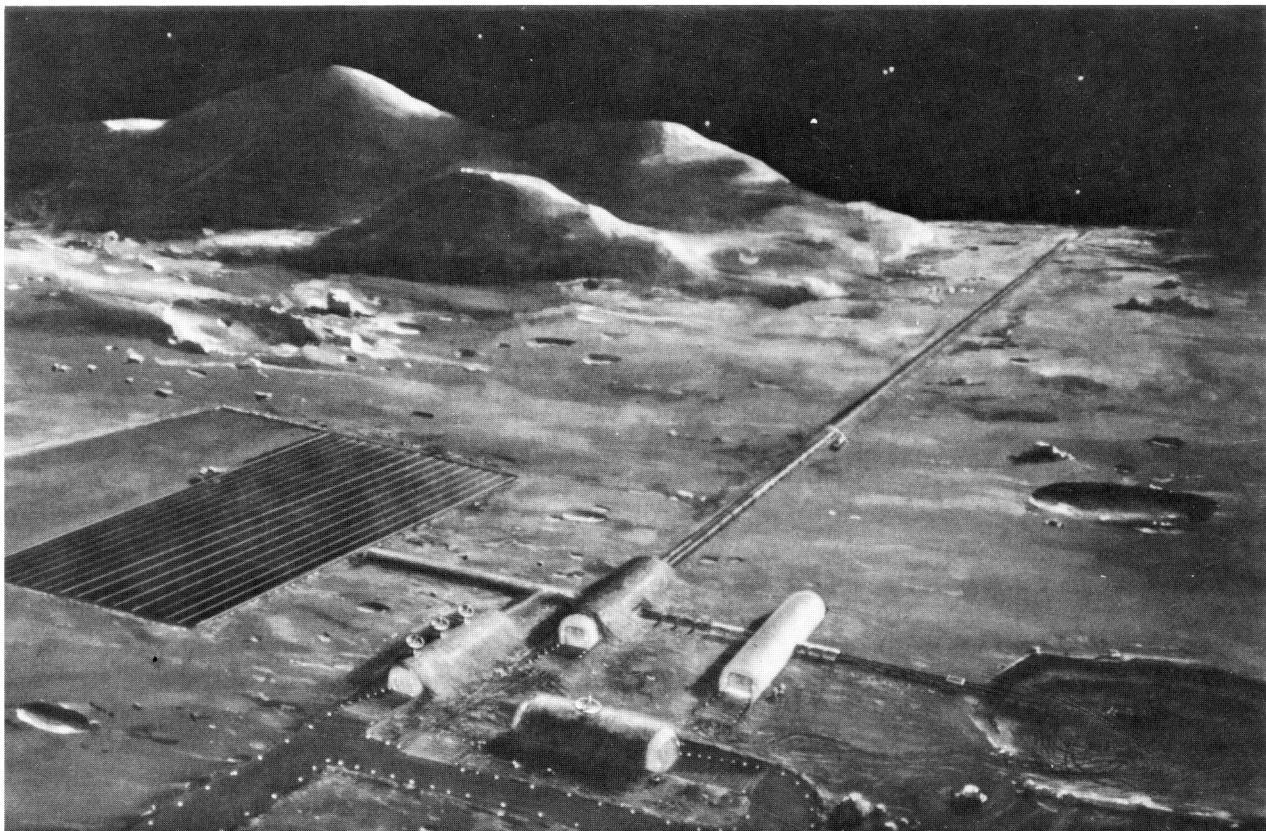
Figure 2 — *Oblique view of the initial lunar base during the second lunar day of assembly as seen from several hundred meters above the landing pad.*

Figure 2 is a painting of the initial lunar supply base during the second lunar day of installation. All major features except three large adjustable mirrors to the east, west, and north of the solar array are depicted. Upon completion of the base, the three adjustable mirrors immediately to the east, west, and north, dominate the scene. Figure 3 is a scaled schematic of the base which will assist in locating the components described in the following tour. The solar array (item 6 in fig. 3) is about 180 m on a side (10 percent efficient cells) with a mass of 108 tons. Each of the three side mirrors (180 m wide, 260 m high) is individually adjustable to focus the maximum amount of sunlight onto the solar array and catch the last glimpses of the Sun after local sunset. Most importantly, it focuses the reflected sunlight from two to four solettas (large mirrors orbiting the Moon) which provide the equatorial base at night with one-ninth the full solar illumination adequate initially to maintain continuous operation of the mining, maintenance, and life systems, but not mass driver operation. Each surface mirror can be elevated from the horizontal to face the solar array at 45° past the local vertical. Although visually imposing because of their enormous width, 70-story height, and constant visible tracking motion night and day, they are very filmy and lightweight structures with a mass of 18 metric tons including hoists (estimated by E. Bock, study participant).

Lunar base is on the Earth side of the Moon near a juncture region between Mare Tranquillitatis and the eastward highlands. At night, a pinpoint of light 8.7 km across is centered on the base and is visible from Earth as a variable star in the dark disk of the Moon. Four large, multifaceted mirrors, each 8.7 km in diameter and 240 metric tons in mass and in lunar orbits that are continuously sunlit, can illuminate the base with reflected sunlight. These orbiting mirrors are named solettas (refs. 8, 9). Continuous tracking of each mirror allows each to be sailed in its orbit about the Moon using the pressure of sunlight, so as to maintain the apolune of each soletta directly above the lunar base during the night. As seen from the lunar surface, the mini-suns sequentially rise in the west, cross the vertical meridian just higher than 30° above the horizon, and set in the east just after the following soletta rises in the west. Thus, there is a continuous input of solar energy for power, locally warming the extreme cold of lunar night and providing illumination for mining. The initial solettas were assembled in low Earth orbit from terrestrial materials, and then solar sailed to the Moon and into lunar orbit prior to the first landing of the lunar base components. The reflective area is increased thereafter using aluminum and fiberglass produced at the space manufacturing facility (SMF).

This soletta approach seems awkward on first consideration. However, the orbiting mirrors can be constructed in low Earth orbit and solar-sailed to lunar orbit without using propellant. They may also be capable of transferring significant cargo on a one-time basis. Such capability is not examined in this paper. Of immediate interest is the fact that use of solettas allows one to eliminate the need for about 400 tons of power storage equipment (example — flywheels) for nighttime operation of the base and also the 280 tons of propellant necessary to land the power storage units. Thus, the mass one transports to low lunar orbit could be decreased from 2600 tons (table 2 of Vajk et al., p. 60) to 1920 tons. It is conceivable that one can reduce the number of MDRE trips to deploy the base from LEO to LLO to two or even less by use of the solettas for illumination and possibly transport.

Restricting early mass driver operation to the lunar day, deploying a directable solar array and utilizing the solettas, enables continuous operations in construction and running of the base, minimizes the need for power storage and support machinery (the latter by a factor of 2) and greatly moderates the thermal day/night extremes at the lunar site.

Also visible from landing altitude is the 2-km-long, 5-m-wide mound of excavated lunar soil which covers the top of the tunnel containing the mass driver (item 1, fig. 3). A very slight dogleg is visible 200 m from the far end where the 3.8 kg slugs of packaged lunar soil are ejected from the deaccelerating buckets (item le, fig. 3). Three kilometers beyond is the first "Drift and Stabilization Section" (item 1f, fig. 3). At the end of the dogleg is a 100-m-diameter loop wherein the buckets are turned around and returned on a passive guideway toward the main tunnel and the loading facility. Almost all other features of the base, including the initial strip mine (item 5, fig. 3) are difficult to discern because of their small size, the blending covers of lunar soil, and the visual confusion of permanent disturbance patterns in the lunar soil resulting from the emplacement of the base and ongoing vehicular operations.

MINIMUM LUNAR BASE TO SCALE

1. MASS DRIVER

    1a. ACCELERATOR SECTION
    1b. DRIFT AND STABILIZATION SECTION
    1c. PAYLOAD RELEASE AND BUCKET DEFLECTION SECTION
    1d. BUCKET DECELERATION SECTION
    1e. RETURN TRACK LOOP
    1f. INITIAL TRIM STATION, SOLAR ARRAY AND MINI-HABITAT
    1g. FINAL TRIM STATION

2. LOADING FACILITY
3. STOCKPILE BEN
4. PACKAGING UNIT
5. TRUCKS AND HAUL-ROAD TO PIT
6. SOLAR POWER ARRAY AND SIDE MIRRORS
7. MAINTENANCE FACILITY
8. HABITAT
9. CRYOGENICS STORAGE VOLUME UNDER ONE SIDE MIRROR
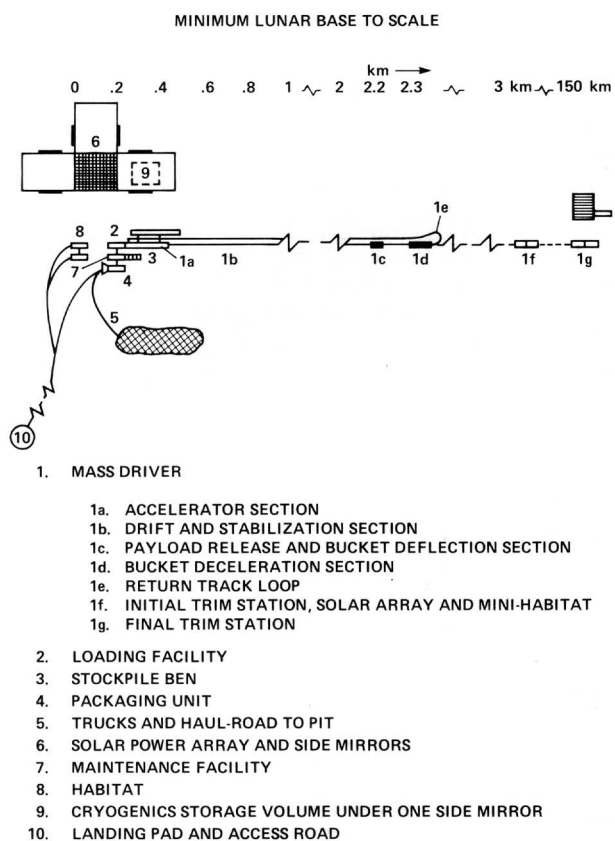10. LANDING PAD AND ACCESS ROAD

Figure 3 — *Schematic scale view (above) of the initial lunar base with main features identified.*

TABLE 2 — MASS-DRIVER SYSTEM

1. *Accelerator Section:* 300 m long, 1000 g, 3.8-kg payloads, 4-kg buckets (payload clamp and release mechanism), mass 100 tons, prefabricated as plug together 20-m units, housed in lightweight tunnel (5 m diameter) for thermal moderation and dust control, waste heat radiators, foundation points (empty cylinders with metal attachment points are buckets filled with lunar soil and binder (10%) at site, four foundation points per accelerator coil, cross-bracing above and beneath coils).

2. *Drift and Stabilization Section:* Passive guide rails, with slight lossiness to allow damping of transverse energy of the bucket, 2 km long, side and top covers to protect against dust and thermal changes, foundation every 20 m, 40 tons.

3. *Payload Release and Bucket Sideways Deflection Section:* Two bucket deceleration magnetic loops (Δv = 100 m/sec); ejection section; 1/2° deflection of bucket over 200 m (90 g side acceleration for 0.043 sec), four foundation points at each magnet section and every 2 m, 20 tons, <10/cm/sec velocity errors at ejection in all axes.

4. *Bucket Deceleration Section:* 150 m long, 2000 g (8 kg overrun capacity), thermal and dust tunnel, four foundation points per deceleration section, waste heat radiators, cross-bracing, power accumulator and electrical refeed circuits, 50 tons.

5. *Return Track:* Passive guideway with thermal and dust tunnel; foundations every 20 m except on curves (eight foundations per 40 m), final deceleration section at entry to loading area and bucket checkout bay; 70 m/sec bucket velocity, 40 tons.

6. *Initial Trim Station:* Electrostatic focusing tube located 3 km downrange of release point, 3 m in diameter and 100 m long, trim velocity to 0.1 cm/sec, 30 tons, velocity sensors and control computer, 0.16 MW at full capacity ($\approx$0.002 percent ejection energy) or 10 kW at 30,000 tons/yr, retraction hoists for focusing tube.

7. *Final Trim Station:* Electrostatic focusing tube located 150 km downrange of release point, trim velocities to 0.01 cm/sec, 30 tons, velocity sensors, 3 m by 100 m lightweight and segmented aluminum tube, 16 kW at 600,000 tons/yr, install to accept maximum capacity at once, retraction hoists for the focusing tube, solar array and power storage are located in a pit below ground level (ref. 11).

Installation physically able to eject 600,000 tons/yr, powered for initial ejection rate of 30,000 ton/yr, extensively pretested on earth and/or LEO; unitized in 20-m sections for plug-together installation. Power (96 percent efficient in electrical to kinetic energy conversion; ejection of 30,000 tons/yr at 2.4 km/sec requires 6.4 MW average input power).

Technical details of the mass driver are given in a companion paper. Here the concentration is on layout related to installation, volume, and mass. The major mass driver acceleration sections are assembled from 23 connected subsections. The coasting sections can be shipped in partially assembled condition to minimize shipping volume if necessary. All components of the mass driver system must be shielded from the extremely fine lunar dust. Thermal fluctuations must also be minimized to simplify design of the electronic and mechanical elements, maintain stable operating conditions, and prolong component lifetime. Radiation protection should also be provided for maintenance personnel. The MD system is laid out in a leveled trench 5 m wide, which is encased by heavy fiber reinforced Kevlar sheets laid directly on the lunar soil in the trench and supported on the side walls and ceiling by graphite epoxy stays (20 m formed hoops of 1 cm² cross section) every meter down the tube. Small openings are provided for ejection of the slugs and escape of gas from space suit and repair operations. The stays and Kevlar mass is less than 20 metric tons. Lunar soil is heaped over the sides and top of the trench to a thickness of 4 m (300 g/cm² column density) thus providing an extremely stable thermal environment of $\leqslant \pm 1$ K (ref. 10) and complete radiation protection for repair and maintenance workers. Portable pressure chambers are provided which can be set up wherever in the tunnel detailed repair or maintenance is required. Accelerator sections can also be unplugged and rolled down the tunnel to the maintenance section.

Bags of lunar soil ($\approx$3.8 kg) are ejected by the mass driver from the Moon. Downrange adjustment of the ejection velocity (i.e., velocity trimming) is accomplished by means of two trim stations. Each bag is electrostatically charged as it enters the trim station. In the station, electric fields parallel and perpendicular to the bag's velocity vector adjust the bag's trajectory and velocity to great precision. The two trim stations are located 3 and 150 km downrange. It is highly desirable to complete most final velocity trim (Δv) of the payloads close to the main base (ref. 11). This is because the trim energy is proportional to $1/2 \, m v \Delta v$ and will be of the order of 10 kW (m = 26.6 kg/sec, 80 percent duty cycle; v = 2.4 km/sec, Δv = 0.1 m/sec). This power is easy to obtain near the main solar array and no storage would be required. By trimming the dispersion velocity of the slugs to less than 0.1 cm/sec, the radius of the downrange guidance unit could be reduced and less energy storage and total station mass and complexity would be required at the downrange station than assumed by Vajk et al. (p. 57). Note that the solettas will not provide continuous sunlight at the downrange station.

Table 2 lists the systems features of the mass driver diagrammed in figure 3. Table 3 presents the estimated mass and power requirements of the major components. Construction of the mass driver was facilitated by the excavation of the trench by means of remotely-operated equipment deployed to the Moon following final site surveys and emplacement planning. The mass driver was fully tested in vacuum on Earth for 1 year prior to shipment. It was constructed in major 20-m sections specifically designed for "plug together" assembly with an absolute minimum of detailed work and extensively wired for remote (terrestrial or lunar base) monitoring of status, performance, and

TABLE 3 — LUNAR BASE COMPONENTS (30,000 TONS/YR INITIAL INSTALLATION)

Lunar surface		
Solar array mirrors[a]	7.2 MW	130 (tons)
Mass Driver[b]	6.4 MW	250
Trim Stations	10.0 kW	60
Loading facility (pressurizable)[b]	100.0 kW	40[c]
Stockpile bin	20.0 kW	40
Packaging unit (pressurizable)[b]	120.0 kW	70[c]
Trucks (4 vehicles at 10 tons each)	250.0 kW	40
Maintenance facility (pressurizable)	150.0 kW	40
Habitat (pressurizable)	150.0 kW	40
Binder for soils	—	50
Miscellaneous	—	40
		800 tons[d]
Low lunar orbit		
Solettas — four orbiting mirrors		
8.7 km diameter, 600 tons each		
33.3° inclination, 3000 km apolune		

a No significant power storage ($\approx$400 tons — Vajk et al., **p. 61**). Initial solettas provide night time power.

b Scale for 600,000 tons/yr — electrical components (230 MT), and 20 MT for tunnel stays and plastic coverings.

c Including 30 tons of packaging material for first year of operation.

d Consumables and crew masses discussed in separate paper.

adjustments. Major components on each section (e.g., magnets, guide rails, radiators, monitors) were designed for quick plug-in and, where necessary, mechanical attachment without intricate assembly. Subassembly maintenance was designed to be done by removing accelerator units to the pressurized maintenance shop or utilizing portable pressure chambers. Foundation points for the mass driver are provided by mixing a binding agent 10 percent by volume (imported from Earth) with lunar soil and casting the foundation blocks in situ in lightweight plastic forms with the attachment points fitted in the mold.

LH_2 tanks of the space shuttles (8 m diameter, 24 m clear length) provide pressure vessels for the four major base units: (1) habitat; (2) loading facility; (3) packaging unit; and (4) maintenance shop. Units 2, 3, and 4 were designed as emergency habitats and to accommodate the extra workers during the initial emplacement period. All these units are connected by continuously pressurized tunnels with airlocks at each end. The loading facility and packaging units were sized initially for the full production capability of the base (1.6 X 10^8 slugs/year at 3.8 kg/slug). In the automatic loading facility slugs are accepted from the stockpile bin, weighed, center of mass determined, the aluminum charging and tracking pattern sprayed on, correctly positioned, a last integrity check of the packaging performed and the slug placed in the bucket of the mass driver. The loading facility accepts buckets from the return tracks of the mass driver, offloads the buckets, checks each bucket (containment and release mechanism, superconductor temperature and field, NDT structure check, scan of sleeve in container section, adjust sleeve for payloads of different density 2-6 g/cm³) and then transfers the bucket to the loading carousels.

Subsequently, the bucket and payload are rechecked for total mass and center of mass and then transferred to the access section, equipped with a short section of superconducting guideway and accelerated into the main portion of the track at a very precise acceleration. Velocity is checked just prior to entry onto the main track and, if necessary, buckets not accelerated to the preducted velocity are shunted immediately to the return track. As needed, the passive cooling system of each bucket is refrigerated to insure the continued superconducting status of the bucket coils. Initially, the loading facility operates for 80 percent of the daytime duty cycle. It is expected that this will approach 90 percent of the full lunar month after 3 years of operation. The mass of the loading units is 40 tons and they consume 100 kW during initial daytime operations and 30 kW at standby.

Between the loading facility (item 2) and the packaging unit (item 4) is a stockpile (item 3) capable of holding a 10-day reserve of slugs (30,000 ton/yr launch rate). The bins are top-loaded and bottom-emptied by conveyor units that can sort slugs by length corresponding to different densities (2-6 g/cm³) of packaged material. All slugs are the same diameter. The bin is about 60 by 6 m and weighs 40 tons complete with conveyors. This unit is not pressurized, but is emplaced in a trench roofed with Kevlar over stays and covered by 3 m of lunar soil.

Packaging of each slug is accomplished by compressing 3.8 kg of material to 500 bars pressure (about twice the base-pressure in the slug at 10^4 m/sec² acceleration) and then sealing in a 2-μm thick package of Kevlar which is then aluminized. Approximately 2 bars of bag tension is provided. Material compression requires 17 kW at the 30,000 tons/yr production rate. All grains packaged are less than 1 mm diameter. It is estimated the packaging unit may consume as much as 400 kW during full operation. Each slug is weighed and sized prior to delivery to the stockpile conveyor. In addition, the packaging units accept bulk soil from the two excavation trucks, screen the soil to remove nonfriable rocks larger than 1 mm, and dump the larger rocks by means of conveyors, in a small crater or returns them as fill to the soil pit.

The initial soil pit operation is very small by terrestrial standards. The solettas allow continuous operations and one small truck (10 tons inert mass, 30 ton payload) is able to satisfy the 30,000 ton/yr input requirement with 3 to 4 trips per terrestrial day, allowing only 80 percent availability. Considerable time is available for hauling. Three other vehicles are available and are generally involved in site preparation for expansion of the base, including leveling for future solar cell arrays and trenching for new facilities. Most of these highly repetitive operations are controlled from Earth. These trucks were used extensively in the emplacement operation and will receive far more use as the base expands. A conveyor system is to be introduced to accommodate the 600,000 tons/yr operation. Naturally, the remotely operating machine used for the preparatory excavations prior to manual landings has been dispatched on a route of unmanned scientific exploration. All the vehicles

are powered by flywheels scaled to about 150 kW output. Repowering is provided from the main solar array (Vajk et al., p. 57).

Maintenance and repair for the trucks, major sections of the mass drivers, and other equipment, is done in a pressurizable and outfitted hydrogen/oxygen shuttle tank (item 7, fig. 3). It is equipped with a large air lock which can accept 3-m-diameter objects and has a clearable depth of 22 m. The back bulkhead contains an air lock and covers a bunk area and control system for depressurization operations and equipment which should not be subjected to vacuum. A 100-m-long approach ramp allows truck access to the main air lock and is stabilized with a binder to minimize dust entry to the maintenance facility. Mass of the facility is about 40 tons and it draws an average 150 kW.

Cryogenics storage (item 9, fig. 3) is provided in the permanently shadowed area under the eastward-facing mirror attached to the main solar array. Chemical rockets touchdown on a 100 m diameter landing pad (item 10) of stabilized lunar soil located 5 km to the south. Stabilization is required to prevent dust disturbance which obscures the landing and might coat the solar array and heat radiators at the lunar base. There are stabilized haul roads between the landing pad, maintenance and loading facilities, packaging unit and the pit (item 11).

The Habitat (item 8) is the residence and communications and control center of the base. It houses the 10 personnel who stay on station for 6 months, but 50 percent of whom are rotated every 3 months, either to Earth or to the space manufacturing facility (SMF). In effect, the lunar crew is an extension of a terrestrial control center which operates and monitors equipment round-the-clock for both site preparation operations by the remotely-controlled excavators and mass-driver operations. No estimate is provided here of the necessary terrestrial manning level. It is noted that studies of the degree of possible automation and man-hours/operating hours of the major lunar units are required and afford a very real opportunity for spinoff to many economically significant tasks on the Earth. Possible examples of terrestrial application include development of remote operation of Earth moving equipment for excavation and leveling, systems monitoring and control of undersea oil production or glass production, quality inspection of agglomerated materials (encased) by thin films. Joint NASA/industry workshops on specific topics would clearly be appropriate. There is high bandwidth continuous communications between the terrestrial center and the lunar crew complete with a full-color, wall-sized television system for weekly staff meetings between the entire lunar crew and the terrestrial staff and, as necessary, the staff at the SMF. Basic functional volumes in the habitat are: (1) communications and control center; (2) main (TV screen) and adjacent recreational rooms; (3) galley and dining area; (4) 12 private rooms; (5) storage locker; and (6) the life-support room. The habitat is similar in design to those employed in low Earth orbit and at the SMF with modifications necessary for horizontal emplacement beneath the lunar surface.

Two unmanned trim stations (items 1f and 1g, fig. 3) are located 3 km and 150 km downrange from the mass driver. Only the long, but lightweight correction tube is present above the surface at each station. Some consideration was given to placing the trim stations behind revetments. However, occasional misses by 3.8 kg slugs moving 2.4 km/sec generate large craters and would require major revetment repairs. Instead, the supporting mechanisms for the initial correction tubes were designed to pull the correction tubes into a trench and beneath the surface in 1/20 sec if a bag is observed either to rupture or to be badly off course on leaving the mass driver. Small blast deflectors are designed into the front of each of the trenches to insure that all the debris will pass over the recessed correction tube.

The lunar supply base would offer a viewer a slowly changing scene of mirrors following the Sun during the day and the solettas at night. The steady expansion of scratch marks on the lunar surface by the mining operation contrast to the occasional quick hops downward by the 100-m-long, but lightweight, correction tubes to avoid certain destruction by a direct hit by one or more misejected bags of lunar soil. The fast action, the packaged slugs of soil leaving the Moon at 2.4 km/sec, would not be visible until the launch rate exceeded 4 or 5 per second. At that time one could stand underneath the entry tube to the first trim station and see a sparkling line of light, something like a stream of water, wobble its way into the mouth of the correction tube. On exiting, the stream would be rock steady and point arrowlike to the eastern horizon and the location of the final trim station. Persistence of vision would tie the thousands of separate slugs into a faint pipeline of light leaving the Moon. A strobe light shining across the exit mouth of the initial trim station could be flashed in synchrony with the exiting packages of soil to produce the visual illusion at night of a single, slightly blurry bag of soil suspended above the ground. Of course, over the interval of 1.25 min the illusion would be composed of the reflections from about 1000 soil packets at an ejection rate of 600,000 metric tons each year.

IMPLACEMENT STRATEGIES

Five general considerations influence the design and operation of the initial base suggested in this study: (1) need for continuous operation in order to minimize the size of the initial and final base; (2) maximum use of remote control and assistance from a terrestrial control center of as much of the process monitoring, equipment status, vehicle guidance (e.g., mining), administrative assistance, and problem analysis as is possible; (3) all initial units should be constructed as separate plug-together units which are as large as possible and still convenient to land, manipulate, and place and plug together in the quickest possible time by a minimum crew; (4) the mass driver, sieving/packaging units should be scaled to handle 600,000 tons/yr; and (5) the basic operating crew should have as their main functions maintenance and site preparation for future expansions. All aspects of the design, emplacement, and operation of the base are greatly facilitated if continuous sunlight is available at the base. Thus, four 8.7-km-diameter mirrors in

continuously illuminated orbits about the Moon are assumed to be operational before emplacement of the first major units of the base. These mirrors are discussed in the "Soletta" section.

Expansion of throughput by a factor of 20 (from 30,000 to 600,000 tons/yr) can be accomplished through three steps: (1) steady additions of nine more 7.2 MW solar arrays (each supplemented by three surface mirrors); (2) addition of a mineral separation facility, haul trucks and a fiberglass/aluminum facility for the production of bags for packaging the soil slugs; and (3) enlargement of the orbiting mirror arrays to provide constant solar illumination during the lunar night. Total mass of the mature lunar operation should be less than 3000 tons on the lunar surface and 8640 tons of solar reflectors in lunar orbit. Total base personnel should increase to about 50 at the end of the 5-year growth phase, requiring additional habitats.

The following scenario for deployment of the initial base following site selection is predicated on the extensive development and checkout on Earth and possibly in Earth orbit, of the unitized (plug-together) base which is shipped as two major freight subsystems from low Earth orbit (LEO) to low lunar orbit (LLO) by the first mass-driver tug. The mass-driver tugs have payloads of approximately 1300 tons from LEO to LLO. Similar problems were faced in development of the petroleum fields on the North Slope of Alaska. Habitats weighing up to 800 tons were preassembled in Seattle, Washington and shipped to the North Slope and installed in 4 months on prereadied sites (ref. 12).

Each freight unit is soft-landed (300 to 600 tons) as a single unit following LLO insertions (ref. 13). Freight unit no. 1 contains two automated (Earth-controlled) excavation units. On landing, these units unload themselves, assist in unfurling from the landing vehicle two 150 kW solar arrays, which operate electrolysis units for regeneration of fuel cell hydrogen and oxygen (or recharging flywheel power units), and then proceed for the next 7 months under terrestrial control to make the major leveling excavations for the mass driver, processing units, large solar array, and habitats. These excavation units will be operated exclusively for site preparation for the 5-year period of base development. The mass driver immediately returns to Earth after deploying the first freight unit. Freight unit no. 2 and the construction force of 25 persons (personnel transported by chemical rocket from LEO) arrive 7 months later and begin emplacing the various units over a 4-month period. The orbital mass-driver tug immediately returns to Earth after deploying two catcher/freight units at L2.

Base construction would consist of the following deployment sequence: (1) on lunar day 1 — habitat and maintenance emplacement and coverage, start of solar array emplacement, layout of the 23 major accelerator units and 200 coast sections of the mass driver along the excavation for the track; (2) on lunar day 2 — emplacement of the solar array completed, mass-driver layout completed, assembly of the thermal and dust tunnel progresses with mass-driver assembly, assembly of the initial trim-facility completed, and emplacement of the screening/packaging facility completed; (3) on lunar day 3 — crew of 6 translates to the site of the final trim facility to prepare the site and emplace the unit (2 lunar days for job), assembly of mass driver is complete and alignment and test shots are made following completion of work at the remote site and deployment of surface mirrors is started; and (4) on lunar day 4 — emplacement of surface mirrors and the final trim station is completed and full operational tests are conducted. At the end of lunar day 4, the remote crew returns to the lunar base and the 15 construction workers then return to Earth. At the start of lunar day 5, 1 year after touchdown of freight unit no. 1, the lunar base is ejecting during the day bulk lunar soil to the two catcher/transporters which can transfer 2300 tons/lunar month of bulk lunar soil to the SMF by 1 year after the start of lunar base construction. This soil will be useful for reaction mass, shielding, checkout of the mineral dressing and chemical processing equipment, oxygen generation, and fiberglass production.

INCREASING CAPACITY AND DECREASING UNIT COSTS

Increasing the capacity of useful material ejected to deep space requires: (1) the addition of nine more solar arrays, (2) introduction of soil separation and beneficiation equipment, (3) an increase in the hauling capacity from the mining areas to the soil processing unit by a factor of 40 to 60, (4) the emplacement of a waste material dump system (very likely a fixed conveyor dumping into a small crater), and (5) enlarging the orbiting mirrors by a factor of 9 in area. It is possible that the availability of lunar samples will permit the design, construction and deployment of electrostatic separators as part of the initial soil sieving and packaging unit. If not, the separation units can be added. Installation of the separation unit will allow one to send only the most useful component (83 percent anorthite, 19 percent ilmenite) of the lunar soil to space, and thus maximize raw material input to the SMF for manufacturing Al, Si, O, Ti, and Fe. This will be equivalent to a factor of 3 to 4 increase in the delivery rate of economically useful materials. Trucks and/or conveyor systems necessary for increasing the haulage capacity, can be delivered yearly from Earth. Trucks and conveyors adequate for the task will have a mass less than 60 tons (Williams et al., p. 219).

It is assumed that most of the solar cells and reflectors (surface and orbital) for the additional power units will be produced at the SMF from processed lunar materials and delivered to the Moon for installation. Preassembly and checkout at the SMF of these units is assumed so that only site preparation and deployment will be required of the lunar crews. The costs of all of the additional arrays (factor of 20 increase in power) should be less than the cost of the original 7.2 MW unit. It is possible that the additional solar arrays will be center-mounted on tall support columns and actively directed toward the Sun. This involves much stronger support columns than the mirrors, but almost eliminates site preparation, makes tracking of the solettas more precise, and maintains a lower temperature for the array.

Cost per unit (\$/kg) of the delivered materials can be progressively reduced by: (1) installation of a plant for the production of a bagging material made of fiberglass/aluminum composite; (2) use of liquid oxygen produced in space from lunar materials and stored in low lunar orbit for the lunar landing rocket; (3) recovery at the lunar surface of hydrogen and oxygen from lunar fines (see Williams et al., p. 219); (4) facility for the fabrication of pressure vessels, structural materials and other redundant items from the fiberglass/aluminum composite and locally produced ceramics and glasses (especially foundations and stabilized soils); and (5) increasing the "closure" ratio of the life-support systems. By the end of year 5 of base operations, the operating costs should be dominated by crew rotation costs, salaries and maintenance expenses (excluding capital investment of further expansion operations).

Approximately 1 ton of liquid oxygen is required to land 1.2 tons of payloads on the lunar surface from low lunar orbit and return a lunar shuttle to low lunar orbit (Vajk et al., p. 57). It is not clear at this time whether the oxygen production can best take place at the SMF, the lunar base, or both, but any of these options in effect increases the useful payload fraction of mass driver freighter to the Moon by a factor of 2. Thus, very large cost savings are possible by quickly initiating production of liquid oxygen from lunar materials for use in operations between the lunar surface and low-lunar orbit.

PACKAGING OF THE LUNAR MATERIALS

Each unit of lunar soil ejected from the Moon must be contained in a thin, aluminized packet. This packet must contain the powdery material for mechanical handling, prevent breakup of the slug and dust generation during ejection by the mass driver, and accept uniform electrical charging for electrostatic velocity trims and high radar and optical reflectivity. In addition, there must be uniformity of packaging from one slug to the next with respect to trajectory perturbations by light pressure, the solar wind, and magnetic and gravity gradients. The packages must break apart uniformly for removal of the encapsulated material, and the packet material should be useful for either recycling to the Moon or in some other derivative application. Packaging must be done in a vacuum so that no outgassing will occur during the coasting phase which would perturb the trajectory of the slug of lunar material. The total mass of bagging material used each year ($\breve{M}_b$) is related to the total mass of lunar material to be ejected each year ($\breve{M}$) by

$$\breve{M}_b = 2\breve{M}(\rho'/\rho) \bullet (\Delta P/Y) \, [(4 + L/R)/(L/R - 2/3)]$$

for cylindrical slugs (ignoring slight taper of the cylinder of soil) with hemispherical end caps where R is radius of the cylinder, L is the length of the cylinder, ΔP is the pressure the bag applies to hold the slug of soil together, Y is the yield stress of the bag material, ρ' is the density of the bagging material, and ρ is the density of the compressed lunar soil. Thus, to first order the required mass of bagging material is independent of the size of the slugs (m) made of the ejected Itmar material. The mass of one bag (m_b) is simply

$$m_b = \breve{M}_b/\breve{N} = \breve{M}_b \, (M_s/\breve{M})$$

where N is the number of slugs produced each year.

Bag pressure will be adjusted to about 2 bars (a factor of 10 in bag yield strength is included for safety), the bulk lunar soil compressed to a density of about 2.2 g/cm³, and $L/R \approx$ 12.66 for the present lunar mass driver. The compression requires a pressure of about 500 bars and is twice the pressure the lunar material will experience at the base of the slug during the 10^4 m/sec² acceleration from the Moon. There should be negligible rebound of the material following acceleration termination or ejection from the bucket. Grinding between soil grains in the bag should provide a sink for vibratory and compressive disturbances during launch and release. A continuous power supply of about 17 kW is needed for the compression of 30,000 tons/year of slugs. Clearly, the bagging material cannot sustain the full stresses of the 1000 g (±60 g's transverse) launch environment. It is assumed that the bucket will be designed to securely contain the bag of soil against these accelerations without tearing the bag, permitting a smooth axial release of the bag at the launch (ejection point) and a means of containing bags which do not eject.

In order to keep the base design and functions simple at first, it is appropriate and economically reasonable to import the packaging material from Earth. A high strength synthetic such as Kevlar ($Y \approx 34,000$ bar and $\rho' \approx 1.5$ g/cm³) seems completely adequate. The total mass of bagging for 30,000 tons of ejected mass would be about 33 tons. This is an acceptable penalty for initial operations. However, as the operations increase in scale, it becomes desirable to install a plant on the Moon to produce an aluminum/fiberglass composite sheet. It is assumed that the fiberglass will be produced on the Moon and the aluminum returned from the SMF by the start of the second year of operation of the lunar base. Assuming the composite has a yield stress of about 10,000 bar (ref. 14), then one must manufacture 2.2 kg of packaging material on the Moon for every ton of ejected materials or 1320 tons/yr for 600,000 tons/yr of ejected material.

Details of lunar fiberglass production from lunar materials are discussed in a companion paper (Ho and Sobon). A 10-20 percent increase in the capacity of this production facility and the addition of fabrication shops would permit the construction of a large number of items for subsequent expansion of the lunar base such as large pressure vessels, structural fiberglass composites, electrical cable, glass and ceramic structural elements, pipes, acoustic panels, and so on. A fiberglass production facility adequate to produce 3000 tons/yr of finished fiber should have a mass of less than 100 tons. Lay-up and fabrication facilities should have a mass of about 70-100 tons. Refer to Criswell (ref. 15) for a general outline of material flow for production of bags on the lunar surface.

LUNAR BASE POWER REQUIREMENTS

Ideally, all operations concerned with the lunar mining and mass ejection should be conducted continuously with only scheduled maintenance shutdowns. In this manner the base could be about one-half the size required for an operation conducted only during the lunar day. Continuous operation is only possible if a source of continuous power is available. Continuous power could be obtained by increasing the size of the solar array and storing power for nighttime operations in fuel cells, flywheels, or batteries. Flywheels appear to provide the highest energy density and infinite recycling but impose a weight penalty slightly less than 1.2 to 1.3 kg/kW-hr including transport fuel for delivery to the Moon (P. Vajk, p. 57). Other schemes, such as a nuclear power plant (legal problems) or a space power platform beaming microwaves to the Moon (depend on start of SPS production) appear less than optimal initially. It is suggested here that mirrors orbiting the Moon and reflecting sunlight to the base during lunar night may be a reasonable solution. First, an overview of the power consumption is presented.

The major blocks of power which must be provided for operation of the minimum base are, first, for the ejection of 30,000 tons/yr (0.967 kg/sec continuously) of material during the lunar day (0.5 duty cycle of the lunar day) and, secondly, for the mining and packaging operations which are best conducted continuously (Williams et al., p. 219). Notice that 2.9×10^6 J/kg are required to accelerate material to the 2.4 km/sec ejection velocity. Assuming the mass driver is 96 percent efficient in converting electrical energy into ejection energy and 10 percent of the daytime ejection period (0.9 operating fraction per terrestrial day) is lost due to maintenance downtime the average input power ($P(MD)$) is:

$$P(MD) = \frac{[(0.967 \text{ kg/sec}) (2.88 \cdot 10^6 \text{kg/sec})]}{[(0.5)(0.9)(0.96)]}$$

$$= 6.4 \; MW$$

Approximately 2.2×10^9 W-hr are required during each lunar day for mass driver operation. It is clear that the mass driver control system must be designed to accept a continuously changing launch rate of payloads in order to avoid the penalty of very large power smoothing units. Base operations are anticipated to require the following units of power: Habitat $\sim$ (16 kW/person, 10 persons) $\approx$ 160 kW; trucks $\sim$ 250 kW; sieving, packaging, and maintenance facility and miscellaneous power requirement $\sim$ 400 kW for a total continuous input of P(B) = 800 kW. About 5.4×10^8 W-hr of electrical energy are required for operation of the base, exclusive of the mass driver, each lunar month. This corresponds to 20 percent of the total monthly power input of the solar array. Thus, the average daytime power requirement is P_0 = 7.2 MW, whereas the nighttime requirement is about an order of magnitude less at $P(N)$ = 0.8 MW.

It is assumed that the power will be provided by a solar cell array (E = 0.1 efficient in solar to electrical energy conversion efficiency including power conditioning; 15

tons/MW area power density). Two innovations are suggested to minimize the size of the solar array and the capacity of power storage devices (e.g., fuel cells, flywheels). First, the solar array will be surrounded on three sides by three lightweight mirrors which are independently adjustable from the horizontal to 45° local vertical. These mirrors are of width equal to that of the side length L_s of the square array and a length of h = 1.414 L_s. Second, two to three orbiting mirrors will provide reflected sunlight during the lunar night adequate to operate the base (0.8 MW), but not the mass driver. By the third year of base operations, these orbiting mirrors (solettas) can be increased in size by a factor of 9 using fiberglass and aluminum from the SMF; this will permit operation of the mass driver during the lunar night and thus increase the mass ejection capacity of the base by a factor of 2 with little or no additional ground installations.

Figure 4 depicts the power profile for the solar array/mirror system augmented by soletta illumination at night. Region 1 corresponds to a sine dependence of the power output of the flat solar array, between sunrise and sunset. The total watt-hours (WH) output in region 1 is $(2/\pi)P_0L_d$ (length of lunar day) where P_0 = 7.2 MW. Actually, the sine distribution of output power would not be realized due to increasing external reflection and scattering of the incident sunlight back to space as the illumination angle of the solar cells approached the horizontal (0°). However, use of the mirrors greatly improves the power input because the sunlight is then never incident on the solar cells at less than 45°. Continuous adjustment of the elevation angles of the mirrors on the western and eastern edges of the solar array allows the reflection of sunlight onto the array to produce additional power in region 2. Lunar reflectors are effective whereas times-2 solar concentrators are not competitive with solar cells alone for space power stations since they can be continuously directed toward the Sun (ref. 16). The Lunar case is different in that the "times-2" concentration need only occur (optional) about lunar noon. Otherwise, the concentrators suggested here simply maintain the solar radiation to the solar array at a high value ($\geq$l solar constant) throughout the lunar day. Let E (=0.1) be the
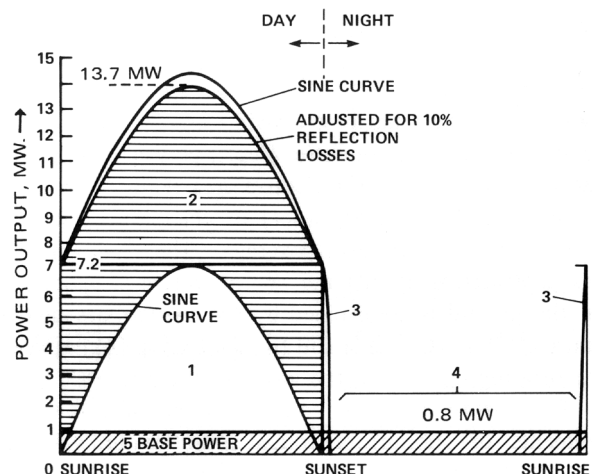

Figure 4 — *Power profile of the lunar base during a complete lunar month (power consumption in megawatts, vertical axis; time past sunrise, horizontal axis).*

conversion efficiency of solar energy into electrical output of the array and allow for 10 percent average reflection losses (c) at the mirrors and the surface of the solar array, then we can estimate the area (A_s) of the solar array (where $P_s = 1.4 \times 10^3$ MW/km is the solar constant) to be:

$$A_s = (P_0/P_s)/\{[1 + (1 - c)(2/\pi)]\ E\}$$

For the stated values of the quantities in the equation we have

$$A_s \sim 0.0327 \text{ km}^2, \quad L_s = 181 \text{ m}$$

The mass of the solar array would be 108 tons. The mass of the three adjustable mirrors, support beams and hoisting mechanisms would be about 18 tons (E. Bock, Convair, San Diego) using two compression beams and side beams for each mirror and cable hoists. Reflectors are useful for power conditioning on the lunar surface, in spite of the large area of the reflectors, due to low gravity and lack of weather and weathering effects. This approach would be impractical terrestrially. Major future considerations in evaluation of this approach are (1) effects of running the solar cell array at two solar concentrations for about 1/4 of the lunar day and (2) conditioning of the front surface of the solar arrays to minimize reflection of sunlight at small angles of incidence. Alternatively, it may be advantageous to center-mount the array (or a segmented array) on a tower of height one-half the length of the array and point the array continuously toward the Sun or the particular soletta providing nighttime illumination. Use of a tower would allow the solar cells to operate at lower temperatures during the lunar day.

Region 3 (sunrise and sunset) corresponds to either the east or west mirror viewing the Sun while the general terrain is dark. Some power can be received during this time due to the slow rotation of the Moon and the large height of the mirrors ($L_h \approx 260$ m). The time interval (t_i) between sunset at the base and the top of the mirror at the equator for a spherical moon is given by

$$t_i = \frac{\text{arc cos}\left[\dfrac{1}{1 + (L_h/R)\cos\phi}\right]}{\dot{\theta}}$$

where $\dot{\theta} \sim 0.53°/$hr is the rotation rate of the Moon, $R = 1738$ km (radius of the Moon), L_h is the vertical dimension of the array, and ϕ the angle of the mirror with respect to the direction to the local sunset direction ($=45°$). Thus, for $L_h = 260$ m we have $t_i = 1.57$ hr. The pre-sunrise and post-sunset operations can add as much as

$$2 \times (1/2)\ (7.2 \text{ MW})\ (1.57 \text{ hr}) = 0.11 \times 10^8 \text{ W-hr}$$

Large elevation differences are available in the lunar highlands. It is not unreasonable to expect that one could locate mountain peaks within 30 km of the base site which might be 2 km higher than the base. The peaks would be exposed to the Sun at least 5.2 hr longer than the base and possibly much longer if the local eastern and western horizons are significantly depressed below the horizon of the spherical Moon. Reflectors on the scale of 600 m (length) by 300 m (height) adjustable over 95° azimuth could contribute

at least 0.74×10^8 W-hr to the nighttime power budget or increase the operating time of the mass driver by 3 percent or more. Such surface mirrors could contribute 2 percent to 14 percent to the estimated nighttime energy budget of 2.7×10^8 kW-hr indicated as region 4 in figure 4, depending on local geometry.

An interesting option to conventional solar cells may be available for use on the Moon by using photoemission and/or thermionic emission. The basic power unit would consist of three aluminum strips which could be vapor deposited on the bottom and sides of a rectangular trench (possibly 3 or 4 cm wide and deep, and about 1 m long). The trench, one of tens of thousands of identical closely spaced trenches, would be oriented with its long axis in the east-west direction. The bottom of the trench would next be evaporatively coated with a photoemissive/thermionic material. Sunlight would produce a flow of electrons from the trench bottom to the sides evoking a small potential difference which can be regulated to control the current flow and thus maximize the power output. The mass of the aluminum and electron emissive materials required would be trivial compared to the equivalent areal mass of solar cells, whereas the mass of ancillary parallel and series hook-up wire and power conditioning equipment should be similar to that needed for solar cells. Conversion efficiencies of about 5 percent are thought to be possible (ref. 17). This photo-similar effect is likely to operate naturally on the Moon in the levitation of lunar dust (refs. 18, 19). Further experimental and theoretical research is needed and should be given high priority for application not only to lunar surface operations, but also for possible space power systems which could be constructed largely of lunar materials.

As noted earlier, about 400 tons of power storage units (1.2-1.5 kW-hr/kg) would be required to power the station over one lunar night. In addition, about 300 tons of propellant would be required to soft-land the extra mass. Finally, as base activities increased, the storage capacity would increase linearly with the scale of nighttime operations. Total mass of power storage units could approach 6000 tons on the lunar surface and 4000 tons of propellant in LLO for delivery. For these reasons, the alternative approach of deploying large mirrors in lunar orbit which could power, illuminate, and warm the base at night and permit 24 hr a day operation even during the lunar night, is suggested.

SOLETTAS

Billman et al. (ref. 9) and Ehricke (ref. 8) both proposed that large mirrors be orbited about the Earth to illuminate cities, agricultural regions, ice fields blocking navigation, and solar power installations. Orbiting mirrors are far better suited for lunar than terrestrial use due to the absence of a lunar atmosphere, availability of continuously illuminated lunar orbits, the long period of such lunar orbits, relatively small change in slant range during the illuminating period, and the option of precessing the apolune of each mirror over the cycle of the lunar month in order to keep the apolune over the longitude of the lunar base (David Ross, Stanford Univ.,

Aeronautics and Astronautics Dept., personal communication). The amount of reflective area required in space is independent (to first order) of the altitude of the solettas for continuous coverage. The fundamental design constraint is that the minimum size of spot (D_S) on the ground is determined by the angular size of the Sun ($\alpha = 9.3 \times 10^{-3}$ rad) and the slant range (h) between the orbiting mirror and the ground spot where $D_S = h\alpha$.

The mirrors must be constructed of individual flat segments or submirrors which must be individually directed toward the desired ground spot. Submirror size is limited by the required flatness of the mirror surface. The segments can be directed toward a reference laser beam at the receiving site. For one solar constant of illumination the mirror must be the size of the ground spot; therefore, the diameter of the mirror (D_M) will also be $D_M = h\alpha$. In the lunar case the use of the three movable mirrors on the ground (or a tilting solar array) which surround each solar array will permit considerable smoothing and effective concentration of the solar power to the array in response to non-normal incidence of the sunlight reflected to the site by the orbiting mirrors. The three ground mirrors become more effective as the maximum viewing angle of the orbiting mirrors above the local horizon increases. Use of ground mirrors or tilting arrays avoids increasing the size of the orbiting mirror above $D_M = h\alpha$. However, attention must be given to array spacing on the lunar surface as the ground installation grows in order to insure that there is no significant shadowing of portions of the array by foreground units.

The suggested lunar system consists of four solettas trailing each other along a high inclination, low altitude orbit. It is assumed the initial solettas are sized to provide one-ninth solar illumination (average) to the arrays to power the lunar base through the night. These one-ninth solettas would be constructed in low-Earth orbit from components supplied from Earth. Figure 5 depicts the low altitude, high inclination orbit. In this example, the average slant range is 2800 km and $D_S = D_M = 26$ km. For the initial one-ninth solar illumination at the base $D_S = 8.7$ km. A slight increase of the eccentricity of this orbit would permit overlap of the viewing periods (57.2 min; 24.4 percent of the orbit). Decreasing the inclination of the orbit increases viewing time but also the slant range to the base and therefore requires an increased mirror size.

Four mirrors, each about 40 km² area (240 tons per mirror at 6 g/m²), could meet the overnight power needs of the base and prevent the extremely prolonged cold soak of lunar night by providing one-ninth the full solar constant. For an orbit with a perilune of 500 km, apolune of 1610 km, and inclination of 33.3°, each mirror would rise in the southwest (or northwest), attain a maximum elevation of 20° in the south (or north), set in the southeast, and be visible above the horizon for 57.2 min per orbit (24 percent of the 3.9-hr orbit). The projected spot from such a satellite would be extremely elongated due to the low sighting angles. However, the three ground mirrors could be continually reconfigured to reflect soletta light into the collecting array thus obviating the low illumination angle. Assuming the launch costs ($650/kg) to an Earth orbit of altitude greater than 1000 km dominate the production and assembly costs of the mirrors, an investment of $624 million would be required for the initial orbiting network. This cost could be reduced sharply by utilizing the aluminum in shuttle tanks in the mirror structure. Savings in base construction time, continuous equipment usage, and minimization of power conditioning and storage should justify the expense. The mirrors would transport themselves by solar sailing from

GIVEN: 2 = 1738 km
1 = 500 km
⑦ = 1838 km
θ = 30°

THEN φ = 33.3°
3 = 3348 km
4 = 555 km
5 = 2793 km (SEMIMAJOR AXIS)
6 = 2122 km (SLANT RANGE AT APOLUNE)
8 = 1055 km

9 = 2737 km SEMIMINOR AXIS
ψ = 43.9° ~ HALF ANGLE OF VISIBILITY
⑩ ~ POSITION OF THE LUNAR BASE

SUMMARY SEMIMAJOR AXIS — 2793 km (a)
SEMIMINOR AXIS — 2737 km (b)
ECCENTRICITY = c/a = 0.1987
FOCUS DISPLACEMENT = 555 km
INCLINATION = 33.3°

VISIBLE PORTION OF THE ORBIT

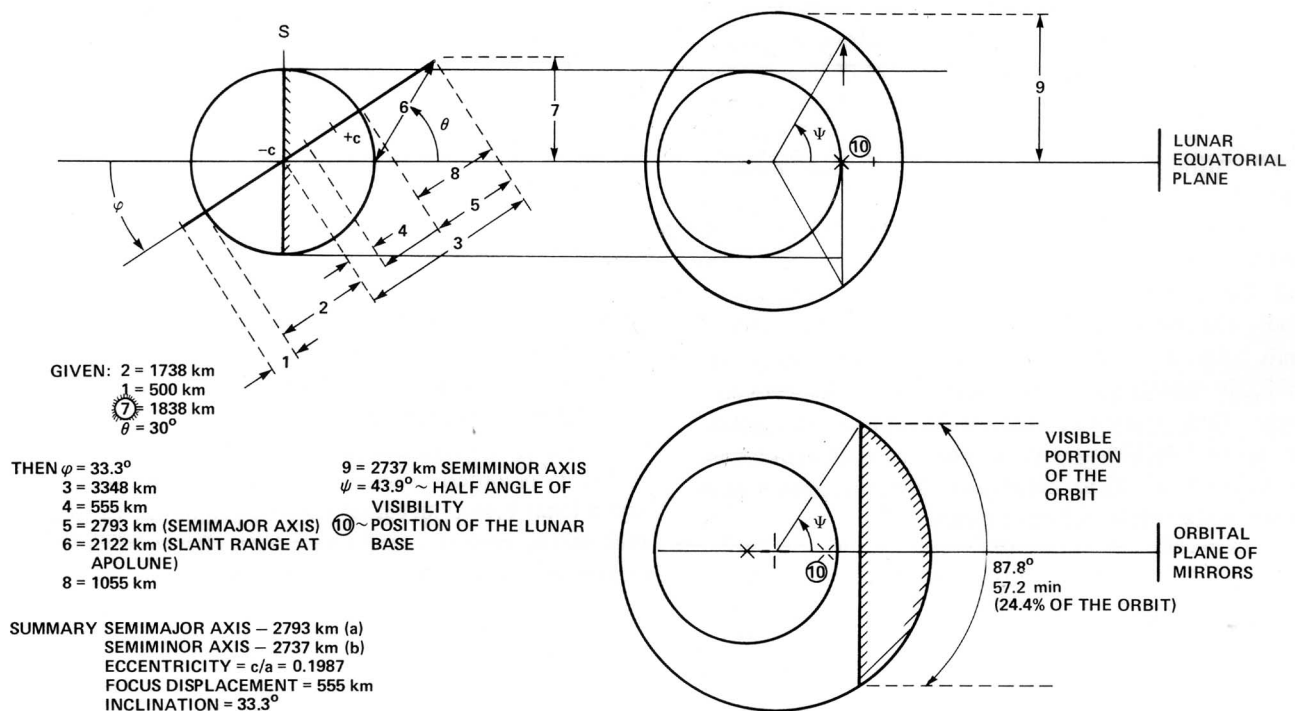ORBITAL PLANE OF MIRRORS

87.8°
57.2 min
(24.4% OF THE ORBIT)

Figure 5 — *Three views of a low altitude soletta orbit about the moon. Four 8.7-km diameter solettas would be required to provide overlapping illumination of the base with one-ninth solar constant input to the solar array.*

Earth orbit to low lunar orbit and might be used to transfer significant payloads as well to lunar orbit depending on the time constraints. It will be necessary to continually track and solar-sail the solettas. There must be a continual reconfiguring of the individual submirrors during the lunar daytime portion of the orbit and when the base is on the day side in order to utilize solar pressure to maintain the proper orbital elements. Presumably this can be a highly automated process.

NASA programs for solar-sail development have established the characteristics of a large space mirror constructed out of aluminum and plastics which could be deployed in the mid-1980's. Areal densities as low as 6 g/m² can be expected (refs. 20-22). Thus, one low altitude soletta providing full solar illumination at the lunar surface would have a mass $M_S = (6 \text{ tons/km}^2)(\pi/4)(26 \text{ km})^2 = 3185$ tons. Extensive use could be made of fiberglass and aluminum from the initial production runs at the SMF to produce the full size solettas for final production expansion of the lunar supply base. If a technique can be developed to produce thin-film aluminum without a substrate, then very little material would have to be brought from the Earth. The solettas could be sailed directly from the SMF to lunar orbit without the expenditure of reaction mass or energy.

The relative efficiency of the solettas in providing energy increases as the size of the lunar base increases to fill the 26-km diameter of the minimum illuminated spot. The initial installation on the lunar surface utilizes only 9×10^{-5} of the incident sunlight and the 600,000 tons/yr installation 2×10^{-3} of the incident sunlight. Thus, a soletta system could support the ejection of up to 3.4×10^8 tons/yr of lunar material with a base installation of 45 to 50 percent less total mass than without the orbital reflector system.

CONCLUSION

Construction of a lunar supply base in support of suggested scenarios for space manufacturing (refs. 23-24) does not appear to present insurmountable problems. The main challenge is in reducing the overall costs, development and deployment times and designing highly automated systems capable of maintaining continuous high throughput of soil into space. The main research items are in the direction of enhancing rather than enabling base deployment and operation. Specific research and development objectives include the following:

1. Preparation of the site of the base by remotely controlled excavation equipment.
2. Determination of reasonable designs for maximum unitization and pretesting of base units for minimum time of implacement.
3. Determination of schemes for remote monitoring and control base operations to minimize base personnel and to maintain highly reliable performance.
4. Development of one-ninth solar illumination solettas for continuous operation of the base and full-scale solettas which would utilize lunar materials for the bulk of the mirror structure and reflective surface.

5. Production of oxygen on the lunar surface and in space for propulsion and secondary life support.
6. Development of aluminum/fiberglass composites for bagging materials and structural materials.
7. Production of nonorganic binders on the Moon for producing foundations, haul roads and other stabilized surfaces, and for binding fiberglass should be researched and developed.
8. Investigation (theoretically and experimentally) of the feasibility of solar power conversion by photoelectric and thermionic devices which could be emplaced on the Moon using 10 to 100 times less materials imported from Earth than would be necessary for conventional solar cells.
9. Exploration of the Moon for concentrations of trace materials — especially volatiles such as water, carbon, nitrogen, sulfur, chlorine and copper, zinc, lead, and hydrogen.
10. General exploration of the options for materials substitutions with respect to expected major products in space and optional processing schemes.
11. Exploration of alternative uses of lunar materials and a lunar base at an earlier stage to extend the capabilities of the present space transportation system and to extend space exploration and exploitation.

It cannot be overemphasized that additional options not mentioned in this study should be explored. Conceptual advances can be expected which would lead to overall space systems that could be less expensive, deployed faster, provide bulk lunar soil at lower costs and over a greater range of space between the Earth and the Moon, and possibly sharply reduce the cost of Earth-to-orbit transportation compared to this scenario. As the cost of unprocessed lunar materials and chemical feedstock obtained from lunar materials decreases, the magnitude of space operations will expand rapidly with only moderate increases in the minimum necessary funding.

REFERENCES

1. Criswell, David R.: Space Industrialization Rationales and Key Technologies. Lunar Utilization, Lunar Science Institute, Houston, Texas, 1976, pp. 3-9.
2. Davis, H. P.: Long Range Aspects of a Large Scale Space Program. Lunar Utilization, D. R. Criswell, ed., Lunar Science Institute, Houston, Texas, 1976, pp. 10-22.
3. O'Neill, Gerard K.: Space Colonies and Energy Supply to the Earth. Science, vol. 190, no. 4218, 1975, pp. 943-947.
4. Criswell, David R.: Demandite, Lunar Materials and Space Industrialization. Third Princeton/AIAA Conference on Space Manufacturing, 1977, pp. 131—137.
5. Goeller, H. E.; and Weinberg, A. M.: The Age of Substitutability. Science, vol. 191, no. 4228, Feb. 20, 1976, pp. 683-689.
6. O'Neill, Gerard K., ed.: Third Princeton/AIAA Conference on Space Manufacturing Facilities.

Princeton, N.J., May 9-12, 1977.

7. Design of a Lunar Colony. NASA/ASEE Systems Design Institute, NGT-44-005-114, 1972, p. 506.

8. Ehricke, K. A.: Space Industrial Productivity New Options for the Future. Presented to the Committee on Science and Technology and the Subcommittee on Space Science and Applications Hearings on Future Space Programs, Washington, D.C., July 22-30, 1975, p. 168.

9. Billman, K. W.; Gilbreath, W. P.; and Bowen, S. W.: Introductory Assessment of Orbiting Reflectors for Terrestrial Power Generation. NASA TM X-73,230, April 1977.

10. Langseth, Marcus G.; Keihm, Stephen, J.; and Peters, Kenneth: Revised Lunar Heat-Flow Values. Proc. 7th Lunar Science Conference, vol. 3, Pergamon, 1976, pp. 3143-3171.

11. O'Leary, Brian; Heppenheimer, T. A.; and Kaplan, David: Trajectory Analyses for Material Transfer from the Moon to a Space Manufacturing Facility, in Space-Based Manufacturing from Nonterrestrial Materials. Progress in Astronautics and Aeronautics, vol. 57, AIAA, New York, 1977, pp. 21-36; also NASA TM X-73,265, Aug. 1977.

12. Floyd, P.: The North Slope Center: How Was It Built? The Northern Engineer, Gina (Brown) Wickwar, ed., vol. 6, no. 3, 1974, pp. 22-36.

13. Faget, Maxine A.; and Davis, Hubert P.: Space Shuttle Applications. In Third Conference on Planetology and Space Mission Planning, Robert D. Enzmann, ed., Annals of the New York Academy of Sciences, vol. 187, 1972, pp. 261-282.

14. Rauch, H. W.; Sutton, W. H.; and McCreight, L. R.: Ceramic Fibers and Fibrous Composite Materials. Academic Press, 1968.

15. Criswell, David R.: Materials Packaging, in Space-Based Manufacturing from Nonterrestrial Materials. Progress in Astronautics and Aeronautics, vol. 57, AIAA, New York, 1977, pp. 125-131; also NASA TM X-73,265, Aug. 1977.

16. Solar Power Satellite — Concept Evaluation. Activities Report July 1976 to June 1977, vol. 1 Summary, NASA, Lyndon B. Johnson Space Center, JSC-12973, section IV, Houston, Texas, 1977.

17. Freeman, J. W.: Photoelectric Electric Energy Conversion. Space Solar Power Research Program — First Quarterly Review Meeting, Dec. 7, 1977, J. W. Freeman, ed., Dept. Space Physics and Astronomy, Rice Univ., Houston, Texas, 1978, p. 68.

18. De, Bibhas R.; and Criswell, David R.: Intense Localized Photo Electric Charging in the Lunar Sunset Terminator Region 1. Development of Potentials and Fields, J. Geophys. Res., vol. 82, no. 7, March 1, 1977, pp. 999-1004.

19. Pelizzari, M. A.; and Criswell, D. R.: Differential Photoelectric Charging of Non-Conducting Surfaces in Space. To be published J. Geophys. Res., 1978.

20. Wright, J. L.: Solar Sailing: Evaluation of Concept and Potential. Battelle (Columbus Lab.), Report No. BMI-NLVP-TM-74-3, Contract No. NASW2018 to NASA, Nov. 1974, p. 38.

21. MacNeal, R. H.: The Heliogyro: An Interplanetary Flying Machine. (ARC-R-249), Astro Research Corp., Santa Barbara, Calif., Contract No. NAS7427, Mar. 1967, p. 65.

22. Uphoff, C.: Solar Sailing: Potential for Future Missions, Jet Propulsion Laboratory, Report No. 760-164, Jan. 1977, pp. 26.

23. O'Neill, G. K., ed.: Space Manufacturing Facilities. Proceedings of the Princeton AIAA/NASA Conference, May 7-9, 1975, American Institute Aeronautics and Astronautics Inc., New York, 1976.

24. O'Neill, G. K., ed.: Space Manufacturing from Nonterrestrial Materials. Progress in Aeronautics and Astronautics, AIAA, 1977.

V-2
Extraterrestrial Fiberglass Production Using Solar Energy

DARWIN HO and LEON E. SOBON

A conceptual design is presented for fiberglass production systems in both lunar and space environments. The raw material, of lunar origin, will be plagioclase concentrate, high silica content slag, and calcium oxide. Glass will be melted by solar energy. The multifurnace in the lunar plant and the spinning cylinder in the space plant are unique design features. Furnace design appears to be the most critical element in optimizing system performance. A conservative estimate of the total power generated by solar concentrators is 1880 kW; the mass of both plants is 120 tons. The systems will reproduce about 90 times their total mass in fiberglass in 1 year. A new design concept would be necessary if glass rods were produced in space.

INTRODUCTION

Fiberglass is an ideal material for use in space construction: It can be used for weaving cylindrical mass-driver containers (ref. 1) and for electrical insulation, and for manufacturing many lunar and space structural components such as reinforced plastic structural panels, large fiberglass cylinders, and small-diameter tubing for struts. The more desirable properties of fiberglass are (ref. 2):

1. High tensile-strength/weight ratio, with tensile strength ranging from 2×10^9 to 3.5×10^9 N/m² (300,000 to 500,000 psi)
2. Excellent stability: durable, dimensionally stable, and corrosion-resistant to moisture, most alkalis, and acids
3. Good thermal properties: incombustible, with low coefficient of thermal expansion; most fiberglass maintains 50 percent of its original tensile strength at 700 K
4. Excellent electrical insulation characteristics: low dielectric constants and high dielectric strength

The purpose of this study was to show, in concept, that fiberglass can be prepared from lunar materials and to define the design of an effective system for such production.

SOURCES OF RAW MATERIALS

Fiberglass can be produced from materials available from lunar soil directly and from by-products of aluminum and titanium extractions:

1. Anorthite, $CaAl_2Si_2O_8$: the main part of the plagioclase concentrate obtained by beneficiation of lunar soil.
2. Slag ($SiO_2 \sim 75$ percent; $Al_2O_3 \sim 15$ percent; $CaO + MgO \sim 10$ percent): a by-product of aluminum extraction from plagioclase based on the following reaction:

$CaO \cdot Al_2O_3 \cdot SiO2(s) + 8C(s) + 8Cl_2(g)$
$\quad = 2AlCl_3(g) + CaCl_2(s) + 2SiCl_4(g) + 8CO(g)$
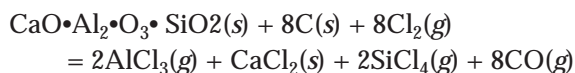
Slag is easily extracted since it is the only solid among the products of this reaction.

3. Calcium oxide, CaO: a by-product of titanium production (refs. 3, 4):

$CaCl_2(s) \xrightarrow{electrolysis} Ca\ (s) + Cl_2\ (g)$
$2Ca(s) + TiO_2(s) \rightarrow 2CaO(s) + Ti(s)$
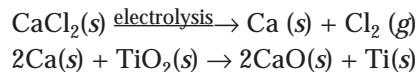
The approximate fiberglass composition (by weight) to be used is 82-percent slag, 16-percent CaO, and 2-percent anorthite (fig. 1). Since the composition can be varied to obtain fiberglass with different properties and since the chemical quality of the slag and anorthite may vary, chemical analysis must be made to determine the exact weight percentage of each material before mixing. After mixing, the material could be ground into finer grains of similar size. This would minimize the melting time.

According to an analysis of the lunar material extraction process (ref. 4), one unit of lunar soil may yield 0.59 unit of material suitable for fiberglass production. Therefore, for a projected annual processing rate of 5.5×10^8 kg (600,000 tons) of lunar soil, 3.2×10^8 kg (350,000 tons) of material for fiberglass production may be obtained. This amount is more than adequate for a throughput of 9.1×10^6 kg (10,000 tons) of fiberglass per year — the estimated need for the initial buildup of lunar and space bases. The remainder of the yearly slag production would be used to produce shielding material and silicon.

DESIGN OF FIBERGLASS PRODUCTION PLANT

Lunar Plant

Figure 2 is a schematic diagram of major components of the fiberglass plant. The unique features of this design are that several small furnaces are used and parabolic solar concentrators are installed horizontally pointing down to the lunar surface (fig. 3) for convenience in handling molten material (ref. 5).
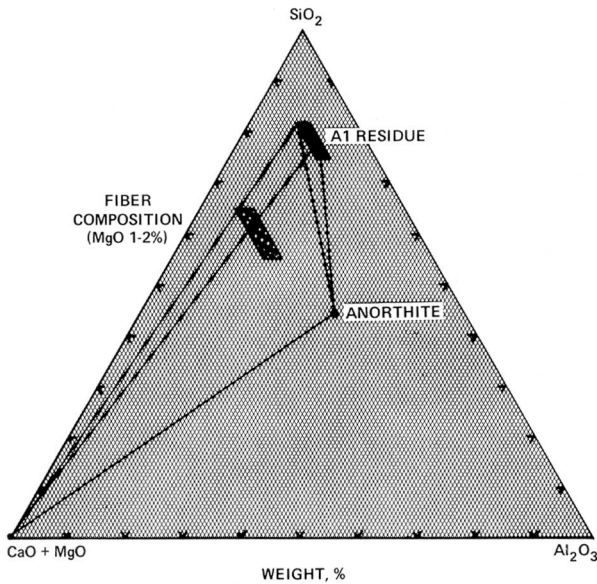
Figure 1 — *Ternary diagram for fiberglass composition (courtesy of Richard J. Williams).*

Production of bubble-free glass for continuous filament drawing — The raw material is first melted in a small furnace by the primary solar concentrator. The batch of molten glass is then transferred by conveyor belts to a smaller solar concentrator for fining and homogenizing.

(Fining is defined as the minimum heating time to obtain bubble-free, inclusion-free glass.) This two-step procedure is used because the power for fining and homogenizing is only about 30 percent of that required for melting, and fining and homogenizing are time-consuming processes (ref. 6). Therefore, it is preferable to use several smaller solar concentrators for fining and homogenizing so that the primary concentrator can be used full time to melt raw material. The number of small concentrators is described by:

$$N_S = \text{INT}\left(\frac{T_F}{M\Delta H}\, N_p P + 1\right)$$

where

N_s number of small concentrators
N_p number of primary concentrators
AH   enthalpy for fiberglass production ($\sim$1340 kW-sec/kg)
INT   integer function
M capacity of furnace, kg
P power of primary concentrator, kW
T_F time for fining and homogenizing

Figure 2 — *Operation of lunar fiberglass plant.*

1. PARABOLIC CONCENTRATOR
2. KAPTON FILM
3. FURNACE
4. CONVEYOR BELT
5. ZERO THERMAL EXPANSION CABLES
   FOR HANGING THE FLAT MIRROR
6. FLAT MIRROR
7. MIRROR ARRAY
8. TURNTABLE
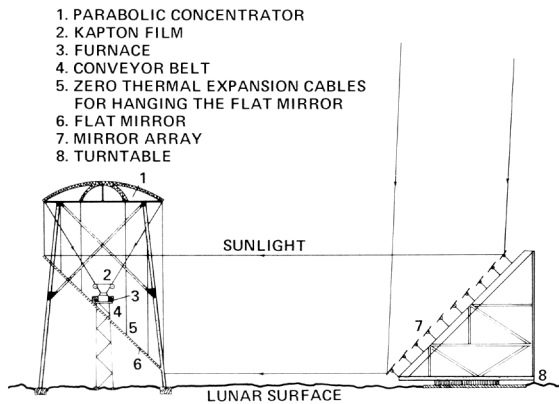
Figure 3 — *Mirror system for melting raw material.*

There will be a furnace under each concentrator at all times. Therefore, the total number of furnaces required would be the total number of concentrators plus the number of furnaces on the conveyor belt and those for preparing the material for the next cycle.

After the fining and homogenizing are completed, the molten glass is poured into molds that can be of any desired shape (one rod-shaped mold to make a product suitable for shipment to the space manufacturing facility (SMF) by the lunar mass driver). The emptied furnace is then sent back for reloading, thereby preparing the furnace for the next cycle. With this multifurnace technique, maximum productivity is achieved with minimum plant mass.

Remelting and mechanical drawing for making continuous textile filaments — Glass marbles or rods are fed into and melted continuously in another solar furnace. Fiberizing elements (bushings) made of platinum plate with orifices, from which filaments are drawn, are installed in the bottom of this furnace. To lubricate individual filaments and to gather them into continuous and untwisted strands, the filaments are sized below the bushing. From the sizing applicator, each strand is wound onto a forming tube by a winder that rotates at a rate up to 4 km/min (refs. 7, 8).

Glass Production in the Space Manufacturing Facilities

Simulated gravity must be present to handle the molten material in a space furnace. Thus, centrifugal acceleration produced in a rotating cylinder is required. As shown in figure 4, two furnaces are located opposite each other inside a rotating cylinder. The parabolic concentrator is always oriented toward the Sun. Concentrated sunlight is reflected to the back of the concentrator by a secondary convex mirror and then to the furnaces by a pair of flat diagonal reflectors. These reflectors can be made of highly polished aluminum, coated on the back with carbon black to dissipate absorbed heat. Winding machines similar to those used on the Moon are positioned under each furnace outside the cylinder. The systems will be automated, but minimum manpower will be required for maintenance. For the comparable lunar plant, maintenance will be required at the beginning of each lunar day to begin the drawing process.

1. CONVEX MIRROR
2. CONVEX MIRROR SUPPORT
3. PARABOLIC CONCENTRATOR
4. CONCENTRATOR SUPPORT,
   ATTACHED TO SMF
5. RADIATOR
6. ROTATING CYLINDER IN FRONT
   OF WINDING MACHINERY
7. DIAGONAL REFLECTORS
8. GLASS ROD STORAGE
9. FAST MOVING KAPTON FILM
10. FURNACE
11. HOUSING FOR WINDING MACHINERY

Figure 4 — *Space fiberglass manufacturing facility.*

Figure 5 — *Lightweight honeycomb-graphite/epoxy structure for MJS 77 high-gain antenna /courtesy of Ford Aerospace).*

MAJOR COMPONENT DESIGNS

Optical System

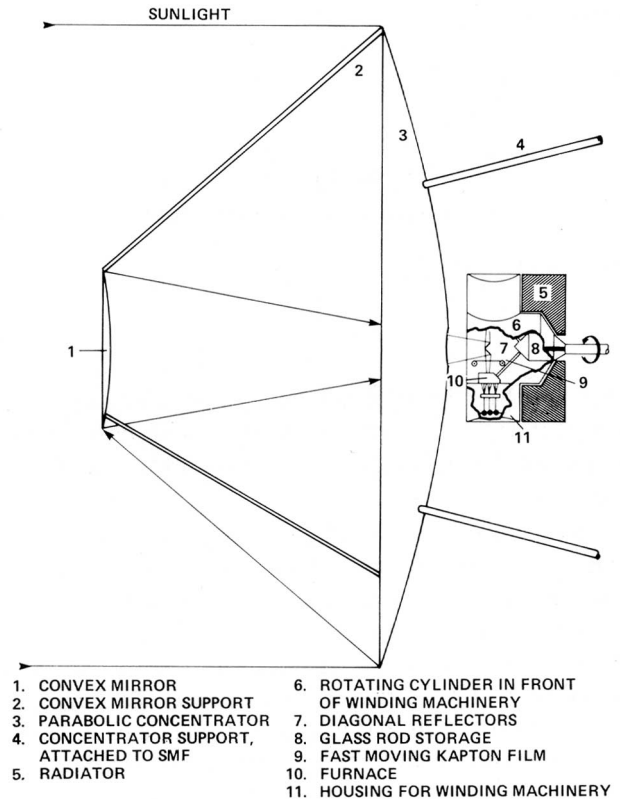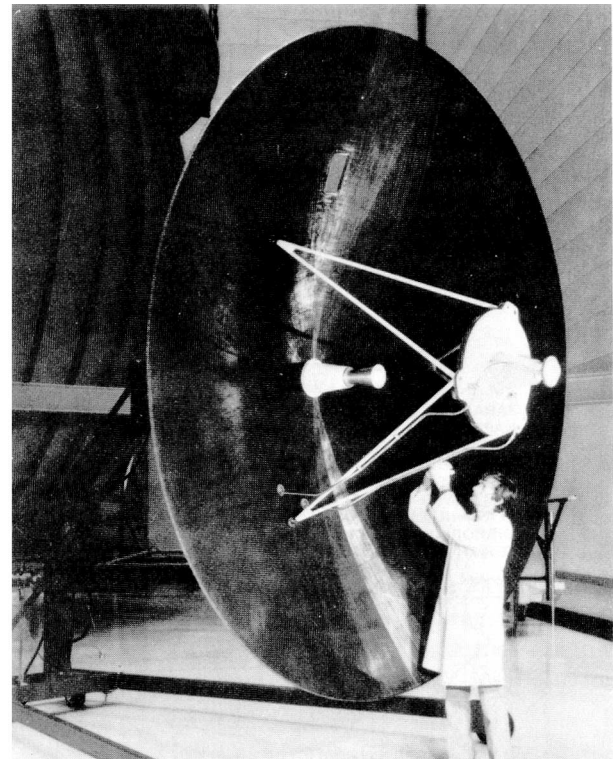*Parabolic collector* — Aluminum honeycomb with an aluminum-coated graphite/epoxy skin was selected for construction of the collector because it is lightweight (0.6 kg/m² for a thickness of 0.064 m). The technique for manufacturing the honeycomb structure would be similar to that used to mold the MJS77 spacecraft high-gain antenna (fig. 5), except the collector will have a much smoother reflecting surface made in small segments that can be reassembled in space. The focal length, diameter of the concentrator, diameter of the solar image at the focal plane, weight of the concentrator, and the maximum attainable temperature are described by (ref. 9):

$$d = 2\alpha f/[(1+\cos\theta)\cos\theta]$$

$$D = 2f\sin\theta/(1+\cos\theta)$$

$$f = \frac{1}{100}\left(\frac{eKAT^4 + m\Delta H}{\pi\rho_O F \sin^2\theta}\right)^{1/2}$$

$$T = \left(\frac{C_a\rho}{K}\right)^{1/9}$$

$$W = \frac{w\pi}{3f}\left[\left(4f^2 + \frac{D^2}{4}\right)^{3/2} - 8f^3\right]$$

where

A external surface area of furnace, m²
C_a concentration ratio = $(4F/\alpha^2)\sin^2\theta$, dimensionless
D diameter of concentrator, m
d diameter of solar image at focal plane, m
e emissivity of external surface of furnace, dimensionless
F efficiency of optical system, dimensionless
f focal length of concentrator, m
ΔH enthalpy for fiberglass production ($\approx$1340 kW-sec/kg)
K Stefan-Boltzmann constant (5.67 X 10⁻¹¹ kW/m²)
m production rate, kg/sec
T maximum attainable temperature in furnace, K
W weight of concentrator, kg
w weight of honeycomb-graphite/epoxy structure per unit area, kg/m²
α angular diameter of Sun's disk (0.00931 rad)
θ concentrator rim angle, deg
ρ_0 total solar radiation received at normal incidence outside atmosphere (1.394 kW/m²)

Figure 6 shows the relation between maximum attainable temperature T and concentration ratio C_a.

From this curve, note that the concentration ratio C_a should be no less than 427.0 or, in other words, the rim angle θ cannot be less than 8.8° to maintain a furnace temperature of 1800 K, which is required to melt glass. C_a and θ should be greater than 650.8 and 10.6°, respectively, for a furnace
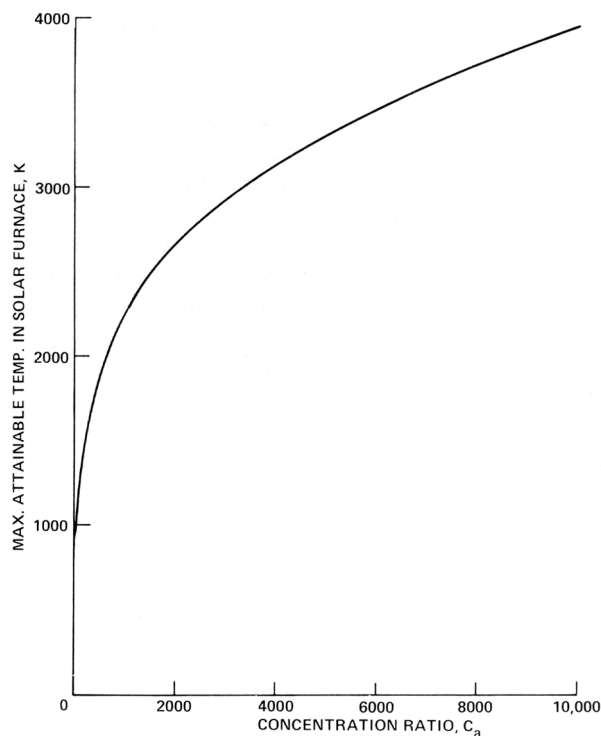
Figure 6 — *Maximum attainable temperature for a solar furnace with 40-percent efficiency.*

temperature at 2000 K, which is required for fining and homogenizing. For heat flux control, shutters will be used.

Flat mirror and heliostat — Aluminum-coated Kapton film stretched on a lightweight structure was chosen as the reflecting surface for minimum weight. Figure 3 shows the plane mirror of the heliostat divided into several bands to eliminate the distortion of a large single frame as it changes position during Sun-tracking. These bands may be constructed on a pyramidlike structure that rests on a rotating disk.

Furnace Design

The time required for fining and homogenizing (exact time determined by experiment) increases exponentially with the mass of the molten glass: the number of concentrators required for fining would be increased exponentially. Therefore, a small furnace cavity is chosen to minimize the number of concentrators and thus increase the annual throughput/plant-mass ratio. For example, a volume of 0.1 m³ has a capacity of 90 kg of raw material, which requires roughly 2.6 min for melting and 30 min for fining and homogenizing.

The cavity paving is a heat-resistant refractory material such as zircon.[1] To minimize the corrosion caused by the molten glass, the coils attached to the outer surface of the paving will be turned on after all raw material has melted, thus

---

1   Mullite $3Al_2O_3\bullet2SiO_2$, which can be produced from lunar resources, may be used as a substitute for zircon (which cannot be readily produced from lunar material). However, there is a potential problem that mullite may dissolve into molten glass and thus affect the glass properties.

forming a protective solid glass layer adjacent to the zircon. The paving should be at least 10 cm thick for a reasonable lifetime of several years. The paving is surrounded by a thick layer of lunar soil (up to 1 m thick) to reduce energy loss due to radiation (fig. 7). The power requirement for fining and homogenizing is expressed by

$$t_c = (KA_e d_2 e t_e^4 / k_s A_a) + t_e$$

$$P_F = [k_z(t_m - t_c)A_e]/d_p$$

where

A_a mean area between paving and external surface of furnace, m²

A_e external surface area of furnace, m²

d_p thickness of paving, m

d_s thickness of lunar soil, m

k_s conductivity of packed lunar soil;
    ~2.09 X 10⁻³ kW/mK

k_z conductivity of zircon; ~2.93 X 10⁻³ kW/mK

P_F power requirement for fining and homogenizing, kW

t_c temperature of cooling coil, K

t_e temperature of external surface of furnace, K

t_m temperature of solid glass film, K

Contamination of the concentrator and diagonal reflector surface by vapor from the glass-melting process can be eliminated by having transparent Kapton film moving above each furnace (ref. 10). A similar furnace could be used to melt glass rods. In this furnace, however, platinum bushings are inserted on the bottom of the furnace, and glass rods are fed in continuously.

Dimensions of the System

To meet the projected fiberglass throughput of 9.1 X 10³ kg (10,000 tons) per year, the lunar plant will produce 0.58 kg of glass rods per second (780 tons/lunar day). One-tenth of these will be processed into fiberglass on the Moon and the rest will be processed at the SMF. If the capacity of the furnace is chosen to be 0.1 m³, the thickness of the insulating lunar soil is 0.5 m (the estimated mass of each furnace is about 2.7 X 10³ kg); if four primary solar concentrators are used on the lunar plant, then the power requirements, concentrator characteristics, and mass of the plants would be as summarized in tables 1, 2, and 3. Since the total mass of the system is about 110 X 10³ kg (120 tons), it will be able to process raw material about 90 times its own mass in 1 year.

1. APERTURE
2. MOLTEN GLASS
3. LAYER OF SOLID GLASS
4. ZIRCON PAVING
5. TITANIUM COOLING COIL
6. PACKED INSULATION, HIGH Al₂O₃ LUNAR DUST
7. CARBON BLACK ON ALUMINUM SKIN
8. RADIATOR FOR COOLING COILS
9. SUPPORT STRUCTURE

CONCENTRATED SUNLIGHT

MOVING KAPTON FILM
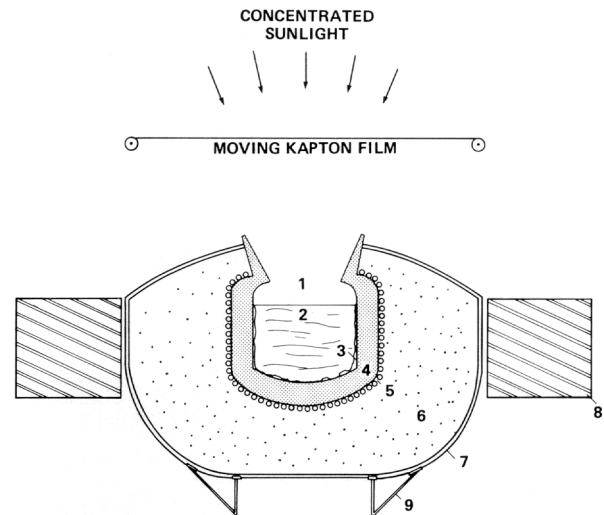
Figure 7 — *Cross section of a furnace.*

TABLE 1 — POWER REQUIREMENTS FOR FIBERGLASS PRODUCTION

Process	Production rate, kg/sec	Power required, kW
Melting raw material	0.58	820
Fining and homogenizing	.58	240
Remelting glass rods on Moon	.06	80
Remelting glass rods at SMF	.52	740

CONCLUSIONS

Abundant amounts of fiberglass can be produced from lunar materials. The key factors in designing the production plants are system mass optimization, technological availability, and highly automated operations.

It has been chosen that glass rods will be produced on the Moon. However, if all lunar raw materials are processed at the SMF, a different system should be designed to produce glass marbles in space. The SMF plant may have a higher production rate/plant-mass ratio since sunlight is available at all times in space. The design of the furnace appears to have the strongest effect on system performance, and further research must be done. Other recommended areas for further study include:

TABLE 2 — CHARACTERISTICS OF SOLAR CONCENTRATOR

Process	Number of concentrators	Mass, kg/unit	Diameter, m	Power output, kW/unit
For melting raw material	4	350	26.5	205
For fining and homogenizing	12	20	6.6	20
For remelting glass rods on Moon	1	135	16.5	80
For remelting glass rods at SMF	1	1520	55	740

TABLE 3 — MASS OF PRODUCTION PLANTS

Equipment	Lunar plant mass, 10^3 kg	SMF plant mass, 10^3 kg
Mirrors and support structure	20	3
Furnaces:	65	5.4
24 on Moon		
2 at SMF		
Winding and auxiliary machinery	5	6
Conveyor belt	7	
Total weight	97	14.4

- Zero thermal expansion honeycomb structure for solar contentration
- Automated operations
- Spinning mechanism for the production plant at the SMF
- Furnace cooling system for solid film formation
- Refractory lifetime
- Sizing type selection
- Detailed study of properties of $CaO\text{-}MgO\text{-}Al_2O_3\text{-}SiO_2$ glasses
- Glass made from lunar material to evaluate the effects of minor constituents in the feedstock on the quality of glass produced

After these areas have been researched, a detailed system-design study should be made.

REFERENCES

1. Criswell, David R.: Materials Packaging. In Space Based Manufacturing from Nonterrestrial Materials. Progress in Astronautics and Astronautics, vol. 57, AIAA, New York, 1977, pp. 125-131.

2. Lubin, George, ed.: Handbook of Fiberglass and Advanced Plastics Composites. Polymer Technology Series, Van Nostrand Reinhold Co., New York, 1969.

3. Rao, D. Bhogeswara; Choudary, U. V.; Erstfeld, T. E.; Williams, R. J.; and Chang, Y. A.: Extraction Processes for the Production of Aluminum, Titanium, Iron, Magnesium, and Oxygen from Nonterrestrial Resources. Space Resources and Space Settlements, NASA SP-428, 1979, pp. 205-2184.

4. Williams, Richard J.; McKay, David S.; Giles, David; and Bunch, Theodore E.: Mining and Beneficiation of Lunar Ores. Space Resources and Space Settlements, NASA SP-428, 1979, pp. 219-229.

5. Edlin, F. E.: Industrial Consideration of Solar Furnaces. J. Solar Energy Sci. Eng., vol. 1 (2-3), April-July 1957, pp. 52-54.

6. Tooley, Fay V.: Handbook of Glass Manufacture; A Book of Reference for the Plant Executive, Technologist, and Engineer. Vol. 1. Ogden Publ. Co., New York, 1961, pp. 241-260.

7. Phillips, Charles J.: Glass: Its Industrial Application. Reinhold Publ. Corp., New York, 1960, pp. 210-233.

8. Shand, E. B.: Glass Engineering Handbook. McGraw-Hill Book Co., Inc., New York, 1958, pp. 381-386.

9. Bliss, R. W.: Notes on Performance Design of Parabolic Solar Furnaces. J. Solar Energy Sci. Eng., vol. 1 (1), Jan. 1957, pp. 22-29.

10. Drexler, K. E.; and Henson, H. K.: Design of Equipment for Vapor Phase Processing of Metals. In Lunar Utilization, D. R. Criswell, ed., The Lunar Science Institute, March 1976, pp. 110-113.

V-3
Lunar Building Materials — Some Considerations on the Use of Inorganic Polymers

STUART M. LEE

The fabrication of lunar building materials and the assembly of structures requires the use of adhesives, binders, and sealants. These terrestrial materials are usually produced from carbon, hydrogen, and nitrogen, elements scarce on the Moon. One possible approach would be to use inorganic polymer systems synthesized from the available lunar chemical elements, viz., silicon, aluminum, and oxygen. This paper considers inorganic polymer systems, their background, status, and shortcomings, and the use of network polymers as a possible approach to synthesis. In addition, other potentially useful considerations were advanced, including glassy metals for unusual structural strength, and the use of cold-mold materials as well as foam-sintered lunar silicates for lightweight shielding and structural building materials.

INTRODUCTION

Ideally, structural systems assembled on the lunar surface would be fabricated from available lunar materials. This process might include synthesis of adhesives for use in filament winding, sealants, binders for incorporating into lunar road-bed materials to minimize dust generation, as well as materials for insulation and radiation shielding. However, lunar materials do not contain the abundance of basic chemical elemental building blocks available in terrestrial minerals. The lunar composition is dominated by five minerals — pyroxenes, olivines, feldspars, ilmenite, and spinel — and consists mainly of metal silicates and titanates. Terrestrial technology concerned with adhesives, sealants, and binders revolves about the ubiquitous carbon atom. All current adhesive systems use macromolecular organic polymeric compounds which are produced from carbon containing small molecules that contain, in addition to carbon, hydrogen, nitrogen, and oxygen. Only oxygen, which is combined as oxides and silicates, is relatively abundant on the Moon, comprising more than 50 percent by weight of lunar materials (ref. 1), while the upper limit of indigenous organics in lunar samples is about 1 ppb (ref. 2).

In the absence of lunar materials for fabricating organic structures, several alternatives were considered:

1. The simplest but most expensive alternative would be to transport all needed materials by means of the Space Shuttle. The present proposed method for producing aluminum from lunar ores involves the use of carbon and chlorine, which would have to be transported to the Moon. However, these elements remain captive within the process and need not be constantly replenished as would be the case if organic polymeric adhesives were produced from carbon starting material.
2. An alternative would be to "dismantle" a carbonaceous containing asteroid into the desired chemical elements. Towing asteroids to a convenient work area is under consideration.
3. Another alternative would be to use available lunar materials with or without a minimum of terrestrial materials to synthesize and fabricate the required building materials.

The purpose of this discussion is to consider alternative 3 and its ramifications.

STATUS OF INORGANIC POLYMERS

Nearly all synthetic plastics and elastomers in use today are organic polymers. These consist of very large molecules containing linear or branched chains with a backbone of carbon atoms. However, it has been long known that carbon is not a required component of materials that exhibit plastic behavior. For example, plastic sulfur, glassy selenium, and polyphosphonitrilic chloride are totally inorganic substances that demonstrate elastomeric properties at moderate temperatures, but are unstable and cannot retain their potentially useful properties for prolonged periods.

Inorganic polymers are defined here as materials composed
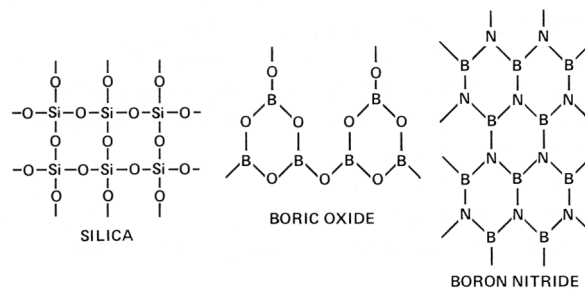
Figure 1 — *Some inorganic polymers.*

of long linear chain molecules that do not contain carbon in the chain but may have carbon in the pendant groups or in the side chain. Polymer systems containing both inorganic elements and carbon in the backbone structure are considered to be semiorganic polymers.

Inorganic polymers have been in use a long time; for example, glass is an inorganic polymer comprised of rings and chains of repeating silicate units, as are most rocks, minerals (including sapphire and ruby), brick, concrete, and ceramics, which are three-dimensional inorganic polymers (cf. fig. 1). In pyroxene, one of the main lunar minerals, similar chains of silicate units are found. Also, ladder polymers or double chains are found in amphibole minerals such as one form of asbestos. In this latter type of structure, the negative charges of the oxygen atoms are neutralized by positively charged metal ions that tend to bind adjacent chains together to form a crosslinked matrix (ref. 3). However, these materials have limited use because of the difficulty in fabricating them into useful objects such as those requiring high temperature. These materials generally are not flexible, elastomeric, or impact-resistant. However, despite the difficulties with naturally occurring inorganic polymers, these facts have not precluded further investigation into synthetic inorganic polymer chemistry.

For years, chemists have sought a middle ground somewhere between organic polymers on one hand and mineralogical inorganic materials on the other. Generally, organic materials cannot resist heat, while inorganics cannot undergo strain. The better material should be between these extremes. The desired structure required is postulated to consist of a linearly structured polymer with nonionic substituent groups to favor flexibility. This is the basic concept behind the design of silicone polymers, the most solid claim to commercial success of an inorganic polymer. The most widely used silicone — polydimethylsiloxane (fig. 2) — consists of a chain of alternating silicon and oxygen atoms with two methyl groups attached to each silicon heteroatom, materials similar to the atomic makeup (not structural) of inorganic materials that occur in nature (quartz, feldspars, and zeolites).

The chemistry required to produce long chains (thought necessary to develop "plastic properties"), based on elements other than carbon, is not so highly developed as that used to prepare carbon-based polymers. Many of the polymerization reactions that would be expected to provide high-molecular-weight inorganic polymers tend to produce only small cyclic molecules or low-molecular-weight

Figure 2 — *Polydimethylsiloxane.*

SILICON
OXYGEN
CARBON
HYDROGEN

Figure 3 — *Rearrangement of silicone polymer.*

Figure 4 — *Aluminum metalosiloxane.*

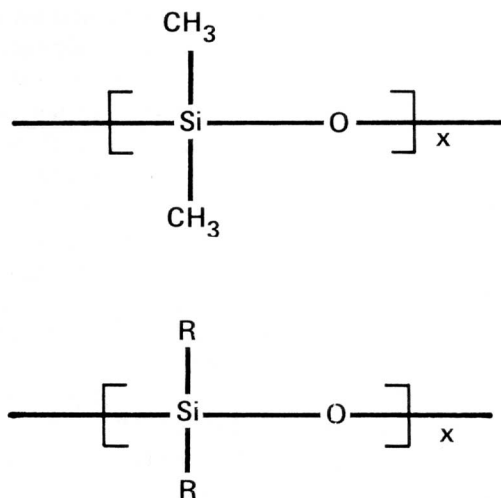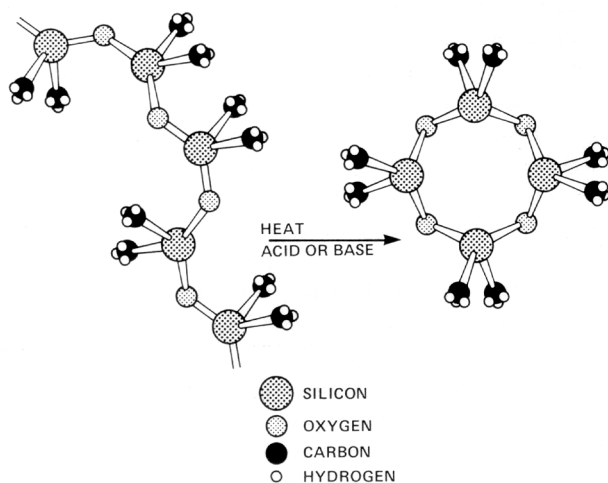products. Conversely, many inorganic polymer chains, including silicones (above about 350° C), show strong tendencies to rearrange to low-motecular-weight polymers or small ring compounds upon heating, due, in the case of silicones, to cleavage of the relatively strong silicon-oxygen bonds, while the supposedly less stable silicon-carbon bonds remain intact (fig. 3).

Up to now, inorganic polymer chemistry has generally been approached by investigating the two basic types: those consisting of chains of a single element (homoatom) chain (as in plastic sulfur or black phosphorus) and those having two or more dissimilar alternating elements (heteroatom) chains that utilize metals (such as the aluminoxanes). However, despite promising claims made by early workers (ref. 4), the aluminoxanes have been found to hydrolyze easily (which may not be a lunar problem).

PRESENT TRENDS IN INORGANIC POLYMER STUDIES

Metalosiloxanes

Few elements have been overlooked in the search for new inorganic polymers. One well-worn approach systematically replaces the silicon or oxygen atoms or both of the basic silicone structure by other elements of periodic groups II and VI. By replacing some silicon atoms with other metallic atoms such as aluminum or titanium, materials known as metalosiloxanes have been prepared (fig. 4).

The synthesis and investigation of polymers with siloxane-like structures built with Al, Ti, P, and O atoms have been the work of Andrianov and others (refs. 5-8).

They reported that double-chain metalosiloxane structures containing aluminum or titanium were stable up to 590° C, while aluminosiloxanes (chains with alternating aluminum and silicon atoms separated by oxygen atoms) were stable above 300° C (ref. 9). *A priori,* these polymers could be potentially useful because of the chemical elements available on the lunar surface.

These metalosiloxane polymers, even though basically inorganic, contain some carbon side chains. The carbon used to synthesize these materials remains in the final polymer and naturally is not available for reuse.

Metalosiloxanes may be prepared by hydrolyzing metal siloxanic compounds at room temperature. Thus, a polyorganic silylaluminoxane may be prepared from nonaethylaluminoxytrisilane according to:

$$6R_3SiOH + 2Al \rightarrow 2(R_3SiO)_3Al + 3H_2$$

$$(R_3SiO)Al + H_2O \rightarrow (R_3SiO)_2AlOH + R_3SiOH$$

$$2(R_3SiO)_2AlOH \rightarrow (R_3SiO)_2AlOAl(OSiR_3)_2 + H_2O$$

$$(R_3SiO_2)AlO \begin{bmatrix} -AlO- \\ OSiR_3 \end{bmatrix} Al(OSiR_3)_2$$
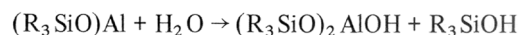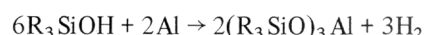
The resulting polymer contains an Al-O-Al main chain protected by organic substituents (O-Si-R_3) which also acts as a chain-stopping group. In this scheme, the aluminoxytrisilane is prepared by treating a trialkylsilanol with aluminum. The material can also be obtained by reacting trialkyl sodium silenoxide with aluminum trichloride (possibly available from proposed lunar aluminum process).

These methods of preparation are not entirely satisfactory since initially they lead to the formation of appreciable

quantities of cyclic or low-polymerized products (as previously indicated in fig. 3) that can be polymerized further. A similar problem was observed when polymer chains containing Al-O-P linkages were prepared. In two recent patents, Dow workers (refs. 10, 11) succeeded in preparing relatively long-chain aluminum-oxygen-phosphorus bond polymers by reacting an aluminum compound with an alkyl orthophosphonate or phosphonic and/or phosphinic acid.

In another study, inorganic polymers containing silicon-oxygen-metal linkages were prepared over several years (ref. 12) and it was found that various techniques can be used to establish the silicon-oxygen-bond. However, Chamberlain (ref. 12) states that "nothing has been found during this study to indicate that the Si-O-metal linkage can be of great utility in the formation of chemically and thermally stable elastomers."

In addition to single-chain polymers, the ladderlike double chains (fig. 5) were synthesized by General Electric. These phenylsilsesquioxanes, or phenyl-T polymers, are reported (ref. 13) to have molecular weights up to 200,000 and even up to 4×10^6 with branching. They do not melt on heating, they are stable up to 400° C, and they form good films by solvent deposition.

Figure 5 — *Silicone ladder polymer.*

Coordination Polymers

Coordination or chelate polymers are unique to inorganic chemistry and are formed when certain electron donor atoms such as oxygen, nitrogen, or sulfur donate an unshared electron pair to a metal ion that can receive these electrons. The donor atoms may be part of an organic molecule, in which case the entire molecule is said to be coordinated to the metal.
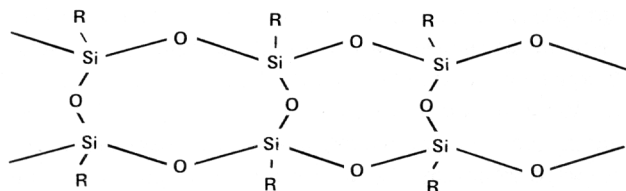
Attempts to crosslink chelate polymers were undertaken by a Monsanto team to develop semiorganic structural adhesives (ref. 14). However, the products obtained were not homogeneous. It appears that the coordination process for preparing inorganic polymers is not fully understood. The problems include the lack of product solubility, infusibility, and depolymerization of product.

Miscellaneous Polymers

Some inorganic polymers that have been synthesized show some promise. For example, polymers of titanium oxide form strong films and are used in the optical industry (ref. 15), while a mixed product containing silicon and titanium yields materials that can be cold-hardened to give strong films suitable as coatings for ceramic electrical insulators and as a water repellent.

SOME PROBLEMS WITH INORGANIC POLYMERS

The outstanding success of polymer chemists in developing organic polymers has been an inspiration to the inorganic polymer chemist. However, research has not yet revealed an entirely new inorganic polymer system other than silicones. The chemistry of inorganic polymers lags a half century behind the chemistry of organic polymers. Since the 1960s, no recent comprehensive texts on inorganic polymers have appeared (refs. 5, 16-18). The lag in technology is apparent not only in our lack of knowledge of the polymerization process, but also regarding bonding of inorganic polymers. For organic polymers, the general covalent s-p sigma bonds and sigma-pi multiple bonds are well characterized. However, the inorganic polymer systems involve d-orbital pi-bonding and other less familiar interactions of bonding electrons.

Bonding types range from wholly covalent at one extreme to ionic at the other. The ability of carbon to bond with another carbon or oxygen makes the production and study of monomers simple. These monomers can then be converted to polymers by reactions that open the double bonds to form polymer linking bonds, addition-polymerization. However, outside of the first raw elements, carbon, nitrogen, and oxygen, multiple bonds of the p-pi type are rare. Multiple bonds involving p-pi-d-pi orbitals are fairly widespread, but do not react by addition-polymerization. As a result, inorganic monomers generally cannot be isolated to study polymerization.

Molecular engineering as applied to inorganic polymer systems might involve the design of molecules with optimum thermochemical bond strengths. However, one considered factor alone cannot suffice; for example, bond energy data may lead one to conclude that polymers based on inorganic elements should be superior to organic polymers in thermal stability. To determine thermal stability, we must ponder other kinetic considerations, for example, the silicon-oxygen bond in the silicones has a value of 110 kcal/mole, which is 75 percent stronger than the silicon-carbon bond (64 kcal/mole). Yet linear polysiloxanes heated above 600 K yield low-motecular-weight cyclic siloxanes. This indicates that the silicon-carbon bonds remain intact while the silicon-oxygen bonds are broken, which involves a bond rearrangement that occurs through a transition state, lowering the energy barrier relative to that required for a direct thermal rupture.

Many inorganic systems tend to polymerize through two or more units. However, most tend to form oligomers and small cyclic molecules, viz., dimers, trimers, tetramers, and other low-molecular-weight polymers rather than desired high-molecular-weight materials. Similar results were encountered in the development of silicone polymers, viz., the formation of small cyclic polymers from two to six units (fig. 3). Present technology has circumvented some of the tendencies of silicones toward cyclization. However, much of the product is still obtained in this undesirable form. The formation of small cyclic units also presents a possible route

for depolymerization. When higher silicone polymers are heated in the range of their upper temperature utility 350° C - 450° C, they can depolymerize to these volatile, cyclic, low polymers. This phenomenon, observed occasionally in completed systems, is called reversion.

In retrospect, it appears that a lack of sufficient background information is the major problem. Previously, there has been a strong emphasis, both commercial and governmental, for high-temperature-resistant materials, with a resultant concentration on synthetic approaches to inorganic polymers, to the detriment of basic research. Additional studies would be most helpful in the areas of inorganic bonding and polymerization reactions and probably would require a joint effort of both inorganic chemists (who understand the inorganic syntheses) and organic polymer chemists.

POTENTIAL CONSIDERATIONS

Glassy Metals

For extremely high-strength composites, there appears to be a proclivity toward more exotic materials such as whiskers and wire reinforcements, which are natural candidates when high structural efficiency is desired. In the same vein of new and unusual materials are the glassy metals (ref. 19). It is feasible that high-strength structures could be fabricated from these metal support materials which could be embedded in an adhesive, preferably inorganic, or a metal matrix such as aluminum.

Normal metallics, which are malleable, ductile, and opaque and are good conductors of heat and electricity, have a crystalline structure in which atoms are regularly arranged in three-dimensional repeating structures. Glasses, because of their covalent bonding, are strong and directional. It has long been known that metals can exhibit properties other than those of their natural state if they are cooled so rapidly that a nonequilibrium state is frozen in. The quenching rates required to produce glassy metals are usually several orders of magnitude higher than those achievable in normal metallurgical practice, that is, by simply plunging the heated metal into water.

An ingenious system for producing continuous ribbons of metallic glasses ("metaglasses") was developed at the Allied Chemical Corporation. The process involves injecting the hot metal in liquid form between counter-rotating drums that are continuously cooled. Long lengths of threadlike ribbon of glassy metal, up to about 2000 m/min, have been produced. The production cost is quite low because, by producing the glassy alloys directly from metal, it is possible to bypass the otherwise expensive and energy-consuming stages (such as casting, rolling, and drawing) necessary when working with the material in solid form.

The most important property of new metallic glasses is their unusual combination of strength and plasticity. Common glass, even in the form of a thin filament, cannot be strained more than 1 percent. However, a metallic glass specimen similarly shaped can withstand a local plastic sheer strength well in excess of 50 percent.

A five-component alloy with a tensile fracture strength about 3 times that of stainless steel has been produced. Moreover, stainless steels cannot withstand strains similar to the 50 percent observed by metallic glasses. Strong and hard metals are expected to be rather brittle; therefore, a material that has both strength and ductility is an unusual advance. Another unusual aspect of these materials is their reported magnetic properties (ref. 19).

Cold-Mold Materials

Primary constituents of many electrical and automotive components from 1910 to 1920 are still used in low-voltage switch gear for arc chutes arc-resistant areas.

These are the "transite" cement asbestos composites similar to some cold-mold formulations (ref. 20). A typical cold-mold composition is a cement asbestos product that is volumetrically loaded in a compression mold, pressed to shape in a punch-press-like operation, and cured in a water or steam-bath oven. Calcium alumino silicate is used to make an asbestos-filled cold compression molded compound cured by steam. These cold-mold materials are silicates, not unlike some of the minerals found on the Moon. It would be worthwhile to study techniques for adapting lunar silicates coupled with a synthesized inorganic polymeric binder to form cold-mold building materials that could then be used to build space structures. In addition, the cold-formed materials could be used in sandwich multilayer construction, consisting of two outer aluminum thin face skins bonded to an intermediate thick layer of low-density, cold-formed material. The latter material could be a foam type, using available oxygen as the foaming gas.

An Approach to Inorganic Polymers — Network Type

Glass technologists deal with highly crosslinked network polymers, yet inorganic polymer chemistry is almost entirely concerned with linear polymers. Research into processible network polymers could result in major advances in inorganic polymer chemistry.

Many common inorganic substances are polymers (fig. 1). Each compound is composed of large numbers of identical structural units linked by covalent bonds, but in these polymers the units are not joined in long chains, but instead form three-dimensional networks. Over the last three decades, the synthesis of inorganic polymers has been based on the belief that the structural units must be linked together into long chain molecules similar to organic polymers.

Although many novel and scientifically interesting structures have been synthesized, no useful new materials other than silicones have appeared; as a result, interest in this area has greatly diminished in recent years. The silicones have truly achieved fruition and embrace an extensive variety of polymers based on chains or networks of alternating silicon and oxygen atoms that match many of the structures found in the mineral kingdom. But, whereas the polysiloxane

skeletons in natural minerals are crosslinked by means of metaloxy groups, the corresponding backbones in silicones are isolated by substitution of organic groups at silicon sites. The siliceous minerals are crosslinked structures so involved that the whole specimen of a pure mineral may be but one continuous molecule, insoluble, infusible, and intractable within reasonable temperature limits. On the other hand, the silicone chains are laterally blocked by organic substituents and can merely associate with each other by weak van der Waals forces. Several organosilicon polymers together with their structural counterparts in the mineral kingdom are shown in figure 6 (ref. 16).

If the inorganic polymeric network structure is an accepted fact in natural inorganic polymers and ceramics, should this type of structure be considered as a logical extension for the synthetic inorganics? This approach has been taken by N. H. Ray (ref. 21), who postulated that the problem was due to the fact that inorganic polymeric structures must be linear to have the required combination of properties. Strangely, this theory is expounded even though the vast majority of inorganic polymers do not contain long-chain molecules but are composed of two- and three-dimensional networks. In fact, long-chain molecules are rare except among carbon and silicon.

Why has research been restricted to a linear approach? The answer probably is processability: most easily processible polymers soften reversibly to viscous liquids and can be processed by extrusion, injection molding, and vacuum forming.

All polymers at low temperatures are rigid solids with their molecular units bound into a three-dimensional structure either by van der Waals forces or sometimes by hydrogen bonds (as for long-chain polymers), or by covalent linkages, or sometimes by ionic forces (as for network polymers). If a polymer is to undergo permanent deformation by viscous flow, it must move bodily. This requires that the polymer be a long-chain molecule. For a network polymer, a higher temperature is required to achieve viscous flow than for a similar chain polymer. Higher temperatures favor more complex reactions and possible degradation.

Inorganic network polymers differ from organic polymers in that the network atoms are not joined directly (as in graphite) but are united through intermediate connecting atoms that may be oxygen (as in the simple compounds of boric acid or silica). The bonds within these polymers are covalent between oxygen and boron or silicon.

The search for processible inorganic polymers need not be restructured to chainlike molecules. The use of linear polymers requires that one or more unreactive substituents be attached to each atom in the chain. These univalent groups are either unstable to oxidation or hydrolysis or are lost on heating. The silicones are exceptional because substituents such as methyl, when attached to silicon, make possible the formation of a linear polydimethylsiloxane chain.

For production of network polymers, a much smaller proportion of unreactive substituents is required because they serve to control the density of network crosslinking. This process is illustrated by the chemical durability of ordinary glass, which is tremendously resistant to hydrolytic attack because of its crosslinked network structure as compared to the corresponding linear polymer sodium metasilicate, which is soluble in water and decomposed by acids.

Factors to consider in design include the expected processing temperature and the crosslink density as defined by P. J. Flory (ref. 22).

The stability as well as desirability of network structures can be attested to by the fact that network linking structures are used to overcome depolymerization of silicones by use of phenylene structural units. The phenylene units in this semi-inorganic silicone polymer appear to suppress the ordinary depolymerization reaction. Some of these materials showed no visible decomposition up to 500° C, but measurements indicated some weight loss up to 20 percent at these higher temperatures.

Network structures of aluminum-oxygen-phosphorus have been prepared by reaction of orthophosphoric acid and aluminum oxide (refs. 23, 24). The products of this reaction from these components is a viscous fluid that can be dried to an amorphous material believed to be a three-dimensional network of Al-O-P chains. These phosphate materials have been used as insulating coatings and as binders (ref. 25).

CONCLUSIONS

1. Inorganic polymer chemistry has not undergone the tremendous explosion of its organic counterpart. The relegated secondary status could possibly be ascribed to the synthetic approach thus far taken toward the synthesis of linear inorganic polymers.
2. Efforts to synthesize lunar inorganic polymers for use as adhesives, coatings, and binders based on current technology and utilizing lunar materials would prove unsuccessful. However, this does not preclude future technology to alleviate this problem. What is needed is not a continuing study based on the present synthetic approach of inorganic polymers but a different, concerted, and positively directed one, possibly using molecular engineered techniques to design inorganic network polymeric systems.
3. Available lunar silicate minerals are potentially useful for use as cold-mold cement composites. An effort should be made to ascertain techniques for utilizing lunar silicates for cold-mold materials and as a core in multilayer composites.
4. Filament wound structures or supports requiring extremely high strength could be fabricated from "glassy metals." Ribbons of this very strong, hard, ductile metal should prove a useful adduct for lunar composites.
5. Another potential by-product of the lunar inorganic polymeric silicates, after subjecting them together with a synthesized inorganic binder mixture to a sintering and
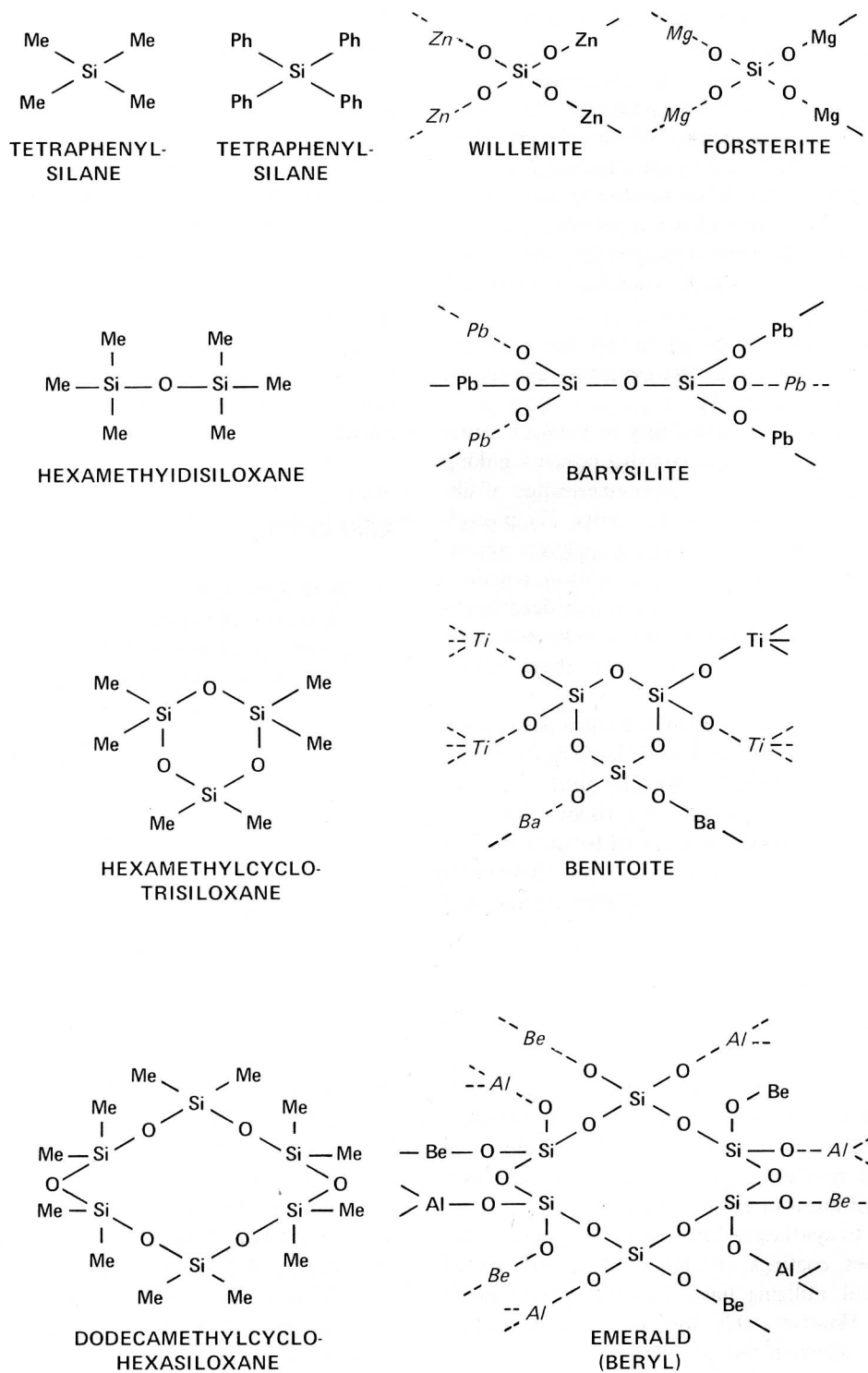
Figure 6 — *Relatunrslrip between synthetic silicon monomers and naturally occuring network polymers.*

foaming process, might be a lightweight building material for sandwich construction, building blocks, or shielding.

REFERENCES

1. Bjerholdm, I. E.: Lunar Science IV, Lunar Science Institute, Houston, Texas, 1973, p. 78.
2. Handbook of Lunar Materials, Lunar and Planetary Science Division, NASA Johnson Space Center, Houston, Texas, June 1977, p. VII-7.
3. Allcock, H.: Inorganic Polymers, Scientific American, 1974, pp. 66-74.
4. McClosky, A. L. et al.: Research on Inorganic Polymer Systems, WADC TR 59-761, Dayton, Ohio, March 1960.
5. Andrianov, K. A.: Metalorganic Polymers. Interscience, New York, 1965.

6. Andrianov, K. A.; Zhdanov, A. A.; Kurasheva, N. A.; and Dulova, V. G.: Synthesis of Polyorganosiloxanoalumoxanes and Polyorganosiioxanotitanoxanes. Doklady Akad. Nauk S.S.S.R., vol. 112, 1957, pp. 1050-1052.

7. Andrianov, K. A.; and Shdanov, A. A.: Synthesis of Polyorganoaluminosiloxanes. Doklady Adak. Nauk S.S.S.R., vol. 114, 1957, pp. 1005-1007.

8. Andrianov, K. A.; and Ganina, T. N.: Polyorganoaluminosiloxanes. Izvestia Akad. Nauk S.S.S.R. Otd. Khim. Nauk, 1956, pp. 74-82.

9. Wood, William G.; Iverson, Marlowe L.; and Kitasaki, Kiyoshi: Heat-Stable Aluminosiloxane Polymers. U.S. Patent 3,184,418, June 29, 1962.

10. Monroe, R. F.; and Schmidt, D. L.: Inorganic Aluminum-Oxygen-Phosphorus Bond Polymers, U.S. Patent 3,497,464, 1970.

11. Schmidt, D. L.; and Flagg, E. F.: Inorganic Bond Polymers, Aluminum-Oxygen-Phosphorus U.S. Patent 3,538,136, 1970.

12. Chamberlain, Mark M.: Inorganic Macromolecules Containing a Silicon-Oxygen-Metal Linkage. AD 601415, 1964.

13. Brown, John F.; Vogt, Lester H., Jr.; Katchman, Arthur; Eustance, John W.; and Kiser, Kenneth M.: Double Chain Polymers of Phenysilsesquioxane. J. Am. Chem. Soc., vol. 82, no. 23, 1960, pp. 6194-6195.

14. Kwan, S. C.; McElhill, E. A.; O'Connell, J. J.; and Tsigdinos, G.: Development of Improved Semiorganic Structural Adhesives for Elevated Temperature Applications. NASA CR-62561, 1965.

15. Lehn, W. L.: Inorganic Polymers, Industrial Research, Oct. 1962, pp. 64-69.

16. Stone, F. G. A.; and Graham, W. A. G.: Inorganic Polymers. Academic Press, New York, 1962.

17. Lappert, M. F.; and Leigh, G. L.: Developments in Inorganic Polymer Chemistry. American Elsevier Publ. Co., New York, 1962.

18. Gimblett, F. G. R.: Inorganic Polymer Chemistry. Butterworths, London, 1963.

19. Cotterill, R. M. J.: Glassy Metals. American Scientist, vol. 64, no. 4, 1976, pp. 430-4 37.

20. DuBois, J. H.: A Review of Uses and Properties of Inorganic Plastics, Insulation/Circuits, Oct. 1974. pp. 31-32.

21. Ray, N. H.: A New Approach to Inorganic Polymers. Endeavor, vol. 34, no. 121, 1975, pp. 9-18.

22. Flory, Paul J.: Principles of Polymer Chemistry. Cornell Univ. Press, Ithaca, New York, 1953.

23. Gregor, H. S.: Preparation of Aluminum Phosphates, U.S. Patent 2,460,344, 1949.

24. Callis, Clayton F.; Van Wazer, John R.; and Arvan, Peter G.: The Inorganic Phosphates as Polyelectrolytes. Chem. Revs., vol. 54, 1954. pp. 777-796.

25. Eubanks, A. G.; and Moore, D. G.: Investigation of Aluminum Phosphate Coatings for Thermal Insulation of Airframes. NASA TN D-106. Nov. 1959.

V-4
A Geologic Assessment of Potential Lunar Ores

DAVID S. McKAY and RICHARD J. WILLIAMS

Large amounts of silicon and aluminum and smaller amounts of other elements will be needed to construct large space structures such as solar power satellites. An analysis of transportation costs indicates that it may be much less expensive to use lunar material. Although bulk lunar soil is not a suitable feedstock for extracting metals, certain minerals such as anorthite and ilmenite can be separated and concentrated. These minerals can be considered as potential ores of aluminum, silicon, titanium, and iron. A separation and metal extraction plant could also extract large amounts of oxygen and perhaps hydrogen from these minerals. Anorthite containing 19 percent aluminum and 20 percent silicon can be concentrated from some highland soils where it is present in amounts up to 60 percent. Ilmenite containing 32 percent titanium and 37 percent iron can be concentrated from some mare soils where it is present in amounts up to 10 percent. The ideal mining site would be located at the boundary between a high-titanium mare and a high-aluminum highlands. Such areas may exist around the rims of some eastern maria, particularly Tranquilitatis. A location on Earth with raw materials as described above would be considered an economically valuable ore deposit if conventional terrestrial resources were not available.

INTRODUCTION

G. K. O'Neill (ref. 1) points out the potential economic advantage of using nonterrestrial resources, particularly lunar resources, in constructing large space structures in Earth orbit. This advantage accrues because the gravitational well of the Moon is only about 1/22 that of Earth. For the very large mass of material necessary to build a large space structure such as a solar power station, this difference in gravitational energy represents a significant savings in launch costs between the Earth and the Moon.

The construction of a large solar power station will require thousands of tons of aluminum and silicon. In addition, a large mass of shielding is necessary to protect the construction crew from exposure to cosmic rays and solar flares. How much of this material can be derived from the Moon? Do economically useful materials exist on the Moon? Can these materials be concentrated and processed to produce the material necessary for constructing large space structures? In the following sections, these questions are considered in the context of the extensive lunar data base resulting from the Apollo program.

BULK LUNAR SOIL AS A RESOURCE

Bulk lunar soil[1] contains as major constituents aluminum, silicon, iron, titanium, magnesium, calcium and oxygen. It has been previously proposed that lunar soil could be used directly as an industrial feedstock from which all of these constituents could be extracted in a single plant using a variety of processes (ref. 2). However, nearly all commercial metal-extraction plants are designed to process a single feedstock containing a small number of elements and to extract a single metal or, at most, two or three metals. The plants can then be optimized by a single process designed specifically for the feedstock and the end-product metal. For maximum extraction efficiency, the feedstock is usually concentrated by beneficiation processes before it enters the extraction plant. A plant designed to extract six or seven elements from bulk lunar soil would be extremely complex, it could not be optimized for a single element, and it would have to overcome such complex problems as cross reactions and blocking reactions.

Extensive experience has shown that it is nearly always far cheaper to concentrate an ore by beneficiation technique than to use the unconcentrated ore directly in the energy-intensive chemical processing plant. For example, energy used to concentrate iron ore is only about 1/10 that used in smelting and refining per ton of processed iron (ref. 3). Without concentration, the smelting and refining costs would be much greater and the processes themselves would need to be redesigned.

Based on these considerations and drawing on the extensive experience of commercial metal extraction, we suggest that it is more practical to limit the extraction effort to a small

---

1 The term "soil" is used here to describe the fine-grained debris layer which overlies much of the surface of the Moon: the term "regolith" is also often used for this layer.

number of elements and to concentrate lunar materials that contain only those elements. The metal-extraction plants can then be designed specifically for those elements using the least complicated processes available.

In following this philosophy, we have chosen aluminum as the primary metal to be extracted from lunar material — the mineral anorthite is the primary aluminum resource. In companion papers (refs. 4, 5), the mining and ore concentration operations are discussed as well as the chemical processing necessary to extract aluminum from anorthite. Silicon and oxygen are valuable by-products of this extraction process. Because aluminum and silicon may not be suitable for some applications (e.g., where high structural strength is required), we will also extract, on a smaller scale, iron and titanium from the mineral ilmenite. Again, references 4 and 5 discuss the procedures for mining and concentrating the ilmenite and for chemically extracting its metals and oxygen. A by-product of ilmenite concentration may be recovery of solar-wind hydrogen which can then be used for propulsion fuel or for life-support needs when combined with oxygen.

ANORTHITE AS AN ALUMINUM RESOURCE

Aluminum may be used extensively to construct a large solar power station. Fortunately, the Moon contains abundant aluminum as an essential constituent of the mineral anorthite, the aluminum-rich end member of the plagioclase series. Pure anorthite — $CaAl_2Si_2O_8$ — contains (by weight) 19.4 percent aluminum metal, 20.2 percent silicon metal, 14.4 percent calcium metal, and 46.0 percent oxygen. Anorthite can be considered to be a potential aluminum ore in the sense that it is a naturally occurring concentration of aluminum from which it may be economically feasible to extract the metal. Bauxite, which contains about 25 percent aluminum, is currently the major terrestrial aluminum ore. However, terrestrial anorthite has been used in some countries as a commercial aluminum ore (ref. 6). The United States Bureau of Mines (ref. 7) recently studied the economics of extracting aluminum from anorthite using a lime-soda sinter process. They concluded that the cost of extracting aluminum from anorthite was within a factor of 2 of the cost of extracting aluminum from bauxite and would become even more competitive as the cost of bauxite increased. The Bureau of Mines is currently planning to build a pilot plant to extract aluminum from anorthite (ref. 8). Alcoa Corp., which recently purchased a large area of land in Wyoming estimated to contain as much as 30 billion tons of recoverable anorthosite (ref. 9), is developing plans to recover aluminum from this source.

If anorthite is becoming attractive as a terrestrial aluminum resource, it is even more attractive as a lunar aluminum resource. The lunar crust contains a much higher proportion of anorthite than does the Earth's crust and the lunar highlands are particularly rich in anorthite.

Table 1 presents Al_2O_3 data on lunar soils sampled by the Apollo and Luna missions (refs. 10-12). Normative anorthite is calculated using a value of 36.6 percent Al_2O_3

---

for pure anorthite and assuming that all the Al_2O_3 in a regolith will go into anorthite. Normative anorthite is a good measure of the theoretical maximum amount of anorthite that can be present. The true or modal anorthite content will always be somewhat less because some aluminum will be present in solution in pyroxenes and glasses. Table 1 shows clearly that the highlands contain notably more normative anorthite than the mare regions. It is also apparent that the highlands show considerable variation in normative anorthite content from site to site and that the Apollo 16 site is the region richest in anorthite.

ANORTHITE IN APOLLO 16 ROCKS

The rocks at the Apollo 16 site consist of a variety of cataclastic breccias, porous breccias, metamorphosed breccias, and crystalline melt rocks. The rocks display a considerable range of anorthite content. Anorthosites are richest in anorthite, containing more than 95 percent modal plagioclase that is more than 95 percent of the anorthite molecule (An_{95}). If we require an aluminum ore that is more than 90 percent anorthite, then anorthosite rocks are an ideal ore. These rocks are represented in the Apollo collection by such rocks as 60015 (mass, 5547 g), which is more than 98 percent plagioclase of An_{96-96}; 60025 (mass, 1836 g), which is more than 98 percent plagioclase of A_{n95-97}; 60215 (mass, 385 g), which is more than 99 percent plagioclase of An_{96-97}; and 65315 (mass, 300 g), which is more than 98 percent plagioclase of An_{97-98} (ref. 13). These rocks contain about 35 percent Al_2O_3 or 18 percent aluminum metal.

Unfortunately, anorthosites are not particularly common among the Apollo 16 rocks. A survey of 342 rock fragments 2-4 mm in size showed that only 9 percent were anorthosites (ref. 13). A more abundant rock type of a slightly lower grade is the light matrix breccia. Light matrix breccias contain about 34 percent Al_2O_3, or about 93 percent normative anorthite (ref. 14). A study of 31 1-2 mm fragments of light matrix breccias showed a mean modal plagioclase content of 79 percent (ref. 15), or somewhat less than the normative anorthite calculated from the Al_2O_3 content. Studies of 2-4 mm fragments at each Apollo 16 station showed a range in the total anorthosite plux light matrix breccia fragments from a low of 25 percent at stations 9 and 10 to a high of 63 percent at station 11 (ref. 14). The other rock types present at the Apollo 16 site generally contain less anorthite plagioclase than either anorthosite or light matrix breccia. These rock types include feldspathic melt rocks with 62-84 percent plagioclase (ref. 16), metamorphosed breccia, and poikilitic rocks with 50-55 percent plagioclase (ref. 17). Consequently, they are lower grade potential ores of aluminum.

ANORTHITE IN APOLLO 16 SOILS

Lunar soil consists mainly of fine particles formed by meteorite impact communion of lunar rocks (for a detailed discussion of the lunar soil or regolith, see refs. 2, 18). Lunar soil has the advantage of being already pulverized with a mean grain size generally between 40 and 100 μm. From an economic point of view, this means that lunar soil is very easy to mine by simple surface mining techniques and furthermore need not be pulverized before being fed into ore concentration devices. This is in contrast to the much coarser rock or megaregolith that lies beneath the fine-grained regolith. The megaregolith would require much more elaborate mining processes and would also require energy-intensive grinding equipment. Therefore, we conclude that lunar soil is the best source of anorthositic aluminum ore.

TABLE 1 — Al_2O_3 CONTENT AND NORMATIVE ANORTHITE OF HIGHLAND AND MARE SOILS SAMPLED BY THE APOLLO MISSIONS[a]

Mission		Stations	No. of Soils	Al_2O_3, percent	Normative anorthite, percent
Highland soils	Ap 14	LM, G	6	17.5	48
	Ap 15	2,6,7	11	16.6	45
	Ap 16	1,2,3,4,8	10	27.5	75
	Ap 16	11	4	29.0	79
	Ap 17	2,3	11	20.7	56
	Ap 17	6,7	7	17.8	49
	Luna 20	---	1	22.8	62
Mare soils	Ap 11	LM	1	13.6	37
	Ap 12	LM	11	14.0	38
	Ap 15	1,4,8,9	7	13.1	36
	Ap 15	9A	2	10.0	27
	Ap 17	0,1.1A,5	7	11.2	31
	Luna 16	---	1	15.3	42

a From references 10-12.

A soil made up of meteorite-pulverized anorthosite rock would be the best ore. However, as shown in table 1, such soils have not been found and the richest soils contain no more than 79 percent normative anorthite. This normative anorthite in the soil is not all available for the extraction processing plant, however. Some of it is dissolved in impact-produced glasses (mainly agglutinates) and some of it is intimately intergrown with pyroxene, olivine, and ilmenite and cannot be liberated without pulverizing. The amount of available anorthite that can be physically separated can be approximated on the basis of particle counts obtained from the 90-150 μm grain size fractions of lunar soils. This grain size is close to the mean grain size of immature lunar soils and may therefore be a good average of the coarser and finer grain size populations. Table 2 presents particle counts on 16 Apollo 16 soils from references 19 and 20. Only the anorthite-rich particles and agglutinates are shown. For comparison, the normative anorthite of each soil from data in references 10 and 21 is also shown.

Column 1 in table 2 shows the percent of individual plagioclase grains in each soil. Based on analysis of plagioclase grains in the rocks, these plagioclase grains can be expected to be about An$_{9\,5\text{-}9\,8}$. Column 2 shows the anorthosite rock fragments, which are generally more than 98 percent plagioclase. Column 3 shows light matrix breccia which, based on analyses of larger rock fragments discussed previously, can be expected to be about 93 percent anorthite. Column 4 represents the total available anorthite concentrate that can be physically separated from the soils without additional grinding. The mean value for the 16 numbers in column 4 is 43.5 percent available anorthite concentrate. The purity of the anorthite concentrate depends on the relative amounts of plagioclase and anorthosite at about 97 percent purity and light matrix

breccias at about 93 percent purity. For the soils in table 2, the concentrate is more than 95 percent pure anorthite.

The Apollo 16 samples are the most anorthite-rich soils of the Apollo missions. They contain 75 percent normative anorthite. An anorthite concentrate making up 43.5 percent of the average soil can be recovered without additional grinding. This concentrate is 95 percent pure anorthite. If soil from only station 11 is considered, a 58 percent anorthosite concentrate can be recovered. This concentrate is more than 92 percent pure anorthite. Thus it would appear feasible to obtain concentrates that are more than 90 percent anorthite and comprise from about 40-60 percent of the soils.

EFFECT OF SOIL MATURITY ON AVAILABLE ANORTHITE

The amount of available anorthite must always be somewhat less than the normative anorthite. However, for a constant normative anorthite content, the amount of available anorthite depends strongly on soil maturity. This relationship is shown in figure 1, where the available anorthite concentrate is plotted against the agglutinate content for the soils in table 1. Agglutinates are impact-produced glassy aggregates of glass, mineral, and lithic grains. The agglutinate abundance has been shown to be a useful index of surface exposure age of soil maturity (ref. 22). As agglutinate content increases, more of the aluminum in a soil is incorporated into the agglutinates, either in the glass itself or in feldspar grains engulfed and buried by the agglutinate glass. This aluminum cannot be concentrated by physical mineral separation techniques, so it is not available as an ore. Equally important is the dilution effect of the agglutinates on the recoverable anorthite

TABLE 2 — GRAIN POPULATIONS FOR SELECTED PARTICLE TYPES
OF THE 90-150-μm SIZE FRACTION IN SOME APOLLO 16 SOILS[a]

Sample		Plagioclase	Anorthosite	Light matrix breccia	Total[b]	Normative anorthite[c]	Agglutinates
Core	60009,455	47.0	6.8	3.8	57.6	82	12.5
	60009,457	76.2	3.8	0.8	80.8	—	2.2
	61161	14.7	4.7	13.6	33.0	72	37.0
	61181	5.3	4.3	7.3	16.9	74	59.6
STA 1	61221	17.0	13.6	10.0	40.6	77	6.3
	61241	12.3	5.0	18.3	35.6	74	27.1
STA 2	62281	16.0	5.6	11.3	32.9	73	40.0
	63321	9.6	11.2	14.0	34.8	79	32.6
STA 3	63341	12.6	5.9	14.9	33.4	79	40.0
	63501	10.3	3.0	16.7	30.0	76	44.6
STA 4	64501	20.3	3.0	6.6	29.9	75	51.6
STA 8	68501	12.3	1.9	29.3	43.5	73	38.6
	67481	15.0	10.9	20.3	45.2	79	23.0
	67601	14.0	3.6	24.0	41.6	79	36.0
STA 11	67701	21.0	3.3	34.0	58.3	78	15.6
	67711	41.0	4.6	36.6	82.2	80	1.6

a References 19 and 20.
b Values represent the total available anorthite of >90 percent purity.
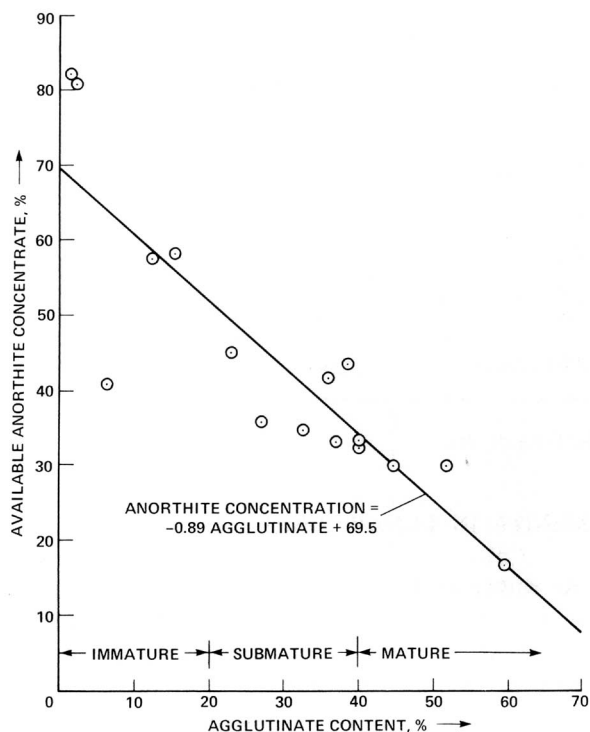c Calculated from data in references 10 and 21.

Figure 1 — *Relationship between available anorthite and maturity of soil.*

concentrate. As shown in figure 1, a mature soil has less available anorthite concentrate by a factor of 2 to 4 compared to an immature soil. The soils richest in available anorthite concentrate are the extremely immature soils with agglutinate contents less than 3 percent. Such soils are created by moderately large impact craters and are found at or near the surface close to fresh large craters.

DO HIGH-GRADE ANORTHITE DEPOSITS EXIST ON THE MOON?

At all Apollo and Luna sites, it is clear that ore beneficiation by mineral separation techniques is necessary to provide anorthite feedstock that is more than 90 percent pure for chemical processing. Do areas exist where the regolith is already more than 90 percent anorthite? If such areas were available as mining sites, there might be no need for ore beneficiation.

As discussed above, at the Apollo 16 site, two rock types have greater than 90 percent normative anorthite: anorthosite and light matrix breccia. No large body of anorthosite has been found, but a 30-m-thick layer of light matrix breccia is postulated to underlie the region around N. Ray crater (refs. 14, 15). If this layer were at the surface, the overlying regolith might be expected to contain 90 percent pure anorthite. However, no surface regolith of this grade has been identified in the Apollo 16 area. Furthermore, no large body of anorthosite has been found at Apollo 16 or any of the other Apollo or Luna sites.

The Apollo 15 and 16 orbital x-ray experiments mapped Al/Si ratios over the Command Service Module ground tract for these missions. Al/Si ratios in highland regions

ranged from 0.52 for the region west of Fecunditatis to a high of 0.71 for the farside highlands west of Mendeleev (ref. 23). For comparison, pure anorthite has a ratio of 0.96, the Apollo 16 site has a ratio of 0.67, and the most anorthite-rich surface soil, 67711, has an Al/Si ratio of 0.80. A material composed of 90 percent anorthite has an Al/Si ratio of about 0.90. Consequently, it is clear that no region has been discovered by orbital mapping which approaches the required concentration. Furthermore, the Apollo 16 area is among the most anorthite-rich areas known, being exceeded only by some areas on the far side of those areas mapped (ref. 23).

We conclude that no large anorthite-rich region is now known. Additional mapping by remote techniques would be desirable to try to locate such areas. Earth-based telescopic spectra sensing has been used to determine iron content in lunar regolith (ref. 24). Since iron content varies inversely with anorthite content, areas extremely low in iron would be rich in anorthite. Additional Earth-based telescopic observations might discover such areas. Surveys from lunar orbiting spacecraft would be highly desirable.

ILMENITE AS A RESOURCE FOR TITANIUM AND IRON

Although rutile is more desirable, ilmenite is also considered to be a commercial ore for producing titanium. Dupont Corp., for example, has used ilmenite ores on a commercial basis and the United States Bureau of Mines has recently reviewed the feasibility of replacing imported rutile with domestic ilmenite as a source for U.S. titanium (ref. 25). Ilmenite — $FeTiO_3$ — contains 31.6 percent titanium and 36.8 percent iron. In a companion paper (ref. 5), an extraction process is discussed that recovers titanium, iron, and oxygen from ilmenite.

LUNAR ILMENITE

Ilmenite is a constituent of most lunar rocks but occurs only in small amounts in highland rocks. Ilmenite is most abundant in mare basalts. Table 3 presents the normative ilmenite identified in each of the large returned mare basalts (ref. 26) and also shows the normative ilmenite calculated from the TiO_2 content by assuming that all TiO_2 is present as ilmenite. The Apollo 11 and 17 basalts are clearly richest in ilmenite. The chemical composition of lunar ilmenite is presented in table 4 (ref. 27).

ILMENITE IN LUNAR REGOLITH

As with anorthite, we consider soil as a source for ilmenite rather than the actual rocks. Again, regolith has the advantage of being easy to mine and of being already pulverized. The disadvantage is that some of the ilmenite is incorporated into glassy agglutinates and cannot be recovered by mineral separation techniques. Additionally, some of the ilmenite is present as fine-grained intergrowths or rock fragments and cannot be separated from pyroxene and plagioclase without additional grinding, which we hope

TABLE 3 — MODAL (MICROSCOPICALLY IDENTIFIED) AND NORMATIVE (CALCULATED FROM TiO_2 CONTENT) ILMENITE IN MARE BASALTS FROM THE APOLLO MISSIONS[a]

Sample	Modal ilmenite content, percent	Normative ilmenite content, percent
10003	14-18	21.5
10017	14-24	22.4
10044	6-12	17.1
10045	7-11	21.3
10049	16-17	21.5
10072	13-22	22.8
AP11 Mean	14.5	21.1
12202	8-11	4.9
12021	5-12	6.6
12022	9-23	9.3
12039	8-10	5.7
12051	8-11	8.9
12063	8-10	9.5
AP12 Mean	10	7.5
15016	6	4.4
15076	0.5	3.6
15475	1.0	3.4
15555	1-5	4.0
15556	2	5.1
AP15 Mean	2.6	4.1
75055	12-20	20.5
70215	13-37	24.7
70035	15-24	24.7
70017	19-23	24.7
AP17 Mean	20.4	23.7

a Reference 26.

to avoid. Consequently, the amount of ilmenite available without additional grinding is considerably less than the normative ilmenite. Table 5 presents the modal ilmenite in the 90-150-μm size fraction for the Apollo 11 soil and for nine Apollo 17 mare soils (A. Basu, unpublished data on 10084, 1977) (ref. 28).

TABLE 4 — CHEMICAL COMPOSITION OF ILMENITE FROM THE APOLLO 11 SITE; DATA ARE MEAN VALUES (IN WEIGHT PERCENT) FROM 17 ANALYSES[a]

TiO_2	53.1
FeO	43.7
Al_2O_3	0.26
Cr_2O_3	0.72
MnO	0.33
MgO	2.0
CaO	0.18
	100.29

a Reference 27.

TABLE 5 — MODAL (MICROSCOPICALLY IDENTIFIED) ILMENITE IN THE 90-150-μm GRAIN SIZE FOR THE APOLLO 11 SOIL[a] AND FOR NINE APOLLO 17 MARE SOILS;[b] NORMATIVE ILMENITE CALCULATED FROM THE TiO_2 CONTENT IS ALSO SHOWN

Sample	Modal ilmenite, percent	Normative ilmenite, percent
10084	2.2	14.7
79221	1.3	12.4
78501	3.7	10.4
75081	7.6	17.9
75061	5.3	19.6
71501	9.0	18.1
71061	4.6	17.7
71041	5.6	18.2
70181	2.3	8.1
70161	5.0	17.1
AP17 Mean	4.9	15.5

a Reference 28,   b Reference 29,   c Reference 10.

TABLE 6 — MODAL ILMENITE ABUNDANCE IN A SINGLE MARE SOIL (71061) AS A FUNCTION OF GRAIN SIZE[a]

Grain size, μm	Ilmenite, percent
45-75	6.0
75-90	3.3
90-150	4.6
150-250	3.3
250-500	2.3

a Reference 18.

The normative ilmenite calculated from the TiO_2 content of the bulk soil is also given. An important point to note in table 5 is that the available ilmenite in the average Apollo 17 mare soil is only 1/3 of the normative ilmenite. All modal data in table 5 are for the 90-150-μm grain size fraction. How does available ilmenite vary with grain size? Table 6 presents modal data for one Apollo 17 mare soil which shows the variation in ilmenite content over five grain size fractions (ref. 18). The overall trend is for more ilmenite to be available at finer grain sizes. This trend is to be expected because a larger proportion of ilmenite grains are liberated from lithic fragments as the overall grain size approaches the average grain size of the mineral grains in the lithic fragments. For sizes below 45 μm, no data are available, but more than 6 percent ilmenite grains should be present if the trend continues. Consequently, the 90-150-μm abundance of 4.6 percent may be a representative average for the whole soil. It appears that 90 percent ilmenite concentrates from mare soils is feasible. On average such concentrates would comprise about 5 percent of the soil; possibly as much as 10 percent could be recovered in favorable areas.

SOIL MATURITY AND AVAILABLE ILMENITE

As with anorthite, the amount of available ilmenite is influenced by the maturity of the soil. As soils mature, they generally become finer grained, which should have the effect of liberating more mineral grains. However, agglutinates are also formed, which tends to reduce the abundance of mineral grains. For Apollo 17 mare soils, the variation in the ratio of available ilmenite to normative ilmenite with agglutinate content is shown in figure 2. No trend is apparent in this figure and, at least for the 90-150-μm fraction, the degree of soil maturity appears to have little effect on the proportion of normative ilmenite available for mineral separation. This contrasts with anorthite, for which soil maturity strongly influenced the amount of available anorthite.
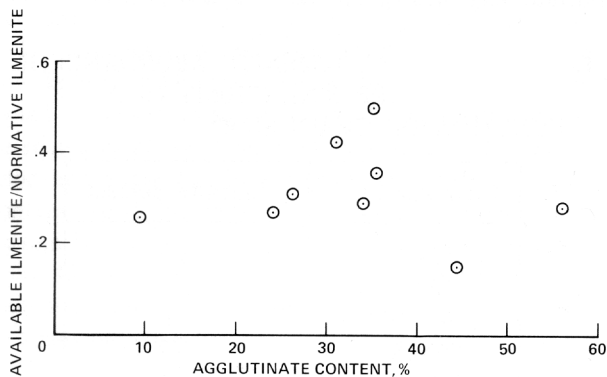

Figure 2 — *Variation in ratio of available ilmenite to normative ilmenite with agglutinate content.*

DO HIGH-GRADE ILMENITE RESOURCES EXIST ON THE MOON?

The most ilmenite-rich mare basalt from the Apollo samples contains about 25 percent ilmenite (table 3), and the most ilmenite-rich soil contains about 9 percent available ilmenite (table 5). Is it likely that more ilmenite-rich rocks and soils exist on the Moon? TiO_2 content can be approximated from optical spectral data using Earth-based telescopic observations (ref. 29). From observations made by this technique, the high titanium basalts of Apollos 11 and 17 appear to represent maximum TiO_2 contents for lunar materials. It is possible that some mare lava flows could have undergone near-surface fractionation and settling of ilmenite to form near-surface ilmenite cumulates. However, little support for this process can be found from the chemistry of the basalt samples (refs. 30, 31). Most researchers favor the theory that the ilmenite-rich basalts originated when a cumulate melted at some depth within the Moon (refs. 30, 31). Therefore, near-surface cumulates of ilmenite may not exist. If they do exist, they have not yet been sampled nor have they been detected by remote-sensing techniques.

BLACK GLASS AS AN ILMENITE RESOURCE

The orange glass and its partly crystallized equivalent, black glass, are apparently abundant in numerous locations, mainly around the rims of circular maria (ref. 32). This material contains 8.8 percent TiO_2 and, in its crystallized form, contains olivine, ilmenite, and other minerals. It has been suggested that this material might be a useful titanium ore (ref. 33). However, the crystallized ilmenite is always very fine-grained and tightly intergrown with olivine. It is therefore not possible to separate and concentrate the ilmenite unless the material were ground to a grain size approaching 1 μm, an extremely impractical undertaking. The bulk orange and black glass would not make a good titanium ore as it contains slightly less titanium than soils from ilmenite-rich basalt regions (such as soil 75080) and contains only about 1/6 as much titanium as ilmenite.

EXTRACTION OF HYDROGEN AND WATER DURING ILMENITE PROCESSING

It is well known that lunar soils contain essentially no water, except possibly in permanently shadowed polar cold traps. However, more mature lunar soils contain some hydrogen implanted from the solar wind. How much hydrogen is present, where is it located, and is it feasible to extract it from the lunar soils? Data on hydrogen content of lunar materials are relatively sparse and mostly limited to bulk soil analyses. Data from various investigators vary by about a factor of 2 for the same soil sample. Typical analyses by Epstein and Taylor (refs. 34-36) and Merlivat et al. (ref. 37) are in the range 30 to 60 ppm with a maximum of 61 ppm. Friedman et al. (ref. 38), DesMarais et al. (ref. 39), and Stoenner et al. (ref. 40) found generally higher values ranging up to 90 ppm for 10084 (ref. 38), 92 ppm for part of the Apollo 15 core (ref. 39), and 145 ppm for part of the Apollo 17 core (ref. 40). Eberhardt (ref. 41) considers 70 ppm to be a typical concentration.

Within a soil, hydrogen concentration varies inversely with grain size. This variation results from the surface correlation of all solar-wind species; these atoms are implanted and trapped near the surfaces of individual grains. For hydrogen, the only published data on this variation are by DesMarais et al. (ref. 39), who found an increase by a factor of about 2 in going from bulk soil to soil finer than 20 μm. Data on the variation with grain size of solar-wind helium are more plentiful. The behavior of hydrogen should be roughly comparable to helium, and helium generally shows an increase by about a factor of 2 in going from bulk soil to soil finer than about 20 μm (refs. 42, 43). The concentration of hydrogen has been measured on individual grains as a function of distance inward from the surface. The outermost zone may contain 400 to 600 ppm (refs. 44, 45).

Hydrogen content also varies with the type of particle. Agglutinates in a single-grain-size fraction may contain more than twice the hydrogen concentration of the bulk-size fraction and more than 10 times the hydrogen concentration

of plagioclase (ref. 40). Although no data exist for hydrogen, the mineral ilmenite is known to retain helium much more readily than other minerals. Hintenberger et al. (ref. 46) found for some Apollo 17 soils that, in the 35-54-μm grain size, the ilmenite grains were enriched in ^{4}He by a factor of about 3 to 6 over the bulk material in that size range. Eberhardt et al. (ref. 47) found that for soil 12001, the 11-μm ilmenite concentrate was enriched in ^{4}He by a factor of nearly 22 over the bulk ^{4}He content of the soil. If hydrogen shows the same enrichment factor as helium in ilmenite, the 11-μm grain size fraction of ilmenite in 12001 might be expected to contain 22 times the bulk hydrogen content of 44 ppm (ref. 48). The fine-grained ilmenite would then contain about 1000 ppm hydrogen. If the bulk soil contained 100 ppm hydrogen and if the 22x enrichment factor occurred, the fine-grained ilmenite would contain over 2000 ppm hydrogen. Whether hydrogen actually follows these trends of extreme enrichment in ilmenite remains to be shown. Only the lighter rare gases show this enrichment; actually, argon, krypton, and xenon show a depletion in ilmenite compared to bulk soil. Because of the enrichment of helium in ilmenite, soils show a correlation between TiO_2 content and helium content. Mare soils are up to an order of magnitude richer in helium than highland soils. The available hydrogen data do not show such a great difference. However, relatively few mare soils have been analyzed for hydrogen.

Maturity also influences hydrogen content. Immature soil 62221 contains only 8 ppm hydrogen and the extremely immature orange glass sample 74220 contains only 0.2 ppm hydrogen (ref. 36).

In summary, solar-wind hydrogen is present in some mature lunar soils in amount exceeding 70 to 100 ppm. The hydrogen is not homogeneously distributed but is concentrated in the finer grain sizes, by a factor of about 2 for the grains of less than 20 μm. Hydrogen is also concentrated by a factor of about 2 in agglutinates. The largest concentration, however, may be in ilmenite grains. For solar-wind helium, finer-grained ilmenite may contain more than 20 times as much helium per gram of ilmenite compared to a gram of bulk soil. Whether hydrogen follows this trend is yet to be determined. If it does follow the trend, however, the finer-grained ilmenite or mature mare soils may contain as much as 1000-2000 ppm hydrogen. Concentrates of this ilmenite could conceivably constitute a hydrogen ore. If this hydrogen were converted to water during the extraction process, the ilmenite concentrate would yield 1 to 2 percent water. Particularly as a by-product of the concentration of ilmenite, hydrogen might be extracted from ilmenite on the Moon with little additional effort. It should be emphasized however that the amount of hydrogen extracted from any concentrate must always be less than the hydrogen present in the bulk soil from which the concentrate came. A thermodynamic analysis of the amount of hydrogen that could be extracted and a discussion of the method and conditions for extraction are found in reference 4.

SELECTION OF A MINING SITE

From the previous discussions, a set of criteria can be constructed for selecting the optimum lunar mining site for Al, Si, Ti, Fe, and H_2 ores:

1. The site should be rich in anorthite, preferably as rich as the Apollo 16 site.
2. The anorthite deposit must consist of relatively immature regolith to increase the amount of available anorthite.
3. The site should also be rich in high TiO_2 mare basalt regolith.
4. The mare basalt regolith should be relatively mature to increase the hydrogen content.
5. The site must be suitable for the location of a lunar mass driver to transport the ore to space (ref. 1).
6. The site must be flat enough to allow easy surface mining.

The requirement for an area rich in both anorthite and ilmenite can only be met at a boundary between a mare region and a highland region. In addition, the mare region must contain a high TiO_2 basalt. These requirements are met at many places on the front side of the Moon, namely, around the margins of the high TiO_2 eastern maria. The requirement that the highland area be very rich in anorthite rather than, for example, KREEP or highland basalt, places an additional restriction on the site. The Descartes highlands area near the Apollo 16 site meets this requirement as determined from the returned samples and from the relatively high Al/Si and low Fe of the orbital x-ray experiment (refs. 23, 49). Whether this high Al region continues northward to Mare Tranquilitatis is not clear from the orbital data. Mare Tranquilitatis is relatively high in its southwestern quadrant near the lobe of highlands extending north from the Apollo 16 region. Consequently, this margin of Tranquilitatis might be an excellent site.

However, mass-driver siting seems to require a location farther east, preferably at long. 33°40′ E and lat. 1°44′ N in southeastern Tranquilitatis (ref. 50). This region appears to be lower in TiO_2 and the closest highland region appears somewhat lower in Al/Si ratio (ref. 23). More detailed remote data are needed to choose the optimum site for high TiO_2 and high Al/Si.

The requirement that the highland site be relatively immature is an important one, but one which can fairly easily be met by location near a relatively large fresh crater that has ejected a large quantity of fresh, immature soil. Mature mare regions should also be easy to locate as they predominate in areas away from fresh craters.

Most mare sites should be flat enough for easy surface mining. A problem might arise with the highland area because highlands at the boundary of mare basins often have a mountain front. However, experience from Apollos 15 and 17 has shown that highland soils are easily accessible in talus slopes or debris aprons at the base of highland mountains. At the Apollo 17 site, relatively pure mare soil

(80 percent mare, 20 percent highland material) was located at station 5 within 7 km of highland soil (92 percent highland, 8 percent mare material) at station 2 (ref. 51). Even over the 4 km between station 6 and the LM, the character of the soil changed from 70 percent highland to 70 percent mare. At the Apollo 15 site, mare soil at station 9 was about 85 percent mare material although it was only 4 km from the highland front (ref. 52). It would appear that a separation of about 5 km between a highland and mare mining pit would be sufficient to provide a reasonably clean separation of soil types. Even less distance might be appropriate for properly chosen sites. A debris apron, typically about 300 m wide, usually separates highland fronts from mare areas (ref. 53). Mining pits separated by only 300 m might be sufficient if located on either side of a debris apron.

SUMMARY AND CONCLUSIONS

We have discussed reasons why bulk lunar soil is not a suitable raw material for chemically extracting metals. On the basis of considerable terrestrial experience, it is much more desirable to concentrate minerals containing the desired metals and then to use extraction techniques specifically, designed for these minerals. A suitable lunar ore would be anorthite feldspar for aluminum and silicon.

Anorthite contains 19.4 percent aluminum and 20.2 percent silicon. It has been used commercially as an aluminum ore and will be used more and more in the future as the supply of bauxite declines. For titanium and iron, lunar ilmenite would be an excellent ore. Ilmenite contains 31.6 percent titanium and 36.8 percent iron. Chemical processing of both anorthite and ilmenite can produce abundant oxygen as a by-product.

Mineral separation techniques should be used on the lunar surface to concentrate the anorthite and ilmenite ores before shipping. Mining and ore beneficiation are greatly assisted by the fine-grained nature of the lunar soil, which eliminates the need for blasting, crushing, and grinding. An anorthite concentration mill located at the Apollo 16 site could recover 40 to 60 percent of the soil as a 90 percent pure anorthite concentrate. An ilmenite concentration mill on a high TiO_2 mare soil could concentrate 5-10 percent of the soils as 90 percent pure ilmenite concentrate. These numbers are based on the available soil data. However, more accurate figures are necessary and can be determined only if lunar soil is analyzed specifically for extractable anorthite and ilmenite content.

The ilmenite concentrate may be rich in solar-wind-derived hydrogen, perhaps containing as much as 1000-2000 ppm hydrogen in the fine-grained ilmenite. This quantity of hydrogen is equivalent to nearly 1-2 percent water. This water could be extracted from the ilmenite concentrate with little additional effort beyond that needed to mine and concentrate the ilmenite. However, actual analyses of hydrogen in ilmenite are necessary before the hydrogen concentration in ilmenite can be known with any certainty. In any case, hydrogen extraction would probably only be worthwhile as a by-product of ilmenite concentration processes.

The ideal mining site must be near both an immature highland area and a more mature TiO_2 mare area. Such sites exist around the margins of some of the eastern maria including Tranquilitatis. The southeastern margin of Tranquilitatis is also ideally suited for a mass-driver location. Additional chemical and soil maturity data are needed to determine whether acceptable mass-driver sites and acceptable geological sites coincide.

After candidate sites are located by Earth-based and lunar-orbiter remote techniques, detailed geologic prospecting, mapping, surveying, and sample analysis would be necessary before a site could be certified for mining operations. Such a site, if transported to Earth, would have such abundant and easily accessible anorthite and ilmenite as to make it a valuable terrestrial ore body, if conventional terrestrial ores did not exist.

REFERENCES

1. O'Neill, Gerard K.: The Low (Profile) Road to Space Manufacturing. Astronautics and Aeronautics, vol. 16, no. 3, March 1978, pp. 24-32.
2. Phinney, William C.; Criswell, David; Drexler, Eric; and Garmirian, James: Lunar Resources and Their Utilization. AIAA Paper 77-537, Third Princeton/AIAA Conference on Space Manufacturing Facilities, Princeton, N.J., May 9-12, 1977.
3. Hayes, Earl T.: Energy Implications of Materials Processing. Science, vol. 191, no. 4228, Feb. 20, 1976, pp. 661-665.
4. Williams, Richard J.; McKay, David S.; Giles, David; and Bunch, Theodore E.: Mining and Beneficiation of Lunar Ores. Space Resources and Space Settlements, NASA SP-428, 1979, pp. 219-229.
5. Rao, D. Bhogeswara; Choudary, U. V.; Erstfeld, T. E.; Williams, Richard J.; and Chang, Y. A.: Extraction Processes for the Production of Aluminum, Titanium, Iron, Magnesium, and Oxygen from Nonterrestrial Sources. Space Resources and Space Settlements, NASA SP-428, 1979, pp. 205-218.
6. Skinner, Brian J.: A Second Iron Age Ahead? American Scientist, vol. 64, May-June 1976, pp. 258-269.
7. Peters, Frank A.; and Johnson, Paul W.: Revised and Updated Cost Estimates for Producing Alumina from Domestic Raw Materials. Bureau of Mines Information Circular IC 8648, 1974.
8. Kirby, Ralph C.; and Prokopovitch, Andrew S.: Technological Insurance Against Shortages in Minerals and Metals. Science, vol. 191, no. 4228, Feb. 20, 1976, pp. 713-719.
9. Patterson, Sam H.: Aluminum From Bauxite: Are There Alternatives? American Scientist, vol. 65, May-June 1977, pp. 345-351:
10. Heiken, Grant H.: Lunar Soil Catalog. Lunar and Planetary Science Division, Johnson Space Center, Houston, Texas, 1972.
11. Vinogradov, A. P.: Preliminary Data on Lunar Ground

Brought to Earth by Automatic Probe 'Luna-16.' Proc. of 2nd Lunar Science Conf., Geochimica et Cosmochimica Acta, Suppl. 2, vol. 1, 1971, pp. 1-16.

12. Laul, J. C.; and Schmitt, R. A.: Chemical Composition of Apollo 15, 16, and 17 Samples. Proc. of 4th Lunar Science Conf., Geochimica et Cosmochimica Acta, Suppl. 4, vol. 2, 1973, pp. 1349-1367.

13. Dixon, James R.; and Papike, J. J.: Petrology of Anorthosites from the Descartes Region of the Moon: Apollo 16. Proc. of 6th Lunar Science Conf., Geochimica et Cosmochimica Acta, Suppl. 6, vol. 1, 1975, pp. 263-291.

14. Delano, J. W.; Bence, A. E.; Papike, J. J.; and Cameron, K. L.: Petrology of the 2-4 mm Soil Fraction from the Descartes Region of the Moon and Stratigraphic Implications. Proc. of 4th Lunar Science Conf., Geochimica et Cosmochimica Acta, Suppl. 4, vol. 1, 1973, pp. 537-551.

15. Taylor, G. Jeffrey; Drake, Michael J.; Hallam, Marie E.; Marvin, Ursula B.; and Wood, John A.: Apollo 16 Stratigraphy: The ANT Hills, The Cayley Plains, and a Pre-Imbrian Regolith. Proc. of 4th Lunar Science Conf., Geochimica et Cosmochimica Acta, Suppl.4, vol. 1, 1973, pp. 553-568.

16. Powell, Benjamin N.; Dungan, Michael A.; and Weiblen, Paul W.: Apollo 16 Feldspathic Melt Rocks: Clues to the Magmatic History of the Lunar Crust. Proc. of 6th Lunar Science Conf., Geochimica et Cosmochimica Acta, Suppl. 6, vol. 1, 1975, pp. 415-433.

17. Albee, A. L.; Gancarz, A. J.; and Chodos, A. A.: Metamorphism of Apollo 16 and 17 and Luna 20 Metaclastic Rocks at about 3.95 AE: Samples 61156, 64423, 14-2, 65015, 67483, 15-2, 76055, 22006, and 22007. Proc. of 4th Lunar Science Conf., Geochimica et Cosmochimica Acta, Suppl. 4, vol. 1, 1973, pp. 569-596.

18. Heiken, Grant: Petrology of Lunar Soils. Reviews of Geophysics and Space Physics, vol. 13, no. 4, Aug. 1975, pp. 567-587.

19. Heiken, G. H.; McKay, D. S.; and Fruland, R. M.: Apollo 16 Soils: Grain Size Analyses and Petrography. Proc. of 4th Lunar Science Conf., Geochimica et Cosmochimica Acta, Suppl. 4, vol. 1, 1973, pp. 251-265.

20. McKay, D. S.; Morris, R. V.; Dungan, M. A.; Fruland, R. M.; and Fuhrman, R.: Comparative Studies of Grain Size Separates of 60009. Proc. of 7th Lunar Science Conf., Geochimica et Cosmochimica Acta, Suppl. 7, vol. I , 1976, pp. 295-313.

21. Blanchard, Douglas P.; Jacobs, Jeffrey W.; Brannon, Joyce C.; and Brown, Roy W.: Drive Tube 60009: A Chemical Study of Magnetic Separates of Size Fractions from Five Strata. Proc. of 7th Lunar Science Conf., Geochimica et Cosmochimica Acta, Suppl. 6, vol. 1, 1976, pp. 281-294.

22. McKay, David S.; and Heiken, Grant H.: The South Ray Crater Age Paradox. Proc. of 4th Lunar Science Conf., Geochimica et Cosmochimica Acta, Suppl. 4, vol. 1, 1973, pp. 41-47.

23. Adler, I.; Trombka, J. I.; Schmadebeck, R.; Lowman, P.; Blodget, H.; Yin, L.; and Eller, E.; Podwysuki, M.; Weidner, J. R.; et al.: Results of the Apollo 15 and 16 X-ray Experiment. Proc. of 4th Lunar Science Conf., Geochimica et Cosmochimica Acta, Suppl. 4, vol. 3, 1973, pp. 2783-2791.

24. Adams, John B.; and McCord, Thomas B.: Vitrification Darkening of the Lunar Highlands and Identification of Descartes Material at the Apollo 16 Site. Proc. of 4th Lunar Science Conf., Geochimica et Cosmochimica Acta, Suppl. 4, vol. 1, 1973, pp. 163-177.

25. Henn, John J.; and Barclay, James A.: A Review of Proposed Processes for Making Rutile Substitutes. Bureau of Mines Information Circular IC 8450, 1970.

26. McGee, Patricia E.; Warner, Jeffrey L.; and Simonds, Charles H.: Introduction to the Apollo Collections; Pt. 1, Lunar Igneous Rocks. NASA TM X-74,633, 1977.

27. Cameron, Eugene N.: Opaque Minerals in Certain Lunar Rocks from Apollo 11. Proc. of Apollo 11 Lunar Science Conf., Geochimica et Cosmochimica Acta, Suppl. 1 , vol. 1, 1970, pp. 221-245.

28. Heiken, Grant; and McKay, David S.: Petrography of Apollo 17 Soils. Proc. of 5th Lunar Science Conf., Geochimica et Cosmochimica Acta, Suppl. 5, vol. 1, 1974, pp. 843-860.

29. Pieters, Carle; and McCord, Thomas B.: Characterization of Lunar Mare Basalt Types: 1. A Remote Sensing Study Using Reflection Spectroscopy of Surface Soils. Proc. of 7th Lunar Science Conf., Geochimica et Cosmochimica Acta, Suppl.7, vol. 3, 1976, pp. 2677-2690.

30. Duncan, A. R.; Erlank, A. J.; Willis, J. P.; and Ahrens, L. H.: Composition and Interrelationships of Some Apollo 16 Samples. Proc. of 4th Lunar Science Conf., Geochimica et Cosmochimica Acta, Suppl. 4, vol. 2, 1973, pp. 1097-1113.

31. Shih, Chi-Yu; Haskin, Larry A.; Wiesmann, Henry; Bansal, Brij M.; and Brannon, Joyce C.: On the Origin of High-Ti Mare Basalts. Proc. of 6th Lunar Science Conf., Geochimica et Cosmochimica Acta, Suppl. 6, vol. 2, 1975, pp. 1255-1285.

32. Heiken, Grant H.; McKay, David S.; and Brown, R. W.: Lunar Deposits of Possible Pyroclastic Origin. Geochimica et Cosmochimica Acta, vol. 38, 1974, pp. 1703-1718.

33. Arnold, James: Lunar Resource Surveys from Orbit. AIAA Paper 77-526, Third Princeton/AIAA Conference on Space Manufacturing Facilities, Princeton, N.J., May 1977.

34. Epstein, Samuel; and Taylor, H. P., Jr.: The Concentration and Isotopic Composition of Hydrogen, Carbon and Silicon in Apollo 11 Lunar Rocks and Minerals. Proc. of Apollo 11 Lunar Science Conf., Geochimica et Cosmochimica Acta, Suppl. 1, vol. 2, 1970, pp. 1085-1096.

35. Epstein, S.; and Taylor, H. P., Jr.: O^{18}/O^{16}, Si^{30}/Si^{28}, D/H and C^{13}/C^{12} Ratios in Lunar Samples. Proc. of 2nd Lunar Science Conf., Geochimica et Cosmochimica Acta, Suppl. 2, vol. 2, 1971, pp. 1421-1441.

36. Epstein, Samuel; and Taylor, Hugh P., Jr.: Investigation of the Carbon, Hydrogen, Oxygen, and Silicon Isotope and Concentration Relationships on the Grain Surfaces of a Variety of Lunar Soils and in Some Apollo 15 and

16 Core Samples. Proc. of 6th Lunar Science Conf., Geochimica et Cosmochimica Acta, Supp1.6, vol. 2, 1975, pp. 1771-1798.

37. Merlivat, L.; Lelu, M.; Nief, G.; and Roth, E.: Deuterium, Hydrogen, and Water Content of Lunar Material. Proc. of 5th Lunar Science Conf., Geochimica et Cosmochimica Acta, Supp1.5, vol. 2, 1974, pp. 1885-1895.

38. Friedman, Irving; Gleason, J. D.; and Hardcastle, K. G.: Water, Hydrogen, Deuterium, Carbon, and C13 Content of Selected Lunar Material. Proc. of Apollo 11 Lunar Science Conf., Geochimica et Cosmochimica Acta, Suppl.l, vol.2, 1970, pp. 1103-1109.

39. DesMarais, David J.; Hayes, J. M.; and Meinschien, W. G.: The Distribution in Lunar Soils of Hydrogen Released by Pyrolysis. Proc. of 5th Lunar Science Conf., Geochimica et Cosmochimica Acta, Suppl. 5, vol. 2, 1974, pp. 1811-1822.

40. Stoenner, R. W.; Davis, Raymond, Jr.; Norton, Elinor; and Bauer, Michael: Radioactive Rare Gases, Tritium, Hydrogen, and Helium in the Sample Return Container, and in the Apollo 16 and 17 Drill Stems. Proc. of 5th Lunar Science Conf., Geochimica et Cosmochimica Acta, Suppl. 5, vol. 2, 1974, pp. 2211-2229.

41. Eberhardt, P.: The Solar Wind as Deduced from Lunar Samples. Solar-Wind Three; Proceedings of a Conference. Institute of Geophysics and Planetary Physics, Univ. of Calif., Los Angeles, July 1974, pp. 58-67.

42. Hintenberger, H.; Weber, H. W.; and Takaoka, N.: Concentrations and Isotopic Abundances of the Rare Gases in Lunar Matter. Proc. of 2nd Lunar Science Conf., Geochimica et Cosmochimica Acta, Suppl. 2, vol. 2, 1971, pp. 1607-1625.

43. Kirsten, T.; Deubner, J.; Horn, P.; Kaneoka, L; Kiko, J.; Schaeffer, O. A.; and Thio, S. K.: The Rare Gas Record of Apollo 14 and 15 Samples. Geochimica et Cosmochimica Acta, Supp1.3, vol. 2, 1972, pp. 1865-1889.

44. Leich, D. A.; Tombrello, T. A.; and Burnett, D. S.: The Depth Distribution of Hydrogen and Fluorine in Lunar Samples. Proc. of 4th Lunar Science Conf., Geochimica et Cosmochimica Acta, Suppl. 4, vol. 2, 1973, pp. 1597-1612.

45. Leich, D. A.; Goldberg, R. H.; Burnett, D. S.; and Tombrello, T. A.: Hydrogen and Fluorine in the Surfaces of Lunar Samples. Proc. of 5th Lunar Science Conf., Geochimica et Cosmochimica Acta, Suppl. 5, vol. 2, 1974, pp. 1869-1884.

46. Hintenberger, H.; Weber, H. W.; and Schultz, L.: Solar, Spallogenic, and Radiogenic Rare Gases in Apollo 17 Soils and Breccias. Proc. of 5th Lunar Science Conf., Geochimica et Cosmochimica Acta, Suppl. 5, vol. 2, 1974, pp. 2005-2022.

47. Eberhardt, P.; Geiss, J.; Graf, H.; Grdgler, N.; Mendia, M. D.; Mdrgeli, M.; Schwaller, H.; and Stettler, A.: Trapped Solar Wind Noble Gases in Apollo 12 Lunar Fines 12001 and Apollo 11 Breccia 10046. Proc. of 3rd Lunar Science Conf., Geochimica et Cosmochimica Acta, Suppl.3, vol. 2, 1972, pp. 1821-1856.

48. Friedman, Irving; O'Neill, James R.; Gleason, Jim D.; and Hardcastle, Kenneth: The Carbon and Hydrogen Content and Isotopic Composition of Some Apollo 12 Materials. Proc. of 2nd Lunar Science Conf., Geochimica et Cosmochimica Acta, Suppl. 2, vol. 2, 1971, pp. 1407-1415.

49. Metzger, A. E.; Trombka, J. I.; Reedy, R. C.; and Arnold, J. R.: Element Concentrations from Lunar Orbital Gamma-Ray Measurements. Proc. of 5th Lunar Science Conf., Geochimica et Cosmochimica Acta, Suppl. 5, vol. 2, 1974, pp. 1067-1078.

50. Heppenheimer, T. A.: Trajectory Dynamics in the Earth-Moon System. AIAA Paper 77-532, Third Princeton/AIAA Conference on Space Manufacturing Facilities, Princeton, N.J., May 1977.

51. Rhodes, J. M.; Rodgers, K. V.; Shih, C.; Bansal, B. M.; Nuquist, L. E.; Wiesmann, H.; and Hubbard, N. J.: The Relationships Between Geology and Soil Chemistry at the Apollo 17 Landing Site. Proc of 5th Lunar Science Conf., Geochimica et Cosmochimica Acta, Suppl. 5, vol. 2, 1974, pp. 1097-1117.

52. Wanke, H.; Baddenhausen, H.; Balacescu, A.; Teschke, F.; Spettel, B.; Dreibus, G.; Palme, H.; Quijano-Rico, M.; Kruse, H.; Wlotzka, F.; and Begemann, F.: Multielement Analysis of Lunar Samples and Some Implications of the Results. Proc. of 3rd Lunar Science Conf., Geochimica et Cosmochimica Acta, Supp1.3, vol.2, 1972, pp. 1251-1268.

53. Young, Richard A.: The Morphological Evolution of Mare-Highland Contacts: a Potential Measure of Relative Mare Surface Age. Proc. of 7th Lunar Science Conf., Geochimica et Cosmochimica Acta, Suppl. 7, vol. 3, 1976, pp. 2801-2816.

V-5
Extraction Processes for the Production of Aluminum, Titanium, Iron, Magnesium, and Oxygen from Nonterrestrial Sources

D. BHOGESWARA RAO, U. V. CHOUDARY, T. E. ERSTFELD, R. J. WILLIAMS, and Y. A. CHANG

The suitability of existing terrestrial extractive metallurgical processes for the production of Al, Ti, Fe, Mg, and O_2 from nonterrestrial resources is examined from both thermodynamic and kinetic points of view. Carbochlorination of lunar anorthite concentrate in conjunction with Alcoa electrolysis process for Al; carbochlorination of lunar ilmenite concentrate followed by Ca reduction of TiO_2; and subsequent reduction of Fe_2O_3 by H_2 for Ti and Fe, respectively, are suggested. Silicothermic reduction of olivine concentrate was found to be attractive for the extraction of Mg because of the technological knowhow of the process. Aluminothermic reduction of olivine is the other possible alternative for the production of magnesium.

The large quantities of carbon monoxide generated in the metal extraction processes can be used to recover carbon and oxygen by a combination of the following methods: (1) simple disproportionation of CO, (2) methanation of CO and electrolysis of H_2O, and (3) solid-state electrolysis of gas mixtures containing CO, CO_2, and H_2O. The research needed for the adoption of Earth-based extraction processes for lunar and asteroidal minerals is outlined.

INTRODUCTION

The success of the space activity depends directly on the successful processing of nonterrestrial resources to obtain essential structural and life-support materials. A variety of structural materials is needed for the construction of solar power stations, mass-driver units, solar flare shelter and for the inside structures of the habitat. Aluminum was considered to be one of the essential metals needed for the construction of such space facilities (ref. 1). It was suggested that an extensive workshop must be provided as a fabrication facility so that many of the heavy components of a rolling mill, extrusion presses, casting beds and other equipment may be made at the space settlement rather than brought from Earth (ref. 1). It is, therefore, imperative that metals such as iron, titanium, and silicon, be available for steel manufacture. Finally, oxygen is one of the most essential elements needed for the life support.

The chemical and physical nature of lunar soils has been described by Levinson and Taylor (ref. 2). The lunar highlands consist mainly of anorthosite (ref. 3). Lunar rocks and fines also contain high titanium content and most of the titanium is present as ilmenite ($FeTiO_3$) (ref. 4). Based on the analysis of some meteoroids it is expected that asteroids may contain considerable amounts of olivine (T. Bunch, NASA-Ames Research Center, private communication). Chemical compositions of these nonterrestrial resources

reveal that aluminum, iron, titanium, and magnesium can be recovered in space. The possibility of manufacturing these elements in space has also been considered in previous studies on the utilization of nonterrestrial resources (refs. 1, 4, 5).

In this study, the suitability of existing terrestrial extractive metallurgical processes for the production of Al, Ti, Fe, Mg, and O_2 in space is examined from both the thermodynamic and kinetic points of view. However, the processes for extracting these elements from the nonterrestrial sources must be different from those conventionally used on Earth for the following reasons:

1. It is estimated that recovery of these elements is more economical in space than transporting them from Earth. The conventional hydrometallurgical operations are therefore not feasible because of the lack of water and hence suitable pyrometallurgical operations must be optimized.
2. Because of the load constraints of the space shuttle, only elements such as hydrogen, carbon, and chlorine, are suitable reductants. These reductants are to be carried from Earth.
3. There is a definite need for a process whereby the reactant carried from Earth can be recycled indefinitely. Thus, the reduction processes must be carefully considered to avoid irrecoverable losses of reductants.

4. The reduction processes must be specially suited for the conditions of space, viz., low gravity and high vacuum.

5. Since the source of oxygen is mainly the oxide minerals, the effluent gases from the reduction processes must be reprocessed to yield oxygen.

These constraints pose enormous problems and demand new processes. This paper evaluates suitable beneficiation processes for lunar and asteroidal minerals and indicates research efforts that must be extended to ascertain the feasibility of these processes. Some of them are based on thermodynamic evaluations and appear to be feasible, but no relevant industrial information exists. Such processes should be further investigated experimentally to identify optimal process conditions.

ALUMINUM

The main source of aluminum in the lunar soil is the plagioclase concentrate which contains mainly anorthite, $(Ca,Na)(Al,Si)_4O_8$. On Earth, aluminum is not normally produced from anorthite, although such resources are being seriously considered because of depleted supplies of bauxite ores (ref. 6). The chemical composition of anorthite is compared with the usual clays and bauxite resources of Earth in table 1. The major difference between anorthite and other minerals is the calcium content, which might prove to be a considerable problem in the extraction of aluminum.

The only processes known on Earth for the beneficiation of anorthite is the soda-lime sintering process (developed by the Bureau of Mines), which was tested both in the laboratory and by pilot plant operation (ref. 7). The general reaction of this process is represented by:

$$CaAl_2Si_2O_8(s) + 3CaCO_3(s) + Na_2CO_3(s) \rightarrow$$
$$2NaAlO_2(s) + 2Ca_2 SiO_4 (s) + 4CO_2(g) \qquad (1)$$
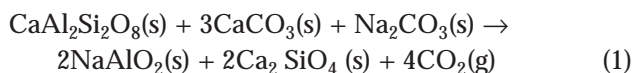
The reaction products are treated to obtain alumina.

In the lime-soda sintering process, it is evident from reaction (1) that large amounts of calcium and sodium carbonates are required. Each mole of anorthite consumes 3 moles of $CaCO_3$ and 1 mole of Na_2CO_3, which are not readily available on the Moon. Additionally, large amounts of water are needed for various leaching operations and water is very limited on the Moon. All these constraints lead one

to search for other suitable processes. The major processes considered are: carbothermic reduction, carbochlorination, aluminum monohalide process, and electrolysis. Out of these processes, carbochlorination, followed by the electrolysis of chlorides, was considered most attractive since a great deal is known about this process.

Carbothermic Reduction of Anorthite

In carbothermic reduction, the oxide reacts with carbon to produce metal and carbon monoxide:

$$M_xO_y(s) + yC(s) \rightarrow xM(s,\ell) + yCO(g) \qquad (2)$$

Since all constituent oxides of anorthite are highly stable, the reduction must be carried out at elevated temperatures (2500 K). At these temperatures, other compounds such as SiC, Al_4C_3, Al_4O_4C in the condensed phase, and Al_2O, SiO, Al, Si, and Ca in the gaseous phase are invariably present. Because of these phases, a reaction of the type (2) is very complicated. Most recently, Grjotheim et al. (ref. 8) explained the complications in the carbothermic reduction of alumina and reviewed the aluminum-producing reactions. Metal losses in the carbothermic reduction do occur because of the substantial vapor pressures of Al_2O and Al. Gitlesen et al. (ref. 9) calculated the partial pressures of Al, Al_2O and CO in the system Al_4O_4C - Al_4C_3 - Al, where Al_4O_4C and Al_4C_3 are the condensed phases formed during the carbothermic reduction of alumina. It is fairly conclusive from their calculations that the aluminum and aluminum suboxide pressures are so high below 1900° C that liquid aluminum cannot be formed at normal operating pressures. Any liquid aluminum added to the system would be consumed by the reactions

$$Al_4O_4C(s) + 2Al (\ell) \rightarrow 3Al_2O(g) + CO(g) \qquad (3)$$

$$Al(\ell) \rightarrow Al(g) \qquad (4)$$
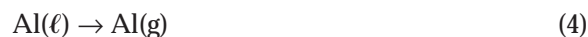
to maintain the equilibrium compositions of the gas phase. Above 2100° C, the solid aluminum carbide decomposes to aluminum and carbon. Also, carbonmonoxide partial pressure increases rapidly with respect to Al and Al_2O, favoring the formation of aluminum. However, metal losses through Al(g) and Al_2O(g) would still be significant unless special conditions are maintained.

Stroup (ref. 10) explained the special conditions for the carbothermic smelting of aluminum. In this process, the presence of a layer of molten aluminum saturated with carbide floating on a layer of molten oxycarbide and oxide in the electric furnace was taken to advantage. Both layers were electrically conductive, so the process was operated in a submerged arc or resistance furnace. Both the electrode and the raw charge pass through the metallic aluminum layer in operation. In the present process, the aluminum layer is allowed to saturate with Al_4C_3 at 2000° C, which reduces the activity of aluminum and maintains the temperature high enough to hinder back-reaction with carbon monoxide. The reaction between alumina and aluminum is also minimized when alumina is converted to oxycarbide.

TABLE 1 — COMPARISON OF THE CHEMICAL COMPOSITION OF LUNAR ANORTHITE WITH THE TERRESTRIAL ALUMINUM MINERALS

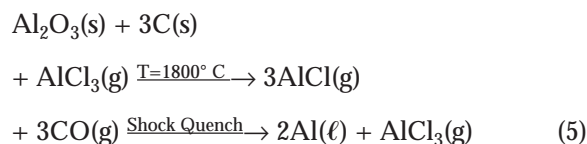| Percent dry basis	Alumina	Bauxite	Clay	Anorthite
Al_2O_3	100	40-58	40	34
SiO_2	—	9-25	44	45
Fe_2O_3	—	0.5-3	0.5	1
TiO_2	—	~2	0.7-2.5	—
CaO	—	0.1	0.1	19
MgO	—	—	—	1
Ignition loss	—	14.28	14	—

Striplin and Kelley (ref. 11) studied the feasibility of forming aluminum-silicon alloys by electrothermal reduction of clays and coke. To produce this alloy, the clay composition should contain at least 30 percent SiO_2. Although this process appears to be feasible provided the conditions are carefully chosen, several unexplained problems make the process unattractive:

1. The extent of reduction of Ca, Mg, Ti, Mn, and Cr and their distribution in the slag and vapor phase is not well established.
2. The formation of carbides, oxycarbides, and suboxides complicates the reaction mechanism which requires detailed study of the proper temperature and proportion of carbon-to-silicate ratio in the feedstocks.
3. Pilot plant operation with alumina and silica showed that the formation of carbides and oxycarbides made it impossible to obtain a melt of Al and Si below 2000° C. Even at 2300° C, the extent of metal losses due to promotion of products into vapor phase is not well established. The metal losses are promoted when the process operates under high vacuum conditions existing in space.
4. Anorthite contains significant amounts of CaO, which further complicates the process. At 2000° C, CaO is also reduced, yielding a Ca-Al-Si alloy that must be further purified.
5. Separation of CaO before the reduction process increases the amount of capital investment and requires large amounts of materials not readily available on the lunar surface.
6. Despite several years of research, no plant for producing aluminum through carbothermic reduction exists.

Carbochlorination Methods

In view of the potential problems anticipated in the carbothermic reduction of anorthite to produce aluminum, a low-temperature carbochlorination with Cl_2 followed by an electrolysis of the aluminum chloride produced appears to be more promising. A carbochlorination method using $AlCl_3$ is considered first.

High-temperature carbochlorination with $AlCl_3$ — A variation of carbochlorination recently tested by Peacy and Grimshaw (ref. 12) was based on an original proposal by Mitterbiller and Fruhwein (ref. 13). In this process, aluminum monochloride produced by high-temperature reduction of bauxite with carbon and $AlCl_3$ is shock-quenched to obtain Al containing small amounts of Si. The process can be essentially represented by:

$$Al_2O_3(s) + 3C(s)$$
$$+ AlCl_3(g) \xrightarrow{T=1800° C} 3AlCl(g)$$
$$+ 3CO(g) \xrightarrow{Shock\ Quench} 2Al(\ell) + AlCl_3(g) \qquad (5)$$

If this process is used to extract Al from anorthite, many problems will arise. Because of the reduced activity of alumina, much higher temperatures are needed to obtain a reasonable yield o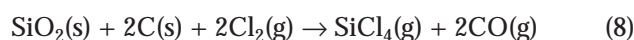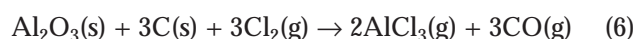f AlCl. This high-temperature process would pose severe problems such as corrosion of the reactor material compared to a low-temperature carbochlorination process. Further, substantial amounts of $SiCl_2$ and $CaCl_2$ will be present in the vapor phase from analogous reactions with SiO_2 and CaO in anorthite, resulting in an aluminum alloy that contains significant amounts of Ca and Si with some minor impurities. An additional purification step would then be required to recover the individual metals.

This process has been demonstrated only on a bench scale with bauxite. The only other attempt with a nonbauxite alumina ore is a single test (conducted at U.S. Bureau of Mines, ref. 14) in which carbochlorination of clay with $AlCl_3$ in the presence of lampblack and sugar did not yield any metal at 1300° C. This process is untested and also is not economically feasible compared to a low-temperature carbochlorination process followed by low-temperature electrolysis. Hence, the other alternative — low-temperature carbochlorination with Cl_2 — is a better method for extracting aluminum from lunar anorthite.

Low-temperature carbochlorination with Cl_2 — This method is essentially the same as the first step in Toth's process (ref. 7) in which $AlCl_3$ obtained from a low-temperature carbochlorination of ores that contain alumina is reduced to aluminum by manganese at about 250° C. The Mn content in Al obtained usually exceeds the theoretical value by 1 weight percent. Because of various technical complications (i.e., a very slow reduction of $AlCl_3$ by Mn), $AlCl_3$ obtained from the first step of Toth's process will be used to extract Al by an electrolysis route.

Previous studies of low-temperature carbochlorination of ores that contain alumina have been mainly confined to bauxite and clays which are essentially CaO-free. Anorthite contains significant amounts of CaO, and any chlorination process for anorthite must consider the formation of highly stable $CaCl_2$. Fortunately, $CaCl_2$ is a very useful by-product of the carbochlorination of anorthite. The various steps in the chlorination process are illustrated in figure 1.

The following reaction equilibria are to be considered in the thermodynamic analysis of the process.

$$Al_2O_3(s) + 3C(s) + 3Cl_2(g) \rightarrow 2AlCl_3(g) + 3CO(g) \qquad (6)$$
$$CaO(s) + C(s) + Cl_2(g) \rightarrow CaCl_2(s) + CO(g) \qquad (7)$$
$$SiO_2(s) + 2C(s) + 2Cl_2(g) \rightarrow SiCl_4(g) + 2CO(g) \qquad (8)$$

The net reaction is

$$CaO{\cdot}Al_2O_3{\cdot}2SiO_2(s) + 8C(s) + 8Cl_2(g) \rightarrow$$
$$CaCl_2(s) + 2AlCl_3(g) + 2SiCl_4(g) + 8CO(g) \qquad (9)$$
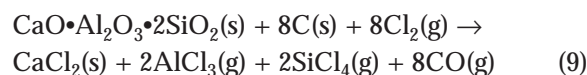
In the original Toth process of CaO-free ores containing alumina, the optimum temperature for carbochlorination was 975° C. However, for chlorination of anorthite, a lower operating temperature is required because $CaCl_2$ is liquid above 772° C, which introduces problems in operation. An optimum temperature between 675° - 770° C is preferable for anorthite chlorination.

In addition to the above mentioned equilibria, chlorination reactions involving some of the alkali, alkaline earth oxides, as well as FeO, MgO, and TiO_2, must be considered since most of these are present as impurities in lunar plagioclase concentrate. Most of the resulting chlorides are volatile and are condensed along with $AlCl_3$. Thermodynamic calculations reveal that the vapor phase contains very little $CaCl_2$ or complexes of $AlCl_3$-$CaCl_2$-$FeCl_3$. Since the recovery of SiO_2 is important for many glass-formation processes, the chlorination of SiO_2 in anorthite can be prevented if the required amounts of $SiCl_4$ are used along with Cl_2. $AlCl_3$ in the gas phase can be recovered by successive condensations to remove other volatile chlorides. Initially, $FeCl_3$ in the gas phase is condensed to a solid by cooling to about 225° C in a heat exchanger/condenser. $AlCl_3$ and chlorides other than $SiCl_4$ and $TiCl_4$ are condensed in a second stage at 90° C, while the latter are recovered in a subsequent stage at -30° C. The reactor residue is heated above 775° C to liquify $CaCl_2$, which can be separated from SiO_2-rich residue by centrifuging. The estimated composition of the residue should contain at least 75-82 weight percent SiO_2 and no more than 5-10 weight percent Al_2O_3 and 10-15 weight percent CaO. The exact composition of the residue should be determined from actual experiments. Pure CaO can be obtained by hydrolysis of $CaCl_2$ followed by calcination. The chlorine and water can be recycled further.

Pertinent thermodynamic calculations along with heat and mass balance are given in the appendix (see tables 4-6).

Alcoa Electrolysis Process

The electrowinning of aluminum from the electrolysis of $AlCl_3$ dissolved in a mixture of alkali and/or alkaline earth chlorides was attempted as early as 1854. These various early attempts are summarized in reference 8.

The most successful process to date is the one developed by Alcoa (at a cost of $25 million and 15 years of research). Since most of the problems encountered in electrolysis were solved by Alcoa and a plant producing 15,000 tons/yr is in operation, we selected this method for producing Al from the $AlCl_3$ obtained by carbochlorination. The Alcoa process has some distinct advantages over the classical Hall-Heroult process for electrowinning of aluminum: the working temperatures are substantially lower, relatively high current densities are used, carbon anodes are not consumed, and a much smaller plant area is required. The electrical energy consumed is claimed to be only 70 percent of that used in the Hall-Heroult process, mainly because of the higher electrical conductivity of the electrolyte and the small interpolar distance of Alcoa cells.

Because the technical details of the process are proprietary, only a brief outline and a discussion are given here. Figure 2 shows typical electrolyte cells. The feed consists of 3-10 weight percent of purified $AlCl_3$ along with the required amounts of alkali and alkaline earth chlorides. Electrolysis
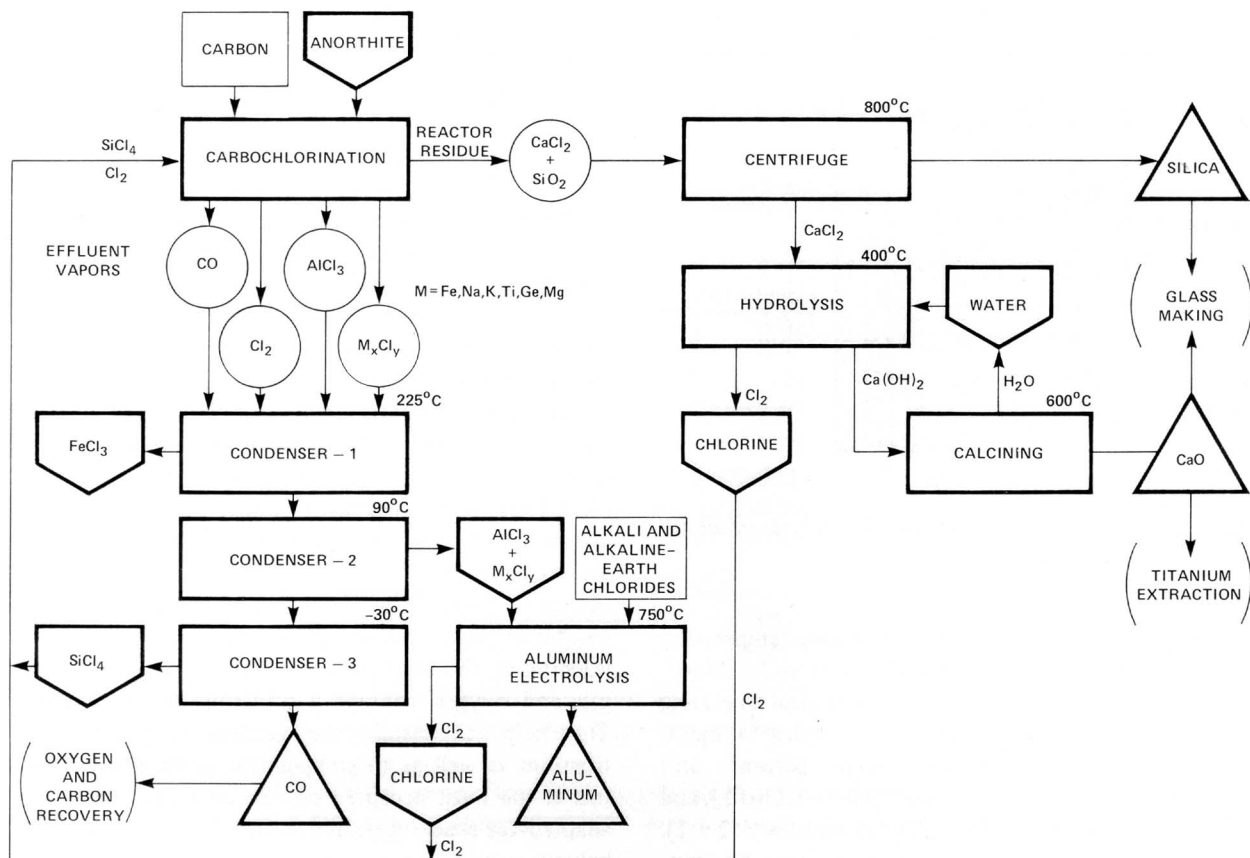

Figure 1 — *Aluminum processing.*

is performed under inert conditions in a sealed cell consisting of 20 to 30 bipolar carbon electrodes stacked vertically at an interpolar distance of 1 cm. Each bipolar electrode behaves as a cathode on its top surface and as an anode on its bottom surface. During normal operation, all electrodes remain immersed in the electrolyte at an operating temperature of $700° ± 30°$ C. A current density of 0.8-2.3 A/cm^2 and a single-cell voltage of 2.7 V are typical operating conditions in the Alcoa process. Two typical compositions of the electrolyte (in weight percent) are: $AlCl_3(5)$, $NaCl(53)$, $LiCl(40)$, $MgCl_2(0.5)$, $KCl(0.5)$, and $CaCl_2(1)$; and $AlCl_3(5 ± 2)$, $NaCl(53)$, and $LiCl(42 ± 2)$. The aluminum chloride concentration must be carefully controlled to ensure trouble-free operation. The $AlCl_3$ concentration must be above a certain limit to prevent the discharge of alkali ions, which are detrimental to the electrodes as they form interchelation compounds with graphite. An upper limit is set by the high pressure of $AlCl_3$. Also, the oxide content of the electrolyte must be as low as possible to prevent significant anode consumption with an attendant formation of an insoluble oxychloride sludge. An operating life of nearly 3 years is claimed for the electrodes when the oxide content of the electrolyte remains below 0.03 weight percent. The energy consumption of the cell is 9 kWhr/kg of aluminum produced.

A useful feature of the cell is that the chlorine generated at the anode sweeps the aluminum away from the cathodes and enhances the coalescence of Al droplets. The pumping effect of the chlorine bubbles maintains a continuous electrolytic flow across the cell, thus preventing the formation of Al pools on the electrodes. Chlorine collects at the top of the cell while molten aluminum falls countercurrently to the chlorine gas into a graphite compartment at the bottom of the cell. Liquid aluminum is passed through a filter to separate it from any excess electrolyte. The electrolyte is recycled to the cell; chlorine gas is also recycled into the carbochlorination step.
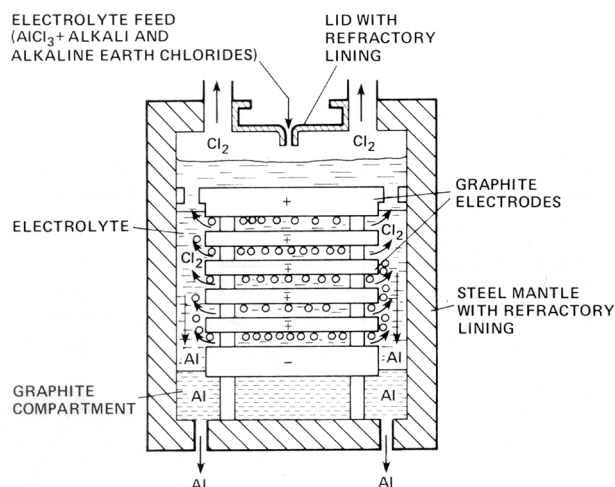

Figure 2 — *Alcoa's bipolar cell for electrolysis of aluminum trichloride.*

TITANIUM AND IRON

The main source of titanium and iron for nonterrestrial extraction is the ilmenite concentrate obtained from the lunar soil. The lunar ilmenite is of fairly high grade when compared to the terrestrial deposits. The chemical composition of lunar ilmenite concentrate is shown in table 2.

Titanium is commercially produced on Earth from ilmenite by a chlorination process and was described in an earlier study (ref. 5). In this process, iron is separated from TiO_2 by leaching with sulfuric acid after reducing ilmenite with coke or hydrogen at high temperatures. The residue (TiO_2) is chlorinated in the presence of carbon to form $TiCl_4$ which is further reduced by magnesium to yield titanium sponge. This process eliminates leaching at the final stages so that the dissolved hydrogen and oxygen content is minimum in the titanium. This helps to sustain the mechanical properties of titanium as well as to get pigment grade titania. While this is the most accepted process on Earth, and can be adapted for space operation; other alternatives are listed below.

NaOH Treatment

The ilmenite can be treated with molten NaOH according to the process patented by Hoekje and Kearley (ref. I5). During this treatment, TiO_2 is preferentially dissolved in NaOH leaving Fe_2O_3 which is insoluble in NaOH. The undissolved Fe_2O_3 is separated and the liquid is leached with hot water. This process also removes impurities such as aluminum and chromium. Since the leaching process uses water instead of acid, the process is easier to perform. However, this process has been tested only on a bench scale.

Carbochlorination Process

The other promising process appears to be the one patented by Daubenspeck and Schmidt (ref. 16) (fig. 3). The ilmenite is treated with CO at $650°$ - $1000°$ C to reduce Fe(III) to Fe(II) (this step may be unnecessary for lunar material). In this process the ilmenite is added at a rate of 5 kg/hr to a tube (4 in. in diameter X 48 in. long) containing 90-95 weight percent TiO_2 and just enough carbon to reduce FeO. It is then chlorinated at $800°$ C in a fluidized bed. The iron is thus selectively chlorinated yielding $FeCl_3(g)$, while TiO_2 remains in the bed. Ferric chloride is condensed and further reacted with oxygen in another fluidized bed at $300°$-$350°$ C to produce Fe_2O_3.

TABLE 2 — BULK COMPOSITION OF PLAGIOCLASE, ILMENITE AND OLIVINE CONCENTRATES[a]

Species	Plagioclase[b]	Ilmenite[b]	Olivine[c]
SiO_2	44.90	3.78	36
TiO_2	0.05	48.10	—
Al_2O_3	33.67	1.07	2
Cr_2O_3	>0.01	0.49	0.3
FeO	1.09	43.28	9
MnO	>0.01	0.03	0.2
MgO	1.35	1.29	23
CaO	18.59	1.07	2
Na_2O	0.45	0.04	1
K_2O	0.16	>0.01	0.2
P_2O_5	0.03	>0.01	—
S	>0.01	>0.02	—
Enrichment factor Al_2O_3	1.96	Enrichment factor TiO_2 3.7 FeO 2.2	— — —

a Ninety percent mineral and 10 percent residue.
b Lunar source.
c Asteroidal Source (based on the analysis of Meteoroids (T. Bunch, NASA-Ames Research Center, private communication)).

Titanium extraction — The reactor residue which is essentially pure TiO_2 can be used to extract titanium. A process reported by Chertien and Wyss (ref. 17) was chosen. In this process, a mixture of powders of calcium metal and TiO_2 is pelletized at 71,000 lb/in.[2] and heated for 2 h at 925° - 950° C. The titanium produced can be recovered by preferentially leaching CaO with a weak-acid wash solution. The main advantages of the process are that the leaching is minimal and all reagents can be recovered and recycled. The calcium metal can be obtained by processing calcium chloride, a by-product in the extraction of aluminum from anorthite.

The production rate of titanium can be enhanced by scaling up the process to handle 69,000 tons of ilmenite per year. Alternatively, several reaction tubes can be employed to process the required ilmenite. Some TiO_2 have to be brought to the space manufacturing facility (SMF) for the initial charge of the first tube. TiO_2 produced subsequently can be used to charge the other tubes.

The processes described in this report involve minimum leaching operations but at the final stages so that some hydrogen and oxygen might dissolve in titanium. Titanium thus produced either by this method or by the process described earlier (ref. 5) must be melted to obtain an ingot. Because of the high vacuum and very low oxygen activity in space, it is expected that the dissolved oxygen and hydrogen will be partly removed during vacuum melting operation.

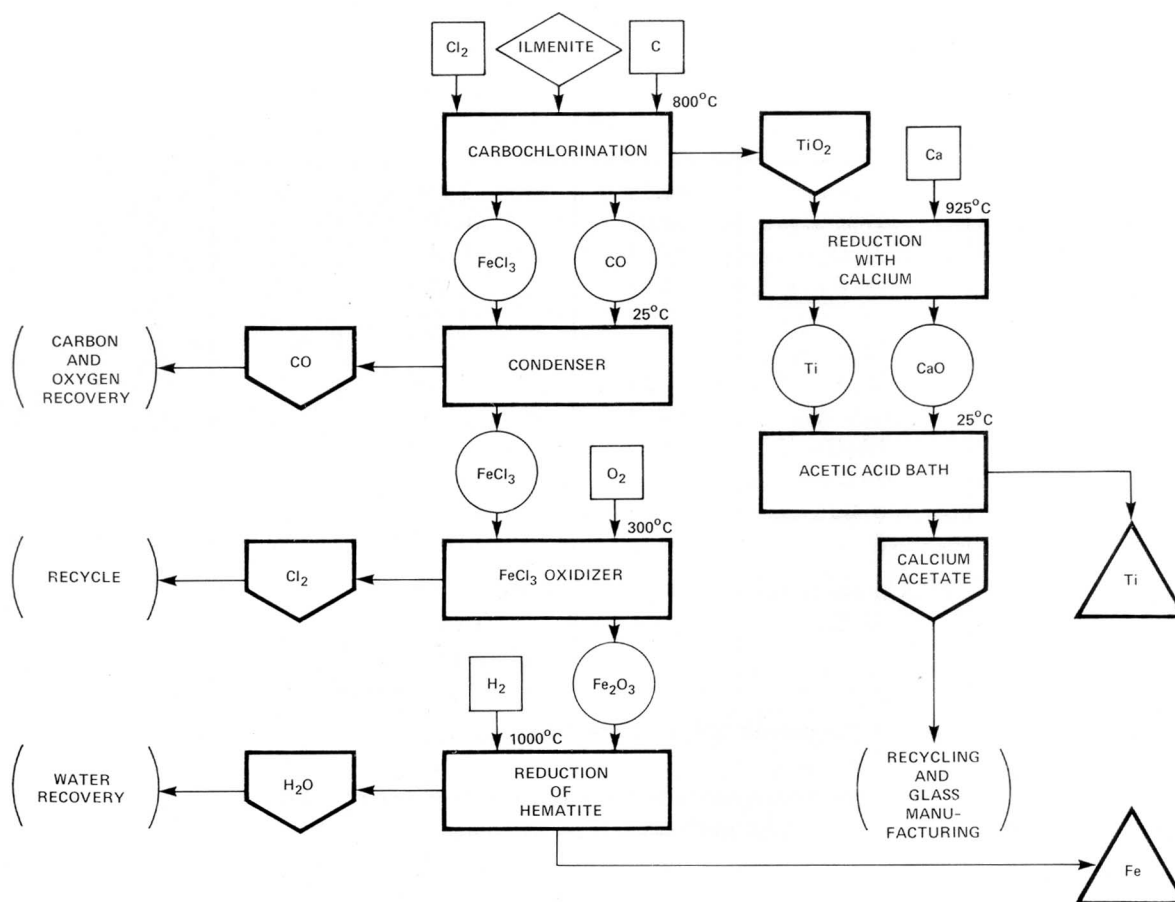*Iron extraction* — The ferric chloride obtained from the carbochlorination of ilmenite can be treated further to

Figure 3 — *Iron and titanium processing.*

extract iron. It can be reduced to metallic iron directly by H_2 at about 700° C. Hydrogen chloride is a useful by-product and can be used in the chlorination process. Alternatively, $FeCl_3$ can be oxidized in a fluidized bed at 300° - 350° C to produce Fe_2O_3, which can be reduced with either C or H_2 below 1000° C to obtain low-carbon steel or iron. In either case, the by-products CO or H_2O can be used to recover oxygen.

MAGNESIUM

Olivine is the main source of magnesium. Olivine is scarce in the lunar samples and is found in the gangue material left after anorthite is extracted. The gangue, a mixture of olivine and several other impurities (such as faylite), does not appear to be a suitable raw material. The best nonterrestrial source of olivine would be from an asteroid. The composition of olivine concentrate from asteroidal sources is given in table 2 (T. Bunch, NASA-Ames Research Center, private communication).

Selection of the Process

Potential reducing agents for olivine reduction are aluminum, calcium carbide, and silicon. Aluminothermic reduction of olivine is interesting from a chemical point of view but does not appear to be economically attractive when compared to the other processes. Of all the processes given, silicothermic reduction is technologically important and economically attractive. Although the other processes are discussed, the silicothermic reduction as shown in figure 4 is recommended.
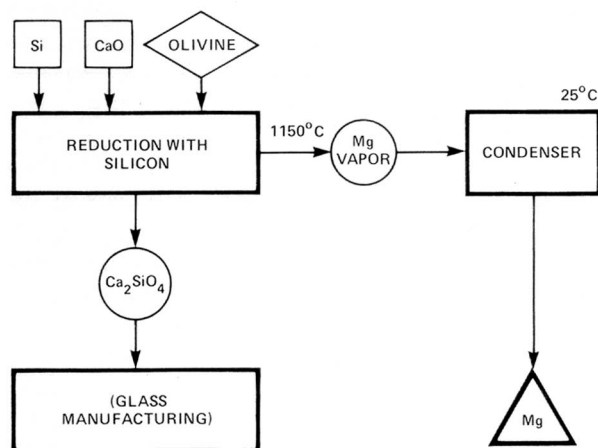

Figure 4 — *Magnesium processing (silicothermic reduction).*

Aluminothermic Reduction of Olivine

The reduction of olivine by aluminum in the temperature range 943° - 1150° C was studied by Grjotheim et al. (ref. 18). They found that olivine and aluminum react according to the scheme:

$$3Mg_2SiO_4(s) + 4Al(\ell) \rightarrow$$
$$2MgAl_2O_4(s) + 4MgO(s) + 3Si(s) \qquad (10)$$
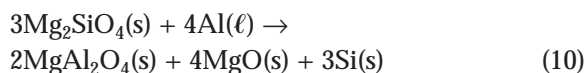
This was confirmed by the fact that, for a mole ratio of 4:3 (aluminum: olivine), no magnesium was obtained even at

1000° C. However, at a ratio of 2:1 and higher, an Al-Si alloy results:

$$3Mg_2SiO_4(s) + 6Al(s) \rightarrow$$
$$2MgAl_2O_4(s) + 4MgO(s) + 2AlSi(\ell) + Si(s) \qquad (11)$$
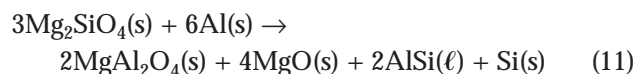
This alloy in turn reacts with magnesium oxide according to the equilibrium:

$$4MgO(s) + 2AlSi(\ell) \rightarrow$$
$$MgAl_2O_4(s) + 3Mg(g) + 2Si(s) \qquad (12)$$
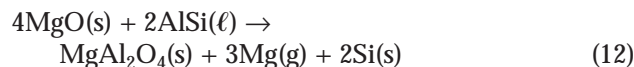
Although this process is attractive from a chemical viewpoint, magnesium cannot be quantitatively recovered because of the formation of $MgAl_2O_4$.

Calcium Carbide Reduction of Olivine

Thermal reduction of olivine by calcium carbide was studied by Grjotheim et al. (ref. 19). From a technical standpoint, calcium carbide is less attractive compared to ferrosilicon, but it was used as a reducing agent for magnesite before and during World War II.

The overall reaction for the process is

$$Mg_2SiO_4(s) + 2CaC_2(s) \rightarrow$$
$$Ca_2SiO_4(s) + 4C(s) + 2Mg(g) \qquad (13)$$
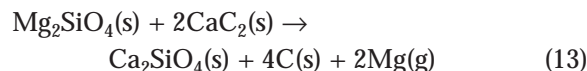
for a mixing ratio of 1:2 (olivine: calcium carbide). Reaction (13) does not represent a valid equilibrium scheme. Reaction (13) is obtained by combining reactions (14) and (15):

$$Mg_2SiO_4(s) + 2CaC_2(s) \rightarrow$$
$$2MgO(s) + 2CaO(s) + SiC(s) + 3C(s) \qquad (14)$$

$$2MgO(s) + 2CaO(s) + SiC(s) \rightarrow$$
$$Ca_2SiO_4(s) + 2Mg(g) + C(s) \qquad (15)$$
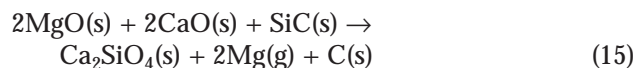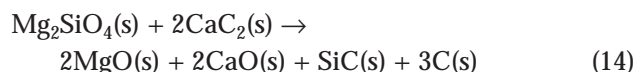
The vapor pressure of magnesium calculated from reaction (15) was much lower than the measured pressure in the presence of excess calcium carbide (ref. 19). In the presence of excess calcium carbide, for a molar ratio of 1:4, calcium carbide is available as a reducing agent for magnesia after conversion; the following reactions take place:

$$Mg_2SiO_4(s) + 2CaO(s) \rightarrow Ca_2SiO_4(s) + 2MgO(s) \qquad (16)$$

$$2MgO(s) + 2CaC_2(s) \rightarrow 2CaO(s) + 4C(s) + 2Mg(g) \qquad (17)$$

Calcium fluoride could be used as a catalyst to enhance the reaction rates.

In this process, one of the by-products is a highly stable silicon carbide. The recovery of carbon from a silicon carbide is rather a difficult operation. The process, therefore, is considered uneconomical unless there is a specific use for silicon carbide at the space manufacturing facility.

Silicothermic Reduction of Olivine

The production of magnesium through silicothermic reduction of dolamite is well known (refs. 20-23). The reducing agent used in industry is ferrosilicon containing

usually about 75 to 80 percent Si. The basic reaction of this process is represented as:

$$2MgO(s) + 2CaO(s) + Si(s) \rightarrow 2Mg(g) + Ca_2SiO_4(s) \quad (18)$$
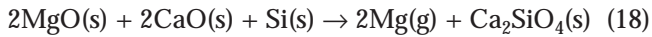
However, Ca-Si alloy is expected to form as an intermediate when the reaction temperature is above 1000° C:

$$4CaO(s) + (2n+1)Si(s) \rightarrow 2CaSi_n(sol) + Ca_2SiO_4(s) \quad (19)$$

where n indicates the silicon-to-calcium ratio in the liquid alloy. The equilibrium reaction for the production of magnesium is then:

$$2CaO(s) + 2MgO(s) + Si(so1) \rightarrow 2Mg(g) + Ca_2SiO_4(s) \quad (20)$$
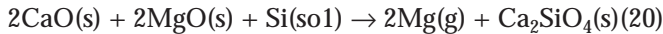
For processing asteroidal resources, the raw material is olivine rather than dolomite. The corresponding reactions for olivine are:

$$Mg_2SiO_4(s) + 2CaO(s) \rightarrow Ca_2SiO_4(s) + 2MgO(s) \quad (21)$$

$$4CaO(s) + (2n+1)Si(s) \rightarrow 2CaSi(sol) + Ca_2SiO_4(S) \quad (22)$$

$$2CaO(s) + 2MgO(s) + Si(sol) \rightarrow Ca_2SiO_4 + 2Mg(g) \quad (23)$$
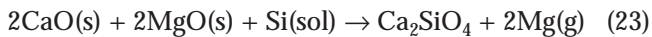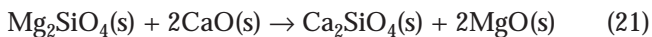
The main reaction that yields magnesium (23) is the same as for dolomite (20) and hence the magnesium pressure for the two processes is identical. The reduction of olivine by silicon in the presence of calcium oxide has been studied by Grjotheim et al. (ref. 19). They found that the absolute magnitudes of the calculated and observed pressures are in fair agreement. They also found that the slope of log P_{Mg} vs 1/T was in rather good agreement between the experimental data for olivine reduction and the various data for dolomite reduction. The establishment of magnesium pressure over the mixture of olivine, calcium oxide, and silicon was observed to be sluggish. The reaction rate was adequate when calcium fluoride of 5 weight percent was added as a catalyst.

Since the Pidgeon process has been used successfully to produce magnesium from dolomite commercially, the same technology could be profitably used for olivine reduction. Calcium oxide and silicon necessary for this process can be obtained from the by-products of anorthite processing.

OXYGEN

The most basic requirement for a space habitat is the availability of oxygen, which must be extracted from the nonterrestrial mineral agglomerates such as lunar raw materials. Further, to maintain the life process in space, humans require an atmosphere of acceptable composition and pressure. The desired composition of the atmosphere given below (ref. 24) is said to be the minimum pressure needed to meet the criteria for atmospheric safety:

$$T = 20° + 5°C$$

Relative humidity = 50 ± 10 percent

Gas	O_2	N_2	H_2O	CO_2
kPa	22.7	26.6	1.0	<0.4

The total atmospheric pressure is maintained at about half that at sea level on Earth (50.8 kPa).

In the following sections, various methods of recovering O_2 and C from the by-products of metal extraction processes are examined.

Extraction of Oxygen, Water, and Methane From CO

As a by-product of the aforementioned metal extraction processes, large amounts of carbon monoxide are generated which can be profitably used to recover solid carbon and to generate O_2, H_2O, and CH_4. For such recovery, three interdependent processes are envisioned (as illustrated in fig. 5). One simple method is to generate CO_2 and deposit

Figure 5 — *Oxygen and carbon recovery* processes.

carbon by the disproportionation of CO on a suitable catalyst that uses the well-known Boudouard reaction:

$$2CO(g) \xrightarrow{\text{catalyst}} CO_2(g) + C(s) \qquad (24)$$

Molecular oxygen and carbohydrates can be further obtained by photosynthesizing CO_2. On the other hand, CO can be reduced with H_2 in a catalytic reactor to produce water and methane:

$$CO(g) + 3H_2(g) \rightarrow CH_4(g) + H_2O(g) \qquad (25)$$

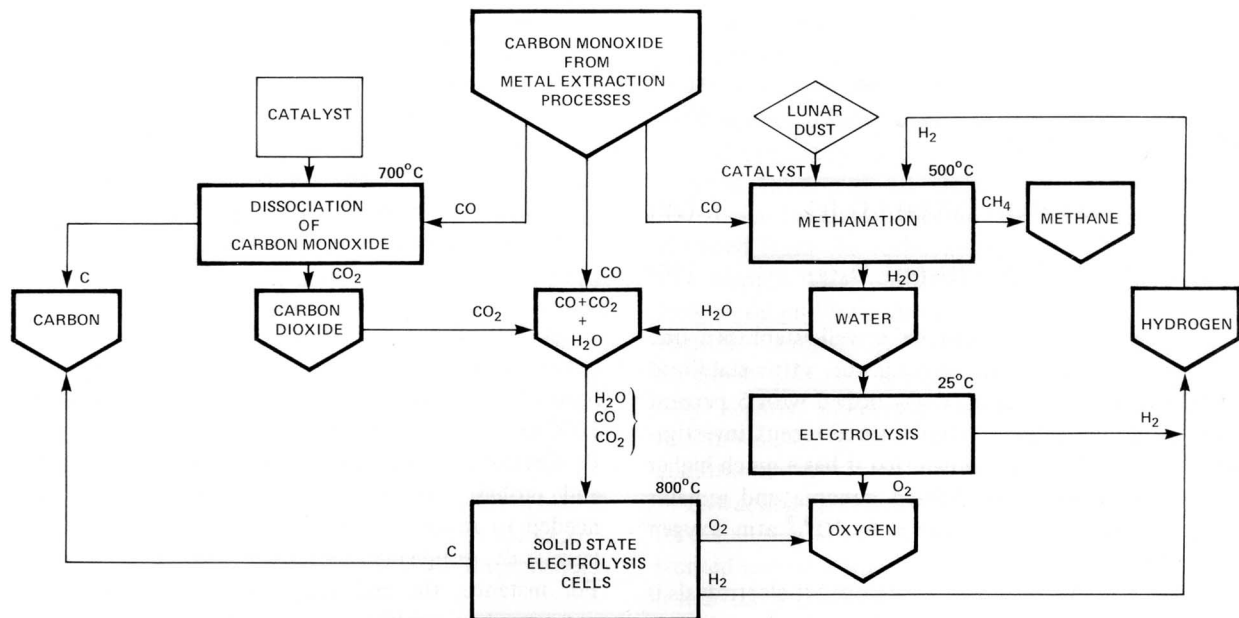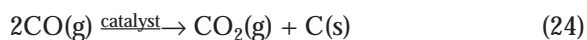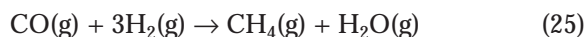This reaction has been used widely for many years in the petrochemical industry. Water is removed in a condenser and electrolyzed in one of several industrial electrolysis cells to obtain hydrogen and oxygen. Hydrogen can be recycled to the catalytic reactor for further reduction of CO.

Rosenberg et al. (ref. 25) investigated the methanation kinetics in the presence of nickel-on-kieselgator catalyst at 250° C. They outlined reaction conditions that resulted in the quantitative conversion of CO to methane and water in a single pass without the formation of by-product carbon or CO. Certain factors must be considered carefully: catalytic poisoning by the impurities in the gas feed, flow rate of gases, catalyst bed depth, and precisely controlling the temperature of the bed. Rosenberg et al. (ref. 25) reported complete conversion of CO to methane even with a space velocity of 2000 hr^{-1} at a H_2/CO ratio of 4. At a lower H_2/CO ratio, bed pressures up to 6 atm were required for higher conversion rates.

Recently, Cabrera et al. (ref. 26) compared the catalytic properties of cobalt, nickel, and lunar dust for the CO methanation reaction. For similar specific surface areas, the reaction rate constant was found to decrease in the order Co > Ni > lunar dust. Although Co and Ni catalyzed the reaction at temperatures near 200° C, detectable quantities of methane appeared only above 440° C with the lunar dust as the catalyst. At temperatures near 800° C, the catalytic activity of lunar dust is increased significantly. In view of the abundance and low cost of lunar dust compared to Co and Ni, further research should be conducted to correlate the catalytic activity with different lunar soil samples of varying grain sizes.

Another convenient method of recovering oxygen from the by-product gases is by solid-state electrolysis. This technique essentially involves the high-temperature electrolysis of the gas mixture consisting of CO, CO_2, and H_2O using a solid oxide electrolyte permeable to oxygen ions only. Since this recent technique has considerable potential, it is discussed in detail in the next section.

Solid-State Electrolysis for the Recovery of Oxygen and Carbon

Oxygen can be generated at the anode by the electrolysis of a gas mixture containing CO_2, CO, and H_2O using a solid electrolyte cell of that type:

$$Pt, O_2 \, / \, \text{Solid electrolyte} \, / \, CO_2, CO, H_2O, Pt$$

$$(O^{2-})$$

The less stable gas species (e.g., CO_2) will decompose first, followed by the more stable ones (e.g., CO). The half-cell reactions can be written:

At cathode:

$$2CO_2(g) + 4e^- \rightarrow CO(g) + 2O^{2-} \qquad (26)$$
$$2H_2O(g) + 4e^- \rightarrow 2H_2(g) + 2O^{2-} \qquad (27)$$

At anode:

$$2O^{2-} \rightarrow O_2(g) + 4e^- \qquad (28)$$

The net reactions are

$$2CO_2(g) \rightarrow 2CO(g) + O_2(g) \qquad (29)$$

$$2H_2O(g) \rightarrow 2H_2(g) + O_2(g) \qquad (30)$$
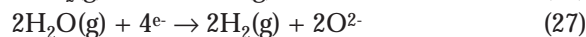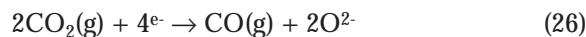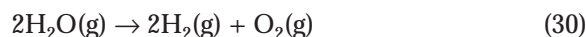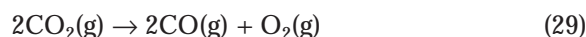
The solid electrolyte can be a well-established one such as calcia-stabilized zirconia or yttria-stabilized thoria. On the other hand, CeO_2 doped with 5 percent Y_2O_3 might be a better choice since recent investigations (refs. 27, 28) have shown that it has a much higher conductivity than CaO-stabilized zirconia and remains purely an ionic conductor down to 10^{-13} atm oxygen potential at 600° C.

Carbon and hydrogen can be removed if electrolysis is performed to remove all oxygen from the gas mixture. However, to completely remove oxygen, the oxygen potential at the cathode must be reduced below the electrolyte conduction domain of CeO_2 materials. It is proposed, therefore, to carry out the electrolysis in two steps: first, the oxygen potential in the gases is reduced by decomposing the less stable oxygen-bearing species using CeO_2-based electrolytes; in the second stage of electrolysis, Y_2O_3-stabilized thoria can be used to completely remove the oxygen.

The following characteristics of the solid electrolyte system for oxygen reclamation are important in any solid-state electrolysis study:

1. Stable gas-tight high-temperature seals
2. Electrolyte stability in terms of vaporization and degradation
3. Stable long-life electrodes
4. Compatibility between the coefficients of thermal expansion of the electrolyte and the cell structure

The only oxygen reclamation investigation based on the solid-state electrolysis is that of Weissbart et al. (ref. 29). They used calcia-stabilized zirconia as the electrolyte and conducted long-term electrolysis experiments with CO_2 and CO_2-H_2O gas mixtures. They found that small amounts of H_2O are needed to catalyze the reaction. For instance, the yield of oxygen with pure CO_2 is only one-fourth that obtained with CO_2 and a small amount of water vapor. Typically, the oxygen yield was 1 mole/min/W. Based on the results of extended tests, the following conservative

design parameters for a one-man operated prototype CO_2 electrolyzer were suggested by Weissbart et al. (ref. 29):

1. Operating temperature of 850° C
2. Current density of 100 mA/cm²
3. OZ Faradaic efficiency ≈ 100 percent
4. Electrolysis power, 250 W
5. Electrolysis power efficiency, 50 percent
6. Conversion of CO_2 to CO and O_2 of 35 percent per pass

At 850° C their cell ran for 200 hr at 100 percent current efficiency without apparent degradation. They found that the glass-ceramic sealing was effective up to 1000 hr of electrolysis. Precious-metal seals and porous Pt electrodes appear to be reliable for runs of 2000 hr and probably much longer. Further experiments are needed to resolve some of the anticipated problems in large-scale, solid-state electrolysis for oxygen recovery. For instance, the cell operation at high temperatures poses certain problems concerning materials, sealants, cell structure, power to maintain high temperatures, increased cell weight, and volume required for "insulation."

On the other hand, the oxygen recovery by solid-state electrolysis offers substantial advantages over conventional methods:

1. Since the electrolyte permits the transfer of oxygen ions only, the separation of oxygen from the gas mixture in a sealed cell is excellent.
2. The problem of gas-liquid phase separation at zero gravity is not encountered since there are no liquids in the electrolyte cell.
3. Unlike the fused salt electrolysis, only a few construction materials are needed for the cell since solid electrolyte is noncorrosive.
4. The continuous electrolysis of CO_2 or H_2O or a mixture of CO, CO_2, and H_2O is possible.

ASSESSMENT OF FURTHER RESEARCH NEEDS

Some of the processes described here have not been tested thoroughly, even for terrestrial applications on a laboratory scale. A few processes, such as Al electrolysis and methanation of CO, have proved to be commercially feasible and plants based on such processes are in operation. Although a partial list of problems likely to be encountered in various processes is given under respective sections, general and specific research areas are outlined here.

Metal Extraction Processes

Before any experimental work is undertaken, the various experimental factors, phase relations, and volatilization reactions must be identified. Once these factors are identified, a systematic method of representing the various reaction equilibria must be devised. Stability field diagrams in which the chemical potentials of the system components are represented as a function of temperature or of a specific species offer one such approach. Hence, as a first step in the

experimental process, it is proposed to construct such diagrams for various tenary systems (M_1-M_2-X_1 and M-X_1-X_2) and quaternary systems (M_1-M_2-X_1-X_2, M-X_1-X_2-X_3) of interest in the extraction processes of Al, Mg, Si, and Fe; M denotes a metal (Ca, Fe, Al, Si, or Mg) while X denotes a nonmetal (O_2, Cl_2, or C). Some of the experimental data needed to construct such diagrams are already available in the literature.

In view of the importance of rate processes in the extraction of metals, the next logical step would be to undertake a systematic and thorough investigation of kinetics and mass-transfer situations. By performing batch segregation tests, the effects of various factors such as reagent additions, particle size, and temperature can be investigated. Based on these results for a single process, a kinetic model can be set up which, in turn, can be used to predict process yields from limited data gathered by different processes.

Carbochlorination of anorthite — There have been few, if any, studies done, either thermodynamic or kinetic, on the low-temperature carbochlorination of anorthite. The first step in the investigation is the synthesis of plagioclase concentrate (90 percent anorthite + 10 percent rock) with its bulk composition closely identical to that of lunar material. Experimental investigations must be performed with the following objectives in mind:

1. Analyze vapor phase, preferably by a mass spectrometer modified for high-pressure sampling
2. Analyze the reactor residue
3. Determine the extent of deviation from thermodynamically calculated values for both condensed and vapor phases
4. Adjust feed rates of various reactants to the fluid bed reactor to selectively remove Al_2O_3 as $AlCl_3$
5. Separate $CaCl_2$ and SiO_2 from the reactor residue and determine the composition of the residue
6. Evaluate chemical engineering aspects of the process as related to lunar or extraterrestrial conditions.
7. Reinforce initial bench scale investigations with pilot plant studies

Alcoa electrolysis process — Since most of the technical aspects of this process for extracting Al from $AlCl_3$ have already been worked out, further studies should be devoted to finding an electrolyte composition more suited to lunar conditions. The aluminum chloride obtained from the carbochlorination of lunar anorthite will contain some alkali and alkaline earth chlorides. Instead of purifying the chlorides, an electrolyte composition compatible with these chlorides must be obtained. This new composition might be obtained by only slightly modifying the electrolyte composition recommended in the Alcoa process for terrestrial conditions.

Extraction of Ti and Fe from ilmenite — The processes for extracting Ti and Fe from ilmenite have already been worked out on a laboratory scale. The processes must be tested on a commercial scale. As in the Al extraction process, the first step in extracting Ti and Fe is the

chlorination of ilmenite in a fluidized bed reactor. The kinetic model set up for anorthite chlorination might be useful in evaluating the process yields based on the limited data concerning ilmenite chlorination.

Extraction of Mg from Olivine — Of all the pyrometallurgical processes for the extraction of magnesium from olivine, silicothermic reduction is the well-investigated process. However, the role of calcium silicide as an intermediate in the overall reduction process needs to be studied.

The following areas need to be investigated for choosing the other alternatives:

1. Kinetics of olivine reduction with aluminum as the reducing agents, and
2. The optimum ratios of reducing agent (Al) needed for the reduction processes.

Oxygen and Carbon Recovery

The kinetics, engineering design, and feasibility of continuous recovery of carbon and oxygen, vital for extraterrestrial activities, have not been thoroughly investigated. Some potential areas of research in the two proposed processes for the reclamation of oxygen and carbon from by-products of metal extraction processes are outlined here.

Methanation of CO — Further investigations are needed to clarify the chemical role of lunar and interstellar dust as a catalyst for the methanation reaction of CO and H_2 to produce CH_4 and H_2O. If the catalytic activity is proportional to the radiation damage sustained by lunar dust in addition to their higher surface area, fine-grained particles

might be a better catalyst because they are exposed to radiation longer than coarse-grained particles. The necessary submicron-sized lunar dust, because of its persistent internal polarization, can be effectively separated by electrostatic purification. Strong research efforts should be undertaken to verify the gain-size correlation of the catalytic effect, which, if proven correct, would lead to a very inexpensive way of catalyzing methanation without resorting to currently used industrial catalysts such as cobalt and nickel.

Solid-state electrolysis — This recent area of research has potential for the recovery of oxygen and carbon from the effluent gases of metal extraction processes. In solid-state electrolysis, the power requirements become excessive as the operating temperature is lowered because of higher cell resistance at lower temperatures. Hence, it is desirable that the cell temperatures be decreased as far as possible, consistent with high Faradiac efficiency. In view of the recent synthesis of solid electrolytes, such as Y_2O_3 doped CeO_2 with high ionic conductivities compared to the conventional ZrO_2-CaO and ThO_2-Y_2O_3 electrolytes, it might be possible to operate the cells at lower temperatures with considerable savings in energy. Hence, the experiments should be conducted with the following objectives in mind:

1. To test the feasibility of CeO_2-Y_2O_3 electrolyte
2. To establish the optimum conditions for long life of the cells
3. To improve the existing design of the metal-ceramic seals
4. To select an optimum temperature — the lowest temperature of cell operation consistent with acceptable IR loss in the electrolyte

TABLE 3 — REACTIONS OF INTEREST IN METAL AND OXYGEN EXTRACTION PROCESSES

1. $Al_2O_3(s) + 3C(s) + 3Cl_2(g) \rightarrow 2AlCl_3(g) + 3CO(g)$
2. $CaO(s) + C(s) + Cl_2(g) \rightarrow CaCl_2(s) + CO(g)$
3. $SiO_2(s) + 2C(s) + 2Cl_2(g) \rightarrow SiCl_4(g) + 2CO(g)$
4. $CaO \cdot Al_2O_3 \cdot 2SiO_2(s) + 8C(s) + 8Cl_2(g) \rightarrow 2AlCl_3(g) + CaCl_2(g) + 2SiCl_4(g) + 8CO(g)$
5. $FeTiO_3(s) + 3C(s) + \frac{3}{2}Cl_2(g) \rightarrow FeCl_3(g) + TiO_2(s) + 3CO(s)$
6. $FeCl_3(s) \rightarrow FeCl_3(g)$
7. $2FeCl_3(s) + \frac{3}{2}O_2(g) \rightarrow Fe_2O_3(s) + 3Cl_2(g)$
8. $Fe_2O_3(s) + 3H_2(g) \rightarrow 2Fe(s) + 3H_2O(g)$
9. $Fe_2O_3(s) + 3CO(s) \rightarrow 2Fe(s) + 3CO_2(g)$
10. $TiO_2(s) + 2Ca(s) \rightarrow Ti(s) + 2CaO(s)$
11. $Mg_2SiO_4(s) + 4CaO(s) + Si(s) \rightarrow 2Ca_2SiO_4(s) + 2Mg(g)$
12. $2CO(g) \rightarrow CO_2(g) + C(s)$
13. $CO(g) + 2H_2(g) \rightarrow CH_4(g) + H_2O(g)$
14. $H_2(g) + \frac{1}{2}O_2(g) \rightarrow H_2O(g)$

APPENDIX

SUGGESTED EXTRACTION PROCESSES

From the several possible methods for extracting metals and oxygen from the lunar and asteroidal resources, the following are considered best suited for nonterrestrial conditions:

1. Carbochlorination of lunar plagioclase concentrate in conjunction with Alcoa electrolysis for Al
2. Carbochlorination of lunar ilmenite concentrate followed by Ca reduction of TiO_2 and subsequent reduction of Fe_2O_3 by H_2 for Ti and Fe, respectively
3. Silicothermic reduction of asteroidal olivine concentrate for Mg
4. Methanation of CO and electrolysis of H_2O and/or solid-state electrolysis of gas mixture containing CO, CO_2 and H_2O for oxygen

The principal reactions of interest in the metal and oxygen extraction process along with the thermodynamic data, mass, and heat balances of the processes considered are detailed in tables 3-7.

TABLE 4 — THERMODYNAMIC DATA FOR SOME PERTINENT REACTIONS
IN METAL AND OXYGEN EXTRACTION PROCESSES

Reaction no.	Temperature, K	$\Delta G°$, Kcal	$\Delta H°$, Kcal	K	Partial pressure of species ($\Sigma P_i = 1$ atm)					
					Gaseous species	P_i	Gaseous species	P_i	Gaseous species	P_i
1	900	−62.2	37.7	1.26×10^{15}	$AlCl_3$	~0.4	CO	~0.6	Cl_2	3.0×10^{-6}
	1000	−73.3		1.07×10^{15}	$AlCl_3$	~0.4	CO	~0.6	Cl_2	1.4×10^{-6}
2	900	−73.3	−63.4	6.5×10^{17}	---	---	CO	~1.0	Cl_2	1.6×10^{-18}
	1000	−74.4		1.8×10^{16}	---	---	CO	~1.0	Cl_2	5.5×10^{-17}
3	900	−41.5	6.2	1.2×10^{10}	$SiCl_4$	~0.333	CO	~0.667	Cl_2	3.5×10^{-6}
	1000	−48.8		1.7×10^{10}	$SiCl_4$	~0.33	CO	~0.667	Cl_2	3.0×10^{-6}
4	900	−190.6	11.9	1.9×10^{46}	$SiCl_4$ or $AlCl_3$	~0.166	CO	~0.667	Cl_2	2.3×10^{-6}
	1000	−213.1		3.7×10^{46}			CO	~0.667	Cl_2	2.0×10^{-6}
5	1000	−69.2	−76	2.7×10^{33}	$FeCl_3$	0.25	CO	0.75	Cl_2	5.3×10^{-21}
	1100	−74.1		2.5×10^{30}	$FeCl_3$	0.25	CO	0.75	Cl_2	1.2×10^{-21}
6	500	11.2	33.2	1.3×10^{-5}	$FeCl_3$	1.3×10^{-5}	---			
	600	6.7		3.8×10^{-3}	$FeCl_3$	3.8×10^{-3}	---			
7	500	−25.6	−8.6	1.5×10^{11}	O_2	3.6×10^{-8}	---		Cl_2	~1
	600	−29.0		3.5×10^{10}	O_2	9.3×10^{-8}	---		Cl_2	~1
8	1000	−3.6	15.3	6.62	H_2	0.348	---		H_2O	0.652
	1200	−7.6		24.0	H_2	0.257	---		H_2O	0.743
9	1000	−5.9	−9.0	19.9	---	---	CO	0.27	CO_2	0.73
	1200	−5.4		94.7	---	---	CO	0.325	CO_2	0.675
10	1200	−70.3	−81.3	6.3×10^{12}						
	1300	−69.4		4.6×10^{10}						
11	1300	+7.7	64.7	5.2×10^{-2}	Mg	0.23				
	1500	−1.1		1.46	Mg	1.21				
12	800	−7.3	−41.0	101.0						
	1200	9.4		1.92×10^{-2}						
13	1000	6.4	−54.6	3.9×10^{-2}						
	1200	8.6		2.8×10^{-2}						
14	1000	−46.0	−59.3	1.16×10^{10}						
	1200	−43.4	−54.3	7.94×10^{7}						

TABLE 5 — THEORETICAL AMOUNTS OF REACTANTS AND PRODUCTS IN VARIOUS METAL EXTRACTION PROCESSES

Extraction process for:	Basis, 1 kg	Reaction	Reactants required, kg				Products formed, k_g			
Aluminum	Anorthite	4	$CaO \cdot Al_2O_3 \cdot 2SiO_2$ (1)	C (0.345)	Cl_2 (2.036)		$AlCl_3$ (0.956)	$CaCl_2$ (0.399)	$SiCl_4{}^a$ (1.221)	CO (0.805)
	Electrolyte	---	$AlCl_3$ (0.05)	Alkali and alkaline earth chlorides (0.95)			Al (0.0101)	Cl_2 (0.0399)		
Titanium and iron	Ilmenite	5	$FeTiO_3$ (1)	C (0.040)	Cl_2 (0.463)		$FeCl_3$ (0.708)	TiO_2 (0.463)		CO (0.093)
		10	TiO_2 (0.463)	Ca (0.463)			CaO (0.650)	Ti (0.277)		
		7	$FeCl_3$ (0.708)	O_2 (0.053)			Fe_2O_3 (0.347)	Cl_2 (0.463)		
		8	Fe_2O_3 (0.347)	H_2 (0.013)			Fe (0.243)	H_2O (0.117)		
Magnesium	Olivine	11	Mg_2SiO_4 (1)	CaO (1.594)	Si (0.200)		Ca_2SiO_4 (2.448)	Mg (0.346)		

a If $SiCl_4$ formation is suppressed, 0.775 kg of SiO_2 can be recovered.

TABLE 6 — THEORETICAL HEAT REQUIREMENTS AND SENSIBLE HEATS FOR SOME REACTIONS IN METAL EXTRACTION PROCESSES

Extraction process for:	Reaction	Temperature, K	H_T-H_{298} reactants, Kcal	Enthalpy of reaction ΔH, °T, Kcal	Sensible heat in products H_T-H_{298}, Kcal
A1	4	1000	119.8	11.9	141.2
Ti	5	1100	37.4	-76.0	158.3
	10	1200	29.9	-51.5	31.4
Fe	7	600	17.8	-8.6	18.4
	8	1000	38.9	15.3	161.8
Mg	11	1500	115.6	64.7	178.7

TABLE 7 — ILMENITE PROCESSING DETAILS[a]

a Based on experiments in references 11 and 12.

b Requirements should at least be doubled; 1 day in use, the next day being recycles.

Year (SMF frame)	2	3	4	5	6
Ilmenite concentrate (X 10^{-3} tons/year)	16	40	61	81	81
Tubes in use	465	1160	1770	2350	2350
Rutile requirement, tons	7.4	18.4	28.1	37.3	37.3
Carbon requirement, tons/day	1.8	4.4	6.7	8.9	8.9
Chlorine requirement, tons/day	20.3	50.8	77.5	103	103
Ferric chloride produced, X 10^{-3} tons/year	11.3	28.3	43.1	57.3	57.3
Rutile produced, X 10^{-3} tons/year	7.4	18.5	28.2	37.5	37.5
Carbon monoxide produced, tons/day	4.1	10.2	15.6	20.7	20.7
Tubes producing hematite	230	580	885	1175	1175
Oxygen requirement,[b] tons/day	4.6	11.4	17.4	23.1	23.1
Hematite produced, X 10^{-3} tons/year	5.6	13.9	21.2	28.1	28.1
Hydrogen requirement, tons/day	0.58	1.44	2.20	2.92	2.92
Iron produced, X 10^{-3} tons/year	3.9	9.7	14.8	19.7	19.7
Calcium requirement, tons/day	20.3	50.8	77.5	103	103
Titanium produced, X 10^{-3} tons/year	4.4	11.1	16.9	22.4	22.4

REFERENCES

1. Driggers, G. W.: Baseline L5 Construction Station, in Space Manufacturing Facilities. Proceedings of the Princeton/AIAA/NASA Conference, May 7-9, 1975, Jerry Grey, ed., American Institute of Aeronautics and Astronautics, Inc., New York, N.Y. 10019.

2. Levinson, Alfred A.; and Taylor, S. A.: Moon Rocks and Minerals. Pergamon Press, New York, 1971.

3. Geake, J. E.: The Physics of Lunar and Planetary Surfaces. Contemporary Physics, vol. 15, no. 2, 1974, pp. 121-158.

4. Grodzka, G. P.: Process Chemistry of L5, in Space Manufacturing Facilities. Proceedings of the Princeton/AIAA/NASA Conference, May 7-9, 1975, Jerry Grey, ed., American Institute of Aeronautics and Astronautics, Inc., N.Y., 10019.

5. Johnson, Richard D., ed.: Space Settlements, A Design Study. NASA-Ames Research Center, Scientific and Technical Information Office, National Aeronautics and Space Administration, Washington, D.C. 1977.

6. Patterson, S. H.: Aluminum from Bauxite: Are There Alternatives? American Scientist, vol. 65, 1977, p. 345-351.

7. Ampain, S. G.: Lime Soda Sinter Process, Correlation of Reaction Products with Extractability of Aluminum from Anorthsite. U.S. Bureau of Mines, RI 6933, April 1967.

8. Grjotheim, K.; Khron, E.; Malinovsky, M.; Matisyovsky, K.; and Thonstand, J.: Aluminum Electrolysis, Aluminum-Verlag Gmbh-Dusseldor, 1977.

9. Gitlesen, G.; Herstad, O.; and Motzfeldt, K.: Selected Topics in High Temperature Chemistry. Forland, T., Grjotheim, K., Motzfedlt, K., and Urnes, S., eds., Oslo, 1966.

10. Stroup, P. T.: Cartothermic Smelting of Aluminum. Trans. Met. Soc. AIME, vol. 230, no. 3, 1964, pp. 356-372.

11. Striplin, M. M.; and Kelley, W. M.: Aluminum Silicon Alloys by Electrothermal Reduction of Clay with Coke. Chem. Eng. Progress, vol. 43, no. 10, Trans. Am. Inst. Chem. Engrs., 1947, pp. 569-578.

12. Peacy, J. G.; and Grimshaw, R. W.: Aluminum from the Rapid Quenching of Carbothermic Aluminum Monochloride Vapors. Twelfth Annual CIM Conference of Metallurgists, Quebec City, August 26-29, 1973.

13. Mitterbiller, K.; and Fruhwein, Walter: Aluminum, German Patents 604,597, 1934; 607,561, 1935.

14. Yerkes, L. A.; and Fursman, O. C.: Refining Crude Aluminum by Sulfide Reaction. U.S. Bureau of Mines, RI 5773, 1961.

15. Hoekje, J. J.; and Kearley, A. A.: Titanium Dioxide From Ilmenite by Caustic Fusion. British Patent 846, 468, Aug. 31, 1960.

16. Daubenspeck, John M.; and Schmidt, Charles L.: Removing Iron From Titanium Ores With Chlorine in a Fluidized Bed. U.S. Patent 2,852,362, Sept. 16, 1958.

17. Chertien, A.; and Wyss, R.: Compt. Rend, vol. 224, 1947 , p. 1642.

18. Grjotheim, K.; Herstad, O.; Skarbo, R.; and Toguri, J. M.: The Aluminum Reduction of Magnesium Compounds. III — The Vapor Pressure of Magnesium Over the System Al-MgSiO$_4$ (olivine). Can. J. Chem., vol. 41, 1963, pp. 739-742.

19. Grjotheim, K.; Johansen, K. H.; Motzfeldt, K.; and Rao, D. B.: Thermal Reduction of Olivine by Calcium Carbide and by Silicon in the Presence of Calcium Oxide. Can. Met. Quart., vol. 9, no. 2, 1970, pp. 389-394.

20. Pidgeon, L. M.: New Methods for the Production of Magnesium. Trans Can. Inst. Min. Met., vol. 47, 1944, pp. 16-18.

21. Pidgeon, L. M.; and King, J. A.: Vapor Pressure of Magnesium in the Thermal Reduction of Magnesium Oxide by Ferrosilicon. Disc. Faraday Soc., no. 4, 1948, pp. 197-206.

22. Wynnyckyi, J. R.; and Pidgeon, L. M.: Equilibria in the Silicothermic Reduction of Calcined Dolomite. Met. Trans., vol. 2, 1971, pp. 979-986.

23. Johansen, K. H.: Chemical Studies Concerning the Thermal Production of Magnesium. Thesis, The Technical University of Norway, 1967 (in Norwegian).

24. Johnson, R. D.; and Holbrow, C., eds.: Space Settlement — A Design Study. NASA SP-413, 1977, p. 53.

25. Rosenberg, S. D.; Gryter, G. A.; and Miller, F. E.: Manufacture of Oxygen from Lunar Materials. Annals N.Y. Academy of Sciences, vol. 123, 1965, pp. 1106-1122.

26. Cabrera, A. L.; Mahle, M. B.; Asunmaa, S. K.; and Arrhenius, G.: Formation of Water and Methane, Catalyzed by Lunar Dust. Abstract in Lunar Utilization, Conf. Mar. 16, 1976, Criswell, D. R., ed., 1976, pp. 96-105, Lunar Science Institute, Houston, 1976.

27. Kudo, Tetsuichi; and Obayashi, Hidehito: Oxygen Ion Conduction of the Fluorite-Type $Ce_{1-x}Ln_xO_{2-x/2}$ (Ln — Lanthanoid Element). J. Electro. Chem. Soc., voi. 122, no. 1, 1975, pp. 142-147.

28. Tuner, H. L.; and Nowick, A. S.: Doped Ceria as a Solid Oxide Electrolyte. J. Electrochem. Soc., vol. 122, no. 2, 1975, pp. 255-259.

29. Weissbart, Joseph; Smart, Wilson; and Wydeven, Theodore: Oxygen Reclamation from Carbon Dioxide Using a Solid Oxide Electrolyte. Aerospace Medicine, vol. 40, no. 1, 1969, pp. 136-140.

V-6
Mining and Beneficiation
of Lunar Ores

RICHARD J. WILLIAMS, DAVID S. McKAY, DAVID GILES, and THEODORE E. BUNCH

The beneficiation of lunar plagioclase and ilmenite ores to feedstock grade permits a rapid growth of the space manufacturing economy by maximizing the production rate of metals and oxygen. A beneficiation scheme based on electrostatic and magnetic separation is preferred over conventional schemes but such a scheme cannot be completely modeled because beneficiation processes are empirical and because some properties of lunar minerals have not been measured. To meet anticipated shipping and processing needs, the peak lunar mining rate will exceed 1000 tons/hr by the fifth year of operation. Such capabilities will be best obtained by automated mining vehicles and conveyor systems rather than trucks. It may be possible to extract about 40 kg of volatiles (60 percent H_2O) by thermally processing the less than 20-μ ilmenite concentrate extracted from 130 tons of ilmenite ore. A thermodynamic analysis of an extraction process is presented.

INTRODUCTION

It has been proposed that lunar rocks and soils will be useful raw materials for manufacturing materials for use in space construction (refs. 1, 2). Many factors relating to the use of lunar materials as industrial feedstocks have been discussed previously (ref. 3). However, a major topic of considerable practical importance to the utilization of lunar resources, the beneficiation of ores, has not been fully discussed in view of recent work on lunar samples and in lunar science. This paper examines the potentials for the mining and beneficiation of lunar materials.

The beneficiation of ores to an industrial feedstock grade is always desirable before such material is chemically processed, both because it reduces the size and energy requirements of chemical processes and because it can significantly reduce the complexity of such processes while increasing their efficiency (ref. 4). Also, since beneficiation usually requires only differentiation of components by physical properties, it is a relatively low-energy process (refs. 5, 6).

The physical and chemical properties of lunar ores are described elsewhere (refs. 3, 6). (The use of the word "ore" here is somewhat unusual, but we are assuming that the economic benefit of the use of these materials is established.) The availability of lunar materials rich in plagioclase and ilmenite (ref. 6); the proposal of chemical processing schemes to obtain Al and SiO_2 from plagioclase and Fe and Ti from ilmenite (ref. 4); the desire to produce CaO-MgO-Al_2O_3-SiO_2 fiberglasses (ref. 7); and the recognition that fine-grained ($<20\mu$) ilmenite is a potential source of lunar H_2 (ref. 6) have determined the type and scale of mining and beneficiation schemes discussed here.

Two very simple mass-flow economics by which lunar materials might be converted into useful products are illustrated in figure 1. Mining is, of course, confined to the lunar surface. Shipping carries material from the lunar surface to a manufacturing facility located in space; shipping includes packaging materials for transport, launch from the lunar surface, and transport within space from the Moon to the manufacturing facility. Launching and transportation are assumed to use "mass drivers" (refs. 1, 2). At the manufacturing facility (labeled "process" in fig. 1), the ores are converted to useful products. Neither the shipping nor the processing portions of these models is considered in any detail here.

Although the locations of mining and manufacturing are defined, beneficiation can occur either after (fig. 1, route A) or before (fig. 1, route B) shipping. Beneficiation on the lunar surface is developed here because, for a given shipping capacity, the removal of waste by beneficiation before shipping allows a larger mass of products to be produced. A consequence of this choice is that the mining output is larger than it would be for the model A in figure 1. Note that if the manufacturing were also on the lunar surface, an even larger
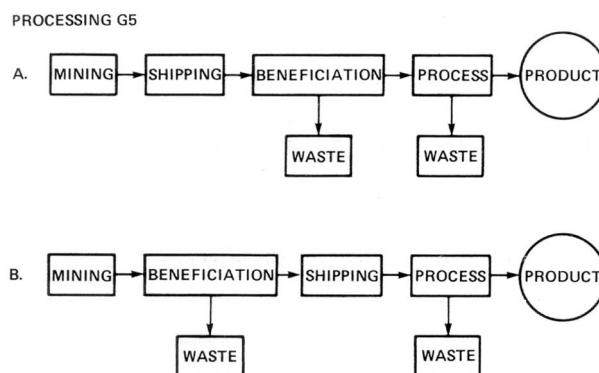
Figure 1 — *Mass flow for two mining and beneficiation, shipping, and processing schemes.*

mass of products could be shipped from the lunar surface. Here we consider only model B in figure 1, where mining and beneficiation occur on the lunar surface; the results of other studies (refs. 1-4, 6, 8, 9) are used to set the scales of the lunar surface operations.

BENEFICIATION SCHEMES

Fortunately, lunar soils are generally fine-grained (<100μ; ref. 3) and crushing is therefore unnecessary. However, disaggregation and size separation are preliminary steps in the beneficiation process. Subsequent beneficiation might involve the separation of a nonmagnetic phase from a weakly magnetic waste for plagioclase ore or of materials with different electrical properties and densities for ilmenite ores. We have proposed two schemes for doing this, one based on established available technology and the other on extrapolations of existing phenomena and technology.

Present Technology

The flow sheet for present technology is shown in figure 2(a). The ilmenite ore is a mature mare soil (ref. 6). The ore is first passed through a coarse sieve to remove fragments larger than 1 cm. After sieving, the material must pass through an airlock; it is then treated with an air cyclone that disaggregates the soil and removes the <20-μ particles. (No commercial, industrial-scale cyclones of this type exist.) These particles are separated into ilmenite and tailings by magnetic separators. The coarse fraction is separated for density on a pneumatic table and the dense fraction is magnetically refined to yield the ilmenite concentrate. All tailings and products must be transferred out through an airlock for shipment. Plagioclase ore is treated in much the same way, except that magnetic refinement is used to

concentrate the plagioclase. In a practical system, several parallel systems will be needed to handle the volume of ore. The cyclones that both disaggregate and separate according to size require large volumes of high-velocity gas (ref. 5). The use of air as a fluid medium for the beneficiation of the ores requires that large amounts of material be transferred from the vacuum of the lunar surface into an atmosphere and then returned to that vacuum. To do this with large amounts of materials at high rates (up to 1000 tons/hr, see below) without significant losses of air (if only as adsorbed gases) is a formidable technical problem.

Advanced Technology

An advanced technology system was designed and analyzed (fig. 2(b)). The ilmenite ore is coarse screened. The ore is sized and disaggregated by an electrostatic device in which the soil is charged and then separated for size based on its trajectory in an electrostatic field under lunar gravity. Figure 3 is a schematic diagram of this device; r and ρ are ranges for lunar materials (ref. 10), and ϵ, for terrestrial minerals (ref. 5).

The device was scaled using lunar gravity and the principles of electrostatics. The primary velocity for particles is supplied by falling in the lunar gravity field; the charging electrodes must supply an electrostatic field gradient in the direction of flow. Separation is achieved by diverting the particle flow into a tangential stream and nullifying a portion of the gravity force with electrostatic force. The resulting particle trajectories should permit separation based on particle size. The feed will vary in all three fundamental parameters (r, ρ, and ϵ) and thus 100 percent efficiency of separation is not possible. Only r and ρ are well known for the various materials that make up lunar soil; ϵ is known
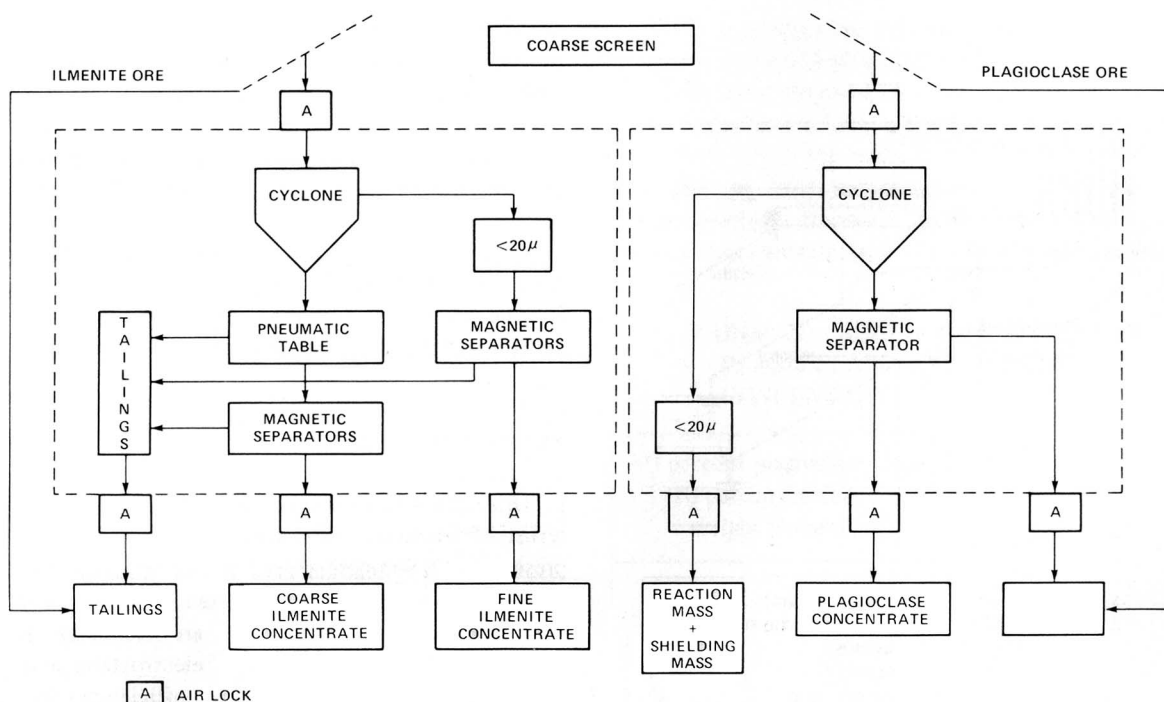
(a) Present technology, using fluid media for disaggregation and separation. This technique requires airlocks in the system.
Figure 2 — *Beneftciation of lunar ore.*
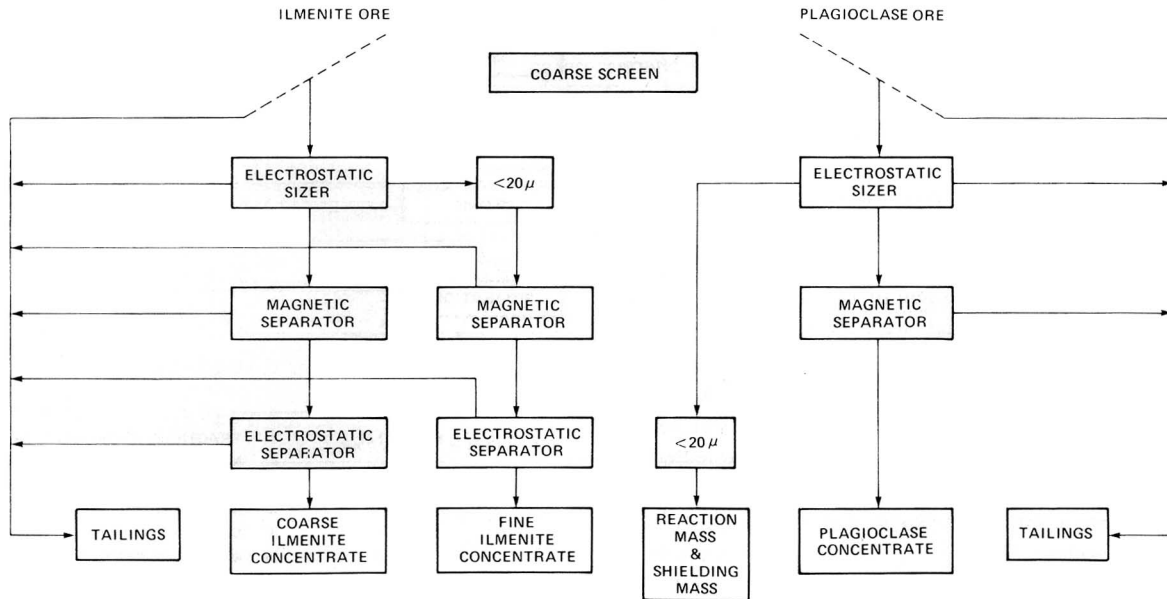
(b) Advanced technology, using electrostatic and magnetic devices to perform disaggregation and separation without media.
Figure 2 — *Beneftciation of lunar ore.*

only for bulk soils and rocks. The range of *r* is much greater than for ρ and thus, if ε is not the controlling parameter, size separation should be possible. The discharge surfaces are only schematic; a grounded metal conveyor may be needed. An interesting alternative might be to use electrostatic

levitation of the particles as a "frictionless" transport mechanism throughout the rest of the system. (A laboratory device that uses electrostatic fields to separate lunar soils according to size is discussed in ref. 11. However, to our knowledge, such a device does not now exist as commercial equipment.) After sizing, particles $>200\mu$ and those $<20\mu$ are first subjected to magnetic separation in a weak field to remove about 50 percent of agglutinitic glasses and, finally, ilmenite is electrostatically refined from the remaining silicates in separate streams.

Although electrostatic separation of a light fraction from a dark fraction has been demonstrated on lunar material (ref. 12), no quantitative data exist for lunar minerals from which

$$E \propto \varepsilon r^2 \;; \quad F \propto \rho r^3$$
$$\therefore (E - F) \propto [\varepsilon - \rho r]$$

F	GRAVITY FORCE
E	ELECTROSTATIC FORCE
r	RADIUS
ρ	DENSITY
ε	INDUCTANCE

RANGE:
ρ: 1.0 – ⩾4.5
r : 20 – 200
ε : 1 – 30 (?)
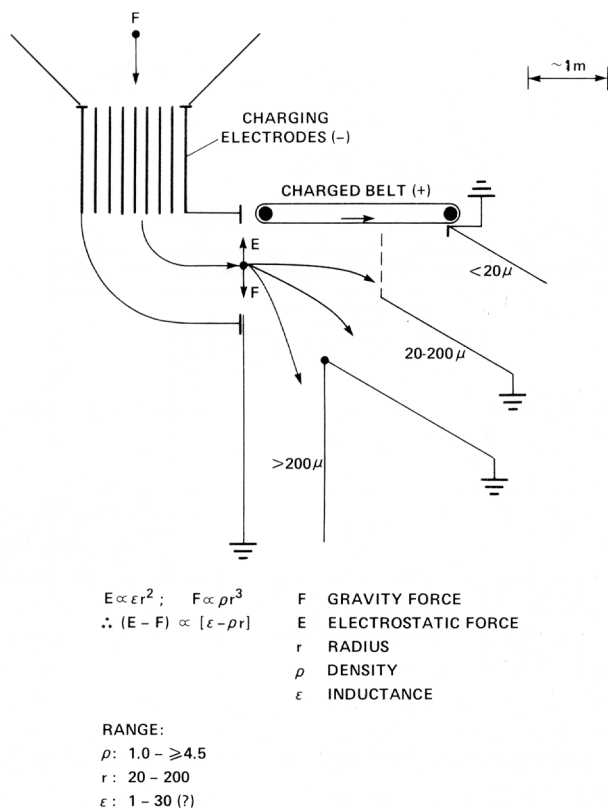
Figure 3 — *Schematic design sketch of the proposed electrostatic sizer. Device is scaled for lunar gravity, using the principles of electrostatics. This scale is only an order of magnitude because ε is not known for lunar materials. Note that, in practice, the charging electrode will have to supply an electrostatic gradient to permit flow-through.*

$$m_a = (f_s\, e_s\, f_e\, e_e\, f_m\, e_m)\, M_A$$
$$T_a = M_a - m_a$$
$$m_a = g_a\, M_a \,; \; g_a -$$
$$E_a = m_a / m_a$$

f	FRACTIONS IN ORIGINAL ORE
e	MASS EFFICIENCY OF SEPARATION
g	GRADE OF ORIGINAL ORE
M	MASS OF ORE MINED
T	MASS OF TAILINGS
m	MASS OF CONCENTRATE
E	OVERALL MASS EFFICIENCY

SUBSCRIPT:
a PLAGIOCLASE

Figure 4 — *Development of parametric approach to plagioclase ore beneficiation.*

to derive operating parameters and detailed sizes of equipment. We note that, in principle, the ilmenite could be beneficiated by a two-step magnetic separation process with fields of different intensities. However, since usual magnetic separators are somewhat heavier and consume more power than electrostatic systems (refs. 5, 13-15), we prefer electrostatic systems.

Plagioclase ore is treated similarly except the electrostatic refinement is unnecessary and the <20-μ fraction is collected for use as mass-driver reaction mass and as shielding at the space manufacturing facility (SMF).

Results of Beneficiation

This advanced system is analyzed in figures 4 and 5 in terms of fractions, efficiencies, and ore grade. Table 1 presents the parameters used in the analysis. The fractions (f) and grade (g) are based on lunar soil data (refs. 3, 6), the efficiencies (e) are estimates. In the absence of specific data on the electrostatic and magnetic properties of lunar minerals, efficiencies based on these properties can only be estimated. We also note that terrestrial beneficiation operations are also largely empirical (ref. 5). It is obvious that primary data should be collected and bench tests conducted.

Table 2 presents the calculated chemical composition of the ilmenite and plagioclase concentrates. These compositions were obtained by combining chemical analyses of the appropriate lunar minerals with those of the soil type from which the minerals would be extracted using the data on light matrix breccias for the plagioclase concentrate and those for high titanium basalts for the ilmenite concentrate (ref. 10). Enrichment factors (the weight ratio of the oxide

TABLE 1 — PARAMETERS FOR ORE BENEFICIATION[a]

Anorthite	Ilmenite			
$f_s = 0.99$	$f_s = 0.99$		$f_m^{\,c} = 0.5$	$f_e^{\,cl} = 0.13$
$f_e = 0.63$	$f_e^{\,c} = 0.63$		$f_m^{\,f} = 0.5$	$f_e^{\,fl} = 0.13$
$f_m = 0.40$	$f_e^{\,f} = 0.15$			
All e's = 0.93	All e's = 0.93			
$g_a = 0.60$	$g_i = 0.05$			

a f = fractions in original ore (from petrologic data, refs. 6 and 10), e = efficiency of process (assumed), and g = grade of ore (defined to be the mass fraction of the desired mineral in the mined soil, ref. 6). Subscripts and superscripts refer to process steps in figures 4 and 5.

TABLE 2 — BULK COMPOSITIONS OF PLAGIOCLASE AND ILMENITE CONCENTRATES

90 percent plagioclase and 10 percent residue, weight percent		90 percent ilmenite and 10 percent residue, weight percent	
SiO_2	44.90	SiO_2	3.78
TiO_2	0.05	TiO_2	48.10
Al_2O_3	33.67	Al_2O_3	1.07
Cr_2O_3	>0.01	Cr_2O_3	0.49
FeO	1.09	FeO	43.28
MnO	>0.01	MnO	0.03
MgO	1.35	MgO	1.29
CaO	18.59	CaO	1.07
Na_2O	0.45	Na_2O	0.04
K_2O	0.16	K_2O	>0.01
P_2O_5	0.03	P_2O_5	>0.01
S	>0.01	S	>0.02
Enrichment factor		Enrichment factors	
Al_2O_3	1.46	TiO_2	3.7
		FeO	2.2
(Relative to a light matrix breccia — e.g., 14063)		(Relative to a high titanium mare basalt — e.g., 70215)	

$m_i^f = (f_s\, e_s\, f_e^f\, e_e^f\, f_m^f\, e_m^f\, f_e^{f1}\, e_e^{f1})\, M_i$

$m_i^c = (f_s\, e_s\, f_e^c\, e_e^c\, f_m^c\, e_m^c\, f_e^{c1}\, e_e^{c1})\, M_i$

$m_i = m_i^f + m_i^c$

$T_i = M_i - m_i$

$m_i = g_i\, M_i$

$E_i = m_i / m_i$

f   FRACTIONS IN ORIGINAL ORE
e   MASS EFFICIENCY OF SEPARATION
g   GRADE OF ORIGINAL ORE
M   MASS OF ORE MINED
T   MASS OF TAILINGS
m   MASS OF CONCENTRATE
E   OVERALL MASS EFFICIENCY

SUBSCRIPTS:
a   PLAGIOCLASE
i   ILMENITE

Figure 5 — *Development of parametric approach to ilmenite beneficiation.*

in the concentrate to that in the appropriate bulk soil, for FeO, TiO_2, and Al_2O_3) over ore are substantial but not spectacular. The primary effect of the beneficiation is shown in figure 6. The useful mass (hashed area) is derived from considerations of reaction mass, shielding mass, and processing mass needed at the SMF and is scaled to the low profile model for lunar mass-driver capability (ref. 8). The dilution effect of useful mass by waste mass without beneficiation is obvious since useful mass is only 17 percent of mined mass.
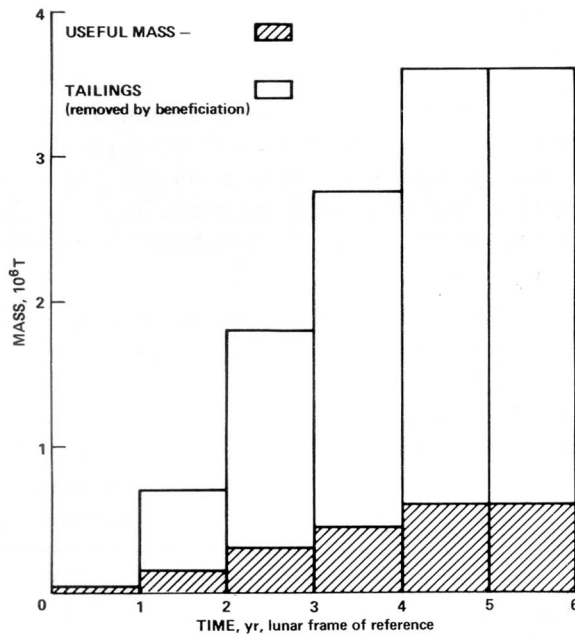
Figure 6 — *Total mined mass divided into waste mass removed during beneficiation and useful mass shipped to SMF Mass derived from the demand model developed from mass launcher, propulsion, shielding, and chemical processing requirements. Time scale refers to lunar surface operations, with year 1 being the first year of mass-driver operation. This time scale is about 1 year ahead of the SMF time line.*

MINING SCHEMES

Quantification of Mass Needs

The processes proposed for extracting Al from plagioclase (ref. 4) and Fe and Ti from ilmenite (ref. 4) and for producing fiberglass from process residues and plagioclase concentrate (ref. 15) can be set into a system to produce feedstock that is 83 percent plagioclase concentrate and 17 percent ilmenite concentrate. The products of such processing are shown in table 3. It appears that the production of fiberglass will require about 4 percent of the total capacity; therefore, the data in table 3 are normalized to this factor. The residue, a rather complex silicate-oxide mixture, is assumed to be an adequate shielding material.

TABLE 3 — PRODUCTS OF SMF PROCESSING

Products/ton, feedstock (83 percent plagiocase 17 percent ilmenite)		
Product	With glass, kg	Without glass, kg
Al	96.1	96.1
Si[a]	—	139.4
Fe	53.8	53.8
Ti	47.1	47.1
Glass	598.7	—
O_2[a]	80.6	207.7
Residue[b]	123.7	454.8

a Assumed efficiency of 80% in production.
b Assumes all intermediaries recovered as residues, for terrestrial imports.

Furthermore, 20 percent of the shipped mass is allocated for use as reaction mass to move mass-driver tugs from L2 to the SMF. We assume that the mass for the first year (30,000 tons) will not be beneficiated or processed by our schemes, and that the residue from chemical processing will meet the shielding needs for the next year. The result is shown in figure 7, a system optimized to deliver maximum processible mass. Note that excess mass accumulates at the SMF during years 2 through 5 (the values are yearly mass budgets that are not cumulative) and that the 20-percent reaction mass is simply an assumption that has not been tested or optimized. After year 5, waste will simply accumulate at the SMF unless further growth occurs; this may present problems if a static future is assumed.

The production from chemical processing is summarized in figure 8. The percentages are normalized to exclude residues. These production data and the beneficiation analysis (figs. 4 and 5) can be back-calculated to scale the mining operations (fig. 9) and waste/useful mass data (fig. 6). Finally, the data are presented in numerical form in table 4. The mining rate was derived from a 3700 hr/yr work time, which is based on the lunar day/night cycle, a loss of one shift at the beginning for startup and one at the end of each day for shutdown, and 7.5-hr production for each 8-hr shift.[1]
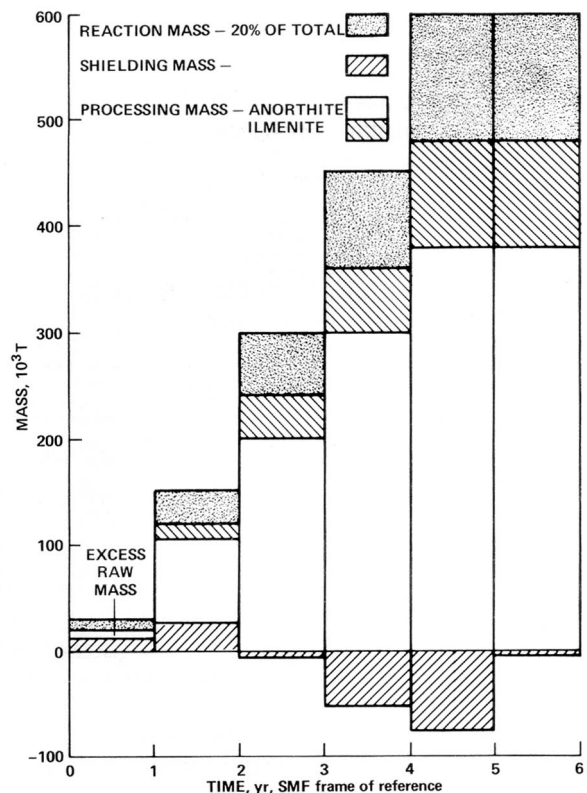

Figure 7 — *Distribution of mass type shipped to SMF as a function of time in the SMF frame of reference. (See text for assumptions.)*

1 This working time could be increased by a factor of 2.2 if a source of continuous illumination and power were available; all rates would decrease by this factor. A potentially more severe problem, however, is the recovery of equipment from the extreme cold of the lunar night.
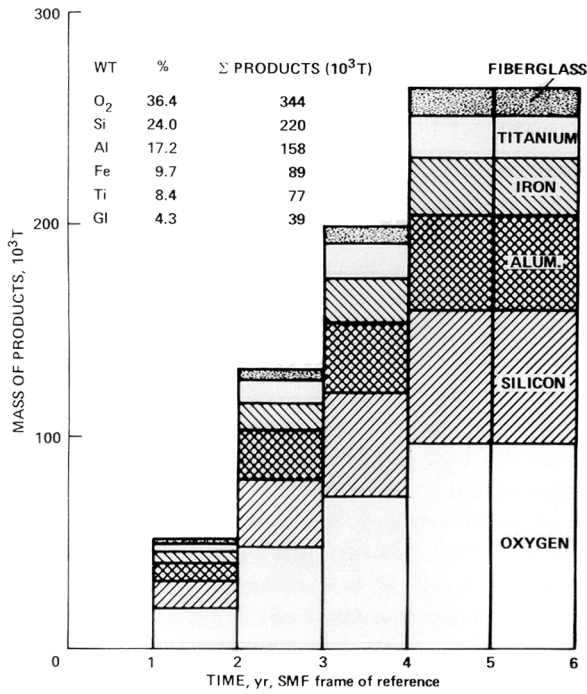
Figure 8 — *Mass of products produced at SMF by chemical processing using thermodynamic efficiencies to scale the outputs. Yearly outputs are not cumulative. Summation of products is for the 6 years of operation. Symbols are normal chemical symbols except G1, which is fiberglass.*
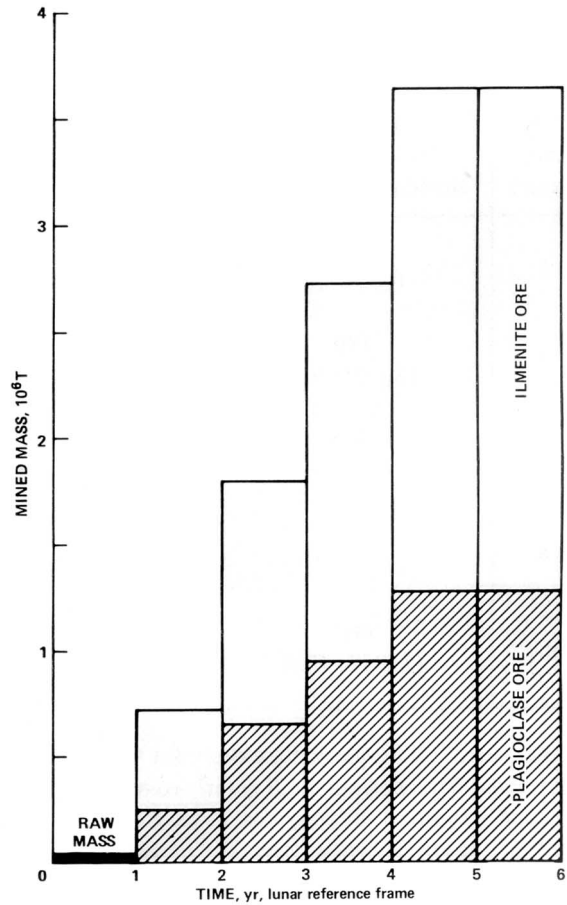

Figure 9 — *Mined lunar mass divided into ilmenite and plagioclase ores as a function of time.*

TABLE 4 — LUNAR MINING AND BENEFICIATIONS SCENARIO, YEARS 1 THROUGH 6

Year (lunar frame)	Shipped mass, 10^3 tons (reaction mass; shielding; processing)	Mined mass, 10^3 tons (ilmenite ore; plagioclase ore)	Beneficiation, 10^3 tons (ilm. conc., plag. conc., fines) (tailings)	Mining rate,[a] tons/hr	Mined area,[b] 10^4 M^2 (plagioclase; ilmenite)
1	30 (6; 24; 0)	30 (0; 0)	---	8	0.1 (---)
2	150 (30; 25; 95)	717 (464; 253)	717 (16; 79; 55) (567)	194	24 (8; 16)
3	300 (60; 0; 240)	1800 (1160; 640)	1800 (40; 200; 60) (1500)	486	60 (21; 39)
4	450 (90; 0; 360)	2726 (1769; 957)	2726 (61; 299; 90) (2346)	737	91 (31; 59)
5 and 6	600 (120; 0; 480)	3656 (2349; 1277)	3656 (81; 399; 120) (3056)	988	122 (43; 79)

a Assumed 3700 hr; plagioclase ore/total = 0.35; rounded to nearest ton.
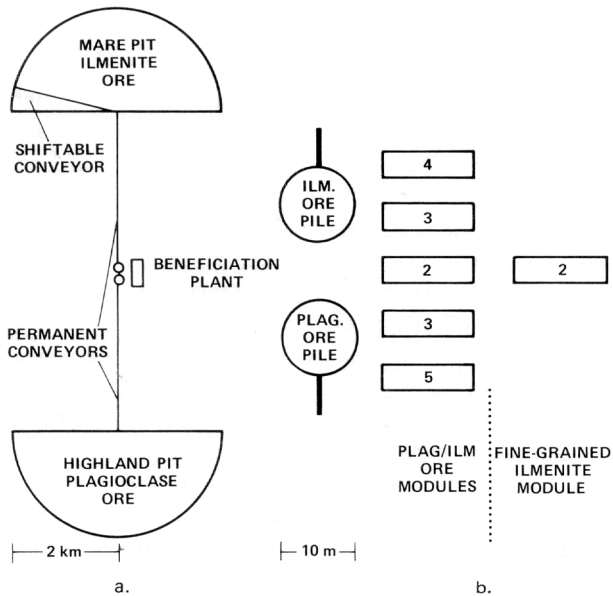b Assumed 2 m depth; ρ = 1.5 g/cm³; rounded.

Figure 10 — *Schematic maps of the lunar mining (a) and beneficiation operations (b). Pits are about 4 km apart; smaller separations may be possible. The shiftable conveyors are rotated through the arc of the pit as shown schematically, one shiftable conveyor per pit. Each pit contains sufficient volume for 5 years of operation at the maximum mining rate of 1000 tons/hr. The numbers shown in (b) represent year of emplacement. Operation for year 1, 30,000 tons/yr, is too small to show. Each module (in (b)) is about 30 m high. Note the ore stockpiles that are necessary for continuous operation.*

Quantification of Mining/Beneficiation System

The mining rates can now be converted to a rough map of the area to be mined (fig. 10(a)). The style and scale of mining changes after year 2; those for year 1 are small and can be handled by simple trucks. Table 5 gives estimates of the size, mass, and power of the processing modules. These values are based on data from references 5 and 12-14, but, in the absence of experimental data on beneficiation of lunar ores, they should be considered no more than order-of-magnitude estimates. Masses could be significantly less on the Moon. The masses of conveyors, supports, and module housing were not considered in table 5. Each module in table 5 is sized to accept over 220 tons/hr; they should meet the maximum mass flow need with about 10 percent excess capacity. The module in table 5B handles a <20-μ ilmenite fraction; only one should be needed even at maximum mass flows. Figure 10(b) summarizes a site layout and emplacement strategy. Although the separation of fine-grained ilmenite is primarily dictated by its potential as an H_2 ore, its separation does supplement ilmenite production by about 25 percent and thus its early emplacement is favored.

Figure 10(b) also illustrates another recommended part of a mining system — stockpiles. Space must be provided for stockpiles since they are essential so that, if a subsystem breaks down, the entire system will not be automatically crippled. The locations of the packaging plant and mass driver were not indicated in figure 10. Although we are certain that optimum sites for a mass driver and mining operations can be found and developed, we are not as confident that both will exist within a few hundred meters of each other. A connecting delivery system should be considered in any final base plans, but cannot be adequately quantified until site locations are defined. Finally, a problem implicit in figure 6 must be considered briefly. Considerable waste mass will be generated during these operations (3×10^6 tons, i.e., $\sim 3 \times 10^6$ m^3/yr at maximum mining rates). Although conveniently located craters can be filled with wastes initially, back-filling the mine site is the only feasible long-term solution. We have not analyzed this problem fully.

Table 6 presents an analysis of bottom scraper design in terms of load, size, speed, mining rate, and haul distance. The minimum pit separation that can be expected is 300 m (ref. 6); we have used this value and the pit sizes (table 4) to compute minimum haul distance and thus to compute trucking needs for lunar mining (table 7). Such vehicles

TABLE 5 — PROCESSING MODULES

	Size, m	Mass, tons[a]	Power, kW
A. Plagioclase and ilmenite ores			
1. Coarse sieve (<1 cm)	4 X 4 X 0.2	2	2
2. Electrostatic sizer	35 X 20 X 2.5	30	50
3. Magnetic separator	20 X 20 X 2	30	200
4. Electrostatic separator	15 X 10 X 2.5	15	20
		77	272
B. Fine ilmenite			
1. Magnetic separator	10 X 10 X 2	15	100
2. Electrostatic separator	10 X 5 X 2.5	10	15
		25	115

a Values are highly uncertain — taken from terrestrial experience where possible (refs. 5 and 12-14). However, the electrostatic sizer envisioned does not exist as a commercial device; it has been sized as an electrostatic separator. Magnetic separators are not superconducting devices. Masses have not been scaled for reduced lunar gravity.

would require about 100 kW per vehicle, within the range of fuel cell systems of reasonable size and mass. However, it is obvious that, for large-scale mining, the vehicles and mass involved become very large and are probably not feasible even without considerations of haul road construction and maintenance.

Since it is more likely that the pits will be several kilometers apart (fig. 10(a), ref. 6), trucks will probably not be a feasible option, and a conveyor system, such as that shown in figure 10(a), will be required. However, because of the general mobility and utility of trucks, several should be included in any base design. For comparison, an equivalent conveyor system is presented. The masses reported are for one belt system of equivalent length; power requirements will be about 100 kW/km. Finally, N' represents the number of 50-ton capacity loaders necessary to load the conveyor, derived by extrapolating to zero-haul distance for the parameterization in table 7.

TABLE 6 — PARAMETERIZATION OF TRUCKING

Parameters (bottom scrapers)
c = capacity, tons	d = depth of cut, m
s = maximum speed, km/hr	ℓ = length of cut, m
L = one-way haul length, m	w = width of cut, m
M_R = mining rate, tons/hr	ρ = density
f = duty cycle	
N = number of trucks	
x = ratio of loading and unloading speed to s	
$\ell = c/(dw\rho)$	

$$N = 2000\ f\ (M_R/cs)\ (xL + \ell)$$

An automated mining system of the required capacity could be developed: possibly a moderate-sized bucket-wheel excavator (ref. 19) that would feed a shiftable conveyor system (ref. 18). A commercial vehicle capable of handling 1000 tons/hr would have a terrestrial mass of 460 tons and would require about 715 kW. Since much of the mass is structural support, a lunar excavator would be less massive. Experience indicates that bucket wheels on the excavator would last about 150-200 hr (ref. 19); however, a longer

lifetime could be expected in excavating loose soil. Replacement parts and facilities for refitting and retooling must be available near the mine site. Maintenance and repair requirements must be considered in any advanced mining and beneficiation models.

A mature mining operation would proceed as follows: a shiftable conveyor would parallel the strip to be mined (fig. 10(a)). The bucket-wheel excavator would mine a 50-m-wide strip parallel to the belt. After the strip had been mined to a depth of 2 m, the excavator would move to the other pit and follow the same pattern. The unworked pit is backfilled with tailing from beneficiation. The shiftable belt would be pulled 50 m radially into its new location by trucks (fig. 10(a)). Each strip should be mined in 12.5 24-hr days. The remaining 1.5 days of the lunation would be used to startup and shutdown the operation. It will take almost 10 years to mine the two 2-km pits shown in figure 10(a) at 1000 tons/hr. Stripping to depths greater than 2 m should be possible; however, we have used 2 m for analysis because regoliths of this depth can be expected at almost any location on the lunar surface.

Summary of Mining and Beneficiation Scenario

Table 8 summarizes the lunar mining and beneficiation scenario and the mass and installed-power requirements. The mass and power estimates were presented earlier and are subject to the constraints as noted. To start the scenario, year -1 was chosen to display the predevelopment mapping required. A rational mining and beneficiation scenario cannot be developed without this step. Mining output for year 1 is too small to be analyzed in the present context: it is quite literally a dump-truck and shovel operation that can be handled by the base construction vehicles.

Although much of the mining and beneficiation operation is amenable to automation, it cannot be unmanned. An integral part of the operation will be to clear boulders and hazards and to survey the mining cuts so that the excavator can be used to its fullest. The basic device used will probably be a clamshell shovel and bulldozer derived from the base construction vehicles; it will probably be manned. Additional personnel will be required to maintain the

TABLE 7 — MINING OPERATIONS

Year (lunar)	Mining, tons/hr	Trucks,[a] no. mass in tons	Conveyor,[b] tons	(N')[a] no.	One-way haul, m
1	8	—	—	—	300
2	194	1; 20	5.1	1	425
3	486	2; 40	11.9	1	990
4	737	3; 60	15.3	1	1275
5	988	6; 120	22.1	1	1840
6	988	7; 140	27.2	1	2265

a Number derived from equation in table 6 (with $c = 50$, $s = 20$, $f = 0.8$, $d = 0.5$, $w = 3$, $\rho = 1$, and $x = 0.1$), rounded to highest integer value; mass rounded. Year 1 capacity is handled by much smaller vehicles. Data scaled from references 16 and 17. N' limit as $L \to 0$.

b Mass is 4 times belt mass. Belt size and speed are scaled to lunar gravity using the maximum mining rate; 2-m-wide V belt; data are from reference 18.

TABLE 8 — MINING AND BENEFICIATION SCENARIO

| Year (lunar)	Activity	Δ Mass, tons	Δ Power, kW
-1	Detailed mapping and exploration of site		
1	30,000 tons/yr, unbeneficiated Only coarse sieves[a]	2	2
	Mining by base construction Vehicles	10	100
2	717,000 tons/yr, beneficiated One plagioclase/ilmenite module[a]	77	272
	Two 2-km permanent conveyor	40	400
	Two large truck systems	40	200
	One tine ilmenite module[a]	77	115
3	1,800,000 tons/yr, beneficiated Two plagioclase/ilmenite modules[a]	154	544
	Two shiftable conveyor systems	40	400
4	2,726,000 tons/yr, beneficiated One plagioclase/ilmenite module[a]	77	272
5	One bucket wheel excavators	460	715
	3,656,000 tons/yr, beneficiated One plagioclase/ilmenite module[a]	77	272
		1054	3492

a Mass not scaled for reduced gravity.

machinery and to ensure quality control of the ore and concentrates. We estimate that at least 10 men/shift (30 total) without support personnel will be required, even with automation.

EXTRACTION OF VOLATILES FROM FINE-GRAINED ILMENITE

Much of the beneficiation effort will be expended in obtaining a fine-grained ilmenite concentrate because of its potential as a hydrogen ore (ref. 6). We performed a thermodynamic analysis of a device that could separate volatiles from the ore. Figure 11 illustrates a separation device and presents the equations that describe its physical behavior. Its chemical behavior is calculated from thermochemistry of C-O-H-S-N gases (ref. 20), assuming local equilibrium and the buffer conditions (ref. 21) given in figure 11. From gas release data and the boundary conditions in table 9, we computed the yields of volatiles. Such a system may offer a way to extract water from a lunar rock; it might be used either on the lunar surface or at the SMF to supplement water supplies.

The device functions as follows: volume V_1 is filled with fine-grained ilmenite and connected to evacuated volume V_2 by a pipe. While V_2 is maintained at 300 K, V_1 is heated to 1000 K, perhaps by a solar concentrator. The temperatures
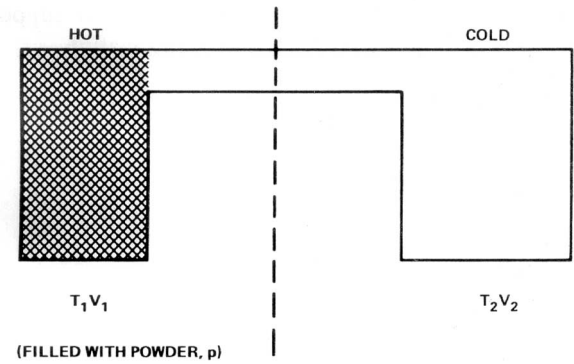
$V_1 = m_p/\rho_p$
$\Delta V = V_1 - m_p/\rho_m$
$p_1 = \Sigma n\, RT_1/\Delta V$
$V_2 = \Delta V(T_2/T_1)\,[(p_1/p) - 1]$
$F = V_2/\Delta V$
$m_i = FV_2 p_i (MW)_i/RT_2$

T TEMPERATURE (K)
V VOLUME
R GAS CONSTANT
ρ_m MINERAL DENSITY
ρ_p POWDER DENSITY
Σn MOLES OF GAS
p FINAL TOTAL PRESSURE
MW MOLECULAR WEIGHT OF SPECIES i
f_i FUGACITY OF SPECIES i

f_{O_2} BUFFERED AT T_1: Fe + TiO_2/FeTiO$_3$

f_{S_2} BUFFERED AT T_1: Fe/FeS

f_{H_2O} BUFFERED AT T_2: LIQUID SATURATION

Figure 11 — *Sketch and equations that describe the thermodynamic behavior of a device that extracts trapped volatiles from lunar materials.*

TABLE 9 — LUNAR GAS EXTRACTOR

Species	10X (g/T)	20X (g/T)
$H_2O(g)$	2	70
H_2	3	109
N_2	24	765
He	31	983
CO	48	1,530
CO_2	81	2,576
$H_2O(\ell)$	5,340	23,270
F	0.82	0.91
V_1	2.83×10^5 cc	2.83×10^5 cc
V_2	3.71×10^5 cc	1.06×10^7 cc

Note: Starting material: $<20\mu$ ilmenite 10x and 20x enrichments over mature mare soil (ref. 10) in C, H, N, S, and He. Only He has been shown to have these enrichments. It may be reasonable to hypothesize that hydrogen will be enriched like He (ref. 6). Assuming that C, N, and S are also enriched by this factor produces a worst case. Assumed release fractions (ref. 10) at 1000 K. H and He — 1.00; C, N, and S = 0.25. T_1 = 300 K; P = 10 atm. Ilmenite is 90 percent pure and the void ratio is 0.5.

are chosen so that liquid water can condense in V_2 and so that almost all the H_2 will be released from the powder in V_1 (the powder being not quite hot enough to sinter rapidly). The released volatiles react among themselves and with the powder to reduce some ilmenite to iron; the hydrogen and carbon are oxidized to water, carbon dioxide, and carbon monoxide. Sulfur reacts with iron to form FeS which

reduces sulfur gas species to negligible levels. Nitrogen and helium are unreacted. The partial pressure of water is great enough to cause liquid water to form in V_2; this extraction of water from the vapor causes most of the hydrogen to react to water. After reaction, the device can then be cooled and liquid water and gases tapped from V_2.

The release of volatiles during mining and beneficiation might decrease the amounts available for extraction. However, this loss should be less than 0.1 percent of the total content (analysis from data given in ref. 22). Finally, the reduction of ilmenite may be kinetically inhibited (ref. 23) to such a degree that local equilibrium cannot be assumed (but this can only be tested experimentally).

SUMMARY AND CONCLUSIONS

The lunar mining operation described here is not enormous in comparison to large terrestrial operations. The mining rates are large enough to warrant the use of bucket-wheel excavators and conveyors. Such systems are commercially available for terrestrial use and are amenable to high degrees of automation. However, the need for maintenance and for clearing and surveying operations suggests that the installation will be manned.

The beneficiation of lunar plagioclase and ilmenite ores is possible with existing technology. However, more advanced techniques based on electrostatics and magnetics should be developed; these techniques require a determination of the properties of lunar minerals and benchtop testing of devices on lunar materials or their similants. Beneficiation produces a system which is maximized in terms of useful mass that reaches chemical processing. The beneficiation of lunar ores on the lunar surface is useful and possible, but a full analysis must await the results of laboratory studies.

The mining and beneficiation of lunar materials is neither an enormously large operation nor is it a small operation. Consequently, it is difficult to evaluate the sensitivity of economic models of nonterrestrial industries to these operations. Further study, particularly of other models and optimization, should be undertaken.

REFERENCES

1. O'Neill, Gerard K.: Testimony on Solar Power from Satellites. Hearings before the Subcommittee on Aerospace Technology and National Needs of the Committee on Aeronautical and Space Sciences. U.S. Senate, Jan. 19 and 21, 1976, pp. 102-139.
2. O'Neill, Gerard K.: The Colonization of Space. Physics Today, vol. 27, no.9, Sept. 1974, pp. 32-40.
3. Phinney, William C.; Criswell, David; Drexler, Eric; and Garmirian, James: Lunar Resources and Their Utilization. AIAA Paper 77-537, Third Princeton/AIAA Conference on Space Manufacturing Facilities, Princeton, N.J., May 9-12, 1977.
4. Rao, D. Bhogeswara; Choudary, U. V.; Erstfeld, T. E.; Williams, R. J.; and Chang, Y. A.: Extraction Processes for the Production of Aluminum, Titanium, Iron, Magnesium, and Oxygen from Nonterrestrial Materials. Space Resources and Space Settlements, NASA SP-428, 1979, pp. 205-218.
5. Taggert, Arthur F.: Elements of Ore Dressing. John Wiley & Sons, Inc., New York, 195 1.
6. McKay, David S.; and Williams, Richard J.: A Geologic Assessment of Lunar Ores. Space Resources and Space Settlements, NASA SP-428, 1979, pp. 194-204.
7. Ho, Darwin; and Sobon, Leon E.: Extraterrestrial Fiberglass Production Using Solar Energy. Space Resources and Space Settlements, NASA SP-428, 1979, pp. 182-187.
8. O'Neill, Gerard K.: The Low (Profile) Road to Space Manufacturing. Astronautics & Aeronautics, vol. 16, no. 3, March 1978, pp. 24-32.
9. Bock, Edward H.; Lambrou, Fred, Jr.; and Simon, Michael: Effect of Environmental Parameters on Habitat Structural Weight and Cost. Space Resources and Space Settlements, NASA SP-428, 1979, pp. 35-57.
10. Handbook of Lunar Materials, Lunar and Planetary Science Division, NASA Johnson Space Center, Houston, Texas, June 1977.
11. Cabrera, A. L.; Maple, M. B.; Asunmaa, S. K.; and Arrhenius, G.: Formation of Water and Methane, Catalyzed by Lunar Dust. Lunar Utilization, Lunar Science Institute, Houston, Texas, 1976, pp. 96-lOS.
12. Gold, T.: Evolution of Moon Surface. In Proceedings of the Second Lunar Science Conference, Geochimica et Cosmochimica Acta, Suppl. 2, vol. 3, 1971, pp. 2675-2680.
13. Coerta, M.: Electric Separation of Fine and Ultrafine Mineral Particles. In Proceedings of the United Nations Interregional Seminar on Ore Concentrations in Water-Short Areas, 1966 (Publ. E.68. Il B.4 United Nations Pubn. Sales, New York, 1968, pp. 226-237.
14. Plaksin, I.: Electric Methods of Concentration. In Proceedings of the United Nations Interregional Seminar on Ore Concentrations in Water-Short Areas, 1966 (Publ. E.68 II B.4 United Nations Pubn. Sales, New York, 1968, pp. 214-226.
15. Magnetics and Electrostatics. World Mining — Catalog, Survey, and Directory, 1976, pp. 105-106, and 1977, pp. 121-122.
16. Carrier, W. David III; and Mitchell, James K.: Geotechnical Engineering on the Moon. Lunar Utilization, Lunar Science Institute, Houston, Texas, 1976, pp. 92-95.
17. Killibrew, C. H.: Tractor Shovels, Tractor Dozers, and Tractor Scrapers. Surface Mining, Eugene P. Pfleider, ed., American Inst. of Mining, Metallurgical, and Petroleum Engineers, Inc., New York, 1968, pp. 463-483.

18. Van Klounen, J. P.: Belt Conveyors. Surface Mining, Eugene P. Pfleider, ed., American Inst. of Mining, Metallurgical, and Petroleum Engineers, Inc., New York, 1968, pp. 484-504.

19. Aiken, G.: Continuous Methods. Open-Pit and Strip-Mining Systems and Equipment, American Inst. of Mining, Metallurgical, and Petroleum Engineers, Inc., New York, 1968, pp. 17-47 to 17-57.

20. Stull, Daniel R.; and Prophet, Harold; eds.: JANAF Thermochemical Tables, 2nd ed., Nat. Stand. Reference Data System, NSRDS-NBS 37, U.S. Government Printing Office, 1971.

21. Robie, Richard A.; and Waldbaum, David R.: Thermodynamic Properties of Minerals and Related Substances at 298.15 K (25.0° C) and One Atmosphere (1.013 bars) Pressure and at Higher Temperatures. U.S. Geological Survey Bulletin 1259, 1968.

22. Carrier, W. David III; Bromwell, Leslie G.; and Martin, R. Torrence: Strength and Compressibility of Returned Lunar Soil. In Proceedings of the Third Lunar Science Conference, Geochimica et Cosmochimica Acta, Supp 1.3, vol. 3, 1972, pp. 3223-3234.

23. Volk, W.; and Stotler, H. H.: Hydrogen Reduction of Ilmenite Ores in a Fluid Bed. Journal of Metals, vol. 22, no. 1, Jan. 1970, pp. 50-53.